Universidad de Alcalá
COMISIÓN DE ESTUDIOS OFICIALES
DE POSGRADO Y DOCTORADO

ACTA DE EVALUACIÓN DE LA TESIS DOCTORAL

(FOR EVALUATION OF THE ACT DOCTORAL THESIS)

Año académico (*academic year):* 2018/19

DOCTORANDO *(candidate PHD)*: **ZAPATA ARRÁEZ, FÉLIX**
D.N.I./PASAPORTE (*Id.Passport*): ******4718D**
PROGRAMA DE DOCTORADO *(Academic Committee of the Programme)*: **D415-QUÍMICA**
DPTO. COORDINADOR DEL PROGRAMA *(Department)*: **QUÍMICA ANALÍTICA, QUÍMICA FÍSICA E INGENIERÍA QUÍMICA**
TITULACIÓN DE DOCTOR EN *(Phd title)*: **DOCTOR/A POR LA UNIVERSIDAD DE ALCALÁ**

En el día de hoy 14/12/18, reunido el tribunal de evaluación, constituido por los miembros que suscriben el presente Acta, el aspirante defendió su Tesis Doctoral **con Mención Internacional** (*In today assessment met the court, consisting of the members who signed this Act, the candidate defended his doctoral thesis with mention as International Doctorate)*, elaborada bajo la dirección de (*prepared under the direction of)* CARMEN GARCÍA RUIZ**.**

Sobre el siguiente tema *(Title of the doctoral thesis)*: *VIBRATIONAL SPECTROSCOPY FOR THE CHARACTERIZATION OF EXPLOSIVE RESIDUES AND BODY FLUIDS*

Finalizada la defensa y discusión de la tesis, el tribunal acordó otorgar la CALIFICACIÓN GLOBAL[1] de (**no apto**, **aprobado, notable** y **sobresaliente)** *(After the defense and defense of the thesis, the court agreed to grant the GLOBAL RATING (fail, pass, good and excellent)*: SOBRESALIENTE / EXCELLENT

Alcalá de Henares, a ...14... de ...Diciembre....de 2018

Fdo. *(Signed)*: ...María López..... Fdo. *(Signed)*: FRANCESCO SAVERIO ROMOLO Fdo. *(Signed)*: .....

FIRMA DEL ALUMNO (candidate's signature),

Fdo. *(Signed)*: ...FÉLIX.....ZAPATA.. ARRÁEZ

Con fecha 21 de enero de 2019 la Comisión Delegada de la Comisión de Estudios Oficiales de Posgrado, a la vista de los votos emitidos de manera anónima por el tribunal que ha juzgado la tesis, resuelve:

☒ Conceder la Mención de "Cum Laude"
☐ No conceder la Mención de "Cum Laude"

La Secretaria de la Comisión Delegada

[1] La calificación podrá ser "**no apto**" "**aprobado**" "**notable**" y "**sobresaliente**". El tribunal podrá otorgar la mención de "cum laude" si la calificación global es de sobresaliente y se emite en tal sentido el voto secreto positivo por unanimidad. (*The grade may be "**fail**" "**pass**" "**good**" or "**excellent**". The panel may confer the distinction of "cum laude" if the overall grade is "Excellent" and has been awarded unanimously as such after secret voting.).*

INCIDENCIAS / OBSERVACIONES:
(Incidents / Comments)

Universidad de Alcalá

COMISIÓN DE ESTUDIOS OFICIALES
DE POSGRADO Y DOCTORADO

En aplicación del art. 14.7 del RD. 99/2011 y el art. 14 del Reglamento de Elaboración, Autorización y Defensa de la Tesis Doctoral, la Comisión Delegada de la Comisión de Estudios Oficiales de Posgrado y Doctorado, en sesión pública de fecha 21 de enero, procedió al escrutinio de los votos emitidos por los miembros del tribunal de la tesis defendida por *ZAPATA ARRÁEZ, FÉLIX*, el día 14 de diciembre de 2018, titulada *VIBRATIONAL SPECTROSCOPY FOR THE CHARACTERIZATION OF EXPLOSIVE RESIDUES AND BODY FLUIDS*, para determinar, si a la misma, se le concede la mención "cum laude", arrojando como resultado el voto favorable de todos los miembros del tribunal.

Por lo tanto, la Comisión de Estudios Oficiales de Posgrado **resuelve otorgar** a dicha tesis la

MENCIÓN "CUM LAUDE"

Alcalá de Henares, 22 de enero de 2019
EL VICERRECTOR DE INVESTIGACIÓN Y TRANSFERENCIA

P. Javier de la Mata de la Mata

Copia por e-mail a:
Doctorando: ZAPATA ARRÁEZ, FÉLIX
Secretario del Tribunal: MARÍA LÓPEZ LÓPEZ
Directora de Tesis: CARMEN GARCÍA RUIZ

Universidad de Alcalá

ESCUELA DE DOCTORADO
Servicio de Estudios Oficiales de Posgrado

DILIGENCIA DE DEPÓSITO DE TESIS.

Comprobado que el expediente académico de D./Dª Félix Zapata Arráez reúne los requisitos exigidos para la presentación de la Tesis, de acuerdo a la normativa vigente, y habiendo presentado la misma en formato: ☒ soporte electrónico ☐ impreso en papel, para el depósito de la misma, en el Servicio de Estudios Oficiales de Posgrado, con el nº de páginas: 462 se procede, con fecha de hoy a registrar el depósito de la tesis.

Alcalá de Henares a 17 de septiembre de 2018

Purificación Reviejo

Fdo. El Funcionario

VIBRATIONAL SPECTROSCOPY FOR THE CHARACTERIZATION OF EXPLOSIVE RESIDUES AND BODY FLUIDS

FÉLIX ZAPATA ARRÁEZ

DOCTORADO EN QUÍMICA
2018

Universidad de Alcalá

FACULTAD DE CIENCIAS
DEPARTAMENTO DE QUÍMICA ANALÍTICA, QUÍMICA FÍSICA E INGENIERÍA QUÍMICA
ÁREA DE QUÍMICA ANALÍTICA

Universidad de Alcalá

Departamento de Química Analítica, Química Física e Ingeniería Química
Área de química Analítica
Edificio Polivalente de Química
Ctra. Madrid-Barcelona Km. 33.600
28871 Alcalá de Henares (Madrid) España

CARMEN GARCÍA RUIZ, Catedrática de Química Analítica de la Universidad de Alcalá, como directora de esta tesis; y Mª PAZ SAN ANDRÉS LLEDÓ, Profesora Titular de Química Analítica de la Universidad de Alcalá, como tutora de esta tesis,

CERTIFICAN:

Que el trabajo descrito en la presente memoria, titulado **"VIBRATIONAL SPECTROSCOPY FOR THE CHARACTERIZATION OF EXPLOSIVE RESIDUES AND BODY FLUIDS"** ha sido realizado, respectivamente, bajo su dirección y tutorización por D. Félix Zapata Arráez en el Área de Química Analítica del Departamento de Química Analítica, Química Física e Ingeniería Química de esta Universidad. Esta Tesis se presenta en formato de compendio de artículos en los que el doctorando ha sido el principal ejecutor y primer autor; salvo en dos artículos en los que el doctorando ha sido segundo autor tras haber compartido con el primer autor la ejecución principal del trabajo. Por ello, autorizan su presentación y defensa para optar al grado de Doctor con Mención Internacional en Química por la Universidad de Alcalá.

Y para que conste y surta los efectos oportunos, firman el presente informe en Alcalá de Henares a 6 de Septiembre de 2018.

Dra. Carmen García Ruiz

Dra. Mª Paz San Andrés Lledó

Universidad de Alcalá

Departamento de Química Analítica, Química Física e Ingeniería Química
Área de química Analítica
Edificio Polivalente de Química
Ctra. Madrid-Barcelona Km. 33.600
28871 Alcalá de Henares (Madrid) España

JESÚS ALBERTO ESCARPA MIGUEL, Catedrático de Química Analítica, Director del Departamento de Química Analítica, Química Física e Ingeniería Química de la Universidad de Alcalá, y Coordinador del Programa de Doctorado en Química,

CERTIFICA:

Que el trabajo descrito en la presente memoria, titulado **"VIBRATIONAL SPECTROSCOPY FOR THE CHARACTERIZATION OF EXPLOSIVE RESIDUES AND BODY FLUIDS"** ha sido realizado en este departamento por D. Félix Zapata Arráez bajo la dirección de la Dra. Carmen García Ruiz, Catedrática en dicho departamento; y bajo la tutorización de la Dra. Mª Paz San Andrés Lledó, Profesora Titular en dicho departamento.

Y para que conste y surta los efectos oportunos, firma el presente informe en Alcalá de Henares a 11 de Septiembre de 2018.

Dr. Jesús Alberto Escarpa Miguel

Universidad de Alcalá

D. Jesús Alberto Escarpa Miguel, Coordinador de la Comisión Académica del Programa de Doctorado en Química

HAGO CONSTAR que la Tesis Doctoral titulada *Vibrational spectroscopy for the characterization of explosive residues and body fluids*, presentada por D. Félix Zapata Arráez, bajo la dirección de la Dr/a. Carmen García Ruiz, ha sido realizada por compendio de artículos, reuniendo los requisitos exigidos a este tipo de tesis, así como los requisitos científicos de originalidad y rigor metodológicos para ser defendida ante un tribunal. Esta Comisión ha tenido también en cuenta la evaluación positiva anual del doctorando, habiendo obtenido las correspondientes competencias establecidas en el Programa.

Para que así conste a los efectos del depósito de la tesis, se firma en Alcalá de Henares a 11 de Septiembre de 2018

Fdo.: Jesús Alberto Escarpa Miguel

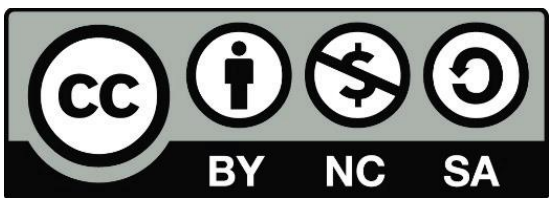

VIBRATIONAL SPECTROSCOPY FOR THE CHARACTERIZATION OF EXPLOSIVE RESIDUES AND BODY FLUIDS

FÉLIX ZAPATA ARRÁEZ

2018

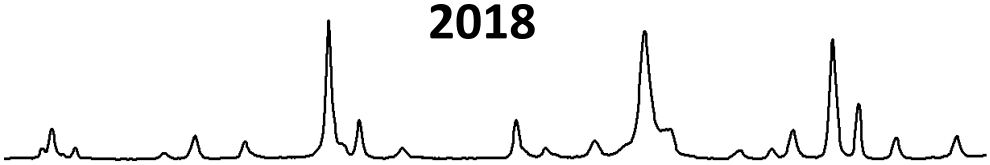

DEPARTAMENTO DE QUÍMICA ANALÍTICA, QUÍMICA FÍSICA E INGENIERÍA QUÍMICA

ÁREA DE QUÍMICA ANALÍTICA

DOCTORADO EN QUÍMICA

El trabajo de investigación que se recoge en esta Tesis ha sido posible gracias al aprovechamiento de las ayudas de Formación de Personal Investigador de la Universidad de Alcalá (durante el curso 2014-2015) y de Formación de Profesorado Universitario (FPU14/00790) del Ministerio de Educación, Cultura y Deporte (en el periodo 2015-2018); así como de la financiación recibida a través de distintos proyectos de la Comisión Europea (proyecto HOME/2011/ISEC/AG/4000002480), del Ministerio de Ciencia e Innovación (proyecto CTQ2014-58688-R), de la Universidad de Alcalá (proyecto CCG2013/EXP-021) y del Instituto Universitario de Investigación en Ciencias Policiales (proyecto IUICP/2016/002).

A mi familia, especialmente a mis padres y mis hermanas…

A los Cuerpos Policiales, que trabajan cada día por hacer de nuestro país un lugar más seguro…

A las víctimas del terrorismo…

A las víctimas de abusos y agresiones sexuales…

A todo aquel que se tome la molestia de leer esta Tesis, aunque sean unas pocas líneas…

Tras varios años de supervivencia
haciendo investigación muy concreta,
¿resultados? La presente libreta…
y la más inolvidable experiencia.

Hacer la tesis requiere paciencia,
pues en la investigación no hay receta,
solo el ingenio de una mente inquieta
y altas dosis de esfuerzo y resiliencia.

Requiere trabajo, duro y constante,
cuarenta y ocho meses intensivos
en pos de algún resultado brillante.

¿Qué tesis, de ambiciosos objetivos?
¿qué tema, tan difícil y acuciante,
se presenta en los versos sucesivos?

La detección, rápida y al instante,
de fluidos biológicos y explosivos
mediante métodos no destructivos,
un desafío, harto relevante.

Es para mí, también reto importante
mi pasión por los versos creativos:
endecasílabos siempre atractivos
ataviados con rima consonante.

Es por ello que, como consecuencia,
quise abordar una primera meta:
la combinación de poesía y ciencia.

Y ya puedo decir: ¡Misión completa!
El fin del soneto así lo evidencia.
Félix, investigador y poeta.

Félix Zapata Arráez

Summary

Resumen

This Doctoral Thesis entitled "Vibrational spectroscopy for the characterization of explosive residues and body fluids" is structured in three sections:

- Analytical studies about the transfer of explosive residues
- Spectroscopic approaches for the identification of explosive residues
- Spectroscopic strategies to identify stains of body fluids

Each section is composed of three chapters, in such a way that this Thesis is composed of a total of nine chapters.

Section 1 includes Chapters 1, 2 and 3, in which the transfer of residues is investigated, either the transfer of gunshot residues as a result of firing, or the transfer of explosive residues through fingerprints.

In Chapter 1, the correlation between the dispersion of gunshot residues in the target and the shooting distance using multispectral imaging was investigated. For this purpose, the same ammunition and weapon was fired at a series of targets placed at different distances in the range of 10-220 cm inside a shooting gallery. The targets were analysed by multispectral imaging and subsequently, the pixels corresponding to gunshot residues were quantified. These values were plotted against the shooting distance, obtaining a decreasing exponential equation in the range of 30-220 cm with an excellent coefficient of determination. The effectiveness of the method was tested with blind samples in which its trigger distance was successfully determined by applying the obtained equation.

In Chapter 2, the transfer of different explosives on two different surfaces (cotton/polycarbonate) through consecutive fingerprints was studied. As in the previous chapter, the quantification of pixels containing explosive particles were calculated using imaging. First, the influence of the subject in the transfer of explosive residues did not seem to be significant when following a defined procedure. Secondly, it was observed that the transfer depended on both the type of explosive and the type of surface. Finely powdered organic explosives showed an exponential / potential decrease in their transfer over cotton / polycarbonate in the ten consecutive fingerprints. On the contrary, the oxidizing salts (hygroscopic and with larger particle size) showed no tendency in their transfer.

In Chapter 3, the complementarity of Raman spectroscopy and ion chromatography for the determination of the inorganic components that are transferred to handprints after handling an explosive was researched. Specifically, several subjects manipulated different inorganic explosives and the explosive residues transferred to their hands (specifically to their handprints) were then analysed. For Raman spectroscopy, the subjects pressed their hands on a plastic adhesive tape. For ion chromatography, the subjects pressed their hands on glass trays, to which a certain volume of water was added later. The respective analyses showed that Raman spectroscopy allowed a better identification of the cation-anion pair of the major inorganic salts, whereas ion chromatography enabled a better quantification of the ions in solution (both major and minor ions).

Section 2 includes Chapters 4, 5 and 6, in which the identification and characterization of explosives is studied by vibrational spectroscopy.

In Chapter 4, the theme of explosives was contextualized providing a general critical review of the most relevant key aspects in the field of explosives, including their definition and classification. Interestingly, a new classification based on the chemical composition of explosives was proposed. On the other hand, the historical evolution of the discoveries of those explosives that are subsequently investigated in this Thesis was contextualized. Finally, the terrorist attacks perpetrated with explosives were compiled to show the transcendence and terrible repercussion that explosives have worldwide and particularly in Europe.

In Chapter 5, the Raman, Fourier transform infrared (FTIR) and near infrared (NIR) spectra of the explosives and oxidizing salts under study are shown and interpreted. First, explosives were analysed by FTIR and Raman. Secondly, oxidizing salts (nitrates, chlorates and perchlorates) were analysed by FTIR and Raman. In both cases, the different spectral bands were assigned with the corresponding fundamental molecular vibrations; and the selectivity and suitability of both techniques for the discrimination of explosives / oxidizing salts was studied. Thirdly, explosives and some oxidizing salts were analysed by NIR. Similarly, the NIR bands were correlated with the corresponding overtones/ combination bands and the selectivity of NIR spectroscopy was studied. In conclusion, either Raman, FTIR or NIR enabled the unequivocal identification

of explosives; except those explosive mixtures having very similar chemical composition, and some oxidizing salts composed of the same anion.

In Chapter 6, the identification of post-blast explosive residues by FTIR and Raman was studied. First, some fundamental theoretical concepts about the detonation of explosives were briefly explained and compared with simple empirical observations of real detonations. For this purpose, safe controlled detonations of a series of explosives were made and photographed, and the different materials exposed to the explosion were collected. Subsequently, these post-blast materials were analysed in search of explosive traces. Particularly, intact particles of the inorganic components of oxidizer-fuel mixtures were identified in post-blast residues of either pyrotechnic devices or improvised explosive devices. However, traces of uni-molecular organic explosives were not detected.

Section 3 comprises Chapters 7, 8 and 9, in which the identification of stains of body fluids is studied by means of vibrational spectroscopy.

In Chapter 7, the scientific literature published to date about the identification of body fluids using spectrometric techniques was revised. In brief, most research was performed using UV-Vis spectroscopy, Raman spectroscopy and IR spectroscopy. Since this review was done at the beginning of the doctorate (2015), a final section is appended that updates the research published during the last years (2015-2018).

In Chapter 8, the suitability of FTIR spectroscopy for discriminating stains of semen, vaginal fluid and urine on cotton fabrics was researched. First, it was visually evidenced that the FTIR spectra of the stains of each body fluid were different from each other and different from that of cotton. The main bands of the spectra of urine stains correlated with the molecular vibrations of urea, while the spectra of stains of semen and vaginal fluid were due to the peptide bonds of the different proteins that compose them. Secondly, different methods of multivariate analysis were investigated, which significantly supported the discrimination of the stains of each fluid. However, the one-spot measurements of FTIR spectroscopy did not allow to resolve mixtures of several fluids, since only one of the fluids was detected.

In Chapter 9, the suitability of NIR-HSI for discriminating stains of semen, vaginal fluid and urine on cotton fabrics was researched. The study mainly

focused on solving the challenge of mixtures of several body fluids. Although it was noted that the spectral differences in the NIR region between the three fluids were less evident than in the MIR region, the multivariate analysis still allowed discrimination of the three body fluids. In addition, this discrimination was even possible in mixtures due to the capability of hyperspectral imaging of simultaneously recording the NIR spectra of all the pixels of the image. This way, those areas of the stain with the highest proportion of semen were determined and visualized by means of chemical mapping.

Esta Tesis Doctoral titulada “Espectroscopía vibracional para la caracterización de residuos de explosivos y fluidos biológicos” se estructura en tres secciones:

- Estudios analíticos sobre la transferencia de residuos de explosivos
- Aproximaciones en espectroscopía para la identificación de residuos de explosivos
- Estrategias espectroscópicas para la identificación de manchas de fluidos biológicos

Cada una de las tres secciones se compone a su vez de tres capítulos, de tal forma que la Tesis se compone de un total de nueve capítulos.

Así, la **Sección 1** comprende los Capítulos 1, 2 y 3, en los que se investiga la transferencia de residuos, bien la transferencia de residuos de disparo a consecuencia de un disparo, o bien, la transferencia de residuos de explosivo a través de huellas dactilares.

En el Capítulo 1 se ha investigado la posibilidad de correlacionar la dispersión de los residuos de disparo en la diana con la distancia de disparo mediante imagen multiespectral. Para ello, se disparó con la misma arma y munición a una serie de dianas dispuestas a diferentes distancias en el rango de 10-220 cm dentro de una galería de tiro. Las dianas se analizaron mediante imagen multiespectral y posteriormente, se cuantificaron los píxeles correspondientes a residuos de disparo. Estos valores se representaron frente a la distancia de disparo, ajustándose, en el rango de 30-220 cm, a una ecuación exponencial decreciente con un excelente coeficiente de determinación. La eficacia del método se comprobó con muestras ciegas en las que se determinó exitosamente su distancia de disparo aplicando la ecuación obtenida.

En el Capítulo 2 se ha investigado la transferencia de residuos de diferentes explosivos sobre dos superficies distintas (algodón/policarbonato) a través de impresiones dactilares consecutivas. Para ello, se empleó también un sistema de imagen y la cuantificación de los píxeles que contenían partículas de explosivo. En primer lugar, se comprobó que la influencia del sujeto no era significativa en la transferencia de residuos de explosivo cuando se seguía un procedimiento definido. En segundo lugar, se observó que la transferencia dependía tanto del tipo de explosivo como del tipo de superficie. Los explosivos orgánicos finamente pulverizados mostraron un decrecimiento exponencial/potencial en su transferencia sobre algodón/policarbonato en las

diez impresiones dactilares consecutivas. Por el contrario, las sales oxidantes (higroscópicas y con mayor tamaño de partícula) no mostraron ninguna tendencia.

En el Capítulo 3 se ha investigado la complementariedad de las técnicas espectroscopía Raman y cromatografía iónica en la determinación de los componentes inorgánicos que se transfieren a las huellas palmares tras la manipulación de un explosivo. En concreto, varios sujetos manipularon distintos explosivos inorgánicos y posteriormente se analizaron los residuos transferidos a sus manos (concretamente a sus huellas palmares). Para los análisis mediante espectroscopía Raman, los sujetos posaron sus manos sobre un film plástico adhesivo. Para los análisis mediante cromatografía iónica, los sujetos posaron sus manos sobre bandejas de vidrio, a las que posteriormente se añadió un determinado volumen de agua. Los respectivos análisis demostraron que la espectroscopía Raman permite una mejor identificación del par catión-anión de las sales inorgánicas mayoritarias, mientras que la cromatografía iónica permite una mejor cuantificación de los iones en disolución (tanto mayoritarios como minoritarios).

La **Sección 2** comprende los Capítulos 4, 5 y 6, en los que se estudia la identificación y caracterización de explosivos mediante espectroscopía vibracional.

En el Capítulo 4, se ha contextualizado el tema de los explosivos dando un repaso crítico general a los aspectos clave más relevantes en el campo de los explosivos incluyendo su definición y clasificación. Se ha propuesto además una nueva clasificación basada en la composición química de los explosivos, que hasta ahora no existía. Asimismo, se ha contextualizado la evolución histórica de los descubrimientos de los explosivos que posteriormente se han investigado en esta Tesis. Por último, se han recopilado los atentados terroristas perpetrados con explosivos con el fin de mostrar la trascendencia y terrible repercusión que éstos tienen a nivel mundial y concretamente en Europa.

En el Capítulo 5, se muestran e interpretan los espectros Raman, FTIR y NIR de los explosivos y sales oxidantes objeto de estudio. En primer lugar, se analizaron los explosivos mediante FTIR y Raman. En segundo lugar, se analizaron las sales oxidantes (nitratos, cloratos y percloratos) mediante FTIR y Raman. En ambos casos, se asignaron las diferentes bandas espectrales con las

correspondientes vibraciones moleculares fundamentales; y se comprobó la selectividad y capacidad de identificación de ambas técnicas en la discriminación de los explosivos/sales oxidantes. En tercer lugar, se analizaron los explosivos y algunas sales oxidantes mediante NIR. Análogamente, se correlacionaron las bandas NIR con los sobretonos/bandas de combinación correspondientes y se comprobó la selectividad de la espectroscopía NIR. Se ha concluido que tanto Raman como FTIR o NIR permiten la identificación inequívoca de los explosivos; excepto las de aquellas mezclas explosivas de composición química muy similar y las de algunas sales oxidantes compuestas por el mismo anión.

En el Capítulo 6, se ha estudiado la identificación de residuos de explosivo post-explosionados mediante FTIR y Raman. En primer lugar, se han explicado brevemente algunos conceptos teóricos fundamentales sobre la detonación de los explosivos, y se han comparado con observaciones empíricas sencillas de detonaciones reales. Para ello, se hicieron y se fotografiaron detonaciones controladas de una serie de explosivos y se recogieron los distintos materiales expuestos a la explosión. Posteriormente se analizaron estos restos post-explosionados en busca de trazas del explosivo, pudiéndose identificar partículas intactas de los componentes inorgánicos de las mezclas oxidante-combustible, tanto en residuos post-explosionados de artefactos pirotécnicos como de artefactos explosivos improvisados. Sin embargo, no se detectaron trazas de los explosivos orgánicos uni-moleculares.

La **Sección 3** comprende los Capítulos 7, 8 y 9, en los que se estudia la identificación de manchas de fluidos biológicos mediante espectroscopía vibracional.

En el Capítulo 7, se ha revisado la literatura científica publicada hasta la fecha acerca de la identificación de fluidos biológicos mediante técnicas espectrométricas. Se han destacado la espectroscopía UV-Vis, la espectroscopía Raman y la espectroscopía IR. Como la revisión se hizo a comienzos del doctorado (2015), se ha incorporado un apartado final que actualiza la investigación publicada durante los últimos años (2015-2018).

En el Capítulo 8, se ha investigado la capacidad de la espectroscopía FTIR para discriminar manchas de semen, fluido vaginal y orina sobre tejidos de algodón. En primer lugar, se comprobó visualmente que los espectros FTIR de las

manchas de cada fluido eran diferentes entre sí y diferentes al del algodón. Las principales bandas de los espectros de las manchas de orina se correlacionaron con las vibraciones de la urea, mientras que los espectros de las manchas de semen y fluido vaginal se debieron a los enlaces peptídicos de las diferentes proteínas que los componen. En segundo lugar, se investigaron distintos métodos de análisis multivariante para ayudar en la discriminación de las manchas de cada fluido. Sin embargo, las medidas puntuales de la espectroscopía FTIR no permitieron resolver mezclas de varios fluidos, pues únicamente se detectó uno de los fluidos.

En el Capítulo 9, se ha investigado la capacidad de la técnica NIR-HSI para discriminar manchas de semen, fluido vaginal y orina sobre tejidos de algodón. El estudio se ha centrado principalmente en resolver las mezclas de varios fluidos. Aunque se comprobó que las diferencias espectrales en la región NIR entre los tres fluidos eran menos evidentes que en la región MIR, el análisis multivariante siguió permitiendo la discriminación de los tres fluidos. De hecho, se consiguieron discriminar los fluidos incluso en mezclas gracias a la capacidad de la imagen hiperespectral de registrar simultáneamente los espectros NIR de todos los píxeles de la imagen. De esta forma, se pudieron determinar y visualizar mediante un mapa químico las zonas de la mancha con mayor proporción de semen.

Acronyms and symbols

2D	Two-Dimensional
3D	Three-Dimensional
A	Absorbance
ACS	American Chemical Society
ALS	Alternate Light Sources
AN	Ammonium Nitrate
ANAl	Ammonium Nitrate - Aluminium powder
ANFO	Ammonium Nitrate - Fuel Oil
ANN	Artificial Neuron Network
ANOVA	Analysis Of Variance
Ar	Aromatic
asym	Antisymmetric
atm	Atmospheres
ATR	Attenuated Total Reflection / Attenuated Total Reflectance
AU	Arbitrary Units
bend	Bending
C4	Composition 4 explosive
CE	Capillary Electrophoresis
CJ	Chapman Jouguet
CLS	Classical Least Squares
CMOS	Complementary Metal-Oxide Semiconductor
comb	Combination
CSI	Crime Scene Investigation
def	Deformation
DMAC	p-Dimethylaminocinnamaldehyde
DNA	Deoxyribonucleic Acid
DNT	Dinitrotoluene
DRIFTS	Diffuse reflection infrared Fourier transform spectroscopy
EGDN	Ethylene Glycol Dinitrate
ELISA	Enzyme-Linked Immunosorbent Assay
EOD	Explosive Ordnance Disposal
FIR	Far Infrared
FOX-7	1,1-Diamino-2,2-dinitroethene
FTIR	Fourier Transform Infrared Spectroscopy
GSR	Gunshot Residue
Hb	Hemoglobin
Hi	Sample Leverage
HMTD	Hexamethylene Triperoxide Diamine
HMX	Cyclotetramethylene Tetranitramine / Octogen
HNIW	Hexanitrohexaaza-isowurtzitane
HPLC	High Performance Liquid Chromatography
HSI	Hyper-Spectral Imaging
IC	Ion Chromatography
IED	Improvised Explosive Device
ip	In plane
IR	Infrared

LDA	Linear Discriminant Analysis
LDH	Lactate Dehydrogenase
LED	Light-Emitting Diode
LOD	Limit Of Detection
LOQ	Limit Of Quantitation
LSD	Fisher's Least Significant Difference
LV	Latent Variable
MANOVA	Multivariate Analysis Of Variance
MCR-ALS	Multivariate curve resolution – Alternate Least Squares
MIR	Medium Infrared
mRNA	Messenger Ribonucleic Acid
MS	Mass Spectrometry
MSI	Multi-Spectral Imaging
NA	Not Available
NC	Nitrocellulose
NIPALS	Non-Linear Iterative Partial Least Squares
NIR	Near Infrared
NG	Nitroglycerine
NMR	Nuclear Magnetic Resonance
NQ	Nitroguanidine
OB	Oxygen Balance
oop	Out of plane
PC	Principal Component
PCA	Principal Component Analysis
PETN	Pentaerythritol Tetranitrate / Penthrite
PLS	Partial Least Squares
PLS-DA	Partial Least Squares Discriminant Analysis
PSA	Prostate Specific Antigen
PVC	Polyvinyl chloride
R	Reflectance
RDX	Cyclotrimethylene Trinitramine / Hexogen
RGB	Red-Green-Blue
RNA	Ribonucleic Acid
ROC	Receiver Operating Characteristic
rock	Rocking
ROI	Region Of Interest
RP-HPLC	Reversed-Phase High Performance Liquid Chromatography
scis	Scissoring
SDev	Standard Deviation
SEM-EDX	Scanning Electron Microscopy-Energy Dispersive X-ray Spectroscopy
SERS	Surface Enhanced Raman Scattering
Si	Sample-to-model distance
SIMCA	Soft Independent Modelling of Class Analogy
SNV	Standard Normal Variate
st	Stretching

SVD	Singular Value Decomposition
SVM	Support Vector Machine
sym	Symmetric
T	Transmitance
TATB	1,3,5-Triamino-2,4,6-trinitrobenzene
TATP	Triacetone Triperoxide
TEDAX	Técnico Especialista en Desactivación de Artefactos Explosivos
THP	Tamm-Horsfall Protein
TNT	2,4,6-Trinitrotoluene
twist	Twisting
umb	Umbrella
UV	Ultraviolet
Vis	Visible
wag	Wagging
XRF	X-ray Fluorescence
ZND	Zeldovich-von Neumann-Döring

E	Energy
h	Planck Constant
ν	Frequency / stretching
δ	Bending
λ	Wavelength
c	Speed of light in vaccum
β	Beta-particle
M	Molar
N	Number of atoms within a molecule
n	Neutron
n_1	Refractive index of medium 1
r	Correlation coefficient
R^2	Pearson Correlation Coefficient
Ω	Ohm
h	Hours
min	Minutes
rpm	Revolutions per minute

Contents

Scope, hypothesis and objectives	III
Alcance, hipótesis y objetivos	VII
Section 0. Fundamental Concepts that Are Needed to Comprehend the Thesis	
Introduction to Vibrational Spectroscopy	3
Infrared Spectroscopy	5
Near Infrared Spectroscopy	12
Raman Spectroscopy	14
Introduction to Chemistry applied to Forensic Science	17
Section 1. Analytical Studies about the Transfer of Explosive Residues	
Chapter 1. Analytical correlation between the transfer pattern of gunshot residues and the shooting distance	23
– Abstract	25
– Introduction	27
– Material and methods	28
– Results and discussion	30
– Conclusions	36
– References	37
Chapter 2. Transfer of explosive residues to different surfaces through consecutive fingerprints	41
– Abstract	43
– Introduction	45
– Materials and methods	46
– Results and discussion	51
– Conclusions	60
– References	61
Chapter 3. Comparison of Spectroscopy and Chromatography for assessing the transfer of explosive residues	65
– Abstract	67
– Introduction	69
– Materials and methods	71
– Results and discussion	75
– Conclusions and future trends	85
– References	86

Section 2. Spectroscopic Approaches for the Identification of Explosive Residues

- Chapter 4. The Chemistry of Explosives 91
  - Abstract 93
  - Fundamental concepts about explosives 95
  - Historical evolution of explosives 99
  - Current classifications of explosives 108
  - New classification of explosives according to their chemical composition 113
  - Terrorist use of explosives (Improvised explosive devices) 122
  - Conclusions 134
  - References 135

- Chapter 5. Spectroscopic Characterization of Explosives 139
  - 5.1. Infrared and Raman Characterization of Explosives 141
    - Abstract 141
    - Introduction 143
    - Experimental section 146
    - Results and discussion 148
    - Conclusions 163
    - References 164
  - 5.2. Infrared and Raman Characterization of Inorganic Oxidizing Energetic Salts 167
    - Abstract 167
    - Introduction 169
    - Experimental section 171
    - Results and discussion 173
    - Conclusions 184
    - References 185
  - 5.3. Near Infrared Characterization of Explosives and Energetic Salts 187
    - Abstract 187
    - Introduction 189
    - Experimental section 190
    - Results and discussion 192
    - Conclusions 202
    - References 203

- Chapter 6. Spectroscopic Identification of Post-Blast Explosive Residues 205
  - 6.1. Key aspects of explosives detonation 207
    - Abstract 207
    - Fundamental concepts about detonations of explosives 209
    - Oxygen balance and chemical reactions in detonations 212
    - Experimental detonations 215
    - Post-blast residues 219
    - Conclusions 221
    - References 222
  - 6.2. Identification of Post-Blast Explosive Residues by Infrared Spectroscopy 225
    - Abstract 225
    - Introduction 227
    - Material and methods 229
    - Results and discussion 232
    - Conclusions 244
    - References 245
  - 6.3. Identification of Post-Blast Explosive Residues by Raman Spectroscopy 249
    - 6.3.1. The influence of the explosive 249
      - Abstract 249
      - Introduction 251
      - Experimental section 252
      - Results and discussion 254
      - Conclusions and future trends 262
      - References 263
    - 6.3.2. The influence of the background material 267
      - Abstract 267
      - Introduction 269
      - Materials and experiments 270
      - Results and discussion 272
      - Conclusions 289
      - References 290

Section 3. Spectroscopic Strategies to Identify Stains of Body Fluids	
💧 Chapter 7. Spectroscopic techniques for the forensic detection of body fluids	295
– Abstract	297
– Introduction	299
– Emerging spectrometric techniques	302
– Review update 2015-2018	319
– Conclusions and future trends	330
– References	332
💧 Chapter 8. Identification of stains of body fluids on fabrics using Infrared Spectroscopy	341
– Abstract	343
– Introduction	345
– Experimental	347
– Results and discussion	351
– Conclusions and future trends	363
– References	364
💧 Chapter 9. Revealing the location of body fluids in stained evidence through near infrared hyperspectral imaging	367
– Abstract	369
– Introduction	371
– Experimental	372
– Results and discussion	376
– Conclusions	385
– References	385
General conclusions	391
Conclusiones generales	395
Annexes	399
Agradecimientos / Acknowledgements	415

"Hay en todos estos ensayos un estímulo personal, porque para poder escribirlos tengo que organizar mis posibles conocimientos sobre el tema y darles consistencia con los materiales que pueda encontrar en mi biblioteca de referencia. En definitiva, debo educarme a mí mismo, y siempre acabo sabiendo más cosas sobre cualquier tema después de haber escrito el ensayo que antes de empezar. Esta autoeducación es un motivo permanente de placer para mí, porque cuanto más sé, más plena es mi vida y mejor aprecio mi propia existencia. Aprender es siempre algo que vale la pena". **Isaac Asimov**

Scope, hypothesis and objectives

Alcance, hipótesis y objetivos

The Doctoral Thesis presented in this report aims to develop different analytical approaches based on spectroscopy to study three currently relevant forensic problems: the transfer of residues; the identification of explosive residues; and the identification of stains of body fluids.

Besides having these techniques in the laboratory, the main reason for having used spectroscopy in this Thesis has been its non-destructive nature and the absence of sample treatment. In forensics, in which the sample is the evidence collected at the crime scene, the intact conservation of sample during its analysis is a fundamental aspect, in such a way that the sample is not altered and can be submitted to further analyses. This is a crucial aspect, since the evidence (usually found in very small quantities) might be subjected to several analyses, including the identification of fingerprints in that sample, the chemical identification of the evidence or the analysis of the DNA that it may contain.

Regarding the three challenges that this Thesis aims to address, they have arisen from demands that different police forces and forensic institutes have conveyed to us. On the one hand, the need to deepen the understanding and research about the transfer of residues. On the other hand, the need to develop new analytical methodologies for identifying the evidence (*i.e.* explosives and stains of body fluids) without altering it in the least.

Thus, **Section 1** includes the Chapters (1-3) about the transfer of residues.

Specifically, Chapter 1 aims to correlate the dispersion of gunshot residues in the target with the shooting distance by multispectral imaging. In the judicial process, determining the shooting distance in a case of death caused by a firearm is fundamental, as it can provide information, not only about whether a murder or suicide has taken place, but also about intentionality, maliciousness and expertise of the person who shoots. One of the ways that exists to determine the shooting distance involves the study of the visual pattern of gunshot residues that remain on the surface on which the projectile has impacted. The dispersion and amount of GSR transferred from the firearm to the surface strongly depends on the shooting distance. In brief, the longer the shooting distance the greater dispersion and smaller amount/density of GSR on the target surface. Thus, the main objective of the first chapter aims to correlate the GSR density with the shooting distance, using multispectral imaging.

Chapters 2 and 3 include several elementary studies about the transfer of explosive residues by fingerprints, after having handled a certain amount of explosive. The transfer of explosives is a fundamental issue that has been vaguely researched by the scientific community. How to optimize the detection of explosives residues if it is not known to what extent these are transferred to the hands and other surfaces? Thus, Chapter 2 focuses on studying the transfer of different explosives on two surfaces (cotton fabric and smooth polycarbonate surface) through consecutive fingerprints by multispectral imaging analysis. The main objective of the study is to determine the amount of residues of each explosive that is transferred to each surface in the consecutive impressions, and to check if there is any tendency. As in Chapter 1, an imaging system is used to non-invasively monitor the amount / density of explosive residues that is transferred in each print. On the other hand, Chapter 3 investigates the qualitative and / or quantitative determination of certain explosives transferred to handprints by combining Raman spectroscopy and ion chromatography. This study also pursues to demonstrate the complementarity of both techniques by highlighting the strengths and limitations of each.

Section 2, which also comprises three Chapters (4-6), addresses the challenge of the identification of explosives by spectroscopic techniques.

First, Chapter 4 aims to review, in a comprehensive manner, fundamental concepts about explosives, including their historical evolution, the most widespread ways of classifying explosives and their social impact. In fact, a new classification of explosives according to their chemical composition is pursued because of the need to i) structure the continuous and scattered allusions found in the literature regarding the chemical composition of explosives, and ii) have a classification that is useful for the chemical-analytical identification of explosives. Chapter 4 also seeks to contextualize the social scourge that the illegal use of explosives in the commission of terrorist attacks represents worldwide and particularly in Europe, during the last two centuries. Inspired by this look at the past, Chapter 4 aims, finally, to synthesize, in an efficiently brief way, the historical evolution of the discoveries of those explosives that are later studied in this Thesis.

Secondly, Chapters 5 and 6 address one of the fundamental themes of this Thesis: the identification of explosives by vibrational spectroscopy. In particular, the main objective of the three sub-chapters of Chapter 5 is the characterization

and interpretation of the Raman, IR, and NIR spectra of the explosives and oxidizing salts under study. It is aimed to assign each band with the fundamental vibration or overtone that produces it, and verify, to what extent, the characteristic spectra of the different explosives and oxidizing salts enable their discrimination. This way, a useful spectral library of explosives is created to later identify the explosives in post-blast residues, which is the purpose pursued in Chapter 6. This aim is based on the need to find out the explosive that has caused a certain explosion, in order to provide information that helps to identify the culprit. Specifically, the three sub-chapters in Chapter 6 have the following objectives: i) to present the key chemical aspects of a detonation, ii) to identify the post-blast residues of pyrotechnic devices by infrared spectroscopy, and iii) to identify the post-blast residues of improvised explosive devices on different surfaces using Raman microscopy.

Finally, **Section 3**, which also includes three Chapters (7-9), addresses the second of the fundamental topics of this Thesis: the identification of stains of body fluids using vibrational spectroscopy. From the forensic point of view, the identification of stains of body fluids by means of non-destructive methods is essential, since, in the case of a positive identification, they are subjected to posterior DNA analysis.

First, Chapter 7 aims to exhaustively revise the existing literature on the use of spectrometric techniques in the identification of body fluids, paying special attention to the most significant advances that have occurred to date. Secondly, Chapters 8 and 9 focus on investigating the identification of those biological fluids usually present in crimes of sexual assault (semen, urine and vaginal fluid) by infrared spectroscopy. Specifically, Chapter 8 pursues the identification of the three body fluids within stains located on cotton fabrics by FTIR spectroscopy, whereas Chapter 9 aims the discrimination of the three body fluids by NIR-HSI imaging. The main objective in both studies is to identify the stains and/or areas of the stain with the highest proportion of semen in order to reduce the interference caused by the victim's fluids in the subsequent extraction and determination of the aggressor's DNA.

Besides the specific research objectives set out in each chapter, another of the objectives, which is inherent when carrying out a Thesis by compendium of articles, is the training in the elaboration, revision and publishing of the accomplished research in varied international scientific journals of high impact

index. Each chapter of this Thesis, either in part or in its entirety, has been published in international scientific journals, in the categories of analytical chemistry (*TrAC, Analytical Chemistry, Talanta,* and *Sensors*); spectroscopy (*Spectrochimica Acta A, Applied Spectroscopy, Journal of Raman Spectroscopy,* and *Applied Spectroscopy Reviews*); or forensic sciences (*Forensic Science International, Science and Justice,* and *Journal of Forensic Medicine*).

La Tesis Doctoral que se presenta en esta memoria persigue desarrollar diferentes aproximaciones analíticas basadas en espectroscopía para estudiar tres problemáticas forenses actualmente relevantes: la transferencia de residuos; la identificación de residuos de explosivos; y la identificación de manchas de fluidos biológicos.

Además de disponer de estas técnicas en el laboratorio, uno de los motivos principales de haber empleado la espectroscopía en esta Tesis ha sido su carácter no destructivo y la ausencia de tratamiento de muestra. En el campo forense, donde la muestra de análisis es la evidencia recogida en la escena del crimen, la conservación intacta de ésta durante su análisis es un aspecto fundamental, de tal forma que la muestra no se vea alterada y pueda ser sometida a posteriores análisis. Este es un aspecto crucial, pues habitualmente una única evidencia (*i.e.* generalmente trazas halladas en muy poca cantidad) puede someterse a varios análisis incluyendo la identificación de huellas dactilares en esa muestra, la identificación química de la evidencia o el análisis del ADN que ésta pueda contener.

Respecto a los tres retos que esta Tesis pretende abordar, éstos han surgido principalmente de la demanda que distintos cuerpos policiales e institutos forenses nos han trasladado sobre la necesidad de, por un lado, profundizar en la comprensión e investigación acerca de la transferencia de residuos, y por otro lado, desarrollar nuevas metodologías analíticas que permitan identificar la evidencia (*i.e.* explosivos y/o manchas de fluidos biológicos) sin alterarla lo más mínimo.

Así, la **Sección 1** comprende los Capítulos (1-3) sobre la transferencia de residuos.

Concretamente, el Capítulo 1 persigue correlacionar la dispersión de los residuos de disparo en la diana con la distancia de disparo mediante imagen multiespectral. En el proceso judicial, conocer la distancia de disparo en un caso de muerte por arma de fuego es fundamental, pues puede proporcionar información, no solo acerca de si se ha producido un homicidio o un suicidio, sino también de la intencionalidad, el dolo y la pericia de la persona que dispara. Una de las formas que existen para conocer esa distancia de disparo implica el estudio del patrón visual de los residuos de disparo que quedan en la superficie sobre la que ha impactado el proyectil. La distancia de disparo determina en

gran medida la dispersión y la cantidad de GSR transferidos del arma de fuego a la superficie. En resumen, a mayor distancia de disparo, mayor dispersión y menor cantidad/densidad de GSR en la superficie de la diana. Así, el objetivo principal del primer capítulo persigue correlacionar la densidad de GSR con la distancia de disparo, empleando para ello un sistema de imagen multiespectral.

En los Capítulos 2 y 3 se presentan varios estudios elementales sobre la transferencia de residuos de explosivo mediante huellas dactilares, tras la manipulación de una determinada cantidad de explosivo. La transferencia de explosivos es un tema fundamental que ha sido escasamente investigado por la comunidad científica. ¿Cómo optimizar la detección de residuos de explosivos si no se conoce en qué medida éstos se transfieren a las manos y a otras superficies? Así, el Capítulo 2 se centra en estudiar la transferencia de distintos explosivos sobre dos superficies (tejido de algodón y superficie lisa de policarbonato) a través de impresiones de huellas dactilares consecutivas mediante imagen multiespectral. El objetivo principal del estudio persigue determinar la cantidad de residuos de cada explosivo que se transfieren a cada superficie en las consecutivas impresiones y comprobar si existe alguna tendencia. Como en el Capítulo 1, se utiliza un sistema de imagen para monitorizar de forma no invasiva la cantidad/densidad de residuos que se transfieren en cada impresión. Por el contrario, en el Capítulo 3 se investiga la determinación cualitativa y/o cuantitativa de ciertos explosivos transferidos en huellas palmares mediante la combinación de la espectroscopía Raman y la cromatografía iónica. Este estudio también persigue demostrar la complementariedad de ambas técnicas destacando las fortalezas y limitaciones de cada una de ellas.

La **Sección 2**, que también se compone de tres Capítulos (4-6), aborda el tema de la identificación de explosivos mediante técnicas de espectroscopía.

En primer lugar, el Capítulo 4 pretende revisar, de forma exhaustiva, conceptos fundamentales sobre los explosivos, incluyendo su evolución histórica, las formas más extendidas de clasificar los explosivos, y su impacto social. De hecho, se propone una nueva clasificación de los explosivos de acuerdo con su composición química debido a la necesidad de, por un lado, ordenar y estructurar las continuas y dispersas alusiones que se encuentran en la literatura respecto a la composición química de los explosivos y, por otro, poder recurrir a una clasificación que sea útil desde el punto de vista de la

identificación químico-analítica de los explosivos. El Capítulo 4 pretende, además, contextualizar la lacra social que supone la utilización ilegal de explosivos en la comisión de atentados terroristas, a nivel mundial y particularmente, en Europa, durante los últimos dos siglos. Inspirado por esta mirada al pasado, el Capítulo 4 pretende, por último, sintetizar, de forma eficientemente breve, la evolución histórica de los descubrimientos de aquellos explosivos que posteriormente se estudian en esta Tesis.

A continuación, los Capítulos 5 y 6 abordan uno de los temas fundamentales de la Tesis: la identificación de explosivos mediante espectroscopía vibracional. En concreto, el objetivo principal de los tres sub-capítulos del Capítulo 5 es la caracterización e interpretación de los espectros Raman, Infrarrojo, e Infrarrojo cercano de los explosivos y sales oxidantes objeto de estudio. Se pretende asignar cada banda con la vibración fundamental o sobretono que la produce, y comprobar, hasta qué punto, los espectros característicos de los diferentes explosivos y sales oxidantes se pueden discriminar entre sí. Todo ello, con el fin de posibilitar su identificación posterior en restos explosionados, que es el propósito que se persigue en el Capítulo 6. Tal propósito se fundamenta en la necesidad de descubrir el explosivo que ha ocasionado una determinada explosión, con la finalidad de aportar información que ayude a identificar a el/los culpable/s. Concretamente, los tres sub-capítulos que componen el Capítulo 6 tienen como objetivos: i) presentar los aspectos químicos clave de una detonación, ii) identificar los residuos post-explosionados de artefactos pirotécnicos mediante espectroscopía infrarroja, e iii) identificar los residuos post-explosionados de artefactos explosivos improvisados en distintas superficies mediante microscopía Raman.

Finalmente, la **Sección 3**, que también se compone de tres Capítulos (7-9), aborda el segundo de los temas fundamentales de esta Tesis: la identificación de manchas de fluidos biológicos mediante espectroscopía vibracional. Desde el punto de vista forense, la identificación de manchas de fluidos biológicos mediante métodos no destructivos es esencial, puesto que, ante una identificación positiva, éstas se someten al posterior análisis de su ADN.

En primer lugar, el Capítulo 7 persigue revisar de forma exhaustiva la literatura existente acerca del empleo de las técnicas espectrométricas en la identificación de fluidos biológicos, prestando especial atención a los avances más significativos ocurridos hasta la fecha. En segundo lugar, los Capítulos 8 y 9 se

centran en investigar la identificación de aquellos fluidos biológicos habitualmente presentes en los delitos de agresión sexual (semen, orina y fluido vaginal) mediante espectroscopía infrarroja. Concretamente, el Capítulo 8 persigue estudiar la identificación de los tres fluidos en manchas sobre tejidos de algodón mediante espectroscopía FTIR, mientras que el Capítulo 9 se enfoca en la discriminación de los fluidos mediante imagen NIR-HSI. El objetivo principal en ambos estudios consiste en identificar las manchas y/o zonas de la mancha con mayor proporción de semen con el fin de reducir la interferencia que provocan los fluidos de la víctima en la posterior extracción y determinación del ADN del agresor.

A parte de los objetivos de investigación específicos planteados en cada capítulo, otro de los objetivos inherentes a la realización de una tesis por compendio de artículos, es aprender a elaborar, revisar y publicar la investigación realizada en revistas científicas internacionales de alto índice de impacto. Cada capítulo de esta Tesis, bien en parte o en su totalidad, se ha publicado en revistas científicas internacionales, en las categorías de química analítica (*TrAC, Analytical Chemistry, Talanta,* y *Sensors*); espectroscopía (*Spectrochimica Acta A, Applied Spectroscopy, Journal of Raman Spectroscopy,* y *Applied Spectroscopy Reviews*); o ciencias forenses (*Forensic Science International, Science and Justice,* y *Journal of Forensic Medicine*).

Section 0. Fundamental Concepts that Are Needed to Comprehend the Thesis

Introduction to Vibrational Spectroscopy

The science that studies the interaction between radiation and matter is named Spectroscopy. When thinking about this definition, I realize that Spectroscopy is a small-scale representative sample of the Universe, because what is the Universe but radiation and matter mutually interacting?

Spectroscopy examines radiation-matter interactions in order to extract information from both the radiation and the matter involved in the interaction (information that would not be possible to obtain by any other method). Radiation and matter interact and the result of that interaction totally depends on the type of matter and radiation involved.

Matter is composed of atoms. These atoms can be found free (*i.e.* elements) or bonded (*i.e.* forming chemical compounds). In the latter case, depending on the type of bond, the compounds can be molecules (covalent bond), ionic compounds (ionic bond), or metals / alloys (metal bond) [1]. When radiation interacts with atoms, the spectroscopy that studies that interaction, with the aim of obtaining atomic information, is called atomic spectroscopy [2]. When radiation interacts with molecules, the spectroscopy that studies that interaction, with the aim of obtaining molecular information, is called molecular spectroscopy [2].

Regarding the radiation involved, electromagnetic radiation is characterized by having a certain frequency (ν) or wavelength (λ). Wavelength is inversely related to frequency through the speed of light in vacuum (c) as given ($\lambda = {}^{c}/_{\nu}$) [1]. In this way, there is a minimum value for frequency that is next to zero, and a minimum value for wavelength that is also next to zero. The range between both limits defines the electromagnetic spectrum, which in turn is divided into several regions: gamma, X-ray, ultraviolet, visible, infrared, microwaves and radio waves [1], as schematized in Figure 1. All these regions are included within the displayed range covering the wavelengths from 10^{3} m (1 km) to 10^{-12} m (1 pm); or the frequencies from 10^{6} to 10^{20} Hz. Gamma radiation includes that radiation generated by radioactive decay of atomic nuclei, whose frequency normally exceeds 10^{19} Hz [1]. X-ray radiation, energetic radiation that does not come from atomic nuclei, usually ranges from 10^{16} to 10^{19} Hz, which corresponds to wavelengths from 10 nm to 10 pm [1]. Ultraviolet radiation (UV)

is the electromagnetic radiation corresponding to wavelengths from 10 nm to 400 nm [1-3]. Visible region, which comprises the electromagnetic radiation that is perceived by the human eye, is defined from 400 to 780 nm (wavelengths) [2, 3]. Infrared radiation (IR) comprises those wavelengths from 780 nm to 1 mm [2, 3]. Microwaves comprises the radiation whose wavelength ranges from 1 mm to 1 m [1]. Radio waves comprise the electromagnetic radiation corresponding to wavelengths that range from millimetres to kilometres [1].

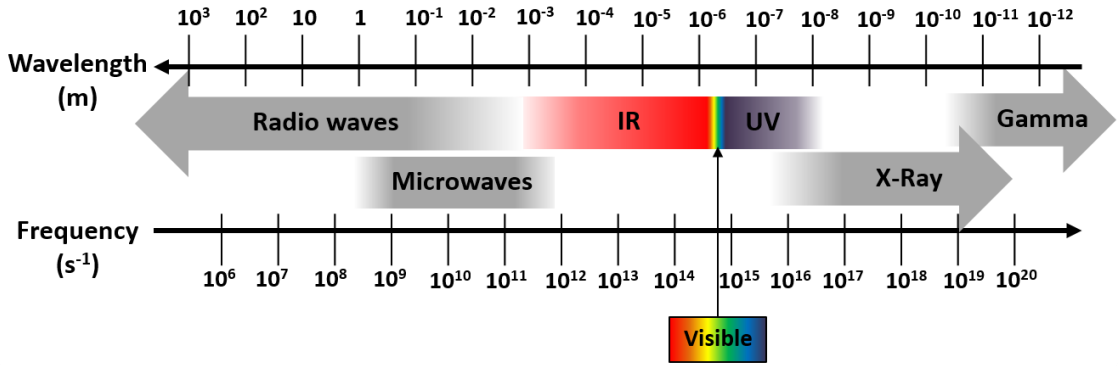

Figure 1. Electromagnetic spectrum and most typical regions.

Infrared region is typically sub-divided in Near-infrared radiation (NIR) covering wavelengths from 700 to 2500 nm; Medium-infrared radiation (MIR) covering wavelengths from 2.5 to 25 μm; and Far-infrared radiation (FIR) covering wavelengths from 25 μm to 1 mm [3].

In the knowledge of the composition of matter and MIR radiation, the result of the interaction between MIR radiation and molecules turns into the vibration of molecules (as later discussed in IR spectroscopy section). The energy associated to MIR radiation was discovered to provoke molecular vibrations. Because of this reason, the science that studies the molecular vibrations through the interaction between molecules and electromagnetic radiation is named Vibrational Spectroscopy [4].

➢ Infrared Spectroscopy

The Infrared range was the first non-visible region of the electromagnetic spectrum that was discovered. William Herschel discovered it, in 1800, when studying the heat of the visible solar rays using a glass prism and mercury-thermometers. He observed that the maximum temperature occurred beyond the red light of visible spectrum [4]. Invisible rays below the visible range were heating those thermometers. We now know that region as Near Infrared (NIR) region (which is further explained at the end of this section). Some decades later, Melloni extended the analysis of that invisible range up to the mid-infrared (MIR) region using a prism made of a rocksalt, and (around 1850) developed the first spectrometer able to collect the absorption bands of the MIR region. Melloni spectrometer was later improved by Langley in the 1880's, particularly in terms of sensitivity, by means of reducing the interference of atmospheric IR absorption and improving the detector. Concretely, carbon dioxide and water vapour provide highly intense absorption bands in the MIR region, in such a way that current software of IR spectrometers automatically remove the atmosphere background to every sample-spectrum. In addition, Langley scaled the IR spectrum in terms of wavelength by calculating the refractive index versus wavelength dispersion curve for the rocksalt [4]. However, it was not until the twentieth century that a chemical molecular interpretation of the IR spectra was accomplished. In 1911, the idea of IR bands associating with the vibrational, rotational and translational energy of molecules was introduced. In 1925, after the publication of Schrödinger wave equation, MIR bands started to be correlated with vibrational (and few closely spaced rotational) levels, whereas NIR bands were correlated with the overtones and combinations of the MIR vibrational fundamentals [4].

The vibrational levels were chemically correlated with either the bond-stretching, angle-bending or torsion molecular vibrations. Additionally, the empirical observation about the lack of IR absorption bands of diatomic molecules evidenced the notable influence of the symmetry and dipole moment of molecules in their IR spectrum. In this respect, the selection rules of IR spectroscopy were established (*i.e.* the molecular vibrations induced by the IR electromagnetic radiation must provoke a change in the dipole moment of the molecule to be IR active) [4, 5]. The assignment of every particular IR band with the corresponding molecular vibration started to be researched; rapidly

extending the limited literature by that time about IR group-characteristic assignment (gathered for years of empirical observations), which included the band at 2900 cm^{-1} for methyl group or the band at 3300 cm^{-1} for hydroxyl group, amongst others.

Furthermore, in the 1920's, Lecomte realized about the capability of using the IR pattern as a molecular fingerprint to unequivocally identify every molecule [4]. From then on, the IR spectra of millions of molecules have been recorded, published in literature, and gathered in spectral libraries/databases.

The combinative study of the IR spectra, the chemical structure of molecules and the development of quantum mechanics, has enabled the comprehensive interpretation and assignment of each band with the corresponding molecular vibration. Furthermore, specific narrow ranges have been established for each molecular vibration. As an example, Table 1 summarizes the more common IR active fundamental vibrations of organic molecules and the spectral wavenumber ranges within which are located [6].

As previously introduced, MIR range covers the region from 4000 to 400 cm^{-1} (wavenumbers). The wavenumber ($\tilde{\nu}$) used in IR spectroscopy is inversely proportional to the wavelength (λ). In turn, according to the Planck-Einstein equation ($\boldsymbol{E} = h \times \frac{c}{\lambda}$), wavelength is inversely proportional to the radiation energy. Thus, wavenumber is directly proportional to the energy [1-5]. In this respect, the energy absorbed in a molecular vibration mainly depends on three factors: the type of vibration, the atoms that are involved, and the vicinity of surrounding atoms.

The type of vibration is, perhaps, the most influencing factor in the energy of vibrations. Molecular vibrations are usually classified in two groups

Table 1. IR spectral ranges of common IR active fundamental vibrations of organic molecules.

Molecular vibration	Spectral range (cm^{-1})
O-H st	3650-3000
N-H st	3500-3100
C-H st (C_{sp2})	3100-3000
C-H st (C_{sp3})	3000-2840
C≡N st	2270-2000
C≡C st	2260-2100
C=O st	1800-1630
C=N st	1690-1540
N-H ip bend	1660-1550
C=C st	1650-1600
NO_2 asym st	1650-1500
C-H ip bend	1500-1300
O-H ip bend	1400-1200
NO_2 sym st	1390-1260
C-O st	1300-970
ar CH ip bend	1250-950
C-H oop bend	1200-650
N-H oop bend	850-700
O-H oop bend	800-600

depending on whether the bond-distance changes during the vibration or keeps constant. Those vibrations during which the bond distance changes are named stretching vibrations. Those vibrations during which the bond distance keeps constant, but angle of bonds changes, are named bending vibrations [4-6].

Stretching vibrations might be further sub-classified into symmetric and antisymmetric stretching vibrations. Similarly, bending vibrations might be also sub-classified into in-plane (ip) and out-of-plane (oop) vibrations, which, in turn, might be differentiated into rocking or scissoring ip bending vibrations, and wagging or twisting oop bending vibrations [4-6]. As a visual example, Figure 2 shows the molecular vibrations of CH_2 group.

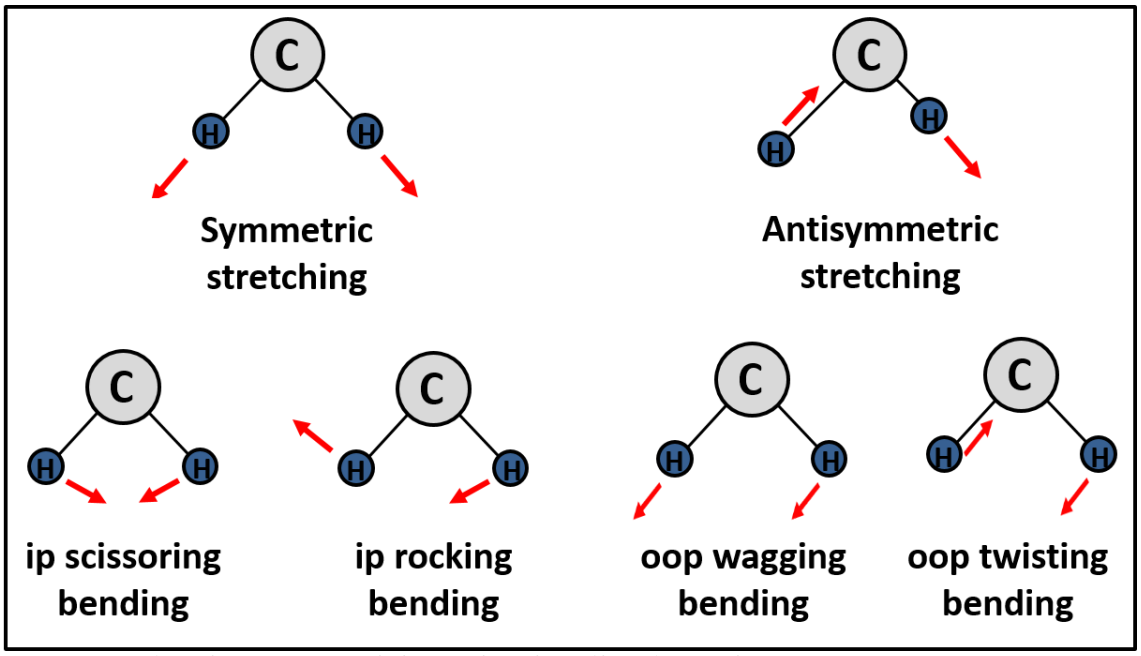

Figure 2. Visual summary of the molecular vibrations of CH_2 group.

The maximum number of molecular vibrations of a certain molecule containing N atoms is theoretically calculated as 3N-6 (for non-linear molecules) or 3N-5 (for linear molecules) [5]. This results from the combination of the three degrees of freedom that are available for every atom (3N) and the removing of those translational/rotational non-detectable modes (-6 or -5). For example, water molecule (H_2O) should have the same six vibrations as CH_2 group (displayed in Figure 2), and it has. However, according to the formula (3N-6), water molecule has three normal modes of vibration. These three modes are symmetric and antysimmetric stretching and ip scissoring bending. The other three bending

modes cannot be detected because are equivalent to a rotation of the entire water molecule (the reader is encouraged to have enough space vision).

Regarding the spectral range in which each vibration allocates, stretching vibrations normally require more energy than bending vibrations. Therefore, those bands corresponding to stretching vibrations are located at higher wavenumbers than the respective bending vibrational bands. For instance, the band due to OH stretching vibration allocates within 3650-3000 cm^{-1}, whereas the band due to OH ip bending allocates within the range 1400-1200 cm^{-1}. In addition, antisymmetric stretching requires more energy (higher wavenumber) than symmetric stretching, as evidenced in Table 1 for NO_2 antisymmetric (1650-1500 cm^{-1}) and NO_2 symmetric (1390-1260 cm^{-1}) stretching vibrations. Similarly, ip bending requires more energy than oop bending, as evidenced for OH ip (1400-1200cm^{-1}) and oop (800-600 cm^{-1}) bending vibrations [6].

The atoms that are involved in the vibration also influence to a large extent the energy of the vibration. In general, the smaller and closer the atoms are, the higher energy they need to vibrate, and hence the higher the wavenumber is. This is in accordance with the Hooke's law for harmonic oscillators in which the required energy to move two linked objects (two bonded atoms) is inversely proportional to the distance of both objects. In addition, the more strongly bonded the atoms are, the higher the wavenumber of vibration is. Thereby, the strength of the chemical bond directly correlates with the wavenumber, whereas the bond distance is inversely correlated. When estimating the strength and distance of chemical bonds two main factors are involved: the size of the atoms that are bonded and the bond order index (*i.e.* whether it is a single, double or triple bond). As an example, C-H stretching vibrations (3100-2840 cm^{-1}) require more energy than C-O stretching vibrations (1300-970 cm^{-1}), as expected for smaller H atom (much shorter bond distance). Similarly, C=O stretching (1800-1630 cm^{-1}) requires more energy than C-O stretching (1300-970 cm^{-1}), as expected for stronger double bond [6].

Finally, the influence of surrounding atoms provides small shifts in the energy of the vibration, which are highly useful from the identification point of view. Due to the introductory scope of this section, every particular case of the influence of surrounding atoms will be explained in the corresponding chapter, as the case of the slightly different spectral ranges for NO_2 stretching in

nitroaromatic (C-NO_2), nitramine (N-NO_2) and nitrate ester (O-NO_2) explosives (see Chapter 5).

Besides these vibrational-theoretical advances in IR spectroscopy, the main technical innovation involved the use of interferometry and mathematical Fourier transformation, which occurred in the 1970s with the arrival of computers to spectroscopy [4]. Interferometry had been largely developed by Michelson in the 1880s. However, the complex interferograms could not be interpreted until computers rapidly calculated the mathematical Fourier transformation. Applying Fourier transformation, interferograms, which represented the variation of the radiation energy as a function of the time lapse between two beams travelling through different optical paths inside the interferometer (one of them to the sample), were converted into IR spectra, in which absorption intensity is displayed as a function of wavenumber (cm^{-1}).

Regarding the physical type of interaction between matter and IR radiation, FTIR spectroscopic techniques may be further sub-classified into transmission, attenuated total reflection, specular reflection or diffuse reflection modes [4, 5].

Before 1960, transmission was the unique mode used in IR spectroscopy due to its simpler instrumental design. In transmission mode, IR radiation simply passes through the sample, reaches the detector and the fraction of the incident radiation that has been absorbed by the sample is determined. Maximum signal reaches the detector since incident and transmitted light travel in one unique straight direction, as schematized in Figure 3. The main disadvantage of transmission IR spectroscopy lies on the fact that a small sample treatment is required. A thick layer of sample would totally absorb IR radiation and no transmitted radiation would reach the detector, thus, a thin layer of sample has to be prepared. The most common procedure to prepare such a thin layer involves powdering the sample in a mortar, mixing a spatula tip of powdered sample with potassium bromide powder (non-IR active) and pressing the mixture to form a pellet [4, 5].

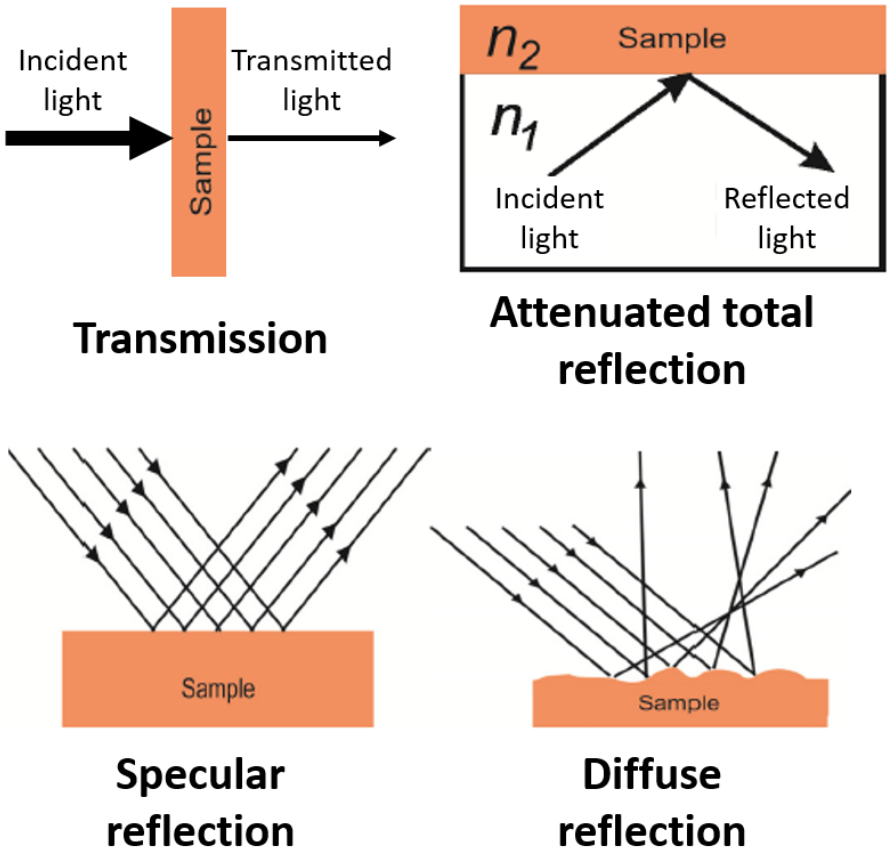

Figure 3. Visual summary of transmission/reflection IR modes. Adapted from [5].

Attenuated total reflection (ATR), which was developed in the 1960s, is based on the refractive index of substances. When two substances of high and low refractive index are placed in contact, incident light travelling through the material of higher refractive index (*i.e.* n_1 in Figure 3) gets almost totally reflected when it reaches the interface between both materials because of the low refraction index of the second material. Concretely, the reflected light penetrates a short distance (of the order of the wavelength) into the substance of lower refractive index in such a way that reflected radiation has been affected by the interaction with that substance [4, 5]. In practise, ATR accessories incorporate a flat ATR plate of a high-refractive-index material such as germanium, zinc selenide or diamond, on which the sample might be placed and pressed (using the pressing device that is typically coupled to the system). Since radiation shortly penetrates into the sample, the pressing of the sample against the ATR plate is crucial to record the IR spectrum of the sample. Hence, contrarily to transmission mode, sample can be directly analysed by ATR with no sample treatment, which is a significant advantage.

Specular and diffuse external reflection modes also record the light that is reflected by the sample. However, incident IR radiation travels through no high-refractive-index material, but only air (as occurred in transmission). In fact, the main difference between transmission and specular/diffuse reflection lies on the angle of the incident radiation with the sample. Transmission is maximum when incident radiation is perpendicular to the sample surface whereas reflection is favoured when the angle of the incident radiation with the normal goes away from zero. In specular reflection (dated from the 1950s), all reflected radiation has been scattered in a unique direction whose angle coincides with the angle of the incident radiation. On the contrary, in diffuse reflection (dated from the 1970s), radiation is scattered in all directions [4, 5]. When any sample reflects radiation, both specular and diffuse reflection occurs. The amount of specular and diffuse reflection depends on the roughness of the sample. Specular reflection prevails in smooth surfaces whereas diffuse reflection prevails in rough surfaces. Nevertheless, due to the generally lower signal of diffuse reflection, diffuse reflection accessories (DRIFTS – Diffuse reflection infrared Fourier transform spectroscopy) are designed in such a way that the detection of diffusely reflected light is optimized and the detection of specularly reflected light is minimized. Like ATR, no sample treatment is required for specular/diffuse reflection analysis.

In either transmission or reflection modes, the Fourier transformation of the interferogram provides an IR spectrum (*i.e.* intensity values as a function of wavenumber). However, depending on the type of radiation that is being recorded, the parameter which is being measured is different. In transmission mode, transmittance is measured. In reflection modes, reflectance is measured. The reflectance spectrum of a sample is not identical to its transmittance spectrum; neither are its ATR, specular and diffuse reflectance spectra. Particularly, the relative intensity of bands may change and small shifts in the wavenumber of certain bands might occur [4, 5]. Nevertheless, they are slight differences, which do not affect the identification of the molecule. Even so, specific mathematical corrections to approximate reflectance spectra to conventional transmittance spectra have been developed including ATR correction and Kramers-Kronig transformation. In addition, when displaying the IR spectra, transmittance is often mathematically converted into absorbance ($A = -\log T$). Similarly, reflectance is often converted into ($-\log R$) or ($1/\log R$).

➢ Near Infrared Spectroscopy

As previously explained, near infrared radiation was the first non-visible radiation that was discovered (1800). However, NIR spectroscopy was not developed until the 1880, when W. Abney discovered that NIR radiation could be measured using photography (like visible light). Particularly, Abney developed photographic silver bromide films that were sensitive to NIR radiation [4]. Contrarily to MIR spectrometers (which record the successive signals at each individual wavelength), the great advantage of photography is its capacity to simultaneously record the spatial information together with the whole range of a spectrum (*i.e.* multiplexing).

By 1880, important advances in photography had been developed such as the possibility of obtaining colour photographs by combining three black-and-white photographs previously taken through red, green, and blue (RGB) filters each, which was first proposed in 1861 by James Clerk Maxwell [7]. In other words, multiple black-and-white images (*i.e.* mono-spectral images only based on the darkening of silver because of the light) could be obtained using different filters (different wavelengths), and later combined to provide multi-spectral RGB images. In this respect, depending on the number of wavelengths and how much spaced they are, multi-spectral imaging (few spaced wavelengths) can turn into hyperspectral imaging (multiple contiguous wavelengths = spectra).

Thereby, combining hyperspectral imaging and NIR radiation, the first NIR spectra of up to 50 organic substances were recorded in 1881 within the spectral range 750-1100 nm [4]. When studying the chemical interpretation of such NIR spectra, W. Abney and R. E. Festing realized that molecules composed of no hydrogen atoms (such as CCl_4 and CS_2) did not provide any absorption band. Therefore, they concluded that NIR bands were due to X-H bonds (including OH, NH and CH). However, it was not until the 1920s (after correlating MIR bands with the fundamental molecular vibrations), that NIR bands were interpreted as overtones and combination bands of the vibrational fundamentals [4].

Regarding the advances in NIR instrumentation, the spatial and spectral resolution of NIR cameras have been constantly improved. Nevertheless, NIR spectrometers have been also developed to maximize the spectral resolution at the expense of removing spatial image and multiplexing [4]. Theoretically, NIR spectrometers might work in the same transmission-reflection modes like those

in MIR spectroscopy. However, NIR spectrometers (like NIR cameras) usually work in external (specular-diffuse) reflection. The wavelength of NIR radiation is shorter than that of MIR radiation. Hence, NIR radiation does not penetrate/transmit through solid substances as much as MIR radiation. This is the reason why transmission and ATR modes are not suitable for the analysis of solid substances using NIR radiation, but specular-diffuse reflection is. In addition, regarding imaging, it is required to measure the light that has been reflected by objects in order to obtain the spatial-spectral image.

Besides the improvement of spatial/spectral resolution of NIR cameras, the spectral range covered by NIR cameras has been also increased. Since 1881, when NIR cameras only covered from 750 to 1100 nm [4], the spectral rage of NIR cameras has been increased up to 2500 nm, which equals 4000 cm^{-1} (wavenumber at which MIR range begins). Thus, the whole NIR range can be recorded today. The same occurs for NIR spectrometers, in which spectral range might be even adjusted to simultaneously measure from UV to MIR wavelengths.

The simultaneous acquisition of spatial and spectral information when using hyperspectral cameras brings forth large amounts of data in the form of a three-dimensional hypercube ($x \times y \times \lambda$), in which ($x \times y$) represents the spatial bidimensional image and λ represents the spectrum [8]. In brief, each pixel of the image has its individual spectrum; and each wavelength has its individual bidimensional image, as schematized in Figure 4. Like a video, which is composed of multiple frames taken over time, hyperspectral images are composed of multiple frames taken along wavelength. In order to interpret all these frames (individually and overall), and extract all the information contained within them, image processing is required. Image processing consists of different steps including selection of the region of interest, spectral/spatial pre-processing, exploratory multivariate analysis, multivariate regression analysis and multivariate classification analysis [8]. The complexity of image processing and the specific methods that should be used in each step will depend on the sample, the objective of the study, the expertise of the analyst (in chemometrics), etc. In any event, the result that is usually pursued when performing image processing is the chemical mapping of the sample. Chemical mapping involves the creation of an image of the sample whose colour scale correlates with the amount of a certain chemical component, in such a way that the distribution of that component might be easily traced along the sample. The greater or lesser

correctness and accuracy of the chemical mapping is determined by the image processing that has been previously performed.

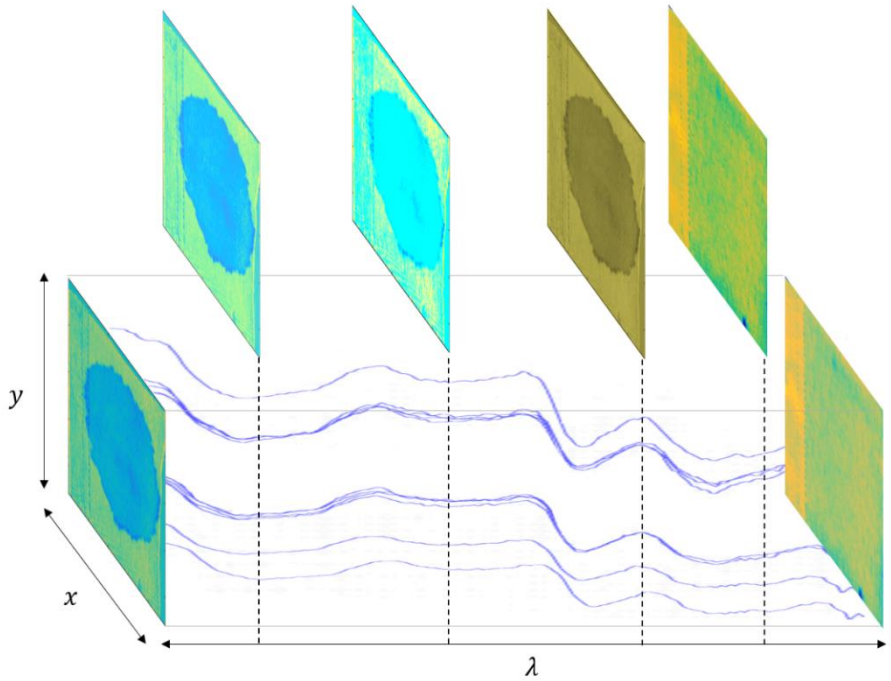

Figure 4. Scheme of a hypercube ($x \times y \times \lambda$).

➢ Raman Spectroscopy

Unlike IR/NIR spectroscopy, in which MIR/NIR radiation is absorbed by the sample, Raman spectroscopy is based on the inelastic scattering of radiation. The inelastic scattering of light was discovered in 1928 by Raman and Krishnan [3, 4]. Unlike transmission/reflection phenomena, in which sample and light interact as if photons were exclusively particles, scattering phenomenon is better comprehended taking into consideration that photons are both particles and electromagnetic waves (*i.e.* duality of light). In this context, when any substance is irradiated with electromagnetic radiation, besides the absorption-reflection or absorption-transmission phenomena, electromagnetic scattering occurs in such a way that sample virtually absorbs and reemits the electromagnetic radiation without reaching an excited energy state (as in absorption), but a virtual state. Such process might be an elastic scattering (also known as Rayleigh scattering) or inelastic scattering (also known as Raman scattering). Most of the radiation is elastically scattered without changing the wavelength of the radiation. However, a small part of the radiation is inelastically scattered at wavelengths that are different from incident radiation

[3, 4]. In order to easily check the shift of scattered wavelengths, a monochromatic radiation (laser) is used as incident radiation. Generally, incident radiation loses a certain amount of energy, which is taken by the molecule to vibrate (Stokes process). The opposite process (in which the molecule transfers energy to the radiation (anti-Stokes)) occurs to a lesser extent due to the lower distribution of virtually excited molecules [3, 4]. Nonetheless, whatever the process, the differences associate to the molecular vibrations of the sample, in such a way that the wavelength shift (also known as Raman shift) correlates to the IR wavenumber of the vibration.

From the beginning, it was observed for certain molecules that their Raman spectra were different from their IR spectra. Particularly, symmetric diatomic molecules, which were non IR-active, displayed intense Raman signals. In addition, vibrations associated to polar bonds, which were highly intense in IR spectroscopy, were little intense in Raman spectroscopy [4]. For instance, unlike IR spectroscopy, Raman spectroscopy was little affected by water in such a way that aqueous solutions could be analysed by Raman. Hence, it was evident that different selection rules operated in IR and Raman. IR active vibrations are those that provoke a change in the molecular dipole moment whereas Raman active vibrations do not, as evidenced by symmetric diatomic molecules. Specifically, Raman active vibrations are those that provoke a change in the polarizability of the molecule (*i.e.* in the electron cloud distribution) [3, 4]. In order to visually comprehend the difference between IR and Raman selection rules, Figure 5 schematizes the stretching vibrations of carbon dioxide and whether they are IR-active or Raman-active. For instance, symmetric stretching is not IR active (because it does not provoke any change in the molecular dipole moment), but it is Raman active (because it provokes a change in the polarizability of the molecule). On the contrary, antisymmetric stretching is not Raman active (because it does not provoke any change in the polarizability of the molecule), but it is IR active (because it provokes a change in the molecular dipole moment). In this case, each CO_2 stretching vibration is exclusively IR or Raman active. Actually, since different selection rules operate for IR and Raman, every molecular vibration might be IR-active, Raman-active or both IR-Raman active. In addition, even though certain vibrations are both IR-Raman active, they usually have different relative intensities in their IR and Raman spectra. Because of these reasons, IR and Raman spectroscopy are typically presented as complementary techniques.

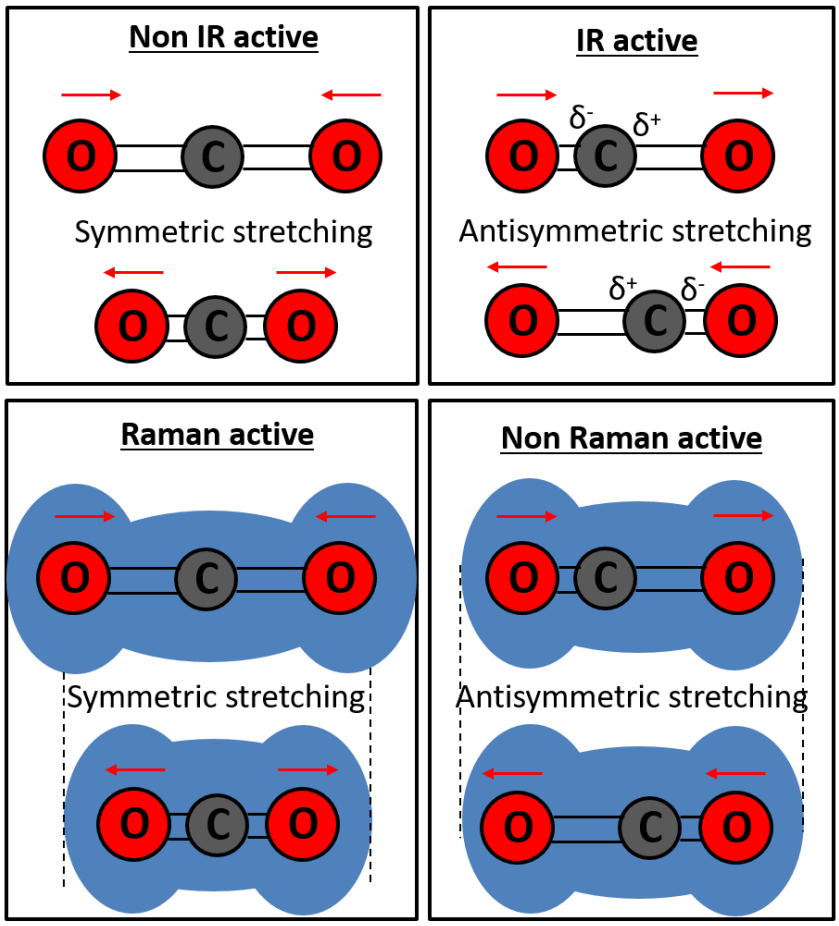

Figure 5. Scheme of CO_2 stretching vibrations and their IR/Raman activity.

From the instrumental point of view, Raman spectroscopy also displays complementary advantages to IR, which were promptly exploited. Unlike IR spectroscopy, Raman spectroscopy might work in the visible region, using visible monochromatic light sources. This fact is very important since it enabled to easily combine Raman spectroscopy and microscopy [4]. Optical microscopes and microscopic lens working in the visible range might be coupled to Raman spectrometers, in such a way that, for the first time, microscopic solid traces could be selectively focused and detected using spectroscopy (with no sample treatment).

Negatively, a challenging disadvantage of Raman spectroscopy was found to be the fluorescence caused by dark-coloured samples, which totally overlapped the weak Raman bands. In those cases, a thorough optimization of the Raman parameters (including wavelength and power of the laser, exposure time, optical aperture, number of scans and sample focusing) is performed with the aim of removing the fluorescence (although the success is not guaranteed).

Introduction to Chemistry applied to Forensic Science

As every chemist knows, chemistry is everywhere. Particularly, determining the chemical composition of matter is an increasingly often requirement in many fields, including forensics. In this respect, chemistry applied to forensics, traditionally known as forensic chemistry, mainly tackles the chemical analysis of the physical evidence related to a criminal act, in order to assist the Justice in the clarification of the crime and identification of the culprits.

Though the term "Forensic chemistry" started to be used in the 20th century, the chemical determination of substances to solve legal disputes is known to date, at least, from the 2nd century BC. At that time, a renowned scientist named Archimedes lived in Syracuse. Because of his fame, the King of Syracuse asked Archimedes assistance to solve a chemical question. The King of Syracuse had ordered to a goldsmith the manufacture of a golden crown, for which he had given a certain amount (weight) of gold. After receiving the crown, (even though it had the expected weight), the King wondered whether the crown was pure gold and whether it had been manufactured using all the gold previously given. The king asked these questions to Archimedes, also advising Archimedes that he could not damage the crown in any way to find the solution [9]. In modern terms, Archimedes had to analyse the crown in a non-destructive way. After a few days, Archimedes demonstrated that crown was not pure gold. The goldsmith had committed a fraud in the manufacture of the crown. Archimedes was able to solve this question in the basis of the different density between pure gold and any other metal. Even if the weight of two objects is the same, their volume is not because they have different densities. Since the crown had an irregular form, Archimedes immersed both the crown and the exact weight of gold into water to compare their volume. In practise, Archimedes found out that crown was not pure gold because its relative weight inside water was different from that of pure gold, as evidenced in Figure 6. Actually, the goldsmith had replaced part of the gold by a lighter and cheaper metal (probably silver) in such a way that the resulted alloy had smaller density than that of pure gold [9].

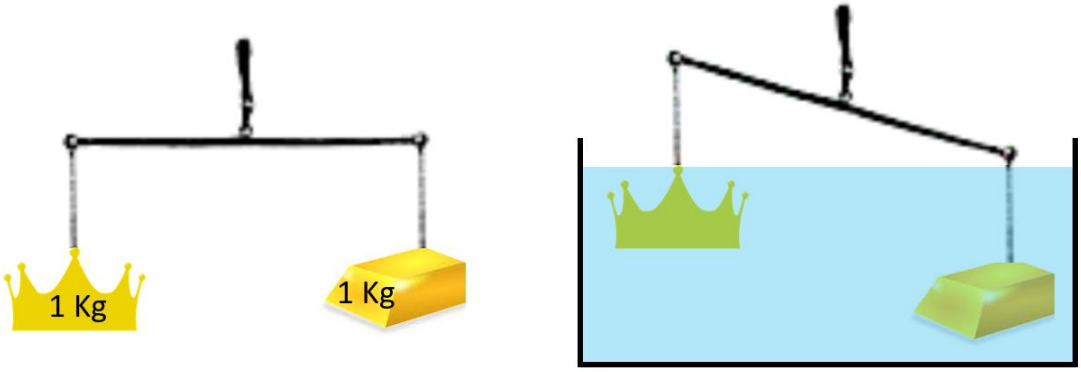

Figure 6. Visual demonstration of Archimedes experiment.

A more recent case about the assistance of chemistry in solving a crime occurred in 1840 in Paris, which is known as the first case of forensic toxicology [10]. Marie Lafarge was accused of murdering her husband using arsenic, a poison used to kill rats at that time. In order to demonstrate whether Mr. Lafarge had died as a consequence of an excess of arsenic, biological samples taken from the corpse were subjected to Marsh test (*i.e.* a test developed few years before by James Marsh to determine arsenic). The test was based on the reaction between arsenic and hydrogen to form arsine, and the decomposition of arsine into metal arsenic when heated. Hydrogen was generated by mixing zinc and sulphuric acid. If arsenic was present, hydrogen reacted with arsenic to form arsine, which later decomposed into metal arsenic when heated. Thereby, Marsh test confirmed that biological samples from the corpse had large amounts of arsenic. In the knowledge of this chemical evidence, Maria Lafarge was convicted of murder by the judge. Though chemical poisons were already known in ancient Greece, Lafarge case was the first case of death by poisoning that was confirmed by scientific methods [10].

Despite these demonstrations of chemistry providing scientific evidence to assist in judicial cases, the basic principles of forensic science were not stablished until 1920 by Edmond Locard (1877-1966). In few words, Locard's exchange principle stablishes that "every contact leaves a trace" [11]. In other words, "the microscopic remains that cover our clothes and our bodies are silent and faithful witnesses of our movements and our meetings".

It should be noted that Arthur Conan Doyle (1859-1930), in 1905, already anticipated this principle in his novel through the following sentence explained by Sherlock Holmes to Hopkins: "*I have investigated many crimes but I have*

never yet seen one which was committed by a flying creature. As long as the criminal remains upon two legs so long must there be some indentation, some abrasion, some trifling displacement which can be detected by the scientific searcher" [12].

According to Locard's principle, a transfer of material between the aggressor, the victim and the crime scene occurs in such a way that are connected by certain evidence that they have unconsciously exchanged among each other. This arises two fundamental questions to investigate in forensic science, what is the evidence? and, how was the evidence transferred to that place? The solution to each question provides complementary information, which assist in solving the crime [10]. Thus, the simultaneous research about both the transfer and the identification of evidence is worth accomplishing, as presented in the following sections of this Thesis.

In addition, like Archimedes' golden crown, trace evidence found in crime scene is unique, unrepeatable and limited. Therefore, non-destructive analyses are highly recommended [10]. The forensic analytical procedure usually involves the presumptive detection, the examination, and the chemical identification of the evidence. In this respect, the more non-destructive analyses are performed, the more information of the evidence is obtained without being destroyed. Among non-destructive techniques, vibrational spectroscopy is likely the one most used in forensics due to its capability to identify and characterize multiple substances, as presented in the following sections of this Thesis.

References

[1] T. Buthelezi, L. Dingrando, N. Hainen, C. Wistrom, D. Zike, Chemistry. Matter and change, Glencoe/Mc Graw Hill, 2008.

[2] D.A. Skoog, F.J. Holler, T.A. Nieman, Principios de análisis instrumental, 5a ed. Mc Graw Hill, 2001.

[3] A.R. Castro, M.C.M. Bondi, B.M.S. Suau, Técnicas espectroscópicas en química analítica. (Vol. 1). Aspectos básicos y espectrometría molecular. Editorial Síntesis. Madrid. Spain. 2012, pp. 437-458.

[4] J. Chalmers, P. Griffiths, Handbook of vibrational Spectroscopy. Five volume set. Wiley, 2002.

[5] T. Theophanides, Infrared spectroscopy – Materials Science, engineering and Technology, In Tech, 2012.

[6] E. Pretsch, P. Bühlmann, M. Badertscher, IR spectroscopy, in: E. Pretsch, P. Bühlmann, M. Badertscher, Structure determination of organic compounds. Tables of spectral data, 4th edition, Springer, 2009, pp. 269-336.

[7] J.M. Eder, History of photography, 3rd edition, Dover publications, 1978.

[8] J.M. Amigo, I. Martí, A. Gowen, Hyperspectral imaging and chemometrics: a perfect combination for the analysis of food structure, composition and quality, in: F. Marini, Chemometric in food chemistry, Elsevier, 2013, pp. 343-370.

[9] T.I. Heath, The works of Archimedes, Dover publications, 2002.

[10] S. Bell, Forensic Chemistry, Pearson Prentice Hall, 2006.

[11] E. Locard, Manual de técnica policiaca. 1935.

[12] A.C. Doyle, Sherlock Holmes: The Return of Sherlock Holmes, 1905.

Section 1. Analytical Studies about the Transfer of Explosive Residues

To Policía and Guardia Civil,
who work every day to make our country a safer place…

¿Quién te dijo que estás sola, Policía Nacional?
Cuéntame del mar las olas, si es que se pueden contar.
Como se cuentan las horas en tu casa, si no estás.
Vas en tu coche patrulla y le llaman patrullar,
pero la noche es oscura sin saber lo que hay detrás,
testigo mudo es la luna, policía nacional
no me digas si no quieres,
si es mentira o es verdad
esos hombres y mujeres
que los llamas y ahí están.
Los que se juegan la vida ayudando a los demás
y hasta parece mentira, mentira que es verdad
la patria sabe de eso y pone en tu frente un beso, policía nacional.
Cuántas veces habrás querido emprender otro camino,
volver a otro lugar y borrar tu pergamino,
pero España te dio un nombre que sólo da a los hombres que no tienen marcha atrás.
Que te digo, policía, de esta tu noble misión,
si comparto día a día escenario y sacrificio,
muchas horas de servicio con el frío y el calor.
Sufriste el terrorismo sin reparar en tu color
yo puedo decir lo mismo, conozco bien ese dolor,
por eso en tu patrón contigo quiero brindar
alzo mi copa al vuelo, policía nacional
brindando por los anhelos los que fueron y no están.
Tu uniforme hoy pone el brillo,
yo me quedo un paso atrás
es tu día, es tu orgullo,
compártelo con los tuyos, policía nacional
y luego vendrás conmigo,
iremos a ese lugar en donde habita el olvido y volvemos a empezar
porque en ese redil vamos al mismo compás.
Yo, guardia civil,
tú, policía nacional,
tú, con el azul del cielo,
yo, con el verde del mar,
tú en tus ángeles, el consuelo
y yo en mi virgen del Pilar.

Author: José Rafael Martínez Jiménez, Capitán de la Guardia Civil. 2016

Chapter 1. Analytical correlation between the transfer pattern of gunshot residues and the shooting distance

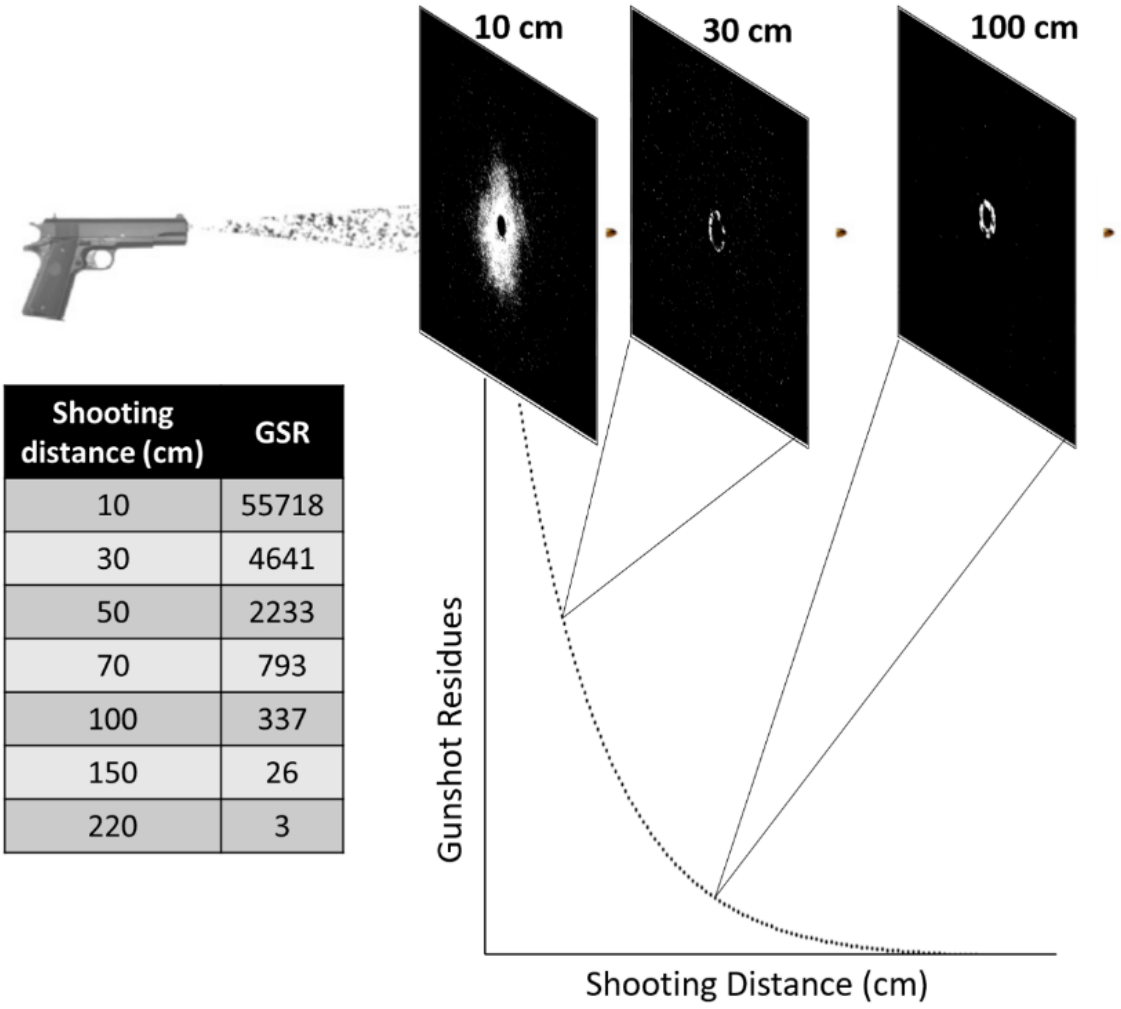

Shooting distance (cm)	GSR
10	55718
30	4641
50	2233
70	793
100	337
150	26
220	3

Main source:

Félix Zapata, M. López-López, J.M. Amigo, C. García-Ruiz, Multi-spectral imaging for the estimation of shooting distances, *Forensic Sci. Int.* 282 (2018) 80-85.

Abstract

Multispectral images of clothing targets shot at seven different distances (from 10 to 220 cm) were recorded at 18 specific wavelengths in the 400–1000 nm range to visualize the gunshot residue (GSR) pattern. Principal component analysis (PCA) showed that the use of violet-blue wavelengths (430, 450 and 470 nm) provided the largest contrast between the GSR particles and the white cotton fabric. Then, the correlation between the amount of GSR particles on clothing targets and the shooting distance was studied. By selecting the blue frame of multispectral images (*i.e.* the blue frame in the red-green-blue (RGB) system which falls at 470 nm), the amount of pixels containing GSR particles was accounted based on the intensity of pixels in that frame. Results demonstrated that the number of pixels containing GSR exponentially decreases with the shooting distance from 30 to 220 cm following a particular exponential equation. However, the targets shot at the shortest distance (10 cm) did not satisfy the above equation, probably due to the noticeable differences of the GSR-pattern of these targets (*e.g.* high presence of soot). Then, the equation was applied to validation samples to estimate the shooting distances, obtaining results with an error below 10%.

Introduction

Significant advances in the visible range of spectroscopy instrumentation such as multi-spectral and hyperspectral imaging systems, make the analysis of large surfaces considerably easy and fast, enabling the discrimination of pixels according to their different visible signatures [1-4]. Furthermore, some applications do not even require the complete visible range, but specific wavelengths that may be selected among the different wavelengths available in multispectral imaging systems. Multispectral imaging involves the collection of multi-frames (*i.e.* mono-coloured images) of each sample, in which each frame is collected under a specific discrete detection wavelength. In this way, each frame of the image at each wavelength (bidimensional frame, 2D), can be examined separately, or, on the contrary, the whole image comprising all frames (tridimensional image, 3D) can be statistically analysed like hyperspectral images [5]. In fact, the information contained in one or few wavelengths is usually enough to overcome specific challenges in many different fields including food quality control [6-8], cultural heritage [9] or forensics [10-12]. These investigations support the use of multispectral imaging as a fast and relatively inexpensive technique for different forensic purposes. However, no attempts have been made to estimate the shooting distance (muzzle to target distance) by multispectral imaging.

Gunshot residues (GSR), which are produced when a gun is fired, are a complex mixture of burned and unburned particles coming from the propellant, primer components, and metals contained in the projectile (*e.g.* bullet, bullet jacket, cartridge case) [13-19]. Depending on the firing distance and other conditions (*e.g.* type of ammunition, firearm, firing angle, atmospheric conditions, etc.), the amount of particles that reach the target differs, creating different patterns [13-19]. The forensic analyst estimates the shooting distance through the visual examination of the characteristics of the GSR pattern and, if possible, its comparison to reference GSR patterns (produced under similar conditions) for more accurate results [15-17]. Colour tests based on chemical reactions have been the main method to assist the expert in the visualization of the GSR pattern for decades [14-17]. However, some spectroscopic and imaging techniques have recently demonstrated their efficacy to reveal GSR patterns on clothing [20-23].

The main advantage of using imaging techniques involves the possibility to automatically examine the GSR pattern through quantitative approaches. Up to

date, some interesting approaches for shooting distance estimation based on the image analysis of photographed targets through mathematical models have been explored. Most of these mathematical models are calculated taking into account either the amount, number, density, distribution or composition of GSR particles in the target [24-29]. The use of numerical data (besides the GSR pattern) enables to study the mathematical tendency for the variation of GSR pattern with the shooting distance, and the possibility to precisely determine the shooting distance within statistical deviation ranges. On the other hand, quantitative approaches for shooting distance estimation are specially affected by the possible loss of particles due to external factors (blood, water (*e.g.* rain or washing), first-aid procedures, recovering and handling victim's clothes, etc. [30-32]). Some interesting approaches based on image analysis and mathematical models are, for instance, the estimation of the firing distance performed with a riffle (0–45 cm distances) considering the GSR stained area [25], or the correlation of the density of IR- luminescent GSR particles with shooting distances from 20 to 300 cm performed with different pistols and revolvers [27]. Both studies seem to evidence an exponential decrease in the amount of GSR particles with the shooting distance.

In this respect, this study explores the potential of multispectral imaging as a forensic tool for the visualization of the GSR pattern and the subsequent mathematical estimation of the shooting distance in the 10–220 cm range through a specific exponential equation. To this aim, multispectral images of the clothing targets shot were recorded in the 400–1000 nm range to determine the wavelength that provided the largest contrast between the GSR particles and the white cotton fabric. Then, the correlation between the amount of pixels containing GSR particles and the shooting distance has been mathematically established. Finally, the equation obtained was applied to a set of validation samples.

Material and methods

- Samples

28 square cardboard pieces of 10 × 10 cm covered with standard white cotton clothing were used as targets. White cotton clothing was used in order to enhance the contrast between GSR and background facilitating thereby the

visualization of GSR particles. The targets were shot using a Glock G17 pistol and 9 × 19 mm semi-jacketed hollow point conventional ammunition manufactured by Sellier&Bellot (Czech Republic). Shots were executed at the shooting range of the Spanish National Scientific Police (Madrid, Spain). Targets were shot at seven different shooting distances, including 10, 30, 50, 70, 100, 150 and 220 cm. Four replicates per distance (28 samples) were prepared. Three replicates (21 samples) were used to create the mathematical model whereas a fourth replicate of each distance was used as validation set (7 samples) to test the model.

- Multispectral imaging

A Videometer Lab 4 (Cambridge, UK) was used to collect a multispectral image of each sample at 18 different specific wavelengths from 400 to 1000 nm (430, 450, 470, 505, 565, 590, 630, 645, 660, 700, 850, 870, 890, 910, 920, 940, 950 and 970 nm). Images contained 960 × 1280 pixels, being the spatial resolution of each pixel 0.12 × 0.12 mm.

- Image processing

Image processing was performed in MATLAB R2016b (Mathworks, USA). After comparing the 18 frames of each multispectral image separately, and all together, using principal component analysis (PCA), the frames at violet-blue wavelengths (430, 450 and 470 nm) were identified as the frames that provided the largest contrast between dark GSR and white cotton fabric. As an example, Figure 1.1 displays the loading and scores plot for the first principal component of one of the targets shot at 30 cm. According to the loading values and keeping in mind the absolute value, the highest contribution was provided by wavelengths at 430, 450 and 470 nm with 0.50, 0.50 and 0.41, respectively. It should be noted that the contribution of the next wavelength (505 nm) decreases to 0.25 of absolute value. Those 3 violet-blue frames were studied by quantifying the pixels that fall below a specific value of intensity and similar results were obtained for the three frames. From those three, the frame at 470 nm was selected as the most relevant frame because, even though it provided the lowest contribution, it corresponds to the blue channel in commercial ordinary digital RGB cameras. In order to carry out the pixel quantification, different ranges of intensity were tested, selecting the range from 0 to 0.45 as the optimum range that gave the best correlation with the presence of GSR. It is important to

highlight that MATLAB works, by default, with intensity values from 0 (black) to 1 (white) after converting an image into a numerical matrix. Therefore, the dark pixels within this frame were quantified. Afterwards, the image was binarized, *i.e.* converted only to black and white (only 0/1 values) for image purposes and these values were inverted for better visualization. Finally, the pixel quantification was plotted against the shooting distance (by calculating the average and standard deviation), and different fitting trendlines using the trendline options of Excel (Microsoft Office 2016) and Origin (OriginPro 9.0) were tested by evaluating their R^2 coefficient.

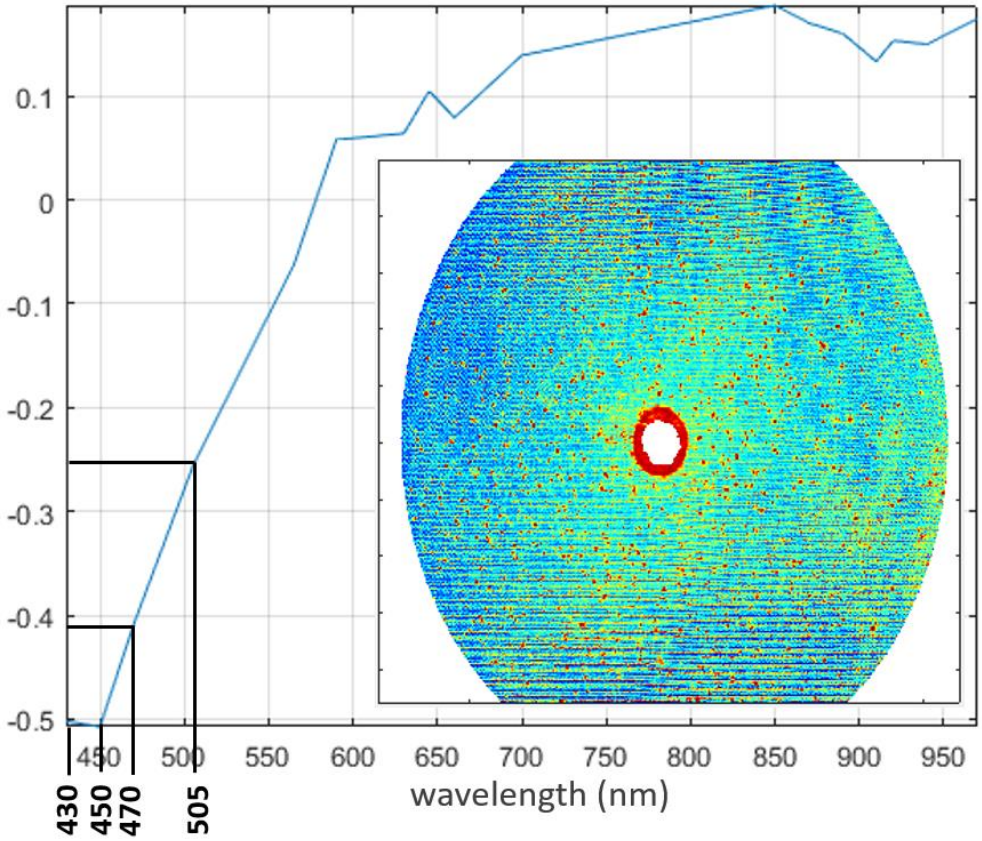

Figure 1.1. Graphical loading plot for the first principal component of one of the targets at 30 cm. Principal component analysis using singular value decomposition (svd) algorithm. GSR particles are observed as red dark pixels in the scores image.

Results and discussion

First, it is important to highlight that the particles imaged in the white cotton targets exclusively came from the shots, since the shootings were performed under controlled conditions to remove any potential interferent. Also worth

noting is the fact that, in this study, the term GSR pattern/GSR particles includes all the particles expelled by the firearm, *i.e.* particles from both primer and propellant and not only those containing lead-antimony-barium. In fact, most of the GSR particles detected at long distances are propellant particles, as evidenced in previous studies [16, 19]. These non-burned or partially burned propellant particles mostly consist of nitrocellulose, the main component in smokeless gunpowders. To avoid confusion, the terms "propellant-GSR particles" and "primer-GSR particles" are used when necessary. The multispectral images obtained for the targets at the different wavelengths in the 400–1000 nm showed that the wavelengths at 430, 450 or 470 nm provided the largest contrast between the GSR particles and the white cotton fabric. However, in order to develop a simple, accessible and broadly usable test for any high-resolution digital camera, the results shown in this study are those from the blue RGB frame at 470 nm. Likewise, no significant improvement was achieved by analysing the whole image (*i.e.* the 18 frames together) using PCA. Therefore, those results obtained by analysing the blue RGB frames are discussed below. To this aim, Figure 1.2(A) displays the images (*i.e.* blue RGB frame at 470 nm) obtained for the first replicate at 10, 30 and 100 cm distances. By comparing the images, the differences in their GSR pattern are highly recognizable. In fact, an expert eye might estimate an approximate range in the firing distance for each pattern. However, in order to develop a mathematical methodology to support that estimation, the pixels in the image attributed to GSR particles were quantified. The quantification of those pixels in the image that contained GSR was performed through calculating the dark pixels (as previously explained in "Image processing" section). Concretely, different ranges of intensity were tested and it was observed that, beyond the intensity value of 0.45, some pixels of pure cotton started to be accounted besides the GSR. Thus, the optimum range giving the best correlation with the presence of GSR was selected from 0 to 0.45. Afterwards, the image was binarized (only black and white) and inverted (*i.e.* pixels were interchanged (black ↔ white)) for better visualization. Figure 1.2(B) displays the binarized and inverted images for the first replicate shot at 10, 30 and 100 cm distances after selecting only those pixels whose intensity was below 0.45. These images enabled to get a reliable idea of the GSR pattern at each shooting distance. Furthermore, by this way, those pixels containing GSR can be quantified and correlated to each shooting distance.

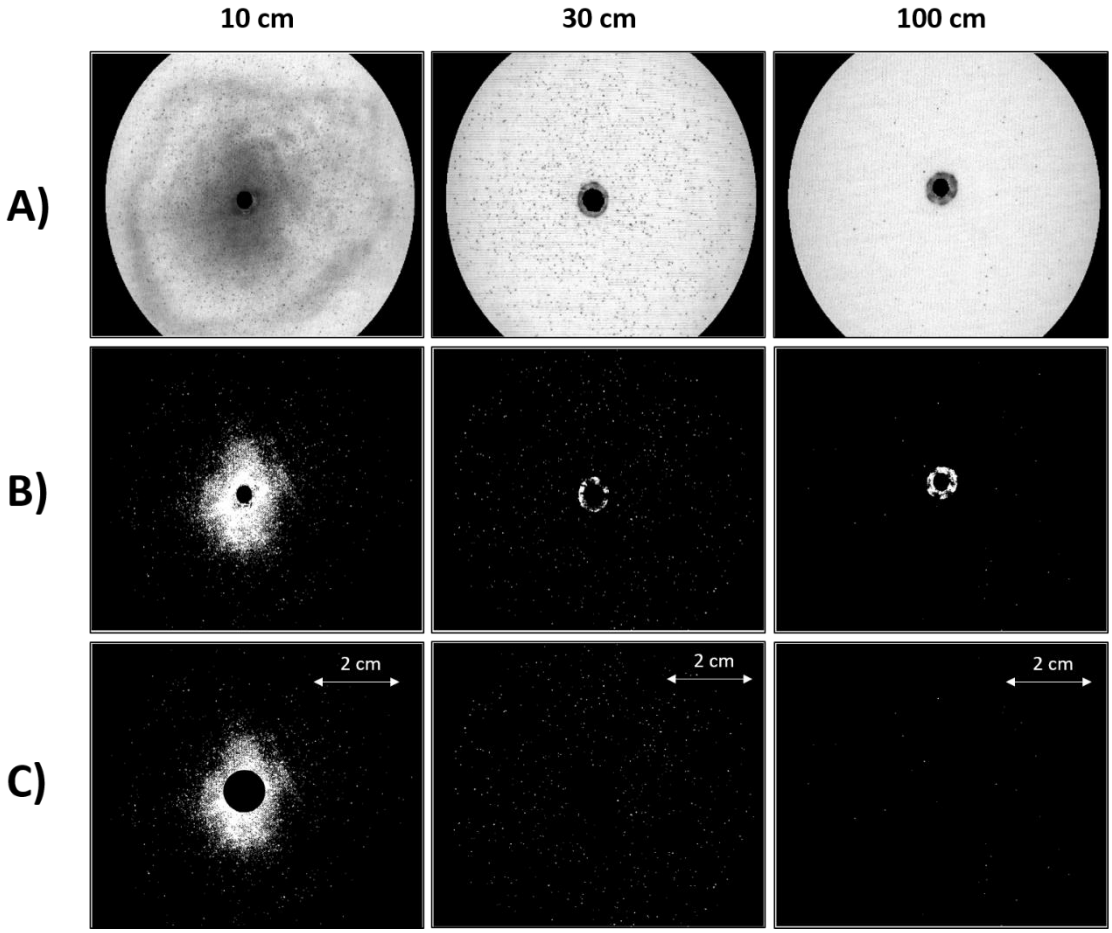

Figure 1.2. Grey-scale images of the blue-RGB frames (at 470 nm) of the first replicate at distances 10, 30 and 100 cm after selecting the ROI (A); after inverting and binarizing the pixels containing GSR (B); and after inverting and binarizing the pixels containing GSR removing the bullet wipe and the entrance hole (C).

Regarding the analysis, first, it is important to consider that the residues present on the surface of the bullet were deposited around the immediate margins of the entrance hole as it passed through the clothing. This dark ring, present to a greater or lesser extent in all the targets, does not offer information directly correlated with the shooting distance. For this reason, the area where the bullet wipe residue was present (including the hole) was removed for data treatment. The size of the removed circle-area for all the samples was the maximum-sized bullet wipe residue observed in one of the targets (diameter of 9.5 mm). The results obtained for the images of targets shot at 10, 30 and 100 cm after removing the bullet wipe residue are shown in Figure 1.2(C). By comparing these three images, the decrease in the number of pixels that contain GSR and a higher dispersion with the shooting distance is clearly noticeable.

The GSR amount and dispersion are two main factors that are usually studied to interpret the shooting distance in clothing patterns. Regarding the amount of pixels containing GSR, they were automatically quantified. The results obtained for all distances and replicates are summarized in Table 1.1.

It is important to highlight that these values are the number of pixels in the image detected as GSR, not the number of GSR particles itself. In fact, it was observed for all the images that GSR particles varied in size (*i.e.* the number of pixels each GSR particle covered) by checking the matrix intensity values of the images. There was not a unique size for the GSR particles, but a range of sizes from 1 pixel (the smallest GSR particles) up to 9 pixels (the largest ones). This estimation was made by evaluating the size of those individual particles that reached 150 and 220 cm distance to minimize the possibility of measuring aggregates of particles. Actually, aggregates of these particles would be even bigger.

Table 1.1. Number of pixels containing GSR for each replicate at the studied shooting distances.

Shooting Distance (cm)	Pixels with GSR Replicate A	Pixels with GSR Replicate B	Pixels with GSR Replicate C
10	58692	63136	45325
30	3864	4509	5551
50	2075	2363	2260
70	797	941	640
100	205	621	184
150	31	18	28
220	1	1	6

The number of pixels containing GSR counted for each replicate (Table 1.1) were plotted against the shooting distance after calculating the average and standard deviation. The resultant graphic could poorly fit both a power ($y = 2 \times 10^8\, x^{-3.051}$) and an exponential equation ($y = 27984\, e^{-0.044x}$) with coefficients of determination (R-squared) of 0.921 and 0.967, respectively. By considering these two fittings, it was noticed that the number of pixels containing GSR at 10 cm shooting distance was lower than those expected for a power equation but higher than those expected for an exponential equation. By visually comparing the targets at 10 cm with the targets at the other distances, the differences are noticeable. The 10 cm-targets evidenced the presence of defined GSR particles also present in the targets at the other shooting distances (organic propellant-GSR particles); and a dark continuous diffuse region stained by

smaller (microscopic) particles (probably soot and inorganic lead-based GSR particles) that was not present in the other targets. As previously indicated, the size of propellant-GSR particles varied from 1 pixel (the smallest particles detected) to 9 (3 × 3) pixels (the largest ones). Since one pixel is 120 µm (the resolution of the camera), the approximate size range for the particles detected was 100–400 µm diameter. Thus, a limit of detection of approximately 100 µm of particle diameter is estimated for this camera. The size of carbon black particles that formed the soot is known to be in the order of nanometres [33]. The size of inorganic primer-GSR particles are known to be in the order of microns, concretely, within the range 0–30 µm (>10 µm when forming aggregates) [14, 19]. This implies that no individual carbon or primer-GSR particles (or even aggregates of them) are being detected with this camera, except when a huge number of them densely covers a specific area, as occurs for 10 cm-shooting distance. This evidences a highly steep decrease of carbon black and primer-GSR particles with the shooting distance since these particles massively reached only the closest targets placed at 10 cm distance. This result is in accordance with previous studies [16, 19, 32] which reported that "at intermediate-long distances, between 0.75 and 3 m depending on the ammunition and the weapon type used, very few microscopic inorganic GSR particles usually deposit on the target" [16].

The reason for the steeper decrease of these microscopic particles is not clear. One possibility involves a different flight behaviour for carbon-black and primer-GSR particles with respect to propellant-GSR particles as a consequence of their different air resistance, explained by their significantly different weight, shape and size. As evidenced in literature, the shooting distance that particles reach strongly depends on their air resistance (influenced by factors such as their morphology) [30]. Nevertheless, further investigations on this issue are required to confirm this hypothesis.

In any event, the huge amount of primer-GSR particles at very short distances leads to an over-count of the pixels containing GSR for the 10 cm-targets in comparison to the other shooting distances, providing larger numbers of pixels containing GSR than those expected using an exponential equation.

Taking this into account, a graph in which the 10 cm targets were removed, was plotted (Figure 1.3). This graph properly fits an exponential equation (R-squared = 0.994).

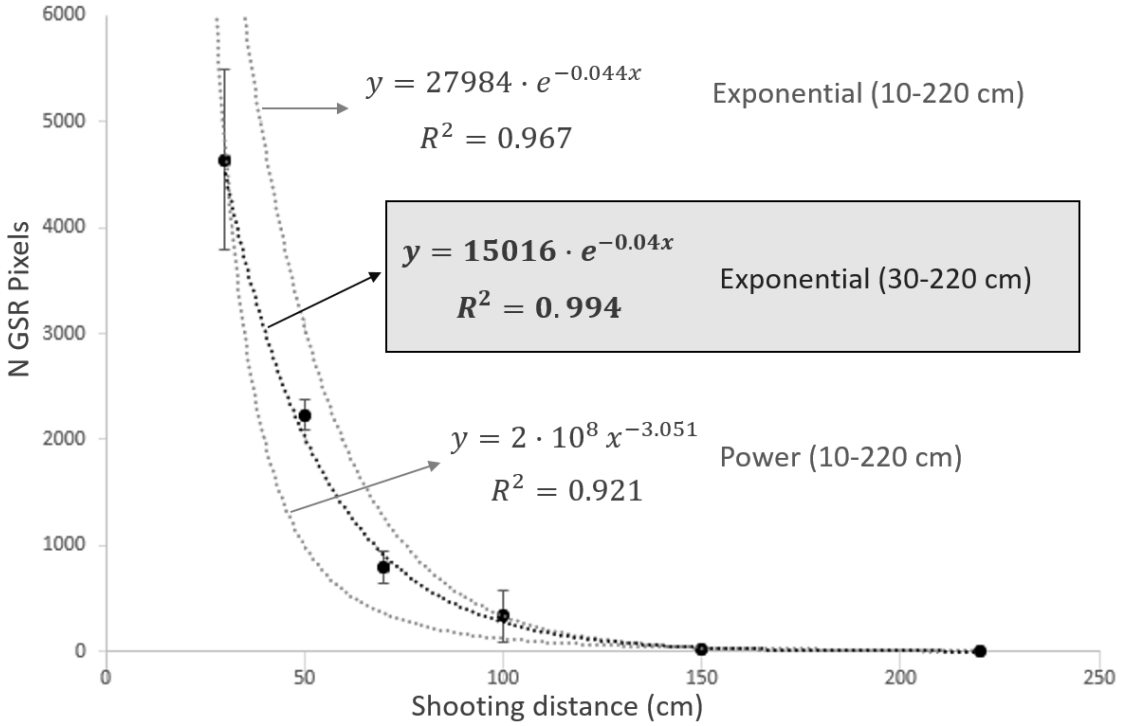

Figure 1.3. Graphical plot: number of pixels containing GSR against the shooting distance from 30 to 220 cm. The best exponential fitting for 30–220 cm is shown as a black solid line. The power and exponential fittings for 10–220 cm (previously calculated) are also displayed as grey dotted lines for comparison purposes.

The number of pixels that contain GSR exponentially decreases with the shooting distance within the range from 30 to 220 cm, following the equation:

$$Number\ of\ pixels\ containing\ GSR\ = 15016\, e^{-0.04(shooting\ distance\ in\ cm)}$$

Operating to find the shooting distance:

$$Shooting\ distance\ (cm) = \frac{\ln(15016/Number\ of\ pixels\ containing\ GSR)}{0.04}$$

Therefore, according to this result: (i) the total amount of GSR correlates with the shooting distance through a specific exponential equation (from 30 to 220 cm), in such a way that the distance might be estimated from the amount of pixels containing GSR; and (ii) for a shooting distance of 220 cm, the amount of GSR is almost zero. Therefore, the detection of no pixels containing GSR would imply a shooting distance larger than 220 cm for this gun and ammunition type.

This hypothesis was tested by interpolating the amount of pixels containing GSR from the fourth replicate of each distance, whose results are summarized in Table 1.2.

Table 1.2. Shooting distances calculated by interpolating the results obtained for the fourth replicate of each shooting distance (pixels containing GSR) into the exponential equation.

Real distance (cm)	Pixels with GSR 4th replicate	Estimated distance	Relative Error (%)	Determined distance range considering the standard deviation (cm)
30	4995	27.5	-8.3	23.6-32.2
50	2072	49.5	-1.0	47.8-51.3
70	793	73.5	5.0	69.2-78.8
100	301	97.7	-2.3	82.8-140.5
150	25	159.9	6.6	153.9-167.9
220	1	240.4	9.3	> 206.5

According to the obtained results, the estimated distance was always determined with a relative error below 10% within the whole range of distances 30–220 cm. Moreover, the standard deviation of the model (*i.e.* from the three replicates used to create the model) might be taken into account by providing a range of shooting distances in the results obtained for the validation samples. Positively, the real shooting distance was always included in the interpolated range except for one of the distances (150 cm).

Conclusions

Targets shot from seven different distances (10–220 cm) with conventional ammunition were analysed using multispectral imaging within the range 400–1000 nm. The acquisition taken at 430, 450 and 470 nm wavelengths provided the largest contrast between the dark GSR particles and white cotton fabric.

The amount of pixels containing GSR particles was calculated based on the greyscale intensity of pixels in the blue RGB frame, at 470 nm. Results showed an exponential decrease in the amount of pixels containing GSR with the shooting distance. This exponential decrease properly fits the specific equation ($Number\ of\ pixels\ containing\ GSR\ =\ 15016\ e^{-0.04(shooting\ distance)}$) for shooting distances between 30 to 220 cm.

In addition, the results obtained in this study indicated that the non-detection of GSR particles in the images would involve a shooting distance longer than 220 cm for the ammunition, weapon, and conditions used. On the other hand, the quantification of an excessive number of pixels (that may even exceed the estimations made by the exponential equation) would imply a shooting distance

within the range 0–30 cm. This is due to the different GSR pattern, observed for very short shooting distances, which contained a grey diffuse region (attributed to carbon black and primer-GSR particles), that considerably increased the number of pixels containing GSR over the estimation provided by the exponential equation. Thus, further studies evaluating additional shooting distances within the range 0–30 cm should be performed in order to find a more accurate mathematical equation applicable to very short-range distances.

Finally, it is important to highlight that favorable and known conditions (*i.e.* ammunition type, gun, white cotton as background, shots performed in a shooting gallery, perpendicular shots to targets, evidence recovery just after shooting, no blood, water or dust contamination, etc.) were employed in this research, due to its preliminary nature. Thus, its immediate application to real casework is, nowadays, unfeasible. How the correlation curve is affected by all these factors needs to be evaluated and think solutions to overcome such problems when estimating the shooting distance in real samples.

References

[1] C. Chang, Hyperspectral Imaging: Techniques for Spectral Detection and Classification, USA Plenum Publishers, New York, 2003.

[2] H.F. Grahn, P. Geladi, Techniques and Applications of Hyperspectral Image Analysis, Wiley, Great Britain, 2007.

[3] B.E. Bernacki, T.A. Blake, A. Mendoza, T.J. Johnson, Visible hyperspectral imaging for standoff detection of explosives on surfaces, Proc. SPIE 7838 (2010) 78380C/1-78381C/7.

[4] G.J. Edelman, E. Gaston, T.G. van Leeuwen, P.J. Cullen, M.C.G. Aalders, Hyperspectral imaging for non-contact analysis of forensic traces, Forensic Sci. Int. 223 (2012) 28-39.

[5] J.M. Amigo, H. Babamoradi, S. Elcoroaristizabal, Hyperspectral image analysis. A tutorial, Anal. Chim. Acta 896 (2015) 34-51.

[6] J. Li, L. Chen, W. Huang, Q. Wang, B. Zhang, X. Tian, S. Fan, B. Li, Multispectral detection of skin defects of bi-colored peaches based on vis-NIR hyperspectral imaging, Postharvest Biol. Technol. 112 (2016) 121-133.

[7] J.C. Noordam, W.H. Van Den Broek, L.M.C. Buydens, Detection and classification of latent defects and diseases on raw French fries with multispectral imaging, J. Sci. Food Agric. 85 (2005) 2249-2259.

[8] J. Liu, Y. Cao, Q. Wang, W. Pan, F. Ma, C. Liu, W. Chen, J. Yang, L. Zheng, Rapid and non-destructive identification of water-injected beef samples using multispectral imaging analysis, Food Chem. 190 (2016) 938-943.

[9] E. Marengo, M. Manfredi, O. Zerbinati, E. Robotti, E. Mazzucco, F. Gosetti, G. Bearman, F. France, P. Shor, Technique based on LED multispectral imaging and multivariate analysis for monitoring the conservation state of the Dead Sea Scrolls, Anal. Chem. 83 (2011) 6609-6618.

[10] L. Caneve, F. Colao, M. Del Franco, A. Palucci, M. Pistilli, V. Spizzichino, Multispectral imaging system based on laser induced fluorescence for security applications, Proc. SPIE 9995 (2016) 999508/1-999508/7.

[11] H. Östmark, M. Nordberg, T.E. Carlsson, Stand-off detection of explosives particles by multispectral imaging Raman spectroscopy, Appl. Opt. 50 (28) (2011) 5592-5599.

[12] Z. Khan, F. Shafait, A. Mian, Automatic ink mismatch detection for forensic document analysis, Pattern Recogn. 48 (2015) 3615-3626.

[13] M. López-López, C. García-Ruiz, Recent non-chemical approaches to estimate the shooting distance, Forensic Sci. Int. 239 (2014) 79-85.

[14] F.S. Romolo, P. Margot, Identification of gunshot residue: a critical review, Forensic Sci. Int. 119 (2001) 195-211.

[15] A. Zeichner, B. Glattstein, Recent developments in the methods of estimating shooting distance, Sci. World J. 2 (2002) 573-585.

[16] D. Muller, A. Levy, A. Vinokurov, M. Ravreby, R. Shelef, E. Wolf, B. Eldar, B. Glattstein, A novel method for the analysis of discharged smokeless powder residues, J. Forensic Sci. 52 (2007) 75-78.

[17] O. Dalby, D. Butler, J.W. Birkett, Analysis of gunshot residue and associated materials—a review, J. Forensic Sci. 55 (2010) 924-943.

[18] M. López-López, C. Alvarez-Llamas, J. Pisonero, C. García-Ruiz, N. Bordel, An exploratory study of the potential of LIBS for visualizing gunshot residue patterns, Forensic Sci. Int. 273 (2017) 124-131.

[19] Z. Brozek-Mucha, Scanning electron microscopy and X-ray microanalysis for chemical and morphological characterisation of the inorganic component of gunshot residue: selected problems, Biomed. Res. Int. (2014) 1-11.

[20] C.S. Atwater, M.E. Durina, J.P. Durina, R.D. Blackledge, Visualization of gunshot residue patterns on dark clothing, J. Forensic Sci. 51 (2006) 1091-1095.

[21] J.A. Bailey, Digital infrared photography to develop GSR patterns, Aust. J. Forensic Sci. 39 (2007) 33-40.

[22] H. Brown, D.M. Cauchi, J.L. Holden, H. Wrobel, S. Cordner, Image analysis of gunshot residue on entry wounds I—the technique and preliminary study, Forensic Sci. Int. 100 (1999) 163-177.

[23] H. Tugcu, C. Yorulmaz, Y. Karslioglu, H.B. Uner, S. Koc, C. Ozdemir, A. Ozaslan, B. Celasun, Image analysis as an adjunct to sodium rhodizonate test in the evaluation of gunshot residues, Am. J. Forensic Med. Pathol. 27 (2006) 296-299.

[24] W. Lichtenberg, Methods for determination of shooting distance, Forensic Sci. Rev. 2 (1) (1990) 37-62.

[25] H. Brown, D.M. Cauchi, J.L. Holden, H. Wrobel, S. Cordner, Image analysis of gunshot residue on entry wounds II—a statistical estimation of firing range, Forensic Sci. Int. 100 (1999) 179-186.

[26] A. Biedermann, F. Taroni, A probabilistic approach to the joint evaluation of firearm evidence and gunshot residues, Forensic Sci. Int. 163 (2006) 18-33.

[27] R. Hofer, S. Graf, S. Christen, The use of unburned propellant powder for shooting distance determination. Part 1: infrared luminescence, Forensic Sci. Int. 273 (2017) 10-19.

[28] R. Hofer, P. Wyss, The use of unburned propellant powder for shooting distance determination. Part 2: diphenylamine reaction, Forensic Sci. Int. 278 (2017) 24-31.

[29] Z. Brozek-Mucha, Distribution and properties of gunshot residue originating from Luger 9 mm ammunition in the vicinity of the shooting gun, Forensic Sci. Int. 183 (2009) 33-44.

[30] M. Bonfanti, A. Gallusser, Problems encountered in the detection of gunshot residues, AFTE J. 27 (2) (1995) 105-121.

[31] A. Vinokurov, A. Zeichner, B. Glattstein, A. Koffman, N. Levin, A. Rosengarten, Machine washing or brushing of clothing and its influence on shooting distance estimation, J. Forensic Sci. 46 (6) (2001) 928-933.

[32] A. Vinokurov, A. Zelkowicz, E. Wolf, A. Zeichner, The influence of a possible contamination of the victim's clothing by gunpowder residue on the estimation of shooting distance, Forensic Sci. Int. 194 (2010) 72-76.

[33] J.B. Donnet, R.C. Bansal, M.J. Wang, Carbon Black: Science and Technology, second edition, revised and expanded, CRC Press, New York, 1993.

Chapter 2. Transfer of explosive residues to different surfaces through consecutive fingerprints

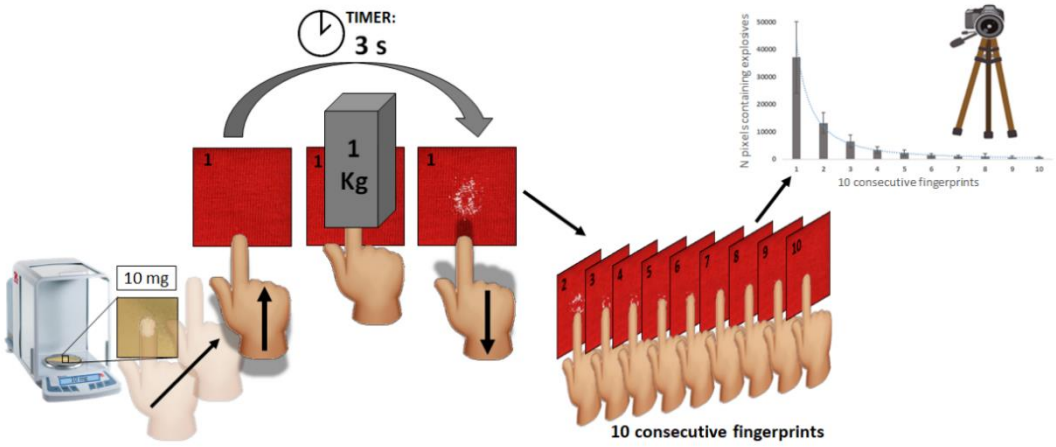

Main source:

H. Lees, **Félix Zapata**, M. Vaher, C. García-Ruiz, Simple multispectral imaging approach for determining the transference of explosive residues in consecutive fingerprints, *Talanta* 184 (2018) 437-445.

Other sources:

H. Lees, **Félix Zapata**, M. Vaher, C. García-Ruiz, Study of the adhesion of explosive residues to the finger and transfer to clothing and luggage, *Sci. Justice* 2018 (In press, DOI: 10.1016/j.scijus.2018.07.002).

Abstract

This novel investigation focused on studying the transfer of explosive residues (TNT, HMTD, PETN, ANFO, dynamite, black powder, NH_4NO_3, KNO_3, $NaClO_3$) in ten consecutive fingerprints to two different surfaces – cotton fabric and polycarbonate plastic – by using multispectral imaging (MSI). Imaging was performed employing a reflex camera in a purpose-built photo studio. Images were processed in MATLAB to select the most discriminating frame – the one that provided the sharpest contrast between the explosive and the material in the red-green-blue (RGB) visible region. The amount of explosive residues transferred in each fingerprint was determined as the number of pixels containing explosive particles. First, the pattern of PETN transfer by ten different persons in successive fingerprints was studied. No significant differences in the pattern of transfer of PETN between subjects were observed, which was also confirmed by multivariate analysis of variance (MANOVA). Then, the transfer of traces of the nine above explosives in ten consecutive fingerprints to cotton fabric and polycarbonate plastic was investigated. The obtained results demonstrated that the amount of explosive residues deposited on successive fingerprints tended to undergo a power or exponential decrease, with the exception of inorganic salts (NH_4NO_3, KNO_3, $NaClO_3$) and ANFO (consisting of 90% NH_4NO_3).

Introduction

In recent years, numerous terrorist attacks have taken place globally, representing a constant threat to citizens in many countries. It is very probable that when a terrorist handles an explosive, there will remain a certain amount of explosive residues on his/her hands and clothes. Therefore, the detection of explosive traces directly from the hands and cloths of suspects [1-3] or through the collection of the explosive traces by swabbing [4-8] has been the subject of many studies. In this regard, Perret *et al.* [4] demonstrated that handling of different explosives resulted in significant transfer of explosives to the hands, and traces were still detectable even after washing hands with soap. Furthermore, explosive residues may be transferred from contaminated hands and clothes to other items, such as laptops, luggage, etc. The search for and detection of trace amounts of explosives on people and objects at airports and other high-risk venues is a major challenge in counterterrorism activities [9, 10]. The transfer of explosive residues through a person's fingerprints enables the detection of concealed explosives through surface sampling [11]. As a matter of fact, fingerprints are one of the main means for transferring trace amounts of explosives during handling and preparation of improvised explosive devices [12].

To date, significant progress has been made in the detection of explosive traces in fingerprints [12-21]. Lately, there has been keen interest in developing methods for the rapid detection of explosive residues in fingerprints by using various spectroscopic, imaging and microscopic techniques, including laser-induced breakdown spectroscopy [12, 22, 23], X-ray fluorescence [24], vibrational spectroscopy (infrared [1, 2, 17, 25-27] and Raman [14, 28-32]) and visible spectroscopy [33]. Most studies are focused on detecting and identifying the explosive residues from fingerprints placed on different surfaces, which is the most important goal for counterterrorism purposes. However, the transfer of explosives in consecutive fingerprints to those materials on which they are detected has been scarcely studied. In this respect, Turano [34] quantified the amount of NH_4NO_3 and $KClO_3$ deposited by successive fingerprints on three different surfaces (filter paper, polypropylene, and polyurethane) by using ion chromatography. Verkouteren *et al.* [10] analysed and characterized fifty composition-4 (C-4) fingerprints by using polarized light microscopy and image analysis. Gresham *et al.* [35] determined the mass of 1,3,5-trinitroperhydro-1,3,5-triazine (RDX) and the particle size distribution of the C-4 residues

deposited on polyethylene films by fingerprint transfer. Mass of RDX was determined by gas chromatography and the particle size distribution of residues was determined by microscopic examination. Choi and Son [36] used ion mobility spectrometry to detect traces of RDX and TNT transferred to three smear matrices – stainless steel mesh, cellulose paper and cotton fabric – by using a stainless steel roller.

Spectral imaging is a well-known non-destructive, fast and inexpensive technique with high potential for studying the transfer of explosive residues since it combines the spectral and spatial information about the imaged sample [17]. Although selective spectral ranges using infrared or Raman vibrational spectroscopy are needed for explosives identification, the identification of explosives was not the objective of this study. This work aims to study the transfer of known explosives through successive fingerprints to different materials. For this purpose, the simplest visible multispectral imaging (MSI) system consisting of red-green-blue (RGB) wavelengths that operate in professional and non-professional cameras as well as mobile phones was applied. The goal of the study was to develop a simple approach for acquiring fundamental knowledge about the transfer of explosive residues in ten consecutive fingerprints to two different surfaces, cotton fabric and polycarbonate plastic.

Materials and methods

- Explosives and inorganic salts

In this research, the transfer of nine different explosive residues –TNT, HMTD, PETN, dynamite, ANFO, black powder, NH_4NO_3, KNO_3, $NaClO_3$ – was examined. Organic explosives and explosive mixtures were obtained from TEDAX, Spanish Explosive Ordnance Disposal (EOD). Inorganic salts (NH_4NO_3, KNO_3, $NaClO_3$) were purchased from Sigma-Aldrich (St. Louis, MO, USA) and were of ACS reagent grade (purity>98%). The composition and average particle diameter of the studied explosive residues are given in Table 2.1. However, during the experiments it was observed that, in some cases, the particles of explosives became aggregated because of the pressing/transfer procedure.

Table 2.1. Composition and average particle diameter of the studied explosive residues.

Explosive residues	Composition[a]	Average particle diameter[b] (μm)
NH_4NO_3	Ammonium nitrate (100%)	≈ 300
KNO_3	Potassium nitrate (100%)	≈ 400
$NaClO_3$	Sodium chlorate (100%)	≈ 500
ANFO	Ammonium nitrate (90%) + diesel (10%)	≈ 500
Dynamite*	Ammonium nitrate (66%) + ethylene glycol dinitrate (29%) + nitrocellulose (1%) + dibutyl phthalate (2.5%) + sawdust (1.2%) + calcium carbonate (0.3%)	≈ 300
Black powder	Potassium nitrate (75%) + charcoal (15%) + sulfur (10%)	≈ 400 (KNO_3) ≈ 50 (charcoal)
TNT*	2,4,6-Trinitrotoluene (100%)	≈ 75
HMTD	Hexamethylene triperoxide diamine (100%)	≈ 20
PETN	Pentaerythritol tetranitrate (100%)	≈ 40

[a] Information provided by the manufacturer or by TEDAX (Spanish EOD).
[b] Experimentally determined by averaging the diameter of 30-50 particles by using a Raman microscope (Thermo Scientific, Waltham, MA, USA).
* Particle diameter after sample preparation (Section 2.2).

- Sample preparation and fingerprint collection

HMTD, PETN, ANFO, black powder, NH_4NO_3, KNO_3 and $NaClO_3$ were obtained already in powdered form and were used without any pretreatment before experiments. Initial experiments showed that big and heavy particles of non-treated TNT (≈ 5mm particles and 12–13 mg) and dynamite (2 cm cylindrical cartridge) did not adhere to the finger and therefore transfer did not occur. Due to this, it was decided to prepare powdered dynamite and TNT in order to study the transfer of explosives with a similar weight (10 mg) and range of particle sizes (< 1 mm). For this, TNT was dissolved in acetonitrile. The solution was left to dry overnight to enable evaporation of acetonitrile. As a result, the powdered TNT remained on Petri dish. Dynamite was mechanically powdered in the mortar. The particle sizes after these pretreatments are indicated in Table 2.1.

Cotton fabric and polycarbonate plastic as the two most common clothing and luggage materials, respectively, were chosen to study the transfer of explosive residues through fingerprints. For experiments, a cotton T-shirt bought from a local supermarket was cut into 3×3 cm pieces. A 5-gallon (*ca* 19 L) polycarbonate plastic water bottle was also cut into 3×3 cm pieces, instead of using a real polycarbonate luggage.

The amount of explosive residues remaining in fingerprints depends on the initial amount present on a person's hands, the number of successive

impressions made after contamination and the force applied by the contaminated finger [10, 11]. Therefore, to take repeatable fingerprints, the applied force (1 kg) and time (3 s), were fixed to standardize the transfer procedure. The controlled force was applied by placing a 1- kg cuboid bottle on the index finger while taking the fingerprints. The time was fixed with a stopper. Additionally, the printing surfaces were all prepared in the same manner and the fingerprints were taken by ensuring the contact of the whole index finger area with the surface. To ensure the presence of the same amount of natural oils and sweat in the finger, a subject's hands were always washed 15 min before each experiment. During these 15 min the normal routine work was allowed to continue. The initial amount of explosive was always balanced at around 10.00 mg on a weighing pan using an Ohaus DV215CD analytical balance with a precision of 5 decimal places (0.00001 g). As previously evidenced in Table 2.1, the average particle size was different for each explosive, and consequently the number of particles contained in 10 mg of substance was different for each explosive. For instance, 10 mg meant 5–40 particles for inorganic salts (KNO_3, NH_4NO_3 and $NaClO_3$), while hundreds/thousands of particles for organic explosives (PETN, HMTD, powdered TNT) and black powder (due to fine particles of charcoal). The number of particles for 10 mg of ANFO and dynamite was intermediate.

- Image collection

Fingerprints of explosive residues on the two studied surfaces were photographed using a Nikon D5000 Digital SLR Camera equipped with a 12.9 megapixel DX-format CMOS sensor and AF-S DX Zoom- Nikkor 18–55 mm f/3.5–5.6G ED II lens. A purpose-built photo studio having controlled light, tripod (a fixed height and perpendicular angle) and remote control was used to minimize the error of imaging. Pictures of samples were taken together with that of a clean blank sample (cotton or polycarbonate) to check the correct intensity value for the background of each picture. Three replicates per explosive and material were prepared. Using the remote control three consecutive photographs of each replicate were taken.

- Image processing

Image processing was performed in MATLAB R2017a (MathWorks, USA) using a self-written code. The used image processing was similar to the previous study

performed in Chapter 1 [37]. Three pictures of each replicate were processed as follows. The region of interest (ROI) was selected by removing the unnecessary edges of the image. Raw images contained 2848×4288 pixels × 3 wavelengths, the spatial resolution of each pixel was 19.2×19.2 μm. ROI involved a square selection of 1000×1000 pixels in the correct frame. In order to select the correct frame, the three RGB frames of each image were compared. The frame that provided the sharpest contrast between the explosive and the background material was chosen. This contrast was evaluated by both the visual inspection of the image and the numerical examination of the values in the matrix. For instance, in case of red cotton fabric and white explosive, the green frame was selected, while for polycarbonate plastic and white explosive, the red frame was selected, as summarized in Table 2.2. In fact, the selection of materials of the above colours was not random. Bearing in mind the aim of maximizing the contrast, materials of different colours (*i.e.* green, blue, red, grey, white and black cotton fabrics or paper sheets placed behind the transparent polycarbonate plastic) were initially examined. Of the tested materials, red cotton fabric provided the highest contrast for both white and dark explosives. Regarding the coloured paper sheet placed behind polycarbonate, black paper for white explosives, and light grey paper for black powder were selected.

Table 2.2. Selected frames and optimized intensity threshold values for counting the explosive particles on each surface.

Explosive particles and surface	RGB frame selected	Intensity threshold value (0-1) 0= completely black, 1= completely white
White explosives on red cotton	Green	> 0.39
Black powder on red cotton	Red Green	< 0.30 (black charcoal particles) > 0.34 (white-grayish KNO_3 particles)*
White explosives on polycarbonate (dark background behind polycarbonate)	Red	> 0.39
Black powder on polycarbonate (light background behind polycarbonate)	Blue	< 0.59 (black charcoal + white-grayish KNO_3 particles)*

*KNO_3 particles were covered with charcoal and were therefore not completely white.

After selecting the proper frame, the amount of pixels containing explosive residues was quantified. To this end, pixels whose values of intensity in the specific frame exceeded a specific value were summed up. Different intensity thresholds were tested by controlling the maximum intensity present in the

blank sample and assuring visually that the program would not count any pixels from the background. Then, the quantification of pixels in each image was performed through automatically counting the pixels whose intensity values were higher (in case of white explosives) or lower (in case of black powder) than the threshold value. For black powder on cotton fabric, the combination of two frames was employed and the number of greyish and black pixels were finally summed up. Table 2.2 summarizes the threshold values optimized for each surface and explosive to count the explosive particles on that surface.

After counting the pixels, the image was binarized, *i.e.* converted only to black and white (values 0 and 1 only) for better visualization. A simplified scheme of image processing in MATLAB for ANFO on cotton fabric is displayed in Figure 2.1.

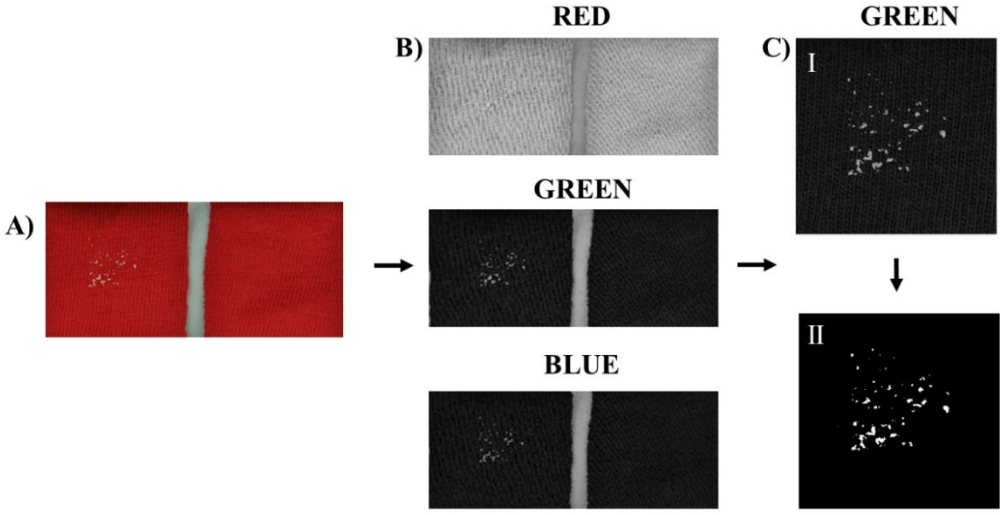

Figure 2.1. Simplified scheme of image processing in MATLAB: A) explosive residues (ANFO) on cotton fabric (left) compared to a blank sample (right), B) RGB frames for evaluation and selection, C) selection of ROI in the correct frame (I) and binarization of the image (II).

It is important to point out that the number of pixels containing explosive residues in the image does not exactly respond to the number of explosive particles itself. The two reasons for this are that (a) the size of the particles is different even within the same explosive and (b) the particles may become aggregated during the pressing/transferring procedure, but only pixels in the upper layer of fingerprints are counted. Nevertheless, despite the above-mentioned shortcomings, some fundamental insights can be established about the transfer of explosive residues.

- Data analysis

The numbers of pixels obtained by MATLAB were imported as a matrix to Excel (Microsoft Office 2016) and STATGRAPHICS Centurion XVI.I (Statpoint Technologies, Inc., USA). Different fitting trendlines using Excel were tested by evaluating the R^2 coefficient. Multivariate Analysis of Variance (MANOVA) was performed in STATGRAPHICS to analyse the variance in the amount of pixels containing explosives among samples and replicates. Before performing MANOVA it was verified that data distribution was normal and linear, there was homogeneity of variances and no outliers were present. The number of dependent variables was 10 (ten fingerprints) to 1 predictive factor (subjects). In brief, an analysis of variance (ANOVA) was conducted for each variable separately, evaluating its performance at an alpha level of 0.05. The multiple comparison procedure to discriminate among the means of transferred explosive residues between subjects was based on Fisher's least significant difference (LSD).

Results and discussion

- Transfer of explosive residues in ten consecutive fingerprints by ten persons

The transfer of PETN in ten consecutive fingerprints to cotton fabric was investigated. Ten consecutive fingerprints were taken of ten persons in triplicate. The test group consisted of five females and five males at the age between 22 and 29 years. A standardized procedure (previously described) for taking fingerprints was followed by all participants. To this end, the index finger of each person's right hand was exposed for 3 s to 10 mg of the explosive powder on a weighing pan. After that, the fingertip with the explosive particles adhered to was pressed consecutively on ten pieces of cotton fabric. The amount of explosive particles remaining on the weighing pan was re-weighed after pressing the finger on the pan to determine the initial amount of explosive adhered to the subject's fingertip. This was done by subtracting the two weight values of the weighing pan (initial and after).

The amount of PETN adhered to the bare finger after pressing varied from 3.7 to 7.5 mg between the subjects. Interestingly, the pattern of transfer of PETN through successive impressions to cotton fabric was similar in all subjects – the amount of explosive residues in the fingerprints decreased with the increasing number of fingerprintings.

The graph showing the average number of pixels containing PETN residues (with standard deviation) in each fingerprint taken of the ten subjects is depicted in Figure 2.2. As an example, the pictures of ten consecutive fingerprints of PETN on cotton fabric taken of one person are also given in the figure.

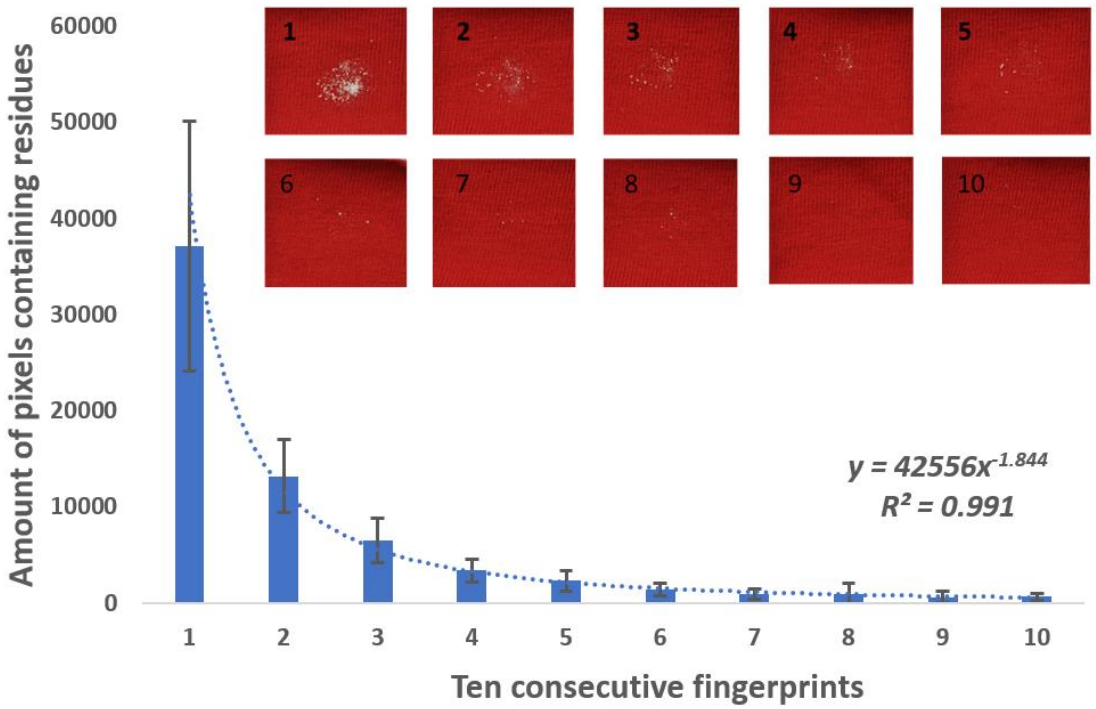

Figure 2.2. Graph showing the variation of the amount of PETN (amount of pixels) transferred through ten successive fingerprints of ten persons. As an example, images of ten consecutive fingerprints of one person are shown (red squares 1–10).

According to the standard deviation bars seen on Figure 2.2, it is evident that there were differences in the amounts of PETN (amount of pixels) transferred by the subjects despite employing the standardized fingerprinting procedure. However, even with those differences, the general results were the same – a similar decrease in the transferred amounts of PETN through successive fingerprints was observed for every person. In fact, this decrease of the transferred PETN amount in consecutive fingerprints may be explained using the power function ($y = 42556\,x^{-1.844}$) with an acceptable coefficient of determination ($R^2 = 0.99$).

In order to check whether the slight differences visually observed among the subjects were statistically significant, MANOVA was performed. Since the p-value for the first variable (the first fingerprint) was less than 0.05 (p-value was 0.0132), there was a statistically significant difference between the subjects considering the first fingerprint at a 95.0% confidence level (*i.e.* rejection of the null hypothesis). ANOVA results for all the other variables gave p-values higher than 0.05, which meant that the differences in the amount of transferred explosive residues between subjects from their second to tenth fingerprint were not statistically significant.

A popular way to investigate the cause of rejection of the null hypothesis is the multiple comparison procedure. Therefore, this procedure was applied to the ANOVA of the first variable (the first fingerprint) to determine which means were significantly different from which others. The Fisher's LSD estimated difference between each pair of means showed that out of 45 pairs (all possible combinations among the ten persons), 14 pairs of means showed statistically significant differences at a 95.0% confidence level. From Table 2.3 it can be seen that five groups were created using columns of X's. Within each column, the levels containing X's form a group of means within which there were no statistically significant differences.

Surprisingly, even though there were significant differences in the explosive amount present in the first fingerprint between some specific subjects, Table 2.3 reveals that none of the subjects differed markedly from the others. The amount of transferred explosive residues in consecutive fingerprints remained in a definite similar range for all subjects. For example, even though there were statistically significant differences (considering the first fingerprint) between subjects 1 and 10, no statistical differences between subjects 1 and 4, neither between subjects 4 and 9 or between subjects 9 and 10 were observed.

Table 2.3. Multiple comparison procedure of the ANOVA results of the first fingerprint for the ten subjects.

	Groups in which transfer is not significantly different				
Subject 1	X				
Subject 2	X	X			
Subject 3	X	X	X		
Subject 4	X	X	X	X	
Subject 5		X	X	X	X
Subject 6			X	X	X
Subject 7			X	X	X
Subject 8			X	X	X
Subject 9				X	X
Subject 10					X

Despite the statistically significant differences that may occur between some persons (regarding the explosive

amount in their first fingerprint), there are no differences that perfectly distinguish people's transfer behaviour. In conclusion, there is not a significant influence from the person when transferring the explosives while following a standardized procedure.

- Transfer of residues of nine explosives in ten consecutive fingerprints to cotton fabric or polycarbonate plastic

The transfer of residues of nine different explosives (HMTD, TNT, PETN, black powder, dynamite, ANFO, NH_4NO_3, KNO_3 and $NaClO_3$) in ten fingerprints to two surfaces, cotton fabric and polycarbonate plastic, was investigated. It was evidenced in the preceding experiment that the transfer of explosive residues was not strongly influenced by the person doing it when following a standardized procedure. Therefore, only one person (doing three replicates per explosive residue and surface) participated in all the experiments.

As in the preceding experiment, the weighing pan with the explosive residues was balanced before and after pressing the finger on it to determine the amount of explosive which had adhered to the subjects' fingertips. Interestingly, residues of NH_4NO_3, KNO_3, $NaClO_3$, ANFO, dynamite, TNT and HMTD adhered to fingertips almost entirely from the weighing pan – the adherence of residues to the fingertip after one touch was 93 ± 4% (n=42). However, the amount of black powder and PETN adhered to the person's fingertip after the first pressing was lower and more variable compared to the other explosives, being 62 ± 11% (n=6) and 72 ± 8% (n=6), respectively.

Figure 2.3 displays, as an example, one replicate of ten successive fingerprints containing HMTD, TNT, black powder and KNO_3 on cotton fabric and polycarbonate plastic. As can be visually observed from the figure, the amount of residues of explosives transferred through fingerprints significantly varies for every explosive. In addition, there seems to be differences in the transferred explosive amount between consecutive impressions. In fact, there are several studies that demonstrated some variability in the amount of transferred explosive from one fingerprint to the next [10, 34, 35]. However, no far-reaching conclusions can be drawn on the basis of visual examination only. Therefore, the information contained in the multispectral image was maximized by quantifying the pixels containing explosive residues.

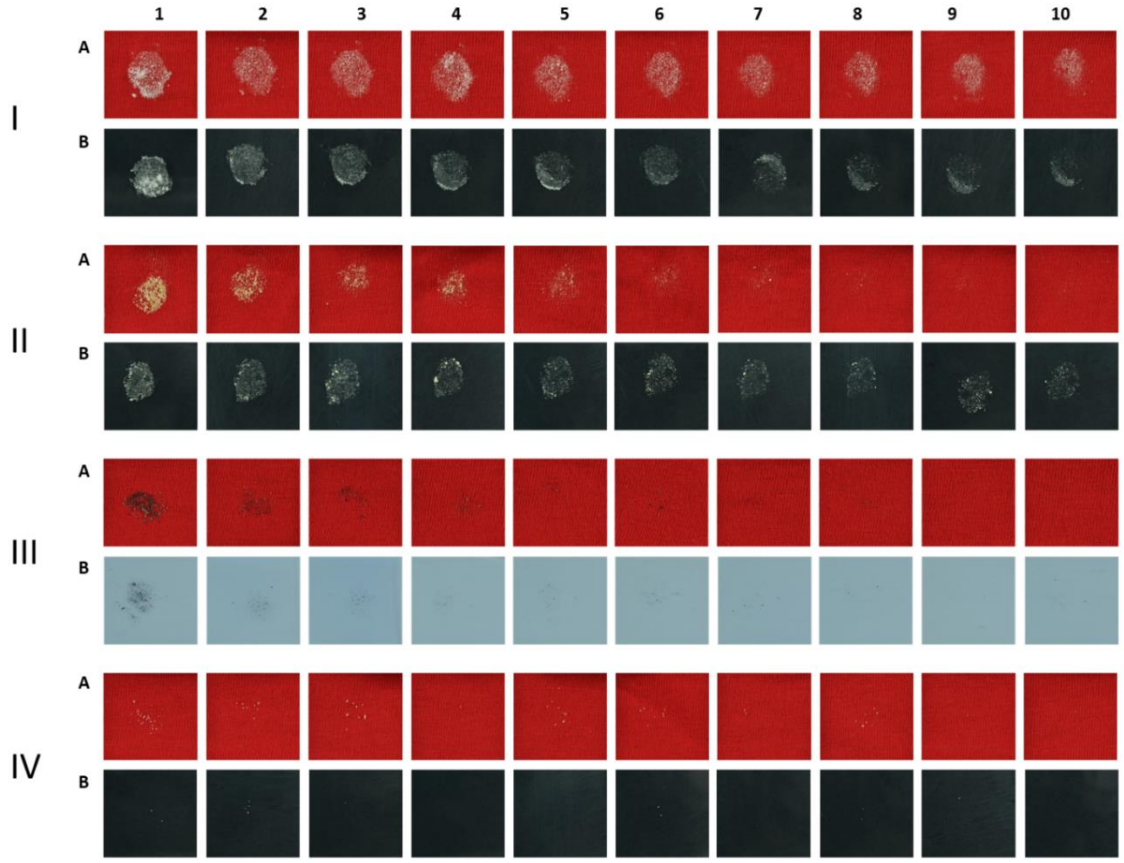

Figure 2.3. Transfer of explosive residues in ten successive fingerprints to cotton fabric (A) and polycarbonate plastic (B). I – HMTD, II – TNT, III – black powder, IV – KNO_3.

According to the obtained results, two entirely different tendencies could be observed in the transfer of explosive residues through consecutive fingerprints when using a standardized procedure. On the one hand, organic explosives (HMTD, TNT, PETN), black powder and dynamite evidenced a particular decrease in the amount of transferred residues through consecutive fingerprints. On the other hand, no clear decrease in the amount of transferred residues of oxidizing inorganic salts (NH_4NO_3, KNO_3, $NaClO_3$) and ANFO (composed of 90% NH_4NO_3) through consecutive fingerprints was noticed. Instead, a random transfer of residues of these explosives was noticed.

The transferred amount of residues of HMTD, TNT, PETN, black powder and dynamite showed a clear decrease (either power or exponential) as illustrated in Figure 2.4. Figure 2.4 displays the quantification of pixels containing explosive residues (y-axis) on consecutive fingerprints (x-axis) together with the respective fitted functions for the transfer of each explosive, as well as their mathematical equations and coefficients of determination.

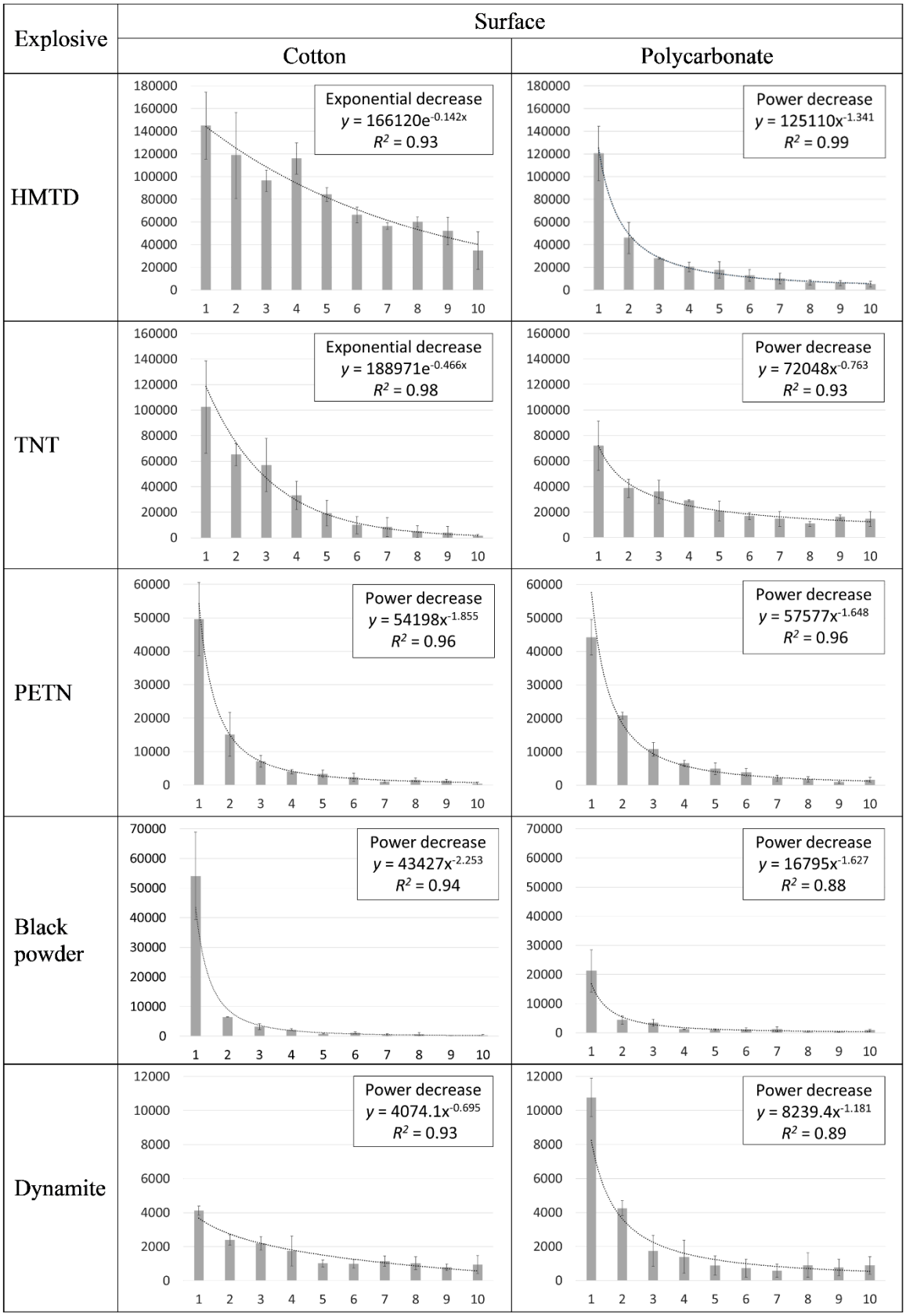

Fig. 2.4. Bar graphs, fitting trendlines, mathematical equations and coefficients of determination showing the amounts of transferred explosive residues undergoing a particular decrease along the ten consecutive fingerprints. X-axis: ten consecutive fingerprints, y-axis: amount of pixels containing explosive residues.

The amount of HTMD transferred to both surfaces under study was clearly the highest. Large number of residues of this explosive could be found in all fingerprints, including the tenth. It should be pointed out that HMTD represented the finest powder (average particle diameter 20 μm), which could explain the higher amounts of transferred residues of this explosive compared to the other explosives. However, the amounts of HMTD residues transferred to cotton fabric and polycarbonate plastic somewhat differed. Specifically, the amount of HMTD transferred to polycarbonate plastic fitted perfectly a power function (R^2 =0.99), while the amount transferred to cotton fabric presented a slighter decrease (exponential) through consecutive fingerprints and underwent some dispersion that accounted for the lower value of R^2.

The amount of TNT transferred to both surfaces was also higher compared to the other explosives. Based on the quantification of the pixels containing explosive residues (Figure 2.4), the transfer of TNT in fingerprints also depended on the target surface. There was a clear decrease through ten fingerprints to cotton fabric – there were only a few particles left by the last fingerprints. This decrease could be explained by an exponential function with R^2 of 0.98. On the other hand, the transfer of TNT to polycarbonate plastic followed a tendency that fitted the power function (R^2 =0.93).

The patterns of transfer of PETN to both materials were very similar and the amounts transferred showed a clear decrease in consecutive fingerprints. The transfer of PETN to cotton fabric and polycarbonate plastic was best described by power functions with R^2 being 0.96 for both surfaces.

The transfer of black powder was characterized by a huge amount of residues left in the first fingerprint on both surfaces (see Figure 2.4), while the second fingerprint contained approximately five to eight times less residues than the first. One explanation to this may be related to the dryness of black powder (due to the charcoal present) and therefore it did not adhere very firmly to the finger, so after the first touch almost the whole amount of explosive fell off from the finger to the surface. Since there were a lot of particles in the first fingerprint and few particles by the last fingerprints, this decay was explained best by power functions, R^2 being 0.94 and 0.88 for cotton fabric and polycarbonate plastic, respectively.

Similarly to PETN and black powder, the transfer of dynamite fitted best power functions to both surfaces (R^2 was 0.93 and 0.89 for cotton fabric and polycarbonate plastic, respectively). However, the amounts of residues transferred to polycarbonate plastic (especially in the first fingerprints) were higher than those transferred to cotton fabric.

In general, it was noticed that the transfer of explosive residues was not only affected by the type of explosive, but also by the surface to which the residues were transferred. In fact, the amount of transferred organic explosives HMTD and TNT underwent an exponential decrease when transferred to cotton fabric, while a power decrease when transferred to polycarbonate plastic. The transfer of PETN, black powder and dynamite fitted best the power decrease in case of both surfaces, indicating that these explosives influenced their transfer more than the surface to which they were transferred.

The transfer of residues of NH_4NO_3, KNO_3, $NaClO_3$ and ANFO was quite chaotic with ten consecutive fingerprints to cotton fabric and polycarbonate plastic (see Figure 2.5).

The pattern of transfer of inorganic salts NH_4NO_3, KNO_3 and $NaClO_3$ to both surfaces under study was rather random and unpredictable. However, as displayed in Figure 2.5, the amount of residues transferred to polycarbonate plastic was very low, on several occasions the number of pixels containing residues was almost zero. Among these three inorganic salts, $NaClO_3$ showed the lowest degree of transfer, while the amount of KNO_3 transferred was the highest. Overall, the transfer of inorganic salts by fingertip was poor (up to 24,000 explosive-pixels for salt explosive residues, while up to 167,000 pixels for organic explosive residues). Due to their high hygroscopicity the salt particles tended to adhere to the bare finger rather than to be transferred to another surface. What is more, the hygroscopic salts formed aggregates which occasionally dropped from the finger during the transfer procedure. This behaviour explained the huge standard deviations obtained for these salts since already one large particle of KNO_3 or NH_4NO_3 could contain 1000 pixels. Therefore, the occasional transfer of a couple of explosive particles increased significantly the standard deviation value. Turano [34] also suggested that variations in his work were likely due to the salt aggregates formed.

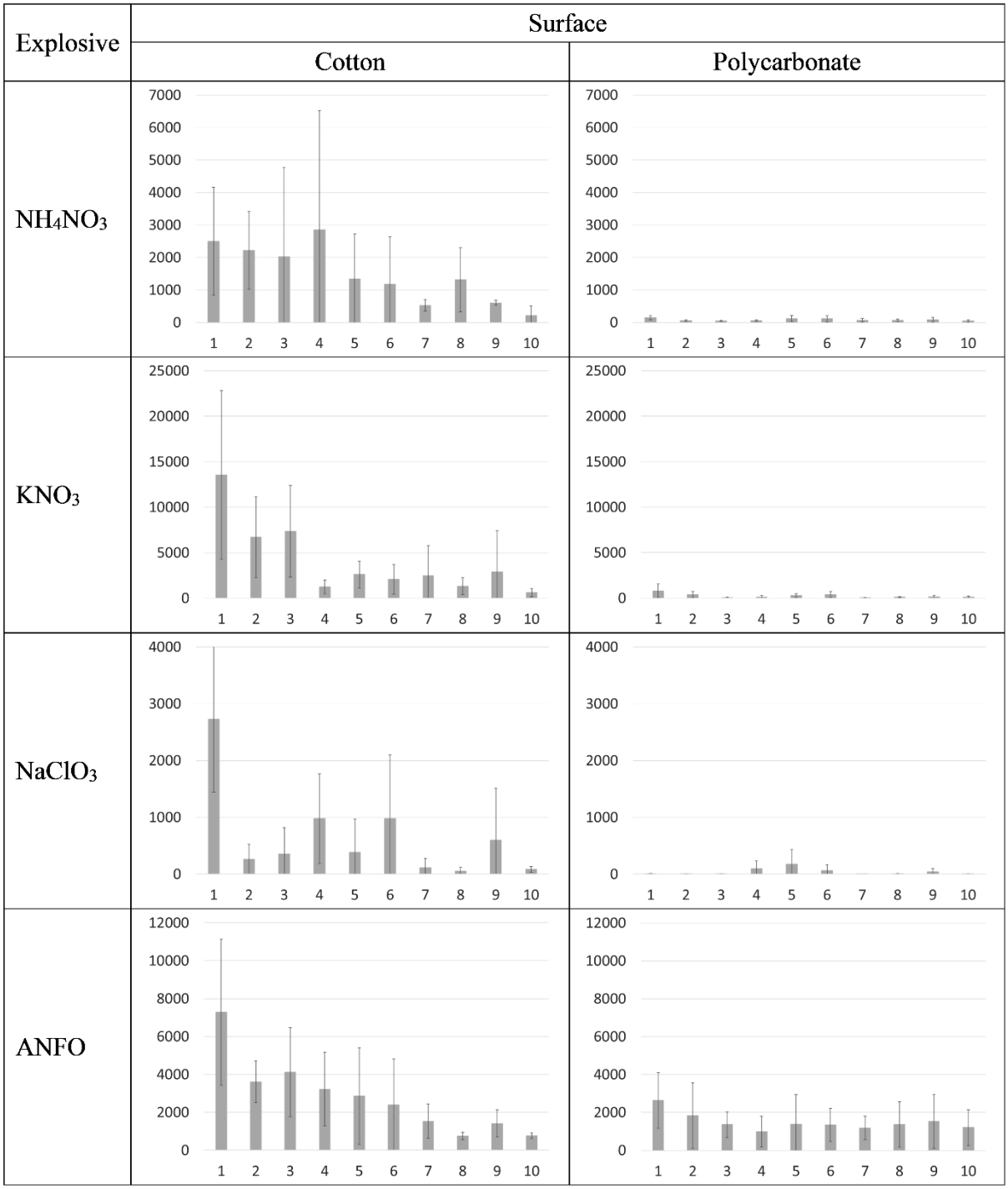

Figure 2.5. Bar graphs and standard deviations showing the transfer of explosive residues of random nature through ten consecutive fingerprints. X-axis: ten consecutive fingerprints; y-axis: amount of pixels containing explosive residues.

The amount of ANFO transferred to cotton fabric showed a doubtful decrease not fitting well to either the power or exponential function. In fact, the pattern of transfer of ANFO to cotton fabric was similar to that of inorganic salts, which is well understood since ANFO consists of 90% NH_4NO_3. However, to both surfaces the amount of ANFO particles transferred was higher compared to

those of NH_4NO_3. The particles of ANFO were oily (one component of which is fuel oil) and when pressuring on them with a warm fingertip, the particles became aggregated. This resulted in the adherence of the particles to the bare finger, making the transfer less controllable. For instance, one big aggregate may correspond to 3600 pixels in the image, while a smaller particle contained about 30 pixels. This explains the large error (standard deviation) in the transferred amounts when an aggregate is inevitably formed and dropped during the transfer procedure. The amount of ANFO particles transferred to polycarbonate plastic in each fingerprint was similar and no decrease in the transferred amount in consecutive fingerprints was observed.

Conclusions

A pioneering fundamental study evaluating the transfer of explosive residues through ten consecutive fingerprints to two different surfaces – cotton fabric and polycarbonate plastic – was carried out using a simple RGB-multispectral imaging approach. The contrast in images was maximized utilizing advantageous coloured backgrounds and selecting the proper frame. This enabled us to estimate the amount of transferred explosive residues through the number of pixels in the image containing explosive residues. Despite the small inequality that may exist between the amount of explosive residues and number of pixels, on the basis of the results obtained, some general conclusions can be drawn.

First, it was shown using PETN as an example that a person does not seem to have a significant impact on the transfer of explosive residues when following a standardized procedure – similar transfer patterns of PETN residues were observed for all subjects. Nevertheless, for stating a general conclusion, further studies with involvement of more subjects and explosives would give more reliable results.

Regarding explosives, large amount of residues of organic explosives HMTD and TNT were transferred showing either an exponential or power decrease. The amount of residues of PETN, black powder and dynamite transferred throughout ten fingerprints was lower, but nonetheless displayed a power decrease on both surfaces, cotton fabric and polycarbonate plastic. On the other hand, no decrease of the transferred amounts of inorganic oxidizing salts

(NH_4NO_3, KNO_3 and $NaClO_3$) and ANFO was observed – the transfer seemed to be mainly governed by random effects.

Regarding the surfaces under study, cotton fabric and polycarbonate plastic, in general, higher amounts of explosive residues were left on the former, which was probably due to the stronger adherence of explosive residues to its fibres than to the smooth surface of polycarbonate plastic. In addition, a sharper decrease in the amount of explosive residues transferred with ten fingerprints to polycarbonate plastic was observed (the transferred amounts of all the explosive residues that presented a decrease, exhibited a power decrease in polycarbonate plastic).

In general, the results obtained may contribute to the scarcely investigated, yet important field – the transfer of explosives through fingerprints to different materials. To date, most investigations have dealt with the trace detection of explosive residues but only few of them have focused on studying the explosives transfer. In fact, still a huge amount of work remains to be done in order to have a more accurate understanding about the transfer pattern of explosives. Further studies including other explosives and ammunitions should be carried out, involving more subjects and more replicates, as well as higher number of fingerprints, to have more representative results. These proposed studies would further increase the knowledge about the transfer pattern of different explosives in various circumstances.

In addition, an interesting study that derives from this research involves the transfer of explosives residues from one surface to another (*i.e.* from cotton to polycarbonate and *vice versa*), which is highly relevant in screening clothing/luggage in airports. To what extent the security controller might unintentionally transfer explosive residues from one luggage to another? Does it depend on whether he/she wears disposable gloves? The interested reader is referred to the reference [38] to solve these questions.

References

[1] M.A. Fernández de la Ossa, J.M. Amigo, C. García-Ruiz, Detection of residues from explosive manipulation by near infrared hyperspectral imaging: a promising forensic tool, Forensic Sci. Int. 242 (2014) 228-235.

[2] M.A. Fernández de la Ossa, C. García-Ruiz, J.M. Amigo, Near infrared spectral imaging for the analysis of dynamite residues on human handprints, Talanta 130 (2014) 315-321.

[3] F. Zapata, M.A. Fernández de la Ossa, E. Gilchrist, L. Barron, C. García-Ruiz, Progressing the analysis of improvised explosive devices: comparative study for trace detection of explosive residues in handprints by Raman spectroscopy and liquid chromatography, Talanta 161 (2016) 219-227.

[4] D. Perret, S. Marchese, A. Gentili, R. Curini, A. Terracciano, E. Bafile, F. Romolo, LC–MS–MS determination of stabilizers and explosives residues in hand-swabs, Chromatographia 68 (2008) 517-524.

[5] F.S. Romolo, L. Cassioli, S. Grossi, G. Cinelli, M.V. Russo, Surface-sampling and analysis of TATP by swabbing and gas chromatography/mass spectrometry, Forensic Sci. Int. 224 (2013) 96-100.

[6] N. Song-im, S. Benson, C. Lennard, Establishing a universal swabbing and clean-up protocol for the combined recovery of organic and inorganic explosive residues, Forensic Sci. Int. 223 (2012) 136-147.

[7] K. Szomborg, F. Jongekrijg, E. Gilchrist, T. Webb, D. Wood, L. Barron, Residues from low-order energetic materials: the comparative performance of a range of sampling approaches prior to analysis by ion chromatography, Forensic Sci. Int. 233 (2013) 55-62.

[8] D.A. Detata, P.A. Collins, A.J. McKinley, A comparison of common swabbing materials for the recovery of organic and inorganic explosive residues, J. Forensic Sci. 58 (2013) 757-763.

[9] J.R. Verkouteren, Particle characteristics of trace high explosives: RDX and PETN, J. Forensic Sci. 52 (2007) 335-340.

[10] J.R. Verkouteren, J.L. Coleman, I. Cho, Automated mapping of explosives particles in composition C-4 fingerprints, J. Forensic Sci. 55 (2010) 334-340.

[11] D.J. Phares, J.K. Holt, G.T. Smedley, R.C. Flagan, Method for characterization of adhesion properties of trace explosives in fingerprints and fingerprint simulations, J. Forensic Sci. 45 (2000) 774-784.

[12] P. Lucena, I. Gaona, J. Moros, J.J. Laserna, Location and detection of explosive contaminated human fingerprints on distant targets using standoff laser-induced breakdown spectroscopy, Spectrochim. Acta – Part B At. Spectrosc. 85 (2013) 71-77.

[13] E.D. Emmons, A. Tripathi, J.A. Guicheteau, S.D. Christesen, A.W. Fountain III, Raman chemical imaging of explosive-contaminated fingerprints, Appl. Spectrosc. 63 (2009) 1197-1203.

[14] A. Tripathi, E.D. Emmons, P.G. Wilcox, J.A. Guicheteau, D.K. Emge, S.D. Christesen, A.W. Fountain, Semi-automated detection of trace explosives in

fingerprints on strongly interfering surfaces with Raman chemical imaging, Appl. Spectrosc. 65 (2011) 611-619.

[15] Y. Mou, J.W. Rabalais, Detection and identification of explosive particles in fingerprints using attenuated total Reflection-Fourier transform infrared spectromicroscopy, J. Forensic Sci. 54 (2009) 846-850.

[16] S. Almaviva, S. Botti, L. Cantarini, A. Palucci, A. Puiu, F. Schnuerer, W. Schweikert, F.S. Romolo, Raman spectroscopy for the detection of explosives and their precursors on clothing in fingerprint concentration: a reliable technique for security and counterterrorism issues, Proc. SPIE 8901 (2013) 890102/1-890102/9.

[17] P.H.R. Ng, S. Walker, M. Tahtouh, B. Reedy, Detection of illicit substances in fingerprints by infrared spectral imaging, Anal. Bioanal. Chem. 394 (2009) 2039-2048.

[18] J.S. Caygill, F. Davis, S.P.J. Higson, Current trends in explosive detection techniques, Talanta 88 (2012) 14-29.

[19] T. Peng, W. Qin, K. Wang, J. Shi, C. Fan, D. Li, Nanoplasmonic imaging of latent fingerprints with explosive RDX residues, Anal. Chem. 87 (2015) 9403-9407.

[20] Y. Ma, H. Li, S. Peng, L. Wang, Highly selective and sensitive fluorescent paper sensor for nitroaromatic explosive detection, Anal. Chem. 84 (2012) 8415-8421.

[21] T.P. Forbes, E. Sisco, Mass spectrometry detection and imaging of inorganic and organic explosive device signatures using desorption electro-flow focusing ionization, Anal. Chem. 86 (2014) 7788-7797.

[22] M. Abdelhamid, F.J. Fortes, M.A. Harith, J.J. Laserna, Analysis of explosive residues in human fingerprints using optical catapulting-laser-induced breakdown spectroscopy, J. Anal. At. Spectrom. 26 (2011) 1445-1450.

[23] J. Moros, J. Serrano, F.J. Gallego, J. Macıas, J.J. Laserna, Recognition of explosives fingerprints on objects for courier services using machine learning methods and laser-induced breakdown spectroscopy, Talanta 110 (2013) 108-117.

[24] C.G. Worley, S.S. Wiltshire, T.C. Miller, G.J. Havrilla, V. Majidi, Detection of visible and latent fingerprints using micro-X-ray fluorescence elemental imaging, J. Forensic Sci. 51 (2006) 57-63.

[25] A. Banas, K. Banas, M.B.H. Breese, J. Loke, B. Heng Teo, S.K. Lim, Detection of microscopic particles present as contaminants in latent fingerprints by means of synchrotron radiation-based Fourier transform infra-red micro-imaging, Analyst 137 (2012) 3459-3465.

[26] N.J. Crane, E.G. Bartick, R.S. Perlman, S. Huffman, Infrared spectroscopic imaging for noninvasive detection of latent fingerprints, J. Forensic Sci. 52 (2007) 48-53.

[27] T. Chen, Z.D. Schultz, I.W. Levin, Infrared spectroscopic imaging of latent fingerprints and associated forensic evidence, Analyst 134 (2009) 1902-1904.

[28] E.D. Emmons, A. Tripathi, J.A. Guicheteau, S.D. Christesen, A.W. Fountain III, Raman chemical imaging of explosive-contaminated fingerprints, Appl. Spectrosc. 63 (2009) 1197-1203.

[29] A. Tripathi, E.D. Emmons, J.A. Guicheteau, S.D. Christesen, P.G. Wilcox, D.K. Emge, A.W. Fountain III, Trace explosive detection in fingerprints with Raman chemical imaging, Proc. SPIE 7665 (2010), 76650N/1-76650N/6.

[30] H. Östmark, M. Nordberg, T.E. Carlsson, Stand-off detection of explosives particles by multispectral imaging Raman spectroscopy, Appl. Opt. 50 (2011) 5592-5599.

[31] I. Malka, A. Petrushansky, S. Rosenwaks, I. Bar, Detection of explosives and latent fingerprint residues utilizing laser pointer-based Raman spectroscopy, Appl. Phys. B Lasers Opt. 113 (2013) 511-518.

[32] M.R. Almeida, L.P.L. Lograd, J.J. Zacca, D.N. Correa, R.J. Poppi, Raman hyperspectral imaging in conjunction with independent component analysis as a forensic tool for explosive analysis: the case of an ATM explosion, Talanta 174 (2017) 628-632.

[33] B.E. Bernacki, T.A. Blake, A. Mendoza, T.J. Johnson, Visible hyperspectral imaging for standoff detection of explosives on surfaces, Proc. SPIE 7838 (2010) 78380C/1-78380C/7.

[34] M.A. Turano, Transfer of Residues in Fingerprints, University of Rhode Island, Kingston, Rhode Island, U.S.A., 2013 ⟨http://digitalcommons.uri.edu/theses/153⟩.

[35] G.L. Gresham, J.P. Davies, L.D. Goodrich, L.G. Blackwood, B.Y.H. Liu, D. Thimsem, S.H. Yoo, S.F. Hallowell, Development of particle standards for testing detection systems: mass of RDX and particle size distribution of composition 4 residues, Proc. SPIE 2276 (1994) 34-44.

[36] S.S. Choi, C.E. Son, Analytical method for the estimation of transfer and detection efficiencies of solid state explosives using ion mobility spectrometry and smear matrix, Anal. Methods 9 (2017) 2505-2510.

[37] F. Zapata, M. López-López, J.M. Amigo, C. García-Ruiz, Multi-spectral imaging for the estimation of shooting distances, Forensic Sci. Int. 282 (2018) 80-85.

[38] H. Lees, F. Zapata, M. Vaher, C. García-Ruiz, Study of the adhesion of explosive residues to the finger and transfer to clothing and luggage, Sci. Justice (2018) In press, DOI: 10.1016/j.scijus.2018.07.002.

Chapter 3. Comparison of Spectroscopy and Chromatography for assessing the transfer of explosive residues

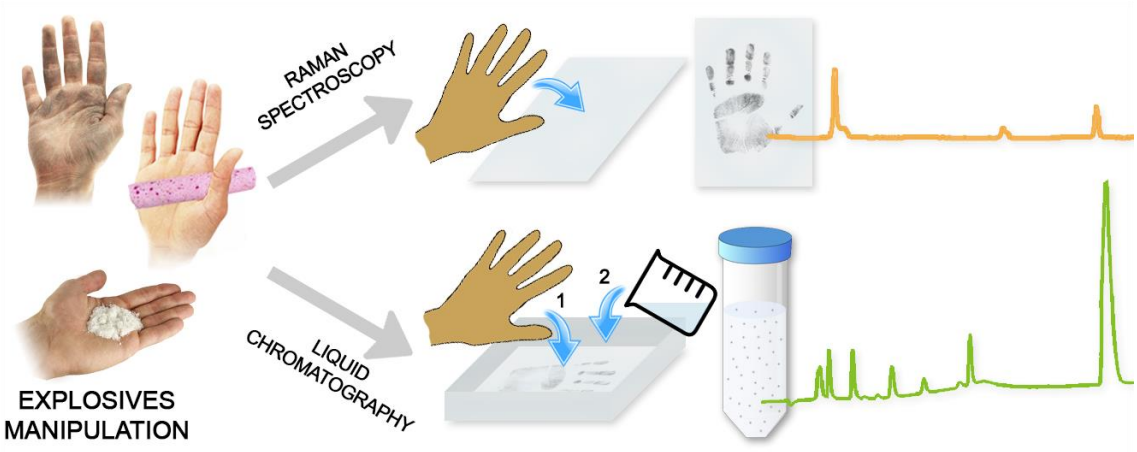

Main source:

Félix Zapata, M.A. Fernández de la Ossa, E. Gilchrist, L. Barron, C. García-Ruiz, Progressing the analysis of Improvised Explosive Devices: Comparative study for trace detection of explosive residues in handprints by Raman spectroscopy and liquid chromatography, *Talanta* 161 (2016) 219-227.

Other sources:

Félix Zapata, F. Ortega-Ojeda, C. García-Ruiz, M. González-Herráez, Selective monitoring of oxyanion mixtures by a flow system with Raman detection, *Sensors* 18 (2018) 2196.

Abstract

Concerning the dreadful global threat of terrorist attacks, the detection of explosive residues in biological traces and marks is a current need in both forensics and homeland security. This study examines the potential of Raman microscopy in comparison to liquid chromatography (ion chromatography (IC) and reversed-phase high performance liquid chromatography (RP-HPLC)) to detect, identify and quantify residues in human handmarks of explosives and energetic salts commonly used to manufacture Improvised Explosive Devices (IEDs) including dynamite, ammonium nitrate, single- and double-smokeless gunpowders and black powder. Dynamite, ammonium nitrate and black powder were detected through the identification of the energetic salts by Raman spectroscopy, their respective anions by IC, and organic components by RP-HPLC. Smokeless gunpowders were not detected, either by Raman spectroscopy or the two liquid chromatography techniques. Several aspects of handprint collection, sample treatment and a critical comparison of the identification of compounds by both techniques are discussed. Raman microscopy and liquid chromatography were shown to be complementary to one another offering more comprehensive information for trace explosives analysis.

Introduction

Terrorist events have increased in frequency during the last two decades and represent an on-going and extremely harmful global threat [1-7]. Terrorist attacks often involve the use of explosives; compounds which have a great destructive power even in small quantities. Currently, there is a growing trend towards using homemade devices called Improvised Explosive Devices (IEDs) [1-7]. Dreadfully, IEDs have been widely used in recent years in different terrorist attacks including those in Madrid (2004), London (2005), Norway (2011), Boston (2013), Santiago de Chile (2014), Paris (2015), Nigeria, Ankara, Brussels and Pakistan (2016) in addition to war zones as Afghanistan, Syria and Iraq where IEDs are constantly used. IEDs are manually manufactured explosive devices, which consist of a variety of elements arranged in a specific way to produce an explosion. Since their destructive effectiveness lies in being unnoticed, IEDs often have varied design and appearance. Thereby, IEDs often evade being neutralized before an explosive attack. IEDs have become an ideal weapon used by terrorists for several reasons, including their low cost, ease of manufacture and subsequent use and difficulty to be detected [1-7]. Therefore, their detection must be tackled as a matter of urgency to avoid such atrocities and guarantee the security of citizens.

Although IEDs can be manufactured from a large variety of explosive materials including military, commercial, or home-made explosives, they usually contain explosive mixtures based on inorganic energetic oxidants including nitrate, chlorate or perchlorate salts [3, 7-9]. In fact, these explosive mixtures are used to manufacture commercial explosives such as dynamites, black powders and other propellants whose purchase is widely available [3]. In addition, the manufacture of home-made mixtures combining any of these oxidazing salts (ammonium nitrate, potassium nitrate, potassium chlorate, potassium perchlorate, etc.) with any fuel (petrol, diesel, sugar, charcoal, flour, etc.) is quite simple [3]. In addition, they are even more freely available than commercial explosives. Ammonium nitrate is used as a fertilizer, but in combination with certain fuels may produce explosive compounds such as dynamite, ammonium nitrate/fuel oil (ANFO) and other nitrate-based explosives [3]. Potassium nitrate, besides also being used as a fertilizer, is a component of black powder widely used to manufacture firecrackers, fireworks and any other pyrotechnic devices. In addition, firecrackers and fireworks usually include potassium chlorate,

perchlorate and other nitrate salts such as barium or strontium nitrates to get different colours and effects [9].

Liquid chromatography, in particular ion chromatography (IC), has been usually employed to identify and quantify energetic salts mainly through the analysis of their characteristic anions (nitrates, chlorates and perchlorates) [10-15]. Complementarily, reversed-phase liquid chromatography (RP-HPLC) is useful for the analysis of organic non-ionic explosives [16, 17]. Until now, only a few preliminary studies have proved their suitability to determine residues in human fingermarks [18, 19]. The detection and identification of explosives in human fingermarks is a comprehensive approach that tackles the challenging task of locating the evidence (illicit substance) as well as potentially identifying a suspect (human fingerprint). The challenge of detecting explosives on fingerprints has been explored using different analytical techniques, being mass spectrometry [20, 21], IR [22-30] and Raman spectroscopy [31-34] those most used up to date. The high sensitivity of mass spectrometry and the speed and non-destructiveness of IR and Raman spectroscopy are highly seductive features. With regards to explosives detection on fingerprints by Raman spectroscopy [31-34], it is important to highlight that the explosives investigated included hexogen (RDX) [31-33], octogen (HMX) [31-33], penthrite (PETN) [31-33], 2,4-dinitrotoluene (2,4-DNT) [34], ammonium nitrate [31-33], potassium nitrate [34] and urea nitrate [34]. In addition, Raman imaging mode was used in those studies and solely the fingerprint area was scanned revealing the presence of explosive residues. Nevertheless, scanning large areas is usually time-consuming, being most effective, in certain cases, the analysis of few selected explosive particles by point measures. Raman microscopy is highly useful to this aim, allowing the rapid detection of microscopic residues. In this study, residues of smokeless gunpowder, black powder and dynamite on human hand-prints, have been analysed due to the high forensic interest of these explosives. In addition, the whole human handprint, instead of a unique fingerprint, was considered with the aim of studying the distribution of the explosive residues adsorbed on the hand and subsequently left on the handprint.

The aim of this work is to study and compare Raman microscopy and liquid chromatography, using both IC and RP-HPLC, for the analysis of explosives residues in handprints.

Materials and methods

- Explosive samples

Smokeless gunpowder, dynamite and ammonium nitrate samples were kindly provided by the Criminalistic Service of Guardia Civil. Two different smokeless gunpowders were used. According to the information included in the official label [35], a single-base gunpowder sample, which was composed by 94% of nitrocellulose and a double-base gunpowder sample containing 85% of nitrocellulose and 10% of dinitrotoluene (DNT) were included in this study. Dynamite was composed by ethylene glycol dinitrate (EGDN), ammonium nitrate, nitrocellulose, dynamite dye, sawdust, calcium carbonate, guar gum and plasticizers, with ammonium nitrate and EGDN declared as its major components [36]. A black powder sample was extracted from a commercial firecracker available in the Spanish market. Black powder is technically defined as a mixture of sulphur, charcoal and potassium nitrate. However, the charge of the pyrotechnic device was composed by sulphur, charcoal and potassium perchlorate. Consequently, and strictly speaking, a black powder substitute product where the potassium nitrate had been replaced by potassium perchlorate, was analysed in this study.

- Reagents

All reagents were of analytical or reagent grade. For Raman spectroscopy, potassium perchlorate, potassium nitrate, potassium chlorate, sodium nitrate and sodium chlorate were purchased from Sigma-Aldrich (St. Louis, MO, USA).

For IC, chloride, nitrite, nitrate, (BDH Chemicals Ltd., Poole, UK), chlorate, perchlorate, cyanate (Sigma-Aldrich, Gillingham, Dorset, UK) were prepared from their sodium salts; sulphate was prepared from its copper salt (BDH Chemicals Ltd., Poole, UK). Acetate (BDH Chemicals Ltd., Poole, UK) and thiocyanate were prepared from their ammonium salts. Formate was prepared from an ammonium solution (Sigma-Aldrich, Gillingham, Dorset, UK). Lactate, oxalate (BDH Chemicals Ltd., Poole, UK), phthalate, and benzoate (Sigma-Aldrich, Gillingham, Dorset, UK) were prepared from their acids. All stock solutions were prepared to a concentration of 1000 mg/L and working standards were prepared daily from these using ultrapure water. Eluents were prepared using a 50 % v/v NaOH solution in ultrapure water (Sigma-Aldrich, Gillingham, Dorset, UK) for anion-exchange chromatography. For RP-HPLC,

EGDN, DNT and nitroglycerine (NG) were purchased from Kinesis (St. Neots, Cambridgeshire, UK). All stock solutions were prepared to a concentration of 100 mg/L and working standards were prepared daily from these using ultrapure water. Mobile phases were prepared using ammonium acetate and methanol (Fisher Scientific, Loughborough, Leicestershire, UK).

All eluents, stocks, standards and samples solutions were prepared using ultrapure water (18.2 MΩ cm) delivered from a Millipore Synergy UV ultra-purification system (Millipore, Bedford, MA, USA). Stock standards were kept in the dark at 5°C and were re-prepared fortnightly.

- Sample preparation and handprint collection

Smokeless gunpowder, dynamite and ammonium nitrate materials were handled without any prior preparation or treatment by seven volunteers (five women and two men). However, black powder had to be extracted from a commercial firecracker. For this, first the fuse was pulled out and then the cartridge was opened with laboratory scissors in such a way that the pyrotechnic charge was collected for handling.

- Procedure for Raman spectroscopy

Prior to the explosive handling, and in order to study whether sweat or common exogenous components can influence the Raman spectra of handprints, the seven volunteers washed their hands in ultrapure water and left to air dry for 15 min with the aim of regenerating the sweat as proposed by Gilchrist *et al.* [18]. During this time, participants were not allowed to handle anything to minimise external contamination. Handprints from both hands were then deposited using a light pressure on the adhesive side of a clear self-adhesive vinyl book cover film of 22 × 38 cm size. For sample conservation and protection, films were covered with another piece of film of the same size. Additionally (and with the aim of testing the influence of common dirt), the handprints (right and left) of two participants who had not washed their hands for at least 3 h and had performed normal daily tasks were also collected. Finally, approximately 5 g of each type of explosive were handled by the volunteers for 10 min. After, volunteers deposited their handprints following the previously explained procedure on a self-adhesive polyvinyl film. Note that before the explosive manipulation, participants cleaned and dried their hands as was first described. Samples containing the denominated “clean”, “natural-contaminated” and

"explosive-contaminated" handprints were then analysed by Raman spectroscopy.

Smokeless gunpowder, dynamite and ammonium nitrate identification was directly performed by Raman spectroscopy. However, since black powder has graphite in its composition, which has a strong fluorescence signal in Raman spectroscopy, it required some sample preparation for its identification. About 0.5 g of black powder were dissolved in 1 mL of ultrapure water and centrifuged at 4000 rpm during 30 min. Three drops of the supernatant were placed on a pre-cleaned microscope slide and the Raman spectra was registered once the solvent was completely evaporated.

- Procedure for liquid chromatography

In order to determine the transfer of anionic explosive residues into handprints and to compare Raman with liquid chromatography results, a similar procedure previously described for Raman analysis was followed for preparing the liquid chromatography samples. Volunteers also washed their hands, manipulated 5 g of each type of explosive during 10 min and, in this case, deposited their handprints on two similar glass trays. One for each hand (left and right). After, 10 mL of ultrapure water was added to each tray and both trays were transferred to an ultrasonic bath (USC 2100D, VWR International, Leuven, Belgium) for 30 min at room temperature (22–23 °C). Extracts were collected into polypropylene vials, along with uncontaminated handprints. Samples were stored in the freezer before being fully defrosted for analysis.

For IC, the extract solutions were dispensed into 0.5 mL poly-propylene vials fitted with in-line filters (Thermo Scientific, Sunnyvale, CA, USA) prior to injection. In some cases it was necessary to dilute the samples to allow for quantification with appropriate reference solutions.

Regarding RP-HPLC, contrary to IC, extracts were transferred into glass vials before direct injection, with no dilution necessary.

- Instrumentation
  - Raman spectroscopy

Raman spectroscopic measurements were performed in a Thermo Scientific DXR Raman microscope (Waltham, MA, USA). It was equipped with a 532 nm excitation wavelength and 900 lines mm^{-1} grating. Control equipment and data

acquisition were performed using the Thermo Scientific Omnic for dispersive Raman 8 software (Waltham, MA, USA). Samples were analysed using 5 mW of laser power and the 10X, 50X or 100X microscope objectives. The spectra acquisition times were 10 spectra of 2 s for all samples. Due to the observation of fluorescent signals, it was necessary to use the confocal pinhole of 50 µm size for the measurement of dynamite samples. However, the slit of 50 µm size was adequate for analysing the ammonium nitrate and the black powder samples. Normalization and baseline correction were applied to all the spectra.

- Liquid chromatography

IC: Suppressed anion-exchange chromatography was performed on a Dionex DX500 system (Thermo Scientific, Sunnyvale, CA, USA), comprising of a GP40 pump and an ED40 conductivity detector fitted with a Dionex AERS 500 (2 mm ID) electrolytic suppressor (current = 50 mA). Instrument control and data acquisition were performed using Chromeleon 6.6. The injection volume was 40 µL. A quaternary ammonium-based Ion Pac AS20 (2 × 250 mm) was used with a flow rate of 0.30 mL/min. In order to separate all species, a hydroxide gradient was employed using two reservoirs of 5 mM and 40 mM NaOH. The optimised gradient profile was as follows: 5 mM hydroxide from 0 to 3 min; a linear ramp from 3 to 8.5 mM hydroxide from 3 to 8.5 min; another linear ramp from 8.5 to 21.5 mM hydroxide from 8.5 to 16 min; a final linear ramp from 21.5 to 40 mM hydroxide from 16 to 25.5 min and maintained at 40 mM hydroxide to 28.8 min. Equilibration time was 15.2 min (total time = 45 min).

RP-HPLC: This was performed on an Agilent HP1100 system (Agilent Technologies, Berkshire, UK) with detection at 210 nm using a diode array spectrophotometric detector. Instrument control and data acquisition were performed using the Chemstation software (Agilent Technologies, Berkshire, UK). A Waters Sunfire C18 column of dimensions 2.1 × 150 mm, 3.5 µm particle size, (Waters, Milford, MA, USA) was used with a flow rate of 0.15 mL/min. An isocratic separation method was used with a mobile phase of 8 mM ammonium acetate in 60:40 MeOH:H_2O. The injection volume was 2 µL.

Results and discussion

- Raman spectroscopy

Since Raman spectroscopy just allows to measure small spots or slits in the region of μm, firstly, the highest concentration of explosive residues area on handprints was evaluated. As black powder was the only coloured sample of all the tested explosives, it was selected to easily visualise the target areas. Figure 3.1 shows the scanned handprints images obtained with a common office scanner (CLX-3175, Samsung, China) of two different volunteers. Note that the three areas with a higher concentration of residues were the fingerprints, phalanx base and thenar (indicated as rectangles in Figure 3.1).

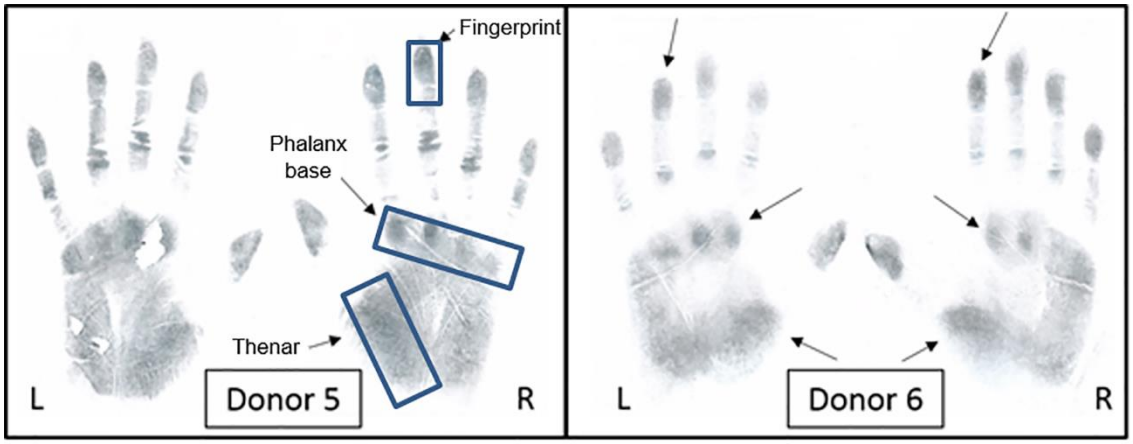

Figure 3.1. Scanned images of handprints from donors 5 and 6 (L, left and R, right) after the donors had handled black powder. Regions of higher concentration of explosive residues indicated in blue rectangles.

As consequence, for the subsequent Raman analysis only these three areas were considered. Furthermore, using these scanned images the influence of sweat or external contamination on the handprints was evaluated. As expected, no differences among the blank (self-adhesive polyvinyl film without handprint), the hand-print collected from a cleaned hand and the handprint from a naturally contaminated hand (at least 3 h performing routine activities and without cleaning) were observed. However, the presence of contamination on the hands of the volunteers affected the amount of explosive residues deposited in their hand palms. It was observed that higher quantity of residues was present on naturally contaminated handprints compared to cleaned hands (see Figure 3.2).

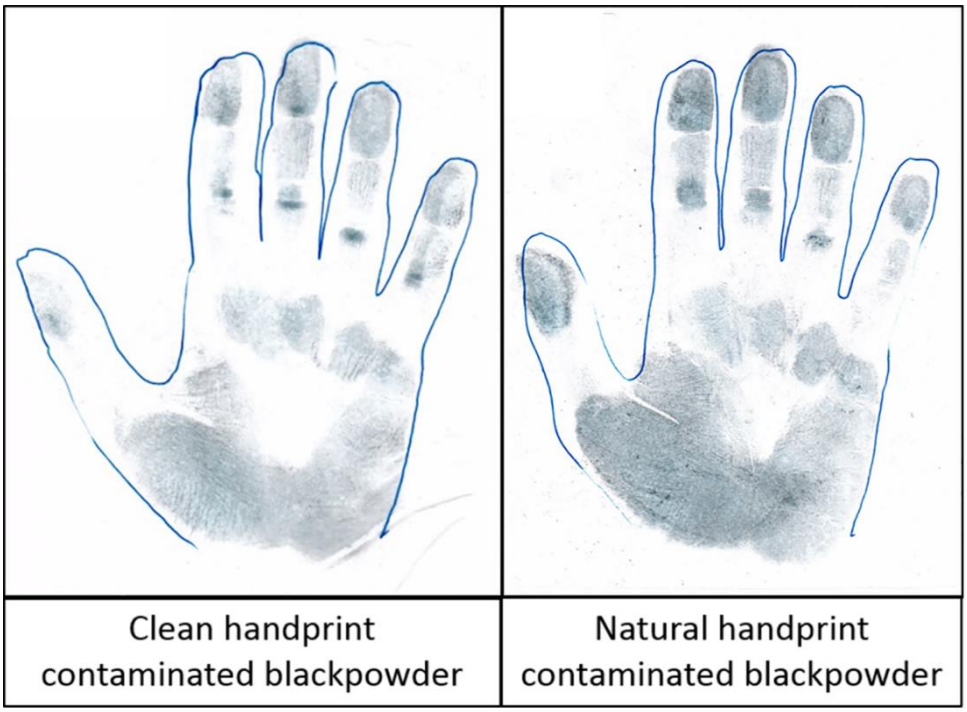

Figure 3.2. Effect of natural contamination on the hands on the amount of explosive residues deposited on handprint. Scanned images of handprints from donor 1 after handling black powder.

To perform the unequivocal identification of each explosive sample and obtain more complete information about the influence of external contamination on the detection of explosive residues, the Raman spectra of blank, clean and natural-contaminated handprints as well as those corresponding to the handling of all explosives were studied. Figure 3.3 shows the spectra obtained for blanks (self-adhesive polyvinyl film of 5 × 10 cm size), clean and natural handprint samples. As can be seen, similar spectra were obtained in all three different samples. Although Raman spectroscopy did not allow the detection of natural residues from dirt or sweat, it did enable the direct detection of explosive residues in handprints with little/no detectable interference.

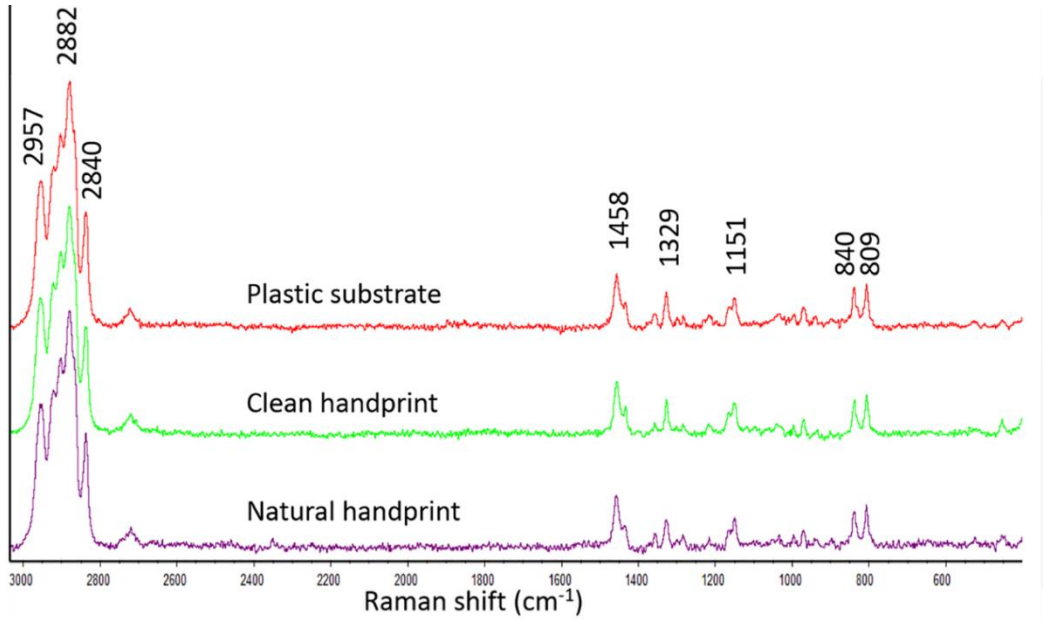

Figure 3.3. Influence of sweat or dirt in the Raman spectra. Spectral comparison (from top to bottom) of the self-adhesive polyvinyl film as blank, a clean handprint and a natural handprint. Raman conditions: laser at 532 nm, 5.0 mW, 10X magnification objective, 25 µm of confocal pinhole aperture, exposure time 2s, 10 acquisitions.

In order to test the efficiency of Raman spectroscopy to detect trace explosive residues on handprints, the handprints deposited on several self-adhesive polyvinyl films of 22 × 38 cm size were collected after the handling of single- and double-base smokeless gun-powder, black powder, dynamite and ammonium nitrate samples by seven different participants. Two handprints (from both hands) were analysed per volunteer. Intense fluorescence signals hiding the characteristic signals of the explosive of interest were observed for both types of smokeless gunpowder and black powder samples (results not shown). Several attempts to reduce this excess of fluorescence were made, such as the reduction of the laser power to 3 mW, the time and number of acquisitions, as well as the exchange of the 532 nm laser for one less powerful of 780 nm, without success. Therefore, smokeless gunpowder samples were excluded from the study by Raman spectroscopy because they presented a very intense fluorescence response to Raman radiation. However, a little sample treatment, as previously mentioned in the method section, was applied to black powder in order to try the identification of any of its components. After complete evaporation, the crystals obtained from the black powder solution were analysed by Raman spectroscopy. Comparing the obtained spectrum with the reference spectra of different inorganic salts (potassium perchlorate, potassium chlorate, sodium chlorate, sodium nitrate, potassium nitrate and ammonium nitrate) commonly

present in pyrotechnic charges, it was possible to identify the presence of potassium perchlorate in its composition (see Figure 3.4). This agrees with the later identification of perchlorate in the extracts from black powder contaminated handprints using IC. In addition, this preliminary study, in which Raman signatures from several salts were compared, seemed to reveal that not only the salts with different anions (nitrate vs chlorate vs perchlorate) could be differentiated by Raman spectroscopy, but also salts based on the same anion and different cation. It is worth comparing, for example, sodium, potassium and ammonium nitrates, whose nitrate bands were not located at the same Raman shift. Bands from sodium nitrate were located at 1383, 1065 and 722 cm^{-1}, whereas bands from potassium nitrate were located at 1357, 1047 and 712 cm^{-1} and bands from ammonium nitrate were located at 1041 and 714 cm^{-1} (see Figure 3.4).

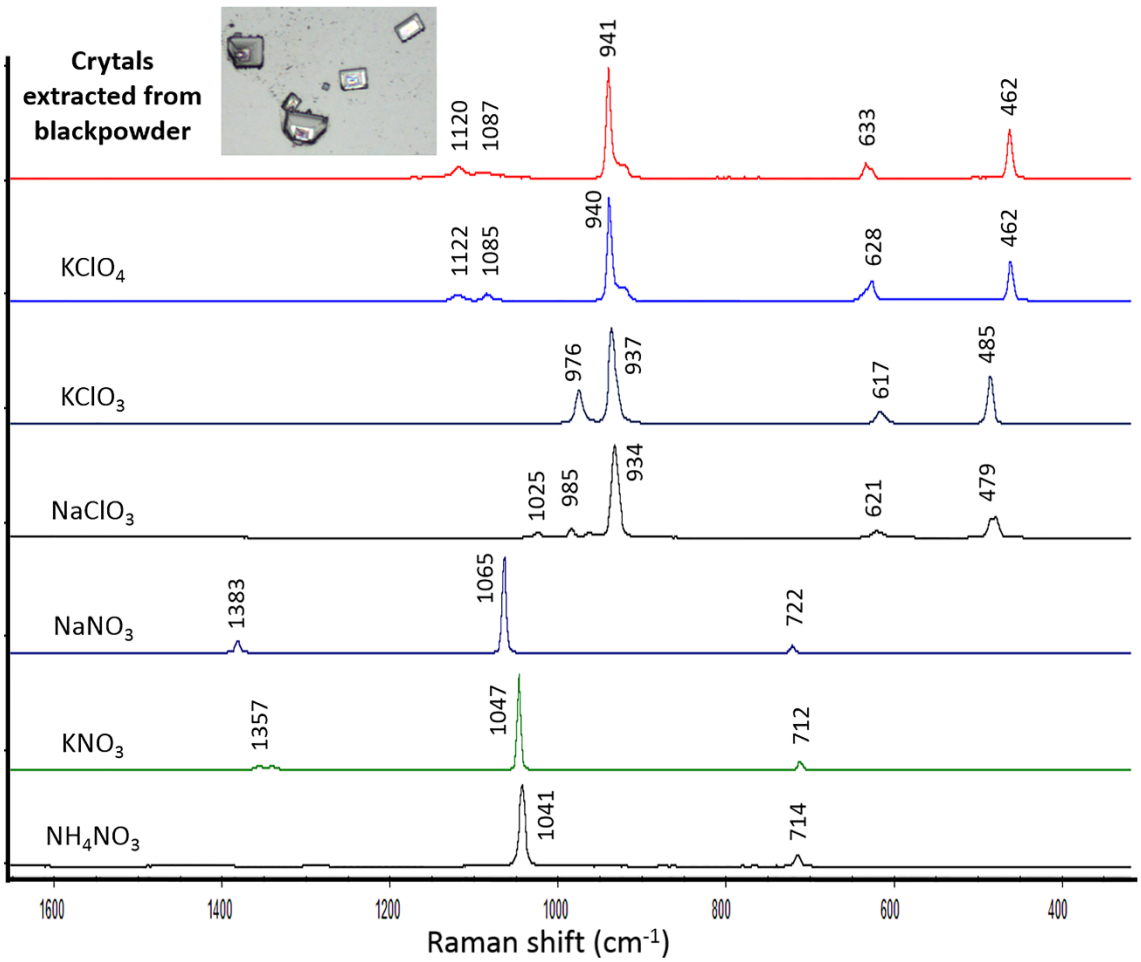

Figure 3.4. Spectrum of black powder extracted from the commercial firecrackers handled in this work (red) compared to other inorganic salts (potassium perchlorate, potassium chlorate, sodium chlorate, sodium nitrate, potassium nitrate and ammonium nitrate) commonly present in commercial firecrackers. Raman conditions as in Figure 3.3.

In fact, by using a Raman spectrometer with an instrumental precision of about ±2 cm^{-1} (the one that our Raman instrument had) even potassium nitrate can be distinguished from ammonium nitrate according to the 6 cm^{-1} shift between their bands at 1047 and 1041 cm^{-1}, respectively. The cation seems to affect the polarizability of the anion and therefore there are slight differences in the Raman shift of the bands of anion depending on the respective cation.

Regarding the handprints contaminated with dynamite and ammonium nitrate, their direct identification was achieved by Raman spectroscopy. Handprint residues were microscopically examined with the aim of searching particles from the explosives, whose Raman spectra allowed their identification by comparison with the Raman spectrum of ammonium nitrate shown in Figure 3.4.

It is interesting to highlight that two types of residues from explosives were detected on handprints using the Raman microscope, including large particles from the explosive which almost overlapped an epidermal ridge, and residues of the explosive quite smaller and contained within the fingerprint ridges. The large particles, which were mainly found in those areas of the hand in which there are deep wrinkles and lines due to muscular and joint contractions, mostly ranged between 10 and 30 μm in size. This fact is probably explained by the largest and deepest surface in those wrinkles in which large particles may be adhered. These particles provided highly intense and well-defined Raman spectra. The largest particles were between 60 and 100 μm. No particles larger than 100 μm were detected, which probably indicates that so big particles are not properly adhered in the skin and fall down immediately. On the other hand, the small particles found within the fingerprint ridges, which are the most abundant residues in latent fingerprints, provided also well-defined but less intense Raman spectra. In fact, these small particles were analysed using 50X or 100X magnification objectives since their size was below 5 μm. As previously reported by Verkouteren [24] for RDX and PETN residues, particles smaller than 10 μm have the highest frequency in fingerprints. Analogously, the largest particles reported by Verkouteren in fingerprints [24] ranged from 50 to100 μm.

Figure 3.5 shows three examples of the spectra obtained for three different particles in both dynamite (a) and ammonium nitrate (b) contaminated

handprints, as well as the spectra registered for the standard sample of dynamite or ammonium nitrate and the self-adhesive polyvinyl film.

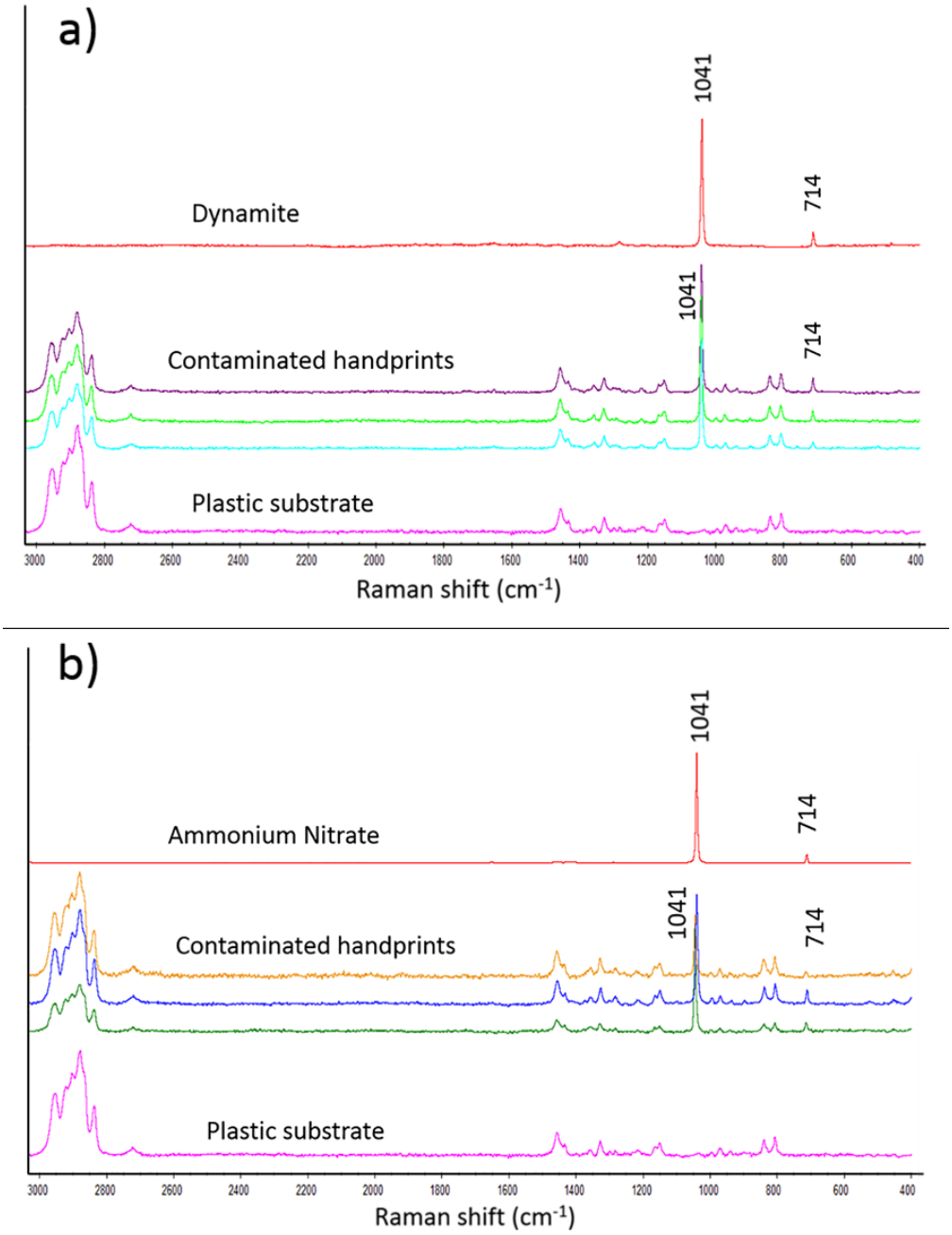

Figure 3.5. Identification of dynamite and ammonium nitrate in handprints. Spectral comparison of (a) standard dynamite, three different handprints (after handling dynamite) and substrate and (b) standard ammonium nitrate, handprints (after handling ammonium nitrate) and substrate. Raman conditions as in Figure 3.3.

Spectra registered for the handprint generated after the handling of dynamite corresponded to ammonium nitrate (bands at 1041 and 714 cm^{-1}) and self-adhesive polyvinyl film (see Figure 3.3: bands at 2957, 2882, 2840, 1458, 1329, 1151, 840, 809 cm^{-1}). In the case of the handprints deposited after handling

ammonium nitrate, these were identical to those registered for the dynamite handprints. This fact was explained through the sample composition, since the main components of dynamite are ammonium nitrate and EGDN. However, EGDN has a high vapour pressure (7.0×10^{-2} Torr at 25°C) and is quickly volatilized at room conditions, used in this research, making its detection difficult after 10 min of dynamite handling and leaving essentially only ammonium nitrate residues on the handprint.

Finally, the mass of the particles detected by Raman microscopy was estimated as follows. Assuming a spherical particle with a diameter of 10 μm, its volume is 523.6 μm^3 (assuming a cubic particle its volume would be 1000 μm^3). In the knowledge that ammonium nitrate has a density of 1.725g/cm^3, the mass of some of the particles analysed by Raman was 0.9 ng (1.7 ng if we assume cubic particles). Moreover, those particles smaller than 5 μm in diameter which were also analysed and identified by Raman weighed less than 0.1 ng.

- Liquid chromatography

Using IC, the analysis of uncontaminated extracts (from "clean" and "natural-contaminated" latent handprints) revealed low μg/mL concentrations of lactate, acetate, formate, chloride nitrite, nitrate and sulphate in agreement with previous work [18]. Oxalate (for n = 2 donors) and thiocyanate (n = 1 donor) were detected at low μg/mL quantities, below the limit of quantitation (LOQ) [19].

The extracts obtained from the latent handprints deposited after handling single- and double-base smokeless gunpowders contained no characteristic anions. There was also no noticeable change in the concentrations of anions present in the control handprints, including nitrite and nitrate.

Using RP-HPLC, the analysis of these extracts showed no traces of nitrocellulose in any of the samples (n = 5). This is not wholly surprising as nitrocellulose, which is the main component in both smokeless gunpowders, is not soluble in water and is therefore itself unlikely to have extracted into solution. DNT, which was supposedly present in the double-base gunpowder, was also not detected. This is likely due to water being an unsuitable extraction solvent for these particular analytes, or perhaps a more sensitive method utilizing mass spectrometry as the detection mode is required.

Regarding the black powder contaminated handprints, the extracts were only analysed by IC due to the inorganic composition of black powder. The extracts

yielded µg/mL concentrations (0–11 µg/mL) of benzoate as well as perchlorate (1–172 µg/mL) as shown in Figure 3.6. These analytes have previously been detected in other black powder substitutes, although nitrate concentrations were not found to similarly increase [18]. As this particular IC method was only applied to determine the anionic components of the handprint extracts, the presence of any counter ions, such as potassium were not confirmed in this case. Concentrations of sulphate, despite the firecracker containing sulphur, did not increase appreciably in any of the seven donors handprint extracts (average increase of 0.15 µg/mL). However, sulphate typically results from oxidation of sulphur and therefore not expected in pre-blast samples.

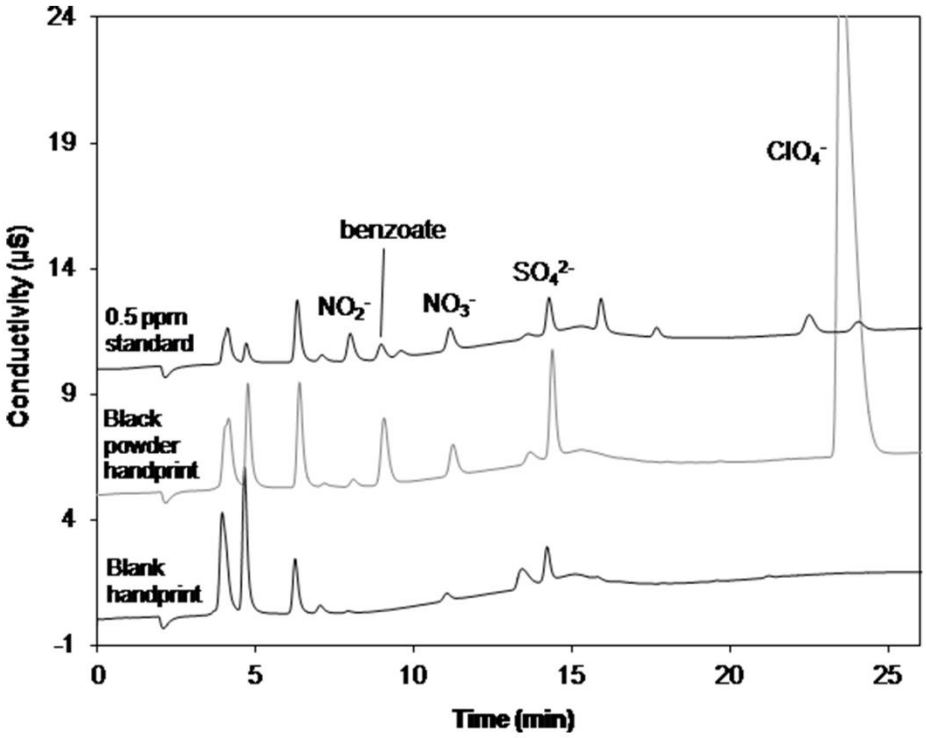

Figure 3.6. Chromatogram showing an uncontaminated handprint; a handprint after the donor had handled black powder; and 0.5 µg/mL anion standard. IC conditions: Injected volume: 40 µL, flow rate 0.30 mL/min, hydroxide gradient: 5 mM from 0 to 3 min; 3–8.5 mM from 3 to 8.5 min; 8.5–21.5 mM from 8.5 to 16min; 21.5–40 mM from 16 to 25.5 min; 40 mM to 28.8 min. Chromatograms offset on signal axis by 5 µS for clarity.

The extracts from the handprints after handling dynamite and ammonium nitrate both showed greatly increased concentrations of nitrate (6–266 µg/mL and 2–479 µg/mL respectively) as shown in Figure 3.7. As the dynamite contained ammonium nitrate, these results were not unexpected. In general, the extracts from the dynamite contaminated handprints contained lower concentrations of nitrate with an average of 95 µg/mL compared to an average

measurement of 213 µg/mL in the extracts from hand-prints after handling the ammonium nitrate sample. There was no noticeable increase in carbonate despite the presence of $CaCO_3$ as a minor component in the dynamite sample, and concentrations of nitrite remained below the method LOQ.

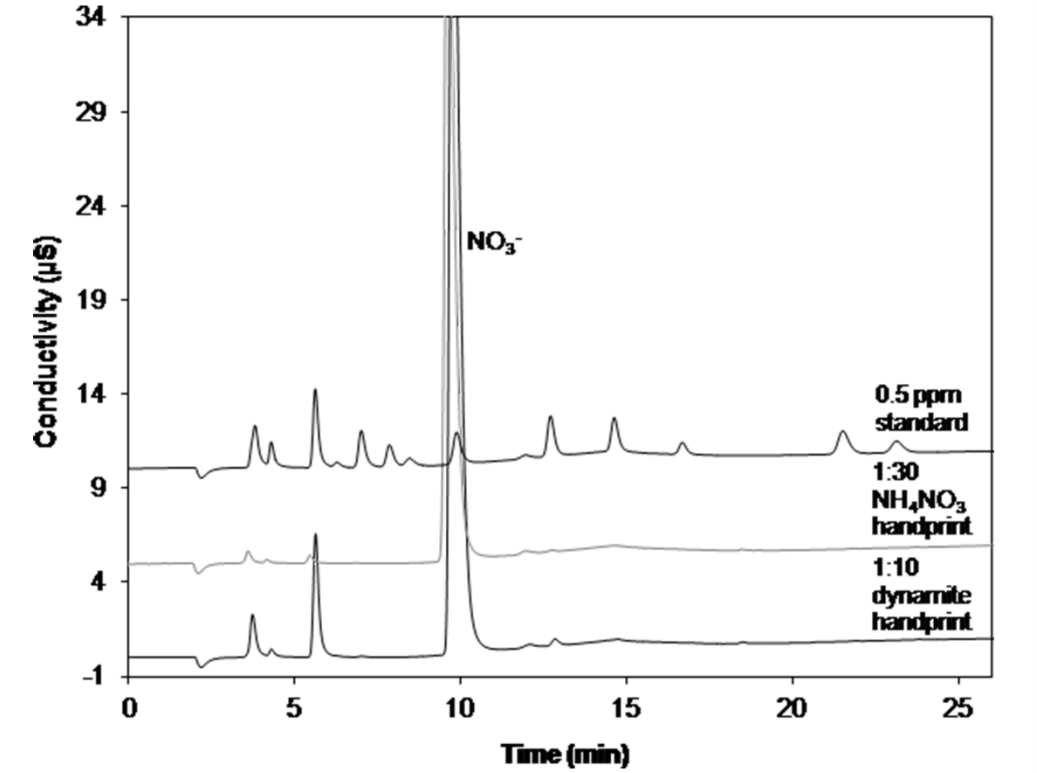

Figure 3.7. Chromatogram showing a 1:10 dilution of a handprint after the donor had handled dynamite; a 1:30 dilution of a handprint after the donor had handled ammonium nitrate; and 0.5 mg/mL anion standard. Chromatographic conditions and chromatograms offset as in Figure 3.6.

The other major component of the dynamite sample was EGDN, which was determined by RP-HPLC. In this case, the chromatograms of the extracts from the handprints left after handling dynamite showed a peak at 4.34 min which matched that of the EGDN standard (4.32 min), as displayed in Figure 3.8. This was surprising as it was expected that EGDN would be mainly lost to the atmosphere, and any remnants would not extract into an aqueous solution. A peak was also present in at 6.42 min, which matched the retention of NG. However, this was also present in the blank handprint, suggesting it to be a component of sweat rather than NG, although this was not identified. In addition, a system peak was present at 5.05 min in all samples.

Results obtained for all three sample types analysed here make it apparent that the transfer between the sample, hand and glass surface is highly variable

between donors, and there was no correlation to suggest certain donors are particularly better or worse at transferring these residues.

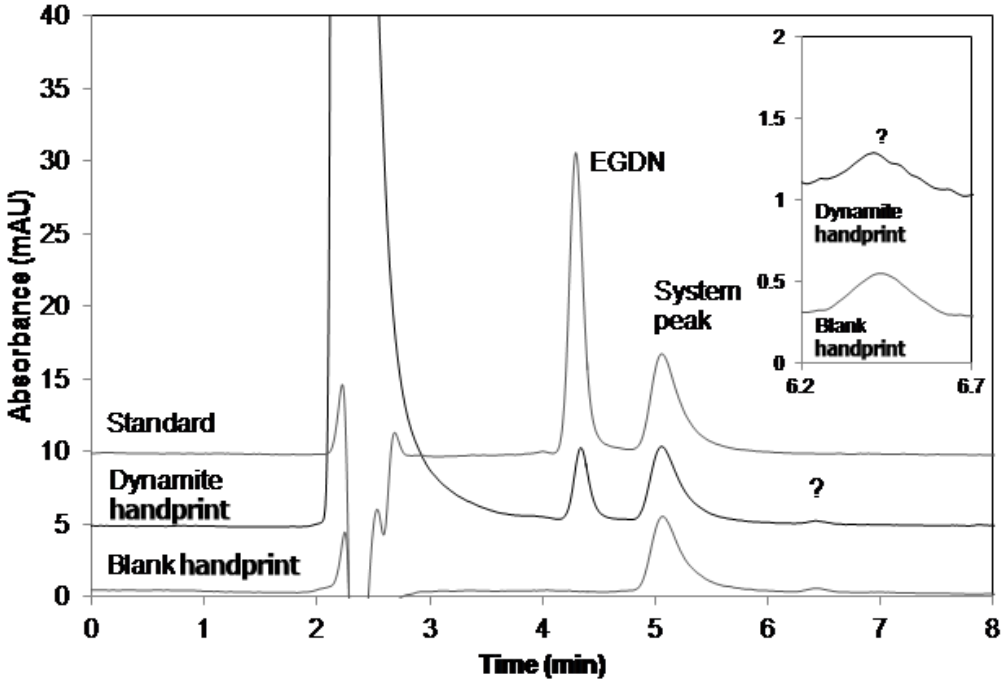

Figure 3.8. Chromatogram showing a blank handprint; a handprint after the donor had handled dynamite; and 5 µg/mL EGDN standard. RP-HPLC conditions: Injected volume: 2 µL, flow rate 0.15 mL/min, isocratic elution with 60:40 (v/v) MeOH/H_2O in 8 mM ammonium acetate. Chromatograms offset on signal axis by 5 mAU for clarity. Insert of the unknown peak at 6.42 min offset by 1mAU.

- Raman spectroscopy and liquid chromatography comparison

A comparative study of the techniques revealed that, using Raman spectroscopy, ammonium nitrate was detected in ammonium nitrate and dynamite contaminated human handprints, while using IC, the nitrate anion was detected in both samples, and EGDN was also detected in dynamite extracts through RP-HPLC. Analogously, black powder was detected through the identification of the perchlorate anion by IC and the potassium perchlorate salt by Raman spectroscopy. Single- and double-smokeless gunpowders were undetected either by liquid chromatography, mainly due to the inefficiency of water extracts to dissolve their non-ionic main components such as nitrocellulose, or by Raman spectroscopy due to their fluorescence. Interestingly, Raman spectroscopy, unlike IC, allowed the identification of the salt (anion+cation). However, liquid chromatography allowed quantitative analysis, being especially useful for trace detection. Regarding the current study, quantitative differences in ammonium nitrate concentrations were found

by IC between ammonium nitrate and dynamite-contaminated handprints. Ammonium nitrate-contaminated handprints had a higher concentration of nitrate than dynamite contaminated handprints. That may be explained according to the dynamite composition, which includes a 60–70% of ammonium nitrate in its composition. Interestingly, by performing the designed procedure to prepare the samples for liquid chromatography analysis, the residues from the entire handprint were collected and determined. On the contrary, the Raman signal was due to the solid particles of residues located within the laser spot. Therefore, only a small part of the residues in the handprint was examined, being enough to identify the compound, and providing the interesting potential to visualise the exact location of residues located in a whole handprint. Given its non-destructive nature, Raman could be previously used for rapid identification of explosives followed by liquid chromatography (either IC or RP-HPLC) for cross-validation or quantitative purposes.

Conclusions and future trends

In conclusion, Raman spectroscopy and liquid chromatography (IC and RP-HPLC) have turned out to be suitable complementary techniques. In fact, in this case Raman spectroscopy has supported the identification of compounds since it was able to identify the salt (anion-cation), whereas IC has supported the quantification of the salt based on the ion concentration. Therefore, both techniques are appropriate to determine the ionic species from explosive residues on handprints and fingerprints. In addition, RP-HPLC enabled the determination of EGDN in extracts from dynamite. As consequence of the different information provided by both techniques, we propose residues should be first identified by Raman spectroscopy (since Raman spectroscopy is more rapid in comparison to liquid chromatography) and, then, quantified by liquid chromatography, in the appropriate mode.

As future trend, it is important to mention that Raman spectroscopy seems to allow the discrimination between salts even when they are composed by the same anion due to the effect of the counter cation. Thus, further studies are being performed considering a wider number of salts in order to confirm this capability of Raman spectroscopy and research this phenomenon more

thoroughly (*i.e.* how the cation shifts the anion band, the influence of charge and size of the cation, etc.).

Despite not having been examined in this chapter, it should be noted that Raman spectroscopy might be also used for quantitative determination of the major anions in solution. To deepen on this, the reader is referred to the reference [37], in which the nitrate anion is quantitatively determined even in the presence of other anions.

References

[1] P.R. Laska, Bombs, IEDs, and Explosives: Identification, investigation, and Disposal Techniques, CRC Press Taylor & Francis Group, Boca Raton, USA, 2016.

[2] J. Yinon, Counterterrorist Detection Techniques of Explosives, Elsevier, Netherlands, 2007.

[3] M. Marshall, J. Oxley, Aspects of Explosives Detection, Elsevier, Netherlands, 2009.

[4] R.S. Golightly, W.E. Doering, M.J. Natan, Surface-enhanced Raman spectroscopy and homeland security: a perfect match? ACS Nano 3 (2009) 2859-2869.

[5] A. Hakonen, P.O. Andersson, M.S. Schmidt, T. Rindzevicius, M. Käll, Explosive and chemical threat detection by surface-enhanced Raman scattering: a review, Anal. Chim. Acta 893 (2015) 1-13.

[6] A. Hakonen, T. Rindzevicius, M.S. Schmidt, P.O. Andersson, L. Juhlin, M. Svedendahl, A. Boisen, M. Käll, Detection of nerve gases using surface-enhanced Raman scattering substrates with high droplet adhesion, Nanoscale 8 (2016) 1305-1308.

[7] M.A. Fernández de la Ossa, J.M. Amigo, C. García-Ruiz, Detection of residues from explosive manipulation by near infrared hyperspectral imaging: a promising forensic tool, Forensic Sci. Int. 242 (2014) 228-235.

[8] N. Nuntawong, P. Eiamchai, S. Limwichean, B. Wong-ek, M. Horprathum, V. Patthanasettakul, A. Leelapojanapom, S. Nakngoenthong, P. Chindaudom, Trace detection of perchlorate inindustrial-grade emulsion explosive with portable surface-enhanced Raman spectroscopy, Forensic Sci. Int. 233 (2013) 174-178.

[9] C. Martín-Alberca, C. García-Ruiz, Analytical techniques for the analysis of consumer fireworks, Trends Anal. Chem. 56 (2014) 27-36.

[10] C. Johns, R.A. Shellie, O.G. Potter, J.W. O'Reilly, J.P. Hutchinson, R.M. Guijt, M.C. Breadmore, E.F. Hilder, G.W. Dicinoski, P.R. Haddad, Identification of homemade inorganic explosives by ion chromatographic analysis of post-blast residues, J. Chromatogr. A 1182 (2008) 205-214.

[11] E. Tyrrell, E.F. Hilder, R.A. Shalliker, G.W. Dicinoski, R.A. Shellie, M.C. Breadmore, C.A. Pohl, P.R. Haddad, Packing procedures for high efficiency, short ion-exchange columns for rapid separation of inorganic anions, J. Chromatogr. A 1208 (2008) 95-100.

[12] H. Meng, T. Wang, B. Guo, Y. Hashi, C. Guo, J. Lin, Simultaneous determination of inorganic anions and cations in explosive residues by ion chromatography, Talanta 76 (2008) 241-245.

[13] E. Tyrrell, R.A. Shellie, E.F. Hilder, C.A. Pohl, P.R. Haddad, Fast ion chromatography using short anion exchange columns, J. Chromatogr. A 1216 (2009) 8512-8517.

[14] G.L. Lang, K.M. Boyle, The analysis of black powder substitutes containing ascorbic acid by Ion Chromatography/Mass spectrometry, J. Forensic Sci. 54 (2009) 1315-1322.

[15] L. Barron, E. Gilchrist, Ion chromatography-mass spectrometry: a review of recent technologies and application in forensic and environmental explosives analysis, Anal. Chim. Acta 806 (2014) 27-54.

[16] D. Gaurav, A.K. Malik, P.K. Rai, High-performance liquid chromatographic methods for the analysis of explosives, Crit. Rev. Anal. Chem. 37 (4) (2007) 227-268.

[17] B. Paull, C. Roux, M. Dawson, P. Doble, Rapid screening of selected organic explosives by high performance liquid chromatography using reversed-phase monolithic columns, J. Forensic Sci. 49 (6) (2004) 1181-1186.

[18] E. Gilchrist, N. Smith, L. Barron, Probing gunshot residue, sweat and latent human fingerprints with capillary-scale ion chromatography and suppressed conductivity detection, Analyst 137 (2012) 1576-1583.

[19] C. Love, E. Gilchrist, N. Smith, L. Barron, Detection of anionic energetic material residues in enhanced fingermarks on porous and non-porous surfaces using ion chromatography, Forensic Sci. Int. 231 (2013) 150-156.

[20] P. Hazarika, D.A. Russell, Advances in fingerprint analysis, Angew. Chem. Int. 51 (2012) 3524-3531.

[21] F. Rowell, J. Seviour, A.Y. Lim, C.G. Elumbaring-Salazar, J. Loke, J. Ma, Detection of nitro-organic and peroxide explosives in latent fingermarks by DART-and SALDI-TOF-mass spectrometry, Forensic Sci. Int. 221 (2012) 84-91.

[22] P.H. Ng, S. Walker, M. Tahtouh, B. Reedy, Detection of illicit substances in fingerprints by infrared spectral imaging, Anal. Bioanal. Chem. 394 (2009) 2039-2048.

[23] E.V. Bertseva, A.V. Savin, Explosives trace detection in the process of biometrical fingerprint identification for access control, Proc. SPIE 6594 (2007) 65940F/1-65940F/10.

[24] J.R. Verkouteren, Particle characteristics of trace high explosives: RDX and PETN, J. Forensic Sci. 52 (2007) 335-340.

[25] T. Chen, Z.D. Schultz, I.W. Levin, Infrared spectroscopic imaging of latent fingerprints and associated forensic evidence, Analyst 134 (2009) 1902-1904.

[26] R. Bhargava, R.S. Perlman, D.C. Fernandez, I.W. Levin, E.G. Bartick, Non-invasive detection of superimposed latent fingerprints and inter-ridge trace evidence by infrared spectroscopic imaging, Anal. Bioanal. Chem. 394 (2009) 2069-2075.

[27] Y. Mou, J.W. Rabalais, Detection and identification of explosive particles in fingerprints using Attenuated Total Reflection-Fourier Transform Infrared Spectromicroscopy, J. Forensic Sci. 54 (2009) 846-850.

[28] A. Banas, K. Banas, M.B.H. Breese, J. Loke, B. Heng Teo, S.K. Lim, Detection of microscopic particles present as contaminants in latent fingerprints by means of synchrotron radiation-based Fourier transform infrared micro-imaging, Analyst 137 (2012) 3459-3465.

[29] A. Banas, K. Banas, M.B.H. Breese, J. Loke, S.K. Lim, Spectroscopic detection of exogenous materials in latent fingerprints treated with powders and lifted off with adhesive tapes, Anal. Bioanal. Chem. 406 (2014) 4173-4181.

[30] M.A. Fernández de la Ossa, C. García-Ruiz, J.M. Amigo, Near infrared spectral imaging for the analysis of dynamite residues on human handprints, Talanta 130 (2014) 315-321.

[31] E.D. Emmons, A. Tripathi, J.A. Guicheteau, S.D. Christesen, A.W. Fountain, Raman chemical imaging of explosive-contaminated fingerprints, Appl. Spectrosc. 63 (2009) 1197-1203.

[32] A. Tripathi, E.D. Emmons, J.A. Guicheteau, S.D. Christesen, P.G. Wilcox, D.K. Emge, A.W. Fountain, Trace explosive detection in fingerprints with Raman chemical imaging, Proc. SPIE 7665 (2010) 76650N-1-76650N-6.

[33] A. Tripathi, E.D. Emmons, P.G. Wilcox, J.A. Guicheteau, D.K. Emge,S.D. Christesen, A.W. Fountain, Semi-automated detection of trace explosives in fingerprints on strongly interfering surfaces with Raman chemical imaging, Appl. Spectrosc. 65 (2011) 611-619.

[34] I. Malka, A. Petrushansky, S. Rosenwaks, I. Bar, Detection of explosives and latent fingerprint residues utilizing laser pointer-based Raman spectroscopy, Appl. Phys. B 113 (2013) 511-518.

[35] Determinación de nitrógeno nítrico y NO3, in: Laboratorio Químico Central DE Armamento, ENAC. Retrieved from ⟨http://www.enac.es/web/enac/acreditados⟩.

[36] M. López-López, J.L. Ferrando, C. García-Ruiz, Dynamite analysis by Raman spectroscopy as a unique analytical tool, Anal. Chem. 85 (2013) 2595-2600.

[37] F. Zapata, F. Ortega-Ojeda, C. García-Ruiz, M. González-Herráez, Selective monitoring of oxyanion mixtures by a flow system with Raman detection, Sensors 18 (2018) 2196.

Section 2. Spectroscopic Approaches for the Identification of Explosive Residues

To victims of terrorism

Al Cairo non lo sanno che ore sono adesso
Il sole sulla Rambla oggi non è lo stesso
In Francia c'è un concerto, la gente si diverte
Qualcuno canta forte, qualcuno grida, "a morte"

A Londra piove sempre ma oggi non fa male
Il cielo non fa sconti neanche a un funerale
A Nizza il mare è rosso di fuochi e di vergogna
Di gente sull'asfalto e sangue nella fogna

E questo corpo enorme che noi chiamiamo Terra
Ferito nei suoi organi dall'Asia all'Inghilterra
Galassie di persone disperse nello spazio
Ma quello più importante è lo spazio di un abbraccio

Di madri senza figli, di figli senza padri
Di volti illuminati come muri senza quadri
Minuti di silenzio spezzati da una voce
Non mi avete fatto niente

Non mi avete fatto niente
Non mi avete tolto niente
Questa è la mia vita che va avanti
Oltre tutto, oltre la gente
Non mi avete fatto niente
Non avete avuto niente
Perché tutto va oltre le vostre inutili guerre

C'è chi si fa la croce, chi prega sui tappeti
Le chiese e le moschee, gli imam e tutti i preti
Ingressi separati della stessa casa
Miliardi di persone che sperano in qualcosa

Braccia senza mani, facce senza nomi
Scambiamoci la pelle, in fondo siamo umani
Perché la nostra vita non è un punto di vista
E non esiste bomba pacifista

Non mi avete fatto niente
Non mi avete tolto niente
Questa è la mia vita che va avanti
Oltre tutto, oltre la gente
Non mi avete fatto niente
Non avete avuto niente
Perché tutto va oltre le vostre inutili guerre

Cadranno i grattacieli, le metropolitane
I muri di contrasto alzati per il pane
Ma contro ogni terrore che ostacola il cammino
Il mondo si rialza col sorriso di un bambino
Col sorriso di un bambino
Col sorriso di un bambino

Non mi avete fatto niente
Non avete avuto niente
Perché tutto va oltre le vostre inutili guerre
Non mi avete fatto niente
Le vostre inutili guerre
Non avete avuto niente
Le vostre inutili guerre

Sono consapevole che tutto più non torna
La felicità volava
Come vola via una bolla

Authors: Andrea Febo / Ermal Meta / Fabrizio Mobrici.
Singers: Ermal Meta / Fabrizio Moro. Winners of Sanremo Music Festival 2018. Eurovision Italy 2018.
Warner/Chappell Music, Inc

Chapter 4. The Chemistry of Explosives

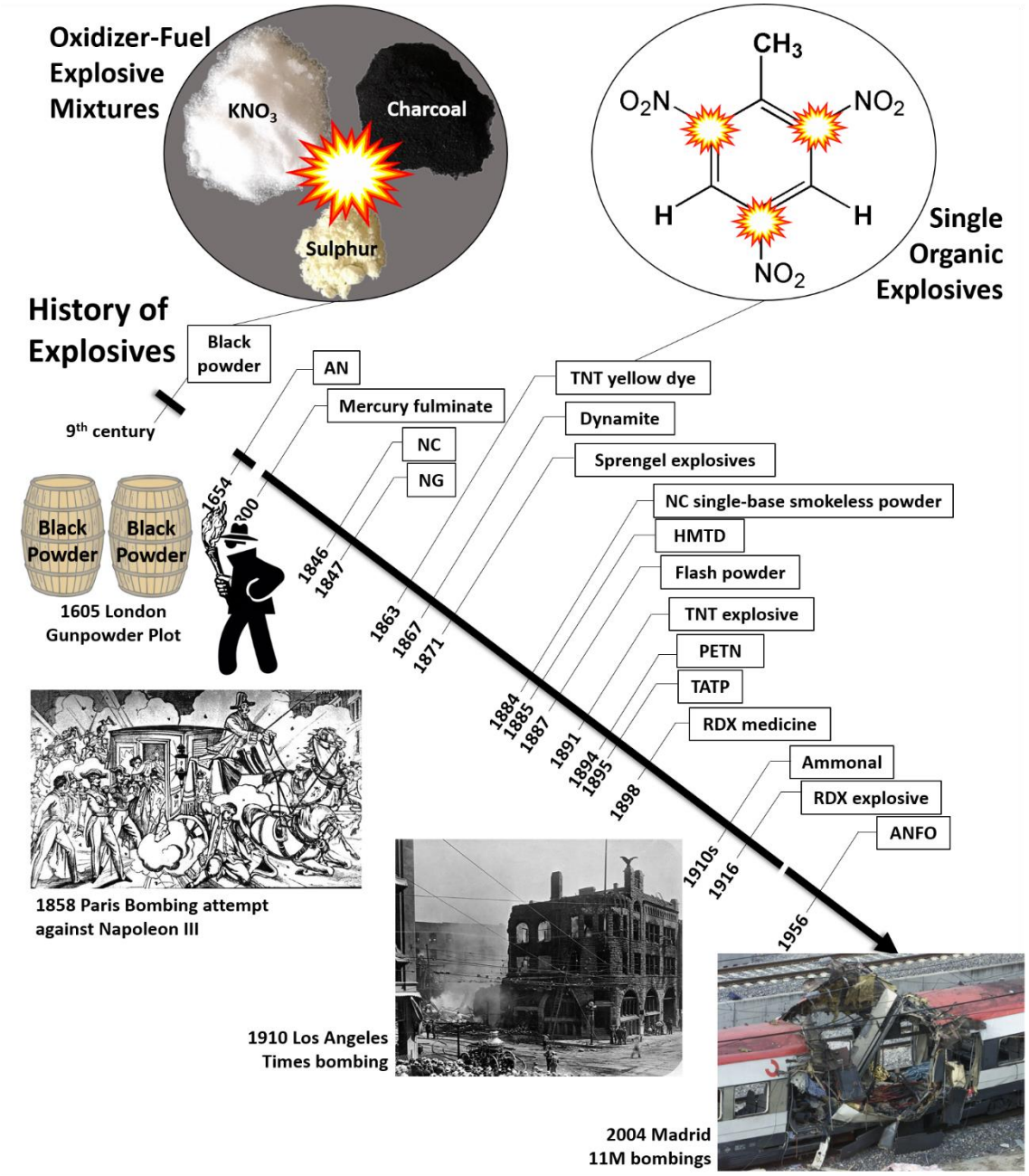

Main sources:

Pending of publication

Abstract

What is an explosive? Are there different types of explosive substances? Why society is concerned about explosives? How long has society been concerned about explosives? This chapter responds to all these questions by explaining and discussing relevant topics within the explosives field such as 1) fundamental concepts about explosives; 2) the historical evolution of explosives; 3) classification of explosives according to either their energy, their use or their chemical composition; and 4) the terrorist use of explosives.

Fundamental concepts about Explosives

An explosive may be simply defined as a substance which is capable of producing an explosion, which means that is capable of producing a large volume of expanding gas in an extremely brief period" [1-4]. Certainly, every explosive may produce an explosion. However, no every material that is capable of producing an explosion is necessarily an explosive. A steam boiler filled with water (put on to the heat) may explode because of the increasing pressure of water vapour generated inside. However, water is not an explosive and no chemical explosion has occurred, but a physical explosion known as BLEVE (acronym of Boiling Liquid Expanding Vapour Explosion) [1, 2]. In such cases, a continuous and external heat flow has been provided, which has slowly increased the inner pressure until the explosion has occurred. Thus, an explosive might be more properly defined as a substance which is capable of producing an explosion by its own chemical energy [1-4].

When talking about explosives and explosions, the term explosion usually refers to chemical detonations, *i.e.* explosions produced as a consequence of a chemical reaction in which the chemical energy of a substance, or mixture of substances, is rapidly released causing a sudden expansive shock wave. The velocity at which the shock wave front travels through the detonating explosive is called velocity of detonation [1-11]. When the velocity of detonation is faster than the speed of sound, a detonation occurs regardless of whether the explosive is confined or not. On the contrary, a deflagration occurs when the velocity of detonation is lower than the speed of sound, being necessary the confinement of the explosive to ultimately produce an explosion [1-11].

Despite the large number of ultra-fast chemical reactions that may ultimately cause an explosion, most of them can be classified in two main groups: unimolecular decomposition reactions and multi-molecular redox (reduction-oxidation) reactions [11-15]. As main requirement, the reaction has to proceed fast enough to produce an expansive shock wave, either because the velocity of reaction is supersonic, or because the generation/accumulation of gas products from a subsonic deflagration is faster than their release when inside a container [1-11].

In this respect, an explosive can be either a pure single substance or a mixture of substances depending on the type of chemical reaction that produces the

explosion [1-13]. A single compound is required for unimolecular decomposition reactions, while two compounds (at least) are required for multi-molecular redox reactions. For instance, the former case is exemplified, below, by RDX decomposition [14] while the latter is explained through the redox reaction of black powder [9]. Although the precise chemical reactions occurring during detonations are notably complex (as subsequently explained in Chapter 6.1), simplified equations are provided below to show chemical transformations of these explosives.

$$C_3H_6N_6O_6(s) \rightarrow 3\,N_2(g) + 3\,H_2O\,(g) + 3\,CO\,(g)$$

$$10\,KNO_3(s) + 8\,C(s) + 3\,S(s) \rightarrow 2\,K_2CO_3(s) + 3\,K_2SO_4(s) + 5\,N_2(g) + 6\,CO_2(g)$$

As observed in both reactions, a solid compound (or mixture of solid compounds) transforms into a large number of gaseous moles (9 moles in the case of RDX; 11 moles in the case of black powder).

In the previous examples, two solid explosives are considered. In fact, the term "explosives" is generally associated to solid explosives, due to the longer history wider applicability, easier handling, larger number and greater awareness of solid explosives over liquid/gas explosives.

In this respect, regarding those explosives whose detonation is based on unimolecular decomposition reactions, they necessarily have to be molecules big enough to decompose into smaller molecules. In this respect, nitromethane, (which has 61 u of molecular weight), is one of the smallest molecules that may suffer an explosive decomposition; and nitromethane is liquid (at atmospheric pressure). Thus, the state of the matter (at atmospheric pressure) of any other explosive molecule that is bigger than nitromethane will be still liquid (like nitro-ethane or nitroglycerine (NG)) or solid (most explosives like TNT, RDX, PETN, TATP, HMTD, etc.) [1-11].

On the contrary, for those explosive mixtures, whose detonation is caused by the redox reaction between an oxidizer and a fuel, there exists a wider variety of oxidizer-fuel combinations, in different states of matter each [2-9]. Most of these explosives are also solid due to the most common oxidizers, which are solid inorganic oxidizing salts (mainly nitrates, chlorates and perchlorates):

- Solid oxidizing salt – Solid fuel. Those explosive mixtures in which both oxidizer and fuel are solid substances (such as black powder).

- Solid oxidizing salt – Liquid fuel. Those explosives in which a solid oxidizing salt is mixed with a liquid fuel (such as ANFO).

However, liquid/gas oxidizing agents (such as nitric acid or oxygen) are also used to produce explosives [4-6].

- Nitric acid – Solid/liquid fuel. Those explosives in which nitric acid is mixed with a solid/liquid fuel (such as nitric acid-nitrobenzene).
- Oxygen Gas – Solid fuel. Those explosive mixtures in which oxygen is mixed with a solid fuel dispersed into a dust cloud (such as flour dust suspended in the air). Such explosions are known as dust explosions.
- Oxygen Gas – Liquid fuel. Those explosive mixtures in which oxygen is mixed with a liquid fuel (such as hydrazine-oxygen mixture).
- Oxygen Gas – Gas fuel. Those explosive mixtures in which both oxidizer and fuel are gas substances (such as hydrogen-oxygen mixture).

Due to the complicate manipulation of gas substances, their use in the manufacture of explosives is unusual. In addition, those explosions caused by oxygen-fuel mixtures are typically unexpected or negligent accidents rather than malicious bombings [9]. In fact, they are usually produced because of an uncontrolled combustion. The term “combustion” typically refers to the oxidation of a combustible substance with the oxygen present in air by means of a flame [11-15]. Nevertheless, depending on the velocity of detonation and confinement, the transition from deflagration (flame) to detonation (explosion) may occur [14]. For instance, a butane gas cylinder maliciously prepared to explode can provoke an explosion, which is chemically based on a rapid combustion of butane.

Nevertheless, the single components are not explosives on their own, but only the mixture is properly classified as an explosive. Neither potassium nitrate, sulphur, butane nor hydrogen are explosives alone. The explosives are black powder, the butane-oxygen mixture or the hydrogen-oxygen mixture. In this respect, although oxygen from air is an always present compound, the chemical reaction that provokes an explosion is so fast that surrounding air has no time to reach and participate in the reaction [8]. Thus, a butane gas cylinder is not an explosive but a fuel. Therefore, explosives are those substances whose detonation do not require the presence of air to explode.

It should be remarked that hydrogen needs oxygen to produce a chemical explosion. Thus, single hydrogen is not a chemical explosive. However, it is a nuclear explosive. Thankfully, hydrogen produces the nuclear explosions occurring in the Sun, which provide enough energy to enable the life on Earth. Unlike chemical reactions, in which the transformation of reagents into different products does not modify the number of atoms of each element (principle of mass conservation), nuclear reactions involve the transmutation of elements. Thereby, nuclear fusion involves the transmutation of atoms of hydrogen into atoms of helium, as displayed in the following general nuclear reaction occurring in the Sun, by which four atoms of hydrogen 1 are fused into one atom of helium and two beta particles [16, 17].

$$4\ {}_{1}^{1}H \rightarrow {}_{2}^{4}He + 2\ {}_{1}^{0}\beta$$

Humans have copied this natural process with two completely opposite purposes: i) as an inexhaustible source of energy with which accelerating the sustainable progress and development of humanity; and ii) the evil destructive purpose of fabricating nuclear bombs. In this respect, the simplest way of nuclear fusion involves the fusion of deuterium and tritium into one atom of helium and one neutron [16].

$${}_{1}^{2}H + {}_{1}^{3}H \rightarrow {}_{2}^{4}He + {}_{0}^{1}n$$

Similarly, nuclear weapons composed of radioactive elements, whose nuclear fission may produce a nuclear explosion (like uranium-235), are not based in chemical reactions, but in consecutive nuclear transmutations of the chemical elements until reaching a stable element. Thus, they are not considered chemical explosives, but nuclear bombs [16].

$${}_{92}^{235}U \rightarrow {}_{90}^{231}Th \rightarrow \cdots \rightarrow {}_{82}^{207}Pb$$

The use of radioactive elements is not exclusive of nuclear bombs. Radioactive elements are sometimes added to chemical explosives to create radiological weapons or “dirty bombs” [17, 18]. Contrarily to nuclear bombs, “dirty bombs” do not have enough initial energy to produce the transmutation of elements as in nuclear fusion/fission. Therefore, the destructive power of “dirty bombs” is provided by the chemical explosive. However, the evil dirty purpose of “dirty bombs” is the spreading of radiological material over an area with the aim of contaminating that area with a harmful material that generates panic in the

population. Therefore, the radiological material is not an explosive, but a harmful extra added to the explosive.

Historical evolution of explosives

Nowadays, a large variety of chemical explosives exists. In fact, many explosives are freely available. However, the situation was completely different few centuries ago. In this respect, the main milestones achieved in the discovery and development of explosives are summarized below. Particularly, the summary focuses on the explosives subsequently analysed in this thesis:

- **Before the 19th century** – A thousand years of **black powder**

As everyone knows, black powder was the first explosive that was discovered. According to the legends, Chinese alchemists accidentally invented black powder when making experiments with the aim of creating gold and, ultimately, the elixir of life. It should be reminded that the elixir of life was thought to be capable of transforming any substance into gold and prolonging life eternally. The origins of black powder date back, at least, to the 9th century, when black powder was already used in the manufacture of Chinese firecrackers [2, 4, 8]. From then on, the knowledge about the existence and use of black powder spread throughout Asia and Europe and different compositions were tested with the main aim of increasing the explosive power of the mixture. This is evidenced by some texts written by Roger Bacon (1214-1292), in which black powder was defined as a mixture of saltpetre, sulphur and charcoal; capable of producing an explosion when inside into a firecracker [1, 2, 4]. Thus, black powder arrived to England before 13th century. From 13th century to 19th century, black powder was not only used in firecrackers but also as gunpowder propellant in canons and firearms worldwide. The classical battles previously based on swords, arrows and lances updated to canons and firearms; and piracy exponentially increased due to the capability of canons of sinking boats from distance. The industry of black powder became one of the most important and powerful resources of every kingdom since no other explosive would be discovered until the 19th century. Consequently, any terrorist bombing perpetrated before 19th century was necessarily committed using black powder, as the *Gunpowder plot* occurred in England in 1605, in which there was an attempt of bombing against

the House of Lords [19, 20]; or the *Plot of the rue Saint-Nicaise* perpetrated in Paris in 1800 with the aim of assassinating Napoleon Bonaparte [21]. After 19th century, black powder was no longer used in firearms and military armament because of the development of safer, cleaner and higher energy explosives. On the contrary, black powder continued being widely used in pyrotechnics [22-25], where its properties as low energy propellant are highly suitable. Regarding current terrorist bombings, though black powder is not usually employed due to its low destruction power, some exceptions have occurred such as the 2013 Boston marathon bombing [8]. In addition, black powder from pyrotechnics is commonly used in urban warfare environments against police. As previously indicated, black powder is an explosive mixture based on potassium nitrate, charcoal and sulphur, whose composition usually ranges around 75% potassium nitrate, 15% charcoal and 10% sulphur [1-8].

- **1800** – **Mercury fulminate**: A primary explosive detonator

Mercury fulminate was first synthesized in 1800 by Edward Charles Howard (1774-1816) [26]. By mixing mercury with nitric acid and ethanol, a white powder with saline taste and explosive properties precipitated. Different stimuli including temperature, electrical shock, sulphuric acid media and physical impact were examined after checking the extreme sensitivity of mercury fulminate to detonate. In addition, E. C. Howard also tested how mercury fulminate worked in firearms, first, in substitution of black powder, and then, as detonator of black powder [26]. After demonstrating its suitability to initiate propellants, mercury fulminate and similar primary inorganic explosives were used as detonators in firearms [27]. Mercury fulminate, $Hg(CNO)_2$, is an inorganic explosive, whose detonation is caused by an unimolecular decomposition:

$$Hg(CNO)_2(s) \rightarrow Hg(s) + N_2(g) + 2\,CO\,(g)$$

- **1846** – **Nitrocellulose** or "gun-cotton": from the cotton apron that rapidly burned to smokeless powders

The discovery of nitrocellulose (NC) in 1846 is the typical example of serendipity. Christian Friedrich Schönbein (1799-1868) was working with nitric and sulphuric acids when he spilled the mixture of acids on the table. He took

immediately a cotton apron to clean the table, and left the apron to dry near the oven. After a while, the apron spontaneously ignited [28]. Schönbein had fortuitously prepared nitrocellulose by the nitration of cotton (>90% cellulose) when mixed with nitric-sulphuric acids. Some years before, Henri Braconnot (1833), Théophile-Jules Pelouze (1838) and Jean-Baptiste Dumas (1843) had discovered that either starch, wood, or paper were transformed by nitric acid into an unstable explosive material, which they named xyloidine/nitramidine [29-31]. However, this unstable NC was low and heterogeneously nitrated because of the low yield of the nitration reaction using nitric acid alone [10]. The stroke of luck of Schönbein was the use of sulphuric acid in combination with nitric acid since we now know that sulphuric acid is a catalyst of the nitration reaction [6]. Thereby, Schönbein created a more stable highly nitrated NC. It should be noted that although Schönbein's fortuitous discovery of NC is the most famous, Rudolf Christian Böttger had also independently discovered, in the same year, the transformation of cellulose into NC using a mixture of nitric-sulphuric acids [1-4]. Despite NC synthesized this way being more stable, the industrial manufacture of NC was not safe until 1865 when Frederick Augustus Abel (1827-1902) patented an improved a safer process for NC manufacture [2]. The applications of single pure highly nitrated NC were limited to powerful military weapons due to the high explosive power of NC. In addition, lower energy more practical explosives based on NC were developed during the following decades by lowering the nitration of NC and/or mixing NC with other components. For instance, Alfred Nobel patented different NC-based explosive compositions such as gelignite (1875) and ballistite (1887) by applying a similar approach to that previously invented for dynamite (as explained below) [1-4]. In addition, Paul Marie Eugène Vieille (1854-1934) invented in 1884 the first NC-based smokeless powder for firearms, which rapidly replaced black powder in firearms because of their advantageous properties [8]. NC-based smokeless powder was more powerful than black powder and left no solid residues and no smoke during its combustion [20]. After the invention of single NC-based smokeless powders, double- and triple-base smokeless powders were developed by mixing NC with other explosive compounds, such as nitroglycerine and nitroguanidine [1-4]. Due to the specific applications of NC as component of either smokeless powders or dynamites, pure single NC is never used in terrorist bombings. Nevertheless, NC is present in every terrorist bombing using

dynamite and every terrorist attack involving shootings and firearms since ammunition is propelled by smokeless powders.

From the chemical point o view, nitrocellulose is a nitrate ester organic explosive, which results from the replacement of hydroxyl groups by nitro groups in cellulose. Depending on the number of replaced hydroxyl groups, low or high nitrated NC is obtained. As an example, Figure 4.1 displays NC with the maximum nitrogen content (14%), where nitro groups have replaced all hydroxyl groups [4, 10].

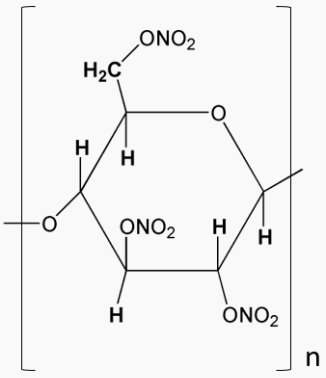

Figure 4.1. Chemical structure of nitrocellulose monomer.

- **1847** – **Nitroglycerine**: the liquid explosive that spontaneously explodes

Ascanio Sobrero (1812-1888) discovered nitroglycerine (NG) in 1847 [32]. In the knowledge of the studies from T. J. Pelouze (his teacher) about cellulose transformation by nitric acid, Ascanio Sobrero tested nitric acid with different organic compounds, including glycerine [32]. Thereby, he obtained nitroglycerine, an extremely sensitive liquid explosive capable of detonating with the least stimulus. Like NC, nitroglycerine is a nitrate ester explosive, which results from the replacement of hydroxyl groups by nitro groups in glycerol molecule. Sobrero was concerned about the danger of NG and the impossibility to handle it safely. He was convinced that no safe application could be developed for NG due to its sensitivity [2, 8, 32]. Regarding terrorism, NG has been used to perpetrate terrorist bombings in combination with other explosives such as the 1993 World Trade Center bombing (a mixture of NG and urea nitrate) [4, 7].

- **1867** – **Dynamite**: the "safe" Nobel's invention

Ascanio Sobrero was wrong in his assumption. There was a safe method to handle NG, which was discovered in 1867 by Alfred Nobel (1833-1896) [1-4]. NG, "the impossible-to-handle explosive" fascinated Alfred Nobel since 1950. From then on, his broad research had a constant topic: finding the way to handle and transport NG safely without reducing the explosive properties of NG. After years of research and several accidental explosions which killed some

workers (including Alfred Nobel's brother) [1], Alfred Nobel patented the solution in 1867, which involved the stabilization of NG through its combination with inert and porous diatomaceous earth [1-4]. Some years later, he named the invention as dynamite. Because of the high explosive power of dynamite and their safe manufacture and transport, dynamite rapidly replaced black powder in military and demolition applications. Consequently, the use of dynamite to perpetrate terrorist bombings started to be constant at the end of the 19th century, as evidenced by the 1886 Haymarket affair Chicago bombing, the 1910 Los Angeles Times bombing, the 1920 Wall Street bombing… and has continued until 21st century, as evidenced by the 11 M 2004 Madrid bombings [33-46]. The initial formula of dynamite (NG-diatomite) has been improved in many occasions with the aim of increasing the safety and applicability of dynamite. Some of these improvements involve the substitution of NG by ethylene glycol dinitrate (EGDN), the addition of NC and paraffin to the mixture, or the substitution of diatomite by ammonium nitrate (AN) [2-6]. In fact, most dynamites today used contain AN instead of diatomite.

- **1871** – **Oxidizer-fuel explosive mixtures**: Sprengel explosives

In the knowledge of the composition of black powder, which contains an oxidizer (saltpetre) and a fuel (charcoal-sulphur), Hermann Johann Philipp Sprengel (1834-1906) was convinced about the rule that every explosion was a sudden combustion, and every explosive was a mixture of oxidizer and fuel constituents, being themselves non-explosive [1, 47]. Thus, Sprengel investigated, in detail, the oxidizer-fuel explosive mixtures, preparing mixtures in such proportions that their mutual reduction-oxidation was complete. In brief, Sprengel made two lists summarizing numerous inorganic oxidizing substances (nitric acid, potassium nitrate, potassium chlorate…) and organic combustible substances (either solid or liquid hydrocarbons and nitro-aromatic compounds) [47]. Due to his comprehensive work about oxidizer-fuel explosive mixtures, oxidizer-fuel explosives are typically known as Sprengel explosives. Additionally to oxidizer-fuel mixtures, Sprengel also detonated picric acid, a nitro-aromatic compound, whose explosive properties were still unknown at that time. According to Sprengel, picric acid was able to explode (combust) alone (without the help of additional oxidizers) because it contains the sufficient amount of oxygen in its molecule [1, 47].

- **1870s-1890s** – **Chloratite**: A chlorate based Sprengel explosive

Though the term "chloratites" includes every chlorate-organic fuel explosive mixture, chloratite typically refers to the specific mixture of sodium chlorate, sugar and sulphur [7-9]. The precise date in which sodium chlorate, sugar and sulphur were combined for the first time to make chloratite is unknown, though it is not unlike that Sprengel did it, since he reported similar mixtures of chlorate and organic fuels [47]. It should be remarked that chloratite (sodium chlorate + sucrose + sulphur) is extremely similar to black powder (potassium nitrate + charcoal + sulphur); however, chloratite was not invented until a thousand years after the discovery of black powder. The reason lies on the fact that, contrarily to saltpetre and charcoal, which may be found in large amounts in nature, sodium chlorate and sucrose were not available until the 19th century. Chlorate based mixtures are significantly more unstable and unpredictably dangerous than the corresponding nitrate based explosives. Because of this reason, chloratite has not been widely used in neither the military, mining, demolition nor pyrotechnic fields [9]. However, chloratite has been often used in terrorist bombings because of the easy acquisition of its precursors nowadays. For instance, chloratite was used by ETA terrorist group.

- **1885** – **HMTD**: a primary-secondary peroxide explosive

Hexamethylene triperoxide diamine (HMTD) was first synthesized by Legler in 1885, while investigating the slow combustion of ether [27]. Unlike previously discovered organic explosives, HMTD was not a nitro-explosive but a peroxide explosive. In addition, unlike nitro-explosives, HMTD was patented as a primary detonator explosive [27]. Actually, HMTD was classified as both a primary and a secondary explosive, which meant that no detonator was necessary to initiate it. However, HMTD was reported to be chemically unstable and easily and slowly decompose [27]. Because of these disadvantages, no practical application (either military or industrial) was reported for HMTD. In this respect, dynamite (secondary explosive) initiated by "Fulminate Blasting Caps" (detonator also patented by Alfred Nobel shortly before patenting dynamite) was preferred [27]. However, the relatively easy synthesis of HMTD has made that some terrorist groups use homemade HMTD to perpetrate terrorist bombings such as 2005 London bombings [7].

- **1887** – **Flash powder**: the shining explosive invented by photographers

The first attempts of creating artificial light to be used in photography date from the middle of the 19th century. Special attention was put on the incandescence of materials, particularly metals. At the beginning of the 1860s, the bright intense white light created by incandescent magnesium became popular among photographers and magnesium wires started to be industrially manufactured [48, 49]. Like a candle, the wire was ignited and magnesium was consumed producing a brightly intense light. The main problem usually involved the incomplete burning of magnesium. In 1865, Charles Piazzi Smyth had the idea of igniting magnesium using black powder in such a way that the combustion of magnesium was optimum [49]. The idea worked perfectly, but the new problem was the interfering residues, dirt and smoke created by black powder, mainly due to charcoal. Adolf Miethe and Johannes Gaedicke solved the problem in 1887 by using a mixture of magnesium powder, potassium chlorate and antimony sulphide [48, 49]. The first relatively clean "flash" had been created and the mixture was called flash powder. For the first time, taking instant photographs was possible. From then on, different flash powder compositions were developed, always maintaining the two required components to produce the flash: the metal powder (magnesium or aluminium are mostly used today) and the oxidizing powder (potassium chlorate or potassium perchlorate are the most common). Due to the lightning effects, flash powder was also rapidly incorporated to pyrotechnics, in combination with black powder. In addition, coloured fireworks were developed by using different metals [22-25]. Due to the low energy of flash powder, it had no application in the military field. Like black powder, flash powder is an explosive propellant mixture of an oxidizer and a fuel. Regarding terrorist bombings, flash powder is not usually employed due to its low destruction power. However, it is commonly used in urban warfare environments in which pyrotechnic devices and firework bombs are thrown against police [23].

- 1863 – **1891** – **TNT**: the yellow dye that turned into an explosive

Like black powder, 2,4,6-Trinitrotoluene (TNT) was invented with a non-explosive purpose. Particularly, TNT molecule was first synthesized in 1863 as a yellow dying agent by Julius Bernhard Friedrich Adolph Wilbrand (1839-1906) [1, 2, 8]. Due to its insensitiveness to be ignited, the explosive properties of TNT

were not discovered until 1891 by Carl Häussermann (1863-1936) [1]. From then on, TNT was industrially manufactured and rapidly incorporated to military field because of its high velocity of detonation and stability. TNT, which is a nitro-aromatic explosive, was the perfect explosive, powerful when detonated while safe when stored and handled [4-9, 50-52]. Since the main application of TNT is military, the sale of TNT is strictly controlled, in such a way that TNT is inaccessible for non-military people. However, TNT has been sometimes used by terrorist groups to perpetrate terrorist bombings (after obtaining it illegally), such as the 1983 Truck bombing in the American marine barracks in Beirut, in which 5400 kg of TNT were detonated [53].

- **1894** – **PETN**: the high energy nitrate ester military explosive

Although pentaerythritol tetranitrate (PETN) is today known to have medical properties as vasodilator, its main application is the explosives field [4]. In fact, PETN explosive was patented in 1894 by a German explosives company manufacturer [2]. Like TNT, PETN is a stable high energy secondary explosive, powerful when detonated while safe when handled [4]. Thus, PETN also satisfied military requirements to be used as a military weapon. Particularly, PETN is typically used today in the manufacture of military detonating cord, which is used to detonate higher insensitive explosives [8, 9]. Unlike TNT, PETN is a nitrate ester explosive. As military explosive, PETN is strictly controlled; however, some terrorist bombings such as the1980 Paris bombing, and several current attempts of blowing up planes have been committed using PETN [8].

- **1895** – **TATP**: The homemade peroxide explosive only used by terrorists

Triacetone triperoxide (TATP) was first synthesized in 1895 by Richard Wolffenstein (1864-1926), who combined acetone and hydrogen peroxide, obtaining, after a few days, a white solid product [27]. Like HMTD, TATP is a peroxide explosive. Like HMTD, TATP is known to be highly unstable and extremely sensitive to impact, friction, static electricity, and temperature changes [8, 27]. Because of such instability and volatility, TATP was never industrially manufactured nor used for military applications [8]. However, TATP is typically homemade by terrorists due to the easy synthesis of TATP from commercially available acetone and hydrogen peroxide precursors. In fact, TATP

has been repeatedly used to perpetrate recent terrorist bombings including 2015 Paris attacks, 2016 Brussels airport bombing, 2017 Manchester Arena bombing, 2017 Brussels Central Station bombing, 2017 Stockholm attack and 2017 Barcelona attacks (where TATP accidentally detonated when being prepared) [42-44].

- **1910s – Ammonal**: AN-based powdered explosive

While potassium nitrate (saltpetre) was already known in China in the 10th century, ammonium nitrate (AN) was not discovered until centuries later. The main reason lies on the fact that the number of natural deposits of ammonium nitrate is significantly lower than those of saltpetre. In this respect, ammonium nitrate is more easily obtained by mixing ammonia and nitric acid. This synthesis was first reported in 1654 by Johann R. Glauber (1604-1670) [2]. However, the use of AN as an explosive ingredient was not reported until 1867, when Ohlsson and Norrbein patented it, and Nobel started to use it in his dynamites (instead of inert diatomite) [2]. In addition, other AN-based explosive mixtures started to be developed, such as ammonal, which was already used by British Army in 1916 [4]. Ammonal generally refers to the mixture of ammonium nitrate and powdered aluminium (ANAl) [7, 8]. However, due to the common addition of TNT to AN-Al mixture within the military field, ammonal often refers to the mixture of AN-Al-TNT [4, 20]. Ammonal, either containing TNT or not, was frequently used by ETA to perpetrate terrorist bombings in Spain, such as the Hipercor bombing in Barcelona or the *Casa-Cuartel* bombing in Zaragoza, both in 1987 [42-44].

- 1898 – **1916** – **RDX**: the high energy nitramine military explosive

Unlike PETN, cyclotrimethylenetrinitramine (today commonly known as RDX, abbreviation of Research Department eXplosive or Royal Demolition eXplosive) was first patented in 1898 as a medicinal compound by Georg Friedrich Henning [2, 4, 54, 55]. In 1916, Henning reported the explosive behaviour of RDX and military forces of different countries started to investigate RDX as an explosive. As previously classified, RDX is an organic nitramine explosive. Like TNT and PETN, RDX is a stable high energy secondary explosive, powerful when detonated while safe when handled, which is typically used in the military field

as a plastic explosive after being combined with different plasticizers [4-9, 50-52]. Despite being a strictly controlled military explosive, RDX has been largely used to perpetrate terrorist bombings including Pan Am flight 103 bombing (Lockerbie 1988), 1993 Bombay bombings, 1999 Russian apartment bombings, 2006 Mumbai train bombings, 2008 Jaipur bombings and 2010 Moscow metro bombings, amongst others [7, 8, 42-44].

- **1956** – **ANFO**: AN-based slurry explosive

In 1956, after decades of using ammonal, Melvin Alonzo Cook (1911-2000) reported the advantages of adding a liquid fuel oil to the AN-Al mixture [2, 8, 56]. Thus, the explosive was called ANFO (acronym of Ammonium Nitrate Fuel Oil). Due to the addition of a liquid fuel, the powdered explosive was transformed into a slurry malleable explosive, which was safer and more easily handle, as previously evidenced by Sprengel for the combination of solid oxidizers and liquid hydrocarbon/aromatic fuels [47]. Particularly, ANFO and AN-based dynamite have similar composition (AN-fuel oil *vs* AN-EGDN), thus they have similar explosive properties. In fact, both explosives are highly suitable for mining/demolition purposes [7-9, 13]. Nevertheless, due to the easy and legal acquisition of ammonium nitrate (from fertilizers) and fuel oil (from petrol stations), ANFO has been typically homemade by criminals to perpetrate terrorist bombings. For instance, ANFO was used in different car bombings perpetrated in Spain and UK by ETA and IRA, respectively. ANFO was also employed in 1992 Taranta Lima bombing (Peru), in 2001 Shijiazhuang bombings (China), 2011 Oslo bombing or 2016 Dublin bombing [42-44].

Current classifications of explosives

Different criteria may be considered when classifying explosives, thus there exist multiple forms of classification. Perhaps, the classification most usually found in literature is the one based on the velocity of detonation, which has been traditionally used in the military field [1-11]. In addition, it is becoming prevalent in the forensic field the classification of explosives according to their source or application [1-10]. Finally, a third classification of explosives according to their chemical composition [4] is proposed in this thesis due to the latent necessity of classifying explosives in a sensible manner that facilitates the

detection of explosive traces. This latter classification is original and self-created (taking, as starting point, the unconnected allusions to the chemical composition of explosives, found in literature).

- **According to the velocity of detonation:**

The velocity of detonation is directly proportional to the destructive power of the explosive. This means, for instance, that for the same mass of two different explosives, a greater destructive power (a more destructive shock wave) will occur for the explosive having higher velocity of detonation. Thus, it is easy to comprehend how important knowing the velocity of detonation of explosives is in certain fields such as military, mining industry or building demolition. This is the reason why infinite resources from these influencing and economically gifted fields have been allocated to study the velocity of detonation of explosives in such great detail. As an example, Table 4.1 summarizes the velocities of detonation of some common explosives.

Table 4.1. Velocities of detonation of some explosives. The highest value found in literature for each explosive are provided, since the velocity of detonation is affected by some other factors besides the chemical composition such as the particle size or the density of the explosive [2-7, 27, 50-52, 54].

Explosive	RDX	PETN	TNT	TATP	HMTD	ANFO	Dynamite	Flash powder	Black powder
Velocity of detonation/ deflagration (m/s)	8700	8400	6900	5300	5100	4200	3800	1000	400

As previously explained, detonation occurs when velocity of detonation exceeds the speed of sound in the unreacted material [2-10]. It should be reminded that the speed of sound in air medium at room temperature is around 340 m/s [5-9]. However, the speed of sound increases when propagated through liquid or solid media because of the higher proximity of atoms/molecules in liquid/solid state. For instance, the speed of sound is around 1500 m/s in water, 3000 m/s in wood while 6400 m/s in aluminium [57, 58]. Regarding explosives (normally prepared in powdered forms), the speed of sound in most of them is expected to range from 1000 to 3000 m/s [7-9]; noticeably lower than the speed of sound in densely packed aluminium metal.

In fact, a tentative velocity of detonation range of 1000-3000 m/s is usually established to discriminate between high and low velocity of detonation explosives [2-9].

- **High energy explosives**

High energy explosives detonate creating a supersonic shock wave that propagates usually exceeding 4000 m/s. Three classes are typically subdivided for high explosives according to their sensitivity to explode: primary, secondary and tertiary explosives [1-10, 27, 50-52, 54].

- **Primary explosives** are extremely sensitive to different weak stimuli (such as heat, spark or friction) by which detonation initiates. In general, primary explosives are not particularly powerful. Because of these properties, they are usually used in little amounts as detonators of secondary high explosives. Some typical primary explosives are mercury fulminate, silver fulminate, lead azide, cuprous acetylide, lead picrate, lead styphnate, diazodinitrophenol, tetrazoles, NG, TATP and HMTD [1-5, 27].

- **Secondary explosives** are practically insensitive to weak stimuli and they usually require the input of a strong shock to detonate. Most secondary explosives are exceptionally powerful (with velocities of detonation that exceed 6000 m/s). Secondary explosives include the most common explosives used in the military field such as RDX, PETN, HMX, TNT, 1,3,5-triamino-2,4,6-trinitrobenzene (TATB), tetryl, picric acid, HNIW and NC [1-15, 27, 50-52, 54].

- **Tertiary explosives** is an extra group, sometimes added in the classification, to include and separate those insensitive explosives widely used for mining and demolition purposes, which have lower velocities of detonation than military secondary explosives. ANFO, ANAl and dynamite compositions are common examples of tertiary explosives [3-5, 13].

- **Low energy explosives**

Unlike high energy explosives, low energy explosives deflagrate creating a subsonic wave front that does not reach the speed of sound. The explosion that low explosives may produce is a consequence of the overpressure generated inside a container by the accumulation of gas products from deflagration. Because of the progressive production of these gas products during their deflagration, low explosives are mostly used as propellants, either in

pyrotechnics, space rockets or ammunition for firearms. Smokeless powder, black powder and flash powder are typical examples of low explosives [1-15].

- **According to the source/application:**

As evidenced in the previous classification, some allusions to the field in which each explosive is preferentially used have inevitably appeared. In this respect, the latent correlation between the explosive detonation properties and its usage is logical and evident. However, the classification of explosives based on the source/application is not a simple rename of the classes previously explained… primary explosives – detonators; secondary explosives – military explosive charges; tertiary explosives – mining explosive charges; and low explosives – pyrotechnic/rocket/firearm propellants. The aim of this new classification, based on the source/application of explosives, is the categorization of explosives according to the easy/complicate, legal/illegal obtaining of each explosive. Such particular interest comes from police, forensic and intelligence investigations, which focus on solving, facing and preventing the criminal use of explosives in terrorist attacks [7-9]. Therefore, depending on how explosives are obtained, explosives may be classified into three different categories: military, commercial and homemade explosives [2-10].

- **Military explosives**

Military explosives are high explosives meeting strict requirements in terms of performance, functionality and safe handle, storage and transport. They have to be powerful while insensitive to weak/medium intense stimuli, requiring the use of detonators to detonate [1-5]. Military explosives are generally organic molecules containing only carbon, hydrogen, oxygen and nitrogen atoms. Particularly, oxygen and nitrogen atoms are typically found as nitro-groups ($-NO_2$) in these molecules. The explosive nature of these molecules is due to those nitro-groups, thus military explosives are usually referred as nitro-explosives [1-10]. Common military explosives are RDX, PETN, HMX and TNT. However, the use of single “powdered” explosives is uncommon. Today, most military explosives are plasticized using inert flexible binders with the aim of making mouldable and easy-to handle explosive compositions. Such compositions are known as plastic explosives and may contain one or more single explosives combined with the plasticizer. Since plasticizers are non-explosive compounds, their addition reduce the explosive power of the mixture. For this reason, the

mass proportion of plasticizers in plastic explosives does not usually exceed 10% [5-9]. Common plastic explosives are C-4, PG-2, Composition B and Semtex. For instance, PG-2 explosive is composed of 91% RDX (explosive), 5.3% bis(2-ethylhexyl) phthalate (plasticizer), 2.1% polyisobutylene (binder) and 1.6% motor oil; while Composition B is composed of 59.5% RDX (explosive1), 39.5% TNT (explosive2) and 1% paraffin wax (plasticizer) [6-9]. Military explosives are strictly controlled in most countries, only having access to them military personnel.

- **Commercial explosives**

Commercial explosives include those explosives that are legally used for non-military purposes including the explosives used in mining industry, construction/demolition applications and firearms/rocket/pyrotechnic propellants [4-9]. Dynamite and ANFO compositions are the most common commercial explosives used today for mining and demolition purposes. They are high explosives with relatively small velocities of detonation (in comparison with military explosives), which enable a more precise control about the required power to move and fragment rocks and buildings [5-9]. Regarding firearm ammunition, the explosive propellants currently used for shooting are smokeless gunpowders based on NC [1-10]. Either dynamite, ANFO or smokeless gunpowders are particularly safe to handle and transport since they are insensitive to weak stimuli and require detonators to explode. On the contrary, the propellants used in pyrotechnics mostly consist of black powder and/or flash powder, which are particularly sensitive and may accidentally deflagrate and explode [1-9, 22-25]. All these explosives are commercially available for non-military citizens. Thus, their acquisition and ultimate usage (either legal or criminal) is particularly easy since they are not as controlled as military explosives. Because of these reasons, commercial explosives are frequently used in terrorist attacks.

- **Homemade explosives**

Homemade explosives include all “do-it-yourself” explosives. With the arrival of Internet last century, it is no longer necessary to be a chemist (or even study some basic concepts of chemistry) to produce or synthetize explosives. Freely accessible recipes guiding step by step about how to obtain, produce and

synthetize different explosives are available online. These recipes typically include oxidizer-fuel explosive mixtures such as ANFO. Examples:

- Recipe for ANFO: "*Into a kitchen mixing drum, add 950 grams of ammonium nitrate with 50 grams of diesel fuel oil at room temperature and blend it for several hours to provide a well-mixed fuel balanced explosive. Use it directly and do not allow it to dry*." [6]

In fact, most recipes also include where you can get each individual component: "*you may find AN as fertilizer in a garden store*", "*you may find diesel fuel oil in any petrol station*".

In addition to these explosive mixtures that you can either purchase or do-it-yourself, there exist homemade explosives that are not commercially available because their instability and sensitivity is extreme. However, they are high energy explosives whose synthesis is simple and from easy attainable reagents such as TATP or HMTD peroxide explosives. In fact, TATP is widely known because of having been used in many recent terrorist attacks [4-9, 27]. TATP is easily synthesized through the reaction between hydrogen peroxide and acetone [27], whose recipe is also available on Internet.

$$3\,H_2O_2(l) + 3\,C_3H_6O(l) \rightarrow C_9H_{18}O_6(s) + 3\,H_2O(l)$$

As previously indicated, TATP does not require a detonator to explode, increasing the danger and ease of use of TATP [27], in spite of the frequent accidents associated to their synthesis.

New classification of explosives according to their chemical composition

An important added value of this chapter is the proposal of a new classification of explosives according to their chemical composition due to the necessity of this chemical-analytical information for the determination of explosives and their residues in post-blast residues.

Thus, the knowledge about the chemical composition of explosives may provide useful information not only to predict the chemical reaction by which such explosive may cause a detonation, but also, and more important, to properly focus the subsequent determination of explosive traces towards the correct

analytes. This involves selecting the appropriate methodology, analytical instrumentation, etc. depending on the chemical compound that is aimed to be determined. For instance, gas/liquid chromatography coupled to mass spectrometry is suitable to determine organic explosives such as TNT or TATP, but completely useless for black powder. Similarly, ion chromatography or capillary electrophoresis is adequate to determine the ionic components of flash powder or black powder, but very ineffective for TNT. Therefore, from the point of view of chemical identification, the classification of explosives according to their chemical composition is needed. In fact, continuous allusions to the chemical composition of explosives are made in previous classifications (either based on velocity of detonation or application). For instance, nitro-explosives, which are secondary explosives used for military purposes; or peroxide explosives, which are homemade explosives [2-10]. In addition, some chemical classifications are based on the particular chemical groups/bonds [4], which provide the explosive character of the substance, in such a way that eight classes have been created (Table 4.2):

Table 4.2. Classification of explosive chemical groups [4].

Class	Nitro/ nitrate	Azide/ Azo	Halogen amine	Fulminate	Chlorate / perchorate	peroxide	Acetylide	Organo-metallic
Chemical bond/group	NO_2, NO_3	–N3, N=N	$-NF_2$ (F = halogen)	–C=N–	ClO_3, ClO_4	–O–O–	–C≡C–	M–C

However, a global, practical and comprehensive classification of explosives based on the entire chemical composition of the explosive is not established yet. Thus, a new classification of explosives according to their chemical composition is proposed in this Thesis. This classification (Scheme 4.1) has been created by gathering the dispersed chemical allusions found in literature, while keeping as main focus whether the explosion of each explosive is caused by an unimolecular decomposition (pure single explosives) or multi-molecular redox reaction (oxidizer-fuel composite explosives).

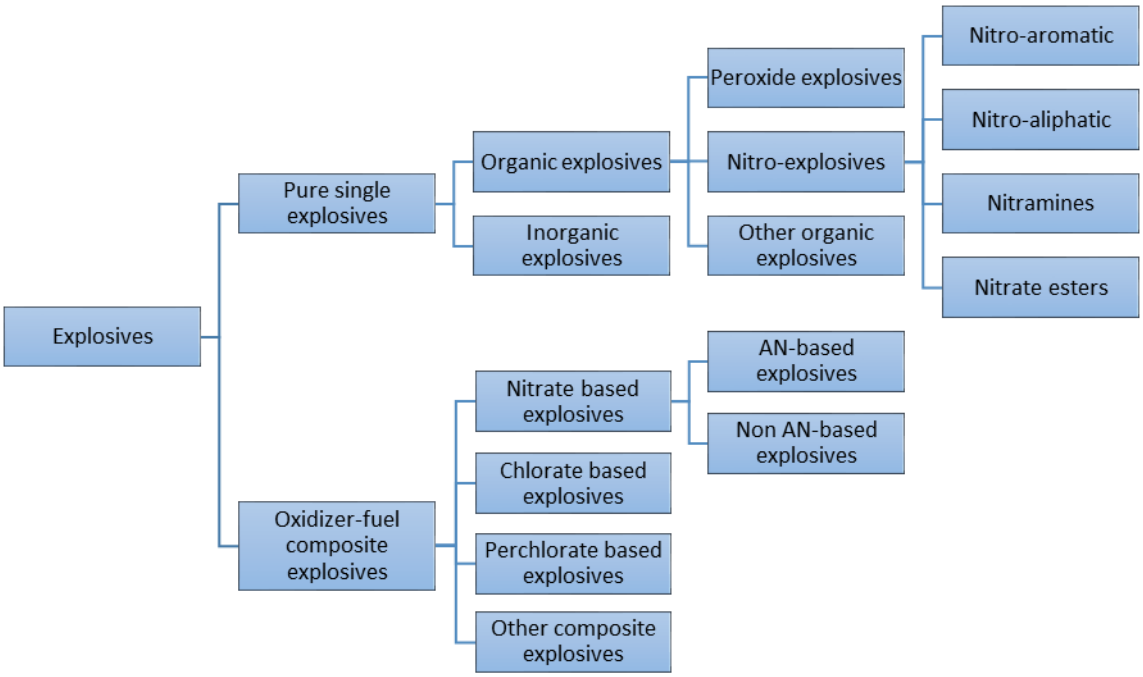

Scheme 4.1. Proposed classification of explosives according to their chemical composition

Pure Single Explosives

Pure single explosives, sometimes also called "molecular explosives", include every explosive compound whose unimolecular decomposition reaction may produce an explosion. This means that they are not a mixture of substances, but a pure compound. As a pure compound, it is composed of different atoms chemically bonded. Depending on the nature of the constituting atoms (*i.e.* elements), the chemical compound can be categorized into two classes: inorganic or organic compound.

- **Inorganic explosives**

Pure single inorganic explosives include those explosive compounds that either 1) do not contain carbon atoms in their structure or 2) contain at least one atom different to carbon, hydrogen, oxygen or nitrogen in their structure. This includes, for example, lead azide ($Pb(N_3)_2$) and ammonium nitrate (NH_4NO_3), which do not contain carbon atoms; but also, silver fulminate (AgCNO), cuprous acetylide (Cu_2C_2), lead styphnate ($PbC_6HN_3O_8$) and lead picrate ($PbC_{12}H_4N_6O_{14}$), which, despite containing carbon atoms, contain at least one atom different to C, H, O, N [4, 27].

- **Organic explosives**

Pure single organic molecular explosives include those explosive molecules that contain at least one atom of carbon and no atoms of an element different to C, H, O, N, in their structure. This includes, for example, TNT ($C_7H_5N_3O_6$), TATP ($C_9H_{18}O_6$) or even nitroguanidine ($CH_4N_4O_2$), which only has one atom of carbon. Because of the large number of organic explosives that exist today, organic explosives are usually sub-divided into two main different classes (nitro-explosives and peroxide explosives). In addition, a third class named "other organic explosives" is also presented in which including those organic explosives that are neither nitro-explosives nor peroxide explosives.

- **Nitro-explosives**

Nitro-explosives are organic explosives characterized by having in their structure one or more nitro-groups (-NO_2) [1-7, 54]. Nitro-explosives are also sub-divided into four different classes depending on the atom to which nitro-group is chemically bonded.

  - **Nitro-aromatic.** Nitro-group is bonded to an aromatic carbon (C(Ar)-NO_2). *E.g.* TNT, picric acid and TATB.
  - **Nitro-aliphatic.** Nitro-group is bonded to an aliphatic carbon (C-NO_2). *E.g.* nitromethane, nitro-ethane and FOX-7 (1,1-diamino-2,2-dinitroethene).
  - **Nitramine.** Nitro-group is bonded to a nitrogen atom (N-NO_2). *E.g.* RDX, HMX and HNIW.
  - **Nitrate ester.** Nitro-group is bonded to an oxygen atom (O-NO_2). Within nitrate esters, we may distinguish between those explosives that detonate (such as PETN and NG), and those powders that deflagrate (such as smokeless gunpowders composed of NC).

- **Peroxide explosives**

Peroxide explosives are organic explosives characterized by having in their structure one or more peroxide groups (-OO-). The most popular peroxide explosives are TATP and HMTD [7, 27].

- **Other organic explosives**

As previously introduced, most organic molecular explosives contain either nitro- or peroxide groups in their structure. In fact, the explosive character of

organic explosives is usually due to those nitro/peroxide groups. Nevertheless, there are some exceptions. Thus, an extra group is created to include every organic explosive that does not contain neither nitro- nor peroxide groups in its structure. For this reason, a wide variety of chemically different compounds has a place in this group including tetrazole (a 5-member ring heterocyclic compound (CH_2N_4) and its derivatives, diazomethane (CH_2N_2) and other azo/diazo alkyl compounds, fulminic acid (HCNO) or cyanuric triazide (C_3N_{12}) and other organic azides [27, 54].

- **Oxidizer-fuel composite explosives or Sprengel explosives**

Oxidizer-fuel composite explosives include every mixture (*i.e.* combination of two or more compounds) whose redox reaction may produce an explosion. As every redox reaction, one of the components in the mixture serves as oxidizing agent while the other component/s serve/s as fuel (reducing agent) [1-10, 22-25]. Therefore, those mixtures containing pure explosives such as Composition B (mixture of RDX and TNT) are excluded from this group, since either RDX or TNT may detonate separately. For this reason, these composite explosives are more properly defined as oxidizer-fuel explosive mixtures. As previously explained, they are also known as Sprengel explosives, in memory of Hermann Sprengel, who explained that the explosiveness of these substances was due to the sudden combustion of the fuel in contact with the oxidizing agent [47]. In fact, the chemical and explosive properties of the explosive are determined by the combination of both oxidizer and fuel. Since there exist many substances that may act as fuels in contrast with the few energetic salts used as oxidizers, Sprengel explosives might be sub-categorized according to the oxidizer. Most oxidizer-fuel explosive mixtures are composed of either a nitrate, chlorate or perchlorate salt. The use of any other oxidizing agent to make explosive mixtures is uncommon, because they are more expensive compounds (such as chromate, permanganate, bromate, iodate or any organic oxidizing compound). Thus, composite explosives might be sub-divided into nitrate, chlorate and perchlorate based explosives. An extra fourth class can be also considered for those oxidizer-fuel explosive mixtures containing uncommon oxidizers.

- **Nitrate based explosives**

Nitrate based composite explosives are composed of an inorganic nitrate salt or nitric acid (oxidizer) mixed with one or more fuel substances. Since organic nitrate esters (-ONO_2), such as PETN, do not need to be mixed with a fuel to detonate, they are excluded from this group. Inorganic nitrate anion (NO_3^-) consists of a nitrogen atom equally bonded to three oxygen atoms. It is the conjugate base of nitric acid and forms nitrate salts with most metals. Nitrate salts, actually, exist naturally on earth. Depending on the cation to which nitrate is bonded, nitrate based explosives might be sub-classified in two groups: those nitrate explosives containing ammonium nitrate and all the rest.

- **AN-based explosives**

Ammonium cation (NH_4^+), which is the conjugate acid of ammonia, consists of a nitrogen atom equally bonded to four hydrogen atoms. In this respect, ammonium nitrate (NH_4NO_3) is the unique inorganic nitrate composed of non-metallic elements. As previously explained, ammonium nitrate (AN) is a single molecular inorganic explosive capable of producing an explosion by unimolecular decomposition (by which AN transforms into water vapour (H_2O), nitrogen (N_2) and oxygen (O_2)). However, many commercial explosives are prepared by mixing ammonium nitrate with a fuel, taking also advantage of the oxidizing capability of ammonium nitrate. Because of these combination (AN unimolecular decomposition + AN-fuel redox reaction), the mass percentage of AN in these mixtures usually ranges from 70 to 95% [4-8]. As a result, AN-based explosives are high energy explosives, which detonate at velocities of detonation around 3000-5000 m/s. In addition, the relevance that AN-based explosives have achieved (for either mining/demolition or terrorist purposes) makes it necessary to create a particular group for them. The most common AN-based explosives are ANFO (*i.e.* mixture of AN and diesel), ammonal (*i.e.* mixture of AN and aluminium powder) and current dynamites (in which NG was long time ago replaced by AN, mixed with EGDN, sawdust and plasticizers) [1-8].

- **Non AN-based nitrate explosives**

Contrarily to AN, nitrate salts whose cation is a metal do not easily decompose, and if so, the decomposition is slow and non-explosive. The addition of a fuel substance is required to have an explosive mixture. Normally in such cases, a deflagration caused by the multi-molecular redox reaction between oxidizer and

fuel produces large amounts of gaseous products, which increase the pressure (if confined) and ultimately provoke an explosion. In fact, these oxidizing-fuel deflagrating mixtures are commonly known as composite propellants, because they are commonly used as propellants due to the large amount of gases they produce [1-15, 22-25]. In order to ensure the complete oxidation of the fuel, oxidizer is usually added in mass percentages ranging from 50 to 75%. Potassium nitrate is the most common nitrate used in nitrate-based propellants as evidenced by black powder (the most renowned and widely known explosive ever, which is a mixture of potassium nitrate, charcoal and sulphur); or rocket candy (a sweet propellant composed of potassium nitrate and sugar sucrose). Nevertheless, other nitrates such as lithium, barium, strontium and copper(II) nitrates, amongst others, are also used in pyrotechnic devices to provide different colour effects due to the characteristic emission colour of the metal ion [22-25].

- **Chlorate based explosives**

Chlorate based explosives are composed of an inorganic chlorate salt (oxidizer) mixed with one or more substances which act as a fuel. Chlorate anion (ClO_3^-) consists of a chlorine atom equally bonded to three oxygen atoms. It is the conjugate base of chloric acid and forms stable chlorate salts with some metals. Similarly to nitrates, chlorates might be sub-divided into ammonium chlorate and metal-chlorates. However, ammonium chlorate is extremely unstable, so much so that ammonium-chlorate-based explosives are not produced. In fact, most chlorate-based explosives are composed of either sodium or potassium chlorate such as chloratite (a homemade explosive composed of sodium/potassium chlorate, sulphur and sugar) and some pyrotechnic powders (in which potassium/sodium chlorate is added to black powder) [22-25].

- **Perchlorate based explosives**

Perchlorate based propellants are composed of an inorganic perchlorate salt (oxidizer) mixed with one or more substances which act as a fuel. Perchlorate anion (ClO_4^-) consists of a chlorine atom equally bonded to four oxygen atoms. It is the conjugate base of perchloric acid and forms perchlorate salts with most metals. Contrarily to ammonium chlorate, ammonium perchlorate (AP) is relatively stable and commonly used as propellant of spatial rockets when mixed with aluminium powder and plasticizers (which act as the fuel) [4-7]. On the

other hand, metal-perchlorates (mainly potassium perchlorate) are used in pyrotechnic compositions, either forming flash powder (a propellant composed of potassium perchlorate and aluminium powder) or in combination with black powder ($KClO_4$ + KNO_3 + charcoal + sulphur) [4-7, 22-25].

- **Composite explosives based on other oxidizing agent**

In the few cases in which an oxidizer-fuel composite explosive is composed of an oxidizing agent other than nitrate, chlorate or perchlorate salts, it would be included in this group. As previously introduced, oxidizing agents such as permanganate, dichromate, chromate or iodate are not usually found in explosive compositions because they are more limited and expensive than the respective nitrate or perchlorate salts. However, some homemade explosive mixtures can be prepared by mixing these oxidizing salts with fuels such as the mixtures of potassium permanganate with either aluminium, antimony or glycerine [4-6, 24].

Finally, as previously explained, some extras can be incorporated to every explosive to either facilitate their handling/transport (such as plasticizers) or increase the damage they produce (such as shrapnel or radiological material), but such extras do not determine the chemical reaction which causes the explosion. Therefore, their incorporation do not alter the chemical classification of the explosive. Negatively, there might be some explosives difficult to classify because of sharing chemical features of different groups, such as urea nitrate, which, despite also being a non-metallic nitrate (like AN), contains a carbon atom, thus it should be theoretically classified as an organic explosive (though it is not a nitrate ester). In addition, two or more different explosives can be combined to produce more harmful explosive mixtures such as ammonal which combines TNT, AN and aluminium powder. In such case, ammonal is an explosive mixture composed of TNT nitro-aromatic organic explosive and ANAl (AN-based) oxidizer-fuel explosive mixture.

As a summary of the three modes of classification of explosives previously explained, a practical user-friendly guide for explosives classification is shown in Scheme 4.2.

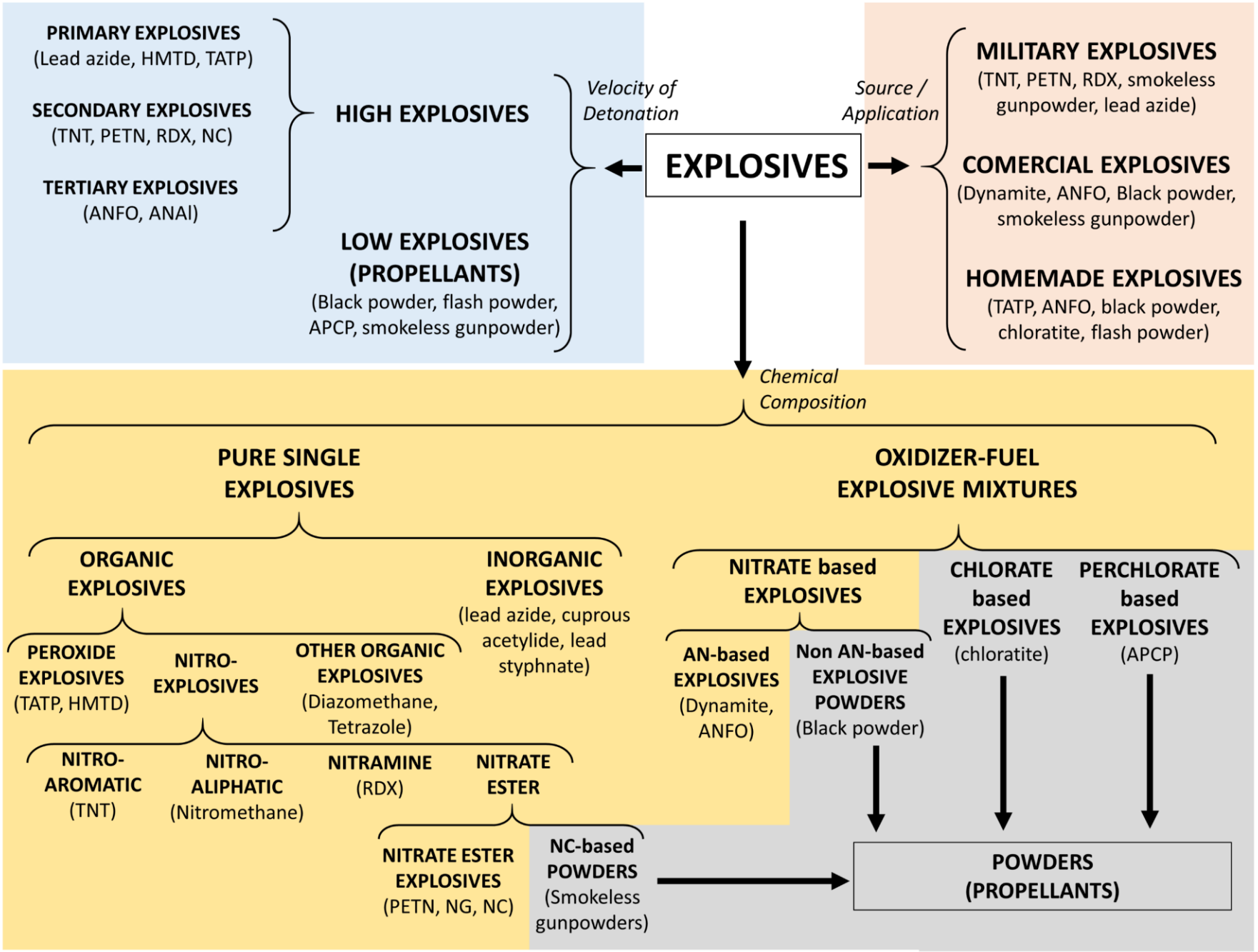

Scheme 4.2. Classification of explosives according to the velocity of detonation, the source/application, or the chemical composition.

Terrorist use of explosives (Improvised Explosive Devices)

Although explosives are theoretically classified into military, commercial and homemade explosives (depending on their use/application), it does not mean that explosives used to commit terrorist bombings are exclusively homemade explosives. Terrorism does not care about classification of explosives. The unique concern of terrorism is the use of violence, especially murder and bombing, in order to demoralize, intimidate, terrorize and subjugate population and governments to achieve political aims [7, 55, 59, 60]. Every explosive may be used to perpetrate a terrorist bombing because every explosive, even in small amounts, may cause terrible damage. In this respect, the explosives used in terrorist bombings are called Improvised Explosive Devices (IEDs) [3-9, 55, 60-62]. Since their destructive effectiveness lies in being unnoticed, IEDs usually offer inoffensive design and appearance using common materials such as bags, suitcases and vehicles, in which the explosive is surreptitiously hidden. Thereby, IEDs avoid being neutralized, and produce the planned explosion and harm (*i.e.* hurting and killing people (soldiers and citizens) and destroying buildings and vehicles) [3-9, 19, 61, 62]. IEDs have become the ideal weapon to fulfil these dreadful objectives, due to several reasons including the advantages of being cheap to manufacture, easy to use and hard to detect. IEDs are manually manufactured explosive devices that consist of a variety of components arranged in a specific way that may produce an explosion. One of the components is the explosive substance (explosive charge). The other essential components of IEDs are a control system, a detonator, a booster, and a container [3-8, 19, 61, 62]. In brief, signal from the control system is converted first into a small explosive shock caused by the detonator, which in turn initiates a more powerful explosion in the booster, which amplifies the shock into the main charge. The booster and the main explosive charge consists of an explosive compound or mixture of several explosive compounds, which produce the explosion. Some IEDs might use a unique explosive as detonator, booster and main charge, such as TATP [6-8].

Despite the current increasing concern about IEDs, the use of IEDs is not new. IEDs have been employed to commit terrorist bombings for more than two centuries. Some of the most ancient terrorist bombings, of which there is evidence, were:

- The plot to assassinate Napoleon Bonaparte in Paris in 1800, in which a barrel containing black powder hidden into a horse drawn cart was detonated. Dozens of bystanders were killed or injured, whereas Napoleon Bonaparte survived [19].
- Clerkenwell explosion (1867), in which a barrel also containing black powder was detonated next to the wall of Clerkenwell prison, with the aim of liberating some prisoners [19].
- Haymarket Affair bombing, which occurred in Chicago in 1886 during a public rally. In such protest rally, a dynamite bomb was thrown against police officers, killing at least eight of them. Police then opened fire against the suspicious bombers within the crowd, increasing the number of casualties [33, 34].
- Los Angeles Times bombing (Figure 4.2), which occurred in 1910. In such attack, the detonation of a suitcase containing dynamite also ignited the natural gas pipes of the building into a fire, causing 21 deaths and more than a hundred injured people [35-37].
- The Wall Street bombing (1920), in which a horse-drawn wagon loaded with 45 kg of dynamite exploded in a crowded street killing 38 people and injuring hundreds more (Figure 4.2) [19, 38, 39, 63].

Figure 4.2. Los Angeles Times bombing 1910 [35] (left); The Wall Street bombing 1920 [39] (right). Public domain.

From then until now, thousands of terrorist bombings using IEDs have been perpetrated in many countries throughout the world, particularly in war zones including the Second World War (1939-1945), Vietnam War (1955-1975), Northern Ireland conflict (1968-1998), Afghanistan War (1978-present), First Lebanon War (1982-1985), First Intifada (1987-1993), First Chechen War (1994-1996), Second Intifada (2000-2005), Second Chechen War (1999-2009),

Iraq War (2003-2011), Somali Civil War (2009-present), Syrian War (2011-present) and Libyan Civil War (2014-present), amongst others [19, 40-43, 55, 61, 64].

The most dreadful and coward reality of IEDs is the fact that, either in war or non-war zones, the targets of terrorist bombings are usually civilians (non-military people). As a brief summary to comprehend the social scourge that IEDs represent, Table 4.3 assembles the two deadliest terrorist bombings (per year) worldwide in which IEDs killed more than 50 people or injured more than a hundred [40-43].

Table 4.3. The two deadliest terrorist bombings per year occurred worldwide that killed more than 50 people or injured more than a hundred [40-43]. No terrorist attacks perpetrated with only firearms or hijacked vehicles are considered. However, some terrorist attacks were committed by combining firearms and IEDs (shooting + bombings). Every incident was reported in either BBC News, CNN, New York Times, The guardian, Los Angeles Times, Fox News, Time, Voice of America, Reuters, Antiwar, El Pais, El Mundo, Chinadaily, Clarín, Semana or RTE News.

Year	Location	Terrorist bombing	Total Deaths	Total Injured
2018	As-Suwayda (Syria)	July 2018 As-Suwayda bombings	+300	+180
2018	Mastung (Pakistan)	2018 Mastung and Bannu bombings	150	+180
2017	Mogadishu (Somalia)	2017 Mogadishu truck bombing	+650	+300
2017	Bir al-Abed (Egypt)	Sinai attack (shooting + bombings)	+300	+120
2016	Baghdad (Iraq)	Karrada bombing (truck bombings)	+340	+245
2016	Jableh & Tartus (Syria)	May 2016 Syrian suicide/car bombings	+150	+200
2015	Kobanî (Syria)	Kobanî massacre (car bombings)	+220	+300
2015	Sinai (Egypt)	Metrojet Flight 9268 bombing	224	0
2014	Baghdad (Iraq)	January 2014 Baghdad car bombings	+150	+370
2014	Peshawar (Pakistan)	Peshawar school massacre (shooting + suicide bombings)	+150	+110
2013	Across Iraq	April 2013 Iraq bombings (shooting + suicide/car bombings)	+450	+1000
2013	Across Iraq	May 2013 Iraq bombings (shooting + suicide/car bombings)	+440	+700
2012	Across Iraq	January 2012 Iraq bombings (shooting + suicide/car bombings)	+290	+730
2012	Across Iraq	June 2012 Iraq bombings (shooting + suicide/car bombings)	+230	+950
2011	Across Iraq	January 2011 Iraq bombings (shooting and suicide/car bombings)	+200	+480
2011	Across Pakistan	March 2011 Pakistan bombings (shooting and suicide bombings)	+180	+500

2010	Across Pakistan	July 2010 Pakistan suicide bombings	+150	+320
2010	Across Pakistan	September 2010 Pakistan suicide/car bombings	+120	+470
2009	Across Pakistan	October 2009 Pakistan suicide/car bombings	+260	+400
2009	Across Iraq	April 2009 Iraq suicide bombings	+220	+500
2008	Across Pakistan	October 2008 Pakistan suicide/car bombings	+180	+250
2008	Mumbai (India)	2008 Mumbai attack (shooting and suicide bombings)	173	+325
2007	Across Iraq	Yazidi communities car bombings	+750	+1500
2007	Baghdad (Iraq)	April 2007 Baghdad car bombings	+200	+250
2006	Baghdad (Iraq)	Sadr City car bombings	+215	+250
2006	Mumbai (India)	2006 Mumbai train bombings	+200	+700
2005	Baghdad (Iraq)	Suicide bombings	+150	+550
2005	Hillah (Iraq)	2005 Hillah car bombing	+120	+200
2004	Beslan (Russia)	Beslan school massacre (shooting and suicide bombings)	334	+780
2004	Madrid (Spain)	11M train bombings	193	+2050
2003	Najaf (Iraq)	Imam Ali mosque car bombings	95	+500
2003	Znamenskoye (Russia)	2003 Znamenskoye bombing	59	200
2002	Bali (Indonesia)	2002 Bali bombing	204	+200
2002	Grozny (Russia)	2002 Grozny truck bombing	83	210
2001	Angola	Angola train derailment by bomb	252	165
2001	Shijiazhuang (China)	Shijiazhuang bombings	108	38
2000	Chechnya (Russia)	July 2000 Chechnya bombings	54	+80
2000	Sri Lanka	Suicide bombings	52	150
1999	Across Russia	Russian apartment bombings	293	+1000
1999	Vladikavkaz (Russia)	1999 Vladikavkaz market bombing	64	168
1998	Kenya and Tanzania	1998 USA embassy truck bombings	224	+5000
1998	Machuca (Colombia)	1998 Machuca bombing and fire	100	+30
1997	Jerusalem (Israel)	Suicide bombing	16	+175
1997	Colombo (Sri Lanka)	Suicide bombing	15	+150
1996	Colombo (Sri Lanka)	Suicide bombings	+90	+1400
1996	Dehiwala (Sri Lanka)	Colombo-Alutgama train bombing	64	+400
1995	Oklahoma (USA)	Truck bombing	168	+900
1995	Navaly (Sri Lanka)	Bombing in church	125	+200
1994	Buenos Aires (Argentina)	Suicide bombing	86	+300
1994	Sarajevo (Bosnia & Herzegovina)	1994 Sarajevo market mortar bombing	68	+140
1993	Bombay (India)	1993 Bombay car bombings	257	+710
1993	New York (USA)	1993 World Trade Center truck bomb.	6	+1000
1992	Buenos Aires (Argentina)	Suicide bombing	22	+350
1992	Lima (Peru)	Truck bombings	25	+150
1991	Colombo (Sri Lanka)	Car bombing	60	85

1991	Rudrapur (India)	Rudrapur bombings	41	140
1990	Bogotá (Colombia)	Car bombings	26	+180
1989	Ténéré (Niger)	UTA Flight 772 bombing	170	0
1989	Bogotá (Colombia)	Truck bombing	+40	+800
1988	Lockerbie (UK)	Pan Am Flight 103 bombing	270	0
1987	Colombo (Sri Lanka)	Car bombing	113	-
1986	Damascus (Syria)	Car bombings	144	-
1986	Arar (Saudi Arabia)	Iraqi Airways Flight 163 bombing	63	53
1985	Atlantic Ocean (Ireland)	Air India Flight 182 bombing	329	0
1985	Beirut (Lebanon)	Car bombing	80	+170
1984	Teheran (Iran)	Teheran train station bombing	18	+300
1984	Florence (Italy)	Florence train 904 bombing	15	267
1983	Beirut (Lebanon)	Beirut barracks truck bombings	307	75
1983	Jebel Ali (United Arab Emirates)	Gulf Air Flight 771 bombing	112	0
1982	Tyre (Lebanon)	Tyre headquarters truck bombing	+90	+50
1981	Damascus (Syria)	1981 Azbakiyah bombing	64	+100
1981	Beirut (Lebanon)	Suicide bombing	61	110
1980	Bologna (Italy)	Bologna train station bombing	85	+200
1980	Munich (Germany)	1980 Oktoberfest bombing	13	215
1979	Madrid (Spain)	Airport and train station bombings	7	+100
1978	Beirut (Lebanon)	Building bombing	175	+80
1976	Al Qaysumah (Saudi Arabia)	Middle East Airlines Flight 438 bombing	81	0
1976	Bridgetown (Barbados)	Cubana Flight 455 bombing	73	0
1974	Ionian Sea (Greece)	TWA Flight 841 bombing	88	0
1974	Phan Rang (Vietnam)	Air Vietnam Flight 706 bombing	75	0
1973	Lake Baikal (USSR)	Aeroflot Tupolev Tu-104B bombing	82	0
1973	London (UK)	1973 Old Bailey car bombing	1	+200
1972	Belfast (UK)	Bloody Friday bombings	9	130
1969	Milan (Italy)	Piazza Fontana bombing	13	+100
1967	Rhodes (Greece)	Cyprus Airways Flight 284 bombing	66	0
1961	Paris (France)	1961 Vitry-Le-François train bombing	28	+100
1960	Havana (Cuba)	La Coubre bombings	+75	+200
1948	Mandatory Palestine (British mandate)	Truck bombing	58	+140
1940	Mandatory Palestine (British mandate)	King David Hotel bombing	91	+45
1925	Sofia (Bulgaria)	St Nedelya Church bombing	150	+500
1921	Bolgrad (Romania)	Bolgrad palace bombing	100	-
1920	New York (USA)	Wall Street horse-wagon bombing	38	+300
1910	Los Angeles (USA)	Los Angeles Times bombing	21	+100
1886	Chicago (USA)	Haymarket Affair bombing	+10	+120
1867	Clerkenwell (UK)	Clerkenwell prison explosion	12	120
1858	Paris (France)	Bombing attempt against Napoleon III	8	+140

As evidenced in Table 4.3, the casualties caused by IEDs have extraordinarily increased for the last decades, particularly in war zones. Actually, in the last two decades more than 70% of terrorist bombings have been perpetrated in Iraq, Afghanistan, Pakistan and Syria. On average, a terrorist bombing occurs in any of these countries every day. In addition, a graphical plot of the casualties caused by the deadliest terrorist bombing per year (Figure 4.3) clearly evidences the increase of cruelty of terrorist bombings for the last decades.

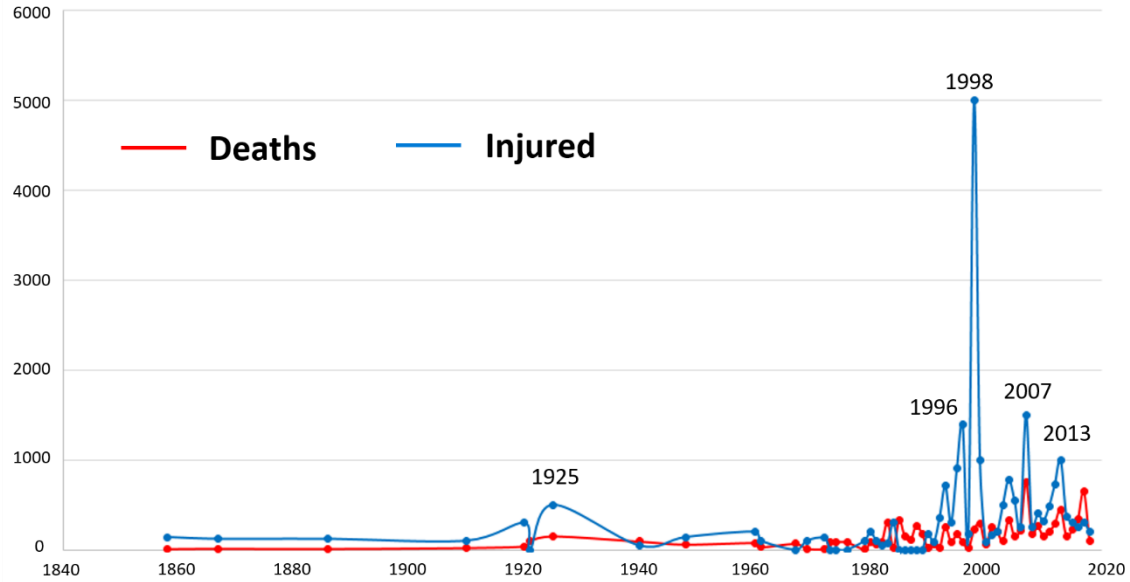

Figure 4.3. Graphical plot of the casualties (deaths and injured) caused by the deathliest terrorist bombing per year.

Despite the calmer situation outside of Middle East countries, no country is totally protected from terrorist attacks. Terrorism phenomenon transcends any geopolitical border in such a way that non-war countries are also affected by terrorist bombings. Regarding Europe, terrorism has also become a major concern for decades [42-46], as evidenced in Table 4.4, which gathers the terrorist bombings perpetrated in Europe which killed more than 10 people or injured more than fifty [42-46].

Table 4.4. Terrorist bombings perpetrated in Europe that killed more than 10 people or injured more than fifty [42-46]. Border European countries (Russia, Turkey, Armenia, Georgia and Azerbaijan) are included. No terrorist attacks perpetrated with only firearms or hijacked vehicles are considered. However, some terrorist attacks were committed by combining vehicles, firearms and IEDs. Every incident was reported in either BBC News, RTE News, France 24 News, CNN, New York Times, The guardian, Sky News, Time, Reuters, Antiwar, El Pais, El Mundo, The Moscow Times, Hürriyet Daily News or The Daily Telegraph.

Year	Location	Terrorist bombing	Total Deaths	Total Injured
2017	Barcelona (Spain)	Barcelona attacks (vehicle attack + bombing)	24	153
2017	Manchester (UK)	Manchester Arena bombing	23	+500
2017	St Petersburg (Russia)	2017 Saint Petersburg metro bombing	16	64
2016	Kayseri (Turkey)	2016 Kayseri car bombing	15	56
2016	Istanbul (Turkey)	Istanbul suicide + car bombings	48	166
2016	Diyarbakir (Turkey)	Diyarbakir car bombing	11	+100
2016	Şemdinli (Turkey)	2016 Şemdinli bombing	16	27
2016	Cizre (Turkey)	Cizre car bombing	11	78
2016	Gaziantep (Turkey)	Gaziantep suicide bombing	57	66
2016	Elazig (Turkey)	Elazig car bombing	11	217
2016	Istanbul (Turkey)	Atatürk Airport attack (shooting + suicide bombings)	48	+230
2016	Istanbul (Turkey)	June 2016 Istanbul bus bombing	13	+50
2016	Greece	EgyptAir flight 804 bombing	66	0
2016	Dürümlü (Turkey)	May 2016 Dürümlü bombing	16	23
2016	Brussels (Belgium)	Brussels Airport suicide bombings	35	340
2016	Ankara (Turkey)	March 2016 Ankara car bombing	38	125
2016	Ankara (Turkey)	February 2016 Ankara car bombing	30	60
2016	Istanbul (Turkey)	January 2016 Istanbul bombing	10	15
2015	Paris (France)	2015 Paris attacks (shooting + suicide bombings)	137	+400
2015	Egypt-Russia	Metrojet Flight 9268 bombing	224	0
2015	Ankara (Turkey)	2015 Ankara suicide bombings	+100	+500
2015	Suruç (Turkey)	2015 Suruç suicide bombing	34	104
2015	Diyarbakir (Turkey)	2015 Diyarbakir rally bombings	5	+100
2013	Volgograd (Russia)	2013 Volgograd suicide bombings	34	85
2013	Cilvegözü (Turkey)	Cilvegözü car bombing	13	28
2013	Reyhanli (Turkey)	Reyhanli car bombings	52	140
2012	Bingol (Turkey)	Bingol suicide bombing + shooting	22	+70
2012	Gaziantep (Turkey)	Gaziantep car bombing	9	+60
2012	Makhachkala (Russia)	2012 Makhachkala suicide bombings	+13	+100
2011	Liège (Belgium)	Liège shooting and grenades bombing	7	125
2011	Oslo & Utøya (Norway)	2011 Norway attacks (shooting + car bombing)	77	+315
2011	Makhachkala (Russia)	2011 Makhachkala car bombings	+3	+120
2011	Minsk (Belarus)	2011 Minsk metro station bombing	15	+200
2011	Domodedovo (Russia)	Domodedovo International Airport bombing	37	173
2010	Hakkâri (Turkey)	Hakkâri bus bombing	10	3
2010	Vladikavkaz (Russia)	2010 Vladikavkaz market bombing	18	173
2010	Kizlyar (Russia)	Kizlyar car bombing	14	37

2010	Moscow (Russia)	Moscow metro suicide bombing	40	+100
2009	Bologoye (Russia)	Nevsky Express train bombing	26	100
2009	Nazran (Russia)	Nazran police station bombing	25	164
2009	Burgos (Spain)	Burgos car bombing	0	65
2008	Vladikavkaz (Russia)	2008 Vladikavkaz market bombing	12	40
2008	Istanbul (Turkey)	2008 Istanbul market bombing	17	154
2008	Diyarbakir (Turkey)	Diyarbakir car bombing	5	110
2007	Tolyatti (Russia)	Tolyatti bus bombing	8	+50
2007	Hakkâri (Turkey)	2007 Hakkâri bombing + shooting	12	32
2007	Moscow (Russia)	Train derailment by bombing	0	60
2007	Ankara (Turkey)	2007 Ankara suicide bombing	9	+120
2006	Madrid (Spain)	2006 Madrid airport bombing	2	52
2006	Moscow (Russia)	2006 Moscow market bombing	13	47
2005	London (UK)	2005 London metro suicide bombings	56	+700
2005	Makhachkala (Russia)	2005 Makhachkala Rus bombing	11	25
2004	Beslan (Russia)	Beslan school massacre (shooting + suicide bombings)	334	+780
2004	Moscow (Russia)	August 2004 Moscow metro bombing	10	50
2004	Tula and Rostov (Russia)	Russian aircraft bombings (suicide bombing inside plane)	90	0
2004	Grozny (Russia)	Grozzny stadium bombing	+10	+100
2004	Madrid (Spain)	11M train bombings	193	+2050
2004	Moscow (Russia)	February 2004 Moscow metro bombing	40	+100
2003	Stavropol (Russia)	Stavropol train bombing	47	+170
2003	Mozdok (Russia)	Mozdok hospital bombing	40	76
2003	Istanbul (Turkey)	2003 Istanbul truck bombings	57	+700
2003	Tushino (Russia)	2003 Tushino suicide bombing	15	+60
2003	Znamenskoye (Russia)	2003 Znamenskoye bombing	59	200
2003	Iliskhan Yurt (Russia)	Suicide bombings	19	78
2002	Grozny (Russia)	2002 Grozny truck bombing	83	210
2002	Vantaa (Finland)	Myyrmanni shopping mall bombing	7	166
2002	Kaspiysk (Russia)	Kaspiysk bombing	44	+130
2001	Madrid (Spain)	2001 Madrid car bombing	0	99
2001	Mineralnye Vody (Russia)	2001 Chechnya bombings	18	86
2001	Podujevo (Yugoslavia)	Podujevo bus bombing	12	40
2000	Chechnya (Russia)	Car bombing	19	30
2000	Madrid (Spain)	2000 Madrid car bombing	3	66
2000	Moscow (Russia)	2000 Moscow street bombing	12	+90
2000	Chechnya (Russia)	July 2000 Chechnya suicide bombings	54	+80
1999	Across Russia	Russian apartment bombings	293	+1000
1999	London (UK)	1999 London bombings	3	+125
1999	Vladikavkaz (Russia)	1999 Vladikavkaz market bombing	64	168
1999	Istanbul (Turkey)	Blue market truck bombings	13	5
1998	Makhachkala (Russia)	1998 Makhachkala car bombing	17	80

1998	Omagh (UK)	Omagh market bombing	29	+210
1996	Paris (France)	1996 Paris metro bombing	4	170
1996	Moscow (Russia)	Moscow cemetery bombing	13	30
1996	Manchester (UK)	Manchester car bombing	0	+200
1996	London (UK)	1996 Docklands truck bombing	2	+200
1995	Grozny (Chechnya)	1996 Grozny car bombing	11	+60
1995	Sarajevo (Bosnia & Herzegovina)	1995 Sarajevo Mortar bombing	43	75
1995	Paris (France)	1995 Paris metro bombing	8	+100
1994	Bagratashen (Armenia)	Bagratashen market bombing	12	46
1994	Baku (Azerbaijan)	Baku metro bombings	27	+90
1994	Sarajevo (Bosnia & Herzegovina)	1994 Sarajevo market mortar bombing	68	+140
1993	Belfast (UK)	1993 Belfast suicide bombing	10	57
1993	Warrington (UK)	Warrington Bridge street bombings	2	56
1992	Manchester (UK)	Manchester car bombings	0	65
1992	London (UK)	1992 London truck bombing	3	91
1991	Dagestan (Soviet Union)	Train bombing	11	8
1991	Vic (Spain)	Cuartel Vic bombing	10	+50
1990	Khanlar (Azerbaijan)	Khanlar bus bombing	+15	+20
1989	Deal (UK)	Deal barracks bombing	11	22
1988	Aegina (Greece)	City of Poros ship attack	10	+80
1988	Lockerbie (UK)	Pan Am Flight 103 bombing	270	0
1987	Zaragoza (Spain)	Casa cuartel Zaragoza bombing	11	88
1987	Enniskillen (UK)	Enniskillen bombing	12	61
1987	Barcelona (Spain)	Barcelona Hipercor bombing	21	+45
1986	Paris (France)	September 1986 Paris bombings	12	+180
1986	Madrid (Spain)	1986 Madrid car bombing	12	+50
1986	Berlin (Germany)	Berlin discotheque bombing	3	230
1985	Rome and Vienna (Italy/Austria)	1985 Rome and Vienna airport attacks	19	+130
1985	Atlantic Ocean (Ireland)	Air India Flight 182 bombing	329	0
1985	Madrid (Spain)	El Descanso restaurant bombing	18	82
1984	Florence (Italy)	Florence Train 904 bombing	15	267
1983	London (UK)	1983 London car bombing	6	90
1983	Paris (France)	1983 Orly airport bombing	8	55
1982	Ankara (Turkey)	1982 Ankara shooting and bombing	10	+70
1982	Paris (France)	1982 Paris car bombing	1	60
1982	Ballykelly (UK)	Droppin Well bombing	17	30
1982	London (UK)	1982 London park bombings	11	50
1981	Antwerp (Belgium)	1981 Antwerp truck bombing	3	+100
1980	Munich (Germany)	1980 Oktoberfest bombing	13	215

1980	Bologna (Italy)	1980 Bologna central station bombing	85	+200
1979	Warrenpoint (UK)	Warrenpoint roadside bombs	19	7
1979	Madrid (Spain)	Airport and train station bombings	7	+100
1978	County Down (UK)	County Down Restaurant bombing	12	30
1975	London (UK)	October-November bombings	5	+70
1975	London (UK)	London Hilton bombing	2	63
1975	Belfast (UK)	1975 Belfast bombing	5	+50
1974	Birmingham (UK)	Birmingham pub bombing	21	182
1974	Guilford (UK)	Guilford pub bombing	5	+50
1974	Madrid (Spain)	"Rolando" cafeteria bombing	13	+70
1974	Ionian Sea (Greece)	TWA Flight 841 bombing	88	0
1974	San Benedetto Val di Sambro (Italy)	Italicus Express train bombing	12	48
1974	Brescia (Italy)	Piazza della Loggia bombing	8	+90
1974	Dublin & Monaghan (Ireland)	1974 Dublin Car bombings	35	+300
1974	Yorkshire (UK)	M62 coach bombing	12	39
1973	Rome (Italy)	Pan Am Flight 110 bombing	34	22
1973	Lake Baikal (USSR)	Aeroflot Tupolev Tu-104B bombing	82	0
1973	Milan (Italy)	1973 Milan Grenade bombing	4	52
1973	London (UK)	1973 Old Bailey car bombing	1	+200
1972	Belfast (UK)	Bloody Friday bombings	9	130
1972	Srbská Kamenice (Czechoslovakia)	Yugoslavian Airlines Flight 364 bombing	27	1
1971	Belfast (UK)	December 1971 Belfast bombings	19	36
1970	Gioia Tauro (Italy)	1970 Gioia Tauro train bombing	6	66
1970	Belfast (UK)	July 1970 Belfast bombings	6	+55
1970	Switzerland	Swissair Flight 330 bombing	47	0
1969	Milan (Italy)	Piazza Fontana bombing	13	+100
1967	Rhodes (Greece)	Cyprus Airways Flight 284 bombing	66	0
1961	Paris (France)	1961 Vitry-Le-François train bombing	28	+100
1939	Coventry (UK)	Coventry bombing	5	70
1931	Biatorbágy (Hungary)	Hungary train bombing	22	+20
1925	Sofia (Bulgaria)	St Nedelya church bombing	150	+500
1921	Bolgrad (Romania)	Bolgrad palace bombing	100	-
1906	Aptekarsky Island (Russia)	Aptekarsky bombings	28	-
1897	London (UK)	Metropolitan train bombing	1	60
1896	Barcelona (Spain)	Barcelona Corpus procession bombing	12	44
1893	Barcelona (Spain)	Gran Teatre del Liceu bombing	20	+40
1867	Clerkenwell (UK)	Clerkenwell prison explosion	12	120
1858	Paris (France)	Bombing attempt against Napoleon III	8	+140
1835	Paris (France)	Boulevard du temps bombing	18	+36
1800	Paris (France)	Plot of the rue Saint-Nicaise	22	+50

Approximately, along the 21st century, a terrorist bombing of such magnitude (>10 deaths / >50 injured) occurs in Europe every 90 days, despite the prevention and intelligence operations accomplished by police counterterrorism experts.

As previously evidenced for worldwide terrorist bombings, a graphical plot of the casualties caused by terrorist bombings in Europe per year (Figure 4.4) also evidences the increase of cruelty of terrorist bombings in Europe for the last decades.

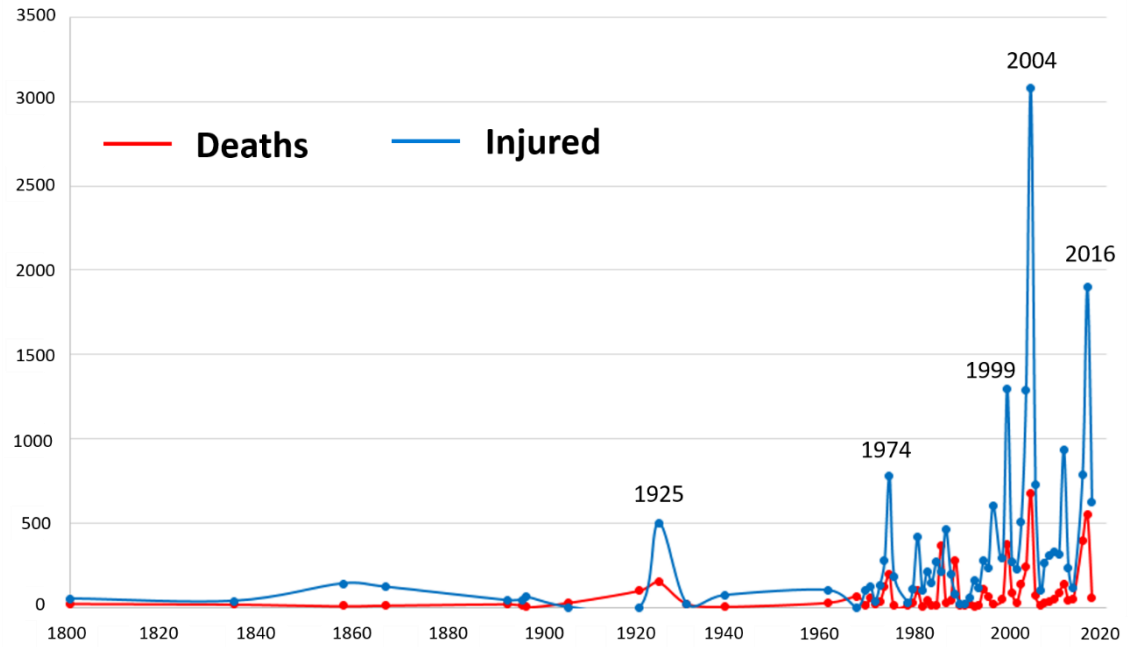

Figure 4.4. Graphical plot of the casualties (deaths and injured) caused by terrorist bombings in Europe (gathered in Table 4.4) per year.

Regarding the european countries that have suffered the most from terrorist bombings, Scheme 4.3 statistically displays the percentage of number of terrorist bombings, and casualties (deaths and injured) per european country from the information compiled in Table 4.4. As evidenced in the three charts, Russia, UK, Turkey and Spain rank the four first positions, followed by France, Italy, Greece and Ireland.

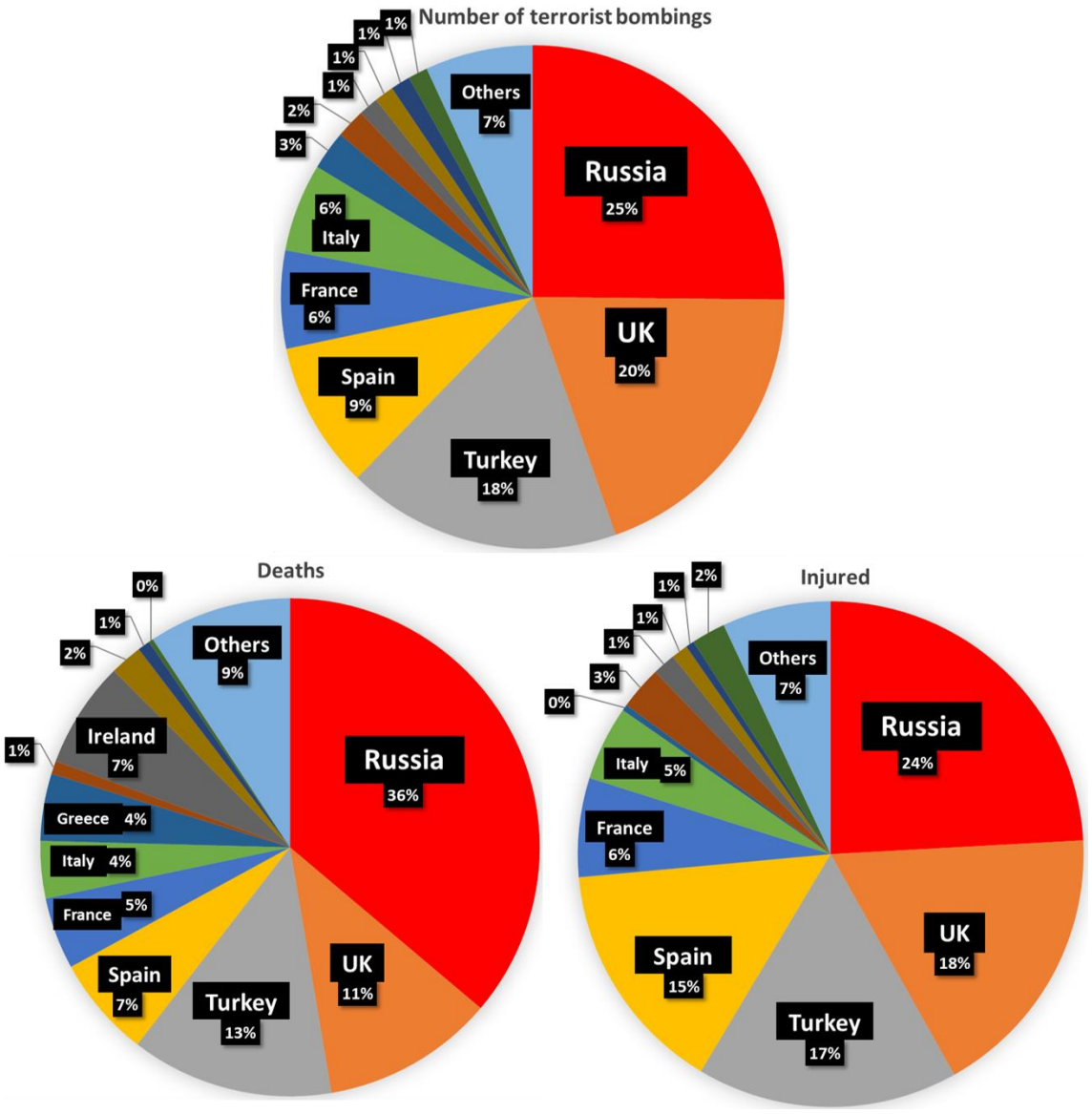

Scheme 4.3. 2D Pie Charts summarizing the percentage of number of terrorist bombings, deaths or injured people (from Table 4.4) per European country.

One of the reasons why the terrorist use of explosives has exponentially increased during the 20th and 21st centuries is the manifest availability of explosives everywhere and for everyone. In fact, explosives are accessible for everyone who has internet connection and has learnt to read. In this respect, I will always keep in mind a real case an EOD police described me once, in which he had have to intervene in a primary school after receiving the emergency phone call of a teacher explaining that the science project of one of their 10 years-old students had been the synthesis of 100 g of TATP explosive. EOD finally detonated the TATP powder directly in the school under safe conditions. EOD certified that the explosive was completely functional. The child explained

that he ignored the destruction power of TATP and he had only found the recipe on the internet as an interesting chemistry project. If an ignorant 10 years-old child is capable today of synthesizing 100 g of TATP, what will an evil and resourceful adult not be able to do?

Conclusions

Though three different types of detonations exist (physical, chemical and nuclear explosions), the term explosives typically refers to chemical explosives.

Regarding the historical contextualization of chemical explosives, only black powder explosive was known before the 19th century. Between 1800 and 1900, a high number of powerful explosives were discovered including dynamite (1867), TNT (1891), PETN (1894) and TATP (1895). After 1900, some other powerful explosives were also developed including ammonal and RDX (1910s) and ANFO (1956).

Chemical explosives are usually classified in literature according to either the velocity of detonation (high/low energy explosives) or the use/application (military/commercial/homemade explosives). However, an efficient way to classify explosives from the point of view of their posterior analytical determination is according to their chemical composition, newly proposed in this Thesis. According to the proposed classification, explosives are first classified into single explosives or oxidizing-fuel explosive mixtures. Secondly, single explosives are classified into inorganic or organic explosives; whereas explosive mixtures further classified according to their oxidizer (nitrate, chlorate or perchlorate based explosive mixture). Within organic explosives, they might be further sub-classified into nitro-explosives, peroxide explosives and others. Within nitrate-based explosive mixtures, they might be further sub-classified into AN-based and Non-AN based explosive mixtures. Finally, nitro-explosives can be also sub-classified into nitro-aromatic, nitro-aliphatic, nitramine and nitrate ester explosives.

Explosives have been widely used to commit terrorist attacks for the 20th and 21st centuries. Particularly, the number of terrorist bombings and the number of casualties have extraordinarily increased for the last decades. This increase

is, in part, due to the ease of obtaining/homemaking explosives and the large variety of powerful explosives that have been developed since the 19th century.

References

[1] T.L. Davis, The chemistry of powder and explosives, Angriff Press, 1943.

[2] J. Akhavan, The chemistry of explosives, 2nd edition, RSC Paperbacks, 2004.

[3] M. López-López, Infrared and Raman spectroscopy for the identification of explosives and related compounds, PhD Thesis, Universidad de Alcalá, 2013.

[4] J.P. Agrawal, High energy materials: Propellants, explosives and pyrotechnics, Wiley, 2010.

[5] R. Meyer, J. Köhler, A. Homburg, Explosives, 6th edition, Wiley, Weinheim, 2007.

[6] J.B. Ledgard, The preparatory manual of explosives. A laboratory manual, 2nd edition, Seattle, 2003.

[7] M. Marshall, J.C. Oxley, Aspects of explosives detection, Elsevier, Oxford, 2009.

[8] J.T. Thurman, Practical bomb scene investigation, 3rd edition, CRC Press, Taylor&Francis, Boca Raton, 2017.

[9] A. Beveridge, Forensic investigation of explosions, Taylor&Francis, 1998.

[10] M.A. Fernández de la Ossa, Electrophoretic and imaging approaches for explosive detection, PhD Thesis, Universidad de Alcalá, 2014.

[11] P.W. Cooper, Explosives engineering, Wiley, 1996.

[12] G.B. Manelis, Thermal decomposition and combustion of explosives and propellants, CRC Press, Tayor&Francis, London, 2003.

[13] P. Persson, R. Holmberg, J. Lee, Chapter 3: Explosives; in, P. Persson, R. Holmberg, J. Lee, Rock blasting and explosives engineering, CRC Press LLC, Boca Raton, USA, 1994, pags. 55-86.

[14] N. Kubota, Propellants and explosives. Thermochemical aspects of combustion, 2nd edition, Wiley, Weinheim, 2007.

[15] A.S. Shteinberg, Fast reactions in energetic materials. High-temperature decomposition of rocket propellants and explosives, Springer, 2008.

[16] M.D. Reboiras, Capítulo 22. Química nuclear, in, M.D. Reboiras, Química. La ciencia básica, Paraninfo, 2006.

[17] M.E. Johll, Bombas sucias y terrorismo nuclear, en: M.E. Johll, Química e investigación criminal, Reverté, 2008, pags. 356-383.

[18] G. King, Dirty bomb: weapons of mass disruption, Chamberlain Bros, Penguin Group, 2004.

[19] J. Revill, Improvised explosive devices. The paradigmatic weapon of new wars, Palgrave Macmillan, 2016.

[20] W.A. Tilden, Chemical Discovery and invention in the Twentieth Century, 1917.

[21] T. Holmberg, M. Sewell (2005). "The Infernal Machine". The Napoleon Series - Research subjects: miscellaneous. www.napoleon-series.org. Retrieved 2006-03-23.

[22] J.B. Ledgard, The preparatory manual of black powder and pyrotechnics, 2006.

[23] C. Martín-Alberca, Analytical solutions for the forensic analysis of improvised incendiary devices and consumer fireworks, PhD Thesis, Universidad de Alcalá, 2015.

[24] J.A. Conkling, Chemistry of pyrotechnics. Basic principles and theory, Marcel Dekker Inc., 1985.

[25] J. Donner, A professional's guide to pyrotechnics: Understanding and making exploding fireworks, Paladin Press, 1997.

[26] E. Howard, "On a New Fulminating Mercury". Philosophical Transactions of the Royal Society of London 90 (1) (1800) 204-238.

[27] R. Matyás, J. Pachman, Primary explosives, Springer, 2013.

[28] Lettre de M. Schoenbein à M. Dumas, Comptes rendus hebdomadaires des séances de l'Academie des sciences, 23 (1846) 678-679.

[29] H. Braconnot. "De la transformation de plusieurs substances végétales en un principe nouveau". Annales de Chimie et de Physique. 52 (1833) 290-294.

[30] T.J. Pelouze, "Sur les produits de l'action de l'acide nitrique concentré sur l'amidon et le ligneux", Comptes rendus. 7 (1838) 713-715.

[31] J.B. Dumas, Traité de Chimie Appliquée aux Arts. 6. Paris: Bechet Jeune (1843) p. 90. Il.

[32] A. Sobrero, "Sur plusieur composés détonants produits avec l'acide nitrique et le sucre, la dextrine, la lactine, la mannite et la glycérine", Comptes rendus, 24 (1847) 247-248.

[33] M.J. Schaack, Anarchy and anarchists: A history of the red terror and the social revolution in America and Europe. Communism, socialism, and nihilism in doctrine and in deed. The Chicago Haymarket conspiracy, and the detection and trial of the conspirators. F.J. Schulte & company, 1889.

[34] Haymarket and May Day. Encyclopedia of Chicago. http://www.encyclopedia.chicagohistory.org/pages/571.html

[35] S. Harrison, The 1910 bombing of the Los Angeles Times. Los Angeles Times. Photography. Framework. 2011. http://framework.latimes.com/2011/09/30/the-1910-bombing-of-the-los-angeles-times/#/0

[36] Twenty-One Killed and More Injured In the Dynamited 'Times' Building, Los Angeles Times, October 2, 1910.

[37] The Crime of the Century, Los Angeles Times, October 16, 1910.

[38] B. Gage, The day Wall Street exploded: A story of America in its first age of terror. Oxford University Press, 2009.

[39] E. Morton, The Wall Street Bombing: Low-Tech Terrorism in Prohibition-Era, New York, 2014,

http://www.slate.com/blogs/atlas_obscura/2014/09/16/the_1920_wall_st_bombing_a_terrorist_attack_on_new_york.html

[40] Every terrorist attack worldwide over 20 years in maps - Business Insider. http://www.businessinsider.com/global-terrorist-attacks-past-20-years-in-maps-2017-5

[41] Terrorism. Our world in data. https://ourworldindata.org/terrorism

[42] Global Terrorism Database. http://www.start.umd.edu/gtd/

[43] Wikipedia, the free encyclopedia. https://en.wikipedia.org/

[44] 46 years of terrorist attacks in Europe. The Washington Post. https://www.washingtonpost.com/graphics/world/a-history-of-terrorism-in-europe/

[45] People killed by terrorism per year in western Europe 1970-2015. Datagraver. http://www.datagraver.com/case/people-killed-by-terrorism-per-year-in-western-europe-1970-2015

[46] Terrorism in Europe - Statistics & Facts. https://www.statista.com/topics/3788/terrorism-in-europe/

[47] W. Gowland, R. Messel, J. Spiller, Obituary notices: Frederic Just Claudet, 1826-1906; Hermann Johann Philipp Sprengel, 1834-1906; George Bowdler Buckton, 1818–1905; J. Chem. Soc., Trans., 91 (1907) 660-665.

[48] M. Brower, Developing Animals: Wildlife and Early American Photography. University of Minnesota Press, 2011.

[49] I. Tolmachev, A brief history of photographic Flash, 2011, https://photography.tutsplus.com/articles/a-brief-history-of-photographic-flash--photo-4249

[50] Department of the U.S. Army, Explosives and demolitions, U.S. Army, Washington, 2007.

[51] M.A. Cook, The science of high explosives, Reinhold Pub. Corp., 1958.

[52] B.T. Fedoroff, O.E. Sheffield, Encyclopedia of explosives and related items, U.S. Army research, New Jersey, 1969.

[53] M. Dzikansky, G. Kleiman, R. Slater, Terrorist Suicide Bombings: Attack Interdiction, Mitigation, and Response, CRC Press, 2012.

[54] J.P. Agrawal, R.D. Hodgson, Organic chemistry of explosives, Wiley, 2007.

[55] Encyclopedia Britannica. https://www.britannica.com/

[56] J. Petes, R. Miller, F. McMullan, User's Guide and History of ANFO (Ammonium Nitrate/Fuel Oil) as a Nuclear Weapons Effect Simulation Explosive, 1983.

[57] W.M. Haynes, Geophysics, astronomy and acoustics, in, W.M. Haynes, Handbook of chemistry and physics, 96th edition, CRC Press, 2015. Pages 1-51.

[58] W. Benenson, J.W. Harris, H. Stocker, H. Lutz, Acoustics; in, W. Benenson, J.W. Harris, H. Stocker, H. Lutz, Handbook of physics, 4th edition, Springer, 2000. Pages 311-334.

[59] Collins Dictionary. https://www.collinsdictionary.com/

[60] National research council, Countering the threat of improvised explosive devices, The national academic press, 2007.

[61] J. Yinon, Counterterrorist detection techniques of explosives, Elsevier, Amsterdam, 2007.

[62] Principles of improvised explosive devices, Paladin Press, 1984.

[63] E. Andrews, The Mysterious Wall Street Bombing, 95 Years Ago, 2015, https://www.history.com/news/the-mysterious-wall-street-bombing-95-years-ago

[64] I. Jones, Malice Aforethought: The history of booby traps from World War One to Vietnam, Greenhill, 2004.

Chapter 5. Spectroscopic Characterization of Explosives and Energetic Salts

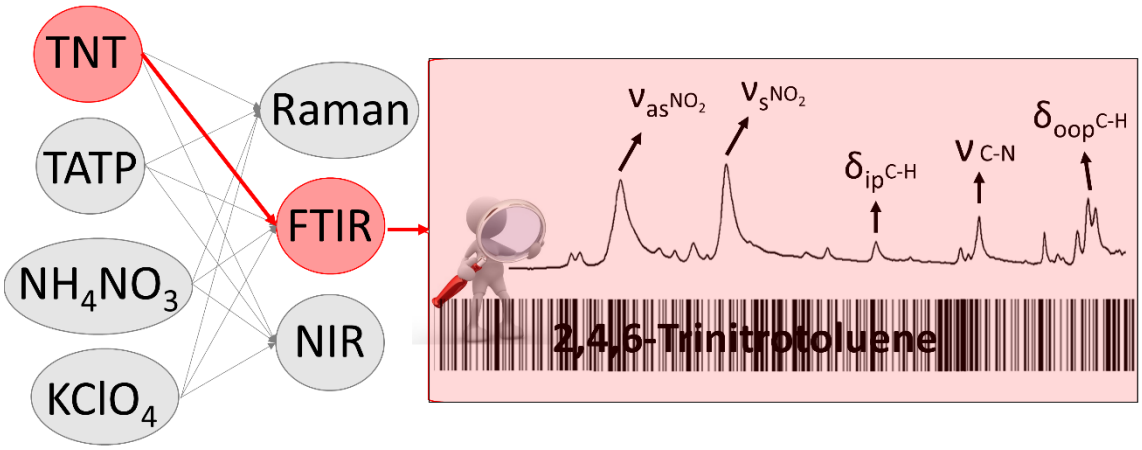

Main sources:

Félix Zapata, C. García-Ruiz, Determination of nanogram microparticles from explosives after real open-air explosions by confocal Raman microscopy, *Anal. Chem.* 88 (2016) 6726-6733.

Félix Zapata, C. García-Ruiz, The discrimination of 72 nitrate, chlorate and perchlorate salts using IR and Raman spectroscopy, *Spectrochim. Acta A* 189 (2018) 535-542.

Félix Zapata, M. Ferreiro-González, C. García-Ruiz, Interpreting the Near Infrared region of explosives, *Spectrochim. Acta A* 204 (2018) 81-87.

5.1. Infrared and Raman characterization of explosives

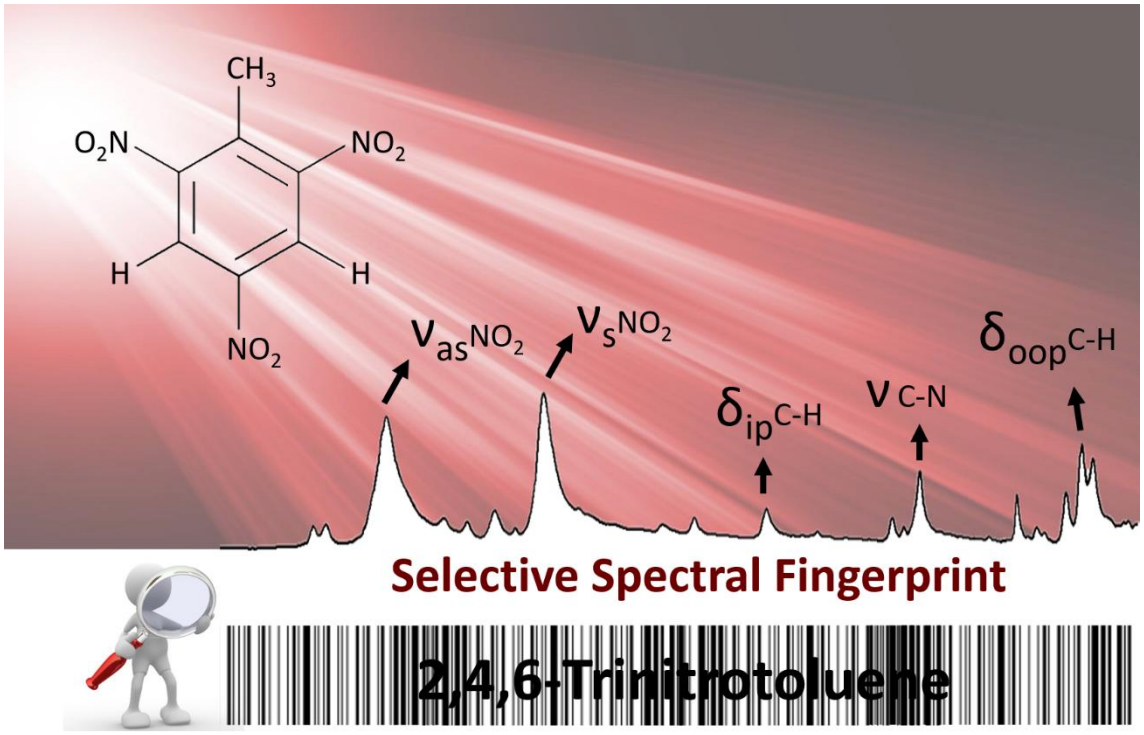

Abstract

The IR and Raman spectra from 2000 to 400 cm^{-1} (*i.e.* spectral fingerprint) of 14 different explosives and smokeless powders were collected and interpreted. Specifically, five single organic explosives (TNT, RDX, PETN, TATP and HMTD), four NC-based smokeless powders composed of NC, NG, NQ and/or DNT; and five oxidizer-fuel explosive mixtures (black powder, dynamite, chloratite, ammonal and ANFO) were studied. The IR/Raman spectra of single organic explosives included those IR/Raman active fundamental molecular vibrations initially examined in their molecular structure. The IR/Raman spectra of NC-based smokeless powders mostly corresponded to NC, except for the triple-base smokeless powder (mostly composed of NQ), whose IR/Raman spectra were dominated by the IR/Raman bands of NQ. In addition, the Raman spectra of some NC-based smokeless powders only displayed fluorescence. Finally, the IR/Raman spectra of oxidizer-fuel explosive mixtures almost exclusively corresponded to the oxidizing salt (potassium nitrate, sodium chlorate or ammonium nitrate), though low intense bands due to the fuel-component were observed in certain explosives.

Introduction

As previously explained, the identification of forensic evidence by non-invasive methodologies is recommended due to the legal and judiciary value of the criminal evidence. Spectroscopic techniques enable a rapid and non-invasive chemical identification of substances. Concretely, IR spectroscopy has been used to characterize chemical compounds for more than a century [1-4]. IR spectroscopy is particularly suitable for the characterization of molecular compounds because of the large number of IR active vibrations in compounds having covalent bonds. As previously explained in Section 0, only such vibrations that modify the molecular dipole moment are IR active. Positively, explosive compounds, either pure organic molecules or inorganic mixtures, contain covalent bonds whose IR active vibrations define their IR spectrum [5, 6]. The correlation between the IR spectrum and the chemical composition of explosives is studied in this chapter. In addition, the capability of IR spectroscopy to unequivocally identify each explosive is examined.

Raman spectroscopy, like IR spectroscopy, has been largely used to characterize chemical molecular compounds, since they present a significant number of molecular vibrations that modify the polarizability of the molecule (*i.e.* Raman active vibrations) [1-3]. Such vibrations are also common in explosive compounds, either pure organic molecules or inorganic mixtures [5]. As previously explained in Section 0, different information is obtained by IR and Raman spectroscopy because Raman active vibrations are not the same as IR active vibrations. Thus, the correlation between the Raman spectrum and the chemical composition of explosives, and the capability of Raman spectroscopy to unequivocally identify each explosive are also studied in this chapter.

IR and Raman spectroscopy are known to be complementary techniques since molecular vibrations may be IR active (only), Raman active (only) or IR-Raman active [1-3]. In this respect, the IR/Raman activity of a particular vibration can be tracked by the presence or absence of the corresponding band in the IR and Raman spectra, respectively. Such IR-Raman comparisons are highly informative for theoretical studies about the symmetry of molecular vibrations and the structural conformation of molecules and crystalline states [3, 4]. However, such comprehensive IR/Raman mutual comparison is out of the scope of this thesis, whose objective seeks evaluating the capability of either IR or Raman spectroscopy to unequivocally identify explosive substances.

When tackling the IR/Raman characterization of any chemical compound, the first basic step (prior to the collection of the spectra) is the familiarization with all the possible molecular vibrations that may take place in the corresponding molecule according to its covalent bonds. In order to facilitate this task, the chemical structure of studied explosives is displayed in Figure 5.1.

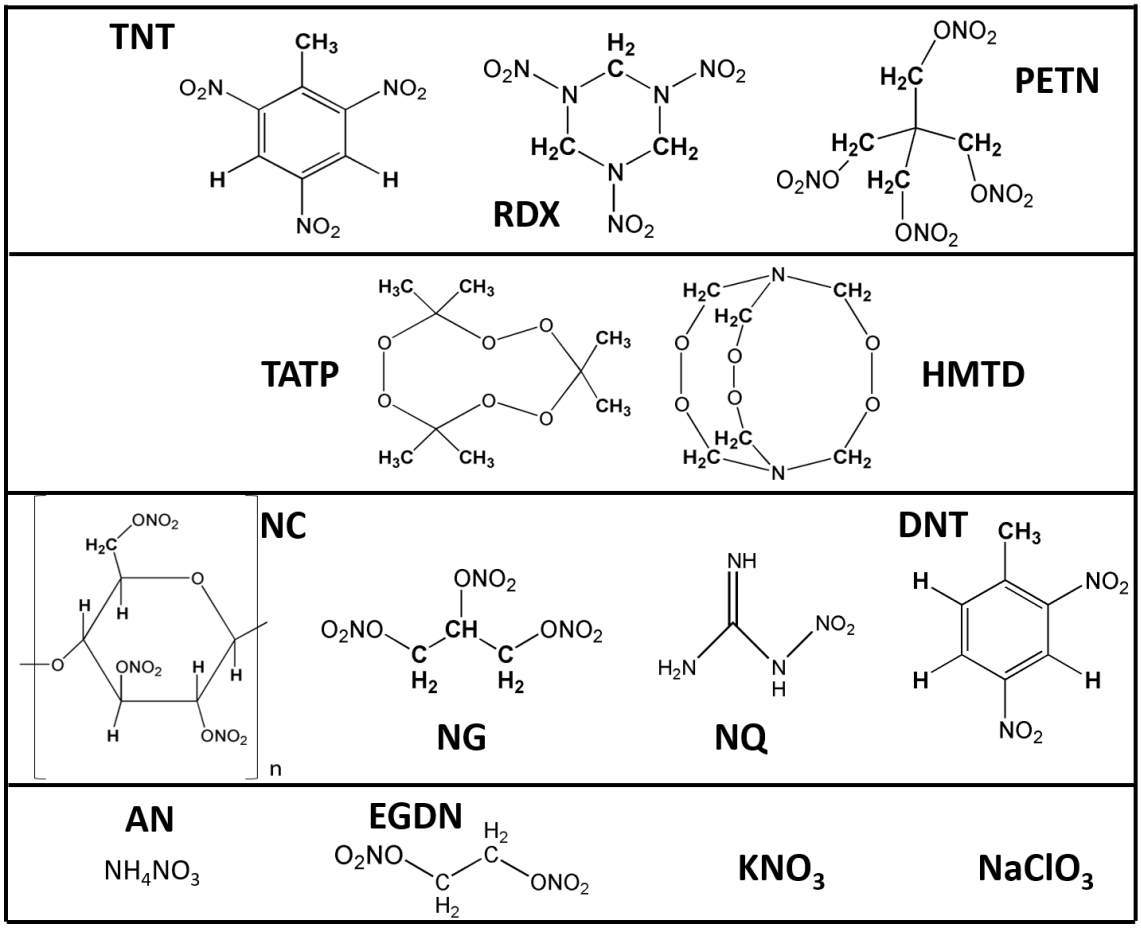

Figure 5.1. Chemical structures/formula of TNT, RDX, PETN, TATP, HMTD, NC (monomer), NG, NQ, DNT, AN, EGDN, KNO_3 and $NaClO_3$.

For instance, TNT molecule is composed of an aromatic ring, one methyl group and three nitro groups, in such a way that the molecular vibrations of TNT, (and therefore, its IR/Raman bands), will exclusively correspond to either NO_2, CH_3, C-C (aromatic), CH (aromatic), C-N or C-C vibrations. As an example, no bands due to C-O, O-H or N-H vibrations can occur in TNT spectrum. After finding which bonds are involved in the molecular vibrations, the knowledge about the approximate spectral range in which their antisymmetric/symmetric stretching, and in-plane/out-of-plane bending will be located is noticeably useful. To this aim, Table 5.1 summarizes the spectral ranges at which the molecular vibrations (occurring in the studied explosives) normally locate [1, 7].

Table 5.1. Spectral range for the molecular vibrations of studied explosives [1, 7].

Molecular vibration	Explosives	Spectral range (cm^{-1})
N-H st	NQ, AN	3500-3100
ar CH st (C_{sp2})	TNT, DNT	3080-3030
C-H st (C_{sp3})	TNT, RDX, PETN, TATP, HMTD, NC, NG, DNT, EGDN	3000-2840
C=N st	NQ	1690-1540
N-H ip bend	NQ	1660-1550
NO_2 asym st (O-NO_2)	PETN, NC, NG, EGDN	1660-1620
NO_2 asym st (N-NO_2)	RDX, NQ	1640-1520
NO_2 asym st (C-NO_2)	TNT, DNT	1620-1490
ar C-C st	TNT, DNT	1625-1500
CH_2 ip bend	RDX, PETN, HMTD, NC, NG, EGDN	1475-1450
CH_3 ip asym bend	TNT, TATP, DNT	1470-1430
NO_3 asym st	AN, KNO_3	1450-1270
CH_3 ip sym bend	TNT, TATP, DNT	1400-1360
NO_2 sym st (C-NO_2)	TNT, DNT	1390-1310
NO_2 sym st (N-NO_2)	RDX, NQ	1320-1260
NO_2 sym st (O-NO_2)	PETN, NC, NG, EGDN	1290-1270
C-O st	PETN, TATP, HMTD, NC, NG, EGDN	1300-970
ar CH ip bend	TNT, DNT	1250-950
CH_3 oop bend	TNT, TATP, DNT	1250-800
C-C st	TNT, PETN, TATP, NC, NG, DNT, EGDN	1200-800
C-N st	TNT, RDX, HMTD, DNT, NQ	1200-800
NO_3 sym st	AN, KNO_3	1075-1020
N-N st	RDX, NQ	1050-800
O-O st	TATP, HMTD	1000-800
ClO_3 asym st	$NaClO_3$	990-950
ClO_3 sym st	$NaClO_3$	940-900
ar CH oop bend	TNT, DNT	900-650
N-O st (ONO_2)	PETN, NC, NG, EGDN	890-850
N-H oop bend	NQ	850-700
NO_3 oop bend	AN, KNO_3	840-800
CH_2 oop bend	RDX, PETN, HMTD, NC, NG, EGDN	800-700
NO_3 ip bend	AN, KNO_3	780-700
ONO_2 oop bend	PETN, NC, NG, EGDN	770-750
ONO_2 ip bend	PETN, NC, NG, EGDN	710-690
ClO_3 oop bend	$NaClO_3$	630-610
ClO_3 ip bend	$NaClO_3$	500-480

As evidenced in Table 5.1 and previously introduced in Section 0, most of the molecular vibrations are located between 1700 and 600 cm^{-1}, within the renowned fingerprint region. Only the X-H (C-H, N-H, etc.) stretching vibrations are located above this range, specifically between 3500 and 2800 cm^{-1}. In fact, since those vibrations are not exceptionally discriminative, the range 3500-2800 cm^{-1} is normally skipped from the fingerprint region, as also did in this chapter. Multiple X-H bending vibrations take place between 1700 and 600 cm^{-1}, which enable the identification of molecular compounds (without the interpretation of their X-H stretching vibrations).

Experimental section

- Explosives.

A total of 14 different explosives were characterized by IR and Raman spectroscopy, including, TNT, RDX, PETN, TATP, HMTD, single-base smokeless powder, double-base smokeless powder 1, double-base smokeless powder 2, triple-base smokeless powder, black powder, chloratite, dynamite, ANFO and ammonal. Explosives were obtained from TEDAX, the Spanish Explosive Ordnance Disposal (EOD). Table 5.2 summarizes the major composition of each explosive, according to the information provided either by the EOD specialists or the manufacturer.

Table 5.2. Composition of the explosives studied in this work. Information provided by the manufacturer or TEDAX (the Spanish EOD). Regarding explosive mixtures, only major components whose mass percentage is over 10% are indicated.

Explosive	Composition
TNT	2,4,6-Trinitrotoluene (100%)
Plastic explosive (RDX)	Cyclotrimethylene trinitramine (91%)
PETN	Pentaerythritol tetranitrate (100%)
TATP	Triacetone triperoxide (100%)
HMTD	Hexamethylene triperoxide diamine (100%)
Triple-base powder 1	Nitrocellulose (19%) + Nitroguanidine (55%) + Nitroglycerine (18%)
Double-base powder 2	Nitrocellulose (85%) + Dinitrotoluene (10%)
Double-base powder 3	Nitrocellulose (71%) + Nitroglycerine (25%)
Single-base powder 4	Nitrocellulose (94%)
Black powder	Potassium nitrate (75%) + charcoal (15%) + sulfur (10%)
Chloratite	Sodium chlorate (80%) + sugar (10%) + sulfur (10%)
Dynamite	Ammonium nitrate (66%) + ethylene glycol dinitrate (29%)
ANFO	Ammonium nitrate (90%) + diesel (10%)
Ammonal (ANAl)	Ammonium nitrate (85%) + aluminium (15%)

- FTIR Instrumentation.

Explosives were analysed using a Thermo Scientific FTIR Nicolet IS10 spectrometer equipped with smart ITR module for ATR measurements (Figure 5.2) and controlled through the Omnic™ spectroscopy for IR spectroscopy 9 (Waltham, MA, USA). IR spectra were collected from 2000 to 600 cm^{-1}, with a resolution of 4 (data spacing of 0.483 cm^{-1}) and 16 scans. Three replicates were analysed per sample by placing around 0.1 g of explosive on the ATR diamond crystal.

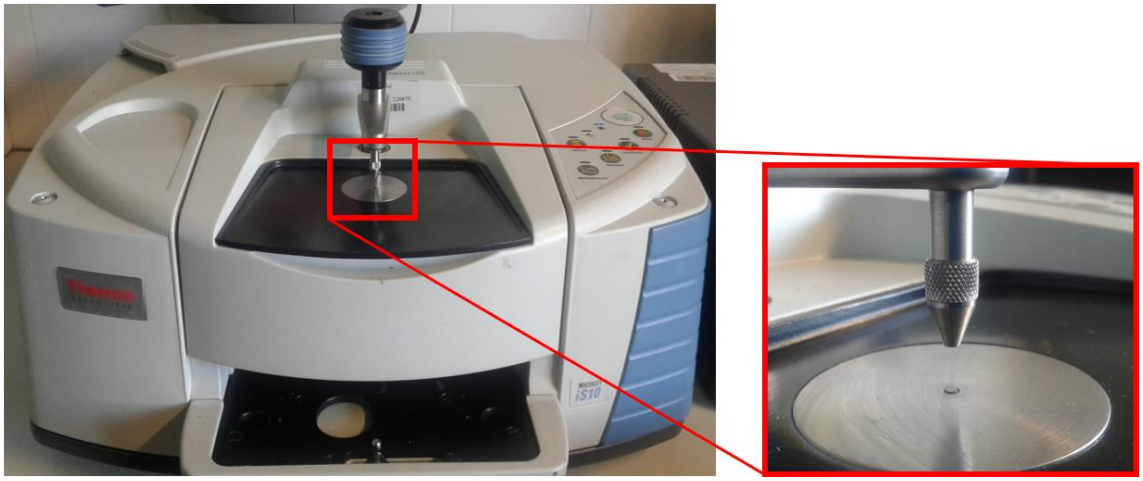

Figure 5.2. FTIR spectrometer equipped with ATR accessory (ATR zoomed).

- Raman Instrumentation.

Raman characterization of explosives was performed with a Thermo Scientific DXR Raman microscope (Figure 5.3) controlled by the Thermo Scientific Omnic for dispersive Raman 8 software (Waltham, MA). Raman spectra were collected using a 780 nm excitation wavelength of 10 mW power, a 400 lines mm^{-1} grating and a 10X microscope objective. The Raman spectra were measured from 2500 to 200 cm^{-1} (with a spectral data spacing of 0.964 cm^{-1}), by accumulating 5 scans of 6 s per scan.

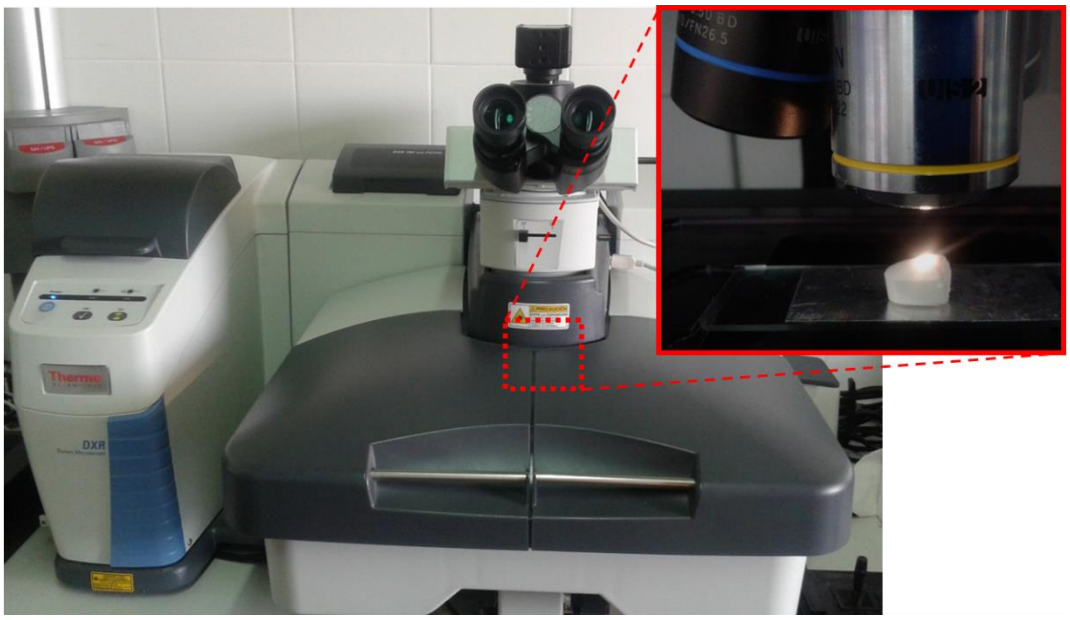

Figure 5.3. Raman spectrometer microscope and magnification objectives focusing an acetaminophen pill (used as calibration standard) zoomed.

Results and discussion

- Infrared characterization of explosives

In the knowledge of the chemical composition of the 14 studied explosives, they were separated into three different groups in order to facilitate the interpretation and analysis of their spectral bands. Particularly, explosives were grouped into single organic explosives, NC-based powders and oxidizer-fuel mixtures, according to the classification previously explained in chapter 4.

Regarding single organic explosives, the IR spectra of TNT, RDX, PETN, TATP and HMTD are displayed in Figure 5.4. As expected for organic molecules with multiple covalent bonds, their IR spectra was noticeably complex due to the large number of IR active molecular vibrations. Such vibrations, which are expected to be different among the five explosive molecules because of their different chemical structure (despite sharing some functional groups), have provided different characteristic IR bands, as evidenced in Figure 5.4.

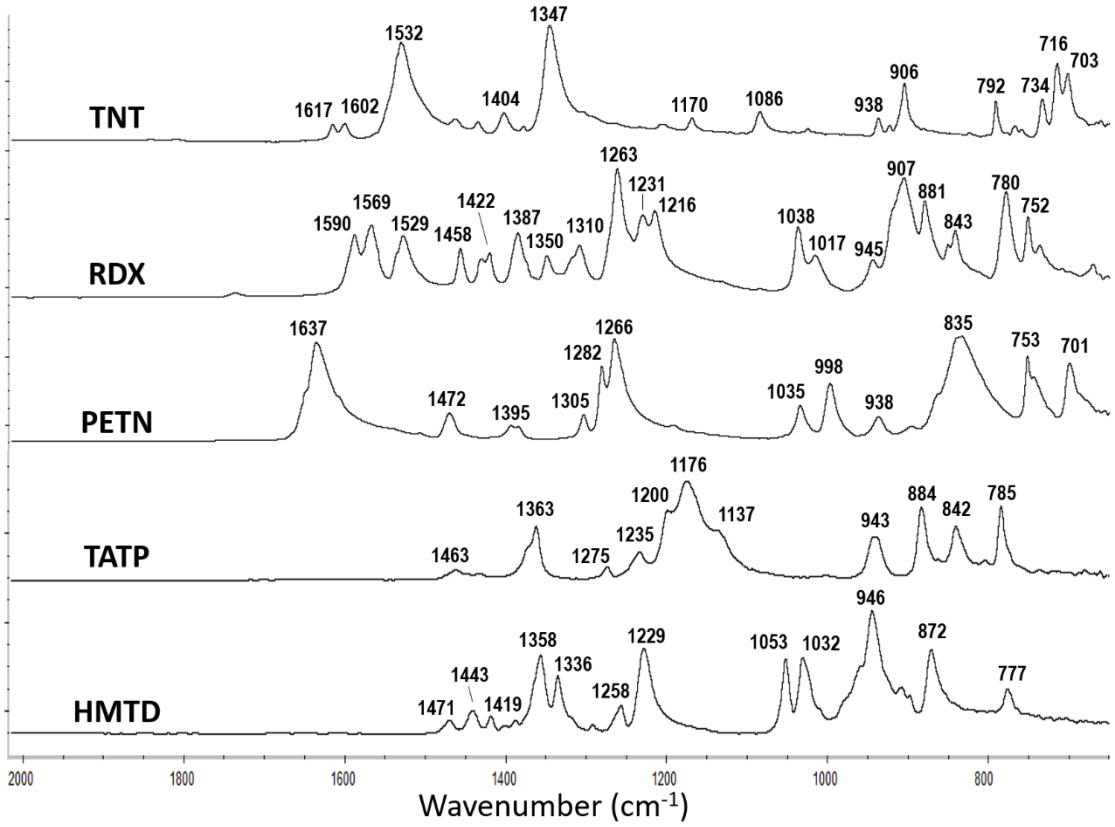

Figure 5.4. Attenuated total reflectance FTIR spectra of TNT, RDX, PETN, TATP and HMTD. IR conditions: resolution 4, 16 scans. Every spectrum is the average of five replicates.

In this respect, TNT, RDX and PETN nitroexplosives all displayed the IR bands corresponding to NO_2 vibrations, but they were located at different wavenumbers in each spectrum. For instance, two bands (1617 and 1532 cm^{-1}) were assigned to antisymmetric NO_2 stretching vibrations in TNT spectrum, while three medium-intense bands (1590, 1569 and 1529 cm^{-1}) in RDX spectrum, and a unique highly intense band (1637 cm^{-1}) in PETN spectrum [8-12]. Similarly, significant differences were observed for the symmetric NO_2 stretching vibration, tentatively assigned to the band 1347 cm^{-1} in TNT spectrum, two bands (1350 and 1310 cm^{-1}) in RDX spectrum and the band 1282 cm^{-1} in PETN spectrum [8-12]. As previously explained, a chemical vibration is not only affected by the identity of vibrating atoms or bonds, but also the chemical surrounding environment. Particularly, TNT is a nitroaromatic explosive ($C-NO_2$), RDX is a nitramine ($N-NO_2$) and PETN is a nitrate ester ($O-NO_2$). Thus, the vibrational change of the dipole moment of nitro group in each explosive is distinctively affected by the electronegativity of the atom to which nitro group is bonded (*i.e.* C, N or O). In addition, multiple IR bands were

selectively assigned to CH_3, CH_2, C–H, C–N, C–O or C–C vibrations that were specific for each explosive molecule. As an example, TNT displayed a band due to C–C aromatic stretching vibration (1602 cm^{-1}), and multiple IR bands due to CH/CH_3 bending vibrations (1404, 1170, 1086, 938, 734, 716 and 703 cm^{-1}). Similarly, RDX and PETN displayed multiple selective bands corresponding to CH_2 bending vibrations and C–N/C–O stretching vibrations. The specific assignment of every particular IR band with the corresponding vibration is summarized in Table 5.3.

Regarding the IR spectra of TATP and HMTD peroxide explosives, multiple bands were also observed including not only peroxide (O–O) vibrations but also CH_3, CH_2, C–O, C–N and C–C vibrations, as summarized in Table 5.3. In fact, the most prominent bands were not due to O–O vibrations (which are theoretically non-IR active because of being a homo-atomic bond), but due to C–O stretching and CH_3/CH_2 bending vibrations. For instance, the most intense bands of TATP, located at 1363, 1176, 884 and 785 cm^{-1}, were all due to CH_3 bending and/or C–O stretching vibrations [13-15]. Similarly, the most intense bands of HMTD (1358, 1229 and 946 cm^{-1}) were due to CH_2 bending and/or C–O/C–N stretching vibrations [15-17].

In brief, the large number of selective IR bands of TNT, RDX, PETN, TATP and HMTD explosives enable the unequivocal identification of each explosive, as has been largely demonstrated in literature for years [8-17].

Table 5.3. Summary of the main IR bands of TNT, RDX, PETN, TATP and HMTD; and their assignment with the fundamental vibrations. (asym: antisymmetric, bend: bending, def: deformation, ip: in-plane, oop: out-of-plane, rock: rocking, scis: scissoring, st: stretching, sym: symmetric, twist: twisting, umb: umbrella, wag: wagging).

Explosive	Formula	Raman shift (cm^{-1})	Assignment to molecular vibrations	References
TNT	$C_7H_5N_3O_6$	1617	2,6-NO_2 asym st, C-C aromatic st	8-11
		1602	C-C aromatic st	
		1532	NO_2 asym st	
		1404	CH_3 ip bend	
		1347	NO_2 sym st	
		1170	C-H ip bend	
		1086	C-H ip bend	
		938	CH_3 oop bend	
		906	C-N st	
		792	NO_2 scis, C-CH_3 st	
		734	C-H oop bend	
		716	C-H oop bend	
		703	C-H oop bend	

RDX	$C_3H_6N_6O_6$	1590	NO_2 asym st	8-11
		1569	NO_2 asym st	
		1529	NO_2 asym st	
		1458	CH_2 ip bend	
		1422	H-C-N bend	
		1387	CH_2 oop bend	
		1350	N-NO_2 st, NO_2 sym st	
		1310	NO_2 sym st, CH_2 wag, CH_2 twist	
		1263	CH_2 scis	
		1231	CH_2 rock, CH_2 scis	
		1216	N-C-N st, N-NO_2 st, CH_2 rock	
		1038	NO_2 rock	
		1017	N-C-N st	
		945	C-N st, CH_2 rock, N-N st	
		907	C-C st, ONO st	
		881	C-N st, N-N st, C-N-C st	
		843	C-N-C st, N-N st, NO_2 scis	
		780	NO_2 scis, CH_2 oop bend	
		752	CH_2 oop bend	
PETN	$C_5H_8N_4O_{12}$	1637	NO_2 asym st	9-12
		1472	CH_2 scis	
		1395	CH_2 wag, CCC st	
		1305	CH_2 wag, NO_2 rock	
		1282	NO_2 sym st	
		1266	C-H bend	
		1035	C-O st, NO_2 rock	
		998	CH_2 rock, C-O st	
		938	CH_2 torsion, CCC st	
		835	N-O st	
		753	ONO_2 umb, CCC st	
		701	CCC def, NO_2 rock	
TATP	$C_9H_{18}O_6$	1463	CH_3 asym bend	13-15
		1363	CH_3 sym bend	
		1275	Sym ring breathing	
		1235	OCO st, Me-C-Me st	
		1200	OCO st, Me-C-Me st, Me-C-O st	
		1176	C-O st, C-O-O st	
		1137	OCO asym st, C-O st	
		943	CH_3 oop bend, O-O asym st, asym ring breathing	
		884	OCO st, Me-C-Me st, Me-C-O st, CH_3 oop bend	
		842	O-O sym st, asym ring breathing	
		785	CH_3 oop, OCO st, Me-C-Me st	
HMTD	$C_6H_{12}N_2O_6$	1471	CH_2 bend	15-17
		1443	CH_2 scis	
		1419	CH_2 wag	
		1358	CH_2 bend	
		1336	CH_2 twist	
		1258	CH_2 bend	
		1229	CH_2 bend	
		1053	C-N st, C-O st,	
		1032	C-N st, C-O st	
		946	C-N st, C-O st	
		872	O-O st	
		777	O-O st, CH_2 rock	

After confirming the possible identification of pure single organic explosives, the suitability of IR spectroscopy was also examined for the identification of organic smokeless gunpowders. As previously indicated, a triple-base, two double-base and a single-base smokeless powders, all of them with different chemical

components, were analysed. The IR spectra of the four smokeless gunpowders are displayed in Figure 5.5.

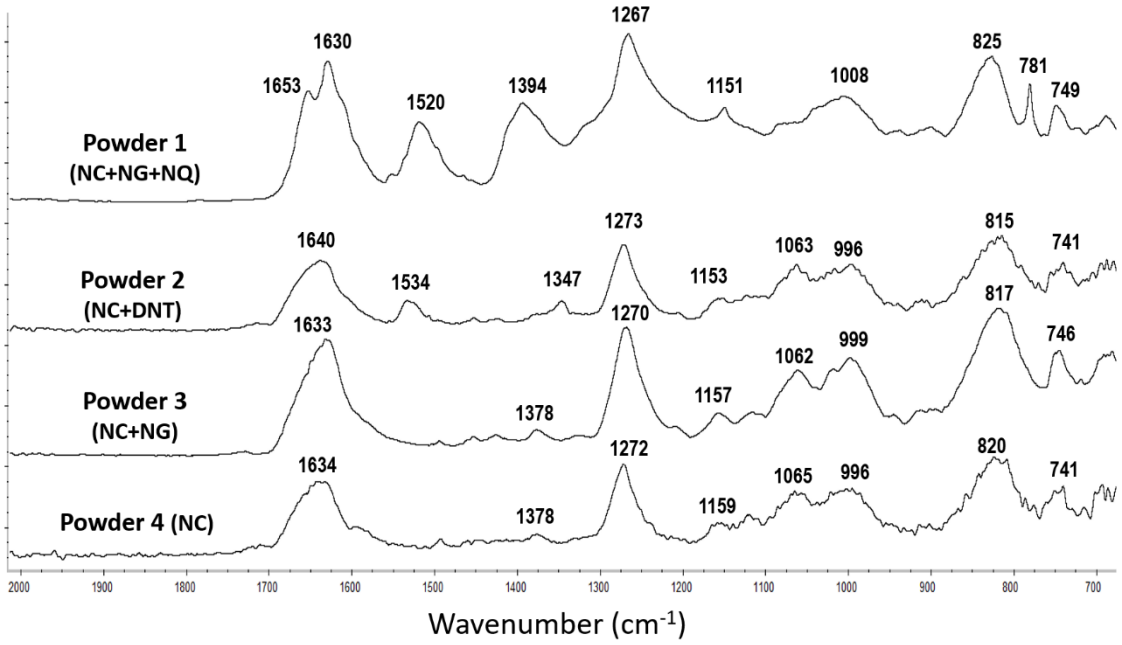

Figure 5.5. Attenuated total reflectance FTIR spectra of triple-base (NC+NG+NQ), double-base (NC+DNT), double-base (NC+NG) and single-base (NC) smokeless powders. IR conditions: resolution 4, 16 scans. Every spectrum is the average of five replicates.

By simultaneously comparing Figure 5.5 and the chemical composition of smokeless powders, it is evident the reason why the IR spectrum of powder 1 is completely different to those of powders 2, 3 and 4 (which are similar). Powder 1 is a triple-base smokeless powder composed of 55% NQ, 19% NC and 18% NG, while powders 2, 3, and 4, are double- or single-base powders whose major component is NC (>70%). In fact, the IR spectrum of either powder 4 (94% NC), powder 3 (71% NC) or powder 2 (85% NC) was dominated by the IR bands of NC, including 1634, 1378, 1272, 1159, 1065, 996, 820 and 741 cm^{-1} (previously referred in literature [18, 19]). Specifically, the bands located at 1634 and 1272 cm^{-1} were due to the antisymmetric and symmetric NO_2 stretching, respectively; while the band at 820 cm^{-1} was due to the N–O stretching [18]. On the contrary, the bands located at 1378, 1159, 1065, 996 and 741 cm^{-1} were either due to C–H bending or C–O stretching vibrations from the pyranose ring (also evidenced by cellulose [20-22]).

As expected, no extra bands (besides NC bands) were observed in the IR spectrum of powder 4 since it is a single-base smokeless gunpowder composed of 96% NC. Likewise but unexpectedly, no extra bands (besides NC bands) were observed in the IR spectrum of powder 3 despite being composed of 71% NC and

25% NG. The reason for the absence of NG bands might be due to the fact that NG is a nitrate ester (like NC) and therefore, the more intense bands of NG (corresponding to ONO_2 stretching vibrations around 1630, 1275 and 825 cm^{-1}) would be overlapped by those of NC (major component). This hypothesis is partially confirmed by the fact that some bands from the minor component DNT are observed in the IR spectrum of powder 2 between the NC bands. In this case, even though powder 2 only contains 10% DNT, the most intense bands of DNT located at 1534 and 1347 cm^{-1} (corresponding to the antisymmetric and symmetric nitroaromatic NO_2 stretching vibrations) [19], are clearly recognizable. No overlapping has occurred between ONO_2 (NC) stretching vibrations and C−NO_2 (DNT) stretching vibrations.

Back to the IR spectrum of powder 1, no band from NC is unequivocally identifiable, even though powder 1 is composed of 19% NC. The reason likely lies on the fact that bands of NC are overlapped by those bands corresponding to the major component NQ (55%). Particularly, the most prominent bands displayed by powder 1, which are located at 1653, 1630, 1520, 1394, 1267 and 825 cm^{-1}, are assigned to NQ (either C=N stretching, N−H bending or NO_2 stretching vibrations) [23]. The particular assignment of every band with the corresponding molecular vibration/s is summarized in Table 5.4.

Table 5.4. Summary of the main IR bands of powder 1 (NC+NG+NQ), powder 2 (NC+DNT), powder 3 (NC+NG) and powder 4 (NC); and their assignment with the fundamental vibrations (asym: antisymmetric, bend: bending, ip: in-plane, oop: out-of-plane, st: stretching, sym: symmetric).

Explosive	Formula	Raman shift (cm^{-1})	Assignment to molecular vibrations	References
Powder 1	55% NQ	1653	C = N st, N-H ip bend (NQ)	
	$CH_4N_4O_2$	1630	N-H ip bend (NQ), NO_2 asym st (NC+NG)	19, 23
		1520	NO_2 asym st (NQ)	
	19% NC	1394	N-H ip bend (NQ)	
	$(C_6H_7N_3O_{11})_n$	1267	NO_2 sym st (NQ+NC+NG)	
		1151	C-N st (NQ), C-O st (NC)	
	18% NG	1008	C-N st (NQ)	
	$C_3H_5N_3O_9$	825	N-H oop bend (NQ), N-O st (NC+NG)	
		781	N-H oop bend (NQ)	
		749	N-H (NQ), C-H (NC+NG) oop bend	
Powder 2	85% NC	1640	NO_2 asym st (NC)	18-22
	$(C_6H_7N_3O_{11})_n$	1534	NO_2 asym st (DNT)	
		1347	NO_2 sym st (DNT)	
	10% DNT	1273	NO_2 sym st (NC)	
	$C_7H_6N_2O_4$	1153	C-O st (NC)	
		1063	C-O st (NC)	
		996	C-O st (NC)	
		815	N-O st (NC)	
		741	C-H oop bend (NC)	

Powder 3	71% NC $(C_6H_7N_3O_{11})_n$ 25% NG $C_3H_5N_3O_9$	1633 1378 1270 1157 1062 999 817 746	NO_2 asym st (NC+NG) C-H ip bend (NG+NG) NO_2 sym st (NC+NG) C-O st (NC) C-O st (NC) C-O st (NC) N-O st (NC+NG) C-H oop bend (NC+NG)	18-22
Powder 4	94% NC $(C_6H_7N_3O_{11})_n$	1634 1378 1272 1159 1065 996 820 741	NO_2 asym st (NC) C-H ip bend (NC) NO_2 sym st (NC) C-O st (NC) C-O st (NC) C-O st (NC) N-O st (NC) C-H oop bend (NC)	18-22

Finally, the oxidizer-fuel explosive mixtures, including black powder, chloratite, ANFO, dynamite and ammonal, were analysed by IR spectroscopy, as displayed in Figure 5.6.

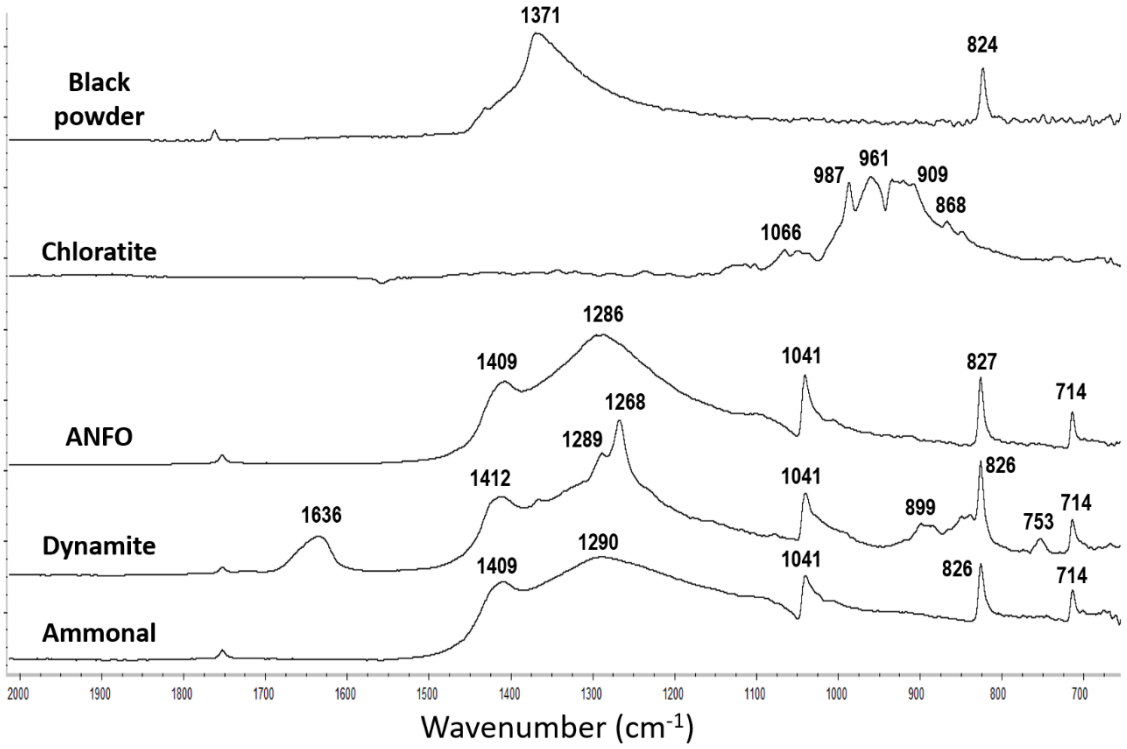

Figure 5.6. Attenuated total reflectance FTIR spectra of black powder (KNO_3+C+S), chloratite ($NaClO_3$+sucrose+S), ANFO (NH_4NO_3+diesel), dynamite (NH_4NO_3+EGDN) and ammonal (NH_4NO_3+Al). IR conditions: resolution 4, 16 scans. Every spectrum is the average of five replicates.

As expected, the most intense bands of explosive mixtures were provided by the molecular vibrations of the oxidizer (the major component in the mixture). In fact, the IR spectrum of black powder was characterized by displaying only the

bands of potassium nitrate (1371 and 824 cm^{-1}), since neither charcoal (C−C) nor sulphur (S−S) have IR active bonds. These bands located at 1371 and 824 cm^{-1} were respectively due to the antisymmetric NO_3 stretching and the out-of-plane NO_3 deformation [3, 24]. Similarly, the IR spectrum of chloratite was dominated by the ClO_3 stretching vibrations of chlorate (987, 961 and 909 cm^{-1}) [3, 24], though some little intense bands (1066 and 868 cm^{-1}) corresponded to C−O stretching and C−H bending vibrations of sucrose [25]. Finally, the IR spectra of AN-based explosives (ANFO, dynamite and ANAl) only displayed the bands of ammonium nitrate, except dynamite whose IR spectrum also displayed medium-intense bands due to EGDN. The bands of ammonium nitrate, which were located at 1409, 1286, 1041, 826 and 714 cm^{-1}, were respectively assigned to the NH_4^+ deformation, antisymmetric NO_3 stretching, symmetric NO_3 stretching, out-of-plane NO_3 deformation and in-plane NO_3 deformation [3, 19, 26]. No bands from diesel were observed in the IR spectrum of ANFO, likely due to the low concentration (10%) and large heterogeneity of diesel fuel. Likewise, no bands from aluminium were observed in the IR spectrum of ANAl, as expected for a metallic non-covalent material. On the contrary, the IR spectrum of dynamite displayed some noticeably intense bands of EGDN besides the bands of AN, likely due to the significant amount of EGDN (29%) in dynamite's composition. Apart from sharing a band at 826 cm^{-1} with AN, the bands of EGDN were located at 1636, 1268, 899 and 753 cm^{-1}. Such bands corresponded to the antisymmetric NO_3 stretching, symmetric NO_3 stretching, C−O stretching and out-of-plane CH_2 deformation [19]. Table 5.5 summarizes the vibrational assignment of every band.

Table 5.5. Summary of the main IR bands of black powder, chloratite, ANFO, dynamite and ammonal, and their assignment with the fundamental vibrations. (asym: antisymmetric, bend: bending, def: deformation, ip: in-plane, rock: rocking, st: stretching, sym: symmetric).

Explosive	Formula	Raman shift (cm^{-1})	Assignment to molecular vibrations	References
Black powder	75% KNO_3 15% C 10% S	1371 824	NO_3 asym st (KNO_3) NO_3 oop def (KNO_3)	3, 24
Chloratite	80% $NaClO_3$ 10% Sucrose 10% S	1066 987 961 909 868	C-O st (sucrose) ClO_3 asym st ($KClO_3$) ClO_3 asym st ($KClO_3$) ClO_3 sym def ($KClO_3$), C-H oop def (sucrose) C-H oop def (sucrose)	3, 24, 25

ANFO	90% NH_4NO_3 10% Fuel oil	1409 1286 1041 827 714	NH_4^+ def (NH_4NO_3) NO_3 asym st (NH_4NO_3) NO_3 sym st (NH_4NO_3) NO_3 oop def (NH_4NO_3) NO_3 ip def (NH_4NO_3)	3, 19, 26
Dynamite	66% NH_4NO_3 29% EGDN	1636 1412 1289 1268 1041 899 826 753 714	NO_2 asym st (EGDN) NH_4^+ def (NH_4NO_3) NO_3 asym st (NH_4NO_3) NO_2 sym st (EGDN) NO_3 sym st (NH_4NO_3) C-O st (EGDN) NO_3 oop def (NH_4NO_3), N-O st (EGDN) ONO_2 oop bend, CH_2 oop def (EGDN) NO_3 ip def (NH_4NO_3)	3, 19. 26
Ammonal (ANAl)	85% NH_4NO_3 15% Al	1409 1290 1041 826 714	NH_4^+ def (NH_4NO_3) NO_3 asym st (NH_4NO_3) NO_3 sym st (NH_4NO_3) NO_3 oop def (NH_4NO_3) NO_3 ip def (NH_4NO_3)	3, 19, 26

- Raman characterization of explosives

As also did for IR spectroscopy, the interpretation of the Raman spectra was facilitated by grouping the explosives into single organic explosives, NC-based powders and oxidizer-fuel mixtures.

Before interpreting the Raman spectra of each group of explosives, it should be remarked an important difference between IR and Raman spectroscopy. Unlike IR spectra, Raman spectra were collected using a confocal microscope, in such a way that Raman spectra were strongly affected by not only the better/worse focusing, but also the selected spot from which collecting the Raman spectrum. Unlike IR spectrophotometer, in which a significant amount of sample was placed onto the large-area of measuring diamond crystal (>3 mm diameter), Raman instrument had a confocal microscope, which enabled the magnification and precise focusing of a micro zone in the sample. In fact, Raman spot size covered less than 10 μm, in such a way that different particles of the sample might be separately analysed. Therefore, contrarily to IR, in which almost the same spectrum was obtained for every replicate along the sample (even in explosive mixtures), Raman spectra of replicates might differ each other depending on the component particle that was being focused. As expected, the homogeneous organic explosives (TNT, RDX, PETN, TATP, and HMTD) provided a unique representative spectrum for all the replicates, no matter which spot was being focused. On the contrary, some smokeless powders and

heterogeneous explosive mixtures (black powder, dynamite, chloratite, ANFO, and ammonal) displayed different Raman spectra among their replicates depending on the major component predominantly present within the focused spot. This selective spatial focusing is a highly significant advantage to detect microscopic explosive particles in real samples, as subsequently demonstrated in Chapter 6. However, the Raman spectra displayed in this chapter are the average of five replicates, and thus, they mostly corresponded to the main component (oxidizer) because the major component was predominant in most of the replicates collected along the sample.

Regarding single organic explosives TNT, RDX, PETN, TATP and HMTD, their homogeneously replicated Raman spectra are displayed in Figure 5.7.

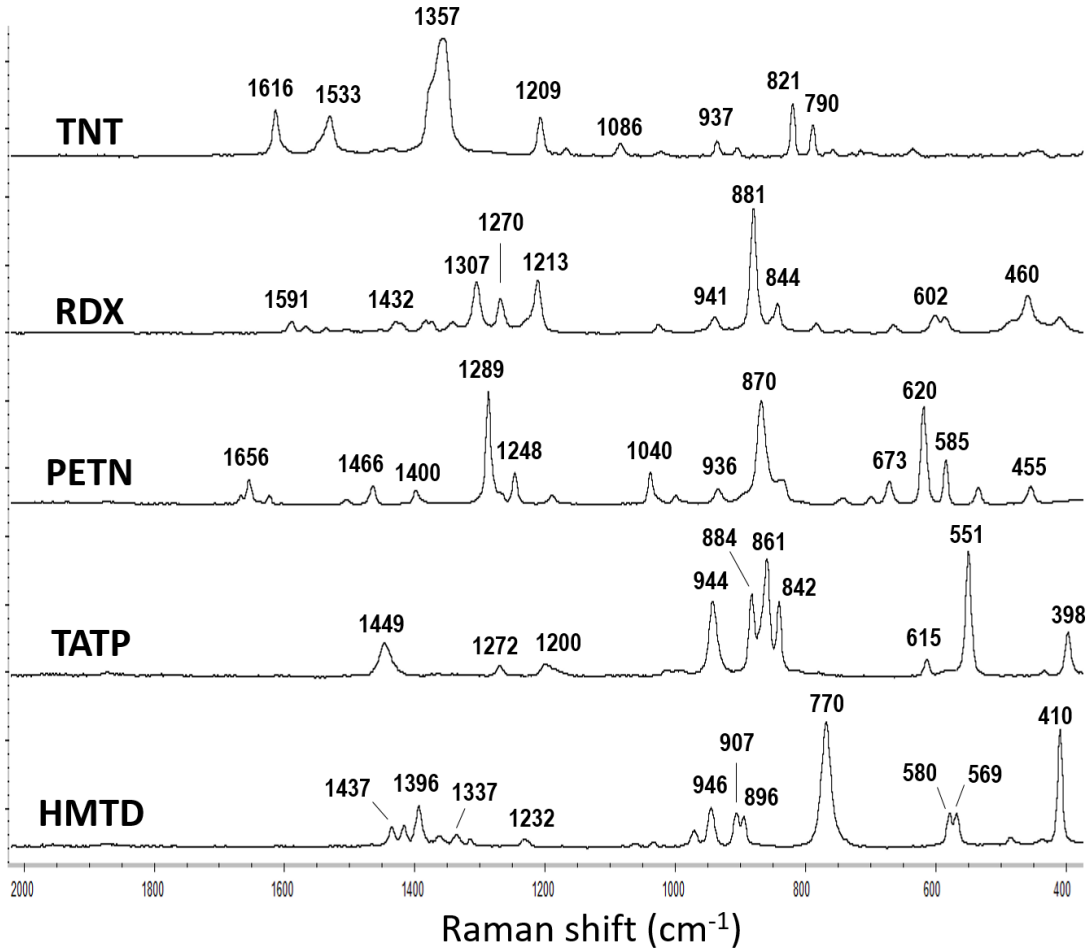

Figure 5.7. Raman spectra of TNT, RDX, PETN, TATP and HMTD. Raman conditions: laser at 780 nm, 14.0 mW, 10× magnification objective, confocal pinhole of 50 µm, 6 acquisitions of 5 s per acquisition. Every spectrum is the average of five replicates.

Although TNT, RDX, and PETN are all nitro-compounds, they provided different characteristic Raman spectra according to their chemical differences (beyond

the nitro-groups), as previously observed for IR spectroscopy. For instance, the Raman spectrum of TNT was dominated by the NO_2 symmetric stretching vibration, whose band was located at 1357 cm^{-1}. Additionally, TNT provided medium intense bands at 1616 and 1533 cm^{-1} (which were due to C−C aromatic stretching and NO_2 antisymmetric stretching vibrations). Similarly intense were those bands located at 1209 and 821 cm^{-1}, which were assigned to ring breathing and NO_2 scissoring, respectively [8-11]. Unlike TNT, the Raman spectrum of RDX displayed the most prominent band at 881 cm^{-1} corresponding to C−N or N−N stretching vibrations; while medium intense bands were found at 1307, 1213 and 460 cm^{-1}, respectively assigned to NO_2 symmetric stretching, CH_2 bending and ring bending [8-11]. Finally, PETN provided a Raman spectrum whose most intense bands were those located at 1289, 870 and 620 cm^{-1} corresponding to NO_2 symmetric stretching, N-O stretching and CCC deformation, respectively [9-12].

The peroxide explosives TATP and HMTD were both characterized by the O−O peroxide bond. Nevertheless, their additional differences in their chemical structures were also clearly reflected in their different Raman spectra. The most intense bands of TATP were located at 944, 884, 861, 842 and 551 cm^{-1}, which were due to either O−O stretching, CH_3 bending, Me−C−Me stretching, Me−C−O stretching or O−C−O stretching/bending [13-15]. On the contrary, HMTD displayed two highly selective intense bands at 770 and 410 cm^{-1} (corresponding to O−O stretching and N−C−O deformation), and medium-intense bands at 1396, 946, 907, 896, 580 and 569 cm^{-1} [15-17].

The particular assignment of every Raman band with its corresponding molecular vibration is summarized in Table 5.6.

Table 5.6. Summary of the main Raman bands from the spectra of TNT, RDX, PETN, TATP and HMTD; and their assignment with the fundamental vibrations. (asym: antisymmetric, bend: bending, def: deformation, ip: in-plane, oop: out-of-plane, rock: rocking, scis: scissoring, st: stretching, sym: symmetric, twist: twisting, wag: wagging).

Explosive	Formula	Raman shift (cm^{-1})	Assignment to molecular vibrations	References
TNT	$C_7H_5N_3O_6$	1616	2,6-NO_2 asym st, C-C aromatic st	8-11
		1533	NO_2 asym st	
		1357	NO_2 sym st	
		1209	ring breathing or C_6H_2-C vibration	
		1086	C-H ip bend	
		937	CH_3 oop bend	
		821	NO_2 scis	
		790	C-CH_3 st, NO_2 scis, C-H oop bend	

RDX	$C_3H_6N_6O_6$	1591	NO_2 asym st	8-11
		1432	H-C-N bend	
		1307	NO_2 sym st, CH_2 wag, CH_2 twist	
		1270	CH_2 scis, N-N st	
		1213	CH_2 rock, N-C-N st, N-NO_2 st,	
		941	N-N st, C-N st, CH_2 rock,	
		881	C-N st, N-N st	
		844	N-N st, NO_2 scis	
		602	O-C-O st	
		460	ip ring bend	
PETN	$C_5H_8N_4O_{12}$	1656	NO_2 asym st	9-12
		1466	CH_2 scis	
		1400	CH_2 wag, CCC st	
		1289	NO_2 sym st	
		1248	C-H bend	
		1040	CH_2 torsion, C-O st	
		936	CH_2 torsion, CCC st	
		870	N-O st	
		673	C-C st, NO_2 scis	
		620	C-C-C def, ONO_2 rock	
		585	ONO_2 rock, C-C bend	
		455	C-C-C def	
TATP	$C_9H_{18}O_6$	1449	CH_3 asym bend, C-C st	13-15
		1272	Sym ring breathing	
		1200	OCO and Me-C-Me asym st, Me-C-O sym st	
		944	CH_3 oop bend, O-O st, asym ring breathing	
		884	OCO and Me-C-Me asym st, Me-C-O st	
		861	O-O st, OCO and Me-C-Me sym st	
		842	O-O st, asym ring breathing	
		615	OCO st	
		551	OCO scis	
		398	ring breathing	
HMTD	$C_6H_{12}N_2O_6$	1437	CH_2 scis	15-17
		1396	CH_2 wag	
		1337	CH_2 twist	
		1232	CH_2 bend	
		946	C-O st, C-N st	
		907	O-O st	
		896	O-O st	
		770	O-O st, CH_2 rock	
		580	Ring st	
		569	Ring st	
		410	NCO def	

Like IR, the large number of selective Raman bands of TNT, RDX, PETN, TATP and HMTD explosives enable the unequivocal identification of each explosive.

Regarding NC-based smokeless gunpowders, the main difficulty was to reduce the fluorescence. Although smokeless powders are mostly composed of non-fluorescent explosive components (NC, NG, DNT and/or NQ), they also contain highly coloured and fluorescent stabilizers and other additives (such as graphite, petroleum jelly, talc and metal oxides), which extraordinarily hinder the analysis of smokeless gunpowders by Raman spectroscopy. Particularly, the darker the gunpowder, the greater the fluorescence. In this respect, the unique smokeless powder properly characterized by Raman spectroscopy was the white

triple-base powder, as displayed in Figure 5.8. Its most intense bands were located at 1152 and 949 cm^{-1}, which were due to C–N/C–O stretching and N–N stretching vibrations, respectively [19, 23]. Additional medium/low intense bands were observed at 1517, 1432, 1282, 1069, 1008, 854, 792 and 710 cm^{-1}, whose vibrational assignment is gathered in Table 5.7. No good-spectrally defined spectrum was obtained for the other three smokeless powders in any of their replicates. Only two clearly noticeable bands (1288 and 853 cm^{-1}) were observed in the Raman spectrum of powder 3 besides the fluorescence. These bands were assigned to the symmetric NO_2 stretching and N–O stretching, respectively [18-22]. Negatively, no bands were detected neither for powder 2 nor powder 4.

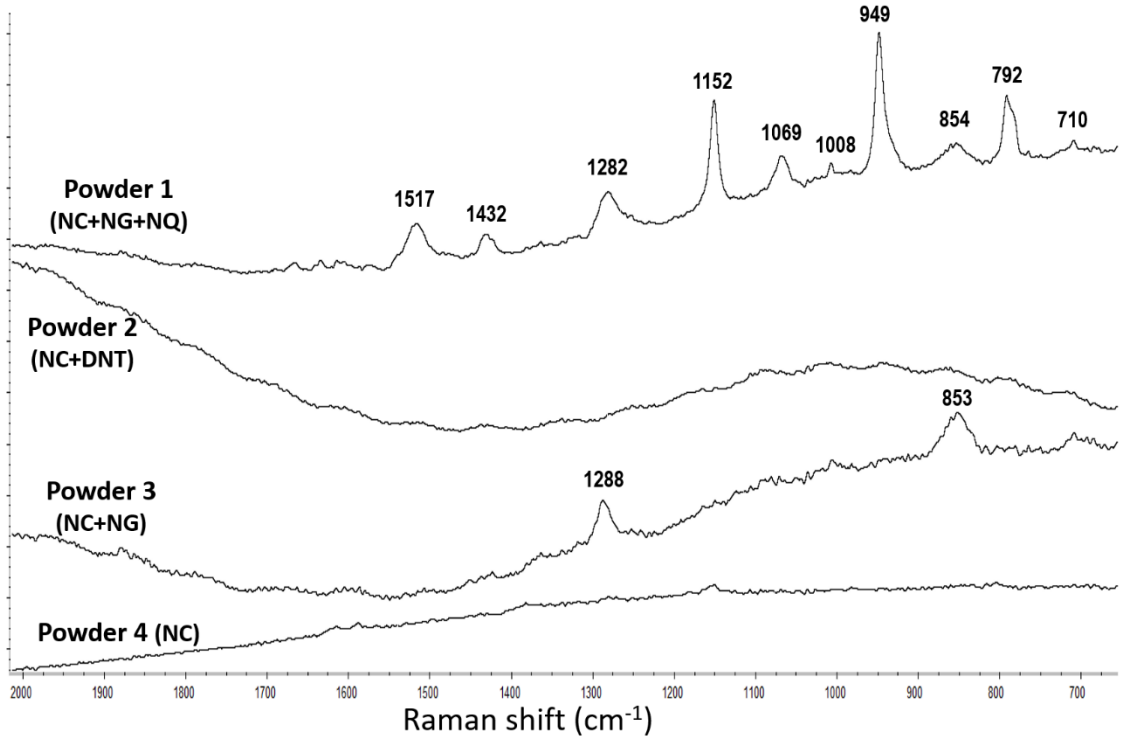

Figure 5.8. Raman spectra of triple-base (NC+NG+NQ), double-base (NC+DNT), double-base (NC+NG) and single-base (NC) smokeless gunpowders. Raman conditions: laser at 780 nm, 8.0 mW, 10× magnification objective, confocal pinhole of 50 µm, 6 acquisitions of 5 s per acquisition. Every spectrum is the average of five replicates.

Table 5.7. Summary of the observed Raman bands of powder 1 (NC+NG+NQ), powder 2 (NC+DNT), powder 3 (NC+NG) and powder 4 (NC); and their assignment with the fundamental vibrations (asym: antisymmetric, bend: bending, ip: in-plane, oop: out-of-plane, st: stretching, sym: symmetric).

Explosive	Formula	Raman shift (cm^{-1})	Assignment to molecular vibrations	References
Powder 1	55% NQ $CH_4N_4O_2$	1517 1432 1282	NO_2 asym st (NQ) N-H ip bend (NQ) NO_2 sym st (NQ+NC+NG)	19, 23
	19% NC $(C_6H_7N_3O_{11})_n$	1152 1069 1008	C-N st (NQ), C-O st (NC) C-N st (NQ), C-O st (NC) C-N st (NQ), C-O st (NC)	
	18% NG $C_3H_5N_3O_9$	949 854 792 710	N-N st (NQ) N-H oop bend (NQ), N-O st (NC+NG) N-H oop bend (NQ) N-H (NQ), C-H (NC+NG) oop bend	
Powder 2	85% NC 10% DNT		Only fluorescence	-
Powder 3	71% NC 25% NG	1288 853	NO_2 sym st (NC+NG) N-O st (NC+NG)	18-22
Powder 4	94% NC		Only fluorescence	-

Finally, the Raman spectra of explosive mixtures (black powder, chloratite, ANFO, dynamite and ammonal) are displayed in Figure 5.9.

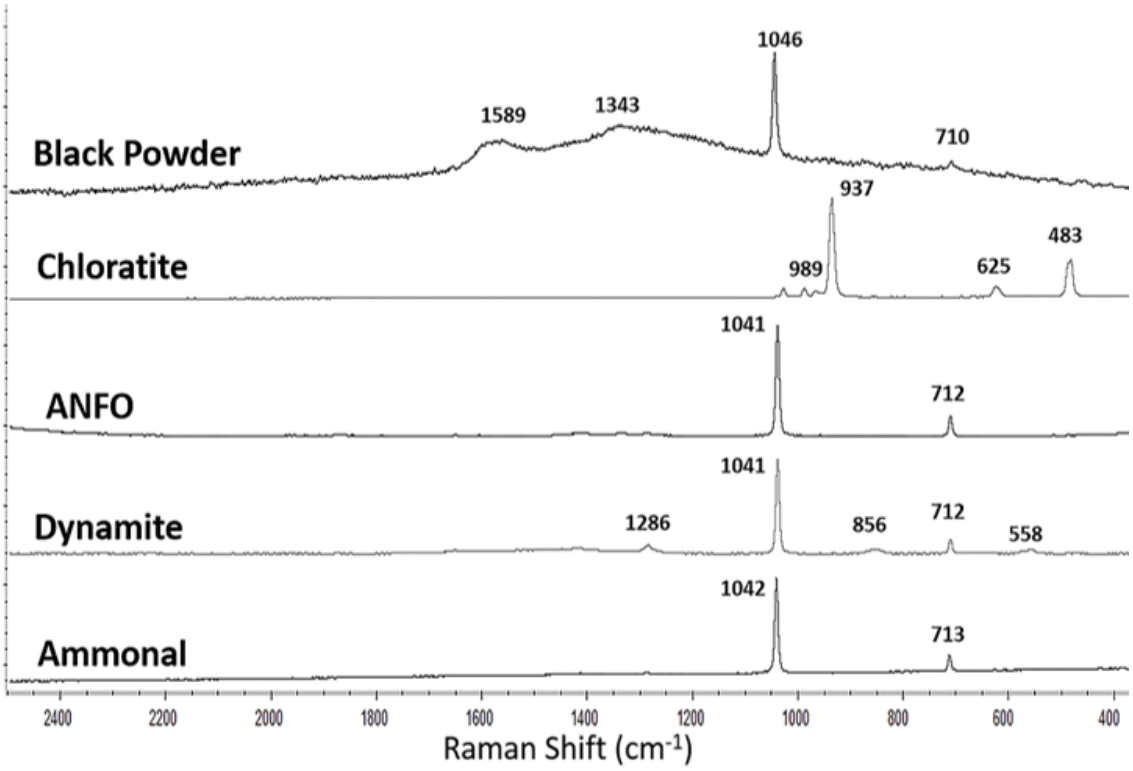

Figure 5.9. Raman spectra of black powder (KNO_3+C+S), chloratite ($NaClO_3$+sucrose+S), ANFO (NH_4NO_3+diesel), dynamite (NH_4NO_3+EGDN) and ammonal (NH_4NO_3+Al). Raman conditions as in Figure 5.8.

As previously introduced, the average Raman spectra of explosive mixtures mostly displayed the Raman signature of the oxidizer (like IR spectroscopy). Even so, the Raman spectrum of black powder clearly displayed the characteristic bands of potassium nitrate placed at 1047 and 711 cm^{-1}, and two wide bands located at 1589 and 1343 cm^{-1} due to charcoal fluorescence. However, no bands from sulfur were detected, probably due to the small amount of sulfur in the mixture and the improbable chance of spotting it. Likewise, chloratite displayed a Raman spectrum dominated by the characteristic bands of sodium chlorate, which were located at 989, 937, 625, and 483 cm^{-1}. No bands from neither sucrose nor sulfur were detected within the five replicates randomly analysed. Finally, the Raman spectra of dynamite, ANFO, and ammonal (ANAl) clearly showed the characteristic bands of ammonium nitrate at 1041 and 713 cm^{-1}. Positively, the Raman spectrum of dynamite also revealed another three weak bands placed at 1286, 856, and 558 cm^{-1}, which are attributed to EGDN [19]. The particular assignment of each band to its corresponding chemical vibration is summarized in Table 5.8.

Table 5.8. Summary of the main Raman bands from the spectra of black powder, chloratite, ANFO, dynamite and ammonal, and their assignment with the fundamental vibrations. (asym: antisymmetric, bend: bending, def: deformation, ip: in-plane, rock: rocking, st: stretching, sym: symmetric).

Explosive	Formula	Raman shift (cm^{-1})	Assignment to molecular vibrations	References
Black powder	75% KNO_3 15% C 10% S	1589 1343 1047 711	Fluorescence from charcoal Fluorescence from charcoal NO_3 sym st (KNO_3) NO_3 ip def (KNO_3)	3, 24
Chloratite	80% $NaClO_3$ 10% Sucrose 10% S	989 937 625 483	ClO_3 asym st ($KClO_3$) ClO_3 sym st ($KClO_3$) ClO_3 sym def ($KClO_3$) ClO_3 asym def ($KClO_3$)	3, 24
ANFO	90% NH_4NO_3 10% Fuel oil	1041 713	NO_3 sym st (NH_4NO_3) NO_3 ip def (NH_4NO_3)	3
Dynamite	66% NH_4NO_3 29% EGDN	1286 1041 856 713 558	NO_2 sym st (EGDN) NO_3 sym st (NH_4NO_3) N-O st, C-C st (EGDN) NO_3 ip def (NH_4NO_3) ONO_2 rock, C-C bend (EGDN)	3, 19
Ammonal (ANAl)	85% NH_4NO_3 15% Al	1041 713	NO_3 sym st (NH_4NO_3) NO_3 ip def (NH_4NO_3)	3

When comparing the Raman bands of potassium and ammonium nitrates, our attention was drawn to the slight but remarkable difference between potassium (1047 cm^{-1}) and ammonium nitrates (1041 cm^{-1}). The high specificity of Raman spectroscopy allowed us to distinguish the slight difference of 6 cm^{-1} in Raman shift between the NO_3 symmetric stretching from potassium and ammonium nitrates, as previously reported in Chapter 3. In fact, this difference, which was properly measured using an instrumental precision of ±2 cm^{-1}, can be probably caused by the cation influence on the anion vibration. This difference was highly relevant because it allowed us to distinguish and identify both nitrates. In fact, the interest about further examining such finding motivated the next study.

Conclusions

Single organic explosives were selectively characterized using either IR or Raman spectroscopy, in such a way that IR or Raman spectroscopy enables the unequivocal identification of TNT, RDX, PETN, TATP and HMTD. The most characteristic IR and Raman bands of nitroexplosives were due to the NO_2 stretching vibrations, while the most characteristic bands of peroxide explosives were due to O-O stretching vibrations. However, C-H bending and C-O/C-N stretching vibrations produced additional intense bands, which were fundamental to properly define the spectral signature of each explosive.

Unlike single organic explosives, organic NC-based smokeless gunpowders were not completely discriminated by neither IR nor Raman spectroscopy. The high fluorescence displayed by graphite and other additives of smokeless gunpowders in Raman spectroscopy hindered the Raman identification of the explosive components. In fact, only white triple-base (NC+NG+NQ) powder was properly characterized. Regarding IR spectroscopy, the four powders provided a comprehensive IR spectrum. Negatively, single-base (94% NC) powder and double-base (71% NC + 25% NG) powder provided visually undistinguishable IR spectra, only due to NC component. No selective bands from NG (25%) were detected. Positively, selective bands from DNT were detected in the IR spectrum of double-base (85% NC + 10% DNT) powder among the NC bands. Finally, triple-base powder mostly provided the IR bands of NQ (55%), which overlapped any band from either NC (19%) or NG (18%).

Like smokeless powders, oxidizer-fuel explosive mixtures displayed IR spectra corresponding almost exclusively to the major component (*i.e.* the oxidizer). Therefore, those explosive mixtures composed of different oxidizer were properly discriminated. However, mixtures composed of the same oxidizer (such as ANFO and ANAl) were not. Nevertheless, dynamite (despite also being an AN-based explosive) was unequivocally identified because of the prevalent bands of EGDN (29%). Similar results were obtained for Raman spectroscopy. Every explosive mixture provided the Raman spectra exclusively corresponding to the oxidizing salt, with the exception of dynamite (in whose spectrum an additional low intense band due to EGDN was perceptible), and black powder (in whose spectrum two fluorescent bands due to charcoal were noticeably intense).

References

[1] N. Sheppard, The historical development of experimental techniques in vibrational spectroscopy, Wiley, 2002.

[2] D. Lin-Vien, N.B. Colthup, W.G. Fateley, J.G. Grasselli, The handbook of infrared and Raman characteristic frequencies of organic molecules, Academic Press, 1991.

[3] K. Nakamoto, Infrared and Raman Spectra of inorganic and coordination compounds. Part A: Theory and applications in inorganic chemistry, 6th edition, Wiley, 2009.

[4] K. Nakamoto, Infrared and Raman Spectra of inorganic and coordination compounds. Part B: Applications in coordination, organometallic, and bioinorganic chemistry, Wiley, 2009.

[5] J.M. Chalmers, H.G.M. Edwards, M.D. Hargreaves, Section III Counter terrorism and homeland security, in: Infrared and Raman spectroscopy in forensic science, Wiley, 2012, pp. 205-314.

[6] S. Zitrin, Analysis of explosives by infrared spectrometry and mass spectrometry, in: A. Beveridge, Forensic investigation of explosions, Taylor&Francis, 1998, pp. 267-314.

[7] E. Pretsch, P. Bühlmann, M. Badertscher, IR spectroscopy, in: E. Pretsch, P. Bühlmann, M. Badertscher, Structure determination of organic compounds. Tables of spectral data, 4th edition, Springer, 2009, pp. 269-336.

[8] W.A. Al-Saidi, S.A. Asher, P. Norman, Resonance Raman spectra of TNT and RDX using vibronic theory, excited-state gradient, and complex polarizability approximations, J. Phys. Chem. A 116 (2012) 7862-7872.

[9] E. Finot, T. Brulé, P. Rai, A. Griffart, A. Bouhélier, T. Thundat, Raman and photothermal spectroscopies for explosive detection, Proc. SPIE 8725 (2013) 872528/1-872528/12.

[10] L.C. Pacheco-Londoño, W. Ortiz-Rivera, O.M. Primera-Pedrozo, S.P. Hernández-Rivera, Vibrational spectroscopy standoff detection of explosives, Anal. Bioanal. Chem. 395 (2009) 323-335.

[11] S. Almaviva, S. Botti, L. Cantrini, A. Palucci, A. Puiu, A. Rufoloni, L. Landström, F.S. Romolo, Trace detection of explosives by Surface Enhanced Raman Spectroscopy, Proc. SPIE 8546 (2012) 854602/1-854602/7.

[12] Y.A. Grudkov, Y.M. Gupta, Vibrational properties and structure of Pentaerythritol Tetranitrate, J. Phys. Chem. A 105 (2001) 6197-6202.

[13] L.C. Pacheco-Londoño, A.J. Peña, O.M. Primera, S.P. Hernández-Rivera, N. Mina, R. García, R.T. Chamberlain, R. Lareau, An experimental and theoretical study of the synthesis and vibrational spectroscopy of triacetone triperoxide (TATP), Proc. SPIE 5403 (2004) 279-287.

[14] G.A. Buttigieg, A.K. Knight, S. Denson, C. Pommier, M.B. Denton, Characterization of the explosive triacetone triperoxide and detection by ion mobility spectrometry, Forensic Sci. Int. 135 (2003) 53-59.

[15] J. Oxley, J. Smith, J. Brady, F. Dubnikova, R. Kosloff, L. Zeiri, Y. Zeiri, Raman and infrared fingerprint spectroscopy of peroxide-based explosives, App. Spectrosc. 62(8) (2008) 906-915.

[16] J. Peña-Quevedo, J.A. Laramee, H.D. Durst, S.P. Hernández-Rivera, Cyclic organic peroxides characterization by mass spectrometry and Raman microscopy, IEEE Sensors 11(4) (2011) 1053-1060.

[17] D. Sülzle, P. Klaeboe, The infrared, Raman and NMR spectra of hexamethylene triperoxide diamine, Acta Chem. Scand. A 42 (1988) 165-170.

[18] D.S. Moore, S.D. McGrane, Comparative infrared and Raman spectroscopy of energetic polymers, J. Mol. Struct. 661-662 (2003) 561-566.

[19] M. López-López, Infrared and Raman spectroscopy for the identification of explosives and related compounds, PhD Thesis, Universidad de Alcalá, 2013.

[20] P. Prego-Meleiro, C. García-Ruiz, Spectroscopic techniques for the forensic analysis of textile fibers, Applied Spectrosc. Rew. 51:4 (2016) 258-281.

[21] S. Salih, Fourier Transform - Materials Analysis, InTech, 2012, pp. 45-68.

[22] P. Peets, I. Leito, J. Pelt, S. Vahur, Identification and classification of textile fibres using ATR-FT-IR spectroscopy with chemometric methods, Spectrochim. Acta A 173 (2017) 175-181.

[23] N. Gupta, R. Dahmani, AOTF Raman spectrometer for remote detection of explosives, Spectrochim. Acta A 56 (2000) 1453-1456.

[24] C. Martín-Alberca, Analytical solutions for the forensic analysis of improvised incendiary devices and consumer fireworks, PhD Thesis, Universidad de Alcalá, 2015.

[25] M. Kacurakov, M. Mathlouthi, FTIR and laser-Raman spectra of oligosaccharides in water: characterization of the glycosidic bond, Carbohydr. Res. 284:2 (1996) 145–157.

[26] J. Max, C. Chapados, Aqueous ammonia and ammonium chloride hydrates: Principal infrared spectra, J. Mol. Struct. 1046 (2013) 124-135.

5.2. Infrared and Raman Characterization of Inorganic Oxidizing Energetic Salts

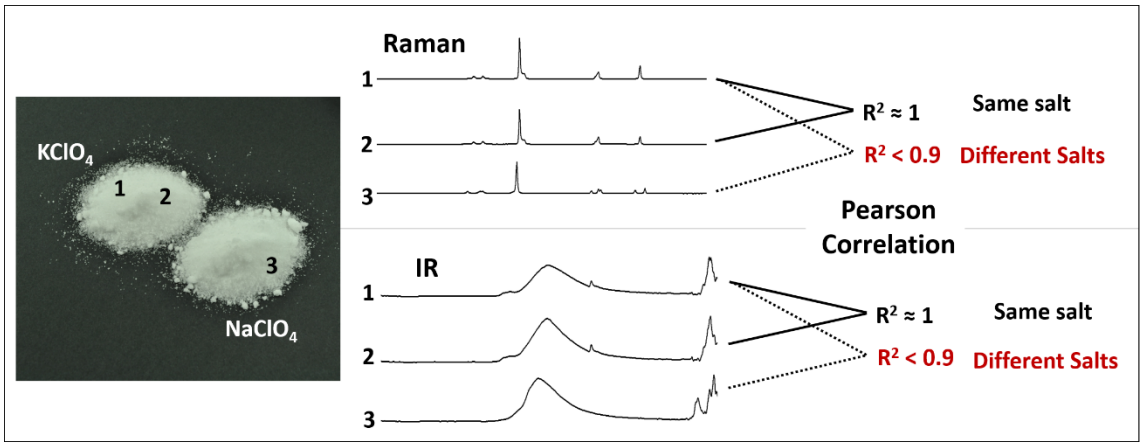

Abstract

Inorganic oxidizing energetic salts including nitrates, chlorates and perchlorates are widely used in the manufacture of not only licit pyrotechnic compositions, but also illicit homemade explosive mixtures. Their identification in forensic laboratories is usually accomplished by either capillary electrophoresis or ion chromatography, with the disadvantage of dissociating the salt into its ions. On the contrary, vibrational spectroscopy, including IR and Raman, enables the non-invasive identification of the salt, *i.e.* avoiding its dissociation. This study focuses on the discrimination of all nitrate, chlorate and perchlorate salts that are commercially available, using both Raman and IR spectroscopy, with the aim of testing whether every salt can be unequivocally identified. Besides the visual spectra comparison by assigning every band with the corresponding molecular vibrational mode, a statistical analysis based on Pearson correlation was performed to ensure an objective identification, either using Raman, IR or both. Positively, 25 salts (out of 72) were unequivocally identified using Raman, 30 salts when using IR and 44 when combining both techniques. Negatively, some salts were undistinguishable even using both techniques demonstrating there are some salts that provide very similar Raman and IR spectra.

Introduction

Inorganic oxidizing energetic salts such as nitrates, chlorates and perchlorates, are of great forensic interest due to their usual and major presence in charge compositions of a large number of improvised explosive devices [1-4]. These salts are commercially accessible (either on their own or as part of the charge of pyrotechnic devices), and, dreadfully, easy "do-it-yourself" recipes to make damaging explosive compositions are freely available [1-7]. In this respect, rapid and selective methodologies to determine them are necessary because forensic investigators may draw relevant conclusions regarding the source, intention, or even the terrorist group or criminals involved; according to the explosive which has been used [1, 3].

In any case, it is useful to determine the particular salt, *i.e.* determining both anion and cation. However, current methodologies used in forensic laboratories usually involve an aqueous extraction (in which the inorganic salts dissociate into their anions and cations) followed by either capillary electrophoresis [8-13] or ion chromatography determination [14-19]. The anions are usually determined because they provide the most relevant information about the explosive [19], *i.e.* whether the explosive is mostly based on a chlorate, a perchlorate or a nitrate salt. More comprehensive results are obtained when using dual working modes, in which both, anions and cations, are determined [9, 18, 19]. Nevertheless, it is important to remark that, using either CE or IC, anions and cations, if both are measured, are separately identified (not constituting the salt), which may induce to misleading results when trying to match them, especially when various cationic and anionic species are involved.

Recently, some research studies have preliminary tested the suitability of spectroscopic techniques, mainly, IR and Raman spectroscopy, to discriminate few of these salts [20-24]. Briefly, using either IR [20] or Raman spectroscopy [21], potassium nitrate, potassium chlorate, and potassium perchlorate have been demonstrated to provide different spectra according to their different bands: 1370 and 823 cm^{-1} for nitrate, 955, 933, 613 and 487 cm^{-1} for chlorate, and 1060, 940 and 621 cm^{-1} for perchlorate using IR [20]; or 1047 and 712 cm^{-1} for nitrate, 976, 937, 617 and 485 cm^{-1} for chlorate, and 940, 628 and 462 cm^{-1} for perchlorate using Raman [21]. Likewise, sodium nitrate and sodium chlorate have also been verified to have different Raman spectra with bands located at 1383, 1065 and 722 cm^{-1} versus 985, 934, 621 and 479 cm^{-1}, respectively [21];

or ammonium nitrate and ammonium perchlorate, whose main bands are located at 1044 and 940 cm^{-1}, respectively [22].

In sum, it has been demonstrated that inorganic salts with different anions are easily discriminated through IR or Raman spectroscopy. The characteristic bands due to the vibrational modes of the anion enable the discrimination of salts. IR and Raman spectroscopy are vibrational techniques, *i.e.* they provide a characteristic spectral signature of each molecule according to the vibrational modes of their covalent chemical bonds [25, 26]. This is ideal to discriminate salts whose anions contain covalent bonds such as nitrates, chlorates and perchlorates. In fact, nitrates can be distinguished from chlorates and perchlorates according to their completely different bonds (N–O versus Cl–O); but also, chlorates can be differentiated from perchlorates due to their different number of atoms and molecular geometry, which lead to different vibrational modes. In brief, vibrational spectroscopic techniques allow to discriminate nitrates, chlorates and perchlorates among each other [25, 26].

However, is vibrational spectroscopy suitable to discriminate salts that have the same anion? Interestingly, preliminary studies have verified that both, IR and Raman spectra of inorganic salts are influenced somehow by the cation. For instance, the nitrate salts of three different cations such as ammonium, potassium and sodium, have significant differences in their Raman spectra even though their spectral bands are due to the nitrate [21, 23]. Ammonium may provide additional specific bands due to their own covalent bonds (N-H), which would discriminate it, but sodium nitrate and potassium nitrate, which do not have covalent bonds except those from nitrate, also provide different spectra. Concretely, the band due to N-O stretching is shifted in the spectrum of each salt (1041 cm^{-1} for ammonium, 1047 cm^{-1} for potassium and 1065 cm^{-1} for sodium nitrate [21], in such a way that this shift is significant enough to spectrally resolve ammonium and potassium nitrate even in mixtures [24], which is a crucial current challenge in forensics). In the same way, significant spectral differences between potassium and barium nitrate have been evidenced in their respective IR spectra (with bands located at 1370 and 823 cm^{-1} for potassium and 1413, 1335, 814 and 728 cm^{-1} for barium nitrate [20]); or between sodium and potassium chlorate, whose bands in their Raman spectra are slightly shifted among each other (985, 934, 621 and 479 cm^{-1} for sodium chlorate versus 976, 937, 617 and 485 cm^{-1} for potassium chlorate [21]). But,

does it mean, for instance, that all nitrate salts provide significant spectral differences to be distinguished? Or do nitrate salts with similar cations provide too slight spectral differences in such a way that they do not enable their discrimination?

In order to solve these questions, this study aims to evaluate all nitrate, chlorate and perchlorate salts commercially available using IR and Raman spectroscopy.

Experimental Section

- Inorganic Oxidizing Salts

In this study, 72 inorganic salts including nitrates (46), chlorates (4) and perchlorates (22) were considered. They were purchased at ACS grade (purity over 98%) either from Sigma-Aldrich or Alfa-Aesar. Salts were purchased anhydrous when possible. However, some salts were only available in their hydrated form and, particularly, ammonium perchlorate was only available in aqueous solution.

The chlorate salts analysed were sodium chlorate, potassium chlorate, barium chlorate monohydrate and silver chlorate.

The perchlorate salts analysed were lithium perchlorate trihydrate, sodium perchlorate, sodium perchlorate monohydrate, potassium perchlorate, magnesium perchlorate, calcium perchlorate tetrahydrate, strontium perchlorate trihydrate, barium perchlorate trihydrate, cerium (III) perchlorate hexahydrate, manganese (II) perchlorate hexahydrate, iron (II) perchlorate hydrate, iron (III) perchlorate hydrate, cobalt (II) perchlorate hexahydrate, nickel (II) perchlorate hexahydrate, copper (II) perchlorate hexahydrate, silver perchlorate, zinc perchlorate hexahydrate, cadmium perchlorate hydrate, mercury (II) perchlorate hydrate, aluminium perchlorate nonahydrate, lead (II) perchlorate hydrate and ammonium perchlorate solution (1 M in H_2O).

Nitrate salts analysed were lithium nitrate, sodium nitrate, potassium nitrate, rubidium nitrate, caesium nitrate, magnesium nitrate hexahydrate, calcium nitrate tetrahydrate, strontium nitrate, barium nitrate, scandium nitrate hydrate, yttrium (III) nitrate hexahydrate, lanthanum (III) nitrate hexahydrate, cerium (III) nitrate hexahydrate, praseodymium (III) nitrate hexahydrate, neodymium (III) nitrate hexahydrate, samarium (III) nitrate hexahydrate,

europium (III) nitrate pentahydrate, gadolinium (III) nitrate hexahydrate, terbium (III) nitrate pentahydrate, dysprosium (III) nitrate hydrate, holmium (III) nitrate pentahydrate, erbium (III) nitrate pentahydrate, thulium (III) nitrate hydrate, ytterbium (III) nitrate pentahydrate, lutetium (III) nitrate hydrate, chromium (III) nitrate nonahydrate, manganese (II) nitrate tetrahydrate, iron (III) nitrate nonahydrate, cobalt (II) nitrate hexahydrate, nickel (II) nitrate hexahydrate, palladium (II) nitrate dihydrate, copper (II) nitrate trihydrate, silver nitrate, zinc nitrate hexahydrate, cadmium nitrate tetrahydrate, mercury (I) nitrate dihydrate, mercury (II) nitrate monohydrate, aluminium nitrate nonahydrate, gallium nitrate hydrate, indium (III) nitrate hydrate, thallium (I) nitrate, thallium (III) nitrate trihydrate, lead (II) nitrate, ammonium nitrate, cerium (IV) ammonium nitrate and bismuth (III) nitrate pentahydrate.

- Instrumentation for Raman and IR Analysis

Raman analysis was performed with a Thermo Scientific DXR Raman microscope using the Thermo Scientific Omnic for dispersive Raman 8 software (Waltham, MA). Raman measurements were performed using a 532 nm excitation wavelength, 10 mW power, 10X magnification objective (3.1 µm diameter spot size) and 400 lines mm^{-1} grating, from 2000 to 400 cm^{-1}, with a spectral resolution of 2 (data spacing of 0.964 cm^{-1}). The spectra acquisition for all samples involved the accumulation of 6 scans of 5 s per scan. Five replicates collected from 5 different spots were analysed per sample (5 Raman spectra per salt).

A Thermo Scientific FTIR Nicolet IS10 spectrometer equipped with smart ITR module for ATR measurements and controlled through the Omnic™ spectroscopy for IR spectroscopy 9 (Waltham, MA, USA) was used for IR analysis. IR spectra were collected from 3000 to 600 cm^{-1}, with a resolution of 4 (data spacing of 0.483 cm^{-1}) and 16 scans. Five replicates were analysed per sample by placing fresh powder on the ATR diamond crystal for each replicate (5 IR spectra per salt).

These Raman and IR parameters were fixed by demonstrating they were suitable to obtain Raman spectra of high signal-to noise ratio for most of the salts.

- Data Analysis

Besides the visual spectra comparison, multivariate statistical analysis using Pearson Correlation (r) was performed to discriminate the salts.

First, the Raman shift and wavenumber values of the bands due to the chemical vibrational modes of nitrates, chlorates and perchlorates were visually compared and studied (see Results and Discussion). Afterwards, spectra were statistically compared using Pearson correlation. First of all, the optimum spectral range (in terms of selectivity for discriminating the salts) was selected after testing different potentially suitable ranges (*i.e.* containing always the most intense and characteristic bands). Either two optimum ranges were suitable for Raman, 1500–400 cm^{-1} or 1100–400 cm^{-1}, since both provided the same results in terms of the number of unequivocally identified salts; whereas the optimum range for IR was from 1500 to 600 cm^{-1}. It should be noted that the IR range was limited to 600 cm^{-1} because of the instrumental features. Then, spectra were normalized between 0 and 1 (using range normalization). Finally, the Pearson correlation analysis was performed. In order to study the selectivity, the intra- and inter-variability between every salt were evaluated. The intra-variability of each salt was accounted by calculating the Pearson correlation among the 5 spectra collected for each salt (10 combinations) avoiding the correlation of each spectrum with itself. Then, the inter-variability between two salts was accounted by calculating the Pearson Correlation between the 5 spectra of salt 1 and the 5 spectra of salt 2 (25 combinations). These calculations were iteratively performed for every salt using MatLab R2016b (Mathworks, USA) through a homemade algorithm based on the "*corrcoef*" function. Finally, the identification/ discrimination of salts was automatically performed in MatLab by comparing the intra-variability and inter-variability Pearson values of all salts using basic mathematical operations mainly based in less/greater than comparisons and conditional statement loops.

Results and Discussion

- Discrimination of Energetic Salts Using Raman Spectroscopy

The Raman spectra of these inorganic salts were dominated by those bands which are due to the vibrational modes of the anion, since it contains the covalent bonds N–O or Cl–O.

In brief, nitrate salts displayed two main bands in their Raman spectra, which were due to the N–O symmetric stretching vibration and the N–O in plane deformation. The symmetric stretching vibration of nitrate (ν_1 (A'_1)), which appeared as a unique band or two separate bands (probably because of a lowering of symmetry in the crystalline state) [25], ranged between 1075 and 1035 cm^{-1} in almost all nitrate salts. The N–O in plane deformation (ν_4 (E′)) ranged between 750 and 705 cm^{-1} for almost all the salts. However, there were some exceptions such as palladium nitrate, whose stretching vibration band was noticeably red-shifted down to 1004 cm^{-1}, or, even, there were new extra bands, as displayed in Figure 5.10. This phenomenon could be explained by the fact that palladium is not so electropositive and thus, their bonds with nitrate have a covalent character, which provide either the unusual shift of the nitrate bands or new bands due to new covalent cation–anion interactions [25]. In addition, a third band due to the antisymmetric stretching vibration of nitrate (ν_3 (E′)) was observed for some nitrate salts within the range 1400–1280 cm^{-1}, but it had a negligible intensity.

Regarding chlorate salts, their Raman spectra were characterized by displaying four bands, which resulted from the symmetric and antisymmetric stretching of Cl–O and the symmetric and anti-symmetric deformation of Cl–O. The anti-symmetric Cl–O stretching (ν_3 (E)) ranged from 980 to 960 cm^{-1} whereas the symmetric Cl–O stretching (ν_1 (A_1)) ranged from 940 to 910 cm^{-1}, except for silver chlorate whose anti-symmetric and symmetric stretching vibrations were located at 921 and 896 cm^{-1}, respectively. This shift to smaller wavenumbers might be due to an increase in the covalent character of the bond silver-chlorate, as previously observed for palladium nitrate. The symmetric Cl–O deformation (ν_2 (A_1)) ranged from 630 to 610 cm^{-1} whereas the anti-symmetric Cl–O deformation (ν_4 (E)) ranged from 500 to 480 cm^{-1}, for all the salts. The Raman spectra of chlorate salts are displayed in Figure 5.10.

Finally, the Raman spectra of perchlorate salts displayed three main bands, the symmetric stretching of Cl–O and two deformations of Cl–O. The symmetric Cl–O stretching (ν_1 (A_1)) ranged from 950 to 930 cm^{-1}, except for silver perchlorate and mercury perchlorate (II) whose bands were located at 923 and 924 cm^{-1}, respectively. Again, a red-shift was observed for the less electropositive metals. The Raman active Cl–O deformation (ν_4 (T_2)) ranged from 635 to 625 cm^{-1} whereas the theoretically Raman inactive Cl–O deformation (ν_2 (E)) ranged from

470 to 445 cm^{-1}, for all the salts except silver perchlorate, as shown in Figure 5.10. In addition, a fourth band due to the anti-symmetric stretching vibration of perchlorate (ν_3 (T_2)) was observed for most perchlorate salts within the range 1150–1040 cm^{-1}, but it had a negligible intensity, probably because this vibrational mode is also theoretically inactive in Raman. Again, the presence of these bands might be explained by the lowering of symmetry in the crystalline state.

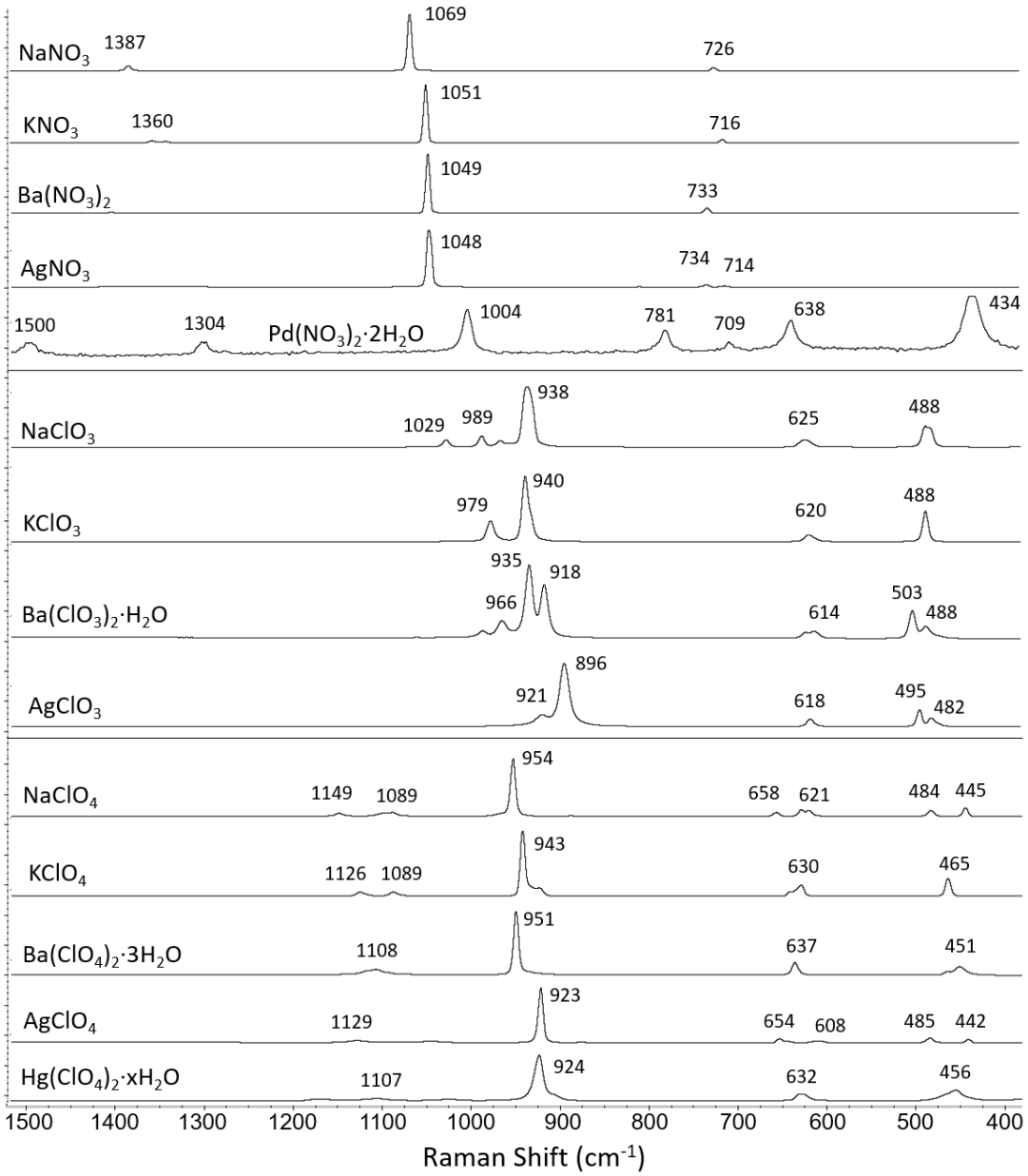

Figure 5.10. Raman spectra of sodium, potassium, barium, silver and palladium nitrates; sodium, potassium, barium and silver chlorates; and sodium, potassium, barium, silver and mercury perchlorates. Each spectrum is the average of five replicates of the salt, and each replicate was collected using 6 scans of 5 s per scan.

The Raman spectra of the 72 salts are displayed in the annexe of this Thesis.

- Discrimination of Energetic Salts Using IR Spectroscopy

As occurred with Raman, the IR spectra of these oxidizing salts were also dominated by those bands due to the vibrational modes of the anion.

However, contrary to Raman, nitrate salts displayed four characteristic bands in their IR spectra, which were due to the four vibrational modes of the nitrate molecule. Instead of the symmetric stretching vibration of nitrate (ν_1 (A'_1)), which appeared as a unique sharp medium-intense band or two sharp little-intense separate bands, within the range 1060 and 1020 cm^{-1}; the most intense band in the IR spectra was a wide band from 1450 to 1270 cm^{-1}, which was due to the antisymmetric stretching vibration (ν_3 (E′)). For many salts such as barium, nickel, copper or gadolinium, this unique wide band split into two or three bands. It should be highlighted that, theoretically, the symmetric stretching vibration of nitrate (ν_1 (A'_1)) is not IR active. However, it was observed in the IR spectra for most nitrate salts. This fact might be explained by a lowering of symmetry in the crystalline state [25]. Finally, the IR spectra of nitrate salts also displayed those bands due to the out-of-plane and in-plane deformation vibrational modes. The out-of-plane deformation band (ν_2 (A''_2)) ranged from 840 to 800 cm^{-1}, whereas the in-plane deformation band (ν_4 (E′)) was located within the range 780–700 cm^{-1}. The unique exception was palladium nitrate, whose bands were located at 899 and 784 cm^{-1}, as shown in Figure 5.11. Unexpectedly, in this case, the shift occurred towards higher wavenumbers.

Regarding the chlorate salts, their IR spectra displayed three main bands due to the vibrational modes of the chlorate. The antisymmetric Cl–O stretching (ν_3 (E)) ranged from 990 to 950 cm^{-1} whereas the symmetric Cl–O stretching (ν_1 (A_1)) ranged from 930 to 900 cm^{-1}, except for silver chlorate whose anti-symmetric and symmetric stretching vibrations were located at 915 and 881 cm^{-1}, respectively. As previously mentioned, this shift to smaller wavenumbers might be due to an increase in the covalent character of the bond silver-chlorate. Finally, the symmetric Cl–O deformation (ν_2 (A_1)) ranged from 630 to 610 cm^{-1} for all the chlorate salts. Unfortunately, since the IR spectrometer used only covered from 4000 to 600 cm^{-1}, the band due to the anti-symmetric deformation

of chlorate (ν_4 (E)) was not observed. The IR spectra of chlorate salts are displayed in Figure 5.11.

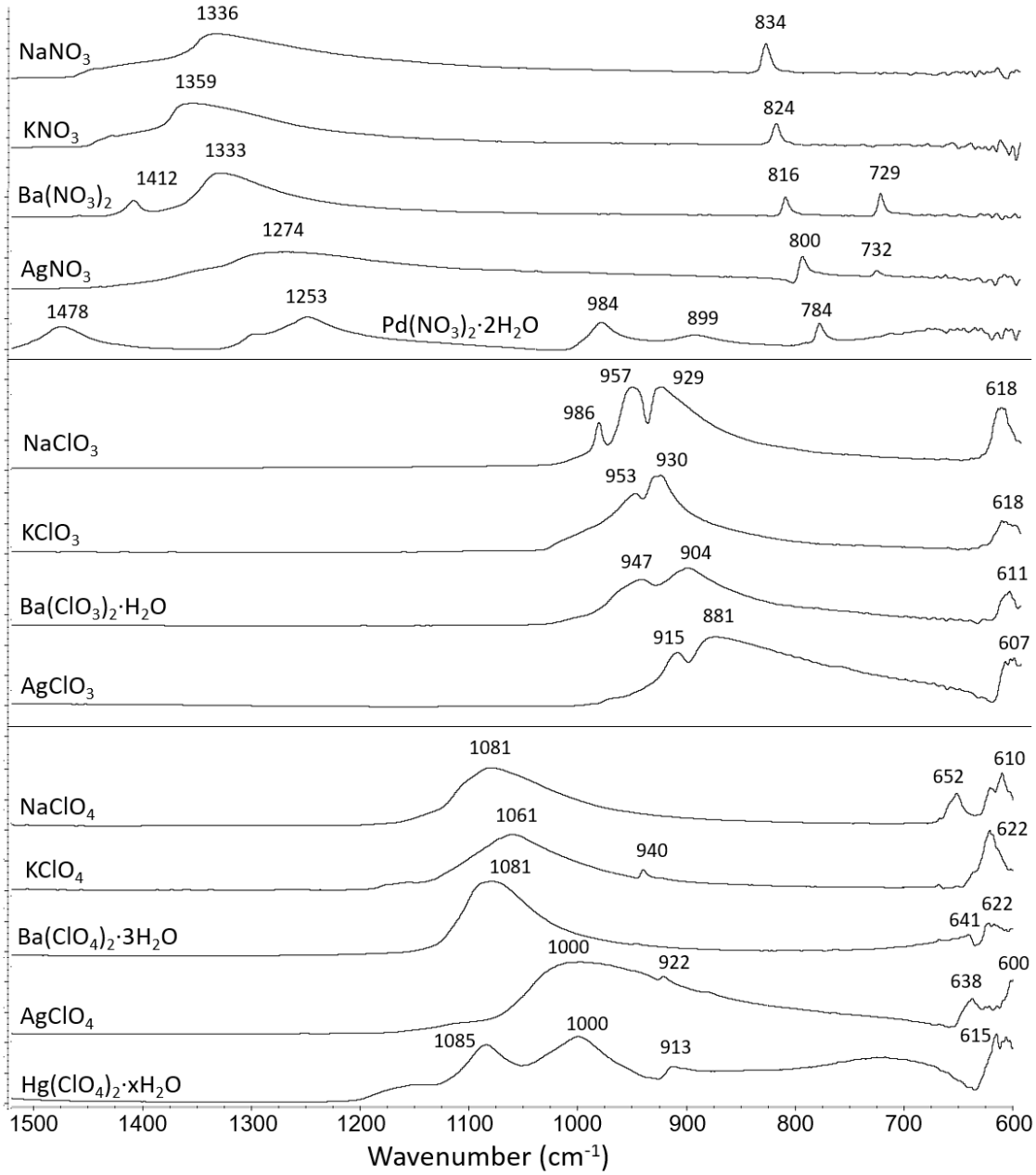

Figure 5.11. ATR-FTIR spectra of sodium, potassium, barium, silver and palladium nitrates; sodium, potassium, barium and silver chlorates; and sodium, potassium, barium, silver and mercury perchlorates. Each spectrum is the average of five replicates of the salt, and each replicate was collected using 16 scans.

Likewise, the IR spectra of perchlorate salts displayed three bands from the vibrational modes of perchlorate. The anti-symmetric stretching vibrational mode of perchlorate (ν_3 (T_2)) displayed a wide intense band that ranged from 1080 to 1030 cm^{-1}, except for silver and mercury perchlorates whose bands were

located at 1000 cm^{-1}, as shown in Figure 5.11. The symmetric stretching of perchlorate (ν_1 (A_1)) was only observed in half of the salts as a little-intense band that ranged from 950 to 930 cm^{-1}; which could be explained by the fact that, theoretically, the symmetric stretching of perchlorate is not IR active. Finally, the perchlorate deformation (ν_4 (T_2)) ranged from 630 to 600 cm^{-1}. Unfortunately, as previously explained for one of the chlorate deformations, the perchlorate deformation (ν_2 (E)) was not observed because of being located below the range measured by the IR spectrometer used.

The IR spectra of the 72 salts are displayed in the annexe of this Thesis.

- The Spectral Influence of Water in Hydrated Salts

As evidenced in experimental section, most of the salts were hydrated. Thus, the influence of water was studied by comparing the spectra of the same salt when hydrated and non-hydrated. Particularly, commercial anhydrous sodium perchlorate was compared with commercial sodium perchlorate monohydrate. As expected, spectra of both salts (either Raman or IR) were quite similar. Both displayed the main bands from the vibrational modes of the perchlorate and the respective shift influenced by the sodium. Nevertheless, despite the evident similarities, there were also significant differences. Regarding IR spectroscopy, the most noticeable change was the presence of the band from water at 1627 cm^{-1} (water is IR active). Fortunately, this change was removed when considering only the IR range of nitrates, chlorates and perchlorates vibrations (from 600 to 1500 cm^{-1}). Also noticeable was the presence of a new band at 652 cm^{-1} in the anhydrous salt in contrast to the hydrated one. This fact was also verified by Raman (658 cm^{-1}). In addition, when comparing their Raman spectra, the most noticeable change was the fact that those bands due to deformation vibrational modes in sodium perchlorate monohydrate split into two bands in anhydrous sodium perchlorate, as displayed in Figure 5.12.

Thus, the presence of this new band located at 658 cm^{-1} in the anhydrous salt and the two bands at 630 and 621 cm^{-1} in Raman is likely explained by the splitting of the tri-degenerate deformation (ν_4 (T_2)) because of a significant lowering of the symmetry in the anhydrous salt. In fact, the presence of water molecules within the ionic crystalline structure seems to unify those small shifts of vibrational modes of the anion that are due to the lowering of symmetry in

the crystalline state. This effect, observed for sodium perchlorate monohydrate, also occurred in other di-, tri- and tetra-hydrate salts. This fact seems to evidence that the presence of water (either mono-, di-, tri-hydrate, etc.) reduces the splitting of bands keeping the degeneration of the vibrational mode in contrast to anhydrous salts. Most nitrate, chlorate and perchlorate salts are highly hygroscopic. Thus, it is expected that they will contain some level of hydration in real samples. Therefore, this aspect should be taken into account when identifying the salts.

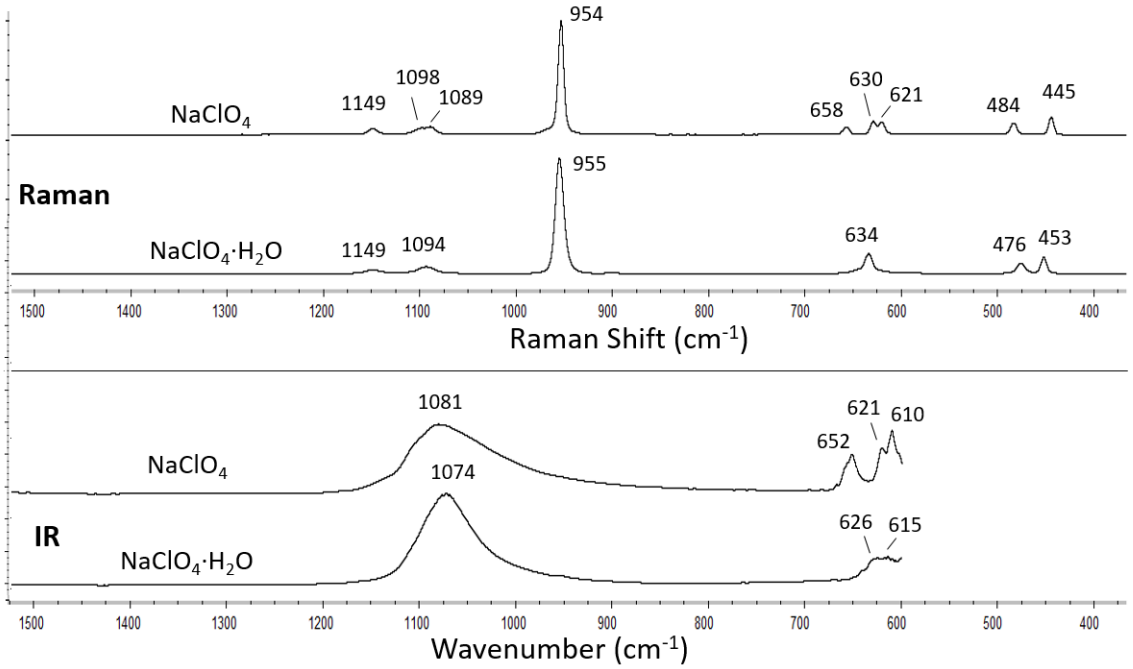

Figure 5.12. Raman and ATR-FTIR spectra of sodium perchlorate anhydrous and hydrate.

- Statistical Discrimination of Energetic Salts Using Pearson Correlation

Positively, by studying either the Raman or IR spectra of an unknown oxidizing salt, the main bands in the spectra easily reveal the nature of the anion, *i.e.* nitrate, chlorate or perchlorate. To this aim, Table 5.9 summarizes the experimental Raman and IR ranges within which the vibrational modes of nitrates, chlorates and perchlorates were located.

Table 5.9. Vibrational modes of nitrates, chlorates and perchlorates [25-27] and the experimental Raman and IR ranges within which were located in this study.

Nitrates	ν_1 (A´$_1$) Symmetric stretch (Raman active)		ν_2 (A´´$_2$) Out of plane deformation (IR active)		ν_3 (E´) Anti-symmetric stretch (Raman-IR active)		ν_4 (E´) In plane deformation (Raman-IR active)	
	Raman	IR[1]	IR		Raman[2]	IR	Raman	IR
	1075-1035	1060-1020	840-800		1400-1280	1450-1270	750-705	780-700
Chlorates	ν_1 (A_1) Symmetric stretch (Raman-IR active)		ν_2 (A_1) Symmetric deformation (Raman-IR active)		ν_3 (E) Anti-symmetric stretch (Raman-IR active)		ν_4 (E) Anti-symmetric deformation (Raman-IR active)	
	Raman	IR	Raman	IR	Raman	IR	Raman	IR[2]
	940-910	930-900	630-610		980-960	990-950	500-480	-
Perchlorates	ν_1 (A_1) Symmetric stretch (Raman active)		ν_2 (E) Deformation (Raman active)		ν_3 (T_2) Anti-symmetric stretch (IR active)		ν_4 (T_2) Deformation (IR active)	
	Raman	IR[1]	Raman	IR[1,2]	Raman[1]	IR	Raman[1]	IR
	950-930	950-930	470-445	-	1150-1040	1080-1030	635-625	630-600

IR[1]: Theoretical IR inactive vibrations violated by the lowering of symmetry in the crystalline state.
Raman[1]: Theoretical Raman inactive vibrations violated by the lowering of symmetry in the crystalline state.
IR[2]: Bands below the IR range considered in this work.
Raman[2]: Negligible-intense bands.

Negatively, the determination of the cation was not so straightforward. No spectral bands came from the cation except for molecular cations as ammonium. However, it was evidenced, for either Raman or IR, that the vibrational modes from the anion were influenced somehow by the cation. A noticeable shift in their Raman shift/wavenumber was observed depending on the cation to which the anion was bonded. Since it is widely known that IR and Raman spectroscopy are complementary techniques; in this study, the capability of both Raman and IR spectral features to unequivocally identify each oxidizing salt was examined, as well as the identification improvement when combining both techniques.

In order to mathematically evaluate the unequivocal identification, *i.e.* whether the spectral differences among salts enable their discrimination; the Pearson correlation coefficients (r) were calculated and studied. To this aim, the r between spectra of the same salt (intra-correlation) was compared with the r between spectra of different salts (inter-correlation). A Pearson value over 0.95 was selected as the condition to confirm the identification.

Positively, the intra-correlation using only Raman was over 0.95 for all the salts except for $Hg(ClO_4)_2$, $Mg(ClO_4)_2$, $Co(NO_3)_2$, $Lu(NO_3)_3$ and $Y(NO_3)_3$,whose average r values were 0.91, 0.84, 0.90, 0.92 and 0.87, respectively. Afterwards, the inter-variability between salts was evaluated. Interestingly, 25 salts were unequivocally identified using Raman as summarized in Table 5.10, *i.e.* their intra-variability was lower than their inter-variability since their intra-correlation was over 0.95 (except for $Hg(ClO_4)_2$ and $Lu(NO_3)_3$) while their inter-correlation with any other salt was below 0.95 (or 0.90 in the case of $Hg(ClO_4)_2$ and $Lu(NO_3)_3$).

Likewise, the intra-correlation using IR was over 0.95 for all the salts except for $Fe(ClO_4)_3$, $Ni(ClO_4)_2$, $Ba(NO_3)_2$, $Er(NO_3)_3$, $Ga(NO_3)_3$, $Nd(NO_3)_3$, $Tm(NO_3)_3$ and $Y(NO_3)_3$, whose average r values were 0.89, 0.86, 0.94, 0.87, 0.94, 0.94, 0.93 and 0.90, respectively. After evaluating the inter-variability, 30 salts were unequivocally identified using IR, as summarized in Table 5.10, *i.e.* their intra-variability was lower than their inter-variability since their intra-correlation was over 0.95 (except for $Ba(NO_3)_2$) while their inter-correlation was below 0.95 (or 0.94 in the case of $Ba(NO_3)_2$).

Table 5.10. Unequivocally identified salts by comparing through Pearson correlation their Raman spectra, IR spectra or both. Intra-correlation was over 0.95 while inter-correlation with any other salt was below 0.95. In order to save space, only the chemical formula of the salt (cation-anion) is displayed, not the number of hydrated water molecules.

Unequivocally Identified Salts *(Intra-variability < Inter-variability)*		
Raman (25/72)	**IR (30/72)**	**Raman + IR (44/72)**
$AgClO_3$, $Ba(ClO_3)_2$, $KClO_3$, $NaClO_3$, $AgClO_4$, $Ba(ClO_4)_2$, $Hg(ClO_4)_2$*, $KClO_4$, $NaClO_4$, $(NH_4)_2Ce(NO_3)_6$, $Bi(NO_3)_3$, $Cr(NO_3)_3$, $Cu(NO_3)_2$, $Er(NO_3)_3$, $Eu(NO_3)_3$, $Hg(NO_3)_2$, $LiNO_3$, $Lu(NO_3)_3$*, $Mg(NO_3)_2$, $NaNO_3$, $Pd(NO_3)_2$, $Sc(NO_3)_3$, $Sm(NO_3)_3$, $Tl(NO_3)_3$ & $TlNO_3$	$AgClO_3$, $Ba(ClO_3)_2$, $AgClO_4$, $Hg(ClO_4)_2$, $Mg(ClO_4)_2$, NH_4ClO_4, $AgNO_3$, $Ba(NO_3)_2$*, $Bi(NO_3)_3$, $Ca(NO_3)_2$, $Cd(NO_3)_2$, $Cu(NO_3)_2$, $Dy(NO_3)_3$, $Hg(NO_3)_2$, $Hg_2(NO_3)_2$, $In(NO_3)_3$, KNO_3, $LiNO_3$, $Lu(NO_3)_3$, $Mn(NO_3)_2$, $(NH_4)_2Ce(NO_3)_6$, NH_4NO_3, $Ni(NO_3)_2$, $Pb(NO_3)_2$, $Pd(NO_3)_2$, $Sc(NO_3)_3$, $Sr(NO_3)_2$, $Tl(NO_3)_3$, $TlNO_3$ & $Yb(NO_3)_3$	$AgClO_3$, $Ba(ClO_3)_2$, $KClO_3$, $NaClO_3$, $AgClO_4$, $Ba(ClO_4)_2$, $Hg(ClO_4)_2$*, $KClO_4$, $Mg(ClO_4)_2$, $NaClO_4$, NH_4ClO_4, $AgNO_3$, $Ba(NO_3)_2$*, $Bi(NO_3)_3$, $Ca(NO_3)_2$, $Cd(NO_3)_2$, $Cr(NO_3)_3$, $CsNO_3$, $Cu(NO_3)_2$, $Dy(NO_3)_3$, $Er(NO_3)_3$, $Eu(NO_3)_3$, $Gd(NO_3)_3$, $Hg(NO_3)_2$, $Hg_2(NO_3)_2$, $In(NO_3)_3$, KNO_3, $LiNO_3$, $Lu(NO_3)_3$*, $Mg(NO_3)_2$, $Mn(NO_3)_2$, $(NH_4)_2Ce(NO_3)_6$, $NaNO_3$, NH_4NO_3, $Ni(NO_3)_2$, $Pb(NO_3)_2$, $Pd(NO_3)_2$, $RbNO_3$, $Sc(NO_3)_3$, $Sm(NO_3)_3$, $Sr(NO_3)_2$, $Tl(NO_3)_3$, $TlNO_3$ & $Yb(NO_3)_3$

* Intra-correlation was between 0.90 and 0.95

Finally, it was decided to study the salts that remained undistinguishable by evaluating together Raman and IR spectroscopy. By combining both spectroscopic techniques, there were 44 salts that were unequivocally identified as summarized in Table 5.10, *i.e.* their intra-correlation (for both Raman and IR) was over 0.95 while their inter-correlation with any other salt (using either Raman, IR or both) was below 0.95.

In addition to Table 5.10, which summarizes the salts that were identified, Table 5.11 was created to summarize the groups of salts that were undistinguishable among each other. For those non-identified salts, it was useful to study the correlation among them and check which ones were undistinguishable and might be erroneously mistaken. Regarding Raman spectroscopy, there were 26 groups of salts with an average of three salts per group which were undistinguishable among each other. However, it was noticeable that groups of perchlorate salts contained a larger number of undistinguishable salts (up to 10) than nitrate groups (in which the number of undistinguishable salts ranged from two to four salts). Concerning IR, there were 23 groups of salts with an average of three salts per group which were undistinguishable among each other. In this case, both perchlorate and nitrate groups contained a similar number of undistinguishable salts (from two to five salts). Finally, when considering together Raman and IR, there were still 15 groups of salts with an average of three salts per group (for perchlorate groups) and two salts per group (for nitrate groups) which were undistinguishable among each other.

By studying the Raman and IR spectroscopic data of each salt, some of the salts that were not discriminated using either only Raman or IR, were properly discriminated when considering the other technique. For instance, barium nitrate might be erroneously identified as gadolinium or lead nitrate using Raman but it was unequivocally identified using IR. On the contrary, potassium perchlorate might be erroneously identified as nickel perchlorate using IR but it was unequivocally identified using Raman. Furthermore, there were some peculiar cases such as caesium nitrate which might be erroneously identified as either calcium, mercury (I) or potassium nitrates using Raman, but as sodium or rubidium nitrates using IR. Positively, by considering both techniques, caesium nitrate was unequivocally identified since no other salt provided a Pearson value over 0.95 for both Raman and IR when compared with caesium nitrate.

Table 5.11. Groups of undistinguishable salts by comparing through Pearson correlation their Raman spectra, IR spectra or both. Inter-correlation between salts within the same group was over 0.95. In order to save space, only the chemical formula of the salt (cation-anion) is displayed, not the number of hydrated water molecules.

Groups of undistinguishable Salts		
Raman (47/72)	**IR (42/72)**	**Raman + IR (28/72)**
$Al(ClO_4)_3$, $Cd(ClO_4)_2$, $Cu(ClO_4)_2$ & $Fe(ClO_4)_3$	$KClO_3$ & $NaClO_3$	$Al(ClO_4)_3$ & $Fe(ClO_4)_3$
$Al(ClO_4)_3$, $Cd(ClO_4)_2$, $Cu(ClO_4)_2$ & $Mg(ClO_4)_2$	$Al(ClO_4)_3$ & $Fe(ClO_4)_3$	$Ca(ClO_4)_2$ & $NaClO_4\_H_2O$
$Ca(ClO_4)_2$, $NaClO_4\_H_2O$ & $Sr(ClO_4)_2$	$Ba(ClO_4)_2$, $Ca(ClO_4)_2$ & $NaClO_4$	$Ca(ClO_4)_2$ & $Sr(ClO_4)_2$
$Cd(ClO_4)_2$, $Ce(ClO_4)_3$, $Co(ClO_4)_2$, $Fe(ClO_4)_2$, $LiClO_4$, $Mg(ClO_4)_2$, $Mn(ClO_4)_2$, $Ni(ClO_4)_2$, $Pb(ClO_4)_2$ & $Zn(ClO_4)_2$	$Ba(ClO_4)_2$, $Ca(ClO_4)_2$ & $NaClO_4\_H_2O$	$Cd(ClO_4)_2$, $Ce(ClO_4)_3$, $Co(ClO_4)_2$ & $Ni(ClO_4)_2$
$Cd(ClO_4)_2$, $Co(ClO_4)_2$, $Cu(ClO_4)_2$, $Mg(ClO_4)_2$, $Ni(ClO_4)_2$ & $Zn(ClO_4)_2$	$Ca(ClO_4)_2$, $Mn(ClO_4)_2$ & $Sr(ClO_4)_2$	$Cd(ClO_4)_2$, $Co(ClO_4)_2$, $Cu(ClO_4)_2$, $Ni(ClO_4)_2$ & $Zn(ClO_4)_2$
$Cd(ClO_4)_2$, $Co(ClO_4)_2$, $Fe(ClO_4)_2$, $LiClO_4$, $Mg(ClO_4)_2$, $Mn(ClO_4)_2$, NH_4ClO_4, $Ni(ClO_4)_2$ & $Zn(ClO_4)_2$	$Cd(ClO_4)_2$, $Ce(ClO_4)_3$, $Co(ClO_4)_2$ & $Ni(ClO_4)_2$	$Cd(ClO_4)_2$, $Co(ClO_4)_2$, $Mn(ClO_4)_2$ & $Ni(ClO_4)_2$
$AgNO_3$, $Mn(NO_3)_2$ & $Nd(NO_3)_3$	$Cd(ClO_4)_2$, $Co(ClO_4)_2$, $Cu(ClO_4)_2$, $Ni(ClO_4)_2$ & $Zn(ClO_4)_2$	$Ce(ClO_4)_3$, $LiClO_4$, $Ni(ClO_4)_2$ & $Pb(ClO_4)_2$
$AgNO_3$ & $Pb(NO_3)_2$	$Cd(ClO_4)_2$, $Co(ClO_4)_2$, $Mn(ClO_4)_2$ & $Ni(ClO_4)_2$	$Fe(ClO_4)_2$ & $Ni(ClO_4)_2$
$Al(NO_3)_3$ & $Ga(NO_3)_3$	$Cd(ClO_4)_2$, $Mn(ClO_4)_2$, $Ni(ClO_4)_2$ & $Sr(ClO_4)_2$	$Al(NO_3)_3$ & $Ga(NO_3)_3$
$Ba(NO_3)_2$, $Gd(NO_3)_3$ & $Pb(NO_3)_2$	$Ce(ClO_4)_3$, $LiClO_4$, $Ni(ClO_4)_2$ & $Pb(ClO_4)_2$	$Ce(NO_3)_3$ & $La(NO_3)_3$
$Ca(NO_3)_2$ & $Cd(NO_3)_2$	$Fe(ClO_4)_2$ & $Ni(ClO_4)_2$	$Co(NO_3)_2$ & $Zn(NO_3)_2$
$Ca(NO_3)_2$, $CsNO_3$, $Hg_2(NO_3)_2$ & KNO_3	$KClO_4$ & $Ni(ClO_4)_2$	$Fe(NO_3)_3$ & $Ga(NO_3)_3$
$Ca(NO_3)_2$, $Dy(NO_3)_3$, $Hg_2(NO_3)_2$ & KNO_3	$Al(NO_3)_3$ & $Ga(NO_3)_3$	$Ho(NO_3)_3$ & $Tb(NO_3)_3$
$Ca(NO_3)_2$, $Dy(NO_3)_3$, $Hg_2(NO_3)_2$ & $Y(NO_3)_3$	$Ce(NO_3)_3$ & $La(NO_3)_3$	$Nd(NO_3)_3$ & $Pr(NO_3)_3$
$Ca(NO_3)_2$, $Dy(NO_3)_3$, $Y(NO_3)_3$ & $Yb(NO_3)_3$	$Co(NO_3)_2$, $Mg(NO_3)_2$ & $Zn(NO_3)_2$	$Tm(NO_3)_3$ & $Y(NO_3)_3$
$Ce(NO_3)_3$, $Fe(NO_3)_3$ & $Ga(NO_3)_3$	$Cr(NO_3)_3$, $Fe(NO_3)_3$ & $Ga(NO_3)_3$	
$Ce(NO_3)_3$, $Fe(NO_3)_3$ & $La(NO_3)_3$	$CsNO_3$, $NaNO_3$ & $RbNO_3$	
$Co(NO_3)_2$ & $Zn(NO_3)_2$	$Er(NO_3)_3$, $Ho(NO_3)_3$, $Tb(NO_3)_3$ & $Tm(NO_3)_3$	
$Dy(NO_3)_3$ & $Gd(NO_3)_3$	$Eu(NO_3)_3$, $Pr(NO_3)_3$ & $Sm(NO_3)_3$	
$Ho(NO_3)_3$ & $Tb(NO_3)_3$	$Gd(NO_3)_3$ & $Y(NO_3)_3$	
$Ho(NO_3)_3$ & $Y(NO_3)_3$	$Nd(NO_3)_3$, $Pr(NO_3)_3$ & $Sm(NO_3)_3$	
$In(NO_3)_3$ & $Zn(NO_3)_2$	$Sm(NO_3)_3$ & $Y(NO_3)_3$	
$Mn(NO_3)_2$, $Nd(NO_3)_3$, NH_4NO_3 & $Pr(NO_3)_3$	$Tm(NO_3)_3$ & $Y(NO_3)_3$	
$Ni(NO_3)_2$ & $Zn(NO_3)_2$		
$RbNO_3$, $Sr(NO_3)_2$ & $Zn(NO_3)_2$		
$Tm(NO_3)_3$ & $Y(NO_3)_3$		

Conclusions

Vibrational spectroscopic techniques such as IR and Raman spectroscopy enable an accurate discrimination of oxidizing salts according to their different anions: nitrates, chlorates and perchlorates. The characteristic chemical vibrational modes of these anions are selective enough to identify these salts either using IR or Raman spectroscopy.

Nevertheless, the discrimination between salts that have the same anion and only differ in the cation was not so straightforward. Thus, besides the visual spectra comparison, a simple statistical analysis based on Pearson correlation helps to objectively discriminate and identify these salts, discriminating the cation. According to the results, the cation influences the shift of the bands from the anion.

Some salts, which contained the same anion and different cations, were not unequivocally identified when using only their IR or Raman spectra, but when combining IR and Raman information. In fact, the discrimination of salts significantly improved when considering both techniques together, despite the fact that there were still 28 salts that were not unequivocally identified.

It is important to highlight that spectral ranges considered in this study were dominated by the vibrational modes of the anions (due to their covalent bonds) and their shift due to the cation-anion interactions. However, in order to improve the discrimination, further information involving the lattice modes of these solid crystalline salts might be studied using high resolution instruments covering the spectral range below 400 cm^{-1}.

A further relevant challenge involves the simultaneous identification of different salts in mixtures. It is essential to study whether two salts in a mixture might be spectrally resolved. Depending on how much their main characteristic bands differ among each other, high or medium spectral resolution might be required. Further research to answer this point is highly necessary.

References

[1] A. Beveridge, Forensic Investigation of Explosions, Taylor & Francis, 1998.

[2] J.B. Ledgard, The preparation of nitrates, chlorates, and perchlorates, in: J.B. Ledgard (Ed.), The Preparatory Manual of Explosives, Paranoid Publications, 2002.

[3] J.T. Thurman, Practical Bomb Scene Investigation, Taylor & Francis, 2006.

[4] TM 31-210, Improvised Munitions Handbook (Improvised Explosive Devices or IEDs), Department of the Army Technical Manual, 2007.

[5] J. Donner, A Professional's Guide to Pyrotechnics: Understanding and Making Exploding Fireworks, Paladin Press, 1997.

[6] J.B. Ledgard, The Preparatory Manual of Black Powder and Pyrotechnics, Lulu, 2006.

[7] R. Meyer, J. Köhler, A. Homburg, Explosives, Sixth edition Wiley, 2007.

[8] M. Pumera, Analysis of explosives via microchip electrophoresis and conventional capillary electrophoresis: a review, Electrophoresis 27 (2006) 244-256.

[9] K.G. Hopper, H. LeClair, B.R. McCord, A novel method for analysis of explosives residue by simultaneous detection of anions and cations via capillary zone electrophoresis, Talanta 67 (2005) 304-312.

[10] J.P. Hutchinson, C.J. Evenhuis, C. Johns, A.A. Kazarian, M.C. Breadmore, M. Macka, E.F. Hilder, R.M. Guijt, G.W. Dicinoski, P.R. Haddad, Identification of inorganic improvised explosive devices by analysis of postblast residues using portable capillary electrophoresis instrumentation and indirect photometric detection with a light emitting diode, Anal. Chem. 79 (2007) 7005-7013.

[11] J.P. Hutchinson, C. Johns, M.C. Breadmore, E.F. Hilder, R.M. Guijt, C. Lennard, G. Dicinoski, P.R. Haddad, Identification of inorganic ions in post-blast explosive residues using portable CE instrumentation and capacitively coupled contactless conductivity detection, Electrophoresis 29 (2008) 4593-4602.

[12] C. Sarazin, N. Delaunay, A. Varenne, J. Vial, C. Costanza, V. Eudes, J.Minet, P. Gareil, Identification and determination of inorganic anions in real extracts from pre- and postblast residues by capillary electrophoresis, J. Chromatogr. A 1217 (2010) 6971-6978.

[13] C. Martín-Alberca, M.A. Fernández de la Ossa, J. Sáiz, J.L. Ferrando, C. García-Ruiz, Anions in pre- and post-blast consumer fireworks by capillary electrophoresis, Electrophoresis 35 (2014) 3272-3280.

[14] D.K. Kuila, A. Chakrabortty, S.P. Sharma, S.C. Lahiri, Composition profile of lowexplosives from cases in India, Forensic Sci. Int. 159 (2006) 127-131.

[15] G.W. Dicinoski, R.A. Shellie, P.R. Haddad, Forensic identification of inorganic explosives by ion chromatography, Anal. Lett. 39 (4) (2006) 639-657.

[16] C. Johns, R.A. Shellie, O.G. Potter, J.W. O'Reilly, J.P. Hutchinson, R.M. Guijt, M.C. Breadmore, E.F. Hilder, G.W. Dicinoski, P.R. Haddad, Identification of homemade

inorganic explosives by ion chromatography analysis of post-blast residues, J. Chromatogr. A 1182 (2008) 205-214.

[17] E. Tyrrell, E.F. Hilder, R.A. Shalliker, G.W. Dicinoski, R.A. Shellie, M.C. Breadmore, C.A. Pohl, P.R. Haddad, Packing procedures for high efficiency, short ion-exchange columns for rapid separation of inorganic anions, J. Chromatogr. A 1208 (2008) 95-100.

[18] H. Meng, T. Wang, B. Guo, Y. Hashi, C. Guo, J. Lin, Simultaneous determination of inorganic anions and cations in explosive residues by ion chromatography, Talanta 76 (2008) 241-245.

[19] L. Barron, E. Gilchrist, Ion chromatography-mass spectrometry: a review of recent technologies and application in forensic and environmental explosives analysis, Anal. Chim. Acta 806 (2014) 27-54.

[20] C. Martín-Alberca, F. Zapata, H. Carrascosa, F.E. Ortega-Ojeda, C. García-Ruiz, Study of consumer fireworks post-blast residues by ATR-FTIR, Talanta 149 (2016) 257-265.

[21] F. Zapata, M.A. Fernández de la Ossa, E. Gilchrist, L. Barron, C. García-Ruiz, Progressing the analysis of improvised explosive devices: comparative study for trace detection of explosive residues in handprints by Raman spectroscopy and liquid chromatography, Talanta 161 (2016) 219-227.

[22] M.R. Almeida, D.N. Correa, J.J. Zacca, L.P.L. Logrado, R.J. Poppi, Detection of explosives on the surface of banknotes by Raman hyperspectral imaging and independent component analysis, Anal. Chim. Acta 860 (2015) 15-22.

[23] F. Zapata, C. García-Ruiz, Determination of nanogram microparticles from explosives after real open-air explosions by confocal Raman microscopy, Anal. Chem. 88 (2016) 6726-6733.

[24] F. Zapata, C. García-Ruiz, Analysis of different materials subjected to open-air explosions in search of explosive traces by Raman microscopy, Forensic Sci. Int. 275 (2017) 57-64.

[25] R.A. Nyquist, R.O. Kagel, Handbook of Infrared and Raman Spectra of Inorganic Compounds and Organic Salts. Chapter 1, Infrared Spectra of Inorganic Compounds, Academic Press, 1971.

[26] K. Nakamoto, Infrared and Raman Spectra of Inorganic and Coordination Compounds, Part A. Theory and Applications in Inorganic Chemistry, 6th edition John Wiley and Sons Inc., New York, 2009.

[27] J.T. Kloprogge, D. Wharton, L. Hickey, R.L. Frost, Infrared and Raman study of interlayer anions CO_3^{2-}, NO_3^-, SO_4^{2-} and ClO_4^- in Mg/Al-hydrotalcite, Am. Mineral. 87 (2002) 623-629.

5.3. Near Infrared Characterization of Explosives and Energetic Salts

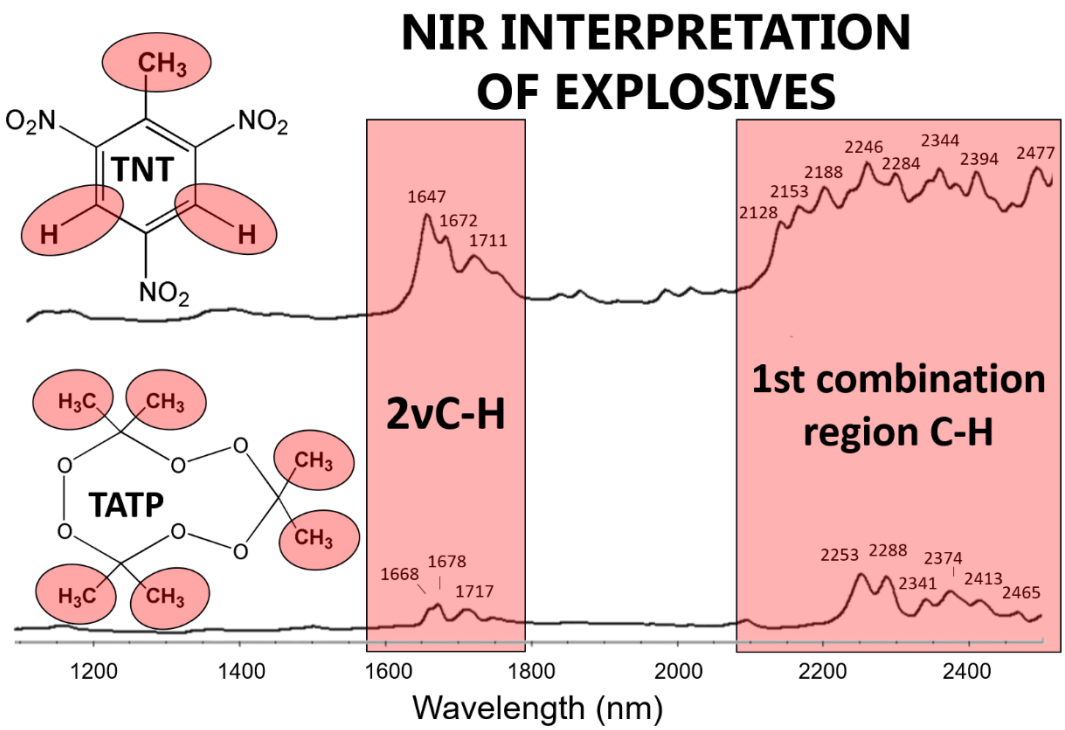

Abstract

The NIR spectra from 1000 to 2500 nm of 18 different explosives, propellant powders and energetic salts were collected and interpreted. NIR spectroscopy is known to provide information about the combination bands and overtones of highly anharmonic vibrations as those occurring in X-H bonds (C-H, N-H and O-H). Particularly intense and complex were the bands corresponding to the first combination region (2500-1900 nm) and first overtone stretching mode (2ν) of C-H and N-H bonds (1750-1450 nm). Inorganic oxidizing salts including sodium nitrate, potassium nitrate, sodium chlorate, potassium chlorate, sodium perchlorate, and potassium perchlorate displayed low intense or no NIR bands.

Introduction

Every fundamental vibrational mode that is active in the mid-infrared region (MIR) from 4000 to 400 cm^{-1} (*i.e.* 2500-25000 nm), have different overtones and combination bands at higher energies (lower wavelengths). Among those IR active vibrations, the fundamental vibrations whose overtones and combination bands lie on the near-infrared (NIR) region from 1000 to 2500 nm (*i.e.* 12500-4000 cm^{-1}), are those belonging to highly anharmonic vibrations [1, 2]. In fact, although overtones and combination bands are theoretically forbidden for harmonic oscillators, they are usually observed in real anharmonic molecular vibrations. In general, these anharmonic vibrations involve the stretching vibrations of strong short bonds, as those occurring between small atoms and hydrogen (X-H). Most of the X-H stretching fundamental vibrations absorb at wavenumbers above 2000 cm^{-1} (MIR) so that their first overtones appear in the NIR region [1, 2]. These chemical bonds usually prevail in organic molecules including C-H, O-H and N-H. In fact, there is such a common prevalence of C-H, O-H and N-H bonds in organic molecules that the selectivity of NIR spectroscopy has been traditionally questioned. However, according to the high number of combination bands that may exist for a certain number of fundamental vibrations, it is even possible (for some molecules) that the combination bands will provide a more specific profile of identification than the fundamental IR spectrum or IR fingerprint [3].

A large number of explosive compounds contain C-H and/or N-H bonds in their structure, including not only organic explosives, such as 2,4,6-trinitrotoluene (TNT) and triacetone-triperoxide (TATP); but also smokeless gun-powders and propellants (composed of nitrocellulose (NC), nitroglycerine (NG) and nitroguanidine (NQ)); and also ammonium nitrate (AN) based explosives, such as dynamite or ammonium nitrate fuel oil (ANFO). An extensive literature can be found for most common explosives and energetic salts about the chemical fundamental vibrations occurring in MIR and Raman spectroscopy [3-11]. However, the analysis and vibrational interpretation of explosives using NIR spectroscopy is very limited (almost missing) in literature. Most of the studies in which NIR spectroscopy has been tested for the analysis of explosives [12-20], usually involve the employment of hyperspectral imaging (HSI) in very short NIR range (800-1700 nm) with the aim of detecting explosive residues on different matrixes such as clothing or fingerprints [15-20]. Advanced pre-

processing and classification chemometric models are performed in order to discriminate the explosive residues over the background [15-20]. However, the fundamental chemical interpretation of the NIR spectra of explosives is not usually reported.

In order to reduce this lack of knowledge, this study focuses on the comprehensive study and interpretation of the NIR spectra displayed by 18 different explosives commonly used in the manufacture of commercial explosives, commercial ammunition and homemade improvised explosive devices (IEDs).

Experimental section

- Explosives

In this study, 18 different explosives, propellant powders and energetic salts were analysed. They are summarized in Table 5.12. Explosives and propellant powders were provided by Spanish Explosive Ordnance Disposal (EOD). Energetic salts were purchased anhydrous at ACS grade (purity over 98%) from Sigma-Aldrich (St. Louis, MO, USA).

Table 5.12. Explosives, propellant powders and energetic salts included in this study. Their chemical composition (provided by EOD) is summarized in column 2. Regarding explosive mixtures, only major components whose mass percentage is over 10% are indicated.

Explosives / energetic salts	**Chemical composition (mass percentage)**	**Type**
TNT	2,4,6-Trinitrotoluene (100%)	Nitroaromatic explosive
RDX-plastic explosive	Cyclotrimethylene trinitramine (91%)	Nitramine explosive
PETN	Pentaerythritol tetranitrate (100%)	Nitrate ester
TATP	Triacetone triperoxide (100%)	Peroxide explosive
HMTD	Hexamethylene triperoxide diamine (100%)	Peroxide explosive
Powder 1 (NC+NQ+NG)	Nitrocellulose (19%) + Nitroguanidine (55%) + Nitroglycerine (18%)	Triple-base smokeless gunpowder
Powder 2 (NC+DNT)	Nitrocellulose (85%) + Dinitrotoluene (10%)	Double-base smokeless gunpowder
Powder 3 (NC+NG)	Nitrocellulose (71%) + Nitroglycerine (25%)	Double-base smokeless gunpowder
Powder 4 (NC)	Nitrocellulose (94%)	Single-base smokeless gunpowder

Dynamite	Ammonium nitrate (66%) + Ethylene glycol dinitrate (29%)	AN-explosive
ANFO	Ammonium nitrate (90%) + diesel (10%)	AN-explosive
NH_4NO_3	Ammonium nitrate (100%)	Nitrate salt
$NaNO_3$	Sodium nitrate (100%)	Nitrate salt
KNO_3	Potassium nitrate (100%)	Nitrate salt
$NaClO_3$	Sodium chlorate (100%)	Chlorate salt
$KClO_3$	Potassium chlorate (100%)	Chlorate salt
$NaClO_4$	Sodium perchlorate (100%)	Perchlorate salt
$KClO_4$	Potassium perchlorate (100%)	Perchlorate salt

- Instrumentation for Near Infrared analysis

A NIRS XDSTM Rapid Content Analyzer spectrometer (Figure 5.13) from Metrohm AG (Herisau, Switzerland) working in the range 400-2500 nm and controlled through the Vision Spectral Analysis Software developed by Foss NIRSystems Inc. (Hilleroed, Denmark) was used for characterizing the NIR spectra of explosives. Around 0.5 g of explosive was placed onto the sampling cell to be analysed. NIR spectra were collected from 1000 to 2500 nm, with a spectral resolution of 2 nm (data spacing of 0.5 nm) and 32 scans. Three replicate spectra were collected per explosive by analysing three different sample portions. The NIR spectra displayed in Results section is the spectral average of the three replicates. No further pre-processing was performed.

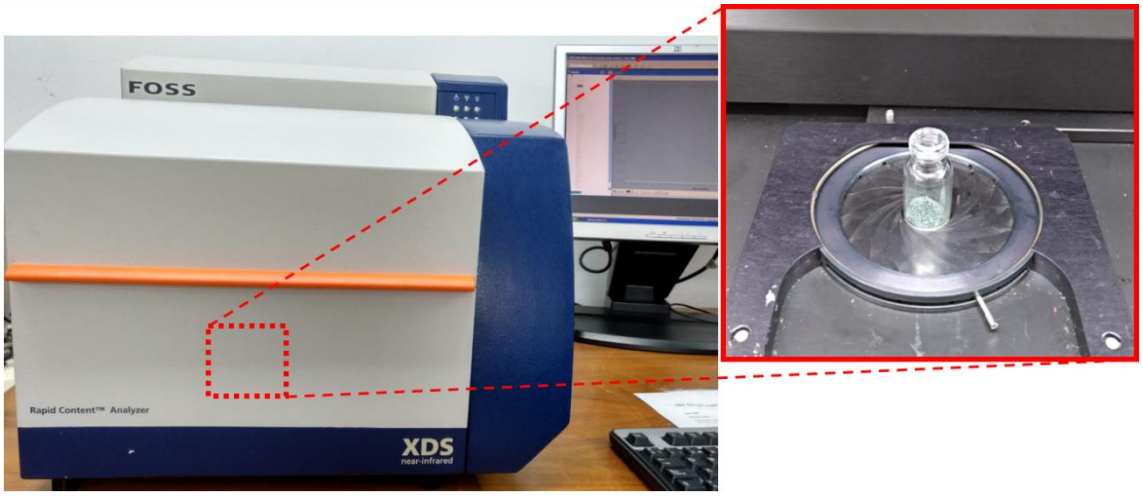

Figure 5.13. NIR spectrometer working in reflection mode (sample cell with a vial containing an explosive powder zoomed).

Results and discussion

As preliminarily explained in the introduction, NIR spectra of organic explosives were dominated by those bands corresponding to the overtones and combination bands of the vibrational modes of C-H bonds. Thus, in order to facilitate their interpretation, the chemical structure of explosives is displayed in Figure 5.14 above their NIR spectra.

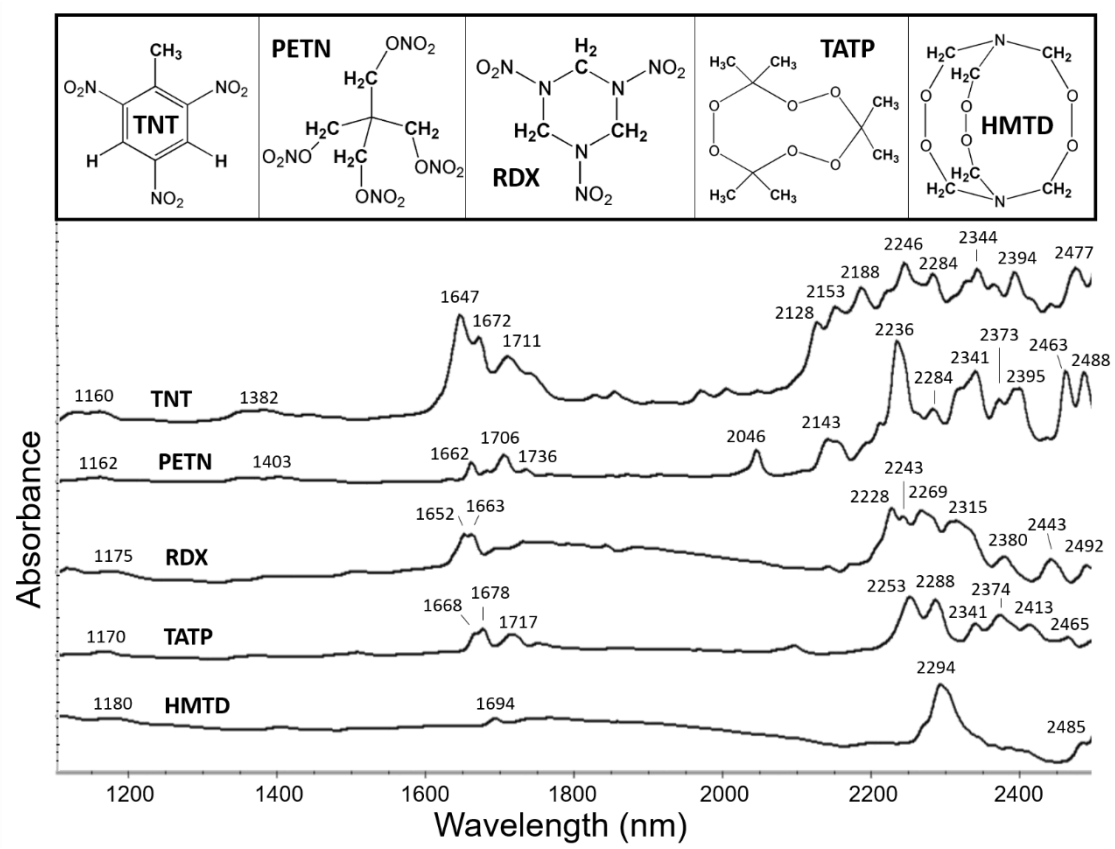

Figure 5.14: Near infrared spectra (1100-2500 nm) of TNT, PETN, RDX, TATP and HMTD explosives. Each spectrum is the average of three replicates. In addition, the chemical structure of explosives is displayed above their NIR spectra.

As a summary of C-H bonds, TNT has one methyl group (CH_3) linked to the aromatic ring and two C-H aromatic bonds. PETN has four CH_2 groups equally bonded to nitrate ester groups {-C-**CH_2**-ONO_2}. RDX has three CH_2 groups equally bonded to nitramine groups {-(O_2N)N-**CH_2**-N(NO_2)-}. TATP has six methyl groups equally bonded to quaternary carbons bonded to two peroxides {(**CH_3**)$_2$-C-$(OO)_2$}. HMTD has six CH_2 groups equally bonded to nitrogen (amine) and peroxide {-N-**CH_2**-OO-}. In the knowledge of the theoretical NIR bands expected from those C-H bonds (revised in literature [2]), the experimental NIR bands of explosives were assigned to their respective vibrations (overtones or combination bands).

As expected, most organic explosives displayed multiple bands within the region 2500-2100 nm, which corresponds to the $CH/CH_2/CH_3$ first combination region. The specific values of all these bands are indicated in Figure 5.14 and their interpretation is summarized in Table 5.13. In brief, each explosive provided selective bands, which were different from each other as expected from their different C-H bonds. Furthermore, even the NIR bands of PETN, RDX and HMTD, which are due to CH_2 groups, were different (according to the different chemical environment of CH_2 groups in each explosive molecule). From the interpretation point of view, this region (2500-2000 nm) is extraordinarily complex and, only a few bands were assigned, based on the NIR assignments reported in literature for very similar molecules. For instance, the interpretation of the NIR bands previously reported for toluene [2] was very helpful in the interpretation of TNT spectrum. Thereby, the bands located at 2477 and 2394 nm were assigned to the combination of aromatic C-H stretching with C-C bending (νArCH+δCC). The band located at 2344 nm was assigned to the combination of aromatic C-H stretching with C-H bending (νArCH+δArCH). The bands located at 2284 and 2246 nm were assigned to the combination of CH_3 symmetric/antisymmetric stretching with CH_3 bending ($\nu CH_3+\delta CH_3$). Finally, the bands located at 2188, 2153 and 2128 nm were assigned to the combination of aromatic C-H stretching with C-C stretching (νArCH+νArCC). Regarding PETN, RDX and HMTD, no chemically similar molecules have been reported by NIR, thus the interpretation of their spectra within 2500-2000 nm range was not specifically assigned band by band, but a general assignment was performed instead. The most intense bands located within 2350-2200 nm theoretically correspond to the combination of symmetric/antisymmetric CH_2 stretching with CH_2 bending ($\nu CH_2+\delta CH_2$), as previously reported for methylene group (CH_2) in literature [2]. The rest of the bands within the combination region (2500-2000 nm) might be due to the second overtone of CH_2 bending ($3\delta CH_2$) and the combination of CH_2 stretching with C-C/C-O/C-N bending/stretching depending on the explosive (see Table 5.13). TATP displayed two highly intense bands located at 2288 and 2253 nm that respectively correspond to the combination of symmetric and antisymmetric CH_3 stretching with CH_3 bending ($\nu_s CH_3+\delta CH_3$ and $\nu_a CH_3+\delta CH_3$), as previously reported for methyl group [2]. The bands of TATP located above 2300 nm are probably due to the second overtone of CH_3 bending ($3\delta CH_3$) and the combination of CH_3 stretching with C-C/C-O bending/stretching, though the specific assignment is unclear.

Table 5.13. Summary of X-H NIR active groups contained in the pure organic explosives under study (TNT, PETN, RDX, TATP and HMTD); the experimental bands obtained for each explosive; and their assignment to the specific vibration (overtone or combination region) according to the literature [2].

Explosive	X-H NIR active groups	Experimental NIR bands (nm)	NIR bands assignment	
TNT	1 CH_3 2 ArCH	2477, 2394 2344 2284, 2246 2188, 2153, 2128	νArCH+δCC νArCH+δArCH $\nu CH_3+\delta CH_3$ νArCH+νArCC	1st comb ArCH/CH_3
		1711, 1672, 1647	2νArCH / 2$\nu_a CH_3$ / 2$\nu_s CH_3$	
		1382	2nd comb ArCH/CH_3	
		1160	3νArCH / 3νCH_3	
PETN	4 CH_2	2488, 2463, 2395, 2373 2341, 2284, 2236* 2143, 2046	(2500-2000) $\nu CH_2+\delta CC$ / $\nu CH_2+\nu CC$ / $\nu CH_2+\delta CO$ / $\nu CH_2+\nu CO$ / $3\delta CH_2$ *(2350-2200) $\nu_s CH_2+\delta CH_2$, $\nu_a CH_2+\delta CH_2$	1st comb CH_2
		1736, 1706, 1662	2$\nu_a CH_2$ / 2$\nu_s CH_2$	
		1403	2nd comb CH_2	
		1162	3νCH_2	
RDX	3 CH_2	2492, 2443, 2380 2315, 2269, 2243, 2228*	(2500-2000) $\nu CH_2+\delta CC$ / $\nu CH_2+\nu CC$ / $\nu CH_2+\delta CN$ / $\nu CH_2+\nu CN$ / $3\delta CH_2$ *(2350-2200) $\nu_s CH_2+\delta CH_2$, $\nu_a CH_2+\delta CH_2$	1st comb CH_2
		1663, 1652	2$\nu_a CH_2$ / 2$\nu_s CH_2$	
		1175	3νCH_2	
TATP	6 CH_3	2465, 2413, 2374, 2341 2288, 2253*	$\nu CH_3+\delta CC$ / $\nu CH_3+\nu CC$ / $\nu CH_3+\delta CO$ / $\nu CH_3+\nu CO$ / $3\delta CH_3$ *$\nu_s CH_3+\delta CH_3$, $\nu_a CH_3+\delta CH_3$	1st comb CH_3
		1717, 1678, 1668	2$\nu_a CH_3$ / 2$\nu_s CH_3$	
		1170	3νCH_3	
HMTD	6 CH_2	2485 2294*	$\nu CH_2+\delta CC$ / $\nu CH_2+\nu CC$ / $\nu CH_2+\delta CO$ / $\nu CH_2+\nu CO$ / $\nu CH_2+\delta CN$ / $\nu CH_2+\nu CN$ / $3\delta CH_2$ *$\nu CH_2+\delta CH_2$	1st comb CH_2
		1694	2νCH_2	
		1180	3νCH_2	

Abbreviations: comb (combination region), 2ν (first overtone of stretching fundamental vibration), 3ν (second overtone of stretching fundamental vibration), 3δ (second overtone of bending fundamental vibration), ν_a (antisymmetric stretching), ν_s (symmetric stretching), ν (stretching), δ (bending).

Besides the first C-H combination region, organic explosives also displayed bands within the range 1750-1600 nm corresponding to the first overtone of $CH/CH_2/CH_3$ stretching vibrations. In the case of TNT, the three bands located at 1647, 1672 and 1711 nm are likely assigned to the first overtones of C-H aromatic stretching, antisymmetric CH_3 stretching and symmetric CH_3 stretching ($2\nu ArCH$ / $2\nu_aCH_3$ / $2\nu_sCH_3$). Among the multiple bands that PETN displayed in this region, the two most intense bands were those located at 1662 and 1706 nm, which are probably due to the first overtones of antisymmetric and symmetric CH_2 stretching modes ($2\nu_aCH_2$ / $2\nu_sCH_2$). Similarly, the bands of RDX located at 1652 and 1663 nm are theoretically assigned to the first overtones of antisymmetric and symmetric CH_2 stretching modes ($2\nu_aCH_2$ / $2\nu_sCH_2$). These two vibrations should be also present in HMTD molecule (since it only contains methylene groups), however, a unique weak band located at 1694 nm was observed in the NIR spectrum of HMTD ($2\nu CH_2$). The bands of TATP located at 1678 and 1717 nm are likely assigned to the first overtone of antisymmetric and symmetric CH_3 stretching modes ($2\nu_aCH_3$ / $2\nu_sCH_3$), though the first band split into two bands.

In addition, a wide weak band within the range 1430-1360 nm, assigned to the $CH/CH_2/CH_3$ second combination region, was observed for most organic explosives. Despite of also being an incredibly complex region, a unique wide weak band was observed, probably because of the low intensity of these bands. Likewise, explosives displayed very weak bands within the range 1200-1150 nm attributed to the second overtone of $CH/CH_2/CH_3$ stretching vibrations ($3\nu CH$ / $3\nu CH_2$ / $3\nu CH_3$). As theoretically predicted [1], the intensity of overtones/combination bands strongly decreases with the number of vibrational levels transgressed: first overtone (0→2) (*i.e.* transition from fundamental to second vibrational level) was much more intense than second overtone (0→3).

After interpreting the NIR spectra of organic explosives, the NIR spectra of smokeless gunpowders were studied. According to the chemical structure of the components of smokeless gunpowders (see Figure 5.15), nitroglycerine (NG) has two CH_2 groups and one CH group, the three of them bonded to nitrate ester groups. DNT has one methyl group (CH_3) linked to the aromatic ring and three C-H aromatic bonds. Nitroguanidine (NQ) has no CH bonds, but NH bonds, including one imine group (=NH), one nitramine group (-**NH**-NO_2) and one

primary amine group (-NH_2). Finally, nitrocellulose (NC) has one CH_2 group and five different CH groups per monomer of glucose. CH_2 group and two CH groups are bonded to nitrate ester groups whereas three CH groups are linked to oxygen (ether). It should be noted that NC structure displayed in Figure 5.15 corresponds to NC with the maximum nitrogen content theoretically possible (14%), which results from the replacement of all hydroxyl groups of cellulose by nitro groups. However, in the real synthesis of highly-nitrated NC, the nitrogen content never reaches the maximum, but usually varies between 12-13.5% [21]. This means that some hydroxyl groups (around one OH group per two monomers of glucose) have not been replaced by nitro groups, and consequently, the NIR bands of OH might be also observed.

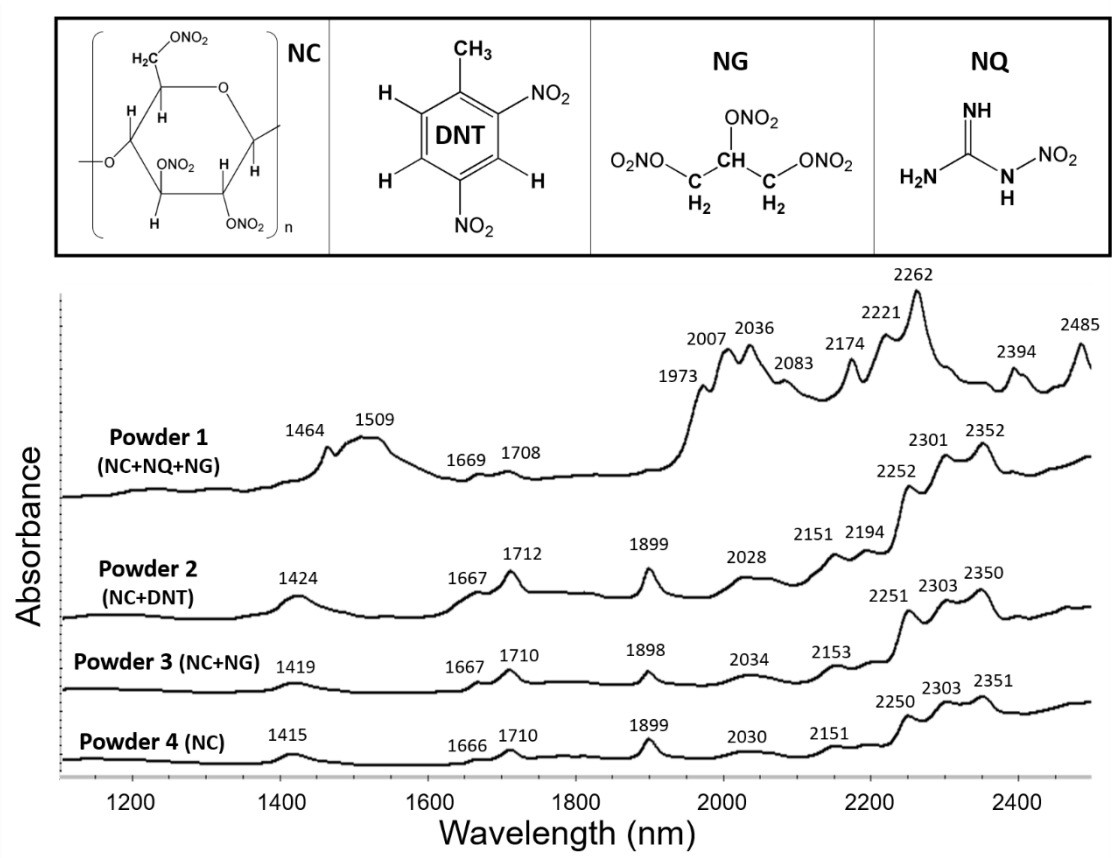

Figure 5.15. Near infrared spectra (1100-2500 nm) of smokeless powders: powder 1 (NC+NQ+NG), powder 2 (NC+DNT), powder 3 (NC+NG) and powder 4 (NC). Each spectrum is the average of three replicates. In addition, the chemical structure of their explosive components is displayed above their NIR spectra.

Regarding the C-H first combination bands of smokeless powders, powders 2, 3 and 4 (whose major component is NC (>70%)) displayed intense bands located at 2351, 2303 and 2250 nm. These bands are likely assigned to the second overtone of CH/CH_2 bending ($3\delta CH$ / $3\delta CH_2$) and the combination of CH/CH_2

stretching with CH_2 bending ($\nu CH+\delta CH_2$ / $\nu CH_2+\delta CH_2$), as previously reported in literature for cellulose [2]. In addition, the two bands located at 1667 and 1710 nm displayed by NC (as evidenced in powder 4 (94% NC)) might be assigned to the first overtone of either CH, antisymmetric CH_2 or symmetric CH_2 stretching modes ($2\nu CH$ / $2\nu_a CH_2$ / $2\nu_s CH_2$), as summarized in Table 5.14.

Table 5.14. Summary of X-H NIR active groups contained in the smokeless powders under study; the experimental bands obtained for each explosive; and their assignment to the specific vibration (overtone or combination region) according to the literature [2].

Explosive	X-H NIR active groups	Experimental NIR bands (nm)	NIR bands assignment	
Powder 1 (triple base)	1n CH_2 (NC) 5n CH (NC) 0.5n OH (NC) 2 CH_2 (NG) 1 CH (NG) 1 =NH (NQ) 1 NH (NQ) 1 NH_2 (NQ)	2485, 2394	$\nu CH+\delta CH_2$ / $\nu CH_2+\delta CH_2$ / $3\delta CH$ / $3\delta CH_2$	1st comb CH/CH_2
		2262, 2221, 2174 2083, 2036, 2007, 1973	$\nu NH+\nu NN$ / $\nu NH+\delta NN$ / $3\delta NH$ $\nu NH+\delta NH$	1st comb NH/NH_2
		1708, 1669	$2\nu CH$ / $2\nu_a CH_2$ / $2\nu_s CH_2$	
		1509, 1464	$2\nu_s NH_2$ / $2\nu_a NH_2$ / $2\nu NH$	
Powder 2 (double base)	1n CH_2 (NC) 5n CH (NC) 0.5n OH (NC) 1 CH_3 (DNT) 3 ArCH (DNT)	2352, 2301, 2252	$\nu CH+\delta CH_2$ / $\nu CH_2+\delta CH_2$ / $3\delta CH$ / $3\delta CH_2$	1st comb CH/CH_2
		2194, 2151, 2028, 1899	$\nu OH+\delta OH$ / $\nu OH+\nu CO$ / $\nu OH+\delta CO$ / $\delta OH+\nu CO$ / $3\delta OH$	1st comb OH
		1712, 1667	$2\nu CH$ / $2\nu_a CH_2$ / $2\nu_s CH_2$	
		1424	2nd comb CH/CH_2	
Powder 3 (double base)	1n CH_2 (NC) 5n CH (NC) 0.5n OH (NC) 2 CH_2 (NG) 1 CH (NG)	2350, 2303, 2251	$\nu CH+\delta CH_2$ / $\nu CH_2+\delta CH_2$ / $3\delta CH$ / $3\delta CH_2$	1st comb CH/CH_2
		2153, 2034, 1898	$\nu OH+\delta OH$ / $\nu OH+\nu CO$ / $\nu OH+\delta CO$ / $\delta OH+\nu CO$ / $3\delta OH$	1st comb OH
		1710, 1667	$2\nu CH$ / $2\nu_a CH_2$ / $2\nu_s CH_2$	
		1419	2nd comb CH/CH_2	
Powder 4 (single base)	1n CH_2 (NC) 5n CH (NC) 0.5n OH (NC)	2351, 2303, 2250	$\nu CH+\delta CH_2$ / $\nu CH_2+\delta CH_2$ / $3\delta CH$ / $3\delta CH_2$	1st comb CH/CH_2
		2151, 2030, 1899	$\nu OH+\delta OH$ / $\nu OH+\nu CO$ / $\nu OH+\delta CO$ / $\delta OH+\nu CO$ / $3\delta OH$	1st comb OH
		1710, 1666	$2\nu CH$ / $2\nu_a CH_2$ / $2\nu_s CH_2$	
		1415	2nd comb CH/CH_2	

Abbreviations: n (per monomer of glucose), comb (combination region), 2ν (first overtone of stretching fundamental vibration), 3δ (second overtone of bending fundamental vibration), ν_a (antisymmetric stretching), ν_s (symmetric stretching), ν (stretching), δ (bending).

Besides the C-H bands, additional bands due to N-H/O-H vibrations were observed in smokeless gunpowders. For instance, triple-base smokeless powder (composed of 55% NQ) displayed multiple bands within the region 2300-1900 nm (assigned to the NH/NH_2 first combination region) and a wide doublet located at 1509 and 1464 nm (assigned to the first overtones of symmetric NH_2, antisymmetric NH_2 and amine/imine NH stretching vibrations ($2\nu_sNH_2$ / $2\nu_aNH_2$ / 2νNH)). As occurred for C-H first combination region, the N-H first combination region (2300-1900 nm) of NQ was extraordinarily complex and the particular assignment of each band to the respective NH stretching-bending combination mode was unfeasible. As a general assignment, the bands located at 1973, 2007, 2036 and 2083 nm were tentatively assigned to a combination of NH stretching with NH bending vibrations (νNH+δNH), based on the available literature reported for amines [2]. The bands above 2100 nm (2174, 2221 and 2262 nm) might be due to second overtones of N-H bending vibrations (3δNH) and the combination of NH stretching with N-N stretching/bending vibrations (νNH+νNN / νNH+δNN). Finally, the NIR spectrum of single-/double- base smokeless powder (NC) displayed additional bands located at 2151, 2030 and 1899 nm. These region (2200-1850 nm) is clearly assigned to OH first combination region. This outcome was not unexpected since, as previously explained, NC usually contains remaining hydroxyl groups that have not been completely replaced by nitro groups. Particularly, these bands are due to the combination of O-H stretching with O-H bending (νOH+δOH) and/or the combination of O-H stretching/bending with C-O stretching/bending (νOH+νCO / νOH+δCO / δOH+νCO) and/or the second overtone of O-H bending (3δOH), though the specific assignment for each band was unclear.

From the identification point of view, most organic explosives provided selective NIR spectral profiles that enabled their discrimination and unequivocal identification. Particularly, the most discriminative regions were those corresponding to C-H first overtone (1600-1750 nm) and C-H/N-H combination region (1900-2500 nm). Almost all organic explosives under study (TNT, PETN, RDX, TATP, HMTD and triple-base smokeless powder) were unequivocally identified based on their different NIR spectra. On the contrary, the NIR spectra provided by single- and double-base smokeless powders were extremely similar. The NIR bands from NC dominated their spectra while no characteristic bands from the second component in double-base smokeless powders (NG or DNT)

were observed. This result seems to evidence that only major components (whose mass percentage is over 30% in the mixture) are detectable by NIR spectroscopy. Thus, those explosives mainly composed of the same major component will not be discriminated by NIR spectroscopy, as occurred for single-base (94% NC) and double-base (85% or 71% NC) smokeless powders. Nevertheless, it should be noted that this result will also depend on how NIR active the minor components are.

Regarding inorganic salts, only ammonium nitrate (NH_4NO_3), which contains NH bonds, was noticeably active in NIR spectroscopy, as displayed in Figure 5.16.

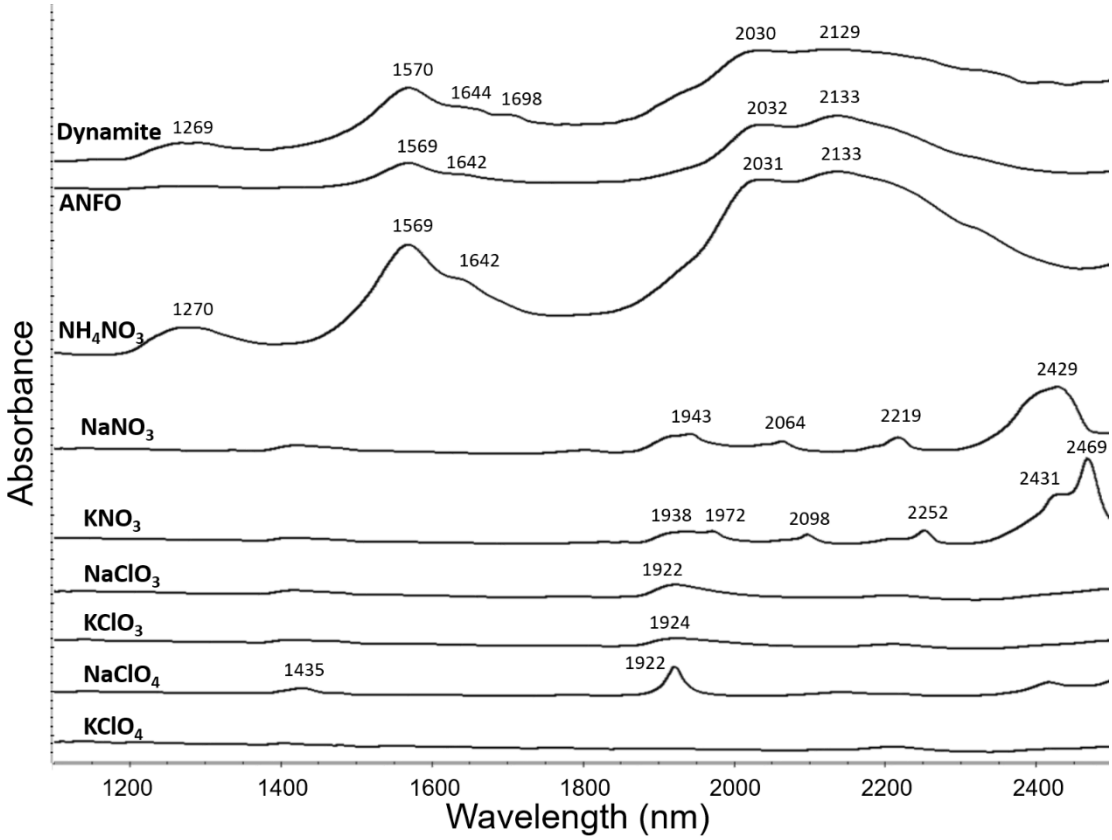

Figure 5.16: Near infrared spectra (1100-2500 nm) of dynamite, ANFO, ammonium nitrate, sodium nitrate, potassium nitrate, sodium chlorate, potassium chlorate, sodium perchlorate and potassium perchlorate. Each spectrum is the average of three replicates.

Particularly, NIR spectrum of ammonium nitrate displayed a doublet located at 1569 and 1642 nm due to the first overtone of symmetric and antisymmetric NH_4 stretching vibrations ($2\nu_sNH_4$, $2\nu_aNH_4$), and a wide doublet located at 2031 and 2133 nm due to the first combination region (*i.e.* the combination of NH_4

stretching and NH_4 bending modes ($\nu NH_4+\delta NH_4$). Table 5.15 summarizes the assignment of the NIR bands displayed by inorganic salts and AN-based explosives. An additional band located at 1270 nm, whose vibrational assignment is unclear, was observed in the NIR spectrum of AN. Likewise, dynamite and ANFO also displayed these NIR bands since ammonium nitrate is the major component of ANFO (~ 90%) and dynamite (~ 66%). Regarding the ANFO composition studied in this work, 10% of ANFO was diesel fuel (a mixture mainly composed by aliphatic and aromatic hydrocarbons). Nevertheless, no bands from the overtones of CH vibrations are observed in the NIR spectrum of ANFO. This is likely due to the low proportion of diesel compared to NH_4NO_3 in ANFO mixture. Unlike ANFO, the NIR spectrum of dynamite displayed an extra band located at 1698 nm (besides the bands of NH_4NO_3). This band seems to correspond to ethylene glycol dinitrate (EGDN), particularly to the first overtone (2ν) of stretching modes of the two CH_2 groups in this molecule (O_2NO-**CH_2-CH_2**-ONO_2). The reason why EGDN bands were observed could be explained by the fact that 29% of dynamite is EGDN, which is almost half of NH_4NO_3 (66%), which is much more than the 10% of diesel fuel mixed with 90% of NH_4NO_3 in ANFO.

The other inorganic salts have few or no bands in their NIR spectra because of the absence of CH, NH or OH bonds in their structure. Actually, they are ionic compounds whose unique covalent bonds are those from the anion (N-O in nitrates or Cl-O in chlorates/perchlorates). The first overtones and combination bands of the fundamental modes of these covalent bonds do not appear in the NIR region. In fact, no bands were observed in the spectrum of $KClO_4$ and the weak bands observed in the spectra of $NaClO_3$, $KClO_3$ and $NaClO_4$ were assigned to water (humidity). These weak bands were located at 1920-1930 nm (combination of antisymmetric H_2O stretching with H_2O bending ($\nu_aH_2O+\delta H_2O$)) and 1435 nm (combination of symmetric and antisymmetric H_2O stretching ($\nu_aH_2O+\nu_sH_2O$), as previously reported in literature for water [2]. Even though every salt was purchased anhydrous, some water molecules (from humidity) likely attached to these hygroscopic salts. However, nitrate salts ($NaNO_3$ and KNO_3) displayed some additional medium-intense bands that did not correspond to water, particularly within the region 1900-2500 nm. To this respect, it should be noted that the spectral signature and specific wavelengths of these bands was different for sodium and potassium nitrates.

Table 5.15. Summary of X-H NIR active groups contained in AN-based explosives (ANFO and dynamite) and inorganic salts included in this study; the experimental bands obtained for each explosive/salt; and their assignment (when possible) to the specific vibration (overtone or combination region) according to the literature [2].

Explosive	X-H NIR active groups	Experimental NIR bands (nm)	NIR bands assignment	
NH_4NO_3	1 NH_4^+	2133, 2031	$\nu NH_4+\delta NH_4$	1st comb NH_4^+
		1642, 1569	$2\nu_aNH_4$ / $2\nu_sNH_4$	
		1270	-	
ANFO	1 NH_4^+ (AN) n C-H (Diesel)	2133, 2032	$\nu NH_4+\delta NH_4$	1st comb NH_4^+
		1642, 1569	$2\nu_sNH_4$ / $2\nu_aNH_4$	
Dynamite	1 NH_4^+ (AN) 2 CH_2 (EGDN)	2129, 2030	$\nu NH_4+\delta NH_4$	1st comb NH_4^+
		1698	$2\nu CH_2$	
		1644, 1570	$2\nu_sNH_4$ / $2\nu_aNH_4$	
		1269	-	
$NaNO_3$	-	2429, 2219, 2064, 1943	-	
KNO_3	-	2469-2431, 2252, 2098, 1972-1938	-	
$NaClO_3$	-	1922	$\nu_aH_2O+\delta H_2O$	
$KClO_3$	-	1924	$\nu_aH_2O+\delta H_2O$	
$NaClO_4$	-	1922	$\nu_aH_2O+\delta H_2O$	
		1435	$\nu_aH_2O+\nu_sH_2O$	
$KClO_4$	-	-	-	

Abbreviations: n (depending on Diesel composition), comb (combination region), 2ν (first overtone of stretching fundamental vibration), ν_a (antisymmetric stretching), ν_s (symmetric stretching), ν (stretching), δ (bending).

This fact necessarily means that neither water nor the nitrate anion are the unique components providing these NIR bands, but the interaction cation-nitrate (sodium-nitrate or potassium-nitrate). Despite being ionic bonds, some kind of NIR-active vibrations are presumed to be occurring between these alkaline cations and nitrate. Actually, it is noticeable the fact that wavelength values of NIR bands of potassium nitrate are shifted to higher values in comparison to those of sodium nitrate. According to Hook's Law, this means

that weaker interactions (*i.e.* the frequency of the strength of the interaction is lower – and consequently, the wavelength is higher) occur between potassium and nitrate than between sodium and nitrate. This is in accordance with the respective size of sodium and potassium atoms (potassium > sodium). Nevertheless further studies are necessary to comprehend in detail the assignment of every particular band for these ionic compounds.

Conclusions

NIR spectroscopy has been demonstrated to be a suitable technique to identify explosives containing C-H and N-H bonds because the combination bands and overtones of the fundamental C-H/N-H/O-H vibrations are located within the NIR range 1000-2500 nm. Particularly, NIR spectra of organic explosives (TNT, PETN, RDX, TATP, HMTD, single-, double- and triple-smokeless powders) were dominated by multiple bands within the range 2100-2500 (due to the $CH/CH_2/CH_3$ first combination region) and 1650-1750 nm (due to the $CH/CH_2/CH_3$ first overtone). In addition, those explosives containing N-H bonds such as NQ and AN-based explosives (NH_4NO_3, ANFO and dynamite) also displayed multiple bands due to the $NH/NH_2/NH_4$ first combination region (1900-2200 nm) and first overtone (1450-1650 nm). $NaNO_3$ and KNO_3 provided few medium-intense NIR bands, which were not clearly assigned, while chlorate and perchlorate salts were not NIR active, since the unique NIR bands that were observed were those corresponding to water.

Regarding the discrimination of single- and double-base smokeless powders, whose major component is NC (>70%), undistinguishable NIR spectra were obtained, which was entirely attributed to NC. This outcome evidenced the limitation of NIR spectroscopy of only detecting the major components in explosive mixtures. In fact, no noticeable NIR signal from the minor components whose mass percentage was below 30% was observed when the mass percentage of the major component was over 70%. On the contrary, when the mass percentage of the major component was below 70%, the NIR characteristic bands of other components started to be perceptible, as occurred for dynamite in which low intense but perceptible bands of EGDN (29%) were detected over the bands of ammonium nitrate (66%).

References

[1] D.A. Burns, E.W. Ciurczak, Handbook of Near Infrared Analysis. Third edit. CRC Press, Taylor & Francis: Boca Raton, USA, 2008.

[2] J. Workman Jr, L. Weyer, Practical guide and spectral atlas for interpretative near-infrared spectroscopy. Second edi. CRC Press, Taylor & Francis: Boca Raton, USA, 2012.

[3] B. Brauer, F. Dubnikova, Y. Zeiri, R. Kosloff, R.B. Gerber, Vibrational spectroscopy of triacetone triperoxide (TATP): Anharmonic fundamentals, overtones and combination bands. Spectrochim Acta - Part A Mol Biomol Spectrosc 71 (2008) 1438-1445.

[4] D. Sülzle, P. Klaeboe, The infrared Raman and NMR spectra of Heamethylene Triperoxide Diamine. Acta Chem Scand A 42 (1988) 165-170.

[5] I.R. Lewis, N.W. Daniel, P.R. Griffiths, Interpretation of Raman spectra of nitro-containing explosive materials. Part I: Group frequency and structural class membership. Appl Spectrosc 51 (1997) 1854-1867.

[6] K.L. McNesby, R.A. Pesce-Rodrigues, Applications of Vibrational Spectroscopy in the Study of Explosives, Handb Vib Spectrosc (2006) 3152-3168.

[7] J. Oxley, J. Smith, J. Brady, F. Dubnikova, R. Kosloff, L. Zeiri, Y. Zeiri, Raman and infrared fingerprint spectroscopy of peroxide-based explosives, Appl Spectrosc 62 (2008) 906-915.

[8] R.J. Stokes, E.L. Normand, R. Lindley, P. Black, M. McCulloch, D.N. Middleton, W.E. Smith, B. Foulger, C. Lewis, The fusion of MIR absorbance and NIR Raman spectroscopic techniques for identification of improvised explosive materials in multiple scenarios, Proc SPIE 7486 (2009) 74860O/1-74860O/12.

[9] F. Zapata, C. García-Ruiz, Determination of Nanogram Microparticles from Explosives after Real Open-Air Explosions by Confocal Raman Microscopy, Anal Chem 88 (2016) 6726-6733.

[10] W.A. Al-Saidi, S.A. Asher, P. Norman, Resonance raman spectra of TNT and RDX using vibronic theory, excited-state gradient, and complex polarizability approximations, J Phys Chem A 116 (2012) 7862-7872.

[11] F. Zapata, C. García-Ruiz, The discrimination of 72 nitrate, chlorate and perchlorate salts using IR and Raman spectroscopy, Spectrochim Acta - Part A Mol Biomol Spectrosc 189 (2018) 535-542.

[12] E.C. Mattos, E.D. Moreira, R.C.L. Dutra, M.F. Diniz, A.P. Ribeiro, K. Iha, Determination of the HMX and RDX content in synthesized energetic material by HPLC, FT-MIR, and FT-NIR spectroscopies, Quim Nova 27 (2004) 540-544.

[13] S.R. Piecuch, J.D. Koch, J.M. Lightstone, J.R. Carney, A fast NIR emission spectrometer for examining explosive events: Emission spectra of PETN explosions

containing silver and aluminium, Shock Compression Condens Matter 1195 (2009) 1297-1300.

[14] M. Snels, T. Venezia, L. Belfiore, Detection and identification of TNT, 2,4-DNT and 2,6-DNT by near-infrared cavity ringdown spectroscopy, Chem Phys Lett 489 (2010) 134-140.

[15] A. Saleem, C. Canal, D.A. Hutchins, R.J. Green, NIR spectroscopy with multivariate calibration and lock-in amplification to detect chemicals concealed behind fabrics, Proc SPIE 8018 (2011) 80181I/1-80181I/18.

[16] C.M. Canal, A. Saleem, R.J. Green, D.A. Hutchins, Remote identification of chemicals concealed behind clothing using near infrared spectroscopy, Anal Methods 3 (2011) 84-91.

[17] H.C. Schau, Remote detection of explosives with multispectral imaging, Proc SPIE 7304 (2009) 730414/1-730414/9.

[18] C.M. Canal, A. Saleem, R.J. Green, D.A. Hutchins, Near-infrared spectroscopy for personal screening, Proc SPIE 7838 (2010) 78380G/1-78380G/11.

[19] M.A. Fernández de La Ossa, C. García-Ruiz, J.M. Amigo, Near infrared spectral imaging for the analysis of dynamite residues on human handprints, Talanta 130 (2014) 315-321.

[20] M.A. Fernández de la Ossa, J.M. Amigo, C. García-Ruiz, Detection of residues from explosive manipulation by near infrared hyperspectral imaging: A promising forensic tool, Forensic Sci Int 242 (2014) 228-235.

[21] M.A. Fernández de la Ossa, M. López-López, M. Torre, C. García-Ruiz. Analytical techniques in the study of highly-nitrated nitrocellulose, TrAC - Trends Anal Chem 30 (2011) 1740-1755.

Chapter 6. Spectroscopic Identification of Post-Blast Explosive Residues

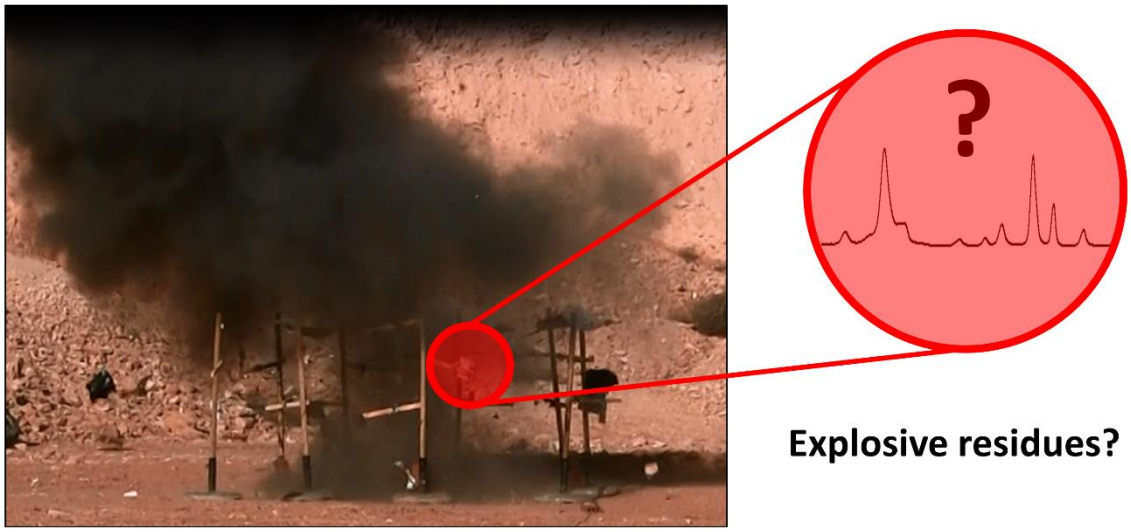

Main sources:

C. Martín-Alberca, **Félix Zapata**, H. Carrascosa, F.E. Ortega-Ojeda, C. García-Ruiz, Study of consumer fireworks post-blast residues by ATR-FTIR, *Talanta* 149 (2016) 257-265.

Félix Zapata, C. García-Ruiz, Determination of nanogram microparticles from explosives after real open-air explosions by confocal Raman microscopy, *Anal. Chem.* 88 (2016) 6726-6733.

Félix Zapata, C. García-Ruiz, Analysis of different materials subjected to open-air explosions in search of explosive traces by Raman microscopy, *Forensic Sci. Int.* 275 (2017) 57-64.

Other sources:

Félix Zapata, M. López-López, C. García-Ruiz, Detection and identification of explosives by surface enhanced Raman scattering, *Applied Spectrosc. Reviews* 51 (2016) 207-242.

D. Videira-Quintela, **Félix Zapata**, C. García-Ruiz, Detection of microscopic traces of explosive residues on textile fabrics by Raman spectroscopy, *J. Raman Spectrosc.* 2018 (In press, DOI: 10.1002/jrs.5455).

6.1. Key Aspects of Explosives Detonation

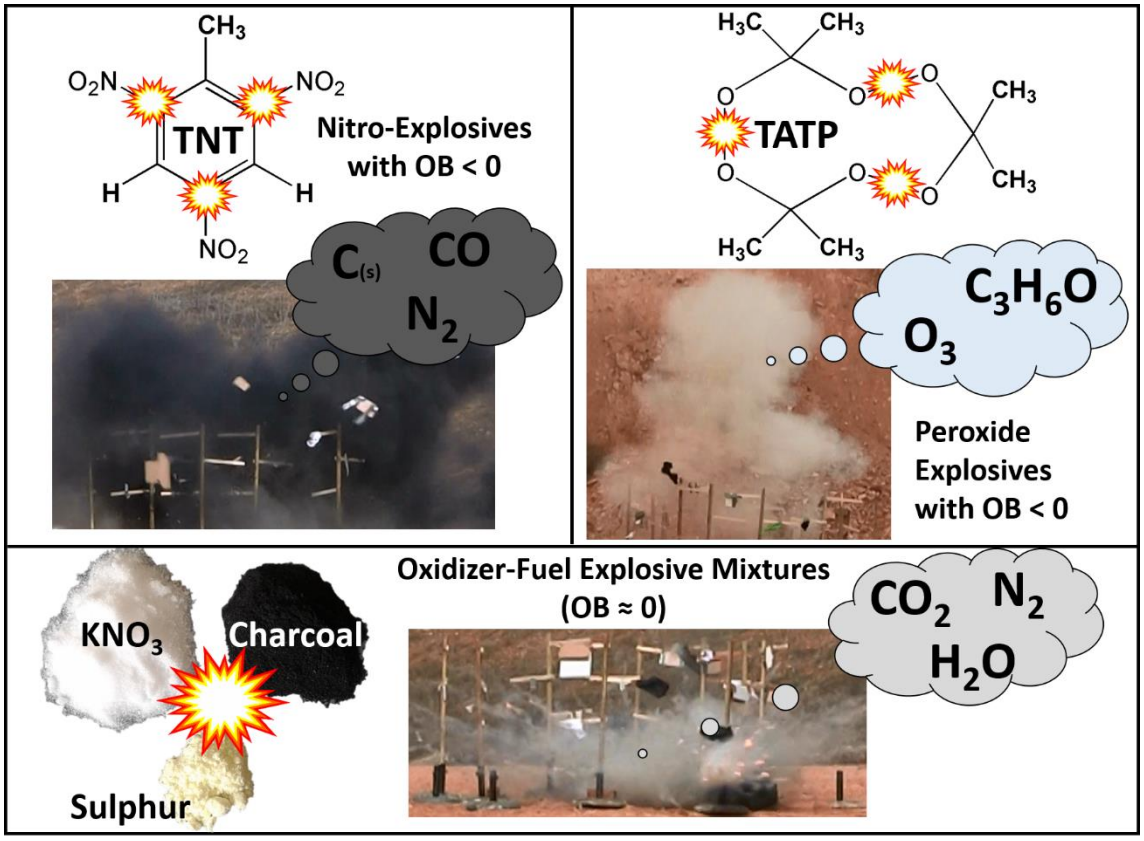

Abstract

Detonation of solid explosives is a highly complex process in which elucidating the chemical reactions that occur inside is an extraordinarily difficult task. From the physics, some theories have been developed to explain the propagation of the detonation shock wave through the explosive material and the role that chemical reactions play in that shock wave. However, the precise chemical reactions undergone by each explosive are uncertain. The most simple and extensively used approach involves the calculation of the explosive's oxygen balance in order to predict the most oxidized products to which may be transformed (in absence of air oxygen). In this chapter, the validity of this approach was empirically evaluated for some explosives by visual examination of the smoke produced in their detonations. Black smoke (which is due to black solid carbon particles) was observed in RDX and PETN detonation, contrarily to the theoretically predicted chemical reactions. On the contrary, no black smoke was evidenced in detonations of TATP and HMTD, though it had been theoretically predicted. Finally, this chapter examines the phenomenon of post-blast residues (*i.e.* the subsistence of undetonated remains of the explosive after its detonation).

Fundamental concepts about detonations of explosives

Detonation of solid explosives (*i.e.* the instantaneous decomposition of a solid reactant into a mixture of gaseous products that may reach temperatures up to 5000 K and pressures up to 500000 atm) is a stunning process that has awaken interest for centuries [1]. From thousand-year-old black powder to novel RDX, a large variety of explosive compounds have been discovered and used for different applications. A deep knowledge exists about the chemical composition and molecular structure of explosives… about the physicochemical explosive properties (such as velocity of detonation)… about the synthesis and manufacture of explosives… about the chemical identification of explosives… However, there is a deep lack of knowledge about the chemical process by which an explosive produces a detonation.

The main difficulty when studying the detonation process is its extremely high speed, which is, at the same time, the requirement for having a detonation. As previously explained in chapter 4, a detonation occurs when the release of energy process propagates at supersonic speeds. The result of such supersonic speed is the creation of an over-pressured front that drives a shock wave, which initiates complex chemical reactions [1-5]. In brief, the shock wave induces chemical reactions and such chemical reactions drive the shock wave through the explosive material. Though real detonations are three-dimensional detonations, simplified unidimensional models help to easily comprehend how detonation proceeds.

Based on the Chapman-Jouguet (CJ) theory, the shock wave front creates two zones in the explosive: the zone ahead of the wave front, (which contains the undetonated explosive at low pressure), and the zone behind the shock wave front (which contains the reaction products at high pressure) [1-5]. These reacting post-blast products (mostly gaseous) move away from the shock wave front at velocities that reach (as maximum) the sound speed in the explosive medium. When those gaseous products reach the local sonic speed, the supersonic velocity at which the shock wave is propagating through the detonating explosive becomes constant. Such velocity is known as Chapman-Jouguet velocity or detonation velocity, and it is characteristic for each explosive, as previously explained in chapter 4. Besides the CJ-velocity, the temperature and pressure at which the detonation proceeds becomes also constant, being also characteristic for each explosive [1-5].

The CJ model was later improved by the Zeldovich-von Neumann-Döring (ZND) theory, which states that the shock wave front is not a simple dividing line between undetonated and post-blast explosive, but consists of different stages [1-5]. The first stage involves the von Neumann spike, in which the undetonated explosive is compressed to a high pressure by the shock wave. After a brief ignition delay, such a high pressure (which exceeds the CJ-pressure) initiates chemical reactions leading to the second stage or "reaction zone", in which the explosive is converted into the gaseous products. Temperature increases whereas pressure decreases as the chemical reaction proceeds. After occurring the reaction, those gaseous products expand, leading to an expansion region. This region finishes at the Chapman-Jouguet plane, in which the detonation velocity, pressure and temperature have reached the corresponding constant CJ-velocity, CJ-temperature and CJ-pressure [1-5]. Figure 6.1 graphically describes the ZND shock wave structure through the pressure variation for each stage.

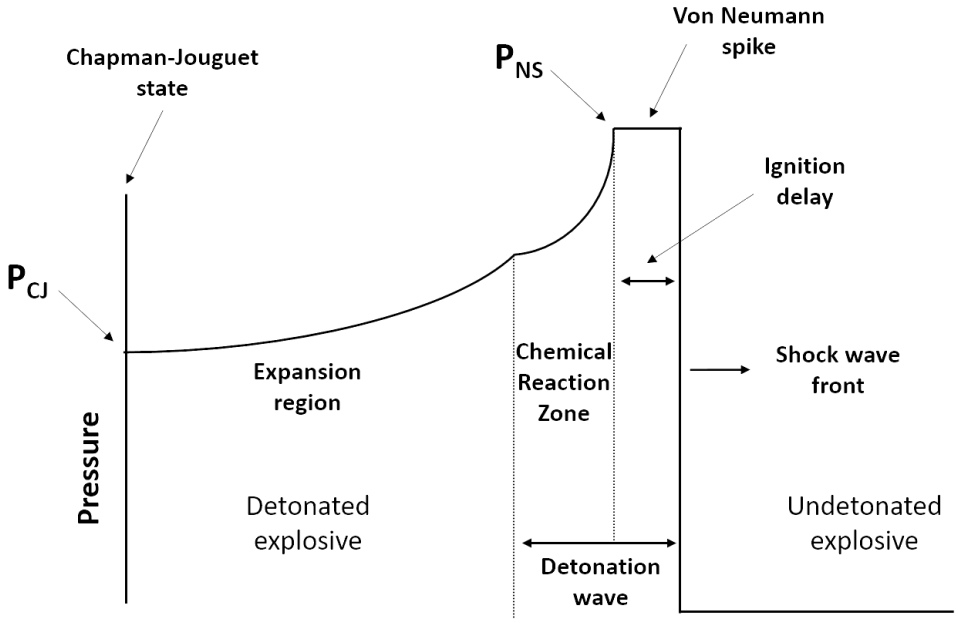

Figure 6.1. Scheme of a shock wave according to Zeldovich-von Neumann-Döring model. P_{CJ} (Chapman-Jouguet pressure), P_{NS} (Neuman spike pressure).

In the knowledge that chemical reactions take place in the reaction zone of the shock wave, determining the identity of the chemical reactions occurring in each explosive detonation is difficult at best. Particularly, the explosive is compressed by the shock wave (up to pressures of 50 GPa), which extraordinarily increases the electron kinetic energy leading to a weakening of chemical bonds. In fact, as

matter is compressed, it becomes increasingly non-molecular [1-8]. This fact, together with the high temperature (>2000 K), multiplies the chemical reactions that may occur because the activation energy of a large number of potential chemical reactions is exceeded. In addition, the high velocity of detonation at which the shock wave proceeds is estimated to produce a reaction zone time-length in the range of μs-ns [1-5]. During such short time, it is not possible to isolate the activated complex or any other intermediate product and study, thereby, the different steps and the specific chemical reaction pathways involved within the detonation process.

The unique perceptible change is the sudden transformation of the solid explosive into gaseous products (mostly carbon dioxide, carbon monoxide, nitrogen and water vapour).

Regarding oxidizer-fuel explosive mixtures such as black powder and ANFO, they contain more than one reactant in its composition (*i.e.* at least an oxidizing compound and a fuel). Such detonation involves the chemical reaction of both reactants, and thus, it is considered a particular case of combustion, which, in turn, is one type of reduction-oxidation (redox) reaction [2]. As an example, within the combustion of black powder, nitrate is reduced to nitrogen while charcoal and sulfur are oxidized to carbonate/carbon dioxide and sulphate, respectively:

$$10\ KNO_3\ (s) + 8\ C\ (s) + 3\ S\ (s) \rightarrow 2\ K_2CO_3\ (s) + 3\ K_2SO_4\ (s) + 6\ CO_2\ (g) + 5\ N_2\ (g)$$

Contrarily, for single explosives, this change involves the conversion of one molecule of explosive into different molecules of gaseous products. In consequence, the single-explosive detonation can be considered a particular case of unimolecular decomposition [2]. As an example, the theoretical chemical reaction for RDX decomposition shows that one molecule of RDX is transformed into three molecules of carbon monoxide, three molecules of water vapour and three molecules of nitrogen. From a redox approach, nitro groups in RDX molecule act like oxidizing agents whereas the hydrocarbon ring acts like fuel. Nitro groups are reduced to nitrogen whereas the hydrocarbon chain is oxidized to carbon monoxide and water vapour.

$$C_3H_6N_6O_6\ (s) \rightarrow 3CO\ (g) + 3\ H_2O\ (g) + 3\ N_2\ (g)$$

How is RDX transformed into carbon monoxide, water and nitrogen? What is the reaction pathway? What is the reaction yield? Does really occur this chemical reaction in RDX detonation? There is no empirical way to respond to all these questions. The unique form to elucidate this matter involves the use of advanced theoretical computational methods for each explosive detonation. Positively, some general and certain outcomes to some of the previous questions might be empirically elucidated by something as simple as the visual inspection, as evidenced below.

Oxygen balance and chemical reactions in detonations

When explaining the differences between explosive and fuel substances, the main difference lies on the role that oxygen (from air) plays in their detonation. Explosives detonate regardless of the presence/absence of air oxygen, whereas fuels necessarily require the presence of oxygen (or any other oxidizer) to undergo their combustion. In the latter case, the combination of fuel and oxidizer is what constitutes an explosive substance. Such oxidizer-fuel explosive combinations are not randomly prepared, but seeking the complete combustion of the fuel.

It should be remarked that complete combustion occurs when the fuel is stoichiometrically transformed to the most oxidized products. Particularly in combustion reactions of organic molecules (mostly composed of carbon and hydrogen atoms), those most oxidized combustion products are carbon dioxide and water vapour [9, 10]. As an example, the complete combustion of propane with oxygen is displayed below:

$$C_3H_8\ (g) + 5\ O_2\ (g) \rightarrow 4\ H_2O\ (g) + 3\ CO_2\ (g)$$

According to the stoichiometry, five moles of oxygen are required to ensure the complete combustion of one mole of propane. In such case, the oxygen balance between reactants and products is zero because there is no excess of oxygen in neither reactants nor completely oxidized products.

On the contrary, when there is a lack of oxygen, propane may undergo an incomplete combustion and produce carbon monoxide. In this case, the oxygen balance is negative since the combustion of propane has not produced the most oxidized products.

$$C_3H_8\ (g) + 4\ O_2\ (g) \rightarrow 4\ H_2O\ (g) + CO_2\ (g) + 2\ CO\ (g)$$

Back to the deflagration of oxidizer-fuel explosive mixtures, fuel component is not oxidized by oxygen from air but by the oxidizer, which is usually composed of a large number of oxygen atoms. For instance, the complete combustion of sucrose in combination with potassium nitrate is oxygen-balanced only when five moles of sucrose react with forty-eight moles of potassium nitrate, as follows:

$$5\ C_{12}H_{22}O_{11}\ (s) + 48\ KNO_3\ (s) \rightarrow 24\ K_2CO_3\ (s) + 24\ N_2\ (g) + 36\ CO_2\ (g) + 55\ H_2O\ (g)$$

Consequently, the mixture of sucrose and potassium nitrate might be prepared on purpose in such stoichiometric proportion to ensure a complete combustion. Particularly, the corresponding mass of each component attending to their respective molecular mass should be weighed.

However, single molecular explosives are composed of both oxidizer groups and fuel groups within the same molecule in such a way that their proportion is always constant. Therefore, the oxygen balance (OB) is specific for each single explosive. In other words, the degree of oxidation of the explosive and its oxidized products (assuming an unimolecular combustion reaction) are also constant. In fact, oxygen balance is usually defined as the amount of oxygen remaining after the oxidation of the hydrogen and carbon atoms to produce H_2O and CO_2. In practice, OB is calculated from the empirical formula displayed below, which, briefly, relates the difference between the available oxygen in the molecule and the total oxygen required for complete oxidation of C to CO_2 and H to H_2O, with the molecular mass (M_m) of the explosive [10].

$$OB\% = \frac{1600}{M_m} \times (Z - 2X - \frac{Y}{2})$$

In previous formula, which is suitable for every explosive containing CHNO atoms, X is the number of carbon atoms, Y is the number of hydrogen atoms and Z is the number of oxygen atoms in the explosive molecule. The oxygen balance of some of the explosives studied in this Thesis is given in Table 6.1. In addition, the theoretical chemical reaction expected for such OB is also presented.

Table 6.1. Explosives grouped according to their negative, zero or positive oxygen balance, and the theoretical expected reaction products for each explosive detonation.

Explosive	Chemical Comp.	Mol. mass (g/mol)	Oxygen balance	Theoretical Chemical Reaction
TNT	$C_7H_5N_3O_6$	227.1	-74	$2\ C_7H_5N_3O_6\ (s) \rightarrow 3\ N_2\ (g) + 5\ H_2O\ (g) + 7\ CO\ (g) + 7\ C\ (s)$
DNT	$C_7H_6N_2O_4$	182.1	-114	$C_7H_6N_2O_4\ (s) \rightarrow N_2\ (g) + 3\ H_2O\ (g) + CO\ (g) + 6\ C\ (s)$
RDX	$C_3H_6N_6O_6$	222.1	-22	$C_3H_6N_6O_6\ (s) \rightarrow 3\ N_2\ (g) + 3\ H_2O\ (g) + 3\ CO\ (g)$
PETN	$C_5H_8N_4O_{12}$	316.1	-10	$C_5H_8N_4O_{12}\ (s) \rightarrow 2\ N_2\ (g) + 4\ H_2O\ (g) + 3\ CO_2\ (g) + 2\ CO\ (g)$
TATP	$C_9H_{18}O_6$	222.2	-151	$C_9H_{18}O_6\ (s) \rightarrow 6\ H_2O\ (g) + 3\ H_2\ (g) + 9\ C\ (s)$
HMTD	$C_6H_{12}N_2O_6$	208.2	-92	$C_6H_{12}N_2O_6\ (s) \rightarrow N_2\ (g) + 6\ H_2O\ (g) + 6\ C\ (s)$
NC	$[C_6H_9N_3O_{12}]_n$	315.2n	-23	$[C_6H_9N_3O_{12}]_n\ (s) \rightarrow 1.5\ N_2\ (g) + 4.5\ H_2O\ (g) + 1.5\ CO_2\ (g) + 4.5\ CO\ (g)$
NQ	$CH_4N_4O_2$	104.1	- 31	$CH_4N_4O_2\ (s) \rightarrow 2\ N_2\ (g) + H_2O\ (g) + CO\ (g) + H_2\ (g)$
EGDN	$C_2H_4N_2O_6$	152.1	0	$C_2H_4N_2O_6\ (s) \rightarrow N_2\ (g) + 2\ H_2O\ (g) + 2\ CO_2\ (g)$
Dynamite*	AN+ EGDN + NC		≈ 0	a AN (s) + b EGDN (l) + c NC (s) → $d\ N_2\ (g) + e\ H_2O\ (g) + f\ CO_2\ (g)$
ANFO*	AN + diesel		≈ 0	$a\ NH_4NO_3\ (s) + b\ C_xH_y\ (l) \rightarrow c\ N_2\ (g) + d\ H_2O\ (g) + e\ CO_2\ (g)$
Ammonal (ANAl)	NH_4NO_3 + Al		≈ 0	$3\ NH_4NO_3\ (s) + 2\ Al\ (s) \rightarrow 3\ N_2\ (g) + 6\ H_2O\ (g) + Al_2O_3\ (s)$
Black powder	KNO_3 + C + S		≈ 0	$10\ KNO_3\ (s) + 8\ C\ (s) + 3\ S\ (s) \rightarrow 2\ K_2CO_3\ (s) + 3\ K_2SO_4\ (s) + 5\ N_2\ (g) + 6\ CO_2\ (g)$
Flash powder	$KClO_4$ + Al		≈ 0	$3\ KClO_4\ (s) + 8\ Al\ (s) \rightarrow 4\ Al_2O_3\ (s) + 3\ KCl\ (s)$
Chloratite	$NaClO_3$ + Sucrose + S		≈ 0	$9\ NaClO_3\ (s) + C_{12}H_{22}O_{11}\ (s) + S\ (s) \rightarrow 9\ NaCl\ (s) + 11\ H_2O\ (g) + 12\ CO_2\ (g) + SO_3\ (g)$
NG	$C_3H_5N_3O_9$	227.1	4	$C_3H_5N_3O_9\ (l) \rightarrow 1{,}5\ N_2\ (g) + 2{,}5\ H_2O\ (g) + 3\ CO_2\ (g) + 0{,}25\ O_2\ (g)$
AN	NH_4NO_3	80.0	20	$NH_4NO_3\ (s) \rightarrow N_2\ (g) + 2\ H_2O\ (g) + 0{,}5\ O_2\ (g)$
KNO_3	KNO_3	101.1	40	$KNO_3\ (s) \rightarrow 0.5\ K_2O\ (g) + NO\ (g) + 0.75\ O_2\ (g)$
$KClO_4$	$KClO_4$	138.6	46	$KClO_4\ (s) \rightarrow KCl\ (s) + 2\ O_2\ (g)$
$NaClO_3$	$NaClO_3$	122.6	39	$NaClO_3\ (s) \rightarrow NaCl\ (s) + 1.5\ O_2\ (g)$

* Chemical reactions for dynamite and ANFO are not stoichiometrically balanced.

By comparing the explosives shaded in different colours in Table 6.1, explosives might be classified in three groups depending on whether they have a positive, negative or zero oxygen balance. As an example, TNT has a negative OB, EGDN has a zero OB, and AN has a positive OB, as evidenced in their theoretical combustion-decomposition reactions:

$2\ C_7H_5N_3O_6\ (s) \rightarrow 3\ N_2\ (g) + 5\ H_2O\ (g) + 7\ \mathbf{CO}\ (g) + 7\ \mathbf{C}\ (s)$ (OB < 0)

$C_2H_4N_2O_6\ (l) \rightarrow N_2\ (g) + 2\ H_2O\ (g) + 2\ \mathbf{CO_2}\ (g)$ (OB = 0)

$2\ NH_4NO_3\ (s) \rightarrow 2\ N_2\ (g) + 4\ H_2O\ (g) + \mathbf{O_2}\ (g)$ (OB > 0)

It should be noticed that AN theoretically decomposes to oxygen, EGDN is oxidized to carbon dioxide, whereas TNT decomposes only to solid carbon and carbon monoxide. AN and EGDN undergo complete combustions while TNT undergoes an incomplete combustion. As evidenced in their chemical reactions, incomplete combustions are characterized by producing toxic carbon monoxide and solid carbon particles whereas complete combustions do not [9, 10]. Solid carbon particles combined with the gaseous products CO_2, H_2O, N_2, and CO, produce a characteristic black smoke. On the contrary, complete combustions produce white-grey smoke. Such difference is highly useful to easily check whether an explosive detonates undergoing a complete or incomplete oxidation.

Experimental detonations

Around 300 g of eight different explosives including TNT, RDX, PETN, TATP, HMTD, dynamite, ANFO and black powder were safely detonated by EOD specialists.

Besides the in-situ visual witnessing of detonations (at a safe distance of 500 m), detonations were recorded with a video camera (located at 100 m). Each video was later examined frame by frame in order to maximize the information previously collected by only visual witnessing.

- *TNT, RDX and PETN*

As expected, the detonations of negative oxygen balance explosives TNT, RDX and PETN, produced large amounts of black smoke, as evidenced in Figure 6.2.

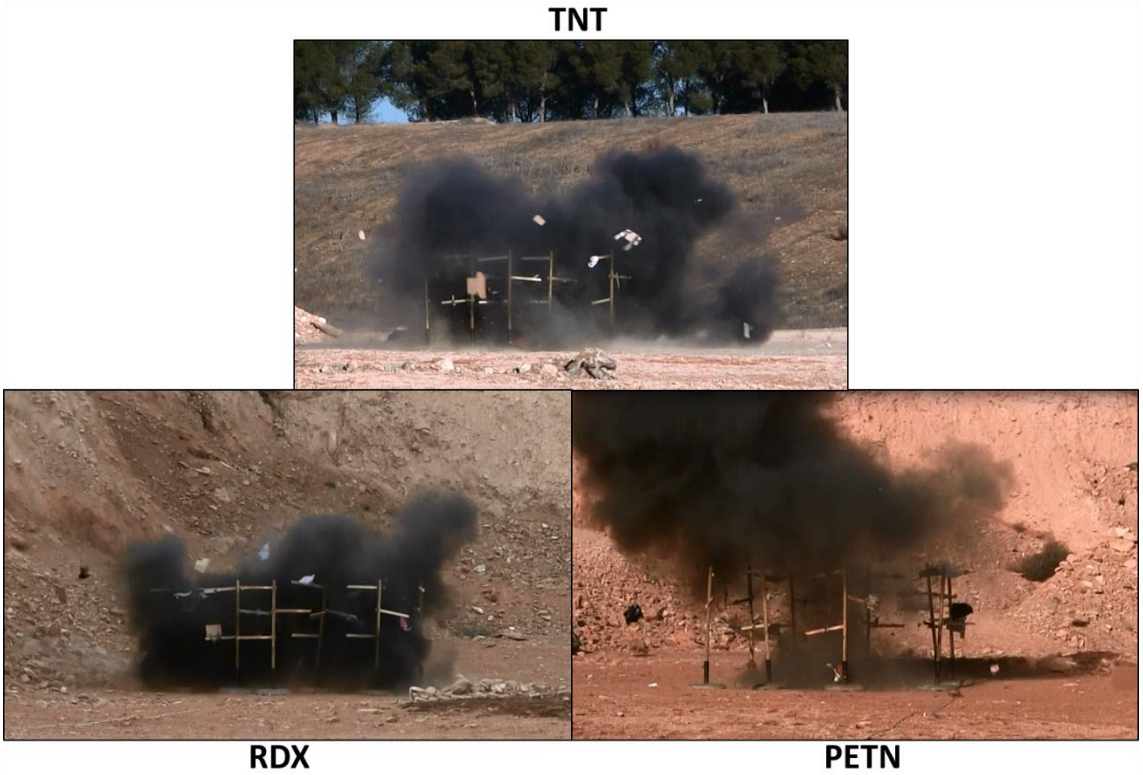

Figure 6.2. Pictures of the detonations of TNT, RDX and PETN explosives, extracted from the corresponding recorded videos. Each picture corresponds to the frame located approximately at 300 ms after initiating the detonation.

This observation is partially in accordance with the theoretical reaction products expected for TNT, RDX and PETN incomplete combustions. Theoretically, only TNT decomposes into solid carbon particles, which provide the black smoke. Neither RDX nor PETN produce solid carbon particles, but only carbon monoxide (which is colourless).

$$2\ C_7H_5N_3O_6\ (s) \rightarrow 3\ N_2\ (g) + 5\ H_2O\ (g) + 7\ \mathbf{CO}\ (g) + 7\ \mathbf{C}\ (s)$$

$$C_3H_6N_6O_6\ (s) \rightarrow 3\ N_2\ (g) + 3\ H_2O\ (g) + 3\ \mathbf{CO}\ (g)$$

$$C_5H_8N_4O_{12}\ (s) \rightarrow 2\ N_2\ (g) + 4\ H_2O\ (g) + 3\ \mathbf{CO_2}\ (g) + 2\ \mathbf{CO}\ (g)$$

Nevertheless, the empirical observation clearly evidences that solid carbon particles are being produced in the detonation of the three explosives. This result implies that, even if the theoretical simplified oxygen balance reaction is the average global chemical reaction for each explosive detonation, multiple non-simplified reactions are actually occurring. As an example, RDX detonation may proceed as follows, in such a way that the three species (C, CO and CO_2) are produced:

$$C_3H_6N_6O_6\ (s) \rightarrow N_2\ (g) + H_2O\ (g) + \mathbf{CO}\ (g) + \mathbf{CO_2}\ (g) + \mathbf{C}\ (s)$$

Actually, computational and isotopic studies found in literature for TNT, RDX or PETN detonations, proposes not only the formation of N_2, H_2O, C, CO and CO_2, but also methane, ethylene, nitrogen oxides, formaldehyde and hydrogen cyanide in lower concentrations [1, 11-13].

- TATP and HMTD

Contrarily to was expected, TATP and HMTD detonated without producing black smoke (see Figure 6.3).

Figure 6.3. Pictures of the detonations of TATP and HMTD explosives, extracted from the corresponding recorded videos. Each picture corresponds to the frame located approximately at 300 ms after initiating the detonation.

According to the remarked negative OB of TATP and HMTD, their detonations should theoretically provide an intense black smoke due to solid carbon particles. However, the empirical evidence refutes those theoretical chemical reactions based on incomplete combustions:

$$C_9H_{18}O_6\ (s) \rightarrow 6\ H_2O\ (g) + 3\ H_2\ (g) + 9\ C\ (s)$$

$$C_6H_{12}N_2O_6\ (s) \rightarrow N_2\ (g) + 6\ H_2O\ (g) + 6\ C\ (s)$$

Other completely different chemical reactions seem to occur during TATP and HMTD detonations. As previously introduced, advanced computational methods are used to confirm or refute a particular conceived reaction pathway by taking into account multiple factors such as the activation energy, enthalpy and entropy. In fact, multiple reactions and pathways might be theoretically possible

and might simultaneously occur, though a main reaction is usually expected. For instance, the main chemical reactions proposed in literature for TATP and HMTD detonations are simplified below [14, 15]:

$$C_9H_{18}O_6\ (s) \rightarrow 3\ C_3H_6O\ (g) + O_3\ (g)$$

$$4\ C_6H_{12}N_2O_6\ (s) \rightarrow 4\ N(CH_3)_3\ (g) + 2\ N_2\ (g) + 6\ H_2O\ (g) + 6\ CO_2\ (g) + 6\ CO\ (g)$$

In both reactions, the reactant explosive molecule initially decomposes to smaller organic molecules (acetone in TATP; trimethylamine in HMTD); instead of fully decomposing to solid carbon. Afterwards, acetone and trimethylamine are completely oxidized to H_2O and CO_2 in combination with air oxygen.

$$C_3H_6O\ (g) + 4\ O_2\ (g) \rightarrow 3\ H_2O\ (g) + 3\ CO_2\ (g)$$

$$4\ N(CH_3)_3\ (g) + 21\ O_2\ (g) \rightarrow 2\ N_2\ (g) + 18\ H_2O\ (g) + 12\ CO_2\ (g)$$

Thereby, solid carbon particles are never formed and black smoke is not produced, which is in accordance with the empirical observations.

- Black powder, dynamite and ANFO

As previously introduced, oxidizer-fuel explosive mixtures are usually prepared in such a way that their proportion ensures the complete combustion of the fuel. Therefore, these explosive mixtures usually have positive OB (proximal to zero). Theoretically, reactants are completely oxidized to H_2O and CO_2 and, consequently, no black smoke should be produced in oxidizer-fuel explosive detonations [9, 10]. As evidenced in Figure 6.4, the empirical detonations of black powder, dynamite and ANFO are in agreement with the complete combustion of the fuel, since no black smoke (due to solid black carbon particles) was observed. A slightly darker-grey smoke was observed in the detonation of black powder with respect to dynamite and ANFO, which could be explained by the fact that black powder leaves solid white-greyish reaction products (due to potassium) whereas dynamite and ANFO are completely transformed into gaseous products.

$$10\ KNO_3\ (s) + 8\ C\ (s) + 3\ S\ (s) \rightarrow 2\ \mathbf{K_2CO_3}\ (s) + 3\ \mathbf{K_2SO_4}\ (s) + 5\ N_2\ (g) + 6\ CO_2\ (g)$$

$$a\ AN\ (s) + b\ EGDN\ (l) + c\ NC\ (s) \rightarrow d\ N_2\ (g) + e\ H_2O\ (g) + f\ CO_2\ (g) \quad (*)$$

$$a'\ NH_4NO_3\ (s) + b'\ C_xH_y\ (l) \rightarrow c'\ N_2\ (g) + d'\ H_2O\ (g) + e'\ CO_2\ (g) \quad (*)$$

(* not stoichiometrically balanced)

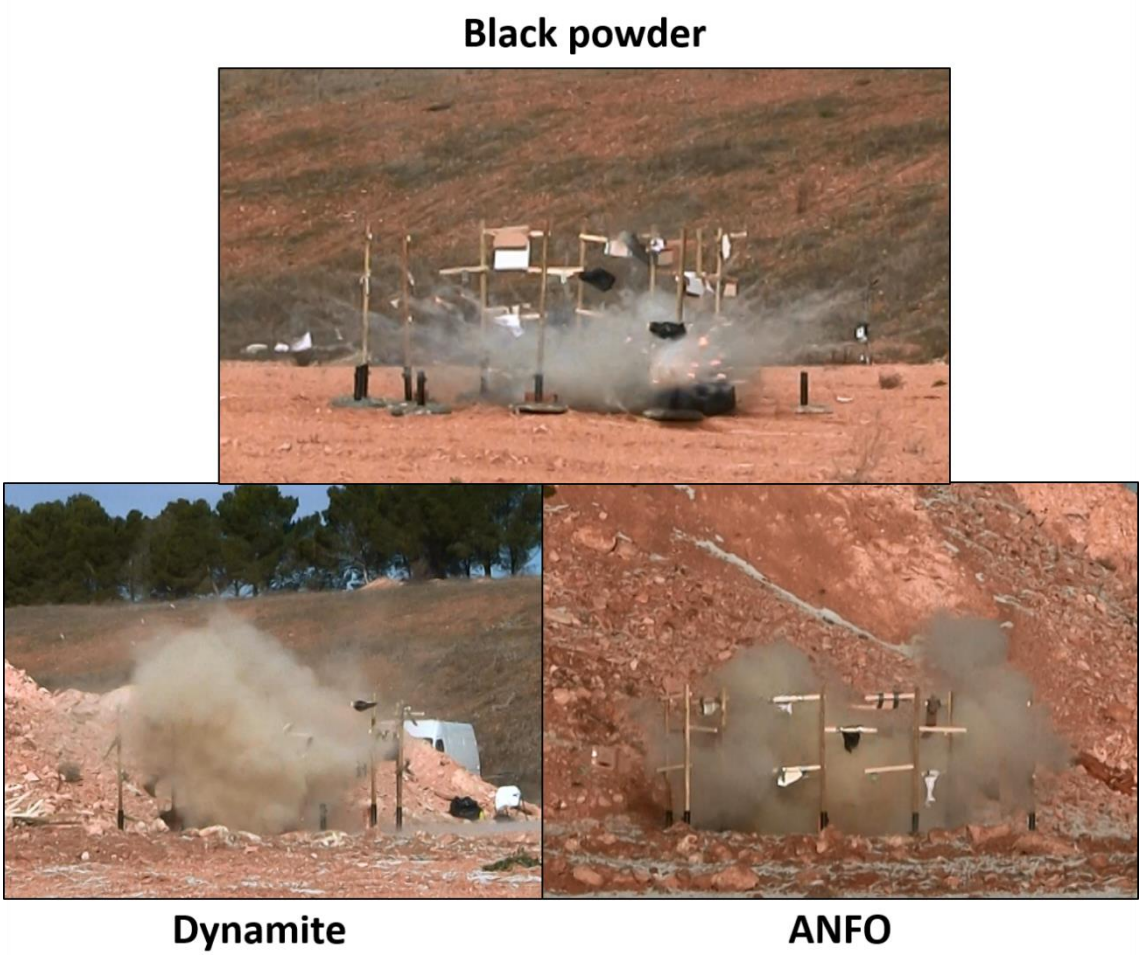

Figure 6.4. Pictures of the detonations of black powder, dynamite and ANFO explosives, extracted from the corresponding recorded videos. Each picture corresponds to the frame located approximately at 300 ms after initiating the detonation.

Post-blast residues

The detection of post-blast residues is today an increasing research topic because of the development and improvement of analytical instrumentation particularly in terms of selectivity, sensitivity and limit of detection. An extensive literature about the positive detection of post-blast residues using different techniques has been reported for the last decades [10, 16-19]. However, what advances does that literature really report? What do post-blast residues really mean?

Chemical reactions occurring in the detonation of explosives (either decomposition or redox reactions) are known to be irreversible, which means that they proceed in only one direction (from reactants to products). There is no chemical equilibrium because there is no reverse reaction. In this context, it seems evident to assume that reactants will be transformed into products as

long as there are reactants. From a chemical point of view, the term “post-blast residues” might refer to the reaction products of detonations (mostly nitrogen, water vapour, carbon dioxide and carbon monoxide). However, in forensics, the term “post-blast residues” is normally referred to the explosive reactant itself (*i.e.* remains of the original explosive found after its detonation), which leads to know the explosive used.

As previously explained for oxidizer-fuel explosive mixtures, fuel is often the limiting reagent since oxidizer is purposely added in some excess to ensure the complete combustion of the fuel. Therefore, the detection of remaining traces of the oxidizer component in post-blast scenes is comprehensible.

On the contrary, single explosives, which undergo a unimolecular reaction, should fully decompose into products (theoretically). No remains of the original explosive are expected to survive during the detonation. The high pressure and temperature reached within the detonation would transform every explosive molecule into its decomposition products. Nevertheless, multiple studies have evidenced that significant amounts of explosive are frequently detected after detonation using highly sensitive instrumentation such as HPLC-MS [16-19]. Hence, this fact demonstrates that explosives do not fully decompose during detonation. The chemical reaction yield of detonations is not 100%.

According to the scant literature published on this matter [20, 21], the subsistence of undetonated explosive particles after an explosion is inherent to the strong blast effect, by which large amounts of matter from explosion are expelled in all directions [20, 21]. This expelled matter is not only composed of reaction products, but also some amounts of undetonated explosive and large amounts of surrounding materials from either the container, the ground or even shrapnel (deliberately added). In this respect, when undetonated particles of explosive are expelled from the explosion, they rapidly get cooled and low pressure; and thus, chemical reaction does not take place. In brief, the velocity of detonation (at which the chemical reactions propagate through the explosive material) competes with the time at which explosive components are expelled due to blasting. In addition, physical factors such as the presence of voids or gaps in the explosive material, the explosive particle size, and the level of compaction of the explosive, influence the amount of undetonated explosive particles that are expelled.

The blasting of undetonated explosive traces occurs with all explosives, but especially with:

1) oxidizer-fuel mixtures (in which the physical separation of reactants ends their redox reaction); and

2) secondary/tertiary explosives (whose detonation only can be initiated by using a detonator, and consequently, the expelled explosive particles may not initiate their detonation alone).

This is in accordance with the empirical studies found in literature mostly concluding that TATP and HMTD primary unstable explosives are more hardly detectable than secondary nitroexplosives TNT and RDX [16-19].

Conclusions

The detonation process is characterized by producing a high energy shock wave that propagates through the explosive material inducing chemical reactions. The identity of those chemical reactions are difficult to elucidate due to the speed at which they proceed (μs-ns).

The oxygen balance of explosives helps to predict the most oxidized products that may be formed during detonation (without the intervention of air oxygen). Such assumption is mostly correct for oxidizer-fuel explosive mixtures in which both reactants undergo a redox reaction. However, the simplified chemical equation theoretically expected for the combustion of individual explosives according to its oxygen balance, does not usually correspond to the empirical chemical reactions occurring in real detonations. Regarding nitro-explosives, other parallel chemical reactions often take place in which not oxidized products such as solid-carbon, methane or ethylene are also produced. Regarding peroxide organic explosives, the theoretical chemical combustion reaction (expected for their OB) does not even take place, and they partially decompose to smaller organic molecules. Nevertheless, the only way to accurately estimate the decomposition reaction products involves the use of advanced theoretical computational methods.

In addition, undetonated remains of the explosive subsist after the explosion due to the rapid blasting/expansion of matter. Such undetonated remains of explosives are usually known in forensics as post-blast residues. The amount

of undetonated explosive is known to be influenced by the explosive type, in such a way that oxidizer-fuel explosive mixtures usually leave more residues than single nitro-explosives, and in turn, nitro-explosives leave more residues than peroxide explosives. In this respect, next chapters (which are focused on the detection of post-blast residues after detonations of either pyrotechnic or explosive artifacts) empirically confirm this outcome.

References

[1] M.R. Manaa, L.E. Fried, The reactivity of energetic materials under high pressure and temperature, Adv. Quantum Chem. 69 (2014) 221-252.

[2] N. Kubota, Propellants and explosives. Thermochemical aspects of combustion, 2nd edition, Wiley-VCH, Weinheim, 2007.

[3] C.M. Tarver, Detonation reaction zones in condensed explosives, 14th APS Topical Conference on SCCM, 2005.

[4] B.G. Loboiko, S.N. Lubyatinsky, Reaction zones of detonating solid explosives, Combust. Expl. Shock Waves 36:6 (2000) 716-733.

[5] J.B. Bdzil, T.D. Aslam, R. Henninger, J.J. Quirk, High-explosives performance. Understanding the effects of a finite-length reaction-zone, Los Alamos Science 28 (2003) 96-110.

[6] M.M. Kuklja, E.V. Stefanovich, A.B. Kunz, An excitonic mechanism of detonation initiation in explosives, J. Chem. Physics, 112:7 (2000) 3417-3423.

[7] M. Akiki, S. Menon, A model for hot spot formation in shocked energetic materials, Combust. Flame 162 (2015) 1759-1771.

[8] N.P. Satonkina, The diagnostic of the chemical reaction zone at the detonation of condensed explosives, Physics Chem. arXiv:1603.08069v2, 2016.

[9] J. Akhavan, The chemistry of explosives, 2nd edition, RSC Paperbacks, 2004.

[10] J.P. Agrawal, High energy materials: Propellants, explosives and pyrotechnics, Wiley, 2010.

[11] V.F. Anisichkin, Isotope studies of detonation mechanisms of TNT, RDX, and HMX, Combust. Expl. Shock Waves, 43:5 (2007) 580-586.

[12] V.F. Anisichkin, Mechanism of the detonation of TNT-RDX mixtures as studied by the isotope tracer method, Russian Phys. Chem. B, 5:2 (2011) 304-307.

[13] R. Cohen, Y. Zeiri, E. Wurzberg, R. Kosloff, Mechanism of thermal unimolecular decomposition of TNT (2,4,6-Trinitrotoluene): ADFT study, J. Phys. Chem. A, 111 (2007) 11074-11083.

[14] F. Dubnikova, R. Kosloff, J. Almog, Y. Zeiri, R. Boese, H. Itzhaky, A. Alt, E. Keinan, Decomposition of Triacetone Triperoxide is an entropic explosión, J. Am. Chem. Soc. 127 (2005) 1146-1159.

[15] J.C. Oxley, J.L. Smith, H. Chen, E. Cioffi, Decomposition of multi-peroxidic compounds Part II. Hexamethylene triperoxide diamine (HMTD), Thermochim. Acta 388 (2002) 215-225.

[16] J. Yinon, Counterterrorist detection techniques of explosives, Elsevier, Amsterdam, 2007.

[17] M. Marshall, J.C. Oxley, Aspects of explosives detection, Elsevier, Oxford, 2009.

[18] J.T. Thurman, Practical bomb scene investigation, 3rd edition, CRC Press, Taylor&Francis, Boca Raton, 2017.

[19] A. Beveridge, Forensic investigation of explosions, Taylor&Francis, 1998.

[20] N. Abdul-Karim, C.S. Blackman, P.P. Gill, E.M.M. Wingstedt, B.A.P. Reif, Post-blast explosive residue – A review of formation and dispersion theories and experimental research, RSC Advances 4 (2014) 54354-54371.

[21] N. Abdul-Karim, C.S. Blackman, P.P. Gill, R.M. Morgan, L. Matjacic, R. Webb, W.H. Ng, Morphological variations of explosive residue particles and implications for understanding detonation mechanisms, Anal. Chem. 88 (2016) 3899-3908.

6.2. Identification of Post-Blast Explosive Residues by Infrared Spectroscopy

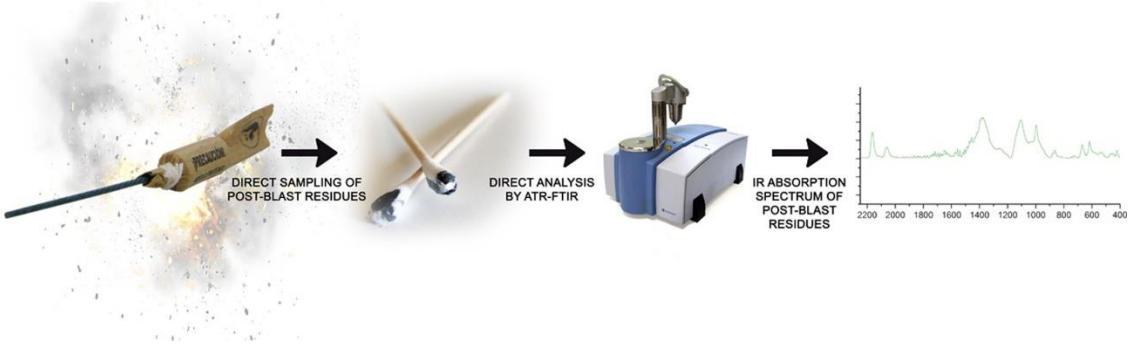

Abstract

Specific analytical procedures are requested for the forensic analysis of pre- and post-blast consumer firework samples, which present significant challenges. Up to date, vibrational spectroscopic techniques such as Fourier transform infrared spectroscopy (FTIR) have not been tested for the analysis of post-blast residues in spite of their interesting strengths for the forensic field. Therefore, this work proposes a simple and fast procedure for the sampling and analysis of consumer firework post-blast residues by a portable FTIR instrument with an Attenuated Total Reflection (ATR) accessory. In addition, the post-blast residues spectra of several consumer fireworks were studied in order to achieve the identification of their original chemical compositions. Hence, this work analysed 22 standard reagents usually employed to make consumer fireworks, or because they are related to their combustion products. Then, five different consumer fireworks were exploded, and their residues were sampled with dry cotton swabs and directly analysed by ATR-FTIR. In addition, their pre-blast fuses and charges were also analysed in order to stablish a proper comparison. As a result, the identification of the original chemical compositions of the post-blast samples was obtained. Some of the compounds found were potassium chlorate, barium nitrate, potassium nitrate, potassium perchlorate or charcoal. An additional study involving chemometric tools found that the results might greatly depend on the swab head type used for the sampling, and its sampling efficiency. The proposed procedure could be used as a complementary technique for the analysis of consumer fireworks post-blast residues.

Introduction

Consumer fireworks are small display pyrotechnic devices available on sale to the general public. They are designed to be lit up and produce some effects such as smoke, noise, colour, sparks or flames by combustion [1]. Some examples are firecrackers, bottle rockets or sparklers. They are made with clever chemical compositions and configurations, which are responsible for the pyrotechnic effects. The most frequently used chemical compounds are oxidizer agents such as nitrate, perchlorate or chlorate salts, fuels such as charcoal, magnesium or aluminium, and auxiliary substances such as potassium benzoate or strontium carbonate [1, 2].

There is high forensic interest in the determination of the chemical composition of consumer fireworks, from both intact items and their post-blast residues. This is important during investigations of caseworks related to vandalism acts, injuries, occupational accidents, illegal trade or improvised explosive devices made with their components [1, 3]. Although the analysis of this type of samples is challenging, forensic experts try to obtain a complete evidence characterization and/or identification by means of applying multiple specific analytical techniques based on different principles and methodologies [4]. Some complications for studying consumer fireworks include the fact that they may have complex configurations and compositions, like several fuses and charges, or that the total amount of pyrotechnic charge is usually low (0.1–2 g [5]), which means that the available amount of post-blast residues is assumed quite lower. Furthermore, studying post-blast residues is a daunting task because some unburnt material from fuses and charges, and reaction products from the original composition are normally mixed with inert materials such as clay plugs or cardboard [6].

Consequently, several specific analytical approaches for the analysis of consumer firework samples were proposed. Colorimetric methods were applied for the quantitative determination of given substances such as sulphur and chlorate in intact items [7]. Scanning electron microscopy/energy dispersive X-ray spectroscopy (SEM-EDX) was used to identify chemical elements in pre- and post-blast consumer firework samples, and to differentiate between pyrotechnic particles and gunshot residues [8-11]. Besides, several sensitive methodologies were proposed for the analysis of consumer firework samples by Capillary Electrophoresis (CE) with UV–vis detection [5, 12-14], and by a portable dual-

channel CE with contactless conductivity detection [15]. These methodologies allowed the identification of their ionic composition. Moreover, it was even possible to associate the identified post-blast ions with their original reagents through the decomposition or combustion derived reaction products [5, 15]. In recent years, the use of spectroscopic techniques has increased in this field especially because they can provide useful atomic and molecular information. Inductively Coupled Plasma, Atomic Fluorescence Spectroscopy and Atomic Emission Spectroscopy were applied to the identification of metallic elements in intact consumer fireworks [6, 16]. Mass spectrometry (MS) coupled to desorption-electrospray-ionization [17] and to laser-electrospray [18] were applied to the analysis of intact consumer fireworks and their post-blast residues, respectively. Furthermore, it is well known that Raman and Fourier transform infrared (FTIR) spectroscopy are suitable techniques to analyse organic or inorganic explosives [19]. In fact, Raman spectroscopy and FTIR spectroscopy (used in transmittance mode) were also applied to detect the molecular composition of intact consumer fireworks [20]. Both techniques have very interesting characteristics in the forensic context, for instance, they allow fast result acquisition without sample destruction, and they are available as portable systems. However, to our knowledge, the use of these techniques for the analysis of post-blast residues of consumer fireworks has not been reported up to date. The reasons might include the challenging issue of analysing this type of samples and the lower sensitivity of these techniques compared with the other previously mentioned. Nevertheless, because they offer interesting strengths for the forensic field, these spectroscopic techniques should be further tested for the specific analysis of post-blast consumer fireworks. A crucial step to achieve the successful analysis of these samples by these techniques is the sampling step. In fact, up to date, several studies have involved the recovery of the explosives' organic and inorganic post-blast residues from numerous surfaces using several swab types [21-23]. All these studies were devised for collecting and then extracting the analytes using solvents for their further analysis by separation techniques. However, they did not tackle the direct analysis of the residues remnant on the swab heads, which might implicate additional challenges.

The aims of this work were to obtain the spectra of several post-blast consumer fireworks samples using a simple and fast sampling and analysis procedure by a portable FTIR instrument with Attenuated Total Reflection (ATR) accessory,

and to achieve the identification of their original chemical compositions. In order to accomplish these goals, the standard reagents of the main compounds found in consumer fireworks and their main combustion products were analysed. Afterwards, some items were exploded, their post-blast residues were swabbed and immediately analysed by ATR-FTIR. In addition, pre-blast fuse and charge samples were analysed, and their spectra compared to their corresponding post-blast counter parts.

Material and methods

- Standards, samples, materials and instrumentation

All standards were of analytical grade. Sodium nitrate, strontium nitrate, barium nitrate, potassium chlorate, sodium chlorate, potassium perchlorate, potassium thiocyanate, sodium thiocyanate, potassium cyanate, sodium cyanate, potassium sulphate, sodium sulphate, sodium thiosulphate, potassium thiosulphate, strontium carbonate and aluminium were obtained from Sigma-Aldrich (St. Louis, MO, USA). Potassium nitrate, Sulphur and copper oxide (II) were purchased from Labkem (Mataró, Barcelona, Spain). Wood charcoal (powder), sodium nitrite, calcium chloride and calcium carbonate were bought from Fisher Scientific (Loughborough, Leicestershire, UK).

Five different consumer fireworks were selected as samples. They were purchased in a local store (Alcalá de Henares, Madrid, Spain). The three simple firecrackers were named as F1, F2 and F3 (commercial names: *100petardos*, cheroki junior and *superfallero*, respectively). One complex firecracker was named as F4 (commercial name: cracks). Finally, a bottle-rocket was named as R1 (commercial name: *voladores surtidos*). Table 6.2 collects the information provided by manufacturers about the used firework's composition. Additional chemical information of these samples was obtained in previous studies [5, 15].

Table 6.2. Composition of the consumer fireworks declared by manufacturers.

Consumer firework	Declared composition (charges)
F1	Al; Sulphur; $KClO_4$
F2	Sulphur; Magnalium; Al; $KClO_4$
F3	Al; Sulphur; $KClO_4$
F4	Cracking effect: $KClO_4$; KNO_3; Sulphur; Charcoal; Magnalium; CuO Green smoke: Sulphur; $Ba(NO_3)_2$; $KClO_4$ Thunder effect: Al; Sulphur; $KClO_4$
F5	Lift mixture: Sulphur; Charcoal; KNO_3 Burst mixture: Sulphur; Charcoal; KNO_3 Green effect: $C_{48}H_{42}O_7$; $(C_2HCl)_n$; $KClO_4$; Magnalium; $Ba(NO_3)_2$

Cotton swabs from three different manufacturers were tested in order to assess the effectivity of the swabbing system and the background signals produced by the swab head material. Specifically, they were obtained from Prionics AG (Schlieren, Zurich, Switzerland), Remel-Thermo Fisher scientific (Santa Fe Drive, P. O., USA), and Baikim-Ruher Iberica S.A. (Barcelona, Spain). It is important to note that the swabs from Prionics AG (named as Cb) were designed for forensic evidence collection, whereas the swabs from Remel (named as Sw) were designed for microbiology purposes, and the swabs from Baikim (named as Hy) were designed for personal care.

A compact portable ALPHA FTIR spectrometer with ATR sampling accessory (Bruker Optics Inc., Ettlingen, Germany) was used to analyse the samples.

- *Sample preparation, sampling and analysis*

In order to obtain post-blast samples, two items of each consumer firework type were exploded on a steel plate (an open metallic sheet, named as Ms). On additional experiments, a glass surface (a large glass desiccator, named as Des) was considered. The methodology used to clean the steel plate and the glass surface between explosions was the reported in reference [5]. Briefly, the post-blast residues were obtained swabbing the surface with a dry cotton swab, trying to collect residues from all over the surface. Then, the dry cotton swab was placed and pressed directly on the cleaned diamond crystal surface of the ATR sampling accessory using the devices' mechanical press. Each swab was analysed thrice by changing (rotating) its position under the press, thus assuring a fresh measurement each time. The instrument was cleaned between analyses with a clean paper tissue and then with isopropanol-soaked tissues.

Furthermore, the pre-blast samples of three additional items of each consumer firework type were also analysed. The following procedure was used for studying the non-exploded items: First, the fuse was separated from the main part of the item. The most external part of the fuse (not contaminated by the main charge of the item) was divided in two. One-half was selected for extracting its containing fuse-powder. Then, the extracted powder was analysed directly on the cleaned diamond crystal surface of the ATR sampling accessory. Afterwards, the item's main part (body) was opened carefully using a scalpel and its powdered content was emptied on a filter paper. Only a small amount (around 50 mg) of such powder was analysed. No other pre-treatment was performed on the samples. Some consumer fireworks contained more than one charge, thus each type of charge was separated for their further analysis, except for those cases where cross-contamination was observed with the naked eye. In those cases, they were mixed further and analysed as a mixed sample.

- *Data acquisition*

IR absorption spectra were recorded from 4000 to 400 cm^{-1} with a spectral resolution of 4 (data spacing of 2.04 cm^{-1}). For every measurement, the system performed 48 scans, which then were automatically averaged using the Opus 7.2 software (Bruker Optics, Ettlingen, Germany). In order to focus on the spectral fingerprint region, the spectral region selected for the data treatment was 2200–400 cm^{-1}. In fact, all the characteristic bands for the inorganic oxidizers and the other components common in these samples are included within this range. Afterwards, a rubber band baseline correction (n=64 points and 15 iterations), and a range normalization between 0–2 (intensity value) were performed. The data was subsequently imported and analysed in the SIMCA 14 software (Umeå, Sweden). For this purpose, different chemometric tools like principal component analysis (PCA) were used. The PCAs were performed to visualize in a straightforward fashion how similar or different the spectra were, and to obtain a first overview of the main sources of variability. First, the noise in the spectra was reduced using the Savitzky-Golay built-in function (2^{nd} order polynomial, and a 15-points window in a symmetric kernel). Then, several PCAs were performed: one PCA for each individual class (*i.e.* type of consumer firework), and one overall PCA containing all data. Other specific PCAs containing certain data of interest such as pre-blast or post-blast samples or even post-blast samples picked up with a specific swab were useful to solve

particular matters. All PCAs were performed using a non-linear iterative partial least squares (NIPALS) algorithm, cross validation with uncertainty test, and 1/SDev as weighing.

Results and discussion

- *Standards analysis*

First, in order to set up a practical compounds library, all the standard reagents of the main compounds found in consumer firework samples were analysed. This library was meant to be useful to subsequently achieve the identification of the compounds contained in the samples. Figure 6.5 shows the ATR-FTIR spectral signatures of the main compounds used to make the selected consumer fireworks such as inorganic salts, charcoal, sulphur or aluminium.

As can be seen in Figure 6.5 a, aluminium showed an interesting IR absorption spectrum. It displayed several noisy signals at approximately 1950–1450 cm^{-1}. However, there is not molecular vibrations in this element that can explain these signals. When another ATR-FTIR instrument was employed for the analysis of the same sample, the same result was obtained. However, when aluminium is measured by transmission using KBr pellet method instead of ATR, these signals do not appear. Therefore, this effect might be produced only when using the ATR-FTIR measurements, which could be explained by some kind of reflected radiation caused by the aluminium in contact with the ATR crystal, although further research would be necessary to confirm this issue. Nonetheless, the spectrum obtained by ATR-FTIR might be useful for the identification of this element, although its signal is not explained by its vibrational properties.

Additionally, Figure 6.5 b shows the IR absorption spectra of some possible reaction products, which were selected based on previous works analysing post-blast residues of consumer fireworks [5, 15].

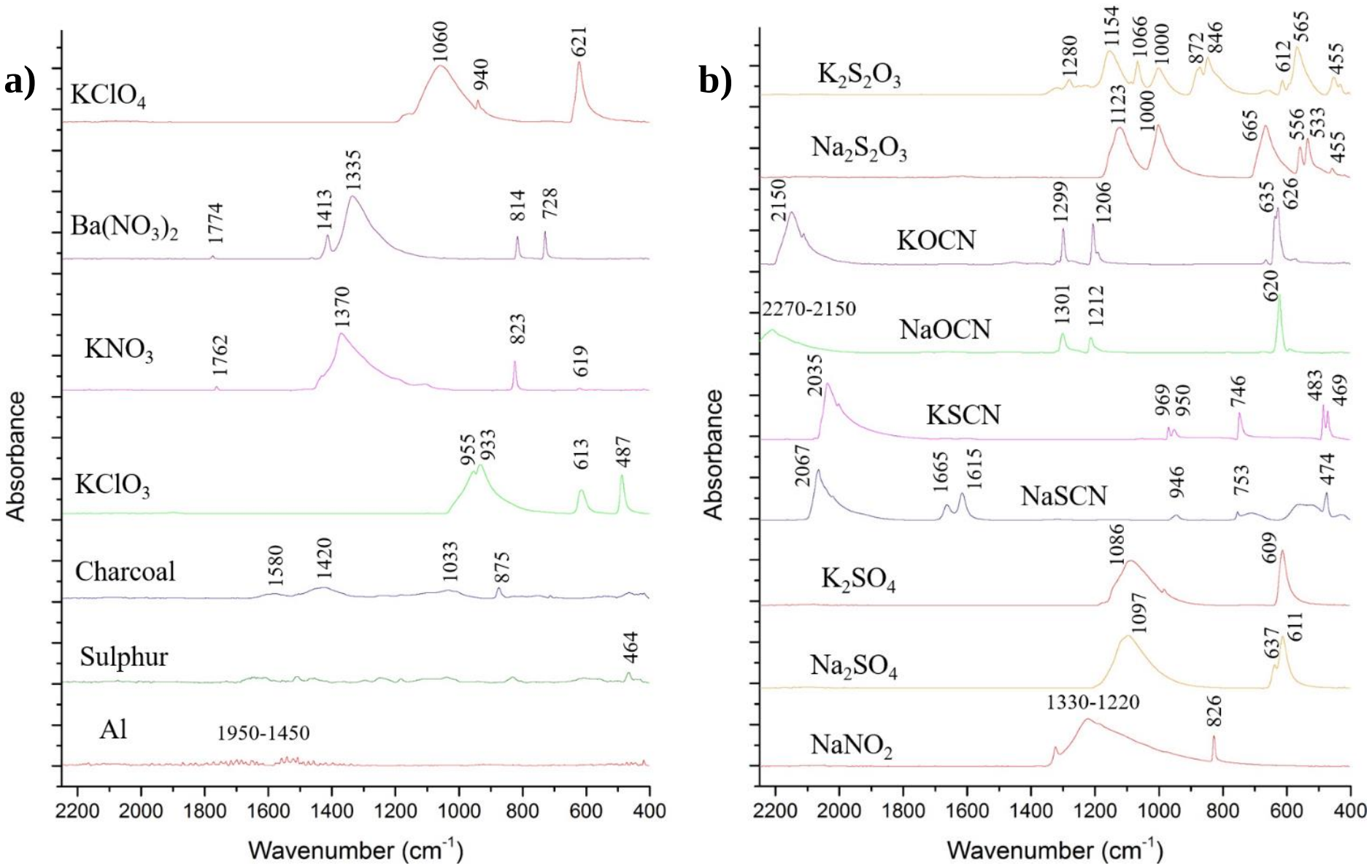

Figure 6.5. ATR-FTIR absorption spectra for a) standard reagents usually found in pyrotechnic mixtures of consumer fireworks, b) standard reagents usually found in consumer fireworks post-blast residues.

Table 6.3 shows the spectral information observed in Figures 6.5, describing the main bands of each compound. Most bands were assigned to anion molecular vibrations. Some other bands, which could not be assigned to covalent molecular vibrations, might be related with vibrations in the crystal structure of the solid.

Table 6.3. Summary of the main compounds used to make consumer fireworks, or that are present in their potential reaction products, as well as their IR bands, and the assignments for the fundamental anion vibrations. (asym: antisymmetric, def: deformation, ip: in-plane, oop: out-of-plane, st: stretching, sym: symmetric). * = band no assigned to fundamental anion vibrations.

Compound	Bands (cm^{-1})	Assignment to anion molecular vibrations	Ref.
$KClO_4$	1060, 940	ClO_4 triply degenerate asym st ($\upsilon_3(T_2)$)	[25]
	621	ClO_4 triply degenerate def ($\upsilon_4(T_2)$)	
$Ba(NO_3)_2$	1774	*	[26-28]
	1413, 1335	NO_3 doubly degenerate asym st (υ_3(E'))	
	814	NO_3 oop def (υ_2(A"$_2$))	
	728	NO_3 doubly degenerate ip def (υ_4(E'))	
KNO_3	1762	*	[26-28]
	1370	NO_3 doubly degenerate asym st (υ_3(E'))	
	823	NO_3 oop def (υ_2(A"$_2$))	
	619	NO_3 doubly degenerate ip def (υ_4(E'))	
$KClO_3$	955	ClO_3 doubly degenerate asym st (υ_3(E))	[28]
	933	ClO_3 sym st ($\upsilon_1(A_1)$)	
	613	ClO_3 sym def ($\upsilon_2(A_1)$)	
	487	ClO_3 doubly degenerate asym def (υ_4(E))	
Charcoal (C and CH)	1580, 1420	Ar C–C aromatic st	[26, 27]
	1033	C–H oop bend	
	875	C–H oop bend	
Sulphur	464	S-S st	[28]
$K_2S_2O_3$	1280	*	[28]
	1154	S_2O_3 doubly degenerate asym st (υ_4(E))	
	1066	*	
	1000	S_2O_3 sym st ($\upsilon_1(A_1)$)	
	872, 846	*	
	612	S_2O_3 def ($\upsilon_3(A_1)$)	
	565	S_2O_3 doubly degenerate def (υ_5(E))	
	455	S-S st ($\upsilon_2(A_1)$)	
$Na_2S_2O_3$	1123	S_2O_3 doubly degenerate asym st (υ_4(E))	[28]
	1000	S_2O_3 sym st ($\upsilon_1(A_1)$)	
	665	S_2O_3 def ($\upsilon_3(A_1)$)	
	556, 533	S_2O_3 doubly degenerate def (υ_5(E))	
	455	S-S st ($\upsilon_2(A_1)$)	
KOCN	2150	C≡N st (υ_1)	[26, 27]
	1299, 1206	O-C st (υ_3)	
	635, 626	O-C≡N def (υ_2)	
NaOCN	2270-2150	C≡N st (υ_1)	[26, 27]
	1301, 1212	O-C st (υ_3)	
	620	O-C≡N def (υ_2)	
KSCN	2035	C≡N st (υ_1)	[26, 28]
	969, 950	*	
	746	S-C st (υ_3)	
	483, 469	S-C≡N def (υ_2)	

NaSCN	2067	C≡N st (υ_1)	[27, 28]
	1665, 1615	*	
	946	*	
	753	S-C st (υ_3)	
	474	S-C≡N def (υ_2)	
K_2SO_4	1086	SO_4 triply degenerate asym st ($\upsilon_3(T_2)$)	[26]
	609	SO_4 triply degenerate def ($\upsilon_4(T_2)$)	
Na_2SO_4	1097	SO_4 triply degenerate asym st ($\upsilon_3(T_2)$)	[28]
	637, 611	SO_4 triply degenerate def ($\upsilon_4(T_2)$)	
$NaNO_2$	1330	NO_2 sym st ($\upsilon_1(A_1)$)	[26, 28]
	1220	NO_2 asym st ($\upsilon_3(B_2)$)	
	826	NO_2 def ($\upsilon_2(A_1)$)	

- *Sample analysis*

Five consumer fireworks available in the Spanish market were analysed: four different firecrackers (named as F1, F2, F3, and F4), and one rocket (named as R1). F1, F2 and F3 are simple firecrackers, which have a fuse and a charge, and F4 is a complex firecracker, which has a fuse and several charges. The simple and fast procedure for obtaining spectra of post-blast residues from consumer fireworks started by swabbing the surface of interest with dry cotton swabs. Then, the swabs were directly placed and pressed on the diamond crystal surface of the ATR-FTIR device. Therefore, first, these items were lit, and after they went off, their post-blast residues were swabbed and analysed. Other consumer fireworks of the same characteristics were also selected and dissected separately for the analysis of their unburnt fuses and unexploded charges.

The F1 item was exploded on a steel plate and its residues were swabbed. Most of the original reagents usually turn into gaseous products such as CO_2 and H_2O. However, part of the total charge may remain unburnt. Figure 6.6 shows the F1 post-blast spectrum in which weak signals appear at around 1950–1450 cm^{-1}. These signals might correspond to Al. It also shows several bands spread over a wide range at approximately 1170–930 cm^{-1}, and a sharp band at around 621 cm^{-1}. These bands might be due to the presence of $KClO_4$. Both, Al and $KClO_4$ are part of the initial components of this item (Table 6.2). Furthermore, the bands observed at around1450–1200 cm^{-1} and the small band at 823 cm^{-1} match up with the KNO_3 spectrum. Therefore, those bands seem to indicate the presence of this salt in the F1 post-blast residues. Additional bands appeared in this spectrum at around 2165 and 2065 cm^{-1}. According to the bibliography and our IR spectral library (Table 6.3), these bands might correspond to vibrations of cyanate and thiocyanate groups. Therefore, these compounds may

belong to the combustion products from the "explosion" of this pyrotechnic composition [5]. For instance, thiocyanate is produced from sulphur in the presence of nitrogenous compounds. Besides, some of those $KClO_4$ related bands (at around 1170-930 and 621 cm^{-1}), could be overlapping with other bands of sulphur reaction products such as sulphate or thiosulphate. A double band at around 880-860 cm^{-1} and bands at approximately 668 and 524 cm^{-1} might also correspond to potassium or sodium thiosulphate salts. Both thiosulphate salts could be produced by combustion because both cations are already present in the item, potassium as KNO_3, and sodium in the clay plugs of this item [15].

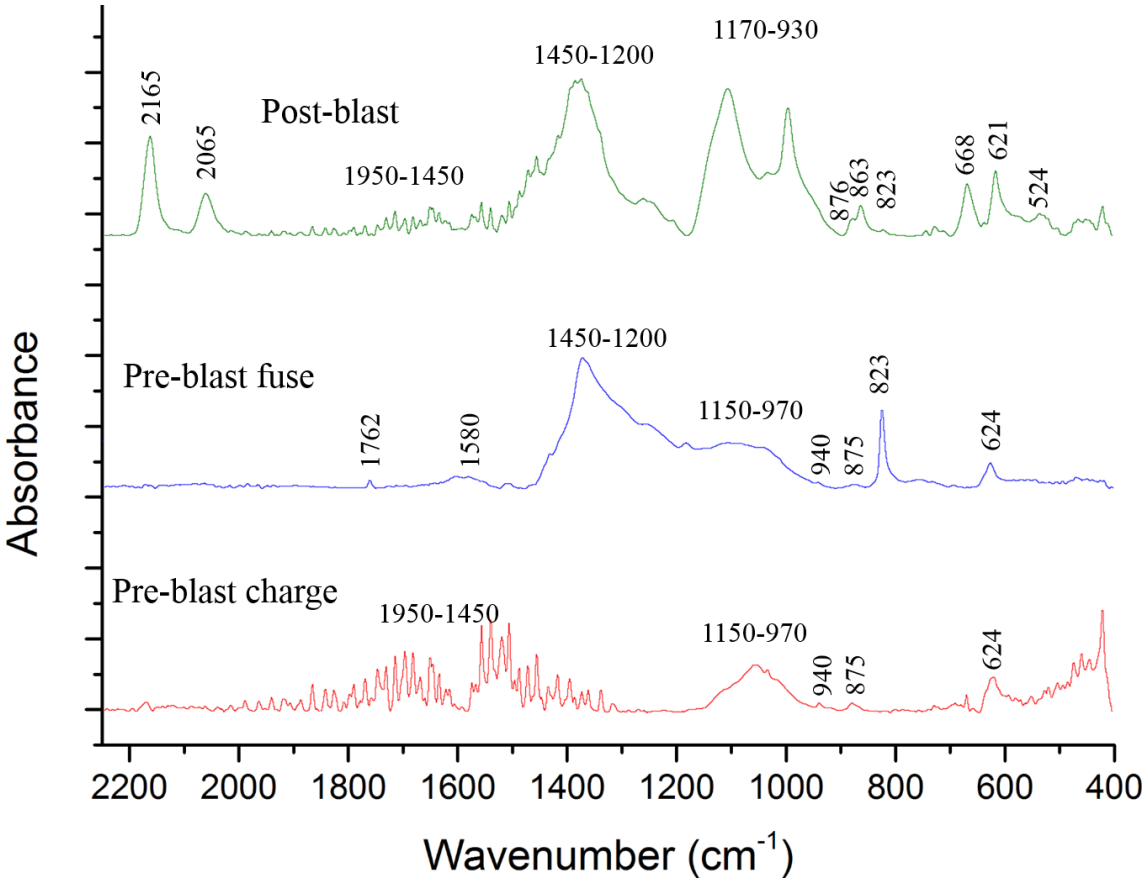

Figure 6.6. ATR-FTIR absorption spectra for the F1 samples.

It is important to note that the bands showed in the spectrum might be related to other reaction products or from cross-contamination, or from additional compounds contained in the item clay plugs or cartridge. Then, pre-blast analysis of the F1 fuse and charge were carried out in order to compare their spectra with the post-blast spectrum (Figure 6.6). In the pre-blast fuse, characteristic IR bands of KNO_3 (at about 1762, 823, and 1450–1200 cm^{-1}), and

some weak bands at about 1150–970, 940, and 624 cm^{-1} were detected. These last bands might correspond to the presence of perchlorate salt. In a previous work by CE, nitrate and perchlorate were identified in the F1 fuse [5]. Besides, some bands that might be related to charcoal (*i.e.* 1580 and 875 cm^{-1}) were also identified. In the pre-blast F1 charge, the unusual signal corresponding to Al (at about 1950–1450 cm^{-1}) was detected, as well as very weak bands at approximately 1150–970, 940 and at 624 cm^{-1}, which might correspond to vibrations of the perchlorate anions. In the light of these results, it seems that this procedure makes it possible to trace the original fireworks composition in their post-blast residues. F1 might be composed of a Pyrodex fuse ($KClO_4$, KNO_3, charcoal and sulphur), and a flash powder charge ($KClO_4$ and Al).

Figure 6.7 shows the IR spectra for the F2 post-blast residues, and fuse and charge pre-blast samples. The F2 post-blast residues spectrum displayed some bands similar to those of F1 post-blast residues. This suggests a composition with analogous unburnt reagents (nitrate and perchlorate salts, and aluminium), and reaction products (cyanate, thiocyanate, and sulphate salts). In fact, both items are very similar in their declared composition (Table 6.2). Regarding the pre-blast fuse spectrum, it showed bands related to KNO_3 (at around 1762, 1375, and 823 cm^{-1}). Besides, some bands possibly related to charcoal are also displayed: a broad band at around 1033 cm^{-1}, and additional bands at approximately 1580 and 875 cm^{-1}. Although, the band at around 1033 cm^{-1} could also be related to perchlorate, the typical sharp band of $KClO_4$ at 621 cm^{-1} did not appear. Finally, this fuse also showed a band at around 465 cm^{-1} which could be related to sulphur. Regarding the pre-blast charge spectrum, it showed the signal related to Al at approximately 1950–1450 cm^{-1}. The very broad bands at around 1150–930 and at 621 cm^{-1} could also indicate the presence of perchlorate. Hence, F2 might be made off a black powder (KNO_3, sulphur, and charcoal) fuse, and a flash powder charge.

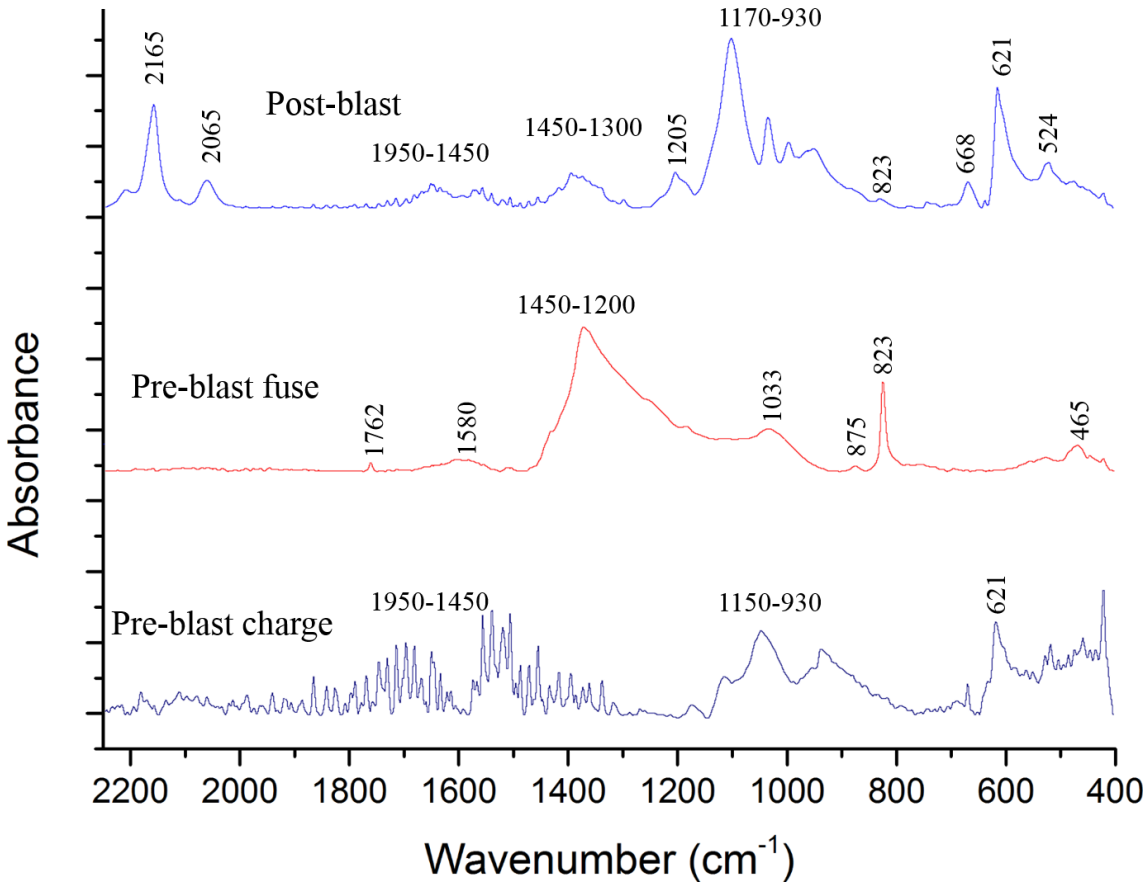

Figure 6.7. ATR-FTIR absorption spectra for the F2 samples.

Figure 6.8 shows the spectra of F3 post-blast residues, pre-blast fuse, and pre-blast charge samples. In the F3 post-blast residues, some detected bands might correspond to initial compounds such as Al (at about 1950–1450 cm^{-1}), and $KClO_4$ (at about 1170–930, and 621 cm^{-1}). Moreover, other identified bands might be related to nitrate salts (at about 1450–1325 cm^{-1}), and reaction products such as sulphate or thiosulphate (at approximately 1170–930, 668, and 524 cm^{-1}), and cyanate and thiocyanate salts (at about 1025 and above 2000 cm^{-1}). The pre-blast fuse spectrum clearly showed bands corresponding to a nitrate salt (at about 1762, 1450–1200, and 823 cm^{-1}), and strong bands related to perchlorate salt (at approximately 1170–930, and 621 cm^{-1}). These compounds seem to be part of the composition of this type of use. Furthermore, the small band at around 465 cm^{-1} and another weak band at about 875 cm^{-1} might indicate the presence of sulphur and charcoal. The pre-blast charge spectrum showed bands related to Al and $KClO_4$, which agree with the results achieved by CE [5]. However, the pre-blast charge spectrum showed also a band, at approximately 875 cm^{-1}, which could be related to charcoal from cross-

contamination between fuse and charge. Hence, F3 might be made off with a Pyrodex fuse and a flash powder charge.

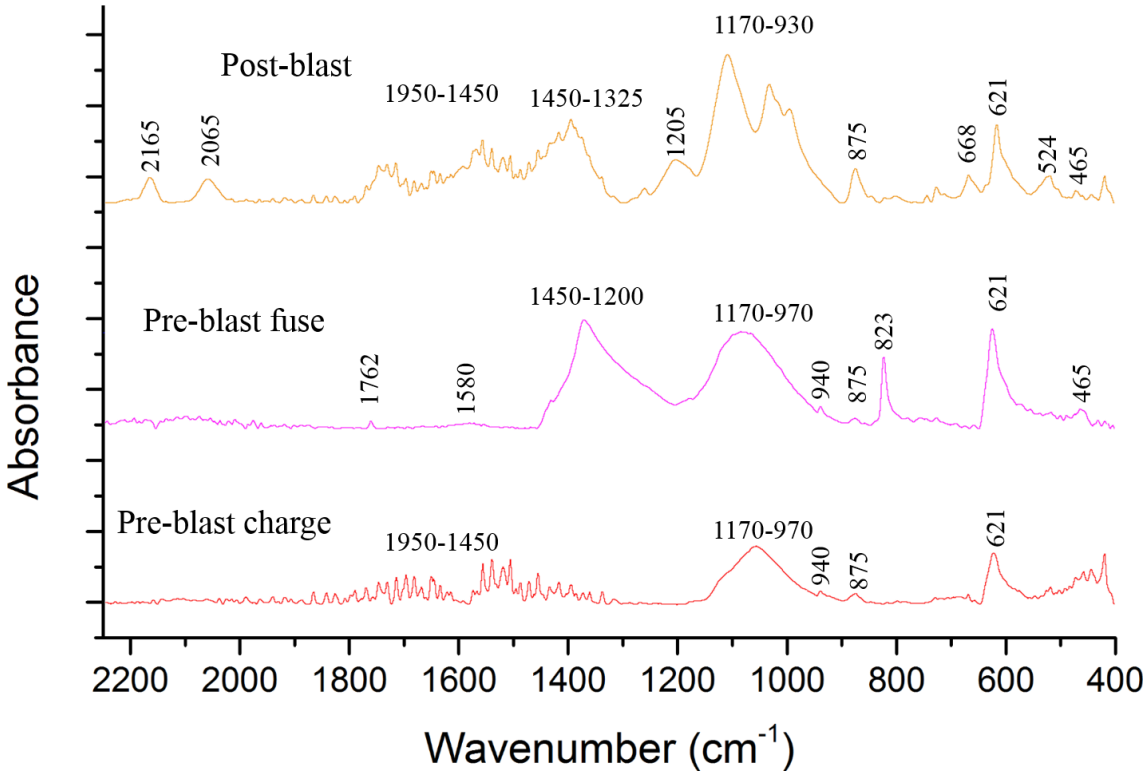

Figure 6.8. ATR-FTIR absorption spectra for the F3 samples.

F4 is a complex firecracker, having three different charges in the same compartment, one after another. These charges produce different pyrotechnic effects (smoke and cracking, and a final thunder), and have different chemical compositions. An item was exploded, and its post-blast residues were analysed. Figure 6.9 shows the spectra of the F4 post-blast residues, pre-blast fuse and thunder charges, and pre-blast smoke and cracking charges samples. The spread signal appearing at about 1950-1450 cm^{-1} may correspond to Al, while the bands at approximately 1170–930 cm^{-1} might be related to $KClO_4$. The spectra also shows some weak bands related to combustion products like sulphate or thiosulphate (at around 1170–930, 668, and 524 cm^{-1}), and cyanate and thiocyanate (at about 1205, 2065, and 2230–2150 cm^{-1}). Another broad band was also observed at around 905 cm^{-1}, and could correspond to $KClO_3$, although the manufacturers had not declared chlorate in its composition, probably because its use in this type of mixtures is banned in some countries [5]. Additionally, a sharp band observed at about 613 cm^{-1} may also be related to the initial compounds (*e.g.* $KClO_4$ or $KClO_3$) or to several reaction products (sulphate, thiosulphate or cyanate).

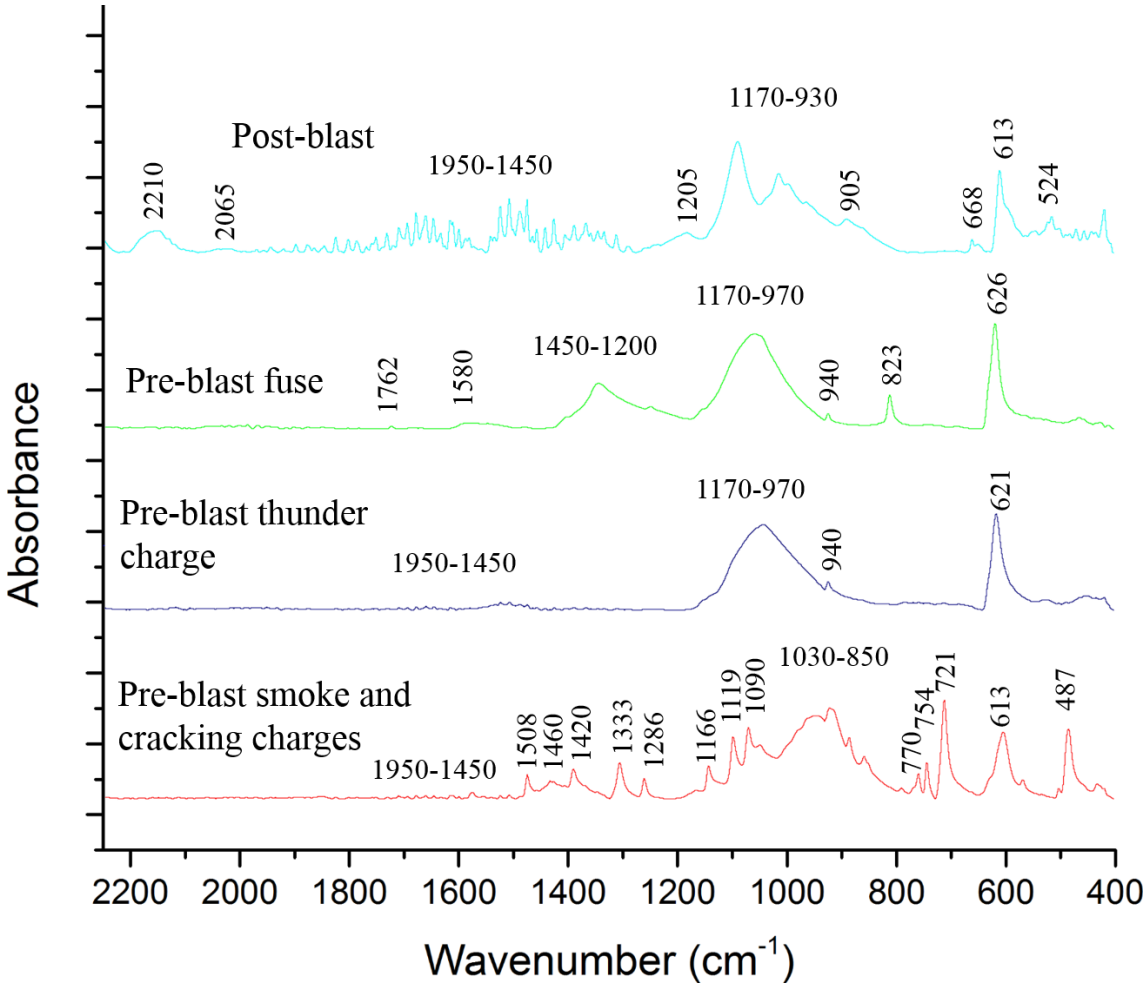

Figure 6.9. ATR-FTIR absorption spectra for the F4 samples.

Regarding the pre-blast fuse spectrum, it displayed bands corresponding to KNO_3 (at about 1762, 1450-1200, and 823 cm^{-1}), and $KClO_4$ (at around 1170-970, 940 and 642-593 cm^{-1}), which agrees with previous findings [5, 15]. A weak band observed at about 1580 cm^{-1} could be related to the presence of charcoal. Regarding the pre-blast thunder effect, and the smoke and cracking mixtures, there was no way to completely separate the smoke and cracking pyrotechnic effect mixtures without causing cross-contamination. Consequently, both mixtures were analysed together, while the thunder effect charge was analysed separately. The thunder effect mixture displayed the signal of Al, and bands at about 1060, 940, and 621 cm^{-1}, which might be related to $KClO_4$. The mixture of the other two powders showed bands at about 487, and 613 cm^{-1}, and in the 1030-850 cm^{-1} range, which might correspond to $KClO_3$. As was suspected after analysing its post-blast spectrum, several bands suggest the presence of $KClO_3$ although it had not been declared by manufacturers. Furthermore, it was not a surprise to find chlorate anions in this type of firecracker since it had been

previously determined by CE [5, 15]. Although, other bands were also observed in this spectrum, they could not be properly assigned. Some of them might correspond to the "inert material" declared by the manufacturers. Hence, F4 seems to be composed of a fuse probably made of Pyrodex (KNO_3 and $KClO_4$), and several charges. One of the charges might be flash powder (thunder effect powder), and the smoke effect powder might contain $KClO_3$ as part of its composition.

R1 is a bottle rocket, a complex item with several charges and an external, and another internal, fuse. Their charge composition is as follows: a lift mixture, a burst mixture, and a main charge with the final effect. Figure 6.10 shows the spectra of post-blast residues, and pre-blast samples of the external fuse, the burst and lift mixtures, and the main charge of the bottle rocket. The spectrum of the post-blast residues showed signals that might be related to Al (at about 1950–1450 cm^{-1}), and bands related to $KClO_4$ (at approximately 1170-930, and 619 cm^{-1}) and related to combustion products like thiocyanate (above 2000 cm^{-1}) or sulphate (at around 1170–930, and 670 cm^{-1}).

The bands found in the pre-blast fuse analysis might be related to $KClO_4$ (at about 1060, 940, and 621 cm^{-1}). The burst and lift mixtures showed bands that might correspond to KNO_3 (at about 1762, 1450-1200, and 823 cm^{-1}). Finally, the pre-blast spectrum of the final effect composition showed bands that could be related to Al, $Ba(NO_3)_2$ (at about 1413 and 1340 cm^{-1}, and sharp bands at 814 and 728 cm^{-1}), and $KClO_4$ (at about 1170–930, and 623 cm^{-1}). These results match with previous findings [5, 15]. Hence, the bottle rocket seems to be composed by a fuse containing $KClO_4$, a body with lift and burst mixtures made off black powder, and a final pyrotechnic effect containing a complex green colouring mixture with Al, $Ba(NO_3)_2$ and $KClO_4$.

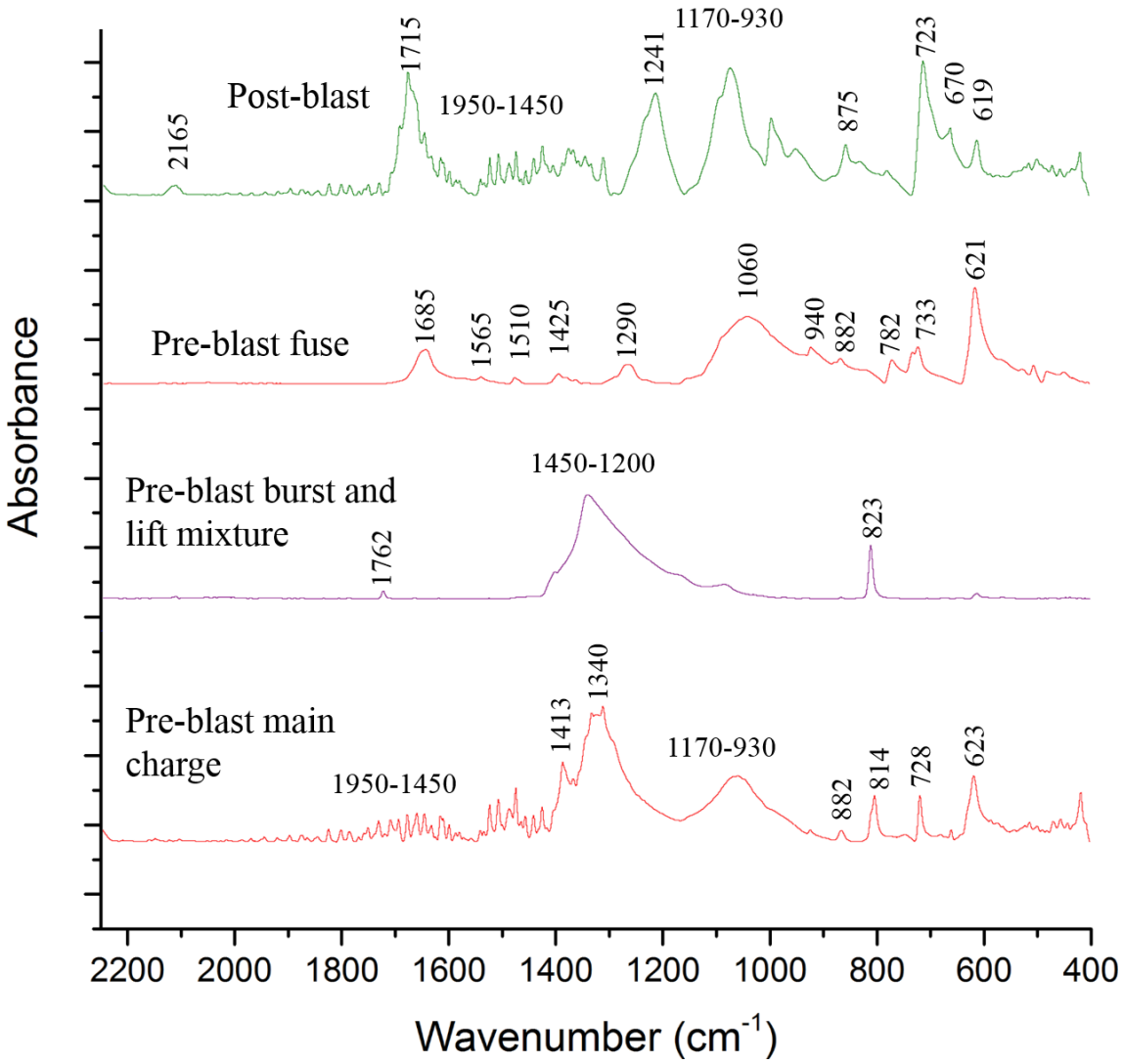

Figure 6.10. ATR-FTIR absorption spectra for the R1 samples.

- *Swabbing, a practical aspect to be considered*

In real cases, the residues amount or the type of collection surfaces are normally unknown variables, and so the residues collection is a crucial factor to be evaluated carefully. In that context, the swab head type/material has to be considered a critical issue during evidence collection [28]. The challenge here is two-fold: the effectivity of the swabbing system on different surfaces (physical aspect), and the background signals produced by the swab head material (chemical aspect). In this work, the post-blast residues were collected using three different dry cotton swabs named as Cb, Sw, and Hy. The swabs were analysed before any swabbing (blank samples), giving several weak bands in their spectral fingerprint region. The Sw swab showed quite similar signals as the Cb swab, thus indicating they were made off with almost the same type of

material. On the contrary, when post-blast residues were swabbed and analysed, the weak in-the-blank bands did not appear. Nonetheless, in a few occasions, and regardless of the swab type, some of the cotton-head bands appeared in the spectrum whenever the amount of collected residues was not enough to cover the cotton head.

Therefore, this work used chemometric techniques for studying a firecracker as a model, focusing on the effectivity of the swabbing procedure using three different swabs on two different surfaces. Two F4 items were exploded on a steal surface (Ms) and a glass surface (Des). The steal surface was an open metallic sheet, while the other surface was an uncovered large glass desiccator. In both cases, a relatively good amount of post-blast residues was available, although the amount of residues is assumed higher in the case of the glass desiccator because of a lower dispersion of the residues. Post-blast residues were collected using three different swabs, gathering residues from the entire surface. In addition, only samples from the fuse residues area and from the item body area were taken. In order to avoid redundancy and overcrowding, the Sw and Cb spectra were not plotted because they were quite similar. Figure 6.11 shows a basic 2D PCA Scores plot performed on the post-blast F4 residues collected on two surfaces (Ms and Des) with two types of swabs (Cb and Hy).

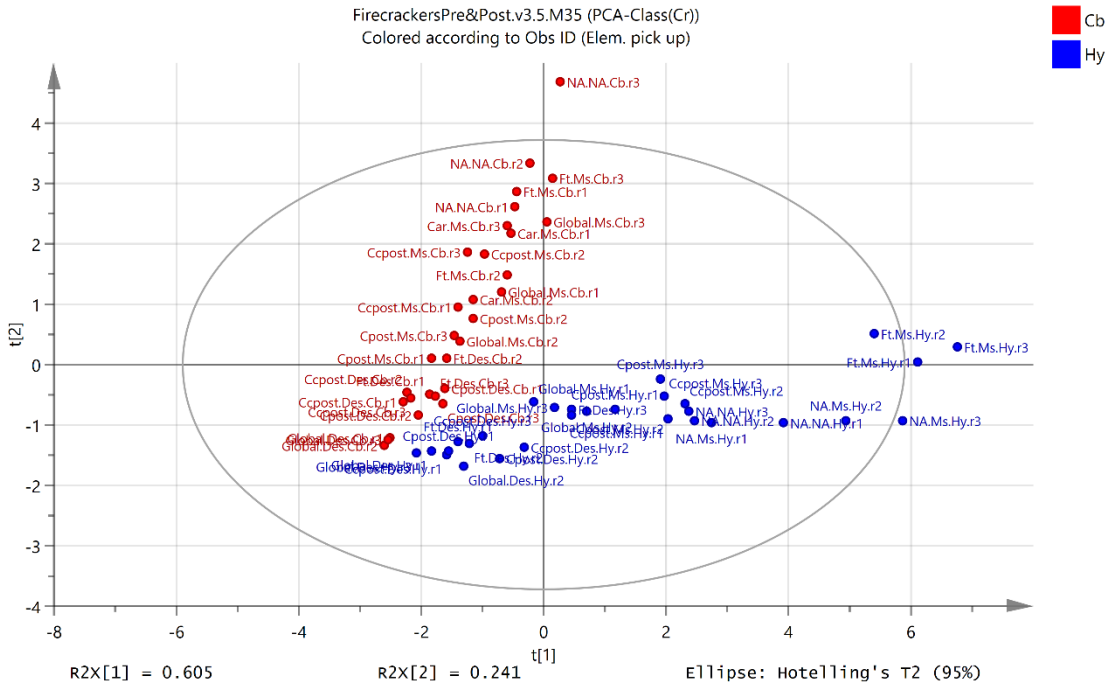

Figure 6.11. Basic 2D PCA Scores plot for the post-blast crack firecracker residues collected from two surfaces (Ms and Des) with two types of swabs (Cb and Hy).

As it was expected, the results indicated that the most important sources of variability are indeed the two collection devices (*i.e.* swab types), and the post-blast residues concentration (Figure 6.11). The planes of the two swab types tend to converge at certain point on the left-hand side of the Scores plot. This suggests that the influence of the collection device gradually decreases when the post-blast residues concentration increases (as inside the desiccator). On the contrary, the importance of the collection device increases with the combination of two factors (Figure 6.11). First, with lower post-blast residues concentration (as on the metallic sheet), moving towards the ultimate blank-swab behaviour. Second, with higher total fuse concentration, showing that the post-blast fuse components were highly concentrated when collected, and that they are rather different compared to the post-blast charge components. Nevertheless, it is clear for the F4 item that the results are very different depending on the swab used for the collection. This behaviour varied with the collection place, which has to do with the post-blast residues concentration (especially for the fuse residues), and the part of the firecracker being analysed. Although the methodology proposed in this work was suitable for studying consumer fireworks post-blast residues under the above-mentioned experimental conditions, more research is needed in order to find an effective collection device useful for a wide variety of surfaces.

Conclusions

In this work, the acquisition of IR absorption spectra from consumer firework post-blast residues was achieved by means of a simple and fast sampling procedure and subsequent analysis by ATR-FTIR.

The acquired post-blast spectra made it possible to trace the post-blast residues back to the original pyrotechnic compositions. This way, the items F1, F2 and F3 were composed of Al, $KClO_4$, KNO_3 and sulphur. In the complex F4 consumer firework, Al, $KClO_4$, $KClO_3$, and sulphur were detected. In the same way, a nitrate salt was identified by the presence of its reaction products. The rocket R1 showed Al, $KClO_4$, sulphur, and the presence of nitrate reaction products. Furthermore, this work shows that the analysis of pre-blast items by ATR-FTIR can provide additional information about the composition of each part. Different fuse compositions were identified in the selected items. Moreover, F4 showed

$KClO_3$ in its smoke pyrotechnic mixture, which is a compound banned in some countries. At the same time, R1 showed $Ba(NO_3)_2$ in one of its charges. An important issue to highlight is the apparition of several signals at approximately 1950–1450 cm^{-1} when Al is analysed by ATR-FTIR. These signals cannot be explained by the vibrational properties of Al, although empirically showed their usefulness to determine the presence of Al in this work. Further research would be necessary to better understand this effect.

This study also found that few analyses showed several weak background bands spread through the fingerprint region, probably because the swabbing procedure was not 100% effective in those cases. Therefore, this work studied one firecracker as a model and focused on the effectivity of the swabbing system on two surfaces using three different cotton swabs. Using chemometric techniques it was found that the results were very different depending on the swab used for the residues collection and on the collection place, which relates to the post-blast residues concentration. Although this methodology was suitable to study post-blast residues from consumer fireworks over some surfaces, more research is necessary for the purpose of finding an appropriate collection device for sampling a wider variety of substrates. This work might be the first step towards proposing ATR-FTIR spectroscopy as complementary technique for the analysis of post-blast residues from consumer fireworks.

References

[1] C. Martín-Alberca, C. García-Ruiz, Analytical techniques for the analysis of consumer fireworks, Trends Anal. Chem. 54 (2014) 27-36.

[2] J.A. Conkling, C. Mocella, Chemistry of Pyrotechnics. Basic Principles and Theory, Second Ed., CRC Press, Taylor & Francis Inc, Boca Raton, FL, 2011.

[3] Y. Tu, D.V. Granados, Fireworks Annual Report: Fireworks-Related Deaths, Emergency Department-Treated Injuries, and Enforcement Activities during 2013, U.S. Consumer Product Safety Commission, Washington, DC, 2013.

[4] TWGFEX (Technical Working Group for Fire and Explosives), Laboratory Explosion Group: Standards & Protocols Committee, Recommended Guidelines for Forensic Identification of Post-Blast Explosive Residues.

[5] C. Martín-Alberca, M.A. Fernández de la Ossa, J. Sáiz, J.L. Ferrando, C. García-Ruiz, Anions in pre- and post-blast consumer fireworks by capillary electrophoresis, Electrophoresis 35 (2014) 3272-3280.

[6] P. Alenfelt, Chemical analysis of consumer fireworks, J. Pyrotech. 11 (2000) 11-15.

[7] D. Chapman, Techniques for the quantitative analysis of sulfur and chlorate in fireworks compositions, J. Pyrotech. 5 (1997) 25-32.

[8] S.A. Phillips, Pyrotechnic residues analysis – detection and analysis of characteristic particles by scanning electron microscopy/energy dispersive spectroscopy, Sci. Justice 41 (2001) 73-80.

[9] K.L. Kosanke, R.C. Dujay, B.J. Kosanke, Characterization of pyrotechnic reaction residue particles by SEM/EDS, J. Forensic Sci. 48 (2003) 531-537.

[10] K.L. Kosanke, R.C. Dujay, B.J. Kosanke, Pyrotechnic reaction residue particle analysis, J. Forensic Sci. 51 (2006) 296-302.

[11] M. Grima, M. Butler, R. Hanson, A. Mohameden, Firework displays as sources of particles similar to gunshot residue, Sci. Justice 52 (2012) 49-57.

[12] T. Kishi, J. Nakamura, H. Arai, Application of capillary electrophoresis for the determination of inorganic ions in trace explosives and explosive residues, Electrophoresis 19 (1998) 3-5.

[13] K.G. Hopper, H. Le Clair, B.R. McCord, A novel method for analysis of explosives residue by simultaneous detection of anions and cations via capillary zone electrophoresis, Talanta 67 (2005) 304-312.

[14] C. Sarazin, N. Dalaunay, C. Costanza, V. Eudes, P. Gareil, Capillary electrophoresis analysis of inorganic cations in post-blast residue extracts applying a guanidinium-based electrolyte and bilayer-coated capillaries, Electrophoresis 32 (2011) 1282-1291.

[15] J. Sáiz, M.T. Duc, I.J. Koenka, C. Martín-Alberca, P.C. Hauser, C. García-Ruiz, Concurrent determination of anions and cations in consumer fireworks with a portable dual-capillary electrophoresis system, J. Chromatogr. A 1372 (2014) 245-252.

[16] R.K. Wharton, D. Chapman, A.E. Jeffcock, Evaluation of the hazards posed by high energy bangers Part 1. Noise, overpressure and TNT equivalence, J. Pyrotech. 15 (2002) 1-8.

[17] E. Sokol, A.U. Jackson, R.G. Cooks, Trace detection of inorganic oxidants using desorption electrospray ionization (DESI) mass spectrometry, Cent. Eur. J. Chem. 9 (2011) 790-797.

[18] P.M. Flanigan, J.J. Brady, E.J. Jude, R.J. Levis, Determination of inorganic improvised explosive device signatures using laser electrospray mass spectrometry detection with offline classification, Anal. Chem. 83 (2011) 7115-7122.

[19] M. López-López, C. García-Ruiz, Infrared and Raman spectroscopy techniques applied to identification of explosives, Trends Anal. Chem. 54 (2014) 36-44.

[20] K. Castro, S. Fdez-Ortiz de Vallejuelo, I. Astondoa, F.M. Goñi, J.M. Madariaga, Analysis of confiscated fireworks using Raman spectroscopy assisted with SEM-EDS and FTIR, J. Raman Spectrosc. 42 (2011) 2000-2005.

[21] K. Szomborg, F. Jongekrijg, E. Gilchrist, T. Webb, D. Wood, L. Barron, Residues from low-order energetic materials: the comparative performance of a range of sampling approaches prior to analysis by ion chromatography, Forensic Sci. Int. 233 (2013) 55-62.

[22] D.A. De Tata, A.P. Collins, J.A. McKinley, A comparison of common swabbing materials for the recovery of organic and inorganic explosive residues, J. Forensic Sci. 58 (3) (2013) 757-763.

[23] N. Song-im, S. Benson, C. Lennard, Establishing a universal swabbing and clean-up protocol for the combined recovery of organic and inorganic explosive residues, Forensic Sci. Int. 223 (2012) 136-147.

[24] G. Raj, A. Bhagi, V. Jain, Group theory and Symmetry in Chemistry, Krishna Prakashan Media Ltd., Meerut, 1998.

[25] D.W. Mayo, F.A. Miller, R.W. Hannah., Course Notes on the Interpretation of Infrared and Raman Spectra, John Wiley & Sons, Inc., Hoboken, NewJersey (2003), pp.297-354.

[26] R.A. Nyquist, R.O. Kagel, Handbook of Infrared and Raman Spectra of Inorganic Compounds and Organic Salts. Chapter 1, Infrared Spectra of Inorganic Compounds, 1971, pp.1-18.

[27] K. Nakamoto, Infrared and Raman spectra of inorganic and coordination compounds, Part A. Theory and applications in inorganic chemistry, 6th edition, John Wiley & Sons Inc., New York, 2009.

[28] N. Song-im, S. Benson, C. Lennard, Evaluation of different sampling media for their potential use as a combined swab for the collection of both organic and inorganic explosive residues, Forensic Sci. Int. 222 (2012) 102-111.

6.3. Identification of Post-Blast Explosive Residues by Raman Spectroscopy

6.3.1. The influence of the explosive

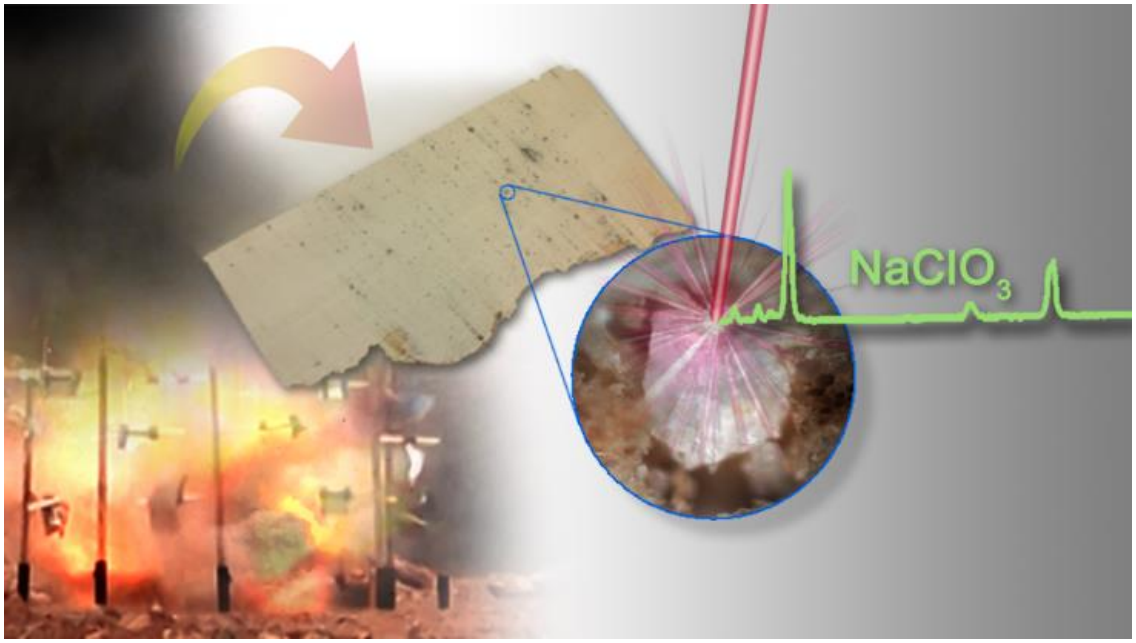

Abstract

Explosives are increasingly being used for terrorist attacks to cause devastating explosions. The detection of their post-blast residues after an explosion is a high challenge, which has been barely investigated, particularly using spectroscopic techniques. In this research, a novel methodology using confocal Raman microscopy has been developed for the analysis of post-blast residues from 10 open-air explosions caused by 10 different explosives (TNT, RDX, PETN, TATP, HMTD, dynamite, black powder, ANFO, chloratite, and ammonal) commonly used in improvised explosive devices. The methodology for the determination of post-blast particles from explosives consisted of examining the samples surfaces with both the naked eye, first, and microscopically (10× and 50×), immediately afterward; and finally, analysing the selected residues by confocal Raman spectroscopy in order to identify the post-blast particles from explosives. Interestingly, confocal Raman microscopy has demonstrated to be highly suitable to rapidly, selectively, and noninvasively analyse post-blast microscopic particles from explosives up to the nanogram range.

Introduction

The use of explosives for terrorist purposes has become a worldwide persistent threat. Numerous dreadful terrorist attacks have shown the harm and destruction that improvised explosive devices (IEDs) may cause [1]. The early detection of suspicious-looking IEDs is mandatory to prevent terrorist attacks. Military and police forces and forensic laboratories along the world spare no effort to achieve the detection of explosives before they cause an explosion. Numerous analytical techniques have been deeply investigated for explosives detection and highly significant improvements in terms of selectivity, sensitivity, and limit of detection, among others, have been achieved [2, 3]. However, the vast majority of studies have focused on the analysis of "pre-exploded" explosives, *i.e.* without having been exploded. The analysis of post-blast residues, which is an overwhelming challenge because of the almost completely consumption and destruction of the original explosive, the vast dispersion of post-blast residues, the trace amount of those explosives residues, and the high contamination of the zone, has been quite less researched. Within the few studies focused on post-blast residues analysis, most of them have been accomplished using liquid [4-6] or gas chromatography [7, 8] coupled with mass spectrometry [9-13] for organic explosives and ion chromatography or capillary electrophoresis for inorganic explosive mixtures [14-22]. Nevertheless, these techniques are time and reagent consuming. They require laborious sample preparations and they are destructive. On the contrary, spectroscopic techniques are rapid, are non-destructive, and do not require any sample treatment. However, they have been barely investigated for post-blast residues detection. Interestingly, despite having been little studied, infrared (IR) spectroscopy and, to a lesser extent, Raman spectroscopy have been preliminary examined for post-blast residues detection.

IR spectroscopy has been studied for the detection of post-blast residues of trinitrotoluene (TNT), dynamite, pentaerythritol tetranitrate (PETN), and cyclotrimethylene trinitramine (RDX) [23-25] as well as black powder and other pyrotechnic compositions [26]. On the other hand, to the best of our knowledge, Raman spectroscopy, in the imaging mode, has been studied only once for rapidly scanning and detecting post-blast residues from different explosives including TNT, PETN, RDX, and black powder along the surface of banknotes after an automatic teller machine explosion [27]. However, the high speed of

scanning of Raman imaging is usually achieved at the expense of both spatial and spectral resolution, being particularly crucial when extremely large surfaces must be analysed. In fact, these few studies have demonstrated that post-blast residues can be easily detected in small explosions of a few grams of explosive performed inside a container [24-26] but extremely complicated when post-blast residues from real open air explosions are spread out over large areas [23]. In this work, confocal Raman microscopy has been studied for the determination of post-blast particles from a large variety of explosives usable in IEDs tackling the analysis of the post-blast residues collected from 10 real open-air explosions of 10 different explosives.

Experimental section

- *Explosives*

A total of 10 different explosives were considered in this study, including, TNT, RDX, PETN, triacetone triperoxide (TATP), hexamethylene triperoxide diamine (HMTD), black powder, chloratite, dynamite, ammonium nitrate fuel oil (ANFO), and ammonal. The 10 explosives were obtained from TEDAX, the Spanish Explosive Ordnance Disposal (EOD). In order to clarify, Table 6.4 correlates each explosive with its composition, according to the information provided either by the manufacturer or by the EOD specialists.

Table 6.4. Composition of the explosives studied in this work. Information provided by the manufacturer [a] or TEDAX (the Spanish EOD) [b].

Explosive	Composition
TNT [b]	2,4,6-Trinitrotoluene (100%)
Plastic explosive (RDX) [b]	Cyclotrimethylene trinitramine (91%) + Bis(2-ethylhexyl) phthalate (5.3%) + polyisobutylene (2.1%) + motor oil (1.6%)
PETN [b]	Pentaerythritol tetranitrate (100%)
TATP [b]	Triacetone triperoxide (100%)
HMTD [b]	Hexamethylene triperoxide diamine (100%)
Black powder [a]	Potassium nitrate (75%) + charcoal (15%) + sulfur (10%)
Chloratite [b]	Sodium chlorate (80%) + sugar (10%) + sulfur (10%)
Dynamite [a]	Ammonium nitrate (66%) + ethylene glycol dinitrate (29%) + nitrocellulose (1%) + dibutyl phthalate (2.5%) + sawdust (1.2%) + calcium carbonate (0.3%)
ANFO [b]	Ammonium nitrate (90%) + diesel (10%)
Ammonal [b]	Ammonium nitrate (85%) + aluminium (15%)

The 10 improvised explosive devices (IEDs) containing around 300 g of each explosive were prepared by the EOD specialists. These IEDs were exploded in 10 separate explosions (one explosion per explosive). They were exploded in open air simulating real explosions. The weather conditions during each explosion are collected in Table 6.5. Various pieces of plywood (20 cm × 15 cm) were used as "catchers", *i.e.* they were placed surrounding the explosive at a distance of 1.5–2 m in order to study the detection of post blast residues on them. Those "catchers" were collected and sealed after each explosion by EOD specialists and they were carried out to the laboratory where they were analysed by Raman microscopy.

Table 6.5. Weather conditions during the explosions.

Explosion	Temp (°C)	Humidity %	Atmospheric pressure (mb)	Wind direction	Wind speed (km/h)
TNT	1.1	54	1017.1	246 WSW	4.8
RDX	2.4	72	1007.0	280 W	24.1
PETN	2.3	53	1017.8	198 SSW	1.6
TATP	5.1	89	1007.8	262 W	22.5
HMTD	5.9	87	1007.7	271 W	20.9
Black powder	7.6	80	1007.0	277 W	17.7
Chloratite	NA	NA	NA	NA	NA
Dynamite	1.8	67	1006.4	265 W	12.9
ANFO	0.7	72	1006.1	250 WSW	9.7
Ammonal	NA	NA	NA	NA	NA

NA: Not available. The weather conditions during explosions of chloratite and ammonal were not registered because the weather station was not available that day.

- *Instrumentation*

Raman microscopic analysis were performed with a Thermo Scientific DXR Raman microscope (Waltham, MA) using the Thermo Scientific Omnic for dispersive Raman 8 software (Waltham, MA). Samples were microscopically observed in minute detail using 10X, 20X, and 50X microscope objectives. After finding a potential suspicious post-blast residue, that spot was analysed by Raman spectroscopy. Raman measurements were performed using a 780 nm excitation wavelength of 10 mW power and 400 lines mm^{-1} grating. The Raman spectra were measured from 2500 to 200 cm^{-1} (with a spectral data spacing of 0.964 cm^{-1}). The spectra acquisition for all samples involved the accumulation of 5 scans of 6 s per scan. These parameters were fixed by demonstrating they were suitable to obtain Raman spectra of high signal-to noise ratio from the first

post-blast residue which was analysed (the ammonium nitrate post-blast residues from ANFO).

- *Data Treatment*

Raman spectra from the post-blast residues were visually and statistically (Pearson correlation) compared with the spectral library, which had been previously created from the standards of the pre-exploded explosives. This comparison was directly performed in the Thermo Scientific Omnic for dispersive Raman 8 software. In order to demonstrate the accuracy of the characteristic Raman spectra from post-blast residues when the particles from residues are properly focused and analysed, these spectra were used for the comparison as they were obtained. They were not processed by any pre-processing method, neither baseline correction, normalization, nor smoothing. Interestingly, the Raman spectra from those correctly focused post-blast particles mostly provided a correlation coefficient above 0.90.

Results and discussion

- *Raman Spectral Library of Pre-Exploded Explosives*

First of all, standards from the 10 explosives prior their explosion were analysed by Raman microscopy in order to create a useful compounds library containing the Raman spectra of those explosives which were necessary to subsequently compare and identify the compounds contained in the post-blast residues. Since the Raman spectroscopic characterization and vibrational interpretation of explosives is explained in detail in Chapter 5.1, only the Raman spectra of explosives is displayed in this chapter (Figure 6.12), in order to facilitate the comparison of Raman spectra between standards and post-blast samples when necessary.

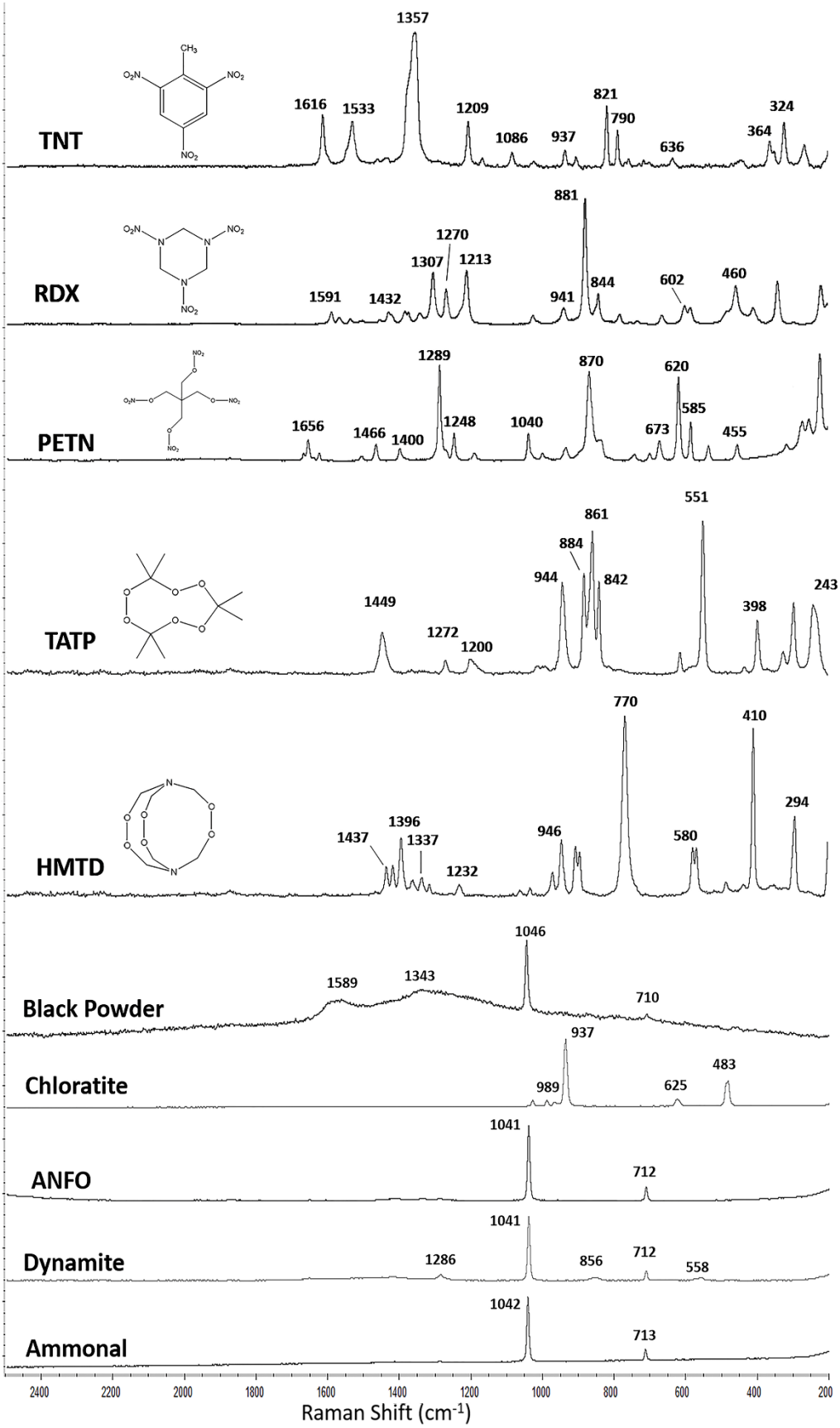

Figure 6.12. Raman spectra of TNT, RDX, PETN, TATP, HMTD, black powder, ANFO, dynamite, ammonal, and chloratite. Raman conditions: laser at 780 nm, 14.0 mW, 10× magnification objective, confocal pinhole of 50 µm, spectra collected by 6 acquisitions of 5 s per acquisition.

➢ *Analytical Methodology*

The real challenge of this study involved the identification of post-blast particles from explosives taking part of IEDs after their open-air explosion by confocal Raman microscopy.

First, it is important to note that most prevalent spots along the surface of post-blast samples were the own material, burnt material, and particles of the ground. Thus, as shown in Figure 6.13, most of the surface of samples was the own material (plywood in this case), whose spots provided the characteristic Raman spectrum of the material, which had quite a lot of noise and displayed a characteristic band at 1598 cm^{-1}. Some parts were burnt material, probably caused by the heat from the explosion. These burnt spots provided Raman spectra with high fluorescence. Some particles which seemed particles of the ground appeared scattered along the surface of collected samples. They were confirmed as particles of calcite (calcium carbonate) from the ground, since they provided the characteristic band located at 1086 cm^{-1}, which had been previously registered for the sample of ground taken as reference and corroborated by analysing calcium carbonate standard. Undoubtedly, the shock wave caused by the explosion made that many particles of the ground flew off in all directions (coming into contact with the samples).

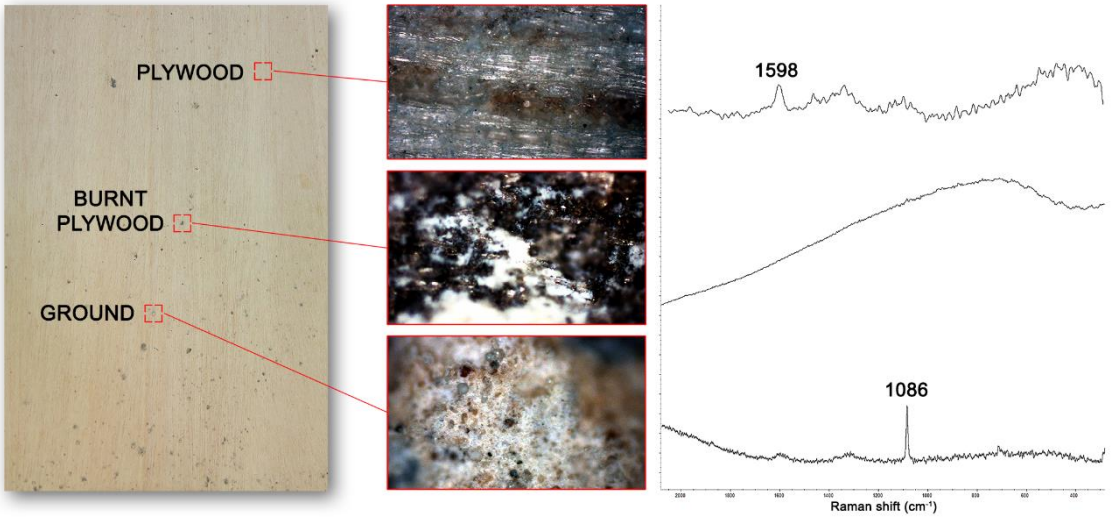

Figure 6.13. Most prevalent spots found on the post-blast samples surface: own material (above), burnt material (middle), and particles of the ground (below). Raman conditions as in Figure 6.12.

In addition to these prevalent spots, traces of post-blast explosives corresponding with few white microscopic particles spread out along the surface

of samples were detected for some of the exploded explosives. Despite being scarce and microscopic, these particles were highly relevant and informative because they were post-blast particles from the explosive which had remained non-reacted during the explosion since they provided the characteristic Raman spectrum of the main components of the original explosive (see Figure 6.14). Because of the difficulties to determine these post-blast explosive particles, an analytical methodology including three consecutive steps was developed.

- *Examination of the Sample with the Naked Eye (Supported by a Magnifying Glass When Necessary)*

The examination of samples with the naked eye was focused on scrutinizing macroscopically the surface of samples in search of those regions where the material showed clear evidence of having come into contact with the explosion. In essence, this examination was focused on anything which was foreign to the material, which could be burnt material, ground particles, or post-blast particles from the explosive. It is highly recommended to use a magnifying glass to improve the vision range and discriminate between regions with post-blast evidence, even for rejecting, right from the beginning, those regions that do not show any post-blast evidence.

- *Microscopic Examination of the Sample for Post-blast Particles Selection*

After finding, with the naked eye, one of those alleged regions with post-blast evidence, that region was subsequently examined under the Raman microscope at 10X and 50X magnifications in order to microscopically verify or dismiss the presence of post-blast particles from the explosive. After a tentative microscopic identification of these particles, they were always analysed by Raman to confirm their identification.

- *Raman Spectroscopic Analysis to Identify Post-blast Particles from the Explosive*

After finding the alleged post-blast-looking particle and selecting and focusing a spot on it, the Raman analysis of that particle was performed providing its characteristic Raman spectrum. This spectrum was compared with the previous database of pre-exploded explosives.

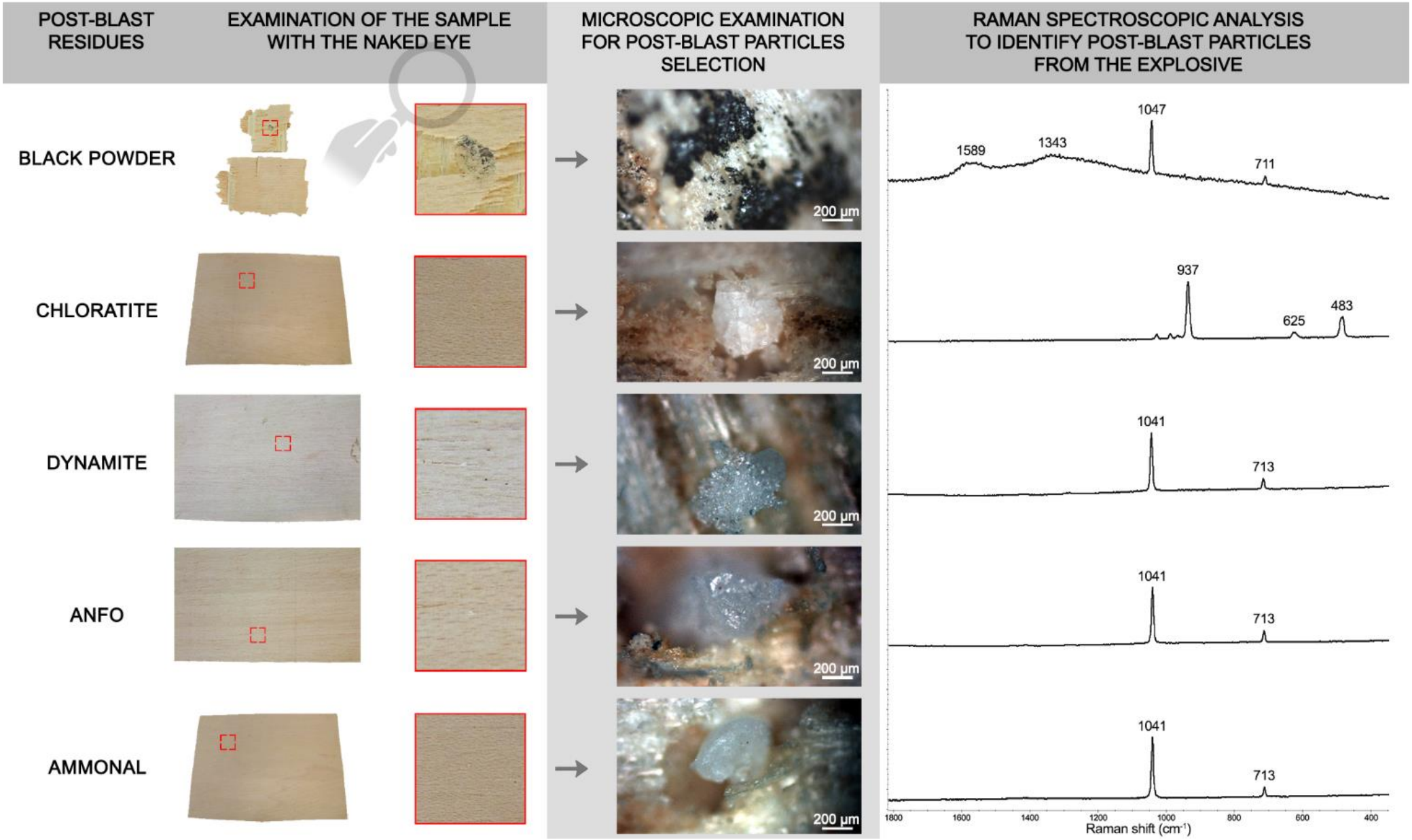

Figure 6.14. Methodological steps and Raman spectra of postblast particles from black powder, chloratite, dynamite, ANFO, and ammonal explosives. Raman conditions as in Figure 6.12.

As an example, Figure 6.14 displays the methodology steps and the results obtained for those explosive mixtures based on oxidizing salts.

As shown in Figure 6.14, the Raman spectra provided by these post-blast particles were surprisingly similar to the spectra previously collected from pre-exploded explosives. Thus, the identification of these particles by checking the spectral database of pre-exploded explosives was extremely fast and straightforward. In general, a visual comparison of the spectra by focusing on the value of the most prominent bands was enough to identify each particle. Nevertheless, a statistical comparison using Pearson correlation, whose value was usually above 0.95 over 1, was directly performed (*i.e.* without spectra pre-processing) using the same Raman software to ensure the identification. These positive results, ultimately provided by the excellent signal-to-noise ratio of the spectra, were due to the exceptional capability of confocal Raman microscopy to focusing just on the post-blast particle of interest in such a way that the Raman spectrum is uniquely determined by the focused particle and not affected by the surrounding material. In fact, this microscopically facilitated recognition of particles in the sample, in addition to the high specificity provided by Raman spectroscopy due to the specific molecular vibrations, have turned Raman microscopy into a highly selective technique for discriminating post-blast particles from explosives.

As also displayed in Figure 6.14, the size of post-blast particles was studied. The size of the post-blast particles detected and analysed by Raman microscopy ranged from 10 to 500 μm (diameter). Particularly, the particles shown in Figure 6.14 had a diameter around 300 μm. Interestingly, taking into account the particles size, the LOD of the developed methodology was estimated through the calculation of the mass of the smallest particles, which was performed as follows. Assuming a cubic or spherical particle with a diameter of 10 μm (the smallest particles detected), its volume is 1000 μm^3 (if cubic) or 524 μm^3 (if spherical). As further discussed in Post-blast Residues Analysis, these particles corresponded to the oxidizing salt from the explosive. Thus, in the knowledge that potassium nitrate, sodium chlorate, and ammonium nitrate have a density of 2.11 g/cm^3, 2.50 g/cm^3, and 1.725 g/cm^3, respectively, the mass of the smallest particles determined by Raman microscopy was 2.1 ng, 2.5 ng, and 1.7 ng, respectively, for potassium nitrate, sodium chlorate, and ammonium nitrate cubic particles (1.1 ng, 1.3 ng, and 0.9 ng if we assume spherical particles).

Consequently, trace amounts in the nanogram range can be detected and identified by Raman microscopy for post-blast residues from explosives.

With regard to the time, it is noteworthy that the whole process only took a few minutes per sample, *i.e.* per piece of plywood of 20 cm × 15 cm dimensions. In fact, several iterations of the three-step process were accomplished per sample. Around 1 min was spent for the visual examination of the whole surface in order to select an interesting post-blast region. A post-blast particle was then selected using the microscope, and it was analysed by Raman spectroscopy. The Raman analysis only took 30 s. Afterward, the process started again in search of another particle. In fact, an expert eye (which was achieved in a very short period of time after examining a pair of samples with post-blast particles) easily found those particles at first.

- *Post-blast Residues Analysis*

The developed methodology was followed to analyse the post-blast samples from the 10 open-air explosions studied in this work. Table 6.6 collects the post-blast particles detected.

Table 6.6. Post-blast particles identified after the open-air explosions by confocal Raman microscopy. Those explosives in which post-blast particles from the explosive were identified are remarked in bold letters.

Explosive	Post-blast particles identified after the explosion
TNT	None
RDX	None
PETN	None
TATP	None
HMTD	None
Black powder	Potassium nitrate and charcoal
Chloratite	Sodium chlorate
Dynamite	Ammonium nitrate
ANFO	Ammonium nitrate
Ammonal	Ammonium nitrate

As shown in Table 6.6, it is important to emphasize that those explosives whose post-blast particles were detected by confocal Raman microscopy were black powder, chloratite, ANFO, dynamite, and ammonal; that is, those energetic explosive mixtures based on inorganic oxidizing salts. On the contrary, post-blast residues from single organic explosives could not be detected by confocal Raman microscopy. No Raman spectra of TNT, RDX, PETN, TATP, or HMTD were registered for any of the post-blast evidence observed in their samples.

The reason for this different behaviour is probably due to the fact that energetic mixtures require the straight contact between their components to produce the combustion reaction between the oxidizing salt and the combustible compound to cause the explosion. Any part of the mixture, which is badly mixed (*i.e.* because of a poor contact between oxidizing and combustible components), will not take part in the reaction and the subsequent shock wave caused by the explosion will expel those non-reacted particles of the mixture all around. Moreover, the higher proportion of oxidizing salt in the mixture (see Table 6.4) contributes to that, being reasonable that post-blast non-reacted particles from the oxidizing salt were more frequently detected than the other minor components. For instance, considering the explosion of the explosive device made of black powder, it is understandable that some particles of its major components (potassium nitrate and charcoal) flew off in all directions and some of those remaining particles ended up on the samples as shown schematically in Figure 6.15. In addition, it may be thought that a considerable amount of these particles came from the explosion since the few pieces of plywood (collectors), which were surrounding the explosion, collected several post-blast particles each. A large number of post-blast particles certainly flew off far away and were lost.

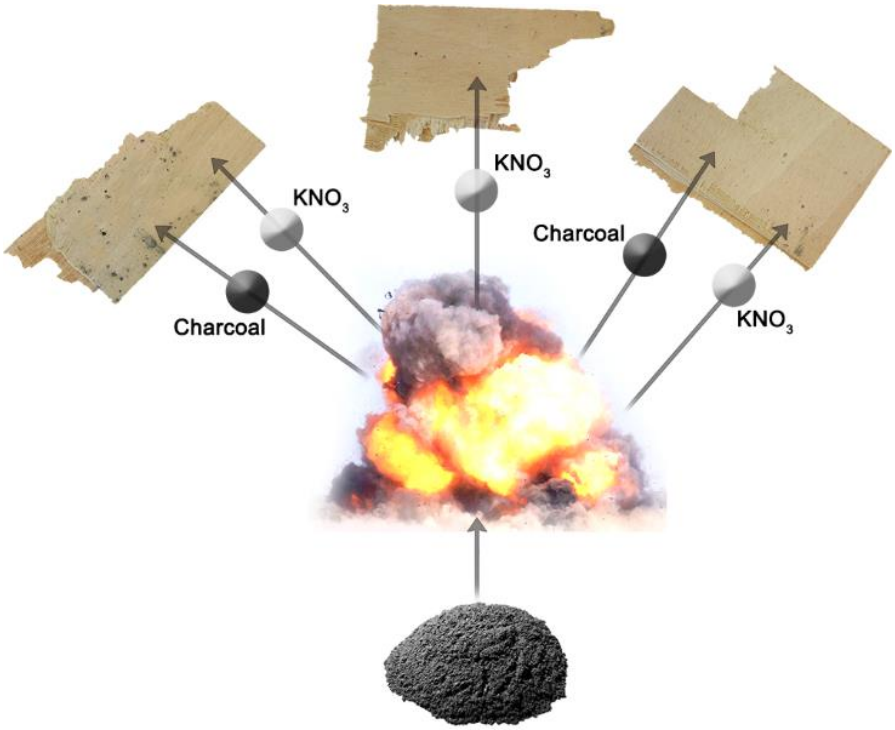

Figure 6.15. Scheme showing a hypothetical projection of black powder particles after its explosion.

On the other hand, TNT, RDX, and PETN military explosives and TATP and HMTD peroxide explosives are pure explosives based on organic compounds (no mixtures). The same molecule reacts as combustible and as oxidizer simultaneously, being a more efficient explosion. Therefore, no non-reacted particles from these explosives remained after the explosion, at least, no particles that were big enough to be detected by Raman microscopy. The LOD of confocal Raman microscopy (ng) was not suitable enough to detect traces of post-blast organic explosives. For that purpose, the sensitivity and LOD of Raman spectroscopy should be first improved. Surface enhanced Raman spectroscopy (SERS) is known to increase the Raman signal of organic molecules (including explosives) in such a way that LOD is also improved several orders of magnitude [42]. In this respect, we thoroughly revised the advances achieved in the detection of explosives using SERS. The reader is encouraged to consult that review [42].

Conclusions and future trends

Confocal Raman microscopy, which combines both microscopic visualization and Raman spectroscopy has enabled a non-destructive, selective, fast, and solvent-free methodology for the detection and identification of microscopic post-blast particles from explosives. Interestingly, the high selectivity and the outstanding estimated LOD in terms of mass of detected particles, through considering the estimated volume of the particle and its density, enabled the detection and identification of post-blast particles up to the nanogram range.

The results achieved from the post-blast analysis revealed that oxidizer-fuel explosive mixtures, after being exploded, were always successfully determined by confocal Raman microscopy through the identification of post-blast non-reacted particles from the oxidizing salt. However, the detection of post-blast non-reacted particles from the pure organic explosives (no mixtures) was not possible by this methodology. A methodology having better LOD is required to detect post-blast traces of organic explosives. Considering Raman spectroscopy, such LOD improvement might be achieved by SERS. Therefore, further research using SERS for the detection of post blast organic explosives is encouraged.

Interestingly, this study has also evidenced the great feature of confocal Raman spectroscopy for differentiating between nitrates (potassium and ammonium

nitrate), which is a great advance over conventional and routinely used chromatographic and/or electrophoretic techniques that require a sample treatment to dissolve the salt and dissociate it into its ions.

The choice of the materials in which detecting the post-blast particles by confocal Raman microscopy seems to be a relevant aspect. Although the plywood has demonstrated to be an appropriate surface in which post-blast particles are both easily retained and detected, further studies examining a wider variety of common materials as catchers are being performed in order to establish the most appropriate materials that should be collected during evidence recovery in real open-air IEDs explosions.

Further studies by using a portable Raman microscope would be also useful in order to test whether the detection of post-blast particles from explosive mixtures can be performed on field, an important aspect in military operations. In fact, current portable Raman spectrometers do not usually combine microscopy and, therefore, they are only suitable for the detection of non-exploded explosives in bulk amounts.

References

[1] M. Marshall, J. Oxley, Aspects of Explosives Detection; Elsevier: Amsterdam, The Netherlands, 2009.

[2] J. Yinon, Counterterrorist Detection Techniques of Explosives; Elsevier: Amsterdam, The Netherlands, 2007.

[3] J.S. Caygill, F. Davis, S.P.J. Higson, Current trends in explosive detection techniques, Talanta 88 (2012) 14-29.

[4] M. Tarvin, B. McCord, K. Mount, M.L. Miller, Analysis of hydrogen peroxide field samples by HPLC/FD and HPLC/ED in DC mode, Forensic Sci. Int. 209 (2011) 166-172.

[5] R. Borusiewicz, G. Zadora, J. Zieba-Palus, Chemical analysis of post explosion samples obtained as a result of model field experiments, Talanta 116 (2013) 630-636.

[6] I.S. Krull, E.A. Davis, C. Santasania, S. Kraus, A. Basch, Y. Bamberger, Trace Analysis of Explosives by HPLC-Electron Capture Detection (HPLC-ECD), Anal. Lett. 14 (16) (1981) 1363-1376.

[7] P. Kolla, A.J. Sprunkel, Identification of Dynamite Explosives in Post Explosion Residues, J. Forensic Sci. 40 (3) (1995) 406-411.

[8] S. Calderara, D. Gardebas, F. Martinez, Solid phase micro extraction coupled with on-column GC/ECD for the post-blast analysis of organic explosives, Forensic Sci. Int. 137 (2003) 6-12.

[9] X. Xu, M. Koeberg, C.J. Kuijpers, E. Kok, Development and validation of highly selective screening and confirmatory methods for the qualitative forensic analysis of organic explosive compounds with high performance liquid chromatography coupled with (photodiode array and) LTQ ion trap/Orbitrap mass spectrometric detections (HPLC-(PDA)-LTQOrbitrap), Sci. Justice 54 (2014) 3-21.

[10] H. Hansson, A. Elfving, D. Menning, H.G. Önnerud, E. Holmgren, M. Brantlind, U. Hedebrant, H. Östmark, R.M. Karlsson, P. Goede, Discrimination of new and aged post-blast explosives residues, Proc. SPIE 8189 (2011) 818903/1-818903/10.

[11] M. Joshi, K. Rigsby, J.R. Almirall, Analysis of the headspace composition of smokeless powders using GC–MS, GC-μECD and ion mobility spectrometry, Forensic Sci. Int. 208 (2011) 29-36.

[12] C.M. Marsh, R.F. Mothershead, M.L. Miller, Post-Blast Analysis of Hexamethylene Triperoxide Diamine using Liquid Chromatography-Atmospheric Pressure Chemical Ionization-Mass Spectrometry, Sci. Justice 55 (2015) 299-306.

[13] H. Téllez, J.M. Vadillo, J.J. Laserna, Secondary ion mass spectrometry of powdered explosive compounds for forensic evidence analysis, Rapid Commun. Mass Spectrom. 26 (2012) 1203-1207.

[14] C. Johns, R.A. Shellie, O.G. Potter, J.W. O'Reilly, J.P. Hutchinson, R.M. Guijt, M.C. Breadmore, E.F. Hilder, G.W. Dicinoski, P.R.J. Haddad, Identification of homemade inorganic explosives by ion chromatographic analysis of post-blast residues, J. Chromatogr. A 1182 (2008) 205-214.

[15] G.W. Dicinoski, R.A. Shellie, P.R. Haddad, Forensic Identification of Inorganic Explosives by Ion Chromatography, Anal. Lett. 2006, 39 (4), 639-657.

[16] M. Pumera, Analysis of explosives via microchip electrophoresis and conventional capillary electrophoresis: A review, Electrophoresis 27 (2006) 244-256.

[17] J.P. Hutchinson, C.J. Evenhuis, C. Johns, A.A. Kazarian, M.C. Breadmore, M. Macka, E.F. Hilder, R.M. Guijt, G.W. Dicinoski, P.R. Haddad, Identification of Inorganic Improvised Explosive Devices by Analysis of Postblast Residues Using Portable Capillary Electrophoresis Instrumentation and Indirect Photometric Detection with a Light-Emitting Diode, Anal. Chem. 79 (2007) 7005-7013.

[18] J.P. Hutchinson, C. Johns, M.C. Breadmore, E.F. Hilder, R.M. Guijt, C. Lennard, G. Dicinoski, P.R. Haddad, Identification of inorganic ions in post-blast explosive residues using portable CE instrumentation and capacitively coupled contactless conductivity detection, Electrophoresis 29 (2008) 4593-4602.

[19] G.A. Blanco, Y.H. Nai, E.F. Hilder, R.A. Shellie, G.W. Dicinoski, P.R. Haddad, M.C. Breadmore, Identification of Inorganic Improvised Explosive Devices Using

Sequential Injection Capillary Electrophoresis and Contactless Conductivity Detection, Anal. Chem. 83 (2011) 9068-9075.

[20] C. Sarazin, N. Delaunay, C. Costanza, V. Eudes, P. Gareil, Capillary electrophoresis analysis of inorganic cations in post-blast residue extracts applying a guanidinium-based electrolyte and bilayer-coated capillaries, Electrophoresis 32 (2011) 1282-1291.

[21] C. Sarazin, N. Delaunay, A. Varenne, J. Vial, C. Costanza, V. Eudes, J.J. Mineta, P.J. Gareil, Identification and determination of inorganic anions in real extracts from pre- and post-blast residues by capillary electrophoresis, J. Chromatogr. A 1217 (2010) 6971-6978.

[22] C. Martín-Alberca, M.A. Fernández de la Ossa, J. Saiz, J.L. Ferrando, C. García-Ruiz, Anions in pre- and post-blast consumer fireworks by capillary electrophoresis, Electrophoresis 35 (2014) 3272-3280.

[23] J. Kuula, H. Rinta, I. Pölönen, H.H. Puupponen, M. Haukkamäki, T. Terävaïnen, Detecting explosive substances by the IR spectrography, Proc. SPIE 9073 (2014) 90730Q/1-90730Q/12.

[24] K. Banas, A. Banas, H.O. Moser, M. Bahou, M. Cholewa, P. Yang, S.K. Lim, Multivariate statistical methods in the forensic investigation of the post-blast residues measured by Fourier transform infrared spectroscopy, Diamond Light Source Proc. 1 (2011) e125.

[25] A. Banas, K. Banas, M. Bahou, H.O. Moser, L. Wen, P. Yang, Z.J. Li, M. Cholewa, S.K. Lim, C.H. Lim, Post-blast detection of traces of explosives by means of Fourier transform infrared spectroscopy, Vib. Spectrosc. 51 (2009) 168-176.

[26] C. Martín-Alberca, F. Zapata, H. Carrascosa, F.E. Ortega-Ojeda, C. García-Ruiz, Study of consumer fireworks post-blast residues by ATR-FTIR, Talanta 149 (2016) 257-265.

[27] M.R. Almeida, D.N. Correa, J.J. Zacca, L.P.L. Logrado, R.J. Poppi, Detection of explosives on the surface of banknotes by Raman hyperspectral imaging and independent component analysis, Anal. Chim. Acta 860 (2015) 15-22.

[28] C. Zhang, K. Wang, D. Han, Q. Pang, Surface enhanced Raman scattering (SERS) spectra of trinitrotoluene in silver colloids prepared by microwave heating method, Spectrochim. Acta, Part A 122 (2014) 387-391.

[29] S. Sil, D. Chaturvedi, K.B. Krishnappa, S. Kumar, S.N. Asthana, S.J. Umapathy, Density Functional Theoretical Modeling, Electrostatic Surface Potential and Surface Enhanced Raman Spectroscopic Studies on Biosynthesized Silver Nanoparticles: Observation of 400 pM Sensitivity to Explosives, Phys. Chem. A 118 (2014) 2904-2914.

[30] F.A. Calzzani, R. Sileshi, A. Kassu, J.M. Taguenang, A. Chowdhury, A. Sharma, P.B. Ruffin, C. Brantley, E. Edwards, Detection of residual traces of explosives by surface

enhanced Raman scattering using gold coated substrates produced by nanospheres imprint technique, Proc. SPIE 6945 (2008) 694510/1-694510/9.

[31] W.A. Al-Saidi, S.A. Asher, P.J.J. Norman, Resonance Raman Spectra of TNT and RDX Using Vibronic Theory, Excited-State Gradient, and Complex Polarizability Approximations, Phys. Chem. A 116 (2012) 7862-7872.

[32] D. Lin-Vien, N.B. Colthup, W.G. Fateley, J.G. Graselli, The Handbook of Infrared and Raman Characteristic Frequencies of Organic Molecules; Academic Press: San Diego, CA, 1991.

[33] S. Almaviva, S. Botti, L. Cantarini, A. Palucci, A. Puiu, A. Rufoloni, L. Landström, F.S. Romolo, Trace detection of explosives by surface enhanced Raman spectroscopy, Proc. SPIE 8546 (2012) 854602/1-854602/7.

[34] Y.A. Gruzdkov, Y.M.J. Gupta, Vibrational Properties and Structure of Pentaerythritol Tetranitrate, Phys. Chem. A 105 (2001) 6197-6202.

[35] B. Brauer, F. Dubnikova, Y. Zeiri, R. Kosloff, R.B. Gerber, Vibrational spectroscopy of triacetone triperoxide (TATP): Anharmonic fundamentals, overtones and combination bands, Spectrochim. Acta, Part A 71 (2008) 1438-1445.

[36] J. Oxley, J. Smith, J. Brady, F. Dubnikova, R. Kosloff, L. Zeiri, Y. Zeiri, Raman and Infrared Fingerprint Spectroscopy of Peroxide-Based Explosives, Appl. Spectrosc. 62 (2008) 906-915.

[37] D. Sülzle, P. Klaeboe, The Infrared, Raman and NMR Spectra of Hexamethylene Triperoxide Diamine, Acta Chem. Scand. 42A (1988) 165-170.

[38] K. Nakamoto, Infrared and Raman Spectra of Inorganic and Coordination Compounds, Part A: Theory and Applications in Inorganic Chemistry, 6th ed.; John Wiley and Sons Inc.: Hoboken, NJ, 2009.

[39] M. López-López, J.L. Ferrando, C. García-Ruiz, Dynamite analysis by Raman spectroscopy as unique analytical tool, Anal. Chem. 85 (2013) 2595-2600.

[40] E.M.A. Ali, H.G.M. Edwards, I.J. Scowen, In-situ detection of single particles of explosive on clothing with confocal Raman microscopy, Talanta 78 (2009) 1201-1203.

[41] F. Zapata, M.A. Fernández de la Ossa, E. Gilchrist, L. Barron, C. García-Ruiz, Progressing the analysis of Improvised Explosive Devices: Comparative study for trace detection of explosive residues in handprints by Raman spectroscopy and liquid chromatography, Talanta 161 (2016) 219-227.

[42] F. Zapata, M. López-López, C. García-Ruiz, Detection and identification of explosives by surface enhanced Raman scattering, Appl. Spectrosc. Rev. 51 (2016) 207-242.

6.3.2. The influence of the background material

Abstract

Post-explosion scenes offer such chaos and destruction that evidence recovery and detection of post-blast residues from the explosive in the surrounding materials is highly challenging and difficult. The suitability of materials to retain explosives residues and their subsequent analysis has been scarcely investigated. Particularly, the use of explosive mixtures containing inorganic oxidizing salts to make improvised explosive devices (IEDs) is a current security concern due to their wide availability and lax control. In this work, a wide variety of materials such as glass, steel, plywood, plastic bag, brick, cardboard or cotton subjected to open-air explosions were examined using confocal Raman microscopy, aiming to detect the inorganic oxidizing salts contained in explosives as black powder, chloratite, dynamite, ammonium nitrate fuel oil and ammonal. Post-blast residues were detected through microscopic examination of materials surfaces. In general, the more homogeneous and smoother the surface was, the less difficulties and better results in terms of identification were obtained. However, those highly irregular surfaces were the most unsuitable collectors for the posterior identification of explosive traces by Raman microscopy. The findings, difficulties and some recommendations related to the identification of post-blast particles in the different materials studied are thoroughly discussed.

Introduction

Amongst the large variety of explosive compositions, explosive mixtures based on oxidizing energetic salts are certainly the explosives most frequently used by civilians (non-militaries) to carry out, not only legitimate commercial purposes such as demolitions and pyrotechnics, but also to commit criminal actions [1-5]. As a result of the wide availability, easy acquisition and lax control of these explosives precursors, oxidizing energetic salts are usually employed by dissidents, extremists and terrorists in the elaboration of improvised explosive devices (IEDs). The mixture of oxidizing energetic salts with fuels produces explosive compositions that can be used as explosive charge in IEDs such as black powder, dynamite or ammonium nitrate fuel oil (ANFO) [1, 3]. Oxidizing salts commonly used in these explosive mixtures are nitrate and chlorate salts [1, 3], which may be combined (in different proportions) with a large variety of fuels such as charcoal, fuel oil or sugar. However, it is important to highlight that whatever the composition is, the oxidizing salt is usually the main and major component in the mixture to ensure the consumption of the fuel and cause the consequent explosion. As a result, post-blast residues from these explosives mostly consist of non-reacted remains of the oxidizing salt [6-12]. Due to their ionic nature, forensic laboratories routinely analyse them by either capillary electrophoresis or ion chromatography, and a wide research involving these two techniques for the analysis of inorganic oxidizing salts from explosives have been published [11-20]. Nevertheless, both techniques are destructive, time-consuming, require a sample treatment and dissociate the salt into its ions. On the contrary, spectroscopic techniques such as Raman spectroscopy has shown an interesting potential for the identification of salts in explosives [10, 12, 21-24]. However, the material in which post-blast particles of these oxidizing salts are adsorbed during an explosion may play an important (and scarcely studied) role in both evidence recovery and spectroscopic measurements [25]. Different materials are expected to offer a different adsorption in relation to the capture of those post-blast particles and, thus, some materials are expected to be more efficient than others. The investigation of this aspect is crucially important for providing forensic investigators know how on the different materials they should preferentially collect during evidence recovery. In addition, each material has a characteristic spectral signature according to its composition, which may occasionally overlap the characteristic

bands of the studied salts. This fact may hinder the spectroscopic detection and identification of post-blast particles, especially when no focusing system is used to exclusively analyse a selected post-blast particle. In this respect, microscopy coupled to Raman spectroscopy has demonstrated to be a useful methodology for the microscopic detection and spectroscopic identification of post-blast microscopic particles of explosives on smooth and homogeneous surfaces [10, 12]. Particularly, in previous Chapter 6.3.1 [10], IEDs based on oxidizing-fuel explosive compositions as well as IEDs based on high organic explosives were exploded and their post-blast residues were subsequently analysed over a smooth homogeneous surface. Results revealed that only those IEDs based on oxidizing-fuel explosive compositions left, after their explosion, microscopic non-reacted particles large enough to be detected by confocal Raman microscopy. Nonetheless, there is a large variety of different materials that may be found in post-explosion scenes that makes evidence recovery an extremely complicate process [2]. The knowledge about the suitability of either homogeneous or heterogeneous materials to catch and retain post-blast residues that are microscopically perceptible by microscopy is a current forensic need. To this end, in this work, a large variety of materials was subjected to different explosions and the appropriateness of each material for post-blast residues detection using confocal Raman microscopy has been deeply examined.

Materials and experiments

- *Materials, standards and explosives*

Eleven different materials (3 replicates per material except for tyre with only 1 replicate) were placed as explosive trace collectors surrounding each explosion at a distance of 1.5 – 2 m in order to study the detection of post blast residues on them. These materials included glass, steel, plastic bag, plywood, chipboard, cardboard, tyre, brick, plaster board, cotton fabric and pig meat, besides the ground from crater. These materials were chosen because they are likely to be found in real terrorist attacks either in the street or within a building. Table 6.7 collects the size of the pieces of each material.

Table 6.7. Size of collectors in cm. R refers to the spoke of the tyre (wheel).

Material	Size (cm)
Glass	18 x 13
Metal (steel)	20 x 6
Plastic bag	30 x 20
Plywood	20 x 15
Chipboard	20 x 15
Cardboard	30 x 20
Tyre	R 30
Brick	25 x 15 x 12
Plasterboard	20 x 20
Cotton fabric	30 x 20
Pig meat	~ 15 x 10

Standards of potassium nitrate and ammonium nitrate were obtained from Sigma-Aldrich in ACS reagent grade (>99.0%).

Five explosions were performed by Spanish EOD specialists using IEDs made of five different inorganic explosives as those reported in previous Chapter 6.3.1 [10], which contained inorganic oxidizing salts including black powder (75% potassium nitrate), chloratite (80% sodium chlorate), dynamite (66% ammonium nitrate), ANFO (90% ammonium nitrate) and ammonal (85% ammonium nitrate).

After each explosion, collectors were recovered and sealed by EOD specialists and were carried out to the laboratory where they were analysed by confocal Raman microscopy.

- *Instrumentation and analysis*

A Thermo Scientific DXR Raman microscope (Waltham, MA, USA) using the Thermo Scientific Omnic for dispersive Raman 8 software (Waltham, MA, USA) was used to analyse the surfaces of materials. First, each material (collector) was analysed to establish the representative Raman spectrum of each material and be used as blank. In addition, to set up the characteristic Raman spectrum of each explosive, small samples from the five explosives were analysed by Raman spectroscopy. Afterwards, the surface of all post-blast samples was observed with both the naked eye and microscopically, as explained in previous Chapter 6.3.1 [10]. Briefly, after visualizing potential post blast residues, that region was microscopically examined through 10X and 50X magnification objectives. Afterwards, the alleged post-blast particles were analysed by Raman spectroscopy in order to confirm or dismiss, based on their Raman spectra, whether they were remains from the explosive. Raman spectra were collected from 2500 to 200 cm^{-1}, accumulating 5 scans of 6 s per scan and using a 780 nm excitation wavelength of 10 mW power. Each Raman spectrum was visually and statistically compared (Pearson correlation) with a spectra database previously registered for the explosives.

Results and discussion

- *Materials and explosives Raman spectra*

The knowledge of these spectra was necessary to later identify residues from the explosives on these materials. As shown in Figure 6.16(a), given the Raman conditions, the materials studied mostly provided no relevant Raman signals except brick. In summary, neither steel, plastic bag, chipboard, cardboard nor tyre provided characteristic Raman bands, except for some fluorescence in chipboard. Plywood displayed a weak band (almost worthless) at 1596 cm^{-1}. Plasterboard, besides providing a bit fluorescence, was dominated by a unique prominent band located at 1006 cm^{-1}. Though cotton and pig meat displayed some characteristic bands along their spectra, they were little intense. Glass was dominated by two characteristic wide prominent bands at 1958 and 1455 cm^{-1}. Finally, brick displayed, unlike previous materials, a large number of bands, some of them noticeably intense such as those at 1668 and 1460 cm^{-1}.

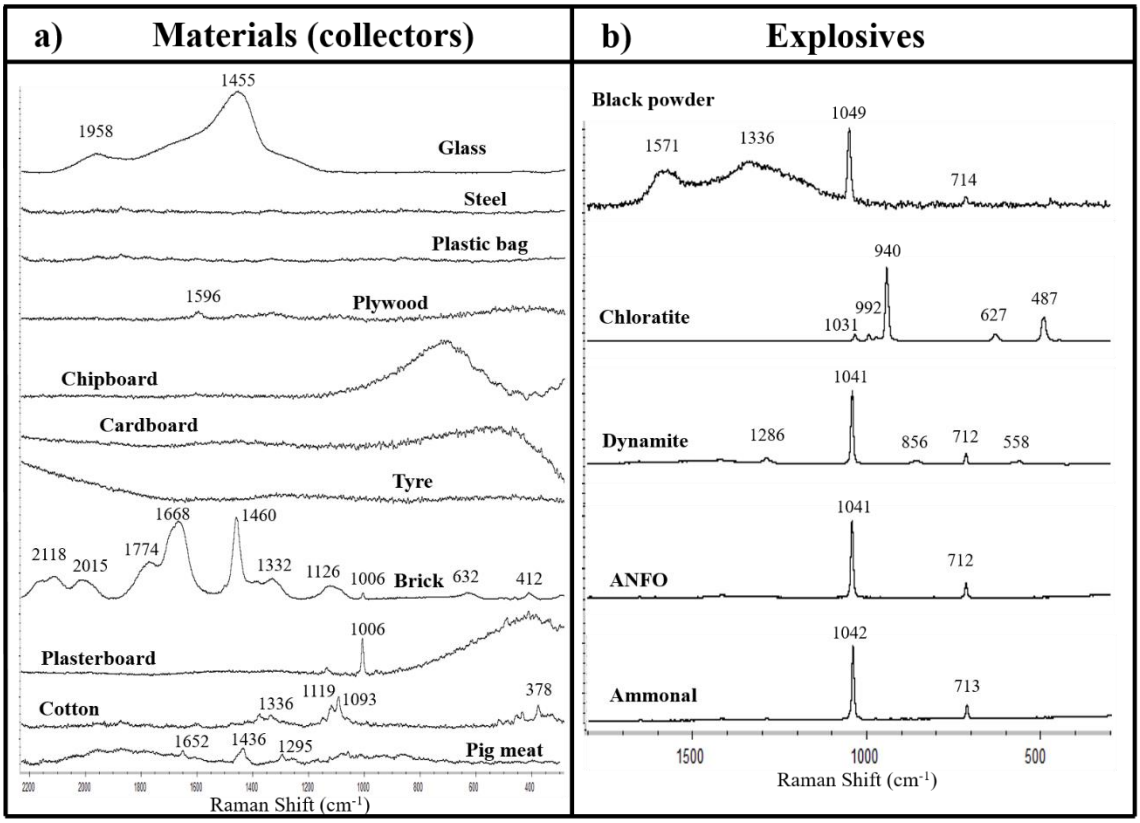

Figure 6.16. Raman spectra of materials (a) and explosives (b) studied in this work. Raman conditions: laser at 780 nm, 14.0 mW, 10X magnification objective, 6 acquisitions of 5 s per acquisition. Materials spectra are displayed on a common scale +offset (a), in order to compare the potential interference each material may cause as background. On the contrary, explosives spectra have been normalized +offset (b) in order to clarify the characteristic bands that enable their identification.

On the contrary, explosives were clearly characterized by the Raman spectra of their respective oxidizing salts, as shown in Figure 6.16(b). This result was not unexpected since oxidizing salts are the major component in these explosives mixtures. What was an unexpected result was the low Raman signals provided by most materials; after all, Raman spectroscopy is being proved as a suitable technique to characterize a wide variety of materials. However, at the selected Raman conditions only those highly Raman active compounds and Raman active vibrations such as those in nitrates and chlorates were properly determined. This result was highly favorable because it meant that most materials would not overlap the Raman spectra from explosives.

As shown in Figure 6.16(b), the different oxidizing salts from explosives (potassium nitrate, sodium chlorate and ammonium nitrate) are easily identified by Raman spectroscopy according to their different Raman spectra. As reported in Chapter 5.1, black powder was characterized by the Raman bands of potassium nitrate (1049 and 714 cm^{-1}) and charcoal (1571 and 1336 cm^{-1}); sodium chlorate from chloratite displayed its main characteristic bands at 940, 627 and 487 cm^{-1} and ammonium nitrate from dynamite, ANFO and ammonal provided its respective bands at around 1041 and 712 cm^{-1}. Interestingly, weak bands due to EGDN were also observed in the dynamite spectrum.

It should be noted that the discrimination between potassium and ammonium nitrates according to the observed shift of 7–8 cm^{-1} of their main nitrate bands may be difficult from a practical point of view, especially when portable Raman spectrometers with low resolution are used. Fortunately, a simple test can be performed to solve this issue. One particle of potassium nitrate can be placed in contact with one particle of ammonium nitrate, both on a microscope slide. Then, Raman microscope needs to be focused just on the contact between both particles. Under these conditions, if the Raman system has enough spectral resolution, spectra as those displayed in Figure 6.17 should be obtained.

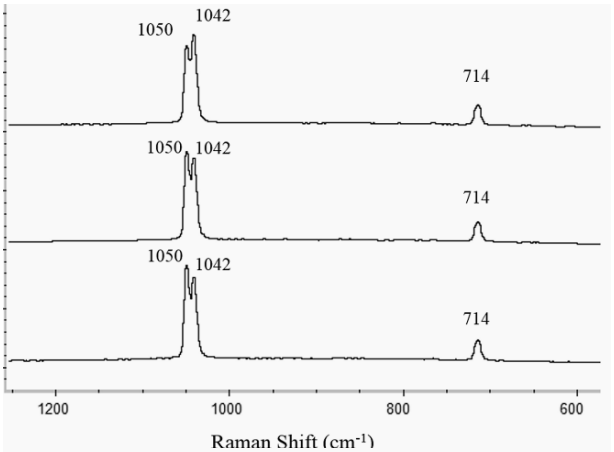

Figure 6.17. Simultaneous identification of potassium nitrate and ammonium nitrate by focusing three nearby spots along the frontier between two particles of potassium and ammonium nitrate.

The characteristic Raman bands of each nitrate (potassium and ammonium) need to be clearly visible and distinguishable according to their bands located at 1050 and 1042 cm^{-1}, respectively. This approach allows to confirm if the simultaneous identification and discrimination of potassium and ammonium nitrates is achievable using the Raman instrument available in the laboratory. That is, this procedure can be a rapid and easy way to check whether our Raman instrument has enough resolution to differentiate both nitrates or not.

- *Detection of explosive components on materials subjected to open-air explosions*

Post-blast residues from different explosions were analysed in order to study the suitability of each material (collector) for post-blast residues detection. The positive/negative results achieved in the detection of post-blast non-reacted particles from each explosive on the different materials studied are summarized in Table 6.8. A positive result involved that at least one post-blast particle was detected; though, that result was uncommon and the most usual positive result involved detecting numerous post-blast particles of the oxidizing salt along the replicate. On the other hand, a negative result involved that no post-blast particle was detected in that replicate.

Table 6.8. Results of post-blast particles detection from explosives on the replicates of the eleven different materials (collectors) studied in this work.

Material (collector)	Replicate (R)	Black powder		Chloratite		Dynamite		ANFO		Ammonal	
Glass	R1	+	2/3	+	3/3	-	0/3	-	2/3	+	3/3
	R2	+		+		-		+		+	
	R3	-		+		-		+		+	
Steel	R1	+	2/3	+	2/3	-	0/3	+	3/3	-	0/3
	R2	+		+		-		+		-	
	R3	-		-		-		+		-	
Plastic bag	R1	-	1/3	+	2/3	+	2/3	+	3/3	-	2/3
	R2	+		-		+		+		+	
	R3	-		+		-		+		+	
Plywood	R1	-	2/3	+	3/3	-	1/3	+	3/3	+	2/3
	R2	+		+		-		+		+	
	R3	+		+		+		+		-	
Chipboard	R1	+	3/3	+	3/3	-	0/3	-	0/3	-	0/3
	R2	+		+		-		-		-	
	R3	+		+		-		-		-	
Cardboard	R1	+	3/3	+	3/3	-	0/3	+	2/3	-	2/3
	R2	+		+		-		+		+	
	R3	+		+		-		-		+	
Tyre	R1	-	0/1	+	1/1	-	0/1	+	1/1	-	0/1
Brick	R1	+	3/3	-	0/3	-	0/3	-	0/3	-	0/3
	R2	+		-		-		-		-	
	R3	+		-		-		-		-	
Plasterboard	R1	+	3/3	-	1/3	-	0/3	-	1/3	-	0/3
	R2	+		+		-		+		-	
	R3	+		-		-		-		-	
Cotton fabric	R1	+	2/3	-	1/3	-	0/3	-	0/3	-	0/3
	R2	+		-		-		-		-	
	R3	-		+		-		-		-	
Pig meat	R1	+	3/3	-	0/3	-	0/3	-	0/3	-	0/3
	R2	+		-		-		-		-	
	R3	+		-		-		-		-	

A comprehensive overview of each material including useful tips and the difficulties overcome during their analysis by confocal Raman microscopy is described below. According to the visual characterization of their surface, the eleven materials were classified to facilitate the interpretation of results into four classes: homogeneous, heterogeneous, highly irregular and biological.

- Homogeneous surfaces

Glass. Glass substrates provided a homogeneous and smooth surface in which both visual and microscopic detection of post-blast residues was quite straightforward. Those foreign particles added on glass were determined by Raman spectroscopy and provided two different spectra: the spectrum of ground or the spectrum of one of the explosive components, as displayed in Figure 6.18. Thus, spectra allowed to confirm whether those particles were post-blast non-reacted particles from the explosive or particles from the ground. Particles from the ground displayed a characteristic spectrum dominated by one main band located at 1087 cm^{-1}, which was due to calcite (calcium carbonate). This was confirmed by testing a standard of calcium carbonate. The reason why particles from ground were found on the surface of materials is probably explained by the fact that ground from crater blew up during the explosion and some particles flew off up to the materials (collectors).

Although this phenomenon (particles of ground on the surface of materials) was observed for almost all the materials, it is not explained for each material to avoid redundancy. Taking into consideration Table 6.8, which summarizes the results of the detection of post-blast residues on the replicates of each material, it can be checked that particles from black powder and ANFO were detected in 2 of the 3 replicates whereas particles from chloratite and ammonal were detected in the three replicates. However, post-blast particles from dynamite were not detected on this material surface.

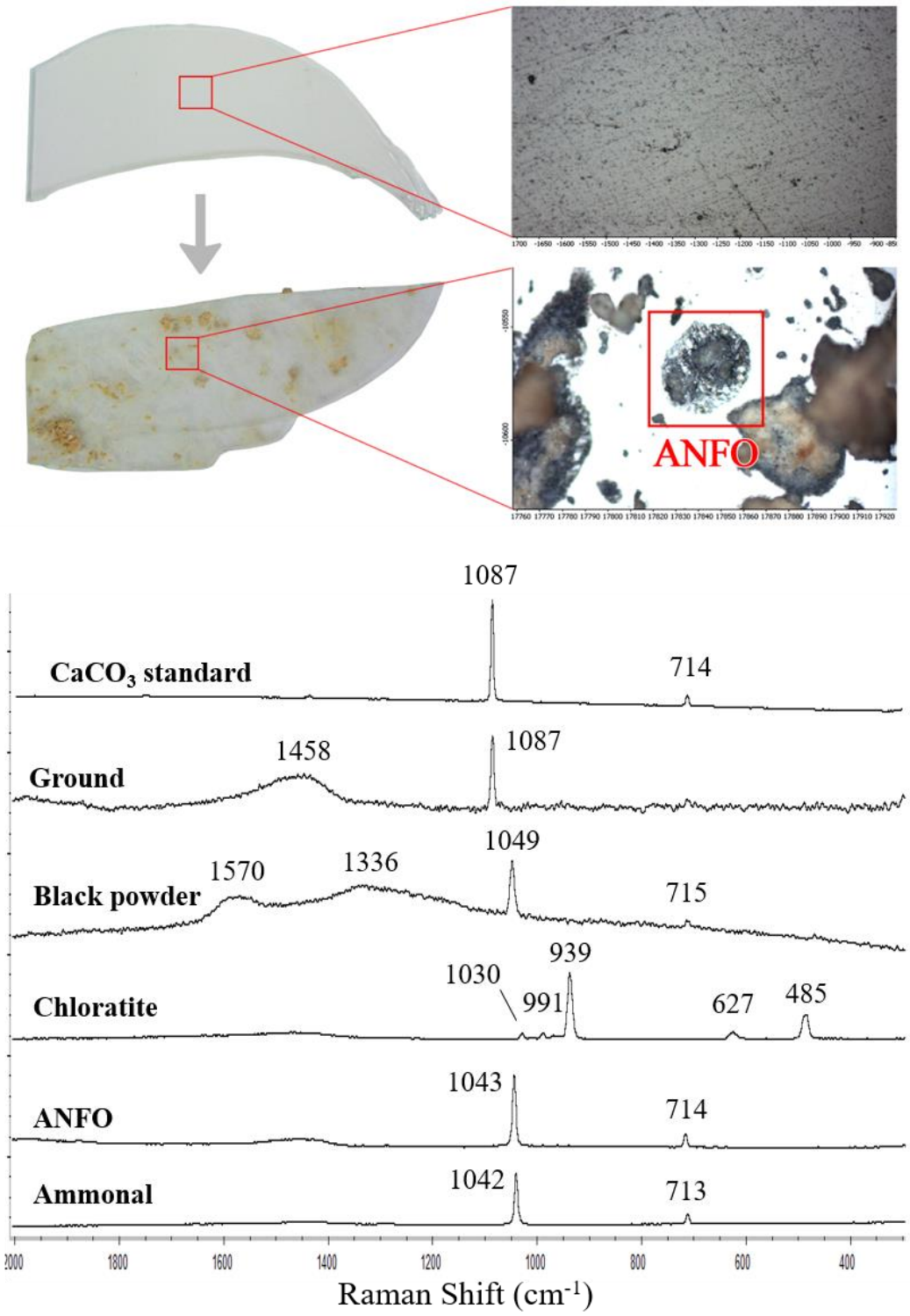

Figure 6.18. Microscopic examination of glass surface and post-blast residues, and Raman spectra of the calcium carbonate standard and the post-blast residues from ground and from the four explosives detected on glass collectors: black powder, chloratite, ANFO and ammonal. Raman conditions as in Figure 6.16.

Steel. Steel substrates also offered a homogeneous and smooth surface which facilitated the detection of post-blast particles on them. As summarized in Table 6.8 and Figure 6.19, post-blast particles from black powder, chloratite and ANFO were detected on steel. Post-blast particles from dynamite and ammonal were not detected on steel. Black powder and chloratite were detected on 2 of the 3 replicates whereas ANFO was detected on the 3 replicates.

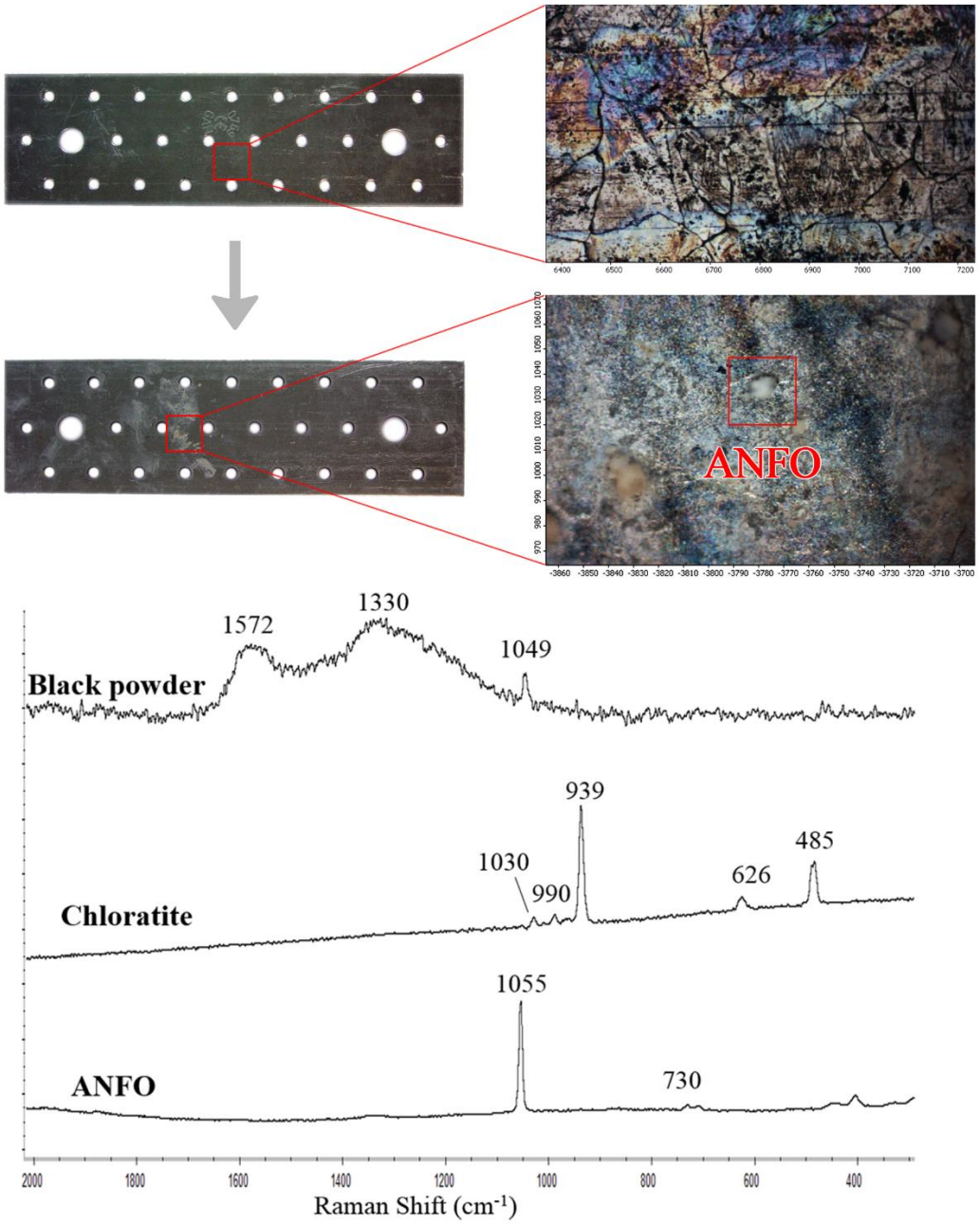

Figure 6.19. Microscopic examination of steel surface (above) and post-blast residues (below) and Raman spectra of the post-blast residues from the three explosives detected on steel collectors: black powder, chloratite and ANFO. Raman conditions as in Figure 6.16.

Nonetheless, the Raman spectra provided by post-blast ammonium nitrate particles from ANFO were slightly inaccurate since their characteristic bands usually located at 1041 and 713 cm^{-1} were shifted around 15 cm^{-1} appearing at 1055 and 730 cm^{-1}. Some studies have revealed the SERS (surface enhanced Raman scattering) effect that steel may provide [26], so this phenomenon could be explained by some sort of SERS interaction between steel surface and ammonium nitrate that may cause the shift. However, the reason why only ammonium nitrate was affected (but not potassium nitrate or sodium chlorate) is unknown. Thus, further investigation focused on comprehending this phenomenon needs to be accomplished.

Plastic bag. Black plastic bags were also highly homogeneous and smooth surfaces in which the detection of white post-blast particles was no trouble. In fact, plastic bags presented an unpredictable result. Although scarce amounts of post-blast particles from explosives were detected on the surface of plastic bags, a large amount of these particles was found inside the plastic bag. Post-blast particles were not found on the outer surface of plastic bags but in the inner surface of the plastic bags, as illustrated in Figure 6.20. In fact, when opening the bags, these particles seemed like spray paint droplets. They were not bound to the second layer, but weakly suspended between the two layers. As hypothesis, this “plastic-bag-effect” may be explained by the fact that particles from the oxidizing salt pierced the first layer of the plastic bag due to their residual heat from the explosion, but they were not able of piercing the second layer and, thus, they got trapped between the two layers of the bag. However, further studies would be necessary to confirm this hypothesis.

As shown in Table 6.8, plastic bags, like plywood, provided the best results since post-blast residues from the five explosives were detected on them. The effect produced by plastic bags likely contributed to trap post-blast particles from the explosives. Post-blast particles from ANFO were identified in the 3 replicates whereas post-blast particles from dynamite, chloratite and ammonal were identified in 2 of the 3 replicates. Finally, post-blast particles from black powder were identified in only 1 of the 3 replicates and only charcoal was identified instead of both charcoal and potassium nitrate.

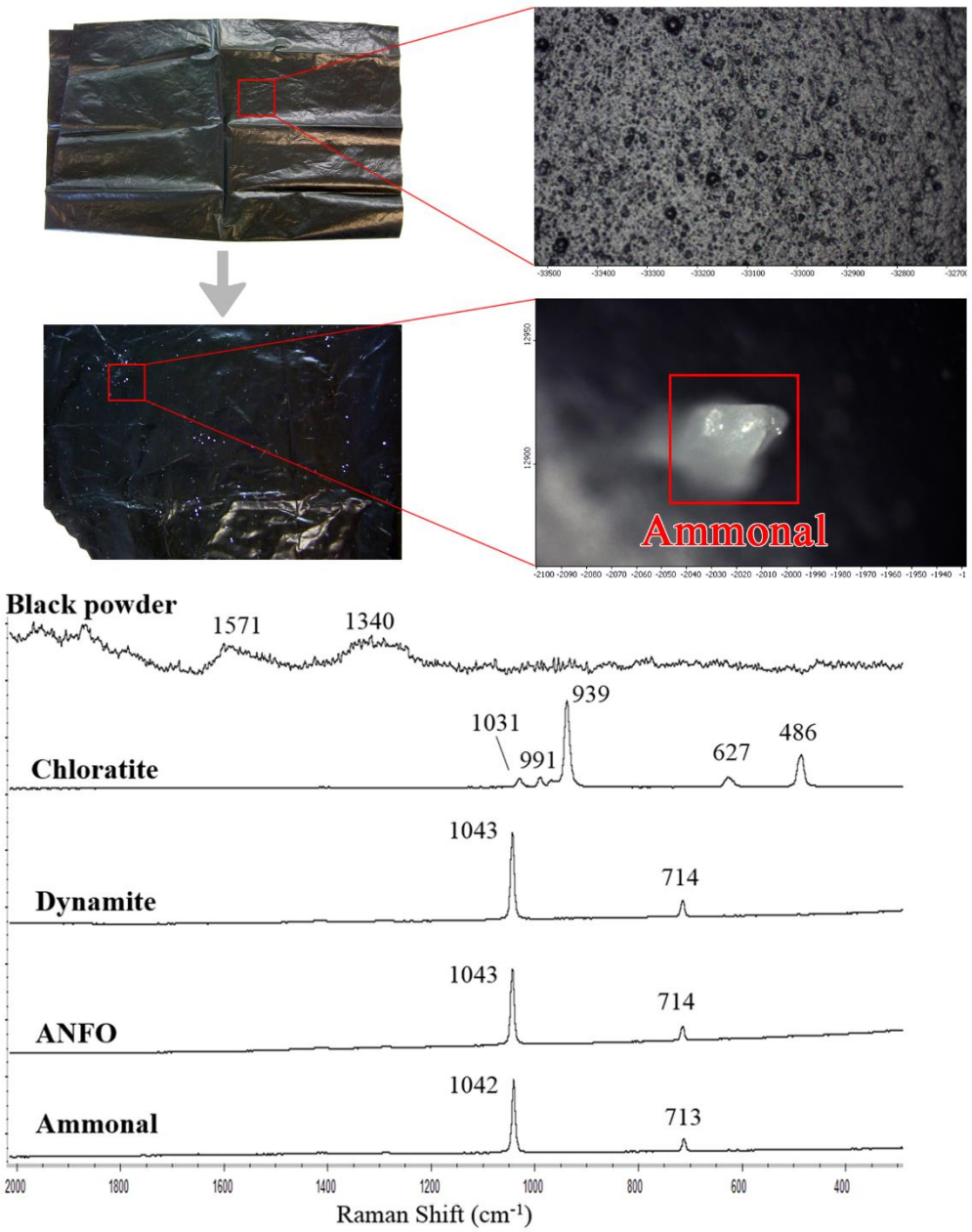

Figure 6.20. Microscopic examination of plastic bag surface (above) and post-blast residues (below) and Raman spectra of the post-blast residues from the explosives detected on plastic bag collectors: black powder, chloratite, dynamite, ANFO and ammonal. Raman conditions as in Figure 6.16.

- Heterogeneous surfaces

Plywood. Plywood substrates offered a bit rougher and more heterogeneous surface than the preceding materials. Nevertheless, post-blast particles from explosives were also easily detected on plywood, since they had a great contrast with the plywood pattern as shown in Figure 6.21. In fact, the plywood collectors provided, as plastic bags, the best results since post-blast residues from the five explosives were detected on them. In particular, post blast particles from

chloratite and ANFO were detected in the 3 replicates, post-blast particles from black powder and ammonal were detected in 2 of the 3 replicates and post-blast particles from dynamite were detected only in 1 of the 3 replicates as summarized in Table 6.8.

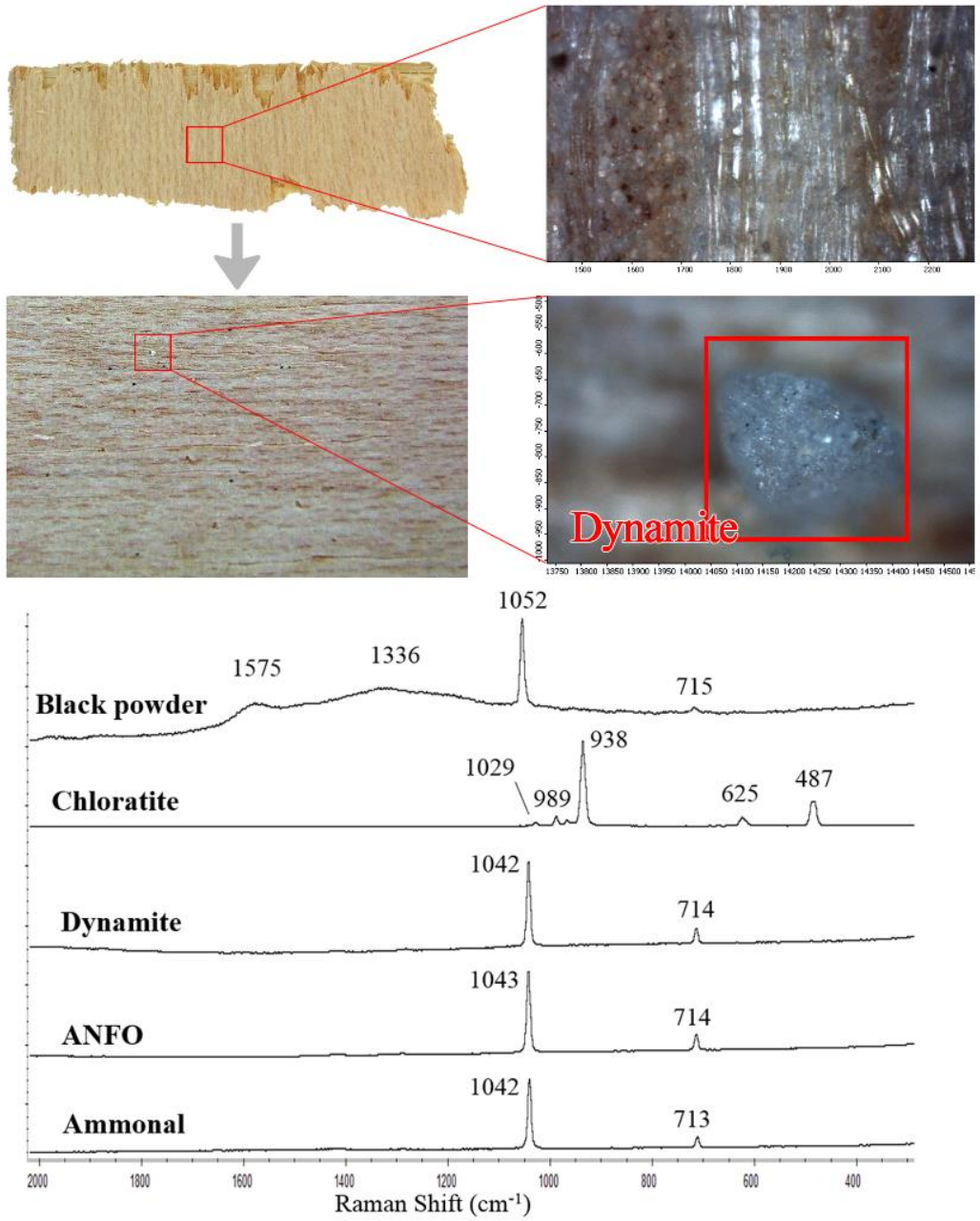

Figure 6.21. Microscopic examination of plywood surface (above) and post-blast residues (below) and Raman spectra of the post-blast residues from the explosives detected on plywood collectors: black powder, chloratite, dynamite, ANFO and ammonal. Raman conditions as in Figure 6.16.

Chipboard. Chipboard substrates provided a highly heterogeneous surface when they were observed with the microscope as displayed in Figure 6.22. This excessive heterogeneity containing numerous and different components hindered the detection of post-blast particles from the explosive. Even so, as indicated in Table 6.8, post-blast particles from black powder and chloratite were identified on the 3 replicates of chipboard. However, post-blast particles from dynamite, ANFO and ammonal were not detected in any of the 3 replicates.

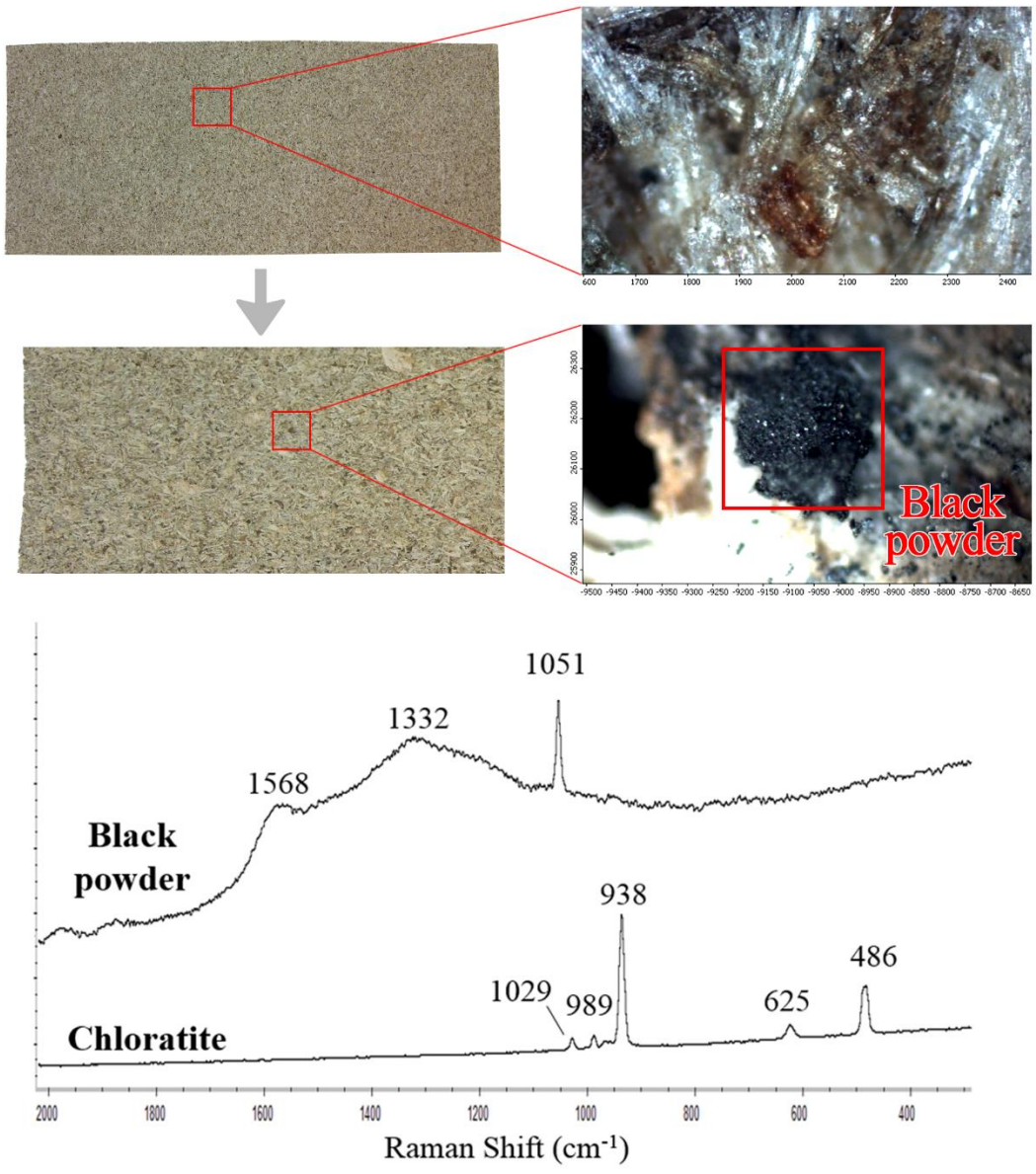

Figure 6.22. Microscopic examination of chipboard surface (above) and post-blast residues (below) and Raman spectra of the post-blast residues from the two explosives detected on chipboard collectors: black powder and chloratite. Raman conditions as in Figure 6.16.

Cardboard. Cardboard substrates were also heterogeneous though not as much as chipboard. In particular, the brown large homogeneous areas within the cardboard samples also contained small white-coloured components, which, to the naked eye, could be sometimes confused with post-blast particles, as displayed in Figure 6.23. Despite that, using the Raman microscope, post-blast particles from all the explosives except dynamite were identified on cardboard. As collected in Table 6.8, post-blast particles from black powder and chloratite were identified on the 3 replicates whereas post-blast particles from ANFO and ammonal were identified only in 2 of the 3 replicates.

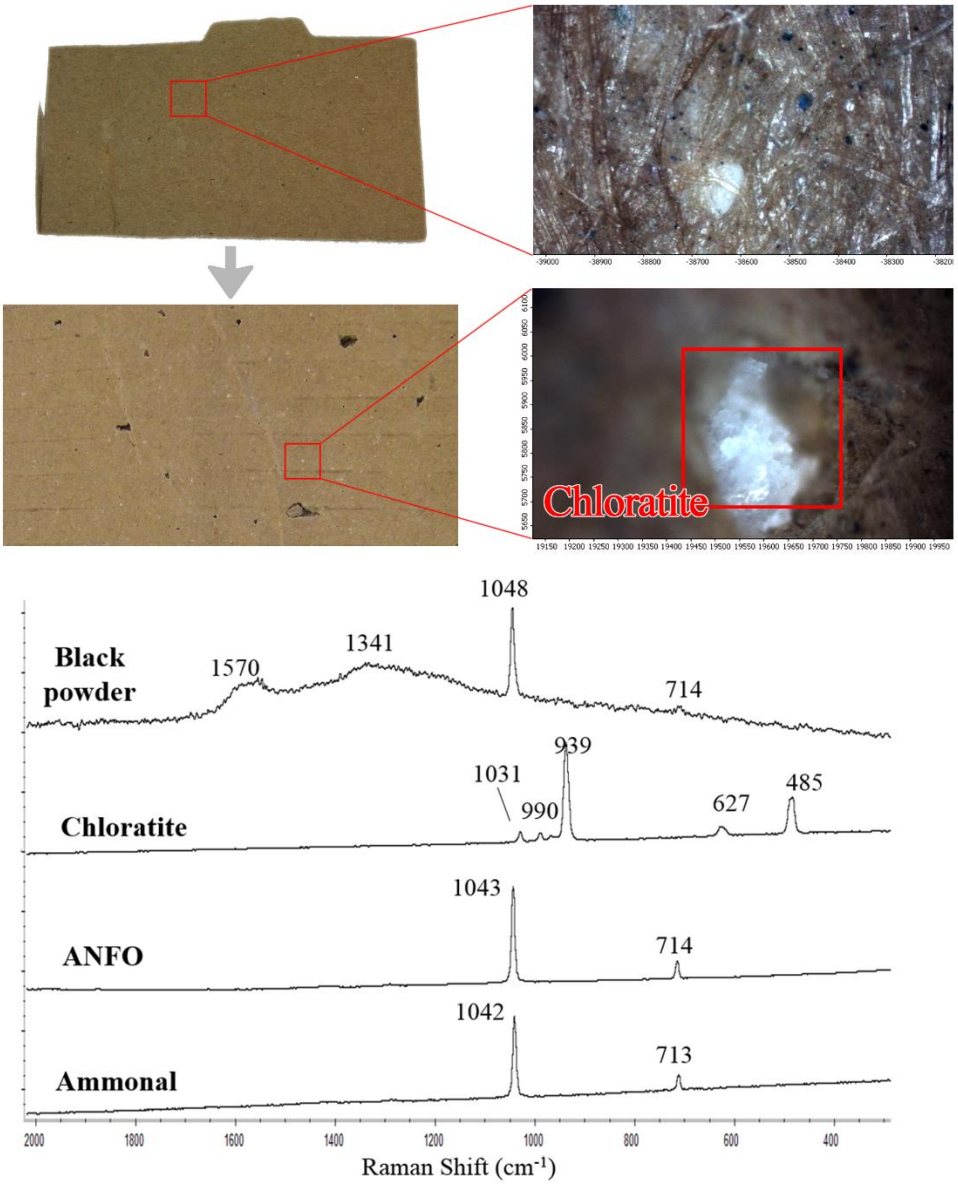

Figure 6.23. Microscopic examination of cardboard surface (above) and post-blast residues (below) and Raman spectra of the post-blast residues from the four explosives detected on cardboard collectors: black powder, chloratite, ANFO and ammonal. Raman conditions as in Figure 6.16.

- Highly irregular surfaces

Tyre. Tyre samples were homogeneous in colour (black) but they offered highly rough and irregular surfaces due to their pattern and tread. In addition, they had been previously used, therefore, they were heterogeneously bald and they had some dirtiness and residues as evidenced in Figure 6.24. To the naked eye, these residues were sometimes confused with post-blast residues. As previously mentioned (see Materials), only one tyre (one replicate) per explosion was used. With regards to the results (see Table 6.8), only post-blast particles from chloratite and ANFO were identified on tyre. No post-blast particles from black powder, dynamite or ammonal were detected.

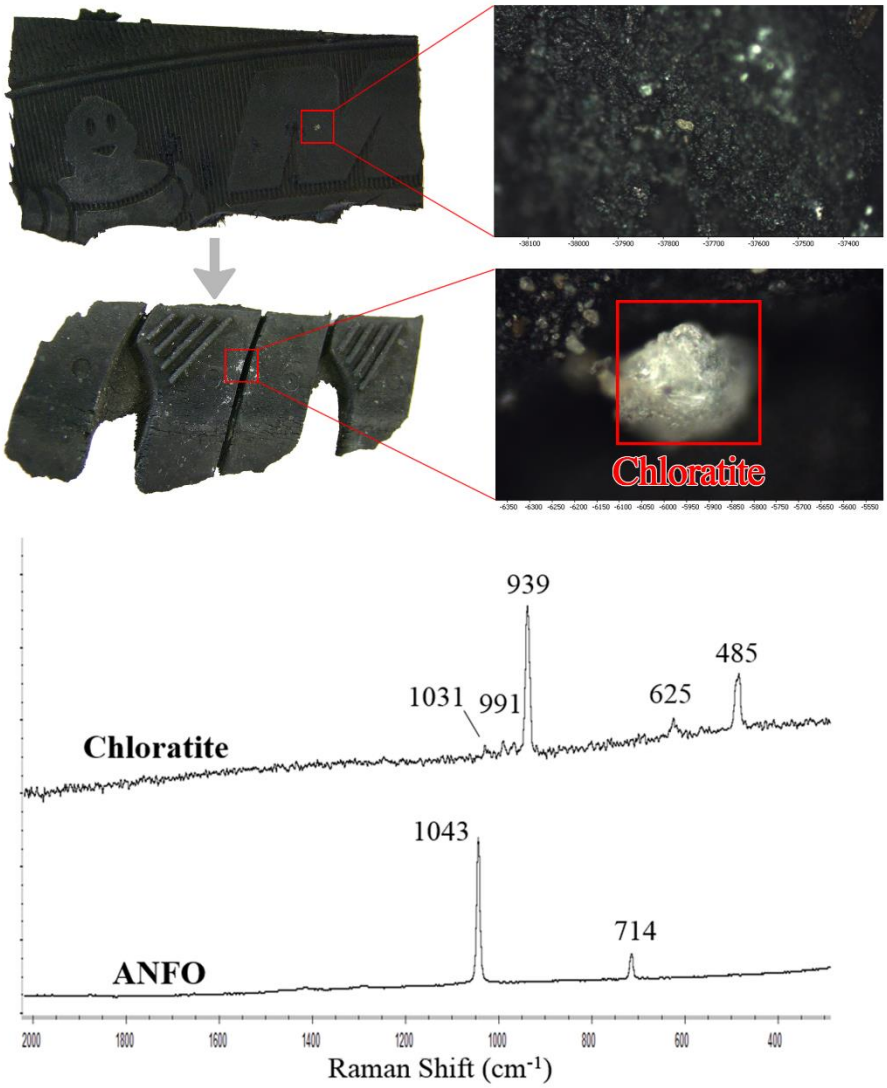

Figure 6.24. Microscopic examination of tyre surface (above) and post-blast residues (below) and Raman spectra of the post-blast residues from the two explosives detected on tyre: chloratite and ANFO. Raman conditions as in Figure 6.16.

Brick. Bricks provided heterogeneous, rough and highly irregular surfaces alternating flat areas and longitudinal grooves of orange colour with small white particles as shown in Figure 6.25. To the naked eye, these particles were sometimes confused with post-blast particles from explosives, as occurred with cardboard. In addition, brick provided a highly intense Raman spectrum, which hindered the Raman determination of those tiny post-blast particles not big enough to display their Raman spectra over the background. In fact, only post-blast residues from black powder were identified on bricks (on the three replicates). However, post-blast particles from any of the other four explosives (chloratite, dynamite, ANFO and ammonal) were not detected on any of the 3 replicates as summarized in Table 6.8.

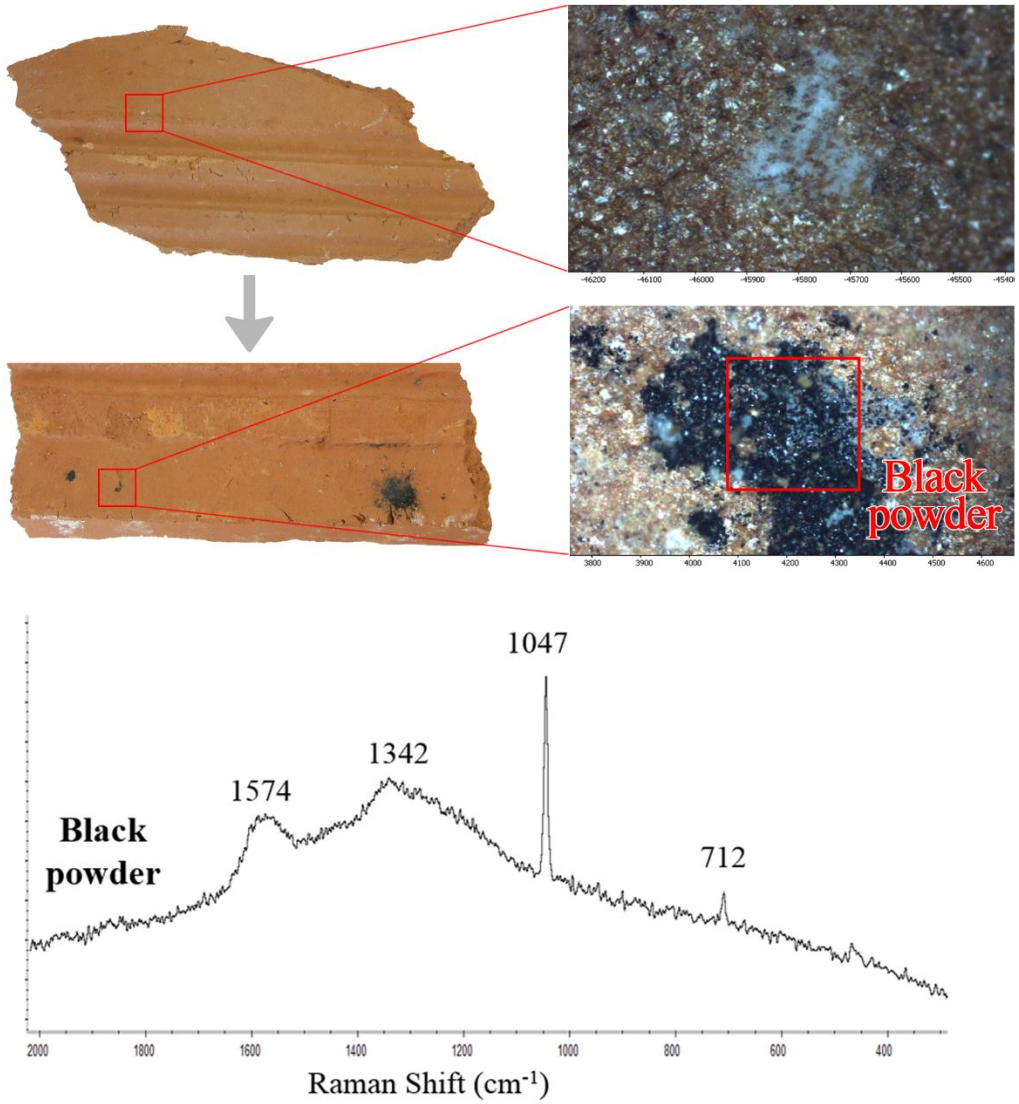

Figure 6.25. Microscopic examination of brick surface (above) and post-blast residues (below) and Raman spectra of the post-blast residues from the unique explosive detected on brick: black powder. Raman conditions as in Figure 6.16.

Plaster board. Plaster board substrates were white and quite homogeneous in colour, but they offered a highly irregular surface consisting of numerous orifices as displayed in Figure 6.26. The white surface of plaster board greatly hindered the detection of white post-blast particles from explosives. In fact, post-blast particles from black powder were easily identified on the three replicates whereas post-blast particles from the other four explosives were hardly detected. According to Table 6.8, post-blast particles from chloratite and ANFO were detected in 1 of the 3 replicates whereas post-blast particles from dynamite and ammonal were not detected in any of the replicates.

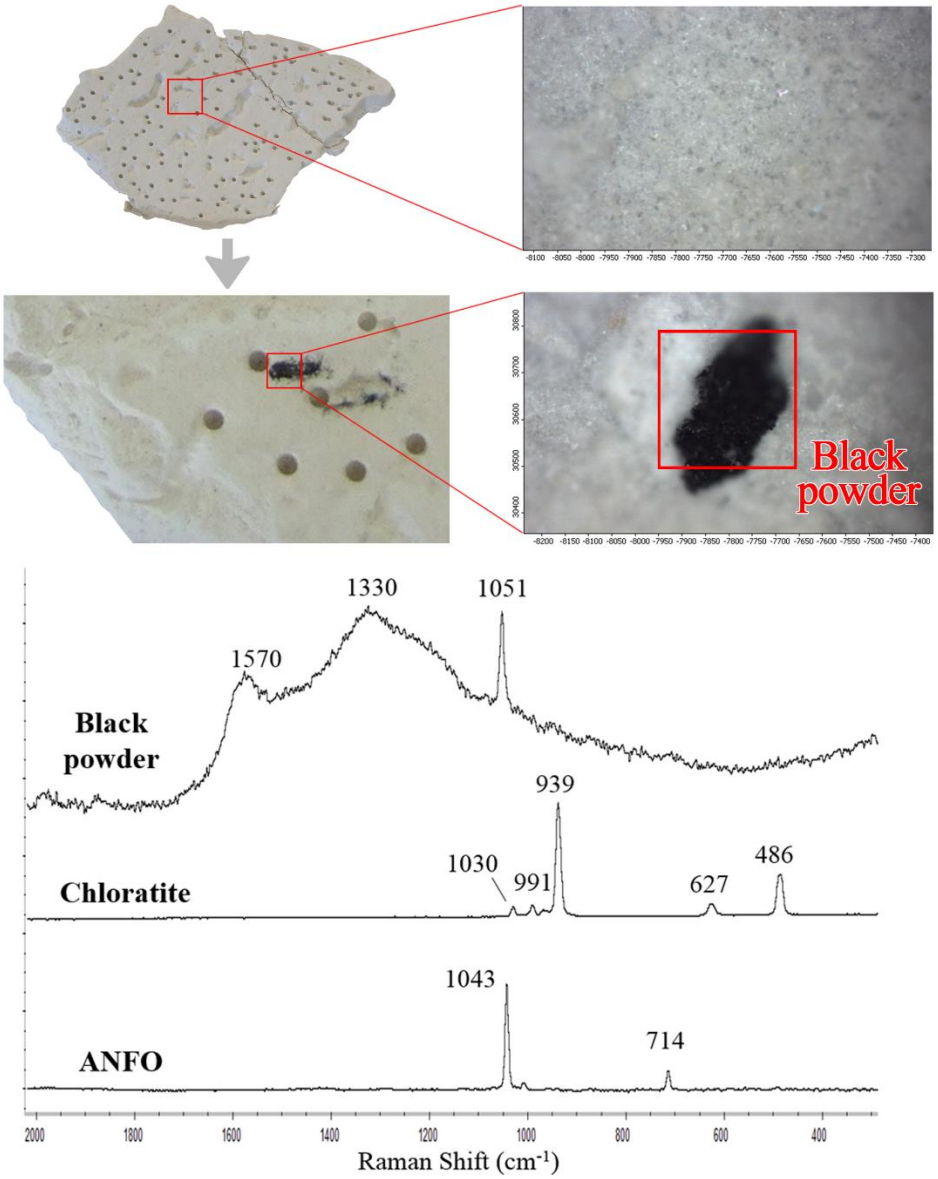

Figure 6.26. Microscopic examination of plasterboard surface (above) and post-blast residues (below) and Raman spectra of the post-blast residues from the three explosives detected on plasterboard collectors: black powder, chloratite and ANFO. Raman conditions as in Figure 6.16.

Cotton fabric. Cotton fabrics were white and homogeneous except for the highly irregular surface, caused by the interlaced fibres, as displayed in Figure 6.27. In fact, post-blast residues were mostly trapped within the fibres and the microscopic detection and Raman analysis became difficult and time-consuming. As shown in Table 6.8, post-blast particles from black powder were identified in 2 of the 3 replicates and post-blast particles from chloratite were detected in 1 of the replicates. Post-blast particles from dynamite, ANFO and ammonal were not detected in any of the replicates. For further information regarding the difficult detection of explosive traces on fabrics, the reader is referred to the reference [27], a further study also accomplished during the Thesis.

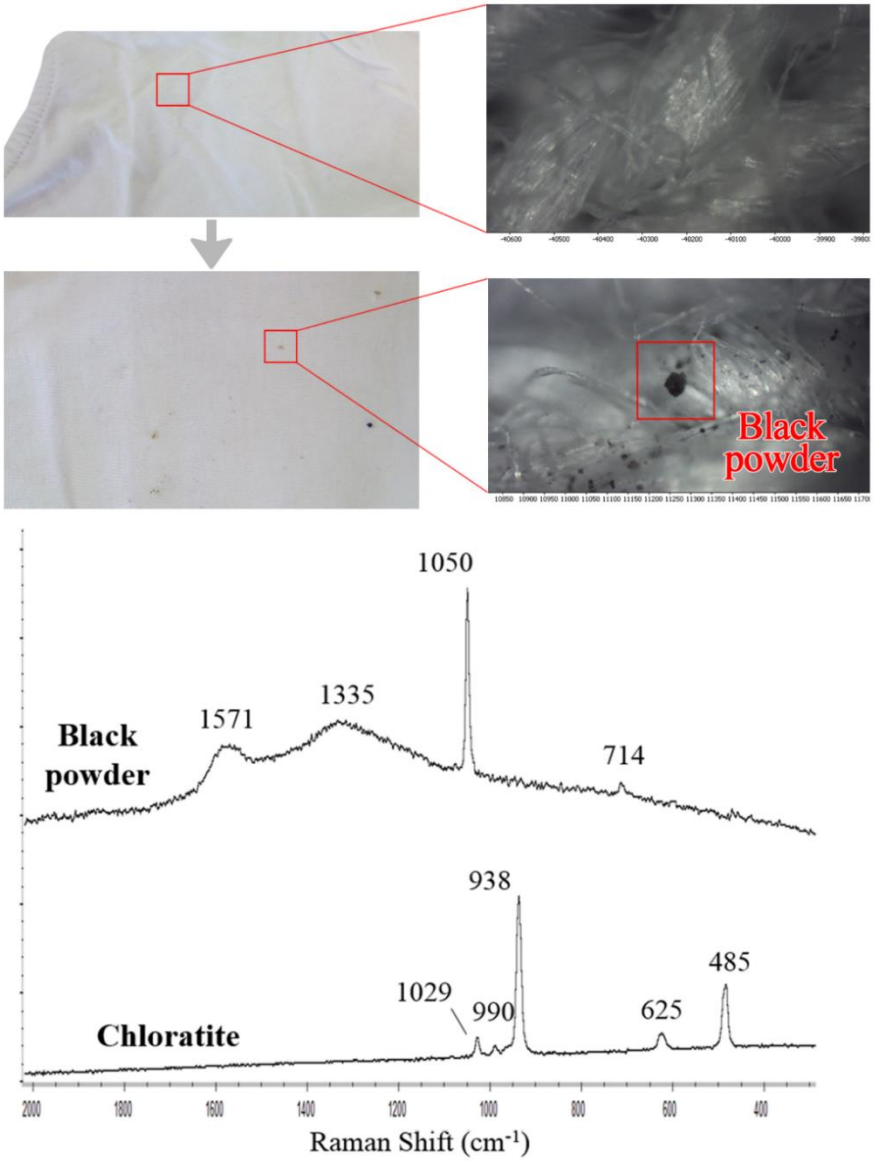

Figure 6.27. Microscopic examination of cotton surface (above) and post-blast residues (below) and Raman spectra of the post-blast residues from the two explosives detected on cotton collectors: black powder and chloratite. Raman conditions as in Figure 6.16.

- Biological surface

Pig meat. The surface of pig meat was highly heterogeneous, as shown in Figure 6.28. Post-blast residues were mostly detected on the skin, though some areas of the skin were burnt. In addition, these samples started to decompose after the explosion even though they were kept in the refrigerator when they were not being analysed. In fact, pig meat samples provided the worst results. In particular, post-blast particles of charcoal from black powder were the unique particles detected on these samples. Even potassium nitrate was not detected, as displayed in Figure 6.28. No post-blast particles from the other four explosives were detected. This result is probably explained by the fact that pig meat has a high water content which would have completely or partially dissolved the particles of inorganic salts in such a way that they were not already detectable by microscopy. Furthermore, the own degradation of meat (even in the refrigerator) could have also degraded the inorganic salts.

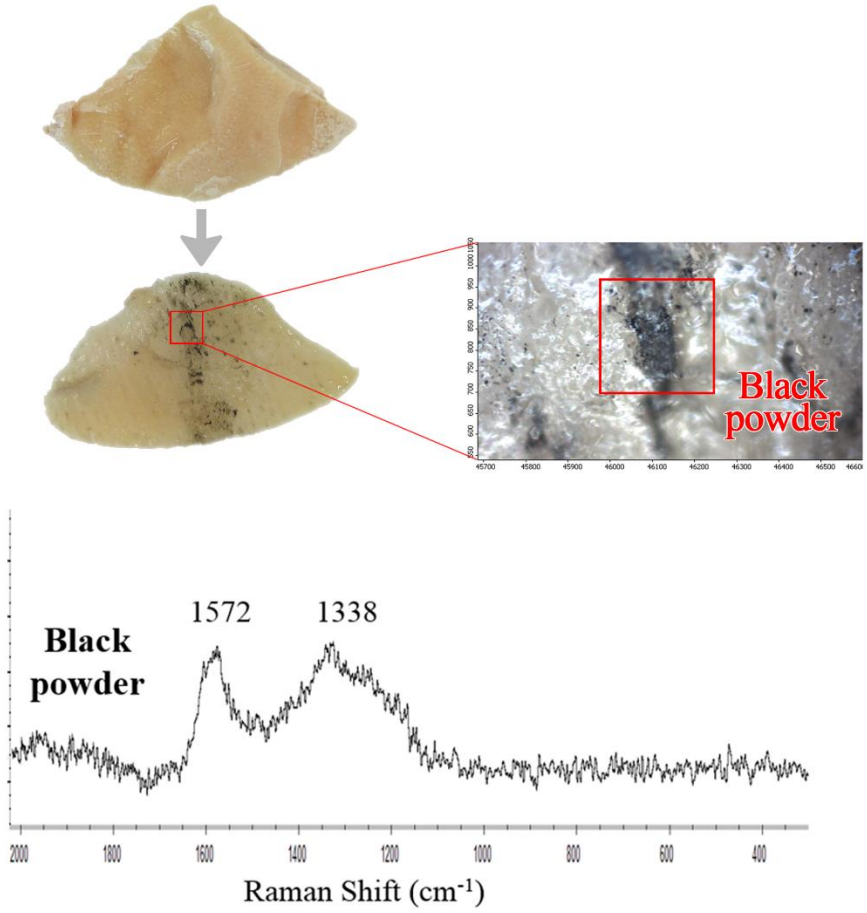

Figure 6.28. Microscopic examination of post-blast residues on pig meat surface and Raman spectra of the post-blast residues from the unique explosive detected on pig meat collectors: black powder. Raman conditions as in Figure 6.16.

Finally, some general outcomes regarding the explosives were drawn. It should be highlighted that charcoal and potassium nitrate from black powder were detected in all materials except for tyre; sodium chlorate from chloratite was detected in all materials except for brick and pig meat; AN from ANFO was detected in all materials except for chipboard, brick, cotton fabric and pig meat; AN from ammonal was detected in glass, plastic bag, plywood and cardboard; and AN from dynamite was only detected in plastic bag and plywood. In summary, post-blast particles from dynamite were detected in 2 of the 11 materials, ammonal in 4 of the 11 materials, ANFO in 7 of the 11 materials, chloratite in 9 of the 11 materials and black powder in 10 of the 11 materials.

In addition, both the best and the worst materials as collectors of post-blast residues detectable by Raman microscopy were assessed. Plastic bag and plywood offered the best results because post-blast non-reacted particles from the five explosives were detected on them. On the contrary, brick and pig meat provided the worst results because only post-blast particles from black powder were detected on them. According to the number of positive/ negative results achieved for the five explosives, the eleven materials (collectors) were listed as follows: Plastic bag and plywood > glass and cardboard > steel and plasterboard > chipboard, tyre and cotton fabric > brick and pig meat. It should be noted that this list had resulted from the obtained results, which depend on the combination of two factors: the material's efficiency to collect post blast residues and the advantages/drawbacks of those materials to be analysed by Raman microscopy. That means that the best materials such as plastic bag and plywood were competent for both factors. However, it does not mean that the worst materials were necessarily unsatisfactory to both factors. For instance, cotton fabric was demonstrated to be highly suitable to trap post-blast residues within the fibres, but it provided bad results, which are likely attributed to the clear difficulty of detecting the post-blast particles across the fibres by Raman microscopy. Thus, post-blast residues on cotton may be more accurately analysed using other techniques or subjected to some extraction methodology.

Conclusions

Enough spectral resolution is essential to differentiate potassium and ammonium nitrates, whose Raman bands are characterized by having a slight

Raman shift of 6–8 cm^{-1}. This can be tested by means of a rapid and simple strategy which may be easily performed with the available Raman spectrometer to check whether both characteristic bands can be simultaneously resolved.

Regarding the appropriateness of each material as collector of post-blast explosive traces, it should be remarked the high quantity of post-blast non-reacted particles from explosives found inside plastic bags, which makes these collectors highly recommendable for the identification of explosive traces in post-blast evidence. In addition, the evidence recovery process may be planned in order to recover first the most worthwhile materials (collectors). In general, either homogeneous or heterogeneous surfaces were demonstrated to provide the best results whereas highly irregular and biological surfaces offered the highest difficulties. The best explosive trace collectors were listed as follows:

Plastic bag and plywood > glass and cardboard > steel and plasterboard > chipboard, tyre and cotton fabric > brick and pig meat.

Considering that microscopy has been the technique used to look for the post-blast residues from explosives, it is understandable that highly irregular surfaces offered a more unfriendly and problematic surface to this aim. In any case, if both homogeneous, heterogeneous and highly irregular materials contain post-blast residues from these explosives, the non-irregular surfaces should be easily and rapidly examined by confocal Raman microscopy whereas the highly irregular surfaces could be reserved for other sort of analysis such as CE or IC. Thus, the samples recovered during evidence recovery can be classified in different groups in order to be suitably analysed using the most appropriate and informative technique in each case.

References

[1] M. Marshall, J. Oxley, Explosives: the threats and the materials, in: M. Marshall, J.C. Oxley (Eds.), Aspects of Explosives Detection, Elsevier, Netherlands, 2009, pp. 11-26.

[2] J.T. Thurman, Practical Bomb Scene Investigation, Taylor & Francis, Boca Raton, USA, 2006.

[3] H.T. Christen, P.M. Maniscalco, Weapons of mass effect-explosives, in: P.M. Maniscalco, H.T. Christen (Eds.), Homeland Security: Principles and Practice of

Terrorism Response, Jones and Bartlett publishers, Sudbury, MA, USA, 2011, pp. 161-170.

[4] U.S. Army, U.S. Army Explosives and Demolitions Handbook, Skyhorse Publishing Inc., Canada, 2010.

[5] J.B. Ledgard, The Preparatory Manual of Black Powder and Pyrotechnics, Lulu Press Inc., Seattle, Washington, 2006.

[6] S.J. Benson, C.J. Lennard, P. Maynard, D.M. Hill, A.S. Andrewe, C. Roux, Forensic analysis of explosives using isotope ratio mass spectrometry (IRMS) – discrimination of ammonium nitrate sources, Sci. Justice 49 (2009) 73-80.

[7] N. Abdul-Karim, C.S. Blackman, P.P. Gill, E.M.M. Wingstedt, B.A.P. Reif, Postblast explosive residue – a review of formation and dispersion theories and experimental research, RSC Adv. 4 (2014) 54354-54371.

[8] J. Cummins, J. Hull, K. Kitts, J.V. Goodpaster, Separation and identification of anions using porous graphitic carbon and electrospray ionization mass spectrometry: application to inorganic explosives and their post blast residues, Anal. Methods 3 (2011) 1682-1687.

[9] C. Martín-Alberca, F. Zapata, H. Carrascosa, F.E. Ortega-Ojeda, C. García-Ruiz, Study of consumer fireworks post-blast residues by ATR-FTIR, Talanta 149 (2016) 257-265.

[10] F. Zapata, C. García-Ruiz, Determination of nanogram microparticles from explosives after real open-air explosions by confocal Raman microscopy, Anal. Chem. 88 (2016) 6726-6733.

[11] J.P. Hutchinson, C. Johns, M.C. Breadmore, E.F. Hilder, R.M. Guijt, C. Lennard, G. Dicinoski, P.R. Haddad, Identification of inorganic ions in post-blast explosive residues using portable CE instrumentation and capacitively coupled contactless conductivity detection, Electrophoresis 29 (2008) 4593-4602.

[12] N. Abdul-Karim, C.S. Blackman, P.P. Gill, R.M. Morgan, L. Matjacic, R. Webb, W. H. Ng, Morphological variations of explosive residue particles and implications for understanding detonation mechanisms, Anal. Chem. 88 (2016) 3899-3908.

[13] G.W. Dicinoski, R.A. Shellie, P.R. Haddad, Forensic identification of inorganic explosives by ion chromatography, Anal. Lett. 39 (4) (2006) 639-657.

[14] C. Johns, R.A. Shellie, O.G. Potter, J.W. O'Reilly, J.P. Hutchinson, R.M. Guijt, M.C. Breadmore, E.F. Hilder, G.W. Dicinoski, P.R. Haddad, Identification of homemade inorganic explosives by ion chromatographic analysis of postblast residues, J. Chromatogr. A 1182 (2008) 205-214.

[15] M. Pumera, Analysis of explosives via microchip electrophoresis and conventional capillary electrophoresis: a review, Electrophoresis 27 (2006) 244-256.

[16] J.P. Hutchinson, C.J. Evenhuis, C. Johns, A.A. Kazarian, M.C. Breadmore, M. Macka, E.F. Hilder, R.M. Guijt, G.W. Dicinoski, P.R. Haddad, Identification of inorganic improvised explosive devices by analysis of postblast residues using

portable capillary electrophoresis instrumentation and indirect photometric detection with a light-emitting diode, Anal. Chem. 79 (2007) 7005-7013.

[17] C. Sarazin, N. Delaunay, A. Varenne, J. Vial, C. Costanza, V. Eudes, J.J. Mineta, P. Gareil, Identification and determination of inorganic anions in real extracts from pre- and post-blast residues by capillary electrophoresis, J. Chromatogr. A 1217 (2010) 6971-6978.

[18] G.A. Blanco, Y.H. Nai, E.F. Hilder, R.A. Shellie, G.W. Dicinoski, P.R. Haddad, M.C. Breadmore, Identification of inorganic improvised explosive devices using sequential injection capillary electrophoresis and contactless conductivity detection, Anal. Chem. 83 (2011) 9068-9075.

[19] C. Sarazin, N. Delaunay, C. Costanza, V. Eudes, P. Gareil, Capillary electrophoresis analysis of inorganic cations in post-blast residue extracts applying a guanidinium-based electrolyte and bilayer-coated capillaries, Electrophoresis 32 (2011) 1282-1291.

[20] C. Martín-Alberca, M.A. Fernández de la Ossa, J. Saiz, J.L. Ferrando, C. García-Ruiz, Anions in pre- and post-blast consumer fireworks by capillary electrophoresis, Electrophoresis 35 (2014) 3272-3280.

[21] B. Zachhuber, G. Ramer, A. Hobro, E.H. Chrysostom, B. Lendl, Stand-off Raman spectroscopy: a powerful technique for qualitative and quantitative analysis of inorganic and organic compounds including explosives, Anal. Bioanal. Chem. 400 (2011) 2439-2447.

[22] S. Wallin, A. Pettersson, H. Önnerud, H. Östmark, M. Nordberg, E. Ceco, A. Ehlerding, I. Johansson, P. Käck, Possibilities for standoff Raman detection applications for explosives, Proc. SPIE 8358 (2012) 83580P/1-83580P/9.

[23] M.R. Almeida, D.N. Correa, J.J. Zacca, L.P.L. Logrado, R.J. Poppi, Detection of explosives on the surface of banknotes by Raman hyperspectral imaging and independent component analysis, Anal. Chim. Acta 860 (2015) 15-22.

[24] F. Zapata, M.A. Fernández de la Ossa, E. Gilchrist, L. Barron, C. García-Ruiz, Progressing the analysis of improvised explosive devices: comparative study for trace detection of explosive residues in handprints by Raman spectroscopy and liquid chromatography, Talanta 161 (2016) 219-227.

[25] J. Kuula, H. Rinta, I. Pölönen, H.H. Puupponen, M. Haukkamäki, T. Teräväinen, Detecting explosive substances by the IR spectrography, Proc. SPIE 9073 (2014) 90730Q/1-90730Q/12.

[26] B. Bozzini, V. Romanello, C. Mele, F. Bogani, A SERS investigation of carbon steel in contact with aqueous solutions containing BenzylDiMethylPhenyl Ammonium Chloride, Mater. Corros. 58 (2007) 20-24.

[27] D. Videira-Quintela, F. Zapata, C. García-Ruiz, Detection of microscopic traces of explosive residues on textile fabrics by Raman spectroscopy, J. Raman Spectrosc. (2018) In press, DOI: 10.1002/jrs.5455.

Section 3. Spectroscopic Strategies to Identify Stains of Body Fluids

To victims of sexual assault

You tell me it gets better, it gets better in time
You say I'll pull myself together, pull it together
You'll be fine
Tell me what the hell do you know
What do you know
Tell me how the hell could you know
How could you know

'Til it happens to you, you don't know
How it feels
How it feels
'Til it happens to you, you won't know
It won't be real
No it won't be real
Won't know how it feels

You tell me hold your head up
Hold your head up and be strong
'Cause when you fall, you gotta get up
You gotta get up and move on

Tell me, how the hell could you talk
How could you talk?
'Cause until you walk where I walk
It's just all talk

'Til it happens to you, you don't know (…)

'Til your world burns and crashes
'Til you're at the end, the end of your rope
'Til you're standing in my shoes, I don't wanna hear nothing from you
From you, from you, 'cause you don't know

'Til it happens to you, you don't know (…)

'Til it happens to you, you won't know how I feel

Authors: Stefani Germanotta / Diane Warren,
Singer: Lady Gaga. 2015 Sony/ATV Music Publishing LLC, Universal Music Publishing Group.

Chapter 7. Spectroscopic techniques for the forensic detection of body fluids

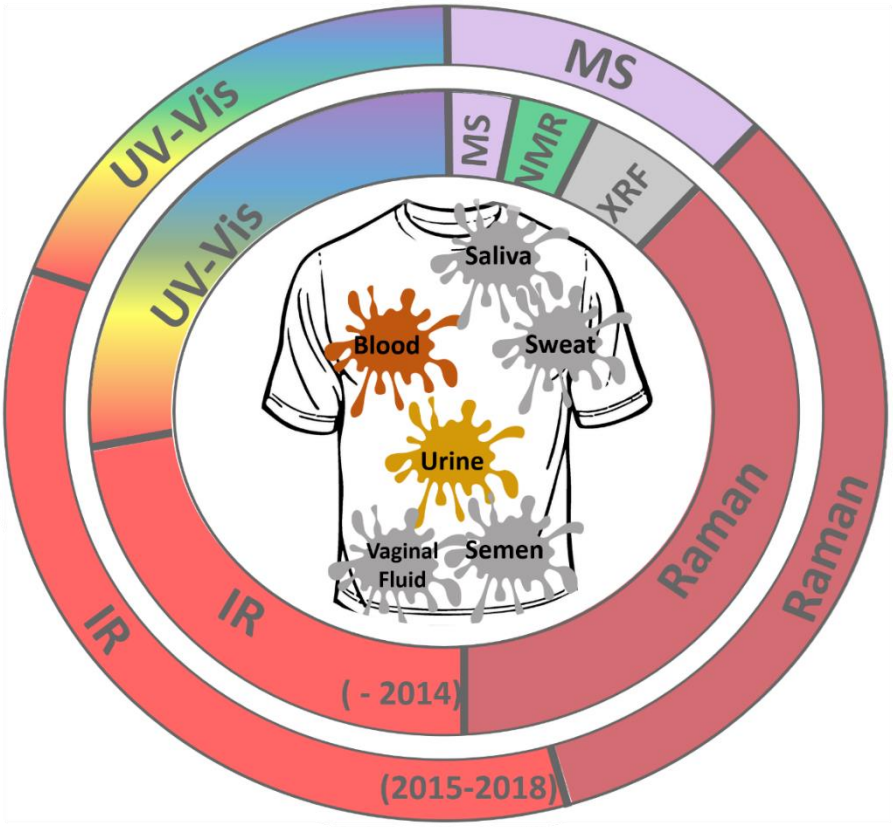

Main source:

Félix Zapata, M.A. Fernández de la Ossa, C. García-Ruiz, Emerging spectrometric techniques for the forensic analysis of body fluids, *TrAC – Trends Anal. Chem.* 64 (2015) 53-63.

Other sources:

Félix Zapata, I. Gregório, C. García-Ruiz, Body fluids and spectroscopic techniques in forensics: a perfect match?, *J. Forensic Medicine* 1 (2015) 1-7.

I. Gregório, **Félix Zapata**, C. García-Ruiz, Analysis of human bodily fluids on superabsorbent pads by ATR-FTIR, *Talanta* 162 (2017) 634-640.

I. Gregório, **Félix Zapata**, M. Torre, C. García-Ruiz, Statistical approach for ATR-FTIR screening of semen in sexual evidence, *Talanta* 174 (2017) 853-857.

Abstract

Body fluids are evidence of great interest in forensics because they allow identification of individuals through the study of DNA. After reviewing the tests and the methods that are currently being used by forensic practitioners for the detection of body fluids (*e.g.* blood, semen, saliva, vaginal fluid, urine and sweat), and after showing their main drawbacks and limitations, this work focuses on the review of emerging spectrometric techniques applied for the forensic analysis of body fluids. These techniques include the use of ultraviolet-visible, infrared (IR), Raman, X-ray fluorescence and nuclear magnetic resonance spectroscopy and mass spectrometry for investigating blood, semen, saliva, urine, vaginal fluid or sweat. Although all these spectrometric techniques seem to have a high potential to differentiate body fluids prior to DNA extraction, IR and Raman spectroscopy have shown the most promising results for discriminating stains from body fluids.

Introduction

Body fluids are exceptionally useful forensic evidence because they provide information that allows police to discover their corresponding owner by analysing the DNA (deoxyribonucleic acid) content. Since DNA testing has acquired huge relevance for solving crimes, the detection of biological evidence at the crime scene has become one of the priorities of law-enforcement officers during ocular inspection. According to Locard's principle, "every contact leaves a trace", so a small part of the offender usually stays in the place while a small part of the place goes with the offender (*e.g.* in homicide, resulting from confrontation between victim and aggressor, residues from the victim are probably found on the attacker and vice versa) [1]. After trace detection, the forensic process continues with evidence analysis to obtain information about the source (identity) or activity (why the trace is where it is) and how it might relate to a proposed crime scene.

Technically, a biological fluid comes from a living being. In the forensic field, the biological fluids of interest are body fluids, which come from a human being, especially those from the attacker. Body fluids generated by human beings include blood, semen, saliva, vaginal fluid, urine, sweat, breast milk, tears and mucus. Undoubtedly, blood, semen and saliva are found in larger amounts than the others at crime scenes, and thus, they have been the most studied [2-4].

Tests currently used to analyse body fluids are classified according to their specificity in two different categories (presumptive and confirmatory) [2]. Presumptive tests provide a large number of false positives (*i.e.* the test is positive although the body fluid is not present in the sample). Presumptive tests are unspecific to a single body fluid, so a positive response is due only to the suspicion that the fluid may be present in the stain. Thus, it is always necessary to apply a confirmatory test to confirm the presence of a body fluid in a stain because, by contrast, confirmatory tests are specific to identify a particular body fluid. A positive response certainly ensures the presence of the searched body fluid in the stain under examination.

Presumptive and mainly confirmatory tests used in body-fluid identification are based on each body fluid having a unique composition, which is the result of specific components of each body fluid and the difference in the relative ratio of common components found in several body fluids [2]. As Lednev and Virkler

indicate [2], urea is found in urine, semen and sweat, its concentration in urine being larger than in either of the other two fluids. Table 7.1 shows the principal components present in blood, semen, saliva, vaginal fluid, urine and sweat [2].

Table 7.1. Major components of body fluids. Adapted from [2].

Blood	Semen	Saliva	Vaginal fluid	Urine	Sweat
Haemoglobin	Acid phosphatase	Amylase	Acid phosphatase	Urea	Chloride
Fibrinogen	Prostate-specific antigen	Lysozyme	Lactic acid	Creatinine	Sodium
Erythrocytes	Spermatozoa	Mucin	Citric acid	Uric acid	Urea
	Choline		Urea		
	Spermine		Vaginal peptidase		
	Semenogelin				
	Urea				

Table 7.2 shows the most relevant tests currently used to detect or to confirm blood, semen, saliva, vaginal fluid, urine and sweat. The columns indicate, respectively, test name, type of test (chemical, spectroscopic, microscopic, crystal test, immunological, chromatographic or electrophoretic), specificity (presumptive or confirmatory), main characteristics of the test and references. All the tests pursue the detection of specific components, ratios of components or characteristics, such as fluorescence, to detect presumptively or to confirm (identify) each body fluid.

Table 7.2. Current tests for identification of body fluids.

Test	Type	Specificity	Characteristics	Ref.
Blood				
Luminol	Chemical	Presumptive	Luminol added together with an oxidant (H_2O_2) becomes luminescent in the presence of haemoglobin.	[2-4]
Kastle-Meyer	Chemical	Presumptive	Phenolphthalein (colourless), with H_2O_2 added is oxidized to a pink compound in the presence of haemoglobin	[2-4]
Leucomalachite green	Chemical	Presumptive	Leucomalachite green (colourless) is oxidized to a green compound in the presence of haemoglobin	[2-4]
Benzidine	Chemical	Presumptive	Benzidine (white) is oxidized in EtOH/HAc medium to a blue compound in the presence of haemoglobin	[2, 4]
Fluorescein	Chemical	Presumptive	Fluorescin is oxidized to fluorescein in the presence of H_2O_2 and haemoglobin that fluoresces under UV light	[2]
Alternate light sources (ALS)	Spectroscopic	Presumptive	Hematoporphyrin fluoresces under UV-Vis radiation	[2]
Microscopic visualization	Microscopic	Confirmatory	Microscopic visualization of blood cells, white blood cells and fibrin	[2]
Takayama crystals	Crystal test	Confirmatory	Fe presents in haemoglobin reacts with pyridine producing pyridine ferroprotoporphyrin (red crystals)	[2, 4]
Teichman crystals	Crystal test	Confirmatory	Haemoglobin reacts with halides producing hematin (brown crystals)	[2]
UV-Vis Absorption	Spectroscopic	Confirmatory	Soret band absorption at 413 nm characteristic of the presence of blood	[2]
Antibodies	Immunological	Confirmatory	Enzyme-antibody specific interaction (precipitin test, ABACard, HemaTrace, Ouchterlony, LDH, Hexagon Obti)	[2-4]

Semen				
Alternate light sources (ALS)	Spectroscopic	Presumptive	Semen fluoresces under UV-Vis radiation	[2, 4]
Acid phosphatase	Chemical	Presumptive	Phosphatase catalyzes the hydrolysis of organophosphates which react with a diazonium salt producing a coloured compound	[2-4]
Florence	Crystal test	Presumptive	Choline produces brown crystals in the presence of potassium iodide	[2]
Choline	Chemical	Presumptive	Choline reacts with luminol analogously to blood (Choline oxidase-luminol)	[2]
Barberio	Crystal test	Presumptive	Spermine reacts with picric acid producing yellow crystals	[2]
Spermine	Chromatographic	Presumptive	Spermine determined by HPLC	[2]
SEM-EDX	Spectroscopic	Presumptive	Elemental analysis of semen (Na, P, S, Cl, K, Ca, etc.) by SEM-EDX	[2]
Microscopic visualization-Christmas tree	Microscopic	Confirmatory	Visualizing spermatozoids under the microscope. Two reagents are used to facilitate its observation turning tails-green and heads-red	[2, 4]
Prostate specific antigen (PSA) or P30	Immunological	Confirmatory	Specific interaction of PSA with its antibody (immunoelectrophoresis, ELISA, Biosign PSA, ABACard)	[2-4]
Other Antibodies	Immunological	Confirmatory	Specific interaction of antibodies with antigens (Inmunoglobulin G1, semenogelin, prostaglandin, LDH-X, γ-glutamyl transpeptidase)	[2, 4]

Saliva				
Alternate light sources (ALS)	Spectroscopic	Presumptive	Saliva fluoresces under UV-Vis radiation	[2, 4]
Amylase	Chemical	Presumptive	Amylase catalyzes the hydrolysis of starch by which the solution remains colourless when adding iodine (Starch-Iodine, Phadebas, Rapignost-Amylase)	[2-4]
SEM-EDX	Spectroscopic	Presumptive	Elemental analysis of saliva (Na, P, S, Cl, K, Ca, etc.) by SEM-EDX	[2]

Vaginal fluid				
Periodic acid Schiff	Chemical	Presumptive	This reagent interacts with the cytoplasm of Glycogenated epithelial cells producing a magenta colour	[2]
Vaginal peptidase	Electrophoretic	Presumptive	Enzyme that hydrolyzes the valine-leucine dipeptide. Reaction is checked by gel electrophoresis	[2]
Oestrogen receptors	Immunological	Presumptive	Specific interaction between oestrogen and antibody (17β-estradiol)	[2]
Lactate/citrate ratio	Electrophoretic	Presumptive	Lactate/citrate ratio measured by capillary isotachophoresis	[2]

Urine				
Alternate light sources (ALS)	Spectroscopic	Presumptive	Urine fluoresces under UV-Vis radiation	[2]
Urea	Chemical	Presumptive	Urea is transformed into NH_3 and CO_2 by urease. Different reagents (Nessler reagent, DMAC, bromothymol blue)	[2]
Jaffe	Chemical	Presumptive	Creatinine reacts with picric acid producing a red precipitate	[2]
Salkowski	Chemical	Presumptive	Creatinine reacts with sodium nitroprusside producing a blue compound	[2]
Tamm-Horsfall (THP)	Immunological	Presumptive	Specific interaction of the glycoprotein THP and its antibody	[2]
Ureic acid/urea ratio	Chemical	Presumptive	Determination of human urine by measuring the urea/ureic acid ratio. Different reagents (uricase-peroxidase, urease-indophenol)	[2]
SEM-EDX	Spectroscopic	Presumptive	Elemental analysis of urine (Na, P, S, Cl, K, Ca, etc.) by SEM-EDX	[2]
17-Ketosteroid	Chromatographic	Presumptive	Identification of this steroid by HPLC-MS	[2]

Sweat				
SEM-EDX	Spectroscopic	Presumptive	Elemental analysis of sweat (Na, P, S, Cl, K, Ca, etc.) by SEM-EDX	[2]

As seen in Table 7.2, the six body fluids can be presumptively detected by different tests, most of them chemical. However, there are available confirmatory tests solely for blood and semen, which involve immunological interactions, microscopic visualization of specific components or formation of specific crystals by chemical reaction. In addition to the lack of confirmatory tests for saliva, vaginal fluid, urine and sweat, there are other disadvantages, such as:

(1) most confirmatory tests (for blood and semen) are destructive; and,

(2) it is necessary to apply different tests to confirm each type of body fluid; this limitation requires division of a sample into several parts, and a portion of the sample having to be kept for possible future analyses.

To date, there is no test or method used by forensic practitioners able to detect and to confirm a body-fluid source without destroying the evidence [2, 5]. This situation makes it necessary to develop confirmatory non-destructive methods applicable to different types of body fluids. Nowadays, there are two principal lines of active research in body-fluid identification. One is dedicated to the development of mRNA (messenger ribonucleic acid) markers [6-12] based on the different mRNA sequences in each body fluid. The other is based on the use of spectrometric analytical techniques.

In this chapter, our goal is to provide a critical review of the works using emerging spectrometric techniques to analyse body fluids.

Emerging spectrometric techniques

Several analytical techniques can be applied to determine the presence in a stain of any of the different types of body fluid included in this review article.

In general, classical analytical chemistry is based on colorimetric assays, the use of many reagents and implementation of a large number of methods, usually specific for only one single analyte. As consequence it leaves room for spectrometric methodologies that are characterized by speed, and absence, or minimum use, of reagents and frequently applicable to the analysis of many analytes at a time. Spectrometric analysis results in a characteristic spectrum, which contains the information related to the chemical composition of the sample under analysis [13, 14]. Since the composition of each body fluid is

different, it is possible to differentiate each type of body fluid by using these techniques.

In recent years, spectrometric techniques underwent strong development in many different fields. Regarding forensic sciences, spectrometric techniques were used for analysing drugs [15-20] and explosives [15, 21-25] and they are still used at forensic laboratories nowadays. However, approved analyses of body fluids used at forensic institutions have continued unchanged, based on the use of classical chemical assays. Their evolution into modern analytical methods has not happened yet. However, some research groups are investigating and developing novel methods for the analysis of body fluids. Specifically, ultraviolet-visible (UV-Vis), infrared (IR), Raman, X-ray fluorescence (XRF) and nuclear magnetic resonance (NMR) spectroscopy and mass spectrometry (MS) are being investigated in this field.

As common data to all studies, body-fluid stains analysed were all dried stains unless otherwise indicated, in order to test conditions similar to those in real forensic crime scenes, and, for some techniques (*e.g.* IR spectroscopy), this condition also avoids the problem of the huge IR signals from water.

- *Ultraviolet-visible spectroscopy*

Illumination with UV-Vis light was the first spectroscopic method used for forensic detection of body fluids. It is based on the two processes that substances subjected to UV-Vis radiation may undergo, absorption or fluorescence emission. Under a UV-Vis source, most body fluids (*e.g.* semen, saliva, and urine) emit fluorescence [26], which is visibly detected as intense brightness of the sample. Blood is not fluorescent at UV-Vis radiation, but it presents a characteristic absorption band in the UV region, which, in good lighting conditions, can create a contrast detectable by the human eye between blood and the background [26].

In 1987, Auvdel [27] first compared the efficiency of using different light sources in the detection of saliva, semen and sweat stains [*i.e.* monochromatic (argon laser), bichromatic (hand-held Mineralight multiband lamp at UV wavelengths 254 nm and 366 nm) and polychromatic (Fotodyne lamp with UV wavelengths at 254 nm and 366 nm and white light of 400–780 nm)]. Stains were prepared at different concentrations on sections cut from 23 multicolored clothes made of cotton, cotton-polyester, polyester, polyester-rayon, nylon, nylon-acrylic fiber

or acrylic fiber. Different concentrations were obtained by consecutive dilutions (from 1/2 to 1/16) of the pure fluids. The argon laser was more efficient than the UV-Vis lamps because it showed better results at detection. Its high intensity allowed detection by visible fluorescence of 17 of 23 semen stains (74%), 7 of 23 saliva stains (30%) and 5 of 23 sweat stains (22%), while the UV-Vis lamps allowed detection of 13 of 23 semen stains (56%), 5 of 23 saliva stains (22%) and 4 of 23 sweat stains (17%). However, a year later, this test was repeated by using a different UV-Vis lamp (Luma-Print, in the wavelength range 400–520 nm) and more favorable results were obtained for the lamp rather than the laser [28]. This UV-Vis lamp allowed detection of 21 of 23 semen stains (91%), 11 of 23 saliva stains (48%) and 7 of 23 sweat stains (30%) – better results than those achieved using the laser. The lamp intensity was enough to produce fluorescence of the stains, and, in comparison to the laser source, a wide range of wavelengths were available. The improvements in UV-Vis lamp manufacture made them more versatile, smaller, lighter and cheaper than UV monochromatic lasers [28].

In 2008, successful results for the detection of body fluids using UV-Vis lamps were also shown by Seidl et al. [29], who compared UV-VIS lamp Lumatec (in the wavelength range 320–700 nm) with a 532-nm laser for detecting blood, semen, saliva and urine stains deposited on glazed tiles, glass, PVC, wood, metal, stone, Formica, carpet and cotton. Comparable results were obtained for the laser and the lamp in the number of semen, saliva and urine stains detected, with the exception that the lamp was more discriminating than the laser. However, the great advantage of the lamp was its capacity to detect blood stains. No blood stain was detected by the 532-nm laser because the absorption band of blood is located at 415 nm. Thus, blood stains were detected by only the lamp [29].

Another UV-Vis lamp successfully used in forensic laboratories for body-fluid detection (Polilight) covers the 310–650-nm region of the electromagnetic spectrum. In 1991, Stoilovic [30] showed its application for locating semen and blood stains placed on different non-photoluminescent and photoluminescent surfaces. In order to overcome the difficulties with respect to the kind of surface, recommended procedures to detect and photograph semen and blood stains were created. Since then, use of this lamp by forensic analysts has spread worldwide. Subsequent studies using the Polilight lamp showed instrumental

optimizations for the detection of semen stains on fabrics (cotton, wool and polyester) [31] and enhancement in the detection of blood, semen and saliva stains deposited on colored clothes made of cotton, nylon or polyester in comparison to conventional tests based on chemical reagents (luminol, acid phosphatase and amylase tests) [26]. In addition, many other UV-Vis lamps other than Polilight have been developed and used for locating body-fluid stains at crime scenes. The Wood's lamp at 320– 400 nm [32] and the Bluemaxx lamp at 320–510 nm [33] were tested for the detection of semen stains on black and white cotton. Beside semen stains, potential false positive substances were analysed (*e.g.* bacitracin zinc, barrier cream, hand cream, castile soap, surgilube, toothpaste and A&D ointment). The results concluded that some of these substances were false positives [32, 33].

Finally, the Lumatec lamp at 320–700 nm [34] was studied for the detection of human and boar semen, and human saliva stains on multicolored fabrics made of cotton, polyamide, polyester and spandex. Semen stains were all detected due to their strong fluorescence, while only the 60% of saliva stains were detected by this lamp. It was demonstrated that the substrate composition did not affect the analysis, but the color did. Dark backgrounds provided the worst results. It was also checked that fluorescence intensity of semen and saliva stains decreased after fabrics were washed [34].

Currently, UV-Vis lamps are known as alternate light sources (ALSs) or forensic light sources, and they are well accepted in the international forensic community as a presumptive and screening test. However, studies reviewed establish that ALSs lack selectivity because fluorescence under UV-Vis radiation is not specific. Fluorescence does not allow confirmation of the body fluid contained in a stain.

In this sense, Powers et al. [35] patented the use of specific light sources (lamps with different bulbs, LEDs and diode lasers) working at different excitation wavelengths to detect the presence of blood, semen, saliva, skin oil and urine stains with the optimum required excitation energies. For this purpose, the excitation wavelengths needed for detecting each body fluid stain were optimized. Table 7.3 summarizes the results obtained.

Table 7.3. Excitation and emission wavelengths for skin oil, semen, blood, urine and saliva. "w" means weak fluorescence. Adapted from [35].

Excitation and Emission Ranges for Select Human Body Fluids						
Excitation range (nm)	Emission range (nm)	Skin oil	Semen	Blood	Urine	Saliva
250-300	320-360	X	X	X	X	X
250-300	380-460				X	
250-290	430-480		X			
360-390	420-510		X		X	
390-410	430-540		X		X	
430-470	480-570		X		X	
520-540	630-700	w				w
570-590	630-700			X		X
640-680	760-840				X	
790-810	860-930		X			

Regarding the use of lasers for the detection of body fluids traces, though at a lower level, it has not totally disappeared. For example, Soukos et al. [36] used a UV laser at 282 nm to detect traces of dried saliva on skin after removing them with a cotton swab.

- *Infrared spectroscopy*

IR radiation has also been applied to the analysis of body fluids. However, its use to study body fluids began two decades ago for clinical purposes [37] and it is later its application to police investigations.

Wang et al. [37] analysed blood drops after drying on a crystal slide by attenuated total reflection (ATR), transmission and diffuse reflection spectroscopy in the wavelength range 500–4000 cm^{-1} (20,000–2500 nm), absorbance at 4000–10000 cm^{-1} (2500–1000 nm) and photoacoustic spectroscopy at 400 Hz. The principal aim was to test the validity of IR spectroscopy for multicomponent determination in blood and plasma. Results showed water-absorption bands to be problematic, and the utility of IR spectroscopy for qualitative assays but also its limitations for quantitative analysis.

It was not until 2007, when a revolutionary, novel methodology based on the use of IR hyperspectral imaging (HSI) began to be investigated for the forensic analysis of body fluids. HSI combines photography with spectroscopy with the aim of obtaining spectral information of the substances that composed the

samples photographed [38]. The spectral information obtained depends on the wavelengths used to photograph the sample. To date, there are commercially available HSI systems working in the UV-Vis and IR regions. In comparison to the UV region, the IR region provides more information about the chemical structure of substances. The IR spectrum is unique for each chemical compound and allows unequivocal identification of a substance.

Lin *et al.* [38] were the first to apply HSI to the forensic analysis of body fluids. For this purpose, they used the near-IR (NIR) region 760–1500 nm and compared with visible light (400–780 nm). This study focused on the analysis of blood stains at different concentrations on black clothes made of different materials, such as cotton, polyester, rayon, velvet, acrylic fiber, wool, lycra and spandex. Different concentrations were prepared by consecutive dilutions (from 1/2 to 1/16) of pure blood. The results obtained showed selectivity and limit of detection (LOD) for NIR better than Vis, specifically for stains on these dark backgrounds. NIR revealed a greater number and more diluted stains than Vis radiation.

Other imaging studies were published using the medium IR region (MIR), 4000–500 cm^{-1} (2500–20,000 nm). Myrick's team developed a method based on applying the thermal MIR imaging to detect blood stains by studying the contrast observed between the stain and the background [39, 40]. In a first study [39], blood stains prepared at different concentrations on dark acrylic fiber were analysed. Different concentrations were produced by consecutive dilutions (from 1/10 to 1/100) of pure blood. In addition, potential false-positive substances, such as rust, cherry soda and coffee, were analysed and compared with blood stains. Results demonstrated that all blood stains analysed were detected and identified by this method even the most diluted samples (1/100). Results also demonstrated that the potential false positives analysed were not confused with blood, so they were not false positives by this method.

In a second study [40], more diluted blood stains (1/200) and more fabric substrates (cotton, nylon and polyester) were analysed. In addition, the statistical method of principal component analysis (PCA) was applied to data treatment. By PCA, the clean substrate and the blood-stained substrate were successfully differentiated at 95% confidence.

In another study (reported by Elkins [41]), blood, semen, saliva, vaginal fluid and urine stains deposited on white cotton were first analysed by ATR-FTIR spectroscopy in the MIR region 4000–400 cm^{-1} (2500–25,000 nm). One stain per fluid was analysed. In order to check false positives, this study also investigated stains of other substances similar in appearance to body fluids by comparing their IR spectra [41]. These substances were barbeque sauce, lotions, mayonnaise, Vaseline, chocolate, coffee, wine, cream cheese, apple juice, ketchup, lipstick and yogurt. This assay also evaluated the effect of temperature (21°C, 40°C and 120°C) in the process of drying the stain. The different FTIR spectra obtained for each body fluid allowed researchers to distinguish between them. Furthermore, the different spectra of body fluids and the substances checked as false positives avoided confusing them. There were no false positives by IR spectroscopy. Regarding the temperature, though its degradation effect reduced the intensity of bands in the spectrum, the variation was insignificant.

Several studies focused on comparing IR and UV-Vis spectroscopy for the analysis of blood stains. De Forest et al. [42] visualized blood stains on dark surfaces by using multispectral imaging in the Vis (RGB LEDs of 400–700 nm) and NIR (850 nm) regions. Four types of blood stain (*i.e.* smear, contact, drop, and small spatter) were deposited on black fabrics made of cotton, leather, wool, silk and polyester. These four types of blood stain cover those expected at a crime scene. In addition to blood, other substances that may produce false positives were also analysed [*e.g.* red-pen inks, paints, nail polishes, lipsticks, crayons, “vampire blood” (false blood), ketchup, raspberry jam and wine]. The image analysis involved measuring the luminosity and the color values of the blood stains. The main conclusion was that blood stains on black substrates were better observed by IR radiation, except “small spatter” stains, which were observed by Vis radiation only. Regarding the potential false positive substances, many of them were perfectly distinguishable from blood and only a few were quite similar to blood stains [42].

The same challenging issue in detecting blood stains located on dark surfaces was approached by Finnis et al. [43]. In this case, there was comparison between the potential of photography by UV (at 395 nm) and NIR (at 720–900 nm) and traditional chemical assays (*e.g.* using luminol, hydrogen peroxide and fluorescein tests). For this purpose, blood samples at different concentrations prepared by consecutive dilutions (from 1/10 to 1/106) of pure blood were

deposited on several dark substrates made of cotton, leather, rubber, vinyl, wool, polyester and suede. In this case, two types of stain were produced (*i.e.* drop and small spatter). The results showed the LOD for blood in water solution was about 10% (v/v) for NIR photography and the hydrogen-peroxide test, 1% (v/v) using UV light and 0.1% (v/v) for fluorescein and luminol tests. The results also showed that all "drop stains" were detected by all methods. However, IR and UV photography did not detect the "small spatter" stains, while the chemical tests did it.

- *Raman spectroscopy*

Raman spectroscopy is increasingly used for the analysis of body fluids. First, Raman spectroscopy was applied for the analysis of body fluids, especially blood, for structural and clinical purposes [44, 45]. Venkatesh et al. [44] focused on studying different hemoglobin (Hb) derivatives (oxy-Hb, carbonmonoxy-Hb, met-Hb, deoxy-Hb, hemichrome, Ni-Hb) by Raman spectroscopy in order to obtain structural information, while Enejder et al. [45] analysed blood from 31 individuals by Raman spectroscopy in order to determine and to quantify nine different compounds simultaneously (glucose, urea, cholesterol, total protein, albumin, triglycerides, hematocrit and hemoglobin) for clinical purposes.

However, in the past six years, Raman spectroscopy has been revealed as a promising technique for the forensic analysis of body fluids. The first study focused on the forensic identification of body fluids, especially blood, by Raman spectroscopy was by De Wael et al. [46] In this work, UV-Vis microspectrophotometry at 380–800 nm and FTIR ATR spectroscopy at 4000–400 cm^{-1} (2500–25000 nm) were applied together with Raman spectroscopy at 2000–400 cm^{-1} (5000–25000 nm) for the identification of blood stains. The blood stains analysed were from three species (human, cat and dog) and were made on clothing, glass slides and a metallic surface. For the blood stains on clothing, small dried particles in the stain were adsorbed on tape to be analysed more easily. The results showed that the three techniques (UV-Vis, IR or Raman) were sensitive enough to allow identification of blood on the basis of its spectrum. However, none of the techniques was able to differentiate the blood of the different species since the UV-Vis, IR and Raman spectra of the three species' blood were visually indistinguishable.

The development of methodologies adapted to the analysis of other body fluids in addition to blood by Raman spectroscopy was mainly tackled by Lednev and his research group. In 2008, they published a first study proving the utility of this technique for the identification of blood, semen, saliva, vaginal fluid and sweat [47] and patented it [48]. One dried drop of each body fluid made on a glass slide was analysed by Raman spectroscopy over the range 100–3200 cm^{-1}. The observation that every body fluid presented an intrinsic heterogeneity made it preferable to perform a mapping methodology where Raman spectra at different spots were registered to obtain finally the spectral average of all points. As a result, the Raman spectra of these body fluids were first obtained and are shown in Figure 7.1.

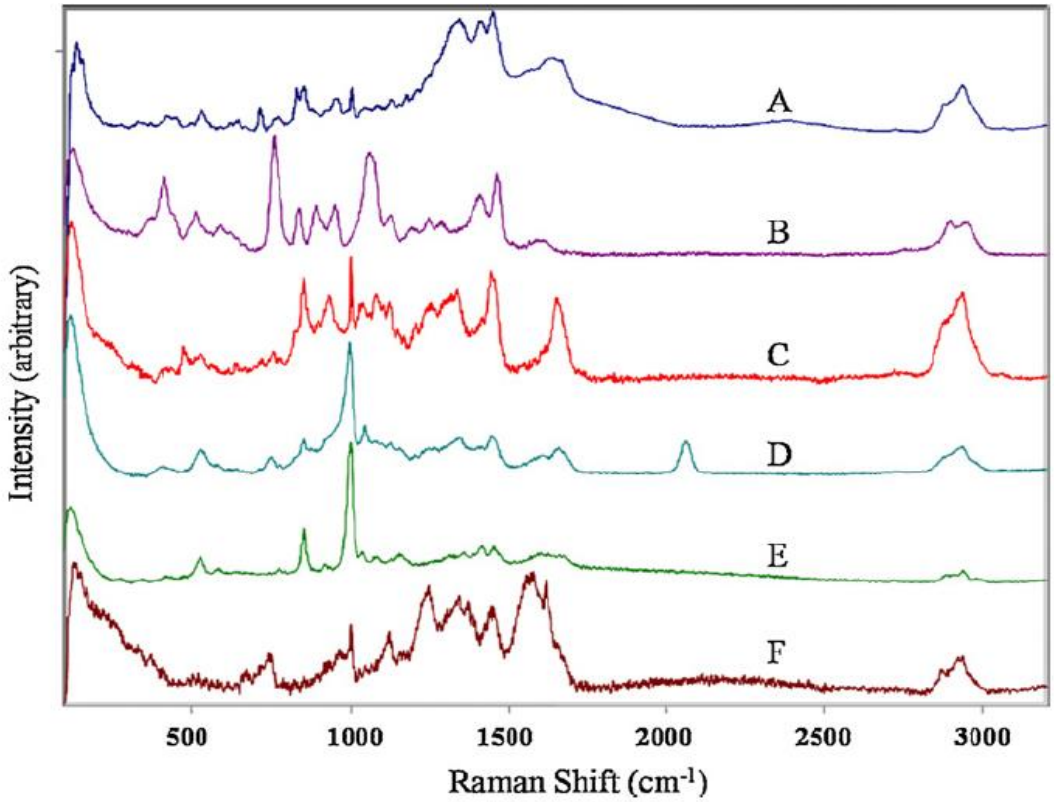

Figure 7.1. Raman spectra of (A) human semen, (B) canine semen, (C) vaginal fluid, (D) saliva, (E) sweat and (F) blood [47].

Canine semen was also analysed and it was differentiated from human semen by observing the spectral differences at the 500–1500 cm^{-1} range. In a further step, the Raman bands were assigned to vibrational modes and certain compounds {*e.g.* hemoglobin, albumin and glucose were identified in the blood spectrum; albumin, fructose, lysozyme and urea were identified in the semen spectrum; amylase and lipase were identified in the saliva spectrum; lactate,

urea, lysozyme, acetate and pyridine were identified in the vaginal fluid spectrum; and, urea was identified in the sweat spectrum [47, 48]}.

Additionally, Virkler and Lednev [49] investigated a problem earlier proposed by De Wael et al. [46] – discrimination among blood stains from human, canine and feline species based on the differences in their Raman spectra. In this study, eight blood samples from each species deposited on glass slides were analysed by Raman spectroscopy at the 250–1800 cm^{-1} range. A PCA was created to compare the spectra statystically. Contrary to De Wael's conclusion [46], which stated the Raman spectra of the blood of the three species were visually too similar to distinguish them, PCA results indicated that it was possible to discriminate among the bloodstains of the different species under study [49]. Figure 7.2 shows the Raman spectra of the three blood species analysed and the PCA results obtained.

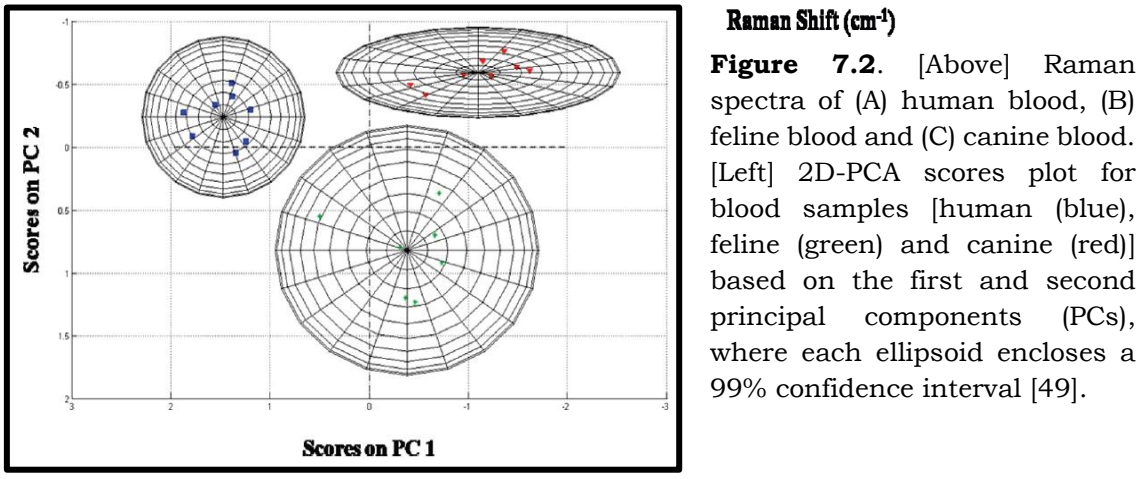

Figure 7.2. [Above] Raman spectra of (A) human blood, (B) feline blood and (C) canine blood. [Left] 2D-PCA scores plot for blood samples [human (blue), feline (green) and canine (red)] based on the first and second principal components (PCs), where each ellipsoid encloses a 99% confidence interval [49].

One study related to the analysis of body fluids in sexual abuse cases involved the investigation of condom lubricants as crime evidence. Coyle et al. [50] analysed 47 different condoms in order to identify them by lubricant composition. Samples were taken by cotton swabs from the condoms (before and after use) and from the simulated vaginal vault and pubic area of the victim (immediately before and after sexual intercourse). All samples were a mixture

among the condom lubricant and body fluids (mainly semen and vaginal fluid). Samples were analysed by Raman spectroscopy at the 200–4000 cm^{-1} range. To determine the effects of condom lubricants and Raman analysis on DNA from body fluids, the DNA was subjected to genetic analysis. The Raman spectra of samples taken from condoms showed bands that corresponded to polydimethylsiloxane, a known component of lubricants. The Raman spectra of samples taken from the simulated victim also showed those bands, so intercourse was established. Finally, the DNA results indicated that condom lubricants and Raman analysis did not affect to the DNA contained in the body fluids.

Virkler and Lednev continued the investigation of body fluids by establishing statistically the Raman spectroscopic signatures of semen [51], saliva [52] and blood [53]. In these studies, 50 samples of semen, 15 samples of saliva and 14 samples of blood deposited on glass slides were analysed by Raman spectroscopy at the 100–3200 cm^{-1} range applying a 36-point mapping methodology for semen and saliva samples and a 16-point mapping methodology for blood samples. One each of the semen and blood samples and five of the saliva samples [51-53] were used to get the spectral signatures of semen, saliva and blood, which were fitted to the remaining samples for comparison. The spectral ranges chosen for the Raman signature of each body fluid was 670–1750 cm^{-1} for semen, 300–1800 cm^{-1} for saliva and 950–1700 cm^{-1} for blood. The spectral signatures of the three body fluids were established by applying a significant factor analysis to determine the number of principal components in the spectra of the samples used as standard, and the alternate least squares function to extract the individual component spectra. Spectra fitting was performed using the curvefitting toolbox in MATLAB, and "goodness-of-fit" statistics (sum of squares due to error, R square (R^2) and root-mean-squared error) were calculated to measure the difference between the fitted spectra and the experimental spectra. The Raman spectral signatures of these body fluids were studied and Raman bands were assigned to certain compounds {*e.g.* tyrosine, choline and spermine in semen [51]; mucin, acetate, saccharides and arginine in saliva [52]; and, hemoglobin and fibrin in blood [53]. Moreover, the fitting results showed that all analysed semen, saliva and blood samples presented good results for their spectral signature (R^2 >0.98) and bad fitting results were obtained for the other body fluid signatures [51-53].

In order to improve differentiation of these three body fluids, a study, published in 2010 [54], focused on the statistical treatment of Raman spectra measured for the semen, saliva and blood samples analysed [51-53]. To classify these data, different statistical methods were applied {*i.e.* SIMCA (Soft Independent Modelling of Class Analogy), LDA (Linear Discriminant Analysis) and PLS-DA (Partial Least Squares Discriminant Analysis) [54]}. Using these three methods, semen, saliva and blood samples were correctly differentiated. As shown in Figure 7.3, practically all the experimental data were successfully clustered. The classification of different samples of blood, semen or saliva was also achieved by the three methods. 100% of the spectra were correctly classified by SIMCA, LDA and PLSDA. The combination of these three methods was a powerful identification and classification tool for blood, semen and saliva samples.

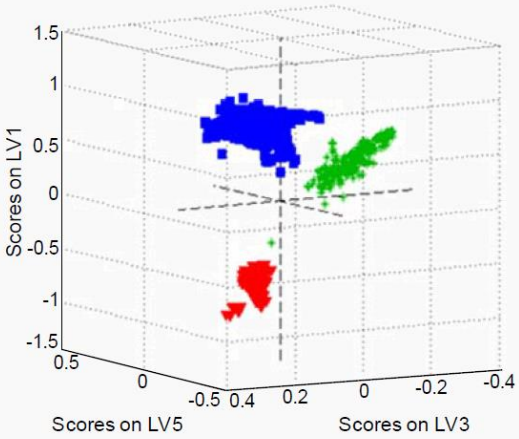

Figure 7.3. A 3D latent variable (LV) plot of PLS-DA model for samples of blood (red), semen (blue) and saliva (green) based on the first, third and fifth LVs [54].

Regarding blood stains detection by Raman spectroscopy, Boyd et al. [55] amplified the investigation by studying various factors in bloodstains, such as concentration and substrate. In that study, eight blood stains at different concentrations (dilutions from 1/50 to 1/500) made on different substrates (*e.g.* glass slides, denim, flannel, cotton, dry wall and plastics) were analysed by Raman spectroscopy at 400–2000 cm^{-1}. The results of diluted blood stains concluded that the maximum dilution for which at least the most intense blood bands were detectable by Raman spectroscopy was 1/250. The results related to the substrates showed that blood bands were more easily detected in spectra of blood stains on non-luminescent substrates (*e.g.* glass, wall and plastics). For blood stains on fabrics, spectra were dominated by scattering bands from the fabric and a larger amount of blood was necessary in the stain to make blood bands clearly visible. Thus, an extraction method of blood from fibers was proposed to avoid the analysis of fabrics by Raman spectroscopy. It involved placing a portion of the stained fiber in a centrifuge tube with 500 µL of water,

flick-mixing it for 1 min and depositing 100 μL on a slide. Using this procedure, the contribution of the fabric spectrum was eliminated.

Lednev's team continued investigation of body fluids by establishing statistically the Raman spectroscopic signatures of vaginal fluid [56] and sweat [57]. In both studies, seven samples of vaginal fluid or sweat deposited on glass slides were analysed by Raman spectroscopy at 100–3200 cm^{-1} range applying a 117-point mapping methodology for vaginal fluid samples [56] and a 32-point mapping methodology for sweat samples [57]. One of the samples was used to get the spectral signatures of vaginal fluid and sweat, which were fitted to the remaining samples for comparison. The spectral range chosen for the Raman signatures of both body fluids was 300–1800 cm^{-1}. The spectral signatures of these two body fluids were established by applying significant factor analysis to determine the number of principal components for the samples spectra used as standard and the alternate least squares function to extract the spectra of individual components. For spectra comparison and fitting, the same approach previously reported [51-53] was performed, based on the curve fitting toolbox in MATLAB and "goodness-of-fit" statistics. The Raman spectral signatures of both body fluids were subjected to assignment of Raman bands and certain compounds were identified {*e.g.* lactic acid, urea and amino acids in vaginal fluid [56] and lactate and urea in sweat [57]}. In this case, the fitting results showed that all analysed samples of vaginal fluid and sweat presented good results for their spectral signature (R^2 >0.98) and bad fitting results for the other body fluid signatures [56, 57].

Once, the spectral signatures of vaginal fluid and sweat were established, it was possible to unify in a single publication the Raman spectroscopic signatures of the five body fluids (blood, semen, saliva, sweat and vaginal fluid) [58]. The five body fluids under study were perfectly differentiated based on their Raman spectral signature. Moreover, it was possible to identify successfully unknown stains by statistical fitting of the corresponding Raman spectra with the specific spectral signature of each body fluid.

With the aim of testing similar conditions to those in real forensic crime scenes, Lednev's team also studied stains containing mixtures of several body fluids; specifically, different mixtures of blood from a woman (potential victim) and sperm from a man (potential attacker) deposited on glass slides were analysed by Raman spectroscopy at the 500–1800 cm^{-1} range by applying a 108-point

mapping methodology [59]. Mixtures were prepared with different blood/semen ratios (5:95, 10:90, 20:80, 30:70, 40:60, 50:50, 70:30, 75:25, 85:15, 87.5:12.5, 92.75:6.25, 96.875:3.125 and 98.4375:1.5625) by thoroughly shaking for 20 s.

Statistical treatment based on using Support Vector Machine (SVM) correctly classified the mixture stains in three different groups according to the blood-semen ratio in the mixture (pure blood, pure semen or mixture at 15–75% blood). Mixtures outside the 15–75% blood range were not considered like other groups because their spectra were too similar to the spectra of pure semen or pure blood. Results therefore showed that to identify the two body fluids (blood and semen) in a stain properly, it had to have a ratio of 15–75% blood. Otherwise, it was high probable that it would only register a signal from the main body fluid in the stain.

These types of study were extended by including the potential effects of pollutants, such as sand, dust and soil, in the analysis of bloodstains [60]. Each contaminant was applied to the fresh blood stain on the glass slide so that it completely covered the surface of the fluid. After drying overnight, samples were analysed by Raman spectroscopy at the 300–3200 cm^{-1} range applying a 108-point mapping methodology. By statistical fitting of the blood signature already established [53] with the experimental spectra, the presence of blood in the stain was determined. In all stains, there were several spots of the 108 measured points that presented a similar Raman spectrum to the blood. In that way, the fitting procedure enabled a PLS-DA classification approach to the identification of nearly pure blood spots within the contaminated stains. Results concluded that a bloodstain can always be identified as blood despite being contaminated or covered with dust, sand and soil.

Lednev wrote a report explaining all the research his group had done in body-fluid identification by Raman spectroscopy and statistical analysis for the US Department of Justice [61]. The main objective was to develop a portable, non-destructive and easy-to-use device for identification of body fluids at crime scenes. To reach this aim, Lednev et al. had already obtained the representative, characteristic Raman spectrum of each body fluid (blood, semen, saliva, vaginal fluid and sweat) on glass. They had automatically classified an unknown fluid into the correct category, even in mixtures. They had extended the method developed for stains on glass to other substrates (*e.g.* cotton, denim or tile). They

had also extended the method developed for clean stains to stains contaminated by dust, sand and soil.

Boyd et al. [62] continued the investigation of bloodstains, evaluating the application of surface-enhanced Raman spectroscopy (SERS) technique to the analysis of these stains. Blood stains prepared at different concentrations were deposited on different fabrics (denim, flannel and cotton). These samples were analysed by a SERS-active substrate composed of nickel nanotips coated with Ag nanoparticles at the 800–1800 cm^{-1} range. Results showed that blood was detected by SERS even in a 1/105-diluted blood stain. SERS amplified the blood signal by two orders of magnitude in comparison with conventional Raman spectroscopy. Results also demonstrated that SERS enabled Raman spectra free of substrate fluorescence, even in luminescent substrates, such as fabrics.

Focusing on blood stains, Lednev's team recently approached differentiation between menstrual and peripheral blood using Raman spectroscopy [63]. 21 peripheral blood samples, 20 menstrual blood samples and 8 vaginal fluid samples deposited on glass slides were analysed by Raman spectroscopy in the 625–1730 cm^{-1} range by applying a 100-point mapping methodology. Band assignment of the spectra obtained revealed that menstrual blood had more compounds than peripheral blood that came from vaginal fluid. Components of menstrual blood were a combination of blood and components of vaginal fluid. PLS-DA and SVM multivariate statistical methods enabled extraction of the statistical information to differentiate and to classify the samples correctly by studying only their Raman spectra. Both statistical methods achieved similar sensitivity and specificity values (>95%).

The discrimination of human and animal blood stains by Raman spectroscopy was recently re-examined by Lednev's team [64], who included more species and improved the statistical methods used in their previous study [49]. In this later study, they analysed 10 blood samples from 11 different animal species (cow, cat, dog, horse, pig, mouse, opossum, raccoon, rabbit, rat and chicken) besides the human. They analysed samples on glass slides by Raman spectroscopy in the 250–1800 cm^{-1} range, applying a 35-point mapping methodology. A PLS-DA model enabled them to classify the spectral Raman data of 20 unknown samples correctly [64].

- *X-ray fluorescence*

The potential of XRF for the forensic detection of body fluids was tested by Trombka et al. [65] in 2002. In that research, gunshot residues (GSRs), blood and semen stains were analysed. Since this technique enabled determination of the inorganic composition of samples based on the study of metallic composition, the main goal of this work was to detect blood and semen on the basis of their inorganic composition. For blood samples, the iron present in hemoglobin was followed, while, for sperm samples, the zinc contained in the zinc protoporphyrin enzyme was the element of study. Blood and semen stains were made on filter paper. The presence of Fe or Zn in a stain may indicate that those stains are blood and semen, respectively [65].

Three years later, a portable XRF device was designed to enable XRF analysis at crime scenes. By using this portable instrumentation, GSRs, blood and semen stains were detected [66]. Due to this technique focusing on one of the sample components (Fe or Zn), it cannot be considered a confirmatory technique because they are not unique to particular body-fluid stains.

- *Nuclear magnetic resonance*

The use of NMR to analyse body fluids in forensics was introduced recently. Scano et al. [5] were the first to investigate the applicability of 1H NMR to differentiate among blood, semen, saliva and urine based on their different NMR spectra. 18 samples of blood, 12 samples of semen, 18 samples of saliva and 21 samples of urine were collected and analysed by NMR. Before the analysis, all samples were centrifuged to remove large proteins and solid debris. The supernatant was analysed by NMR after drying and subsequently being reconstituted in D_2O. Binary mixtures 1:1 (v/v) of saliva-semen, blood-semen, urine-semen, blood-urine, saliva-urine and blood-saliva were also analysed. The ^1H NMR spectra of blood, semen, saliva and urine were then obtained. Based on these spectra, some metabolites, such as propionate, lactate, citrate and several amino acids, were assigned to the spectral bands.

By using a PCA model, it was possible statistically to differentiate these four types of body fluid. As shown in Figure 7.4, all samples were successfully clustered in four separate groups, in line with the four body fluids. In addition, binary mixtures were situated between the two fluids of their compositions.

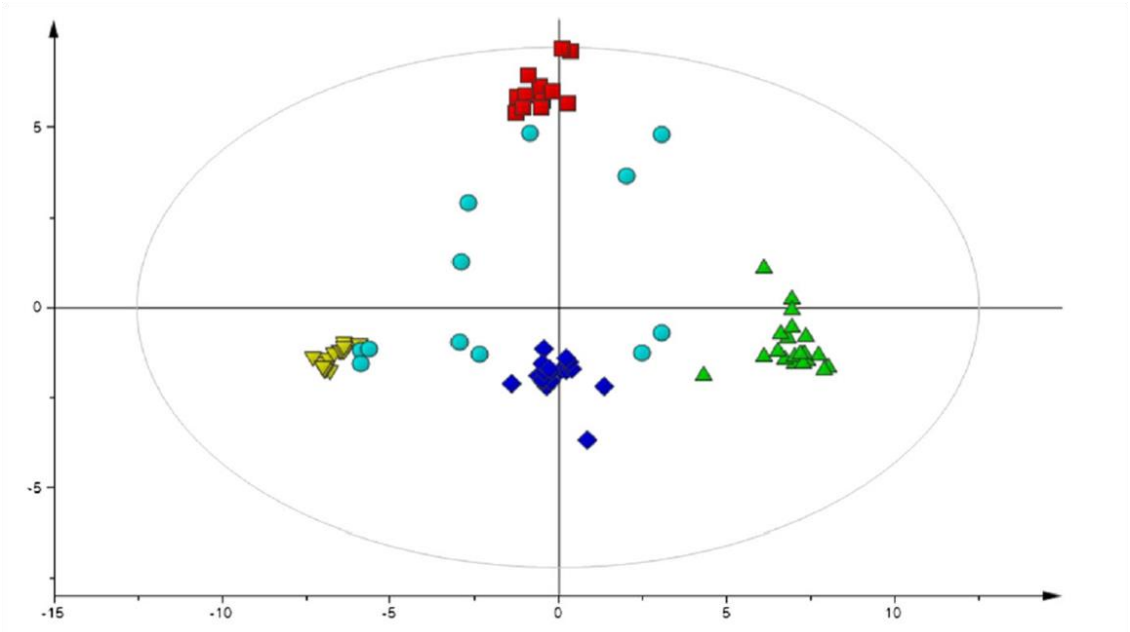

Figure 7.4. A two-dimensional principal component analysis (PCA) scores plot for samples of blood (yellow inverted triangle), semen (red box), saliva (blue diamond), urine (green triangle) and mixtures (blue circle) based on the first (41%) and third (14%) PCs [5].

In a further step, a fitting procedure for body-fluid identification was tested with some of the samples and the binary mixtures analysed. This fitting procedure was based on the average spectral profiles of the four body fluids and the results were reported in terms of root square difference. In this way, the samples tested were correctly identified and the two body fluids were correctly determined in the binary mixtures.

- *Mass spectrometry*

MS was also recently applied to the analysis of body fluids. Yang et al. [67] applied MS to analyse blood, semen and saliva, and specific proteins present in these body fluids were identified. In this work, instead of analysing RNA, specific proteins were considered as body-fluid markers. Blood, semen and saliva samples at different concentrations were used in two forms: liquid samples or "mock samples" (deposited on cotton swabs). Different dilutions for blood (from 1/10 to 1/104), semen (from 1/10 to 1/1000) and saliva (from 1/10 to 1/100) were studied. This study included analysis of the aging of body fluids, by analysing the samples over 16 months, and analysis of binary mixtures (*i.e.* blood-semen, blood-saliva and semen-saliva at different ratios).

A method based on protein extraction and digestion by chemical reagents, protein separation in a C18 reversed-phase HPLC column and protein identification by matrix-assisted laser desorption/ionization-time of flight spectrometer was used. Samples were also analysed by gel electrophoresis in order to determine the protein amounts in each body fluid. The proteins chosen as markers were α and β sub-units of hemoglobin for blood, semenogelin-1 and semenogelin-2 for semen and α-amylase 1 for saliva, among others. MS showed high sensitivity, LOD and specificity values for the identification of blood, semen and saliva based on their specific proteins. MS had the best sensitivity values in comparison with conventional chemical, enzymatic and mRNA profiling methods.

For liquid samples, 0.01×10^{-3} µL of blood, 0.1×10^{-3} µL of semen and 1×10^{-3} µL of saliva were detected by MS. Results also demonstrated that time did not affect the proteins studied. The same results were obtained for the samples throughout the 16 months.

Regarding mixture samples, the main conclusion was that specific proteins of both fluids were always detected by MS with the exception of saliva-blood mixtures with a high proportion of blood where only blood was detected. However, in comparison to the spectroscopic methods, the proposed method is destructive, because it requires a protein-extraction and digestion treatment by chemical reagents, and it is slow because, in addition to the sample-treatment step, it needs a protein HPLC separation for 40 min.

Review Update 2015-2018

It has been three years since this review was accepted and published. Three years, during which, the research focused on the detection of body fluids using spectrometric techniques has exceptionally increased. In brief, more studies have been published within these last four years (2015-2018) than in the previous ten (2005-2014). I really think this “boom” was foreseeable and unstoppable, and little or no influence our review has had on that. Nevertheless, having contributed to such “boom”, with our review and the subsequent experimental studies we have accomplished on this topic [68-72], is a personal gratification. This “update” revises those studies that have been published after the acceptance of our review and that have not been performed in our group.

Additionally, few studies that were missed in the previous review are included. Like the structure of the review, the "update" is also structured according to the spectrometric technique that was used.

But first, it should be mentioned the comprehensive and exhaustive revision accomplished by Zadora and Menżyk about the bloodstains aging and its dating using spectroscopic techniques [73]. Particularly, the extensive research field of estimating the age of bloodstains (after detecting the "unknown" stain as a bloodstain) was out of the scope of our review. A specially dedicated revision of such a relevant and substantial topic was highly necessary, and the recent publication of Zadora and Menżyk [73] eminently covers the topic, becoming a mandatory reading within the field of forensic analysis of bloodstains.

- *Ultraviolet-visible spectroscopy*

Besides the studies previously summarized in the review, ALS were also examined for the detection of stains of semen directly on skin [74, 75], urine and saliva also on skin [74] and blood stains on both skin [74] and other material surfaces [76]. Particularly, Wawryk and Odell [74] tested 11 different LED sources and a lamp from 370 to 482 nm for the detection of stains of semen, urine, saliva and blood either after a few minutes of having been deposited on skin and after one day. The first day, fluorescence from saliva was not detected with any light, fluorescence from urine and semen was detected in some subjects with some light sources (450-467 nm), and blood was easily visualized using all light sources due to its red color. The second day, neither saliva, semen, urine nor blood were detected with any light source, except for a few semen stains that displayed extremely low fluorescence with certain light sources (450-467 nm). Similarly, Lincoln *et al.* [75] detected semen stains on skin and four different surfaces (green cotton, blue denim, transparent plastic film and white paper) using an ALS working at 450 nm. Additionally, they reported two real sexual assault cases in which the ALS successfully assisted in the location of semen traces along the victim's body. Finally, Lee *et al.* [76] statistically compared three different light sources (fluorescent white light, 385 nm LED light and 410 nm LED light) with the aim of enhancing the photographic contrast of bloodstains on four different materials (white cotton, brown carpet, tar road and wood). The 410 nm light provided the best results.

It should be also mentioned the interesting and helpful revision, accomplished by Lee and Khoo [77], in which the milestones and limitations of using ALS for the detection of stains of body fluids (blood, semen, saliva and urine) are efficiently summarized.

Actually, the use of visible light sources to locate body fluids at a crime scene remains the most used methodology in ocular inspection, and has been accompanied in the last four years by significant scientific publications.

In fact, soon after our review was accepted for publication, Miranda *et al.* published an study [78] evaluating the capability of detecting stains of blood, semen, saliva and urine after several days/weeks since they were deposited on different surfaces (tile, wood, paper, white cotton fabric and black cotton fabric). The authors photographed the variation of fluorescence displayed by the stains along time illuminating them at 455 nm (using a Megamaxx™ ALS System) and wearing orange glasses. Results demonstrated that brightness of photographed stains (directly correlated to their fluorescence) variates within the first 24h until they get dry, but later it keeps constant from 24 h to 60 days (the maximum time analysed). Thus, ALS are useful to locate stains of body fluids even several days/weeks after a crime.

Li *et al.* (who previously focused on the estimation of the age of blood stains [79, 80]) have substantially contributed during these last four years to the detection of blood stains (particularly blood stained fingerprints) using visible HSI (from 400 to 500 nm) [81-84]. Briefly, authors successfully discriminated blood from another 40 reddish substances (including red inks and lipsticks), and detected 1/32 diluted blood stains on red tissue, 1/512 diluted blood stains on white filter paper, and blind blood stains on a red T-shirt [81]. Furthermore, authors have proposed and proved (for the first time) the simultaneous detection of blood stained fingerprints and the identification of the fingerprint ridges [82-84], evidencing the benefits of HSI over both normal digital RGB-cameras [82-84] and destructive chemical-based methods of enhancing blood-latent fingerprints such as Amido-Black [84]. In those studies, blood stained fingerprints on different colored non-porous/porous surfaces (including glass, plastic bags, paper, cardboard, wood, and cotton) were tested [83], as well as fingerprints made with potential false positive reddish substances [82].

In addition, Sterzik *et al.* have published a thorough study [85] examining nine different ALS (including visible light, 320-400, 415, 440, 460, 490, 550, 570 and NIR light (>830 nm)) for the detection of stains of semen, urine, saliva, sweat, blood and diluted blood on 29 different materials (such as cotton, linen, wool, paper or PVC). Three different colored filters (red, yellow, orange) were also tested in combination with the ALS. Results evidenced that visualization of the stains depended on four factors: the body fluid, the fabric material, the illuminating wavelength and the colored filter used (if any). Table 7.4 summarizes the results they achieved, indicating both the illuminating wavelength and filter that was applied to visualize each stain on each fabric.

Table 7.4. Stains clearly visible without any tool (blue). Stains do not detected in any way (red). Colored filters (R-red, O-orange, Y-yellow). Table adapted from [85].

Fabric	Blood	Blood 1/10	Blood 1/100	Semen	Urine	Saliva	Sweat
Patterned dishtowel				490 nm + O	460 nm + O		
Brown gunnysack	415 nm			440 nm + Y	440 nm + O		
Blue-grey pullover	415 nm + Y / NIR			415 nm + Y 460 nm + R			
White Kleenex			415 nm + Y	440 nm + O 460 nm + R	460 nm + O		
Grey wallpaper		415 nm + Y		460 nm + O 490 nm + R	460 nm + O		
Beige leather				415 nm + Y 460 nm + R	460 nm + O 490 nm + R	460 nm + R 490 nm + O	
Brown leather				415 nm + Y 460 nm + R	440 nm + Y		
Yellow bedclothes		415 nm + Y		440 nm + Y 490 nm + O	490 nm + R		
White T-shirt			440 nm + O	440 nm + O	440 nm + Y		
Blue towel	440 nm + Y / NIR	415 nm + O / NIR					
Light blue jeans pant		415 nm		440 nm + O	440 nm + Y	440 nm + Y	
Dark blue jeans pant	440 nm / NIR	415 nm		440 nm + Y			
Blue T-shirt		415 nm	415 nm	440 nm + Y	440 nm + Y		
Grey carpet	NIR	570 nm + R	415 nm	415 nm + Y 460 nm + O	415 nm + O		
Grey needlepunch				440 nm + O			

Brown microfiber	490 nm + R / NIR			415 nm + Y 460 nm + R			
Dark blue jersey	415 nm + R / NIR	415 nm		440 nm + Y			
Red textile	415 nm + Y / NIR			440 nm + Y			
Red textile				440 nm + Y			
Purple textile							
Brown PVC		415 nm		415 nm + O 490 nm + R			
Black wallpaper	415 nm / NIR			415 nm + Y 440 nm + O	460 nm + O		
White wallpaper			460 nm + O	460 nm + O 490 nm + R	440 nm + Y 460 nm + O	460 nm + O	
White leatherette				415 nm + O 460 nm + R	All	415 nm + Y	490 nm + O
Red leatherette		550 nm		415 nm + Y 460 nm + R	415 nm + O		
Brown leatherette				415 nm + Y	440 nm + O		
Beige linoleum				570 nm + R	415 nm		
Grey linoleum			415 nm	440 nm + Y	415 nm 460 nm + O	440 nm	
Blue glove			415 nm	440 nm + O			

- *Infrared spectroscopy*

As evidenced in the previous study, NIR wavelengths are often tested together with visible wavelengths for detecting stains of body fluids. In fact, most publications included in the infrared section of the previous review referred to NIR rather than MIR region. Furthermore, besides those publications previously summarized in the review, the efficacy of NIR wavelengths for the detection of blood stains were also verified and reported by different authors [86-89] (previously missed). Concretely, Raymond and Hall verified that contrast between blood and dark-surfaces in real violent scenes was maximized when using NIR wavelengths (900 nm), instead of visible light [86]. Albanese and Montes improved the limit of detection of visualization of diluted blood stains down to 1/32 by using NIR photography (<900 nm) in high dynamic range, which involves the collection and combination of several pictures taken at different light exposures (under-, normal, and overexposed) [87]. Farrar *et al.*

demonstrated the capability of NIR photography (>820nm) to assist in the detection of bloodstains in painted-over bloodstains beneath up to six layers of paint [88]. Finally, Schuler *et al.* proved the suitability of NIR-HSI (from 650 to 1100 nm) to visualize blood stains in black surfaces that were invisible to the naked eye in the visible range [89].

After 2015, the published research focused on studying and improving the detection of stains of body fluids using IR spectroscopy (either NIR-HSI or MIR-FTIR) has notably increased as evidenced by the high number of publications within this period (2015-2018), which exceeds the number of publications before 2015. As previously indicated, our group accomplished a modest small part of such research [68-72], and thus it will not be further discussed in this chapter. On the contrary, the significant advances achieved in the identification of body fluids using IR spectroscopy do not accomplished by our group are indeed revised.

Regarding NIR spectroscopy, Zhang *et al.* [90] used a NIR spectrometer working from 900 to 1700 nm to successfully identify blood from different species (human, macaque and mouse). Spectral differences between species were not intense enough to distinguish them visually, but significant enough to unequivocally classify them using multivariate PLS-DA analysis. One year later (in 2017), Pereira *et al.* [91] also used a NIR spectrometer within the range 900-1700 nm combined with different multivariate analysis (including PCA, SIMCA and PLS-DA) to unequivocally identify and discriminate human blood from animal (cat/dog) blood and other common potential false positive substances (including red wine and pepper sauce). Moreover, authors performed these studies by depositing blood stains on four different surfaces (porcelain, ceramic, glass and metal).

Unlike the two previous studies, Silva et al. [92] focused on the detection of semen stains on ten different colored fabrics using NIR-HSI from 900 to 2500 nm and comparing different multivariate models (including PCA, MCR-ALS, PLS-DA, sPLS-DA and SVM-DA). Concretely, white/black/green/red/yellow cotton, and white/beige fabrics (made of cotton, satin or cotton-polyester) were studied. In addition, the selectivity of NIR-HSI for human semen stains was assessed taking into consideration the number of false positive identifications when also analysing stains of lubricants, breast milk, and animal semen (horse and goat). According to the results, MCR-ALS provided better results than PCA

in the presumptive visualization of stains on fabrics, while sPLS-DA was the most appropriate method to unequivocally identify and discriminate human semen. Figure 7.5 shows the visualization of semen stains using MCR-ALS.

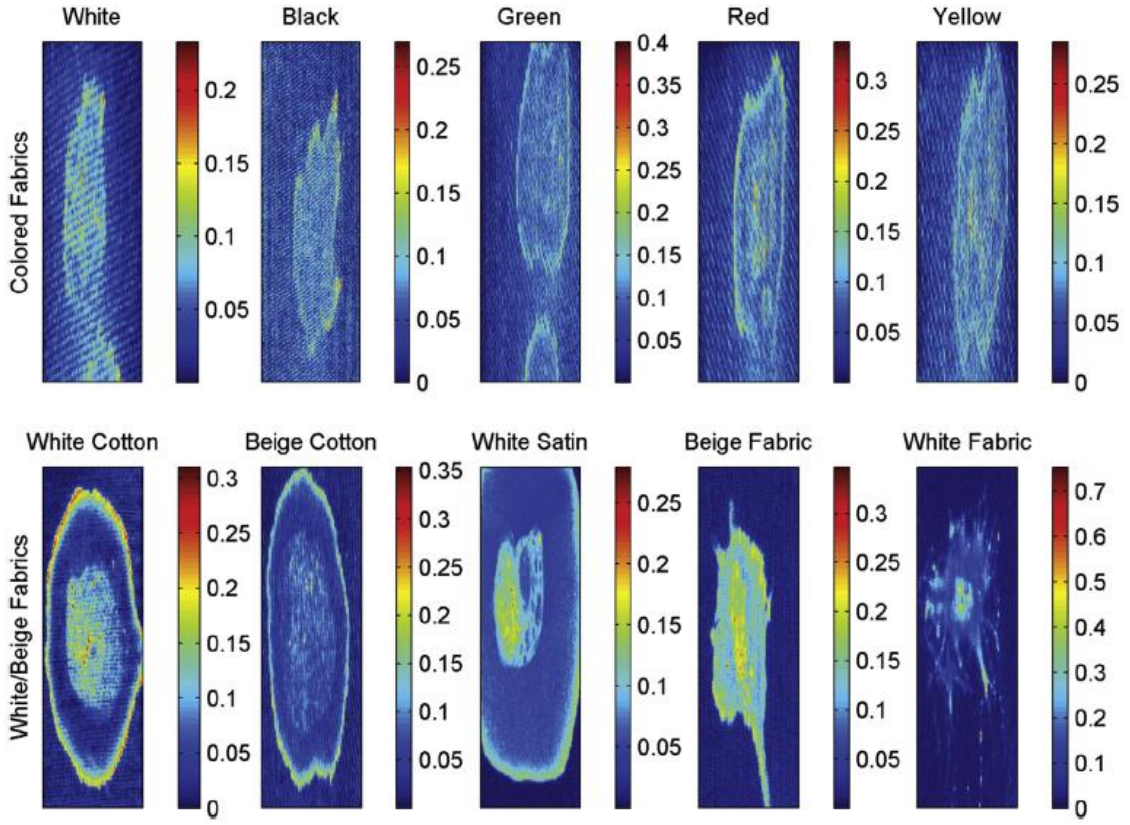

Figure 7.5. Chemical-distribution maps of semen stains using MCR-ALS model for each fabric [92].

Regarding MIR-FTIR spectroscopy, most published studies has used the ATR mode (rather than transmission or external reflection modes). In 2015, Orphanou [93] investigated the discrimination of blood, saliva, semen and vaginal secretions by directly placing body fluids onto the ATR and waiting until they were dry (5h). The FTIR spectra obtained for each body fluid was later interpreted in terms of vibrational bands assignment. Interestingly, the major spectral differences were due to amide I and amide II bands from proteins (which were located within 1700-1500 cm^{-1}). The four body fluids have different protein composition, which provides significant spectral differences in their FTIR spectra. Actually, the visual comparison of the ATR-FTIR spectra of blood, saliva, semen and vaginal fluid (especially within the amide region) was enough to discriminate the four body fluids. Nevertheless, it should be noted that pure body fluids were analysed (in the absence of an interfering substrate).

Also in 2015, ATR-FTIR spectroscopy was tested for blood species identification. Particularly, Mistek and Lednev [94] accomplished the discrimination between human, cat, dog and chicken blood stains with 100% accuracy when using PLS-DA multivariate analysis. Blood stains were prepared on glass slides and allowed to dry overnight before being analysed. Interestingly, the same research group had demonstrated some years before the discrimination of blood species using Raman spectroscopy [49], in such a way that the current demonstration of the capability of ATR-FTIR to also discriminate human blood from animal blood is a significant proof of the complementarity of both techniques in the field of body fluids detection.

In fact, this was also verified by Quinn and Elkins [95], who demonstrated that ATR-FTIR spectroscopy was capable to discriminate menstrual from venous blood (a result previously achieved by Raman [63]). Particularly, the IR discrimination between menstrual and venous blood was mostly based on the characteristic IR band at 1039 cm^{-1} found in menstrual blood (attributed to phosphoric acid). In addition, Quinn and Elkins also accomplished the discrimination of semen, saliva and breast-milk, according to their IR spectral differences, which were mostly attributed to proteins. Visual discrimination of the FTIR spectra of body fluids was straightforward when comparing pure body fluids (directly placed and dried onto the ATR). Nonetheless, those spectral differences were still perceptible to the naked eye when comparing the stains of body fluids on different surfaces (including cotton, nylon, wood, paper and glass). This result evidences the low interference that surface materials provide when using FTIR spectroscopy.

- *Raman spectroscopy*

As revised in the previous review, the section about Raman spectroscopy for identification of body fluids was the most extensive, and gathered the highest number of published studies, mainly due to the prolific research accomplished by Lednev and colleagues. In fact, another study, published by them in 2013, which was missed in the previous revision, should be appended. In that study [96], Raman spectroscopy was reported to be suitable to identify not only pure blood, but also blood stains on different fabrics (including tile, cotton and denim). Different wavelength lasers (including 407, 458, 488, 514, 647 and 785

nm) were tested. While the laser at 407 nm (the most energetic) was the optimum to characterize pure blood, it was useless in the detection of blood stains on cotton due to the extreme fluorescence of cotton. In fact, the optimum laser for the detection of blood stains on cotton was the 785 nm laser, despite having been one of the worst laser-wavelengths for the Raman characterization of pure blood. Positively, cotton substrate did not display fluorescence when using the 785 nm laser, and the Raman characteristic bands of cotton were easily subtracted from the Raman spectra of blood stains. This way, the Pearson's correlation coefficients obtained between pure blood and blood stains (after cotton subtraction) exceeded 0.99, clearly demonstrating the positive detection of blood. Diluted blood stains (down to 1/60) were also identified on cotton, though moderate Pearson's correlation coefficients (>0.6) were achieved.

Concerning the current update comprising the last four years, most of the published research dealing with the identification of body fluids using Raman spectroscopy has continued to be led by Lednev's research group. In brief, besides their work on blood stains aging [97, 98], and some reviews [99, 100], they have accomplished relevant advances in four main topics: the improvement in the detection of blood stains [101], the discrimination of body fluids [102], the discrimination of human from animal blood [103, 104], and the sex/race determination of stains of blood, semen or saliva [105-108].

Concerning the detection of blood stains, Muro and Lednev [101] had a creative idea to determine the limit of detection using Raman microscopy. Contrarily to the typical method when determining the LOD, which involves the preparation of diluted blood stains, Muro and Lednev focused on proving the detection of an individual red blood cell. For that, they took advantage of the capability of Raman microscopy to perform the microscopic (100×) visualization of a red blood cell and the collection of its Raman spectra simultaneously. Interestingly, the Raman spectrum of individual red blood cells were similar to that of pure blood, which is mostly attributed to hemoglobin. According to authors, an individual red blood cell is 5000 times smaller than the minimum amount of blood required to perform DNA analysis, in such a way that every trace of blood suitable enough for DNA testing (*i.e.* that contains multiple red blood cells), can be detected by Raman microscopy.

Regarding the discrimination of body fluids, a recent study [102] reminding the capability of Raman spectroscopy to differentiate pure blood, semen, saliva,

vaginal fluid and sweat has been published, which corroborates their previous study published five years before [58]). Concretely, in this last study, the discrimination of the five body fluids is improved by using advanced multivariate classification analysis such as PLS-DA and SVM-DA.

Similarly, the previous study gathered in the revision [64], which preliminary evidenced the capability of Raman spectroscopy to differentiate human blood from other 11 species' blood, has been improved by the application of an advanced classification model (PLS-DA) [103]. According to the results, no false positive/negative identification for human blood occurred, but only true positive identification. Blood from neither cat, dog, horse, pig, rabbit, rat, mouse, opossum, raccoon, chicken, nor cow were confused with human blood. Furthermore, few years later, this methodology (based on Raman spectroscopy coupled to multivariate PLS-DA classification) has been successfully updated by including six more species (deer, elk, ferret, fish, macaque and chimpanzee) [104]. Concretely, the ROC curve associated to the Raman-PLS-DA model displayed 99% accuracy in correctly predicting human/non-human blood samples used for testing.

The sex determination of body fluids using Raman spectroscopy is also a remarkable breakthrough accomplished by Lednev and colleagues (particularly for saliva [105] and blood [106]). As expected, the average Raman spectra of saliva or blood were visually undistinguishable between male and female. Positively, the combination of Raman spectroscopy and advanced multivariate classification analysis (including SVM-DA and artificial neuron networks ANN) have enabled the accurate differentiation of samples of saliva [105] and blood [106] from male/female donors (training data set), as well as the correct sex determination (>92%) of the donors of saliva/blood samples used for testing (test data set).

In the same vein, the race differentiation of blood [107] and semen [108] samples between Caucasian/Black donors using Raman spectroscopy and SVM-DA has been reported. In brief, 83% probability of correct race classification was obtained for blood samples while 100% of tested semen samples were correctly classified as either Caucasian or Black.

In addition to the research accomplished by Lednev and colleagues, other authors have also published (within 2015-2018) occasional but relevant

advances in Raman identification of body fluids. Fujihara *et al.* [109] also verified the capability of portable Raman spectroscopy combined with chemometrics (PCA) to discriminate human blood from other 10 species' blood including chicken, rabbit, horse, mouse, rat, cat, dog, pig, cow and sheep. Moreover, authors reported that discrimination between species' blood using Raman-PCA was achievable after three months of bloodstains aging (the maximum time they tested). On the contrary, Feine *et al.* [110] focused on the Raman identification of semen, and its discrimination from urine. Particularly, they examined the capability of Raman spectroscopy to further confirm/dismiss the semen identification previously accomplished by PSA test. Though PSA immunoassay is a confirmatory test for PSA, PSA is not exclusively found in semen, but also in urine (from male). Consequently, PSA test is not adequate to discriminate between semen and urine. This was evidenced by the fact that either semen or urine stains analysed by Feine *et al.* were positive to PSA. Positively, the posterior Raman analysis of the PSA-positive stains enabled to discriminate between semen and urine according to their different Raman spectra. Conclusively, author suggest that Raman spectroscopy is highly useful in combination with PSA test to further discriminate between semen and urine.

Finally, Atkins *et al.* [111] have recently published an outstanding revision about the Raman characterization of blood and blood components (plasma, red cells or erythrocytes, white cells or leucocytes, and platelets). The revision thoroughly covers every topic in which blood or blood components have been analysed by Raman spectroscopy (including not only the forensic identification of blood, but also the biochemical analysis of blood components and/or the medical analysis of blood in search of certain diseases). In addition to conventional Raman spectroscopy, the revision also comprises those publications using SERS, from which the study accomplished by Premasiri *et al.* [112] about the SERS characterization of whole blood, blood plasma, and red blood cells, is a notable example.

- *Mass spectrometry*

The forensic investigation of the identification of body fluids using mass spectrometry practically emerged at the time at which the non-updated revision was written, as evidenced by the fact that only one publication had been

published by that time. Positively, within the last four years, the research focused on the identification of body fluids by MS has grown significantly. Legg *et al.* [113] accomplished remarkable advances by studying and proposing a list of highly specific protein biomarkers to discriminate saliva, urine, seminal fluid, vaginal fluid, pheripheral blood, and menstrual fluid, within each other. In brief, from the hundreds of proteins they identified when analysing the six body fluids by HPLC-QTOF, authors proposed focusing on 29 protein markers. As an example, they proposed semenogelin, prolactin, PSA, and acid phosphatase for semen; cystatin and statherin for saliva; cornulin, involucrin, and periplakin for vaginal fluid; osteopontin and uromodulin for urine; hemoglobin and hemopoxin for peripheral blood; and calpastatin for menstrual fluid.

Similarly, Igoh *et al.* [114] used HPLC-TOF to discriminate the specific proteins of nasal fluid, saliva, urine, semen, sweat, and vaginal fluid; with the main aim of finding highly specific protein markers for vaginal fluid. To this respect, two human small proline-rich protein isoforms (with m/z 17237±2 and 18063±2), and a human fatty acid-binding protein (with m/z 15075±1) were exclusively detected in vaginal fluid, in such a way that they can be used as specific protein markers for vaginal fluid.

In a further step, Kamanna *et al.* [115] identified stains of blood, semen, urine, and saliva on different fabrics (cotton, nylon, and cellulose-acetate), using MALDI-TOF through the detection of specific protein markers for each body fluid. Concretely, hemoglobin was used as marker for blood; semenogelin, PSA and acid phosphatase for semen; uromodulin for urine; and α-amylase for saliva. Furthermore, they successfully detected the blood protein markers (hemoglobin (both α/β subunits) and heme group) in blood stains of up to 11-years-old. This result evidences the stability and persistence of proteins even in old body fluid stains, which encourages the detection of protein markers to identify stains of body fluids.

Conclusions and future trends

Spectrometric techniques are emerging tools for the forensic analysis of body fluids. In the last century, the fluorescence of some body fluids, such as semen and saliva under UV light, was discovered. This discovery has been used by forensic practitioners to detect traces of body fluids.

From the revision of the research up to 2014, main conclusions and future trends were:

All studies reviewed based on UV-Vis radiation concluded that it is possible to detect body-fluid stains, but also reported that it is difficult to confirm their presence. This limitation is due to the limited information that UV-Vis and fluorescence emission provides, which is insufficient to differentiate among similar stains. The same applies to X-ray fluorescence, which is based on elemental analysis of the body fluid. Because of these limitations, the potential of other spectrometric techniques has been explored in order to analyse and to differentiate between body fluids.

In spite of the high potential of IR spectroscopy for identification of compounds present in samples, it has scarcely been applied in body-fluid samples. Almost all the studies reviewed were focused on analysing blood stains.

In other work, in addition to blood, stains of semen, saliva, vaginal fluid and urine were subjected to preliminary analysis, using only one stain per fluid. Further analyses are needed to establish the IR spectral signature of each body fluid, which is necessary to identify and to characterize them.

The application of Raman spectroscopy to analyse and to differentiate body fluids has been investigated more deeply than has IR spectroscopy, mainly due to the works of the Lednev's team. The Raman spectral signatures of blood, semen, saliva, vaginal fluid and sweat were established by statistical procedures. The identification and the classification of these body fluids were also accomplished by mathematical methods of multivariate analysis. In these works, several stains per fluid and stains from few different donors were analysed.

NMR and MS recently appeared as promising techniques in the investigation of body fluids. Both techniques count on one publication each one where a very complete study reflects the potential of each technique. The NMR study discriminated between blood, semen, saliva and urine by PCA, while the MS study demonstrated its great sensitivity for blood, semen and saliva fluids. However, NMR and MS require sample treatment prior to analysis, which makes them more time-consuming than UV-Vis, IR and Raman spectroscopy.

This review shows the evolution of these emerging analytical techniques, mainly IR and Raman spectroscopy, for the forensic analysis of body fluids.

For the revision updated for 2015-2018, main conclusions revealed that:

The forensic identification of stains of body fluids using spectrometric techniques has been an increasingly active research field within the period 2015-2018.

Some studies focused on the presumptive detection of stains of body fluids using either ALS or HSI (working in the UV-Vis range) have been reported. It is not perceived neither an increase nor a decrease in the rate of publications dealing with UV-Vis and body fluids.

On the contrary, the research focused on identification of body fluids using IR spectroscopy (both NIR and MIR-FTIR spectroscopy) has notably increased within the last four years.

Raman spectroscopy has continued to be as prolific as it was some years before (mainly due to the research accomplished by Lednev and colleagues).

In addition, a noticeable increase has been observed within this period for the publications concerning identification of body fluids using MS.

References

[1] E. Locard, L'enquête criminelle et les Méthodes scientifiques, 1920.

[2] K. Virkler, I.K. Lednev, Analysis of body fluids for forensic purposes: from laboratory testing to non-destructive rapid confirmatory identification at a crime scene, Forensic Sci. Int. 188 (2009) 1-17.

[3] A.R.W. Jackson, J.M. Jackson, The examination of body fluids, in: A.R.W. Jackson, J.M. Jackson (Editors), Forensic Science, Pearson Prentice Hall, Harlow, England, 2008, pp. 115-136.

[4] R. Li, Forensic serology, in: L. Kobilinsky (Editor), Forensic Chemistry Handbook, Wiley, New Jersey, 2012, pp. 269-290.

[5] P. Scano, E. Locci, A. Noto, G. Navarra, F. Murgia, M. Lussu, et al., 1H NMR metabolite fingerprinting as a new tool for body fluid identification in forensic science, Magn. Reson. Chem. 51 (2013) 454-462.

[6] M. Bauer, RNA in forensic science, Forensic Sci. Int. Genet. 1 (2007) 69-74.

[7] J. Juusola, J. Ballantyne, Messenger RNA profiling: a prototype method to supplant conventional methods for body fluid identification, Forensic Sci. Int. 135 (2003) 85-96.

[8] C. Haas, B. Klesser, A. Kratzer, W. Bär, mRNA profiling for body fluid identification, Forensic Sci. Int. Genet. Suppl. Series 1 (2008) 37-38.

[9] J.H. An, K. Shin, W.I. Yang, H.Y. Lee, Body fluid identification in forensics, BMB Rep. 45 (2012) 545-553.

[10] K. Watanabe, Y. Iwashima, T. Akutsu, K. Sekiguchi, K. Sakurada, Evaluation of a co-extraction method for real-time PCR-based body identification and DNA typing, Leg. Med. 16 (2014) 56-59.

[11] J. Juusola, J. Ballantyne, Multiplex mRNA profiling for the identification of body fluids, Forensic Sci. Int. 152 (2005) 1-12.

[12] R.I. Fleming, S.A. Harbison, The development of a mRNA multiplex RT-PCR assay for the definitive identification of body fluids, Forensic Sci. Int. Genet. 4 (2010) 244-256.

[13] S. Bell, Instrumentation, in: S. Bell (Editor), Forensic Chemistry, Pearson, New Jersey, 2006, pp. 132-211.

[14] A. Koçak, The Role of Vibrational Spectroscopy in Forensic Chemistry, in: L. Kobilinsky (Editor), Forensic Chemistry Handbook, Wiley, New Jersey, 2012, pp. 251-268.

[15] N.N. Daéid, Review papers, 17th INTERPOL international forensic science managers symposium, Lyon, France, 2013. 280-610.

[16] F.P. Smith, Handbook of Forensic Drug Analysis, Elsevier, 2005.

[17] D.E. Bugay, Characterization of the solid-state: spectroscopic techniques, Adv. Drug Deliv. Rev. 48 (2001) 43-65.

[18] A.G. Ryder, G.M. O'Connor, T.J. Glynn, Identifications and quantitative measurements of narcotics in solid mixtures using near-IR raman spectroscopy and multivariate analysis, J. Forensic Sci. 44 (1999) 1013-1019.

[19] M.L. Smith, S.P. Vorce, J.M. Holler, E. Shimomura, J. Magluilo, A.J. Jacobs, et al., Modern instrumental methods in forensic toxicology, J. Anal. Toxicol. 31 (2007) 237-253.

[20] H.R.H. Ali, Non-invasive in situ identification and band assignments of diazepam, flunitrazepam and methadone hydrochloride with FT-near-infrared spectroscopy, Forensic Sci. Int. 206 (2011) 87-91.

[21] J. Yinon, Counterterrorist Detection Techniques of Explosives, Elsevier, Amsterdam, The Netherlands, 2007, pp. 41-366.

[22] J.I. Steinfeld, J. Wormhoudt, Explosives detection: a challenge for physical chemistry, Annu. Rev. Phys. Chem. 49 (1998) 203-232.

[23] D.S. Moore, Instrumentation for trace detection of high explosives, Rev. Sci. Instrum. 75 (2004) 2499-2512.

[24] S. Wallin, A. Pettersson, H. Östmark, A. Hobro, Laser-based standoff detection of explosives: a critical review, Anal. Bioanal. Chem. 395 (2009) 259-274.

[25] J.S. Caygill, F. Davis, S.P.J. Higson, Current trends in explosive detection techniques, Talanta 88 (2012) 14-29.

[26] N. Vandenberg, R.A.H. van Oorschot, The use of polilight in the detection of seminal fluid, saliva, and bloodstains and comparison with conventional chemical-based screening tests, J. Forensic Sci. 51 (2006) 361-370.

[27] M.J. Auvdel, Comparison of laser and ultraviolet techniques used in the detection of body secretions, J. Forensic Sci. 32 (1987) 326-345.

[28] M.J. Auvdel, Comparison of laser and high-intensity quartz arc tubes in the detection of body secretions, J. Forensic Sci. 33 (1988) 929-945.

[29] S. Seidl, R. Hausmann, P. Betz, Comparison of laser and mercury-arc lamp for the detection of body fluids on different substrates, Int. J. Legal Med. 122 (2008) 241-244.

[30] M. Stoilovic, Detection of semen and blood stains using polilight as a light source, Forensic Sci. Int. 51 (1991) 289-296.

[31] H.J. Kobus, E. Silenieks, J. Scharnberg, Improving the effectiveness of fluorescence for the detection of semen stains on fabrics, J. Forensic Sci. 47 (2002) 819-823.

[32] K.A. Santucci, D.G. Nelson, K.K. McQuillen, S.J. Duffy, J.G. Linakis,Wood's lamp utility in the identification of semen, Pediatrics 104 (1999) 1342-1344.

[33] D.G. Nelson, K.A. Santucci, An alternate light source to detect semen, Acad. Emerg. Med. 9 (2002) 1045-1048.

[34] A. Fiedler, J. Rehdorf, F. Hilbers, L. Johrdan, C. Stribl, M. Benecke, Detection of Semen (human and boar) and saliva on fabrics by a very high powered UV-/VIS-Light source, Open Forensic Sci. J. 1 (2008) 12-15.

[35] L.S. Powers, C.R. Lloyd, Method and apparatus for detecting and imaging the presence of biological materials, U.S. Patent documents, 2007.

[36] N.S. Soukos, K. Crowley, M.P. Bamberg, R. Gillies, A.G. Doukas, R. Evans, et al., A rapid method to detect dried saliva stains swabbed from human skin using fluorescence spectroscopy, Forensic Sci. Int. 114 (2000) 133-138.

[37] J.Wang, M. Sowa, H.H. Mantsch, A. Bittner, H.M. Heise, Comparison of different infrared measurement techniques in the clinical analysis of biofluids, Trends Anal. Chem. 15 (1996) 286-296.

[38] A.C. Lin, H. Hsieh, L. Tsai, A. Linacre, J.C. Lee, Forensic applications of infrared imaging for the detection and recording of latent evidence, J. Forensic Sci. 52 (2007) 1148-1150.

[39] H. Brooke, M.R. Baranowski, J.N. McCutcheon, S.L. Morgan, M.L. Myrick, Multimode imaging in the thermal infrared for chemical contrast enhancement. Part 3: visualizing blood on fabrics, Anal. Chem. 82 (2010) 8427-8431.

[40] S.L. Morgan, M.L. Myrick, Rapid visualization of biological fluids at crime scenes using optical spectroscopy, report to the U.S. Department of Justice, 2011.

[41] K.M. Elkins, Rapid presumptive “fingerprinting” of body fluids and materials by ATR FT-IR spectroscopy, J. Forensic Sci. 56 (2011) 1580-1587.

[42] P.R. De Forest, R. Bucht, F. Kammerman, B. Weinger, L. Gunderson, Blood on black-enhanced visualization of bloodstains on dark surfaces, report to the U.S. Department of Justice, 2009.

[43] J. Finnis, J. Lewis, A. Davidson, Comparison of methods for visualizing blood on dark surfaces, Sci. Justice 53 (2013) 178-186.

[44] B. Venkatesh, S. Ramasamy, M. Mylrajan, R. Asokan, P.T. Manoharan, J.M. Rifkind, Fourier transform Raman approach to structural correlation in hemoglobin derivatives, Spectrochim. Acta A 55 (1999) 1691-1697.

[45] A.M.K. Enejder, T. Koo, J. Oh, M. Hunter, S. Sasic, M.S. Feld, et al., Blood analysis by Raman spectroscopy, Opt. Lett. 27 (2002) 2004-2006.

[46] K. DeWael, L. Lepot, F. Gason, B. Gilbert, In search of blood – detection of minute particles using spectroscopic methods, Forensic Sci. Int. 180 (2008) 37-42.

[47] K. Virkler, I.K. Lednev, Raman spectroscopy offers great potential for the nondestructive confirmatory identification of body fluids, Forensic Sci. Int. 181 (2008) e1-e5.

[48] I.K. Lednev, K. Virkler, Identification of body fluids using Raman spectroscopy, U.S. Patent documents, 2009.

[49] K. Virkler, I.K. Lednev, Blood species identification for forensic purposes using Raman spectroscopy combined with advanced statistical analysis, Anal. Chem. 81 (2009) 7773-7777.

[50] T. Coyle, N. Anwar, A novel approach to condom lubricant analysis: in-situ analysis of swabs by FT-Raman Spectroscopy and its effects on DNA analysis, Sci. Justice 49 (2009) 32-40.

[51] K. Virkler, I.K. Lednev, Raman spectroscopic signature of semen and its potential application to forensic body fluid identification, Forensic Sci. Int. 193 (2009) 56-62.

[52] K. Virkler, I.K. Lednev, Forensic body fluid identification: the raman spectroscopic signature of saliva, Analyst 135 (2010) 512-517.

[53] K. Virkler, I.K. Lednev, Raman spectroscopic signature of blood and its potential application to forensic body fluid identification, Anal. Bioanal. Chem. 396 (2010) 525-534.

[54] V. Sikirzhytski, K. Virkler, I.K. Lednev, Discriminant analysis of raman spectra for body fluid identification for forensic purposes, Sensors 10 (2010) 2869–2884.

[55] S. Boyd, M.F. Bertino, S.J. Seashols, Raman spectroscopy of blood samples for forensic applications, Forensic Sci. Int. 208 (2011) 124-128.

[56] A. Sikirzhytskaya, V. Sikirzhytski, I.K. Lednev, Raman spectroscopic signature of vaginal fluid and its potential application in forensic body fluid identification, Forensic Sci. Int. 216 (2012) 44-48.

[57] V. Sikirzhytski, A. Sikirzhytskaya, I.K. Lednev, Multidimensional Raman spectroscopic signature of sweat and its potential application to forensic body fluid identification, Anal. Chim. Acta 718 (2012) 78-83.

[58] V. Sikirzhytski, A. Sikirzhytskaya, I.K. Lednev, Multidimensional raman spectroscopic signatures as a tool for forensic identification of body fluid traces: a review, Appl. Spectrosc. 65 (2011) 1223-1232.

[59] V. Sikirzhytski, A. Sikirzhytskaya, I.K. Lednev, Advanced statistical analysis of Raman spectroscopic data for the identification of body fluid traces: semen and blood mixtures, Forensic Sci. Int. 222 (2012) 259-265.

[60] A. Sikirzhytskaya, V. Sikirzhytski, G. McLaughlin, I.K. Lednev, Forensic identification of blood in the presence of contaminations using raman microspectroscopy coupled with advanced statistics: effect of sand, dust, and soil, J. Forensic Sci. 58 (2013) 1141-1148.

[61] I.K. Lednev, Application of Raman spectroscopy for an easy-to-use, on-field, rapid, nondestructive, confirmatory identification of body fluids, report to the U.S. Department of Justice, 2012.

[62] S. Boyd, M.F. Bertino, D. Ye, L.S. White, S.J. Seashols, Highly Sensitive Detection of Blood by Surface Enhanced Raman Scattering, J. Forensic Sci. 58 (2013) 753-756.

[63] A. Sikirzhytskaya, V. Sikirzhytski, I.K. Lednev, Raman spectroscopy coupled with advanced statistics for differentiating menstrual and peripheral blood, J. Biophotonics 7 (2014) 59-67.

[64] G. McLaughlin, K.C. Doty, I.K. Lednev, Discrimination of human and animal blood traces via Raman spectroscopy, Forensic Sci. Int. 238 (2014) 91-95.

[65] J.I. Trombka, J. Schweitzer, C. Selavka, M. Dale, N. Gahn, S. Floyd, et al., Crime scene investigations using portable, non-destructive space exploration technology, Forensic Sci. Int. 129 (2002) 1-9.

[66] J.S. Schweitzer, J.I. Trombka, S. Floyd, C. Selavka, G. Zeosky, N. Gahn, et al., Portable generator-based XRF instrument for non-destructive analysis at crime scenes, Nucl. Instrum. Meth. B 241 (2005) 816-819.

[67] H. Yang, B. Zhou, H. Deng, M. Prinz, D. Siegel, Body fluid identification by mass spectrometry, Int. J. Legal Med. 127 (2013) 1065-1077.

[68] F. Zapata, M.A. Fernández de la Ossa, C. García-Ruiz, Differentiation of body fluids stains on fabrics by external reflection FTIR spectroscopy and chemometrics, Appl. Spectrosc. 70 (2016) 654-665.

[69] F. Zapata, F.E. Ortega-Ojeda, C. García-Ruiz, Revealing the location of semen, vaginal fluid and urine in stained evidence through near infrared chemical imaging, Talanta 166 (2017) 292-299.

[70] F. Zapata, I. Gregório, C. García-Ruiz, Body fluids and spectroscopic techniques in forensics: a perfect match?, J. Forensic Med. 1 (2015) 1-7.

[71] I. Gregório, F. Zapata, C. García-Ruiz, Analysis of human bodily fluids on superabsorbent pads by ATR-FTIR, Talanta 162 (2017) 634-640.

[72] I. Gregório, F. Zapata, M. Torre, C. García-Ruiz, Statistical approach for ATR-FTIR screening of semen in sexual evidence, Talanta 174 (2017) 853-857.

[73] G. Zadora, A. Menżyk, In the pursuit of the holy grail of forensic science – Spectroscopic studies on the estimation of time since deposition of bloodstains, TrAC Trends Anal. Chem. 105 (2018) 137-165.

[74] J. Wawryk, M. Odell, Fluorescent identification of biological and other stains on skin by the use of alternative light sources, J. Clin. Forensic Med. 12 (2005) 296-301.

[75] C.A. Lincoln, P.M. McBride, G.R. Turbett, C.D. Garbin, E.J. McDonald, The use of an alternative light source to detect semen in clinical forensic medical practice, J. Clin. Forensic Med. 13 (2006) 215-218.

[76] W.C. Lee, B.E. Khoo, A.F.L. Abdullah, Z.B.A. Aziz, Statistical evaluation of alternative light sources for bloodstain photography, J. Forensic Sci. 58 (2013) 658-663.

[77] W. Lee, B. Khoo, Forensic light sources for detection of biological evidences in crime scene investigation: A review, Malaysian J. Forensic Sci. 1 (2010) 17-27.

[78] G.E. Miranda, F.B. Prado, F. Delwing, E.D. Júnior, Analysis of the fluorescence of body fluids on different surfaces and times, Sci. Justice 54 (2014) 427-431.

[79] B. Li, P. Beveridge, W.T. O'Hare, M. Islam, The estimation of the age of a blood stain using reflectance spectroscopy with a microspectrophotometer, spectral pre-processing and linear discriminant analysis, Forensic Sci. Int. 212 (2011) 198-204.

[80] B. Li, P. Beveridge, W.T. O'Hare, M. Islam, The age estimation of blood stains up to 30 days old using visible wavelength hyperspectral image analysis and linear discriminant analysis, Sci. Justice 53 (2013) 270-277.

[81] B. Li, P. Beveridge, W.T. O'Hare, M. Islam, The application of visible wavelength reflectance hyperspectral imaging for the detection and identification of blood stains, Sci. Justice 54 (2014) 432-438.

[82] S. Cadd, B. Li, P. Beveridge, W.T. O'Hare, A. Campbell, M. Islam, The non-contact detection and identification of blood stained fingerprints using visible wavelength reflectance hyperspectral imaging: Part 1, Sci. Justice 56 (2016) 181-190.

[83] S. Cadd, B. Li, P. Beveridge, W.T. O'Hare, A. Campbell, M. Islam, The non-contact detection and identification of blood stained fingerprints using visible wavelength reflectance hyperspectral imaging: Part II effectiveness on a range of substrates, Sci. Justice 56 (2016) 191-200.

[84] S. Cadd, B. Li, P. Beveridge, W.T. O'Hare, A. Campbell, M. Islam, A comparison of visible wavelength reflectance hyperspectral imaging and Acid Black 1 for the detection and identification of blood stained fingerprints, Sci. Justice 56 (2016) 247-255.

[85] V. Sterzik, S. Panzer, M. Apfelbacher, M. Bohnert, Searching for biological traces on different materials using a forensic light source and infrared photography, Int. J. Legal Med. 130 (2016) 599-605.

[86] M.A. Raymond, R.L. Hall, An interesting application of infra-red reflection photography to blood splash pattern interpretation, Forensic Sci. Int. 31 (1986) 189-194.

[87] J. Albanese, R. Montes, Latent evidence detection using a combination of Near Infrared and high dynamic range photography: An example using bloodstains, J. Forensic Sci. 56 (2011) 1601-1603.

[88] A. Farrar, G. Porter, A. Renshaw, Detection of latent bloodstains beneath painted surfaces using reflected infrared photography, J. Forensic Sci. 57 (2012) 1190-1198.

[89] R.L. Schuler, P.E. Kish, C.A. Plese, Preliminary observations on the ability of hyperspectral imaging to provide detection and visualization of bloodstain patterns on black fabrics, J. Forensic Sci. 57 (2012) 1562-1569.

[90] L. Zhang, S. Zhang, M. Sun, Z. Wang, H. Li, Y. Li, G. Li, L. Lin, Blood species identification using Near-Infrared diffuse transmitted spectra and PLS-DA method, Infrared Phys. Technol. 76 (2016) 587-591.

[91] J.F.Q. Pereira, C.S. Silva, M.J.L. Vieira, M.F. Pimentel, A. Braz, R.S. Honorato, Evaluation and identification of blood stains with handheld NIR spectrometer, Microchem. J. 133 (2017) 561-566.

[92] C.S. Silva, M.F. Pimentel, J.M. Amigo, R.S. Honorato, C. Pasquini, Detecting semen stains on fabrics using near infrared hyperspectral images and multivariate models, TrAC Trends Anal. Chem. 95 (2017) 23-35.

[93] C. Orphanou, The detection and discrimination of human body fluids using ATR FT-IR spectroscopy, Forensic Sci. Int. 252 (2015) e10-e16.

[94] E. Mistek, I.K. Lednev, Identification of species' blood by attenuated total reflection (ATR) Fourier transform infrared (FT-IR) spectroscopy, Anal. Bioanal. Chem. 407 (2015) 7435-7442.

[95] A.A. Quinn, K.M. Elkins, The differentiation of menstrual from venous blood and other body fluids on various substrates using ATR FT-IR spectroscopy, J. Forensic Sci. 62 (2017) 197-204.

[96] G. McLaughlin, V. Sikirzhytski, I.K. Lednev, Circumventing substrate interference in the Raman spectroscopic identification of blood stains, Forensic Sci. Int. 231 (2013) 157-166.

[97] K.C. Doty, G. McLaughlin, I.K. Lednev, A Raman "spectroscopic clock" for bloodstain age determination: the first week after deposition, Anal. Bioanal. Chem. 408 (2016) 3993-4001.

[98] K.C. Doty, C.K. Muro, I.K. Lednev, Predicting the time of the crime: Bloodstain aging estimation for up to two years, Forensic Chem. 5 (2017) 1-7.

[99] K.C. Doty, I.K. Lednev, Raman spectroscopy for forensic purposes: Recent applications for serology and gunshot residue analysis, TrAC Trends Anal. Chem. 103 (2018) 215-222.

[100] S.R. Khandasammy, M.A. Fikiet, E. Mistek, Y. Ahmed, L. Halámková, J. Bueno, I.K. Lednev, Bloodstains, paintings, and drugs: Raman spectroscopy applications in forensic science, Forensic Chem. 8 (2018) 111-133.

[101] C.K. Muro, I.K. Lednev, Identification of individual red blood cells by Raman microspectroscopy for forensic purposes: in search of a limit of detection, Anal. Bioanal. Chem. 409 (2017) 287-293.

[102] C.K. Muro, K.C. Doty, L. Fernandes, I.K. Lednev, Forensic body fluid identification and differentiation by Raman spectroscopy, Forensic Chem. 1 (2016) 31-38.

[103] G. McLaughlin, K.C. Doty, I.K. Lednev, Raman spectroscopy of blood for species identification, Anal. Chem. 86 (2014) 11628-11633.

[104] K.C. Doty, I.K. Lednev, Differentiation of human blood from animal blood using Raman spectroscopy: A survey of forensically relevant species, Forensic Sci. Int. 282 (2018) 204-210.

[105] C.K. Muro, L. Fernandes, I.K. Lednev, Sex determination based on Raman spectroscopy of saliva traces for forensic purposes, Anal. Chem. 88 (2016) 12489-12493.

[106] A. Sikirzhytskaya, V. Sikirzhytski, I.K. Lednev, Determining gender by Raman spectroscopy of a bloodstain, Anal. Chem. 89 (2017) 1486-1492.

[107] E. Mistek, L. Halámková, K.C. Doty, C.K. Muro, I.K. Lednev, Race differentiation by Raman spectroscopy of a bloodstain for forensic purposes, Anal. Chem. 88 (2016) 7453-7456.

[108] C.K. Muro, I.K. Lednev, Race differentiation based on Raman spectroscopy of semen traces for forensic purposes, Anal. Chem. 89 (2017) 4344-4348.

[109] J. Fujihara, Y. Fujita, T. Yamamoto, N. Nishimoto, K. Kimura-Kataoka, S. Kurata, Y. Takinami, T. Yasuda, H. Takeshita, Blood identification and discrimination between human and nonhuman blood using portable Raman spectroscopy, Int. J. Legal Med. 131 (2017) 319-322.

[110] I. Feine, R. Gafny, I. Pinkas, Combination of prostate-specific antigen detection and micro-Raman spectroscopy for confirmatory semen detection, Forensic Sci. Int. 270 (2017) 241-247.

[111] C.G. Atkins, K. Buckley, M.W. Blades, R.F.B. Turner, Raman spectroscopy of blood and blood components, Appl. Spectrosc. 71 (2017) 767-793.

[112] W.R. Premasiri, J.C. Lee, L.D. Ziegler, Surface-enhanced Raman scattering of whole human blood, blood plasma, and red blood cells: cellular processes and bioanalytical sensing, J. Phys. Chem. B 116 (2012) 9376-9386.

[113] K.M. Legg, R. Powell, N. Reisdorph, R. Reisdorph, P.B. Danielson, Discovery of highly specific protein markers for the identification of biological stains, Electrophoresis 35 (2014) 3069-3078.

[114] A. Igoh, Y. Doi, K. Sakurada, Identification and evaluation of potential forensic marker proteins in vaginal fluid by liquid chromatography/mass spectrometry, Anal. Bioanal. Chem. 407 (2015) 7135-7144.

[115] S. Kamanna, J. Henry, N.H. Voelcker, A. Linacre, K.P. Kirkbride, Direct identification of forensic body fluids using matrix-assisted laser desorption/ionization time-of-flight mass spectrometry, Int. J. Mass Spec. 397-398 (2016) 18-26.

Chapter 8. Identification of stains of body fluids on fabrics using Infrared Spectroscopy

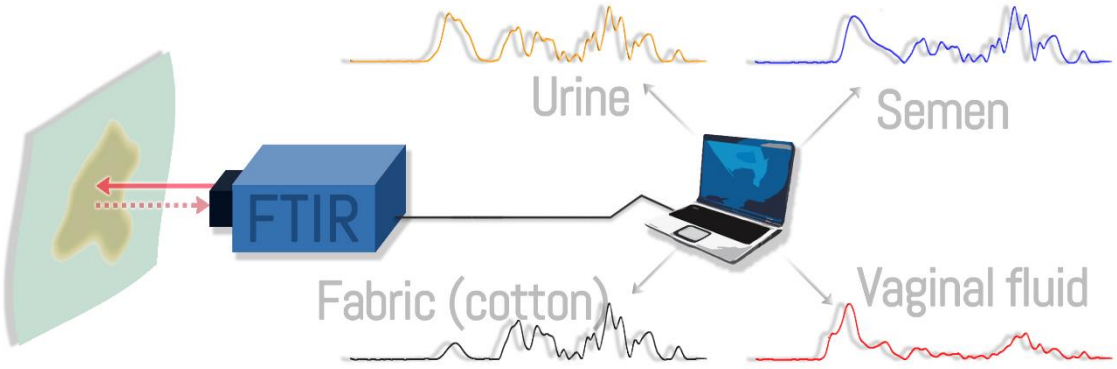

Main source:

Félix Zapata, M.A. Fernández de la Ossa, C. García-Ruiz, Differentiation of body fluids stains on fabrics by external reflection FTIR spectroscopy and chemometrics, *Applied Spectrosc.* 70 (2016) 654-665.

Abstract

Body fluids are evidence of great forensic interest due to the DNA extracted from them, which allows genetic identification of people. This study focuses on the discrimination among semen, vaginal fluid, and urine stains (main fluids in sexual crimes) placed on different colored cotton fabrics by external reflection Fourier transform infrared spectroscopy (FTIR) combined with chemometrics. Semen–vaginal fluid mixtures and potential false positive substances commonly found in daily life such as soaps, milk, juices, and lotions were also studied. Results demonstrated that the IR spectral signature obtained for each body fluid allowed its identification and the correct classification of unknown stains by means of principal component analysis (PCA) and soft independent modeling of class analogy (SIMCA). Interestingly, results proved that these IR spectra did not show any bands due to the color of the fabric and no substance of those present in daily life which were analysed, provided a false positive.

Introduction

Because DNA can be used for individual identification, body fluids have become extremely useful evidence in the forensic field. Stains of body fluids are subjected to different presumptive and confirmatory tests [1] prior to DNA analysis. The study of semen, vaginal fluid, and urine stains is particularly crucial because forensic investigators have to face them in sexual abuse cases. In these cases, fabric evidence stained by semen, vaginal fluid, or urine are commonly found. Semen has been studied for many years and the available confirmatory tests allow forensic practitioners to identify it in a stain [1, 2]. However, vaginal fluid and urine have been scarcely studied and nowadays they do not have available confirmatory tests. Both fluids usually appear in the victim's underwear mixed with semen, making the identification of DNA from semen traces left by the perpetrator difficult. Consequently, in these cases the genetic profile of the victim may be the only result obtained after performing the DNA extraction and DNA typing, even though the presence of semen in the stain has been verified by a confirmatory test. Therefore, it is a current forensic need to develop a methodology allowing to differentiate among semen, vaginal fluid, and urine samples in order to optimize the extraction of the DNA from the perpetrator.

The presumptive and confirmatory tests currently used by forensic crime investigators to identify these body fluid stains have several limitations and disadvantages [1, 2]. Therefore, other techniques, mainly spectroscopic techniques, have been evaluated for the identification of body fluids. These techniques present several attractive features as their nondestructive, non-invasive, fast, and portable nature, and their applicability to analyse multiple body fluids [2]. Ultraviolet visible (UV-Vis) spectroscopy was the first spectroscopic technique applied to the localization of body fluids stains [3, 4] and evolved to the alternate light sources (ALS), routinely used by forensic community. However, ALS lack selectivity, produce false positives [5], and have limitations on identifying stains on colored backgrounds [6, 7].

For these reasons, infrared (IR) wavelengths are being investigated by using IR and Raman spectroscopy in order to evaluate their application to the identification of body fluids. A large part of the studies is focused on analysing body fluids with clinical and medical purposes [8-15], instead of forensic aims. Although IR and Raman spectroscopy are accepted techniques at forensic

laboratories to analyse evidence such as drugs [16-18] and explosives [16, 19, 20], their application to the analysis of body fluids still remains challenging. Therefore, further investigation related to the identification of body fluids using IR and Raman spectroscopy must be accomplished in order to put it on practice for solving real forensic cases. Up to now, Raman spectroscopy has been mainly researched by Lednev's group [21]. As a summary of all their work, the representative and characteristic Raman spectra from blood, semen, saliva, vaginal fluid, and sweat have been established [22] and multivariate classification models which correctly classify unknown fluids, even in mixtures, have been developed [23, 24]. Stains of body fluids made on different fabrics such as glass slides, cotton, denim, or tile have also been analysed [25]. On the contrary, IR spectroscopy applied to the forensic identification of body fluids, has been less studied than Raman spectroscopy. Studies reported in literature were mainly focused on analysing blood stains [2], apart from two of them which were focused on several body fluids including blood, semen, saliva, vaginal fluid, and urine [26, 27]. In fact, the former was the first study where those five body fluids were analysed by attenuated total reflection (ATR) Fourier transform infrared spectroscopy (FT-IR) and it represented a preliminary research of body fluids by IR spectroscopy. Since only one stain and donor per body fluid were analysed in the reported work, further research using IR spectroscopy is necessary. Moreover, white 100% cotton was the unique fabric where stains were deposited and no chemometric methods were applied in order to extract information from the data [26]. Recently, a second study focused on the discrimination of blood, saliva, semen, and vaginal fluid by ATR FTIR has been published [27]. Results demonstrate the capability of ATR FTIR to distinguish these body fluids according to their characteristic FTIR spectrum. However, the study was accomplished by depositing the fresh body fluids on to the ATR stage and analysing them during different time intervals until they were completely dry [27]. Therefore, the challenge of identifying stains of these body fluids on real casework materials such as clothes remains.

Besides ATR FTIR spectroscopy, external reflection IR spectroscopy might be a useful novel methodology to differentiate stains of body fluids, especially when they are located on the surface of different materials including clothes. External reflection FTIR is also a nondestructive, non-invasive, fast, portable, and easy-to-use technique where no sample preparation is required. In addition, external reflection spectroscopy benefits from the fact that no contact between sample

and instrument is required to work, contrary to ATR where the contact sample-ATR crystal is essential. As consequence, external reflection can be potentially used for stand-off detection (at distance), especially the detection of samples which are difficult to be pressed against the ATR crystal. In particular, stains on clothes and other materials usually offer difficulties because of the formation of folds and creases which hinder a proper contact. Furthermore, the capability of detecting stains at some distance can potentially contribute to evidence recovery. External reflection spectroscopy is due to a combination of diffuse and specular reflection processes since, theoretically, the amount of reflection type occurring on the sample depends on the roughness of the sample surface. In addition, its combination with chemometric analyses such as principal component analysis (PCA) and soft independent modeling of class analogy (SIMCA) is a powerful strategy for spectra differentiation and classification. As consequence, our study focuses on analysing semen, vaginal fluid, and urine stains collected from several volunteers to establish the external reflection FT-IR spectral signature of stains of these body fluids on white cotton fabrics prior to their detection on colored cotton pieces from T-shirts and jeans; and their differentiation from daily products, which can potentially provide false positives by visual inspection. PCA and SIMCA models are applied to classify the experimental data and show if the spectral interpretation made visually can be corroborated.

Experimental

- *Samples*

The body fluids studied were human semen, vaginal fluid, and urine obtained from 10 anonymous donors (5 men, 5 women). Some cosmetic substances and foodstuffs including sunflower oil, cold cream, sunscreen, soap, milk, mayonnaise, lotions, toothpaste, soup, Vaseline, yogurt, orange juice, and pineapple juice were analysed in order to check potential false positives. Semen–vaginal fluid mixture stains made by adding fresh semen to both fresh and dry vaginal fluid stains, which were then completely dried overnight, were also analysed.

Samples were prepared by placing 0.6 mL of each body fluid (semen and urine), cosmetic substance, or foodstuff on pieces of 11 × 8 cm^2 cut from T-shirts and

jeans made of 100% cotton. Vaginal fluid samples were directly prepared by the donor placing the body fluid on the cotton pieces. In order to know the mass of body fluid which was deposited on the fabric and subsequently analysed in the dry stain, one stain of each body fluid was weighted just after the addition of body fluid and after drying, 24 h later. In summary, 76 stains (62 from body fluids and 14 from cosmetic substances and foodstuffs) with a diameter of approximately 2–3 cm were created in the middle of the mentioned cotton pieces. Specifically, stains of each body fluid came from five different donors as summarized in Table 8.1.

Table 8.1. Donors-stains distribution on fabrics.

Donor	Stains distribution on fabrics
1	3 stains of semen on white cotton
2	3 stains of semen on white cotton
3	3 stains of semen on white cotton
4	3 stains of semen on white cotton
5	3 stains of semen on white cotton
6	3 stains of vaginal fluid on white cotton
7	3 stains of vaginal fluid on white cotton
8	3 stains of vaginal fluid on white cotton
9	3 stains of vaginal fluid on white cotton
10	3 stains of vaginal fluid on white cotton
1	3 stains of urine on white cotton
2	3 stains of urine on white cotton
6	3 stains of urine on white cotton
7	3 stains of urine on white cotton
8	3 stains of urine on white cotton
1	5 stains of semen on coloured fabrics
6	5 stains of vaginal fluid on coloured fabrics
6	5 stains of urine on coloured fabrics

All stains were made on white cotton fabric except for those which were made on colored cotton fabrics including red, blue, green, black, and blue jeans. These stains were studied in order to test whether colored fabrics are problematic substrates when identifying stains of body fluids by external reflection IR spectroscopy. The statistical distribution of all the stains were subsequently visualized by PCA in order to study the differentiation of body fluids even in colored fabrics. Finally, the stains were divided in two groups. One of them was used to create the SIMCA classification model, which was subsequently applied to the second group used as a test set with the aim of classifying these stains. The first group included stains from four donors whereas the second group included stains from the fifth donor. Furthermore, the test set also included two independent semen–vaginal fluid mixtures and 14 stains of cosmetic substances and foodstuffs in order to check their classification by the SIMCA classification model.

All stains were dried completely overnight in a biological safety cabinet before being analysed.

The unstained cotton fabrics (white and colored) were also analysed to study the cotton response. Likewise, IR spectral signature of cotton was achieved and cotton was used in the PCA and SIMCA analyses.

- *Instrumentation for MIR Spectra Collection*

Infrared external reflection measurements were performed on a Bruker ALPHA FT-IR spectrometer (Ettlingen, Germany) using an ALPHA-R external reflection accessory equipped with the OPUS software version 7.2 (Bruker, Billerica, MA, USA). Log (1/R) spectra were recorded from 4000 to 400 cm^{-1} with a resolution of 4 cm^{-1} (data spacing 2.04 cm^{-1}) and signal averaged over 24 accumulations. The three-term Blackmann–Harris function was applied as an apodization function. The sampling spot, *i.e.* the diameter of the beam at the sample, was 5 mm. All stains were analysed in several places in order to ensure that the IR spectrum of body fluid was collected. For the stains on white fabrics, 10 random points along the stain were measured in order to cover different places along the visibly stained area. On the other hand, after noticing that all points provided almost the same spectra, only three random points were analysed for the stains on colored fabrics which were subsequently studied. All points were measured in triplicate. Data were saved as an Opus file for further analysis. All spectra were ratioed against the single beam spectrum measured from a gold-coated mirror. It was cleaned with alcohol wipes between samples. In addition, the transmission spectra of these body fluids were measured by replacing the external reflection accessory with the transmission one in order to know exclusively the spectrum of the body fluid (without cotton) and compare both types of spectra. Stains of these body fluids measured using transmission were prepared by following the same procedure previously explained, but depositing them on KBr plates instead of cotton. Unfortunately, vaginal fluid was not analysed using transmission because it could not be conveniently deposited on the KBr plate. Therefore, only semen and urine were analysed using transmission FTIR.

- *Data Treatment*

Infrared spectral measurements of dry stains were processed performing various treatments. In OPUS 7.2 a range of 800–2000 cm^{-1} was selected before

performing a rubber-band baseline correction [28] (n=64 points and 15 iterations) and a range normalization of 0–2 (intensity value). The rubber-band baseline correction consists of finding a convex envelope of the spectrum and subtracting the convex part of the envelope lying below the spectrum from the spectrum in the portion to be corrected [28]. These treated spectra were imported as a matrix form to The Unscrambler X 10.1 (CAMO Software, Oslo, Norway). Then, a smoothing task was performed to reduce the random noise, prior to the spectral differentiation of body fluids, using a Savitzky–Golay algorithm (polynomial order 2 and 15 smoothing points in a symmetric kernel). These values were selected because they provided the best results in the chemometric analyses after checking that no relevant spectral information was lost by applying the smoothing.

After the spectral treatment, the IR spectra of cotton, semen, vaginal fluid, and urine were studied. The main bands of the three body fluids appeared between 1500 and 1800 cm^{-1}, and the subsequent multivariate analyses PCA and SIMCA were performed considering this range from the spectra. First, PCA, an unsupervised technique of visualization, was performed using the nonlinear iterative partial least squares (NIPALS) algorithm, leverage correction, and the standardization 1/SDev. Interestingly, the typical standard deviation for the strongest bands in the spectra was 0.08 for cotton fabric, 0.25 for vaginal fluid, 0.07 for semen, and 0.13 for urine. In fact, PCA was performed to visualize how similar or different the spectra were and to obtain a first overview of the main sources of variability. Principal component analysis allowed the reduction of the matrix dimensions consisting of hundreds of wavenumber values from the spectra into three principal components (PC) without losing relevant information and showing them in graphical plots (scores). The distribution of samples in relation to PCs was based on loadings, which related wavenumber values (original variables) and new PCs. Both scores and loadings are necessary to explain the correlation between samples and PCs information.

Finally, a SIMCA classification procedure was performed establishing the four classes previously mentioned (cotton, semen, vaginal fluid, and urine). This procedure was achieved by calculating separately the PCA of each class in order to use each PCA to define the four classes in the SIMCA model. This process was mandatory since SIMCA is a modeling procedure of discrete classes where a rule which allows discriminating between the inclusion or non-inclusion of a

sample in a given class is needed, instead of a rule which discriminates among classes. Therefore, an unknown sample can be classified in one class, in no class, or even in several classes, because its inclusion in each class is checked separately. In order to perform the SIMCA model it was necessary to use some samples to create the model whereas the remaining samples were considered as test samples. The samples used to create the model (calibrating set) consisted of six samples of cotton (one sample from each colored cotton including the white one), 17 stains of semen, 17 stains of vaginal fluid, and 17 stains of urine (12 on white cotton from four different donors and five stains on each colored cotton). Note that every stain was analysed in several places, obtaining several spectra for each sample. These samples were divided into cotton, semen, vaginal fluid, and urine classes, and a PCA was calculated for each class by using the same parameters of the global PCA. The number of PCs considered for each class to create SIMCA were five for cotton, three for vaginal fluid, three for urine, and four for semen. This choice was selected because they were the number of PCs needed to explain in each class at least the 95% of the information contained in the data. Regarding the test set, those samples consisted of six samples of cotton (one from each color), three stains of semen, three stains of vaginal fluid, three stains of urine, 14 stains of cosmetics and foodstuff, and two stains of semen–vaginal fluid mixture. These three stains of each body fluid, which belonged to a fifth donor, were tested in order to validate the model for identifying stains of semen, vaginal fluid, and urine from other people besides the four donors considered to create the model. In fact, SIMCA was performed in order to check if the identification of unknown stains (even mixtures) was possible by means of an easy chemometric classification tool where discrete classes were defined by separate PCAs based on the IR spectral signature of each body fluid.

Results and Discussion

- *Determination of the Mass of Body Fluids Analysed in Dry Stains on Fabrics*

Two stains per body fluid were weighted before and after drying in order to determine the mass of body fluid analysed by external reflection FT-IR prior to perform their spectral characterization. The water content for the three body

fluids was also calculated. These results are summarized in Table 8.2. The approximate volume of 0.5 mL of semen and urine deposited to create the stains weighed around 500 mg. On the contrary, the amount of vaginal fluid deposited on the stains was less controlled because it was impossible to deposit a specific volume. However, by weighting these stains we could know the mass of vaginal fluid deposited in stains of that size, a mass which was in the range of 140–180 mg. After drying, the amount of sample weighted in each stain was around 20 mg of urine, 20-35 mg of vaginal fluid and around 41 mg of semen. That depended on the water content of body fluids, which was found to be around 91% for semen, 96% for urine, and a wider range of 80–86% for vaginal fluid, which notably changed depending on the day of the menstrual cycle.

Table 8.2. Summarized results about the mass of body fluids in stains on fabrics.

Stains	Mass before drying (mg)	Mass after drying (mg)	Water content	Content of non-volatile components
Semen 1	516.2 ± 0.2	42.5 ± 0.2	91.8%	8.2%
Semen 2	459.9 ± 0.2	40.8 ± 0.2	91.1%	8.9%
Urine 1	598.2 ± 0.2	22.3 ± 0.2	96.3%	3.7%
Urine 2	521.8 ± 0.1	16.4 ± 0.1	96.9%	3.1%
Vaginal fluid 1	141.3 ± 0.2	19.8 ± 0.2	86.0%	14.0%
Vaginal fluid 2	178.2 ± 0.2	35.1 ± 0.2	80.3%	19.7%

- *IR Characterization of Semen, Vaginal Fluid, and Urine Stains on Fabrics*

In order to determine the IR spectral signature of semen, vaginal fluid, and urine stains on white cotton fabrics, a spectral average of the 450 spectra measured for each fluid (which came from considering the 30 spectra from the 10 points in each stain along the 15 stains from the five donors) was calculated. These spectral signatures are shown in Figure 8.1. Since the stains of these fluids were made on cotton, the bands of cotton appeared in all spectra. Almost all these bands were located in the interval 800–1500 cm^{-1}. This interval was named "fabric range". As can be seen in Figure 8.1, specific bands for semen, vaginal fluid, and urine were also observed in the spectra, specifically in the interval 1500–1800 cm^{-1}, which was designated as "ID range". The main bands of cotton as well as the specific bands of urine, semen, and vaginal fluid were indicated in Figure 8.1.

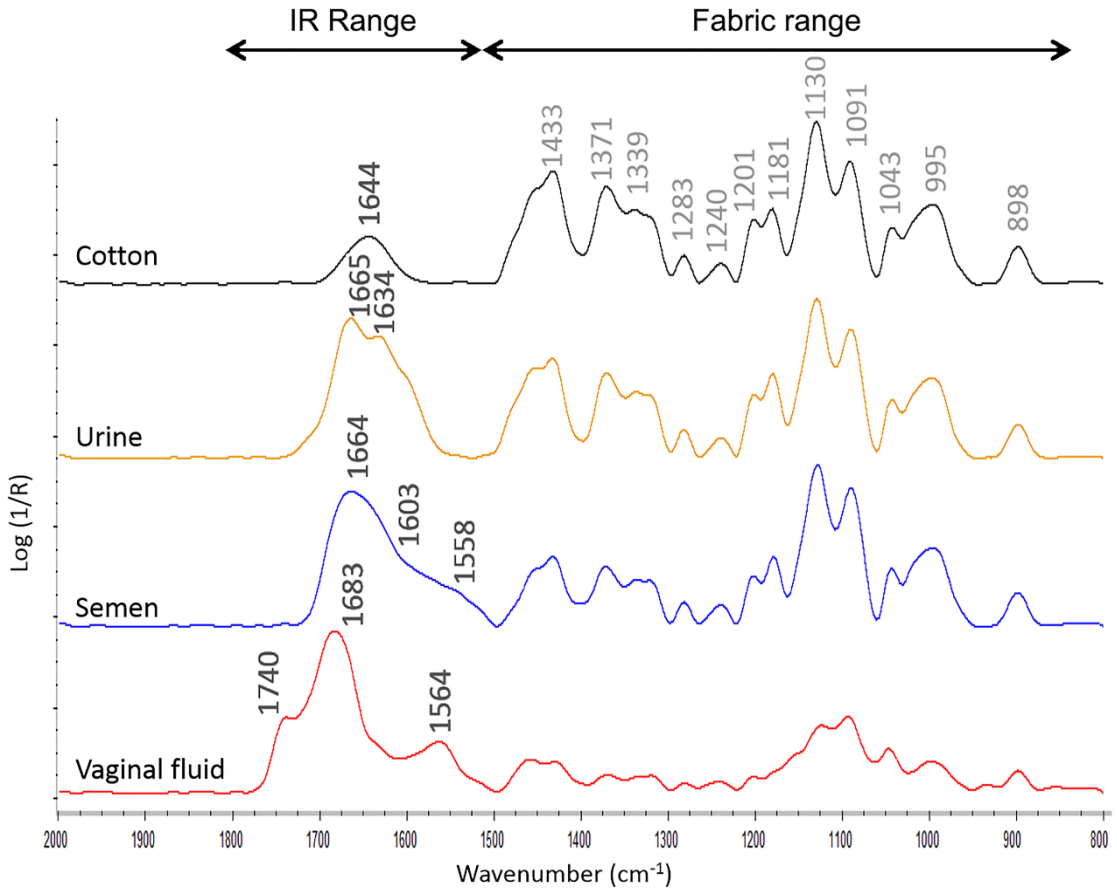

Figure 8.1. Infrared spectral signature by using external reflection of cotton, and stains of urine, semen, and vaginal fluid on cotton.

The spectrum of cotton was not subtracted from the spectra of semen, vaginal fluid, and urine stains because cotton did not supply exactly the same contribution to all stains. Even in the same stain, the contribution of cotton bands to the spectra differed along the stain which it was attributed to the amount of body fluid placed in each part of the stain. For that reason, the indiscriminate subtraction of the cotton contribution was unfeasible.

As can be seen in Figure 8.1, the main IR bands of cotton appeared at wavenumbers below 1500 cm^{-1} except for one band located at 1644 cm^{-1} that was due to water absorbed by the cotton fabric. Since the spectral region of interest in this work is 1500–1800 cm^{-1}, only that band from cotton above 1500 cm^{-1} was further studied. Although this band from water may interfere at first appearance with the identification of bands from body fluids, the spectral signatures from body fluids are quite different, more intense and complex. In fact, the spectrum of vaginal fluid stains was significantly different to the cotton spectrum. It presented specific bands located at 1740, 1683, and 1564 cm^{-1}. On

the contrary, the cotton contribution to semen and urine spectra was higher than its contribution to vaginal fluid spectrum. In spite of that, characteristic bands were observed for semen and urine. The spectrum of semen showed a wide band (1664, 1603, 1558 cm^{-1}) along the "ID range" whereas characteristic bands of urine were located at 1665 and 1634 cm^{-1}. We think that the reason why bands of cotton are not so evident in vaginal fluid stains, contrary to semen and urine stains, lies in the lower water content of vaginal fluid whose stains hide the cotton fabric to a greater extent than urine and semen stains. Therefore, the signal from cotton in vaginal fluid stains is lower. By considering the water content in each body fluid, we checked that vaginal fluid has the lowest water content, so a higher amount of residue remains on the surface of the dry stain. Moreover, those fluids with higher water content, such as semen and urine, were soaked up to a greater extent by the fabric leaving a lower amount of body fluid on the surface.

Semen and urine were also measured by transmission FTIR after being deposited on a KBr plate and dried. The transmission spectra from semen and urine are shown in Figure 8.2. It is important to mention that by comparing both types of spectra (external reflection and transmission) we realized that they matched each other along the range 1500–1800 cm^{-1} though small shifts (≤10 cm^{-1}) were found for some bands in semen and urine. On the other hand, the relative intensities of some bands were quite different between both types of spectra as can be seen in urine spectra. Interestingly, bands from semen and urine below 1500 cm^{-1} became visible since cotton fabric was not present.

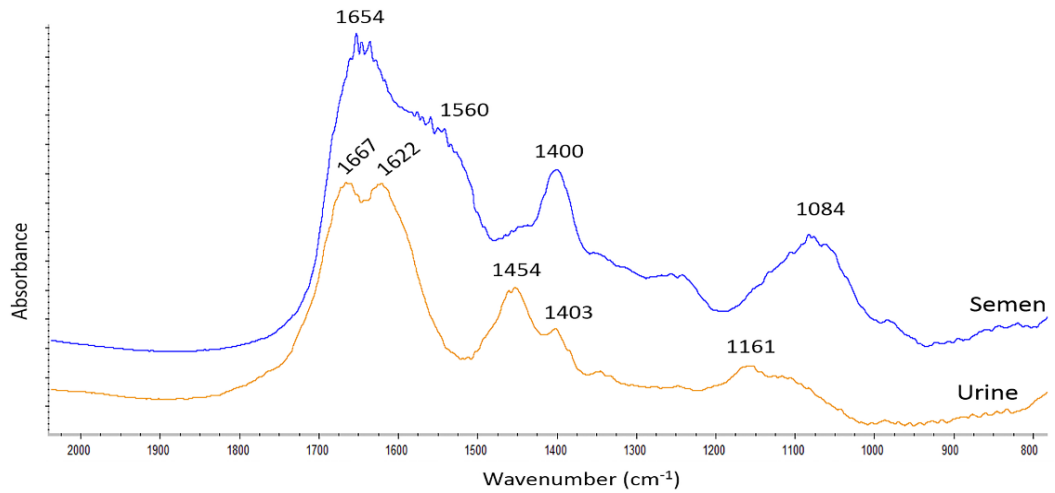

Figure 8.2. Absorbance IR spectra by using transmission mode from dry stains of semen and urine on KBr plates.

Because of these small shifts between reflection and transmission modes, it was difficult to accomplish an accurate assignment of the bands based on the known spectral ranges found in literature for some functional groups. Therefore, only a general bands interpretation was made. Thus, vaginal fluid bands were probably the result of COO^- (of lactate) vibration and C=O stretching and N–H bending (of the amino acids that make up the proteins such as phosphatase, peptidase, and immunoglobulins present in vaginal fluid). Bands from semen probably belonged to C=O stretching and N–H bending vibrations from the amino acids contained in proteins as phosphatase, prostate antigen, semenogelin, and immunoglobulins which are in semen. Finally, the main bands in urine probably belonged to urea, the main component in the dried stains of urine, due to C=O stretching and N–H bending vibrations (from NH_2 groups) [29]. A more detailed study accomplished by Orphanou [27] about the composition of body fluids by FT-IR demonstrates the large contribution of proteins such as acid phosphatase and albumin to semen spectrum or acid phosphatase and lysozyme to vaginal fluid spectrum. Nevertheless, ATR FT-IR was used in that study instead of external reflection. The different interaction between radiation and the sample when using different reflection accessories is probably the reason why we have found some significant differences from our external reflection spectra to those ATR spectra reported by Elkins [26] and Orphanou [27].

Taking the obtained results into account, a visual inspection of the external reflection spectral signature of the three body fluids allowed their characterization by a few defined spectral bands because the spectral signatures were different among each other even to the naked eye. Consequently, it was possible to differentiate each body fluid stain on fabric by its IR spectrum.

After establishing the IR spectra of the studied body fluids, the stains of these three body fluids on colored cotton fabrics were subsequently tested. First, the colored cotton fabrics (without stains) were analysed. Fortunately, the spectra from the colored cotton fabrics were almost identical (Figure 8.3a). A new band was observed for blue jeans, which seemed to demonstrate that there are slight differences between denim fabric and cotton fabric, in spite of both being 100% cotton. Regarding stains on colored cotton fabrics, they provided the characteristic signature of the respective body fluid. As an example, the stains of semen deposited on the different colored fabrics are shown in Figure 8.3b.

It is known that most dyes are IR active, so the lack of interference due to color is probably due to the fact that dyes are present at such low concentration in fabrics that they are undetectable by IR spectroscopy. Therefore, IR spectroscopy is suitable to detect a body fluid stain on the fabric but not the dyes from the fabric. This study is especially interesting since it has already been demonstrated that the color of the fabric presents several disadvantages by UV-Vis spectroscopy [6, 7] but it can be overcome by external reflection FTIR.

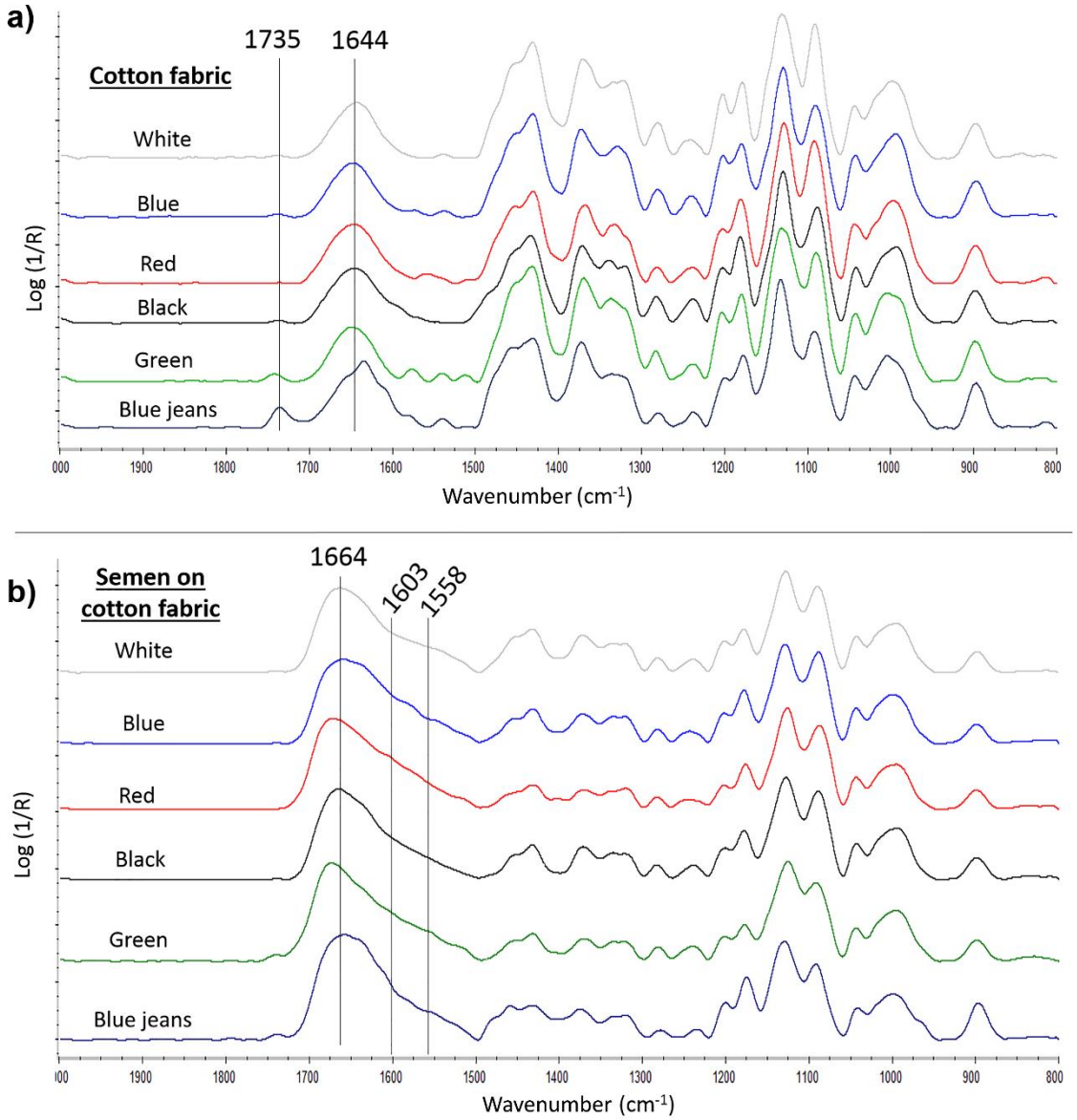

Figure 8.3. IR spectra of coloured cotton fabrics: white, blue, red, black, green and blue jeans (a), and stains of semen on these coloured cotton fabrics (b).

- *Differentiation of Semen, Vaginal Fluid, and Urine Stains on Fabrics*

In order to facilitate the discrimination among stains of body fluids by external reflection FTIR even on colored fabrics, and to check its discrimination

capability in mixtures of several body fluids, different multivariate chemometric approaches were performed. These statistic approaches were undergone by considering the "ID range" from spectra, between 1500 and 1800 cm^{-1}.

A global PCA was calculated including all the spectra of stains of body fluids on white and colored fabrics and the (white and colored) cotton pieces. Thereby, it was possible to represent all the spectra in a three-dimensional plot, where PCs represented the combination of the most discriminative wavenumber values. Figure 8.4 shows the PCA scores plot from cotton and stains of body fluids on cotton fabrics. Principal component 1, PC2, and PC3 summarized the 95% of the PCA model.

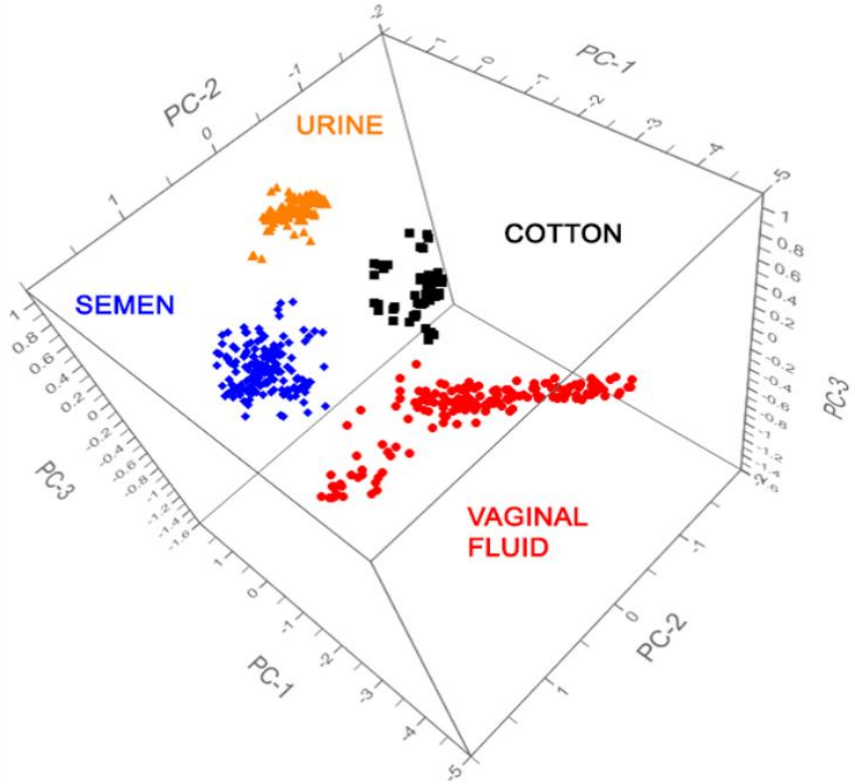

Figure 8.4. Three-dimensional scores PCA plot of the IR spectra from the unstained white and coloured cotton pieces (black ■), vaginal fluid stains (red ●), urine stains (orange ▲) and semen stains (blue ◆) placed on white and coloured cotton. The PCA model is explained by PC1 (77%), PC2 (11%) and PC3 (7%).

Figure 8.5 shows the loadings plots from PC1, PC2, and PC3. The relationship between PCs and body fluids can be tentatively evaluated by observing Figures 8.4 and 8.5 together, and considering the spectral signatures of body fluids previously showed in Figure 8.1. In particular, PC1 that summarized the 77% of the initial variation seemed to mainly differentiate vaginal fluid (loading bands

below zero) from urine (band over zero) and semen (bands over and below zero) as shown in Figure 8.5. That is why the scores plot, displayed in Figure 8.4, showed the vaginal fluid samples along negative values of PC1, urine samples on positive values of PC1, and semen samples close to zero, like cotton samples.

Subsequently, as can be seen in Figures 8.4 and 8.5, PC2 that summarized the next 11% of the variation mainly contributed to differentiate semen (band over zero) from urine and cotton, both close to zero value of PC2. Vaginal fluid was also affected by PC2 because its bands seem to be along both negative and positive values.

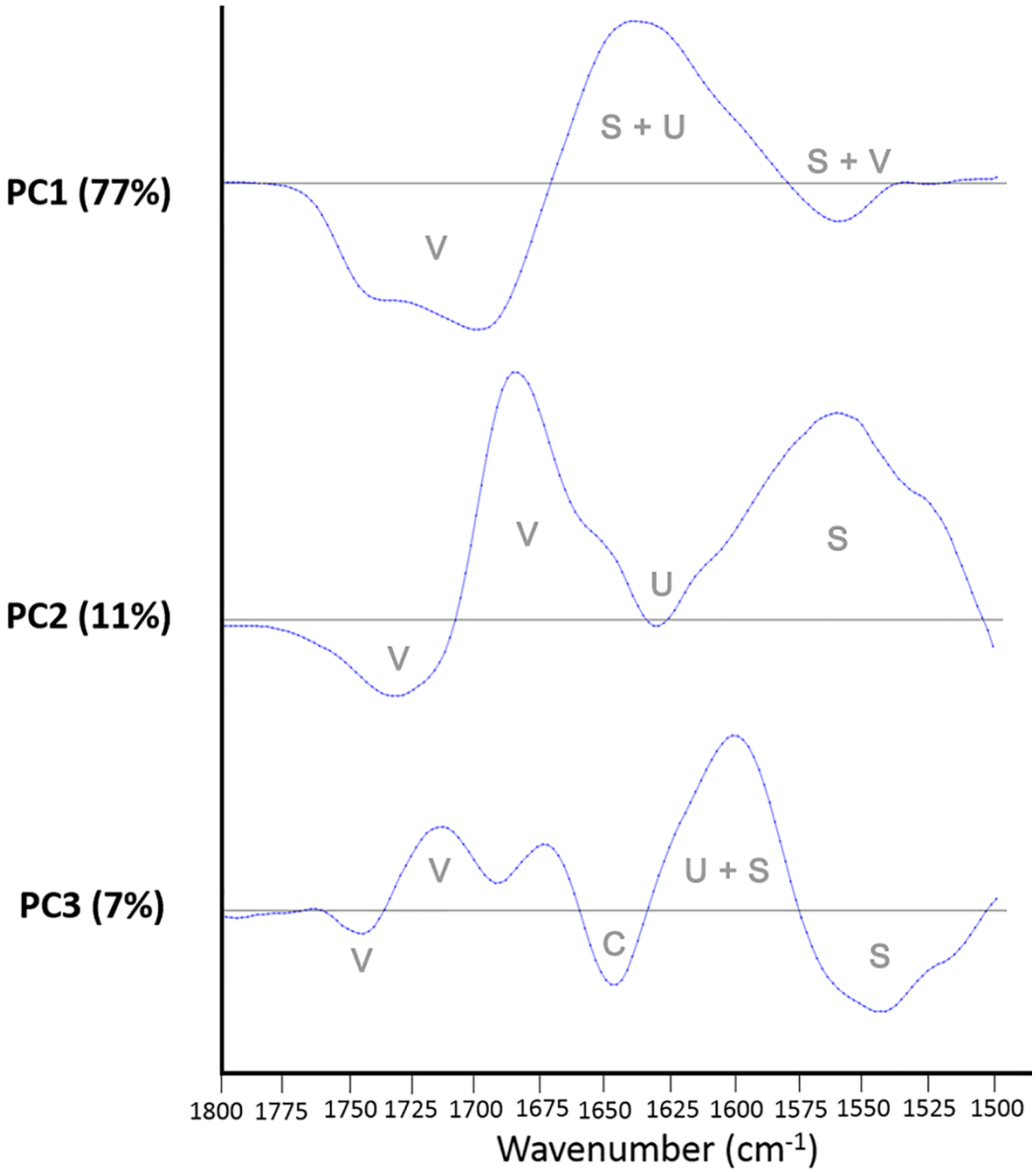

Figure 8.5. Line loadings plot from PC1 (above), PC2 (centre) and PC3 (below). The tentatively relationship between loadings features and body fluids are indicated as "V" for vaginal fluid, "S" for semen and "U" for urine. Cotton is indicated as "C".

Consequently, as shown in Figure 8.4, vaginal fluid samples were widely dispersed along the PC2 axis. Finally, PC3, which summarized the next 7% of the variation, helped to separate the three body fluids a bit more, though its effect was much smaller than the previous ones of PC1 and PC2. In summary, according to Figure 8.4, the pieces of cotton, semen, urine, and vaginal fluid stains were clustered in separate groups. This result confirmed that the differentiation of these three body fluids based on their IR spectra was possible by using external reflection FT-IR and chemometrics, even though the stains of the body fluids were on colored cotton fabrics. As previously explained, stains on different colored fabrics (white, black, blue, red, green, and blue jeans) were included in the PCA.

Considering Figure 8.4 again, it was also observed that vaginal fluid stains were the body fluid samples with the highest variability according to their wide dispersion. This dispersion seems to be related to two factors. First, it was known that the stains of vaginal fluid had a different quantity of fluid since its deposition was less controlled than those for semen and urine. Therefore, some of the dispersion is explained by the differences in the amount of vaginal fluid. We observed that the effect of decreasing the quantity of the deposited fluid produced a shift towards a higher intensity of cotton fabric. The lower the quantity of fluid, the higher the contribution of cotton. Consequently, those spectra are closer to cotton cluster. This result implies that the worst that could occur is a stain without enough quantity of fluid which would be placed close to the cotton group (false negative) leading to necessary subsequent analyses. On the other hand, there is also a dispersion which is not explained by the amount of fluid because it does not tend towards cotton cluster. That dispersion seems to be explained by little differences among the IR spectra from vaginal fluid stains, which may be due to a different chemical composition based on the vaginal fluid physiologic process, where vaginal fluid composition varies with the phases of the menstrual cycle. However, the dispersion that appeared within each cluster, also considering vaginal fluid, did not affect the differentiation observed among classes, which were separate enough to be clearly distinguished. Figure 8.4 shows that there is no overlapping among clusters. Most stains of the same body fluid were closely distributed and every stain was closer to its analogous stains than to the other stains. This fact seems to indicate that the within cluster variability is lower than inter-cluster variability, which is obviously needed to discriminate among different samples.

Regarding the stains of potentially false-positive substances, most of them (including lotions and foodstuffs) were displayed far away from body fluids, as displayed in Figure 8.6. Because of the perspective, some of them (orange juice (1), soup (2), and yogurt (3)) seem to be quite close to urine group. However, (1) and (2) are above the urine group and (3) is below the urine group (the reason why is almost completely covered). In fact, there is enough distance among their scores to avoid their confusion. Regarding soap 1 (6), Vaseline (7) and toothpaste (8), they seem to be quite close to cotton. Again, they are below the cotton group although it is difficult to notice due to the displayed perspective in Figure 8.6. Actually, the proximity of a sample to the cotton group implies that the stain does not provide significant discriminative signals with respect to those of cotton, which is also a positive result regarding the discrimination of these substances and body fluids.

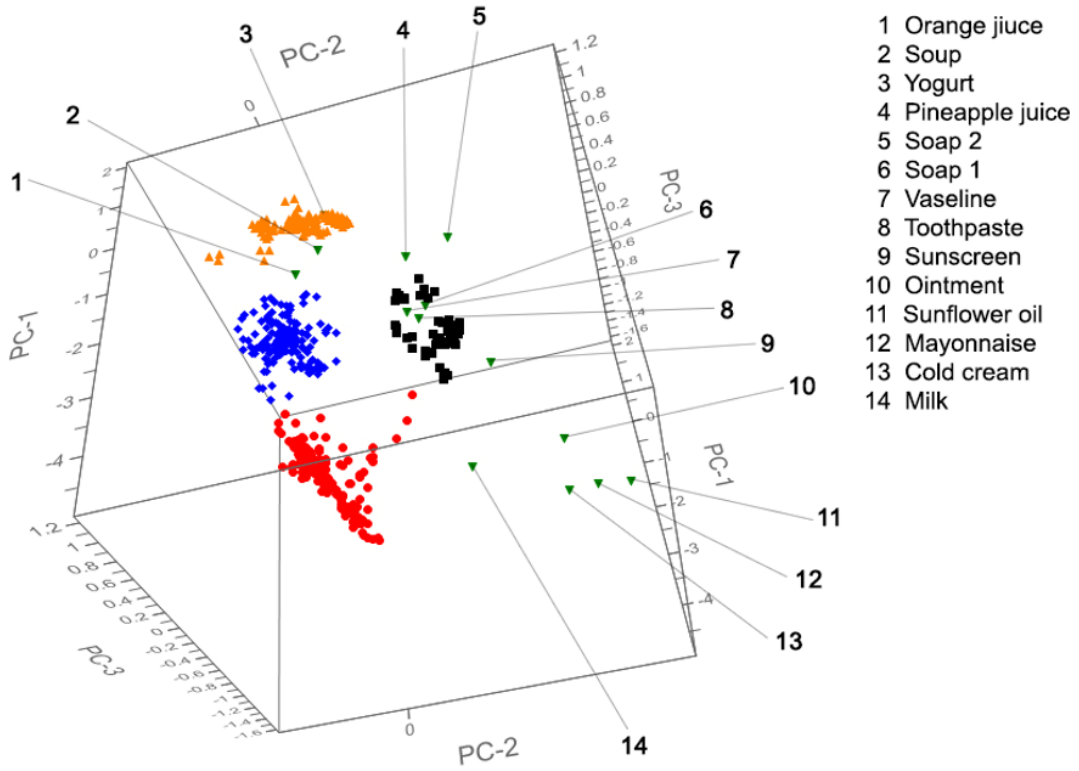

Figure 8.6. Three-dimensional scores PCA plot of the IR spectra from lotions and foodstuffs samples (green ▼) included within the PCA plot of the unstained white and coloured cotton pieces (black ■), vaginal fluid stains (red ●), urine stains (orange ▲) and semen stains (blue ◆) placed on white and coloured cotton.

- *Classification of Unknown Stains on Fabrics*

The most ambitious goal of this work was focused on developing a precise and accurate SIMCA classification model to differentiate and classify unknown stains of the three body fluids studied. The SIMCA model was calculated using separate PCAs of each class (cotton, vaginal fluid, urine, and semen), which were made considering white cotton and the stains from four of the donors. Subsequently, SIMCA was applied to the remaining stains used as test set in order to specifically classify three stains of each body fluid from a fifth donor, colored cotton samples, stains of the substances that may provide false positives, and stains of semen–vaginal fluid mixtures.

Table 8.3 shows the results of the SIMCA classification for these test samples. The classification of the samples in each class was established according to two measures: the sample-to-model distance (Si) and the sample leverage (Hi). "Si" is a measure of how far the sample lies from the modeled class and it is computed as the square root of the sample residual variance. A small distance means that the sample is well described by the class model. The Si is the basis of the statistical criterion used to decide whether a sample can be classified as a member of the class or not [30]. It is an intrinsic value of each sample in the SIMCA classification. "Hi" is a measure of how far the projection of a sample onto the model is from the class center. In fact, it expresses how different the sample is from the other members, regardless of how well it can be described by the class model [30]. The Hi has a linear relationship to the Hotelling T^2 statistic, which is related to the Mahalanobis distance. Its critical limit is based on an F-test and that is why Hi accepts different significance levels. In classification methodology, the significance level is the probability of rejecting a sample from a class when it belongs to that class. However, it is more important in this case to reduce the opposite error: including a sample in a class when it does not belong to that class; because that would mean a false positive. In methods of identification, false negatives are preferred to false positives. In this case, a significance limit of 5% was established.

As Table 8.3 shows, the SIMCA model accurately classified the stains of vaginal fluid, urine, semen, and the unstained cotton samples. In addition, the 14 potential false positive substances were not classified in any class although some of them were false positives by UV-Vis spectroscopy [5]. Finally, the SIMCA model partly classified semen–vaginal fluid mixture stains as vaginal fluid. Mixture stains were only classified as vaginal fluid instead of both semen and vaginal fluid. Erroneously, semen was not detected in the mixture. The spectra from all of these test samples are shown in the annexe of this Thesis.

Table 8.3. SIMCA classification matrix result of the prediction of test samples. The asterisks indicate the classes where samples were classified after establishing a significance limit of 5%.

Test set	Cotton	Vaginal fluid	Urine	Semen
Vaginal fluid 1		*		
Vaginal fluid 2		*		
Vaginal fluid 3		*		
Urine 1			*	
Urine 2			*	
Urine 3			*	
Semen 1				*
Semen 2				*
Semen 3				*
White Cotton	*			
Blue Cotton	*			
Red Cotton	*			
Black Cotton	*			
Green Cotton	*			
Blue Jeans	*			
Sunflower oil				
Cold cream				
Sunscreen				
Soap 1				
Soap 2				
Milk				
Mayonnaise				
Toothpaste				
Soup				
Ointment				
Vaseline				
Yogurt				
Orange juice				
Pineapple juice				
Mixture 1		*		
Mixture 2		*		

Finally, it is important to highlight that no sample was classified into an erroneous class. According to these preliminary results, if the SIMCA model classified a stain in a particular fluid class, it would mean that that fluid is present in the stain. However, the non-identification of a fluid in a stain could also take place, as happened with the mixture stains where semen was not identified.

Conclusions and Future Trends

In this study, dry stains containing about 20–40 mg of vaginal fluid, semen, and urine on cotton fabrics were detected and differentiated by external reflection FTIR. By visual comparison of their spectra, it was observed that they were different. Although the band assignments only provided information about the major compounds in the fluid, the global IR spectral signature using the range of 1500–1800 cm^{-1} enabled the characterization of each body fluid.

The differentiation of stains on fabrics of the three body fluids studied (semen, vaginal fluid, and urine) was confirmed both visually and by chemometrics. In fact, spectra from unknown samples could be added to the PCA model to statistically see its proximity to each body fluid cluster. In addition, it was also demonstrated that the color of the fabric on which the stain was does not influence the body fluid identification by external reflection FTIR. The weak external reflection power, which does not allow the differentiation of colored fabrics, might be a limitation when detecting body fluids at low concentrations.

Finally, a SIMCA classification model was applied to the identification and classification of unknown stains of body fluids on cotton fabrics by external reflection FTIR. Semen, urine, and vaginal fluid stains were not misclassified and no cosmetic substance or foodstuff (of the 14 analysed) constituted a false positive. Unfortunately, mixture stains were only classified as one of its components (vaginal fluid). Therefore, further research is needed to improve and refine the classification model, particularly with semen–vaginal fluid mixtures where only the female's fluid was identified.

External reflection measurements can be used for standoff detection. In this study, stains were analysed at a distance of only 1.5 cm from the spectrometer because of the configuration of the instrument. However, external reflection can be designed to work at longer distances because it does not require a physical contact between sample and instrument. This great advantage makes external reflection particularly suitable for evidence recovery in which finding and locating the evidence together with a preliminary identification is very desirable. Consequently, as a future trend it seems very promising to combine this IR spectroscopy mode with photography by means of hyperspectral imaging, which allows the measuring of the IR spectrum of every pixel in the image. Using this approach, differences in chemical composition could be visualized in the image.

References

[1] K. Virkler, I.K. Lednev, Analysis of body fluids for forensic purposes: From laboratory testing to non-destructive rapid confirmatory identification at a crime scene, Forensic Sci. Int. 188 (2009) 1-17.

[2] F. Zapata, M.A. Fernández de la Ossa, C. García-Ruiz, Emerging spectrometric techniques for the forensic analysis of body fluids, TrAC Trends Anal. Chem. 64 (2015) 53-63.

[3] M.J. Auvdel, Comparison of laser and ultraviolet techniques used in the detection of body secretions, J. Forensic Sci. 32 (1987) 326-345.

[4] M. Stoilovic, Detection of semen and blood stains using Polilight as a light source, Forensic Sci. Int. 51 (1991) 289-296.

[5] D.G. Nelson, K.A. Santucci, An alternate light source to detect semen, Acad. Emerg. Med. 9 (2002) 1045-1048.

[6] N. Vandenberg, R.A.H. van Oorschot, The use of Polilight in the detection of seminal fluid, saliva, and bloodstains and comparison with conventional chemical-based screening tests, J. Forensic Sci. 51 (2006) 361-370.

[7] A. Fiedler, J. Rehdorf, F. Hilbers, L. Johrdan, C. Stribl, M. Benecke, Detection of semen (human and boar) and saliva on fabrics by a very high powered UV-/VIS-light source, Open Forensic Sci. J. 1 (2008) 12-15.

[8] C.E. Thorn, S.J. Matcher, I.V. Meglinski, A.C. Shore, Is mean blood saturation a useful marker of tissue oxygenation? Am. J. Physiol. Heart Circ. Physiol. 296 (2009) 1289-1295.

[9] S. Kloss, B. Kampe, S. Sachse, P. Rösch, E. Straube, W. Pfister, M. Kiehntopf, J. Popp, Culture independent Raman spectroscopic identification of urinary tract infection pathogens: A proof of principle study, Anal. Chem. 85 (2013) 9610-9616.

[10] K. Gilany, R.S.M. Pouracil, M.R. Sadeghi, Fourier transform Infrared spectroscopy: A potential technique for noninvasive detection of spermatogenesis, Avicenna J. Med. Biotechnol. 6 (2014) 47-52.

[11] Z. Huang, X. Chen, Y. Chen, J. Chen, M. Dou, S. Feng, H. Zeng, R. Chen, Raman spectroscopic characterization and differentiation of seminal plasma, J. Biomed. Opt. 16 (2011) 110501/1-110501/3.

[12] B.R. Wood, L. Chiriboga, H. Yee, M.A. Quinn, D. McNaughton, M. Diem, Fourier transform Infrared (FTIR) spectral mapping of the cervical transformation zone, and dysplastic squamous epithelium, Gynecol. Oncol. 93 (2004) 59-68.

[13] E.M. Kanter, E. Vargis, S. Majumder, M.D. Keller, E. Woeste, G.G. Rao, A. Mahadevan-Jansen, Application of Raman spectroscopy for cervical dysplasia diagnosis, J. Biophotonics 2 (2009) 81-90.

[14] J.L. Pezzaniti, T.-W. Jeng, L. McDowell, G.M. Oosta, Preliminary investigation of Near-Infrared spectroscopic measurements of urea, creatinine, glucose, protein, and ketone in urine, Clin. Biochem. 34 (2001) 239-246.

[15] W.R. Premasiri, J.C. Lee, L.D. Ziegler, Surface-enhanced Raman scattering of whole human blood, blood plasma and red blood cells: Cellular processes and bioanalytical sensing, J. Phys. Chem. B. 116 (2012) 9376-9386.

[16] N.N. Daéid, Review Papers, 17th Interpol International Forensic Science Managers Symposium. Lyon, France. 2013. Pp. 280–610.

[17] F.P. Smith, Handbook of forensic drug analysis. Amsterdam, The Netherlands, Elsevier, 2005.

[18] D.E. Bugay, Characterization of the solid-state: Spectroscopic techniques, Adv. Drug Delivery Rev. 48 (2001) 43-65.

[19] J. Yinon, Counterterrorist detection techniques of explosives. Amsterdam, The Netherlands, Elsevier, 2007.

[20] J.I. Steinfeld, J. Wormhoudt, Explosives detection: A challenge for physical chemistry, Annu. Rev. Phys. Chem. 49 (1998) 203-232.

[21] K. Virkler, I.K. Lednev, Raman spectroscopy offers great potential for the nondestructive confirmatory identification of body fluids, Forensic Sci. Int. 181 (2008) e1-e5.

[22] V. Sikirzhytski, A. Sikirzhytskaya, I.K. Lednev, Multidimensional Raman spectroscopic signatures as a tool for forensic identification of body fluid traces: A review, Appl. Spectrosc. 65 (2011) 1223-1232.

[23] V. Sikirzhytski, K. Virkler, I.K. Lednev, Discriminant analysis of Raman spectra for body fluid identification for forensic purposes, Sensors 10 (2010) 2869-2884.

[24] V. Sikirzhytski, A. Sikirzhytskaya, I.K. Lednev, Advanced statistical analysis of Raman spectroscopic data for the identification of body fluid traces: Semen and blood mixtures, Forensic Sci. Int. 222 (2012) 259-265.

[25] I.K. Lednev, Application of Raman spectroscopy for an easy-to-use, on-field, rapid, nondestructive, confirmatory identification of body fluids. Report to the U.S. Department of Justice. 2012.

[26] K.M. Elkins, Rapid presumptive “fingerprinting” of body fluids and materials by ATR FT-IR spectroscopy, J. Forensic Sci. 56 (2011) 1580-1587.

[27] C. Orphanou, The detection and discrimination of human body fluids using ATR FT-IR Spectroscopy, Forensic Sci. Int. 252 (2015) e10-e16.

[28] M. Pirzer, J. Sawatzki, Method and device for correcting a spectrum. US Patent: US 7,359,815 B2. Apr. 15, 2008.

[29] E. Pretsch, P. Bühlmann, C. Affolter, A. Herrera, R. Martinez, Structure determination of organic compounds. Berlin, Germany, Springer-Verlag, 2000.

[30] The Unscrambler X 10.1 Software (Oslo, Norway). Help contents. 2009.

Chapter 9. Revealing the location of body fluids in stained evidence through near infrared hyperspectral imaging

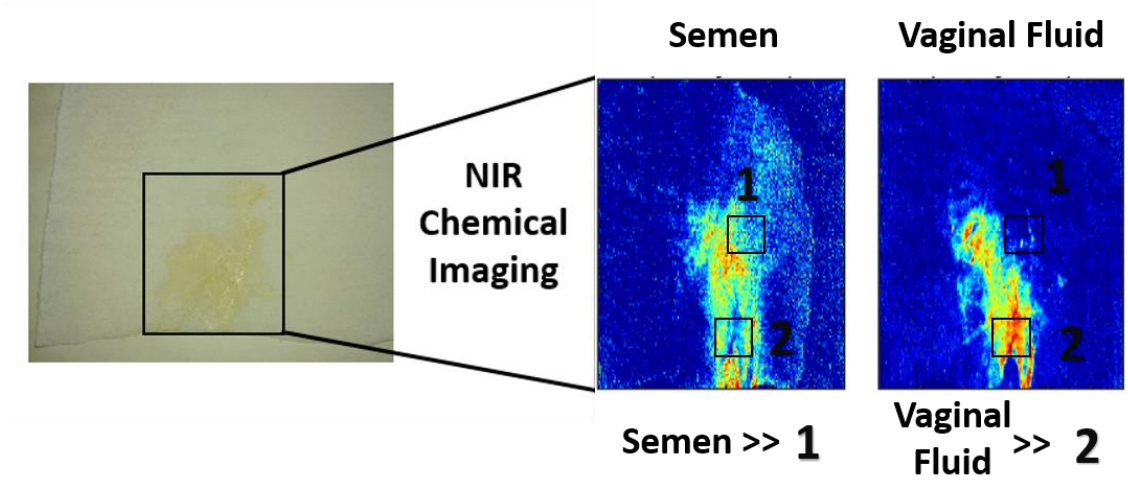

Main source:

Félix Zapata, F.E. Ortega-Ojeda, C. García-Ruiz, Revealing the location of semen, vaginal fluid and urine in stained evidence through near infrared chemical imaging, *Talanta* 166 (2017) 292-299.

Abstract

Crime scene investigation (CSI) requires the ultimate available technology for a rapid, non-destructive, and accurate detection of a wide variety of evidence including invisible stains of body fluids. Particularly crucial is the discrimination of semen in stained evidence from sexual abuse cases. This is because those evidence have high odds of containing the DNA from the aggressor. To this aim, we demonstrated the potential of near infrared hyperspectral imaging (NIR-HSI) to make visible stains of semen, vaginal fluid, and urine on fabrics, which lays the bases to face the challenging visualization and discrimination of semen within body fluids mixtures. Combining the NIR-HSI data and simple chemometric techniques such as principal component analysis and classical least squares regression, we have revealed the location of semen, vaginal fluid and urine in body fluids stained evidence.

Introduction

The utilization of highly informative up-to-date analytical techniques for crime scene investigation in forensics seems evident to nonscientific people to such an extent that mostly think, influenced by TV series and brilliant super-detective characters, that forensic investigation is immediate and fool-proof. Nevertheless, despite being fiction, these series, showing "in situ" fool-proof instrumentation suitable for instantly identifying any evidence, might be just futuristic. In fact, novel significant and highly useful approaches and methodologies towards that aim are being developed and implemented just from the first step in the crime investigation process, *i.e.* evidence recovery, as anticipated in the auspicious "CSI The Hague" project [1].

Evidence recovery usually deals with the detection of minute, concealed and invisible traces, which require the expert and thorough inspection of forensic investigators. Different methodologies, devices and tests that assist the forensic inspection are currently being used for both location and identification purposes. Regarding body fluids evidence, UV light sources and chemical tests are well-known and well-established methodologies in the forensic community for the detection of stains of body fluids such as blood, semen, saliva or urine [2-4]. However, most of these tests are only presumptive, *i.e.* do not provide an unequivocal identification of the fluid. In addition, most of these tests are destructive, which is a huge disadvantage for body fluids, especially for those containing deoxyribonucleic acid (DNA), so useful for subsequent genetic analysis [2-4].

The novel technique called near infrared hyperspectral imaging (NIR-HSI) seems to be a promising approach to reach this evasive goal. This is due to the capability of NIR-HSI of photographing the trace while characterizing its spectral profiles providing chemical information [5]. NIR radiation provides specific chemical information about the photographed samples improving their discrimination based on their chemical composition. That is a great advantage over both traditional visible (Vis) and ultraviolet-visible (UV–Vis) photography, in which the discrimination of body fluids deals with various false positive substances and limitations for coloured backgrounds. This occurs because UV–Vis HSI identification is only supported by the colour and the non-specific UV-fluorescence of body fluids [6-8]. Although it is true that NIR spectroscopy is less specific than MIR for characterization and interpretation purposes [9, 10],

it might be selective enough to characterize and discriminate different molecules according to their either evident or slight NIR spectral differences. Evident spectral differences may involve the presence or absence of the overtone from certain vibration while slight spectral differences might be small shifts in the wavelength value of a certain band and its band-shape. To this aim, multivariate pre-processing and chemometric methods are encouraged to enhance the discrimination from the NIR-HSI data [10-13].

Preliminary useful studies showing the advantages of using HSI for blood stains identification have been reported [14-17]. Nonetheless, other extraordinarily significant body fluids involved in sexual crimes such as semen, vaginal fluid and urine, usually mixed, remain unexplored by NIR-HSI. Interestingly, some Raman or MIR spectroscopy studies that focused on the spectral identification of these body fluids have proved the successful discrimination among them based on their different chemical composition [18-23]. However, those techniques target at a single point and thus, they lack imaging. Therefore, they do not enable the visualization of stains, but only the identification of one point in the stain, which is almost completely useless in mixtures. In fact, the detection of semen still remains challenging when it is mixed with vaginal fluid. The higher proportion and, consequently, the higher signal from vaginal fluid in relation to semen hinders the identification of semen, and ultimately provides no satisfactory genetic results.

This work proposes, for the first time, a comprehensive study examining the potential of NIR-HSI to locate and discriminate semen from vaginal fluid even in mixtures.

Experimental

- *Samples*

In this work, we studied stains of semen, vaginal fluid, and urine from ten anonymous donors (5 women and 5 men), as well as a mixture of semen-vaginal fluid. All stains were prepared following the procedure reported in previous literature [23]. Briefly, 0.6 mL of semen or urine were dropped on pieces of 11×8 cm^2 cut from T-shirts made of 100% cotton, whereas vaginal fluid was directly placed on the cotton pieces by each donor. In addition, a mixture containing semen and vaginal fluid was prepared with the aim of testing the suitability of

NIR-HSI to discriminate those regions containing semen from those containing vaginal fluid along the same stain. This mixture-stain was prepared by dropping 0.6 mL of semen over the cotton piece just after having been stained with vaginal fluid. This way of preparation was selected in order to create similar stains to those found in real evidence, in which the fabric already stained with vaginal fluid might be subsequently stained with the aggressor's semen. The size of every stain ranged between 2 and 3 cm in diameter. All stains were left to air dry overnight before being analysed. Altogether, we studied five stains per body fluid (one stain per donor).

- *Instrumentation for HSI analysis*

We used a hyperspectral camera (Specim, Oulu, Finland) kindly provided by INFAIMON (Barcelona, Spain) working from 1000 to 2500 nm wavelengths to analyse the stains. The camera had a Mercury Cadmium Telluride (MCT) cryogenically cooled detector. The in-built software of the HSI system enabled collecting the data, and then saving it in binary hdr-raw ENVI format (Exelis, Boulder, Colorado, USA). The hyperspectral data collected for each sample yielded a 3D hypercube (x, y, λ) with 243 different wavelengths.

- *Data analysis*

The hyperspectral data analysis was performed in Matlab (MathWorks, MA, USA) using specific in-house algorithm sequences assisted by some freely-available HYPER-Tools functions [11-13, 24]. We designed the algorithm sequences to perform data pre-processing and data classification analysis. Briefly, this process consisted of three main tasks:

– Masking/Selecting the region of interest. In order to ensure the HSI images contained the stain, the images comprised the whole fabric area. However, some areas of the fabric containing useless information were removed to save both processing and data analysis time. The area containing the stain was selectively masked/selected using principal component analysis (PCA). A PCA was performed to each 3D-hypercube image (considering its 243 wavelengths). This enabled a rapid visualization of the stain due to the spectral differences of the body fluid with respect to the fabric. Interestingly, it is remarkable that most stains were highlighted using the second or third principal component even though they had not been still preprocessed. (The first principal component was always correlated with the whole cotton sample). That is, the study of the first

three principal components was enough to reveal the stains over cotton whilst explaining the characteristic spectral differences of the body fluids with regard to the cotton. As explanatory draft, Figure 9.1 displays the colour map scores obtained for one stain of each body fluid using the principal component that correlates with the stain. For instance, for these samples, the stains of either semen or urine were revealed using the third principal component while the stain of vaginal fluid was revealed using PC2. This way to visualize stains was certainly impressive since some stains were invisible to the naked eye (*i.e.* in visible wavelengths), or even invisible at each NIR wavelength on its own. This fact demonstrated the great assistance of PCA when dealing with hyperspectral images since it performed, in only a few seconds, the multivariate analysis of the 3D-hypercube, looking for the major differences along the 243 wavelengths at once.

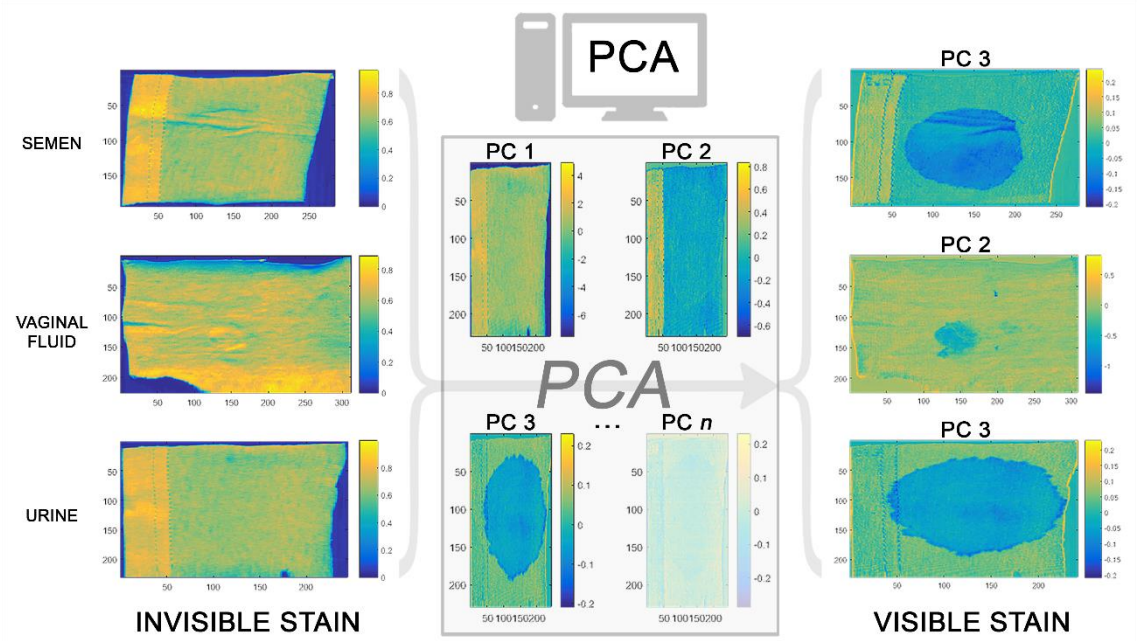

Figure 9.1. The use of PCA for visualizing the stains of semen, vaginal fluid, and urine on cotton fabrics. One stain per body fluid is included. The stains of semen, vaginal fluid and urine are revealed through PC3, PC2 and PC3, respectively. The intermediate PCA colour maps for PC1, PC2 and PC3, shown as example, are those from the urine stain.

– Data Pre-processing prior to discrimination and classification analysis. After testing different alternatives, we selected the most appropriate pre-processing sequence as follows: Selection of the spectral range (1270–2300 nm), Standard Normal Variate (SNV) normalization, and Savitzky-Golay smoothing (2nd degree polynomial fitting using a symmetrical window of 5 points).

– Data classification to discriminate the body fluids and visualize the traces of semen even in mixtures. After proving the discrimination of stains from cotton and optimizing the pre-processing, the next step focused on verifying that the stains from each body fluid could be differentiated from each other according to their respective characteristic NIR spectrum. First, a PCA exploratory analysis containing the spectra collected from one of the stains of each body fluid was performed in order to check whether the stains of semen, vaginal fluid and urine can be discriminated through NIR spectroscopy. Finally, a classical least squares (CLS) classification analysis was carried out in order to improve the discrimination of these stains to such an extent that they may be discriminated and classified even in mixtures. To this aim, 50 representative spectra of both cotton and stains of body fluids (taken from 1 of the 5 stains per body fluid) were gathered into an ad-hoc home-made NIR spectral library. The selection of these representative spectra for each body fluid stain was facilitated by PCA (*i.e.* spectra were manually selected within the stain region delimited by PCA keeping in mind the need to cover the middle of the stain as well as the periphery in order to include the intra-variability of the body fluid along the stain). Afterwards, the other four stains of each body fluid were compared against the body fluids NIR spectral library as blind tests, as summarized in Table 9.1. Finally, a stain containing a mixture of semen-vaginal fluid was compared against the model in order to test the suitability of this methodology to classify mixture stains. This comparison was performed using a classical least squares regression (CLS) between the spectra from the pixels in each image and the NIR spectral library previously created. As a result, a matching value based on the CLS regression was provided for each pixel in the image to each class (cotton, semen, urine and vaginal fluid). By plotting this matching values, a coloured

Table 9.1. Distribution of stains used to create the spectral library / to test the model.

Stain	Used for
Cotton blank	Library
Semen stain donor 1	Library
Semen stain donor 2	Blind test A
Semen stain donor 3	Blind test B
Semen stain donor 4	Blind test C
Semen stain donor 5	Blind test D
Urine stain donor 1	Library
Urine stain donor 2	Blind test A
Urine stain donor 3	Blind test B
Urine stain donor 4	Blind test C
Urine stain donor 5	Blind test D
Vaginal fluid stain donor 1	Library
Vaginal fluid stain donor 2	Blind test A
Vaginal fluid stain donor 3	Blind test B
Vaginal fluid stain donor 4	Blind test C
Vaginal fluid stain donor 5	Blind test D
Mixture (semen-vaginal fluid) stain	Blind test

chemical map was visualized for each body fluid (besides cotton). The colour in every map ranged from blue (smallest value) to red (maximum value), indicating the estimated weight of body fluid in that pixel. In other words, a value close to 1 would imply a perfect matching between the spectrum from a red pixel and the NIR spectra from the library of that fluid. Interestingly, all samples tested displayed an intense red region when comparing with the correct body fluid spectral library, but a blue-to-yellow region when comparing with the incorrect body fluid. Furthermore, in order to numerically assess the classification power within a randomly selected region of a stain, the CLS results provided by that region to each class (cotton, semen, urine or vaginal fluid) are compared to each other. To this aim, the maximum weight value for the selected region at each coloured chemical map, is shown above every coloured map. In addition, the histogram containing the total number of pixels within the selected region, classified into the specific class with a certain value (*i.e.* every pixel with non-zero value to that class), is displayed below every coloured map.

Results and discussion

First of all, it was verified whether the stains from body fluids (semen, urine, and vaginal fluid) were active enough in NIR to be differentiated from each other according to their respective characteristic NIR spectrum. Although the NIR spectra from the three body fluids on cotton were quite similar (Figure 9.2), a thorough inspection revealed some slight differences at the spectral regions around 1500, 1600–1900, 1950 and 2100–2300 nm.

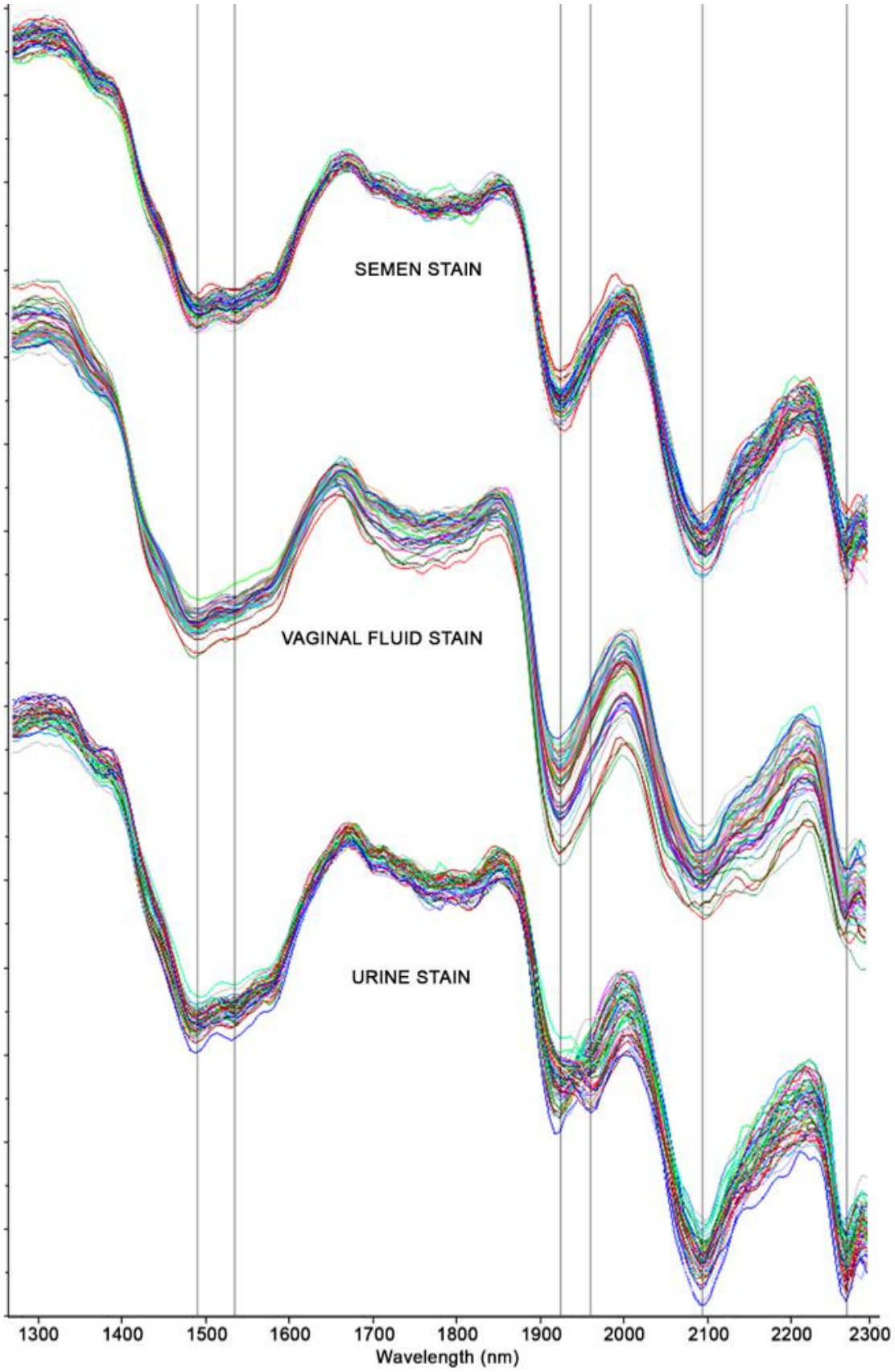

Figure 9.2. NIR spectra from stains of semen, vaginal fluid and urine on cotton fabrics from 1270 to 2300 nm.

Despite being negligible to the naked eye, a simple PCA study (see Figure 9.3) evidenced the significance of these slight differences to discriminate these stains. In fact, the scores corresponding to the spectra of body fluids, which are determined by the spectral loadings, were placed conforming slightly separated groups according to each body fluid. In brief, the spectra of vaginal fluid stains were distributed along negative values of PC1; the spectra of semen stains were distributed around zero and low positive values of PC1; and the spectra of urine stains were distributed along higher positive values of PC1. Consequently, the discrimination of stains from the three body fluids seems to be achievable using NIR spectroscopy supported by chemometrics.

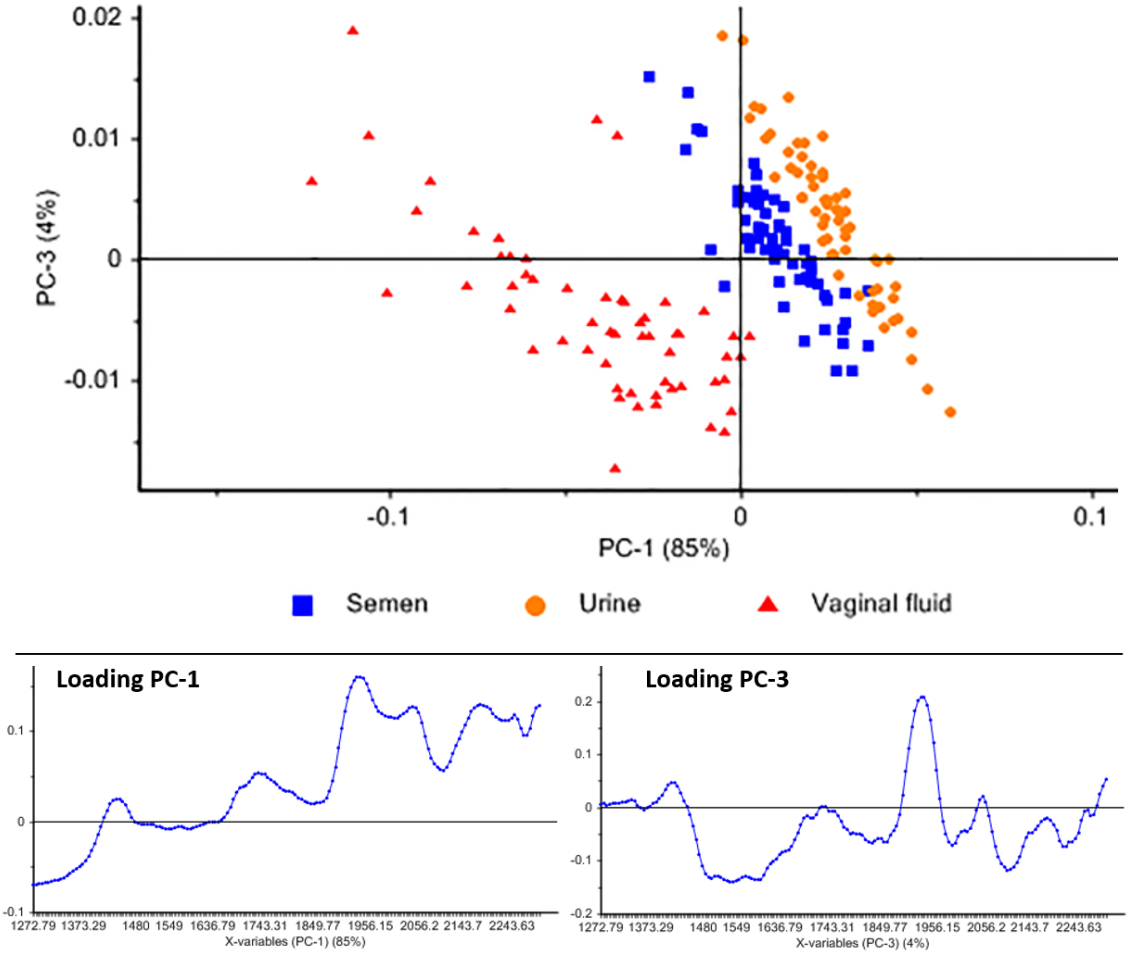

Figure 9.3. Two-dimension scores PCA plot along PC1 and PC3 considering the NIR spectra from stains of semen, vaginal fluid, and urine on cotton.

In order to improve the discrimination, a classification methodology based on CLS was performed by identifying the body fluid in a stain (blind sample) applying a particular level of certainty. As an example, Figure 9.4 summarizes the results for a semen stain used as blind sample.

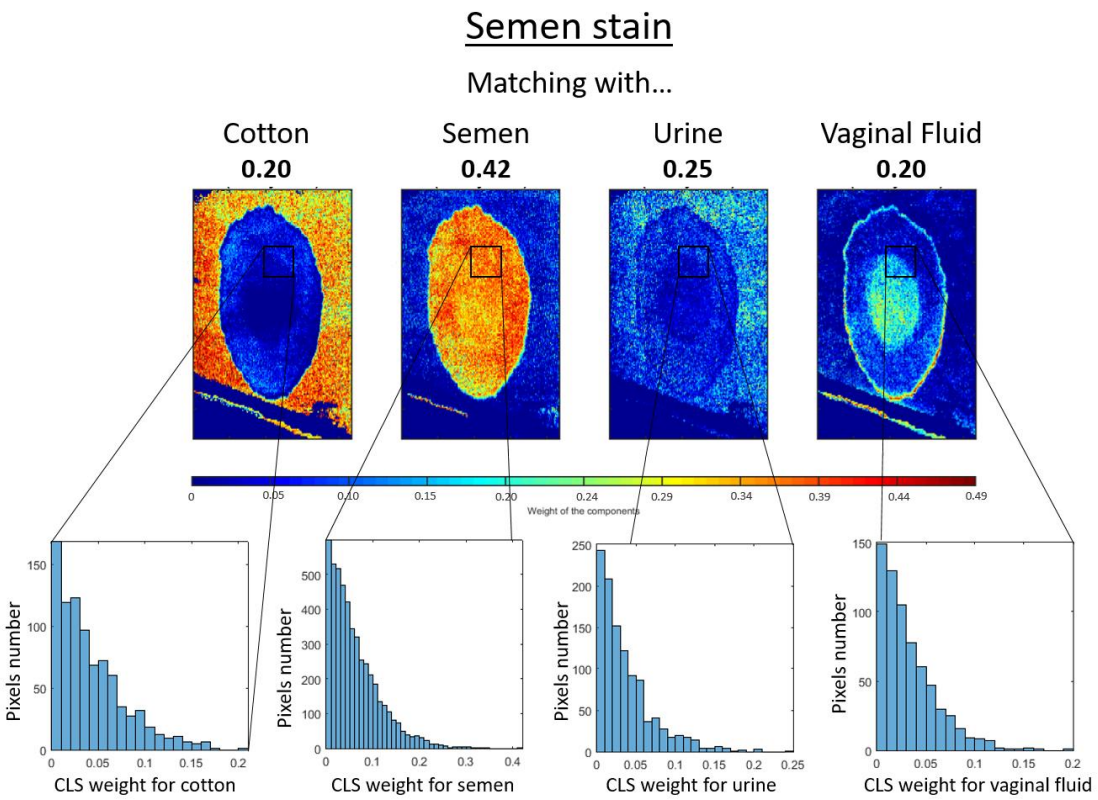

Figure 9.4. CLS classification model applied to a semen stain on cotton fabric. The CLS coloured maps for each class (cotton, semen, urine and vaginal fluid) are displayed. The maximum CLS weight values obtained for each class within the selected stained region is indicated above every colour map. The histogram containing the number of pixels within the selected region and their corresponding CLS weight to each class are provided below every colour map.

As expected, cotton, which is the background, was identified outside the stain as displayed in orange-to-red colours in the first subplot of Figure 9.4. Remarkably, cotton appears like surrounding the stain of body fluid, *i.e.* the body fluid provided characteristic spectral features that are distinctively different from those of cotton. In fact, regarding the selected region within the stain, the maximum weight value for cotton was 0.21. In the same way, the histogram shows the small number of pixels within this region (870) classified as cotton with a low value from 0 to 0.21. However, the most significant result involved the identification of the stain as semen as displayed in Figure 9.4, second subplot, by the orange-red area which perfectly defined the stain. In addition, the maximum weight semen value within the selected area (0.42) and the high number of pixels included in its histogram (4884) support the identification as semen. Negatively, the classification into vaginal fluid (Figure 9.4, fourth subplot) also provided the shape of the semen stain, which could

lead to confusion. Fortunately, the low weight of vaginal fluid within the selected region (0.20 of maximum weight) and the low number of pixels (672) reduce its quantitative identification as vaginal fluid. In fact, semen and vaginal fluid were already reported to have similar composition [2], which would likely explain the noticeable similarities between their NIR spectra. Finally, urine (Figure 9.4, third subplot) was heterogeneously and vaguely accounted by the CLS model as shown in the dispersed pixels, mainly placed outside the stain. Nevertheless, a significant weight (0.25) and number of pixels (1099), were provided for urine within the selected region, which also shows certain similarities between the NIR spectra of semen and urine. Accordingly, the identification of semen within a region must be supported by both the maximum classification weight value and the number of pixels. See Table 9.2 to check the maximum weight classification values as well as the number of pixels within the selected region for each class (cotton, semen, urine and vaginal fluid) for the other three stains of semen included in this study. Similar results were obtained for the four stains.

Table 9.2. CLS classification results for stains of semen, urine, vaginal fluid and the semen-vaginal fluid mixture. The first column of each class, called "Max.", indicates the maximum intensity of the CLS classification model within the selected region to that class. The second column of each class called "Pixels" specifies the total number of pixels from the selected region within the stain whose CLS classification intensity to that class was non-zero (*i.e.* those pixels that were classified into that class with a certain value).

Number of pixels from the selected region (20x20) classified with a certain value as…								
	Cotton		Semen		Urine		Vaginal fluid	
	Max.	Pixels (Int > 0)	Max.	Pixels (Int > 0)	Max.	Pixels (Int > 0)	Max.	Pixels (Int > 0)
Semen stain A	0.21	870	0.42	4884	0.25	1099	0.20	672
Semen stain B	0.12	37	0.49	4683	0.17	977	0.17	370
Semen stain C	0.25	1239	0.43	4272	0.31	1827	0.15	446
Semen stain D	0.18	302	0.55	5405	0.20	1092	0.15	449
Urine stain A	0.26	974	0.24	709	0.45	5018	0.12	153
Urine stain B	0.40	1435	0.18	355	0.53	4081	0.10	72
Urine stain C	0.16	196	0.13	382	0.42	5494	0.06	32
Urine stain D	0.04	3	0.12	49	0.54	3998	0.14	242
Vaginal fluid stain A	0.34	1232	0.19	1059	0.27	1429	0.62	2923
Vaginal fluid stain B	0.30	693	0.17	606	0.21	679	0.41	4586
Vaginal fluid stain C	0.28	1193	0.14	218	0.32	560	0.50	3703
Vaginal fluid stain D	0.30	563	0.20	213	0.24	229	0.66	3661
Mixture (semen region)	0.37	1866	0.41	2639	0.36	1797	0.22	707
Mixture (vaginal fluid region)	0.09	31	0.36	1576	0.11	86	0.69	2122

Similarly, we tested blind stains of urine and vaginal fluid using CLS analysis and similar images to those shown in Figure 9.4 were obtained (See Figures 9.5 and 9.6). Regarding the urine stain (Figure 9.5), besides cotton which appeared highly red-intense surrounding the stain, but with a low weight (0.26) and small number of pixels (974) within the selected region inside the stain, only urine (with a maximum weight value of 0.45 and 5018 pixels within the selected region) was properly quantified all over the stain. Neither the matching with semen (maximum weight value of 0.24 and 709 pixels within the selected region) nor with vaginal fluid (maximum weight value of 0.12 and 153 pixels within the selected region) provided quantitative results high enough for their identification.

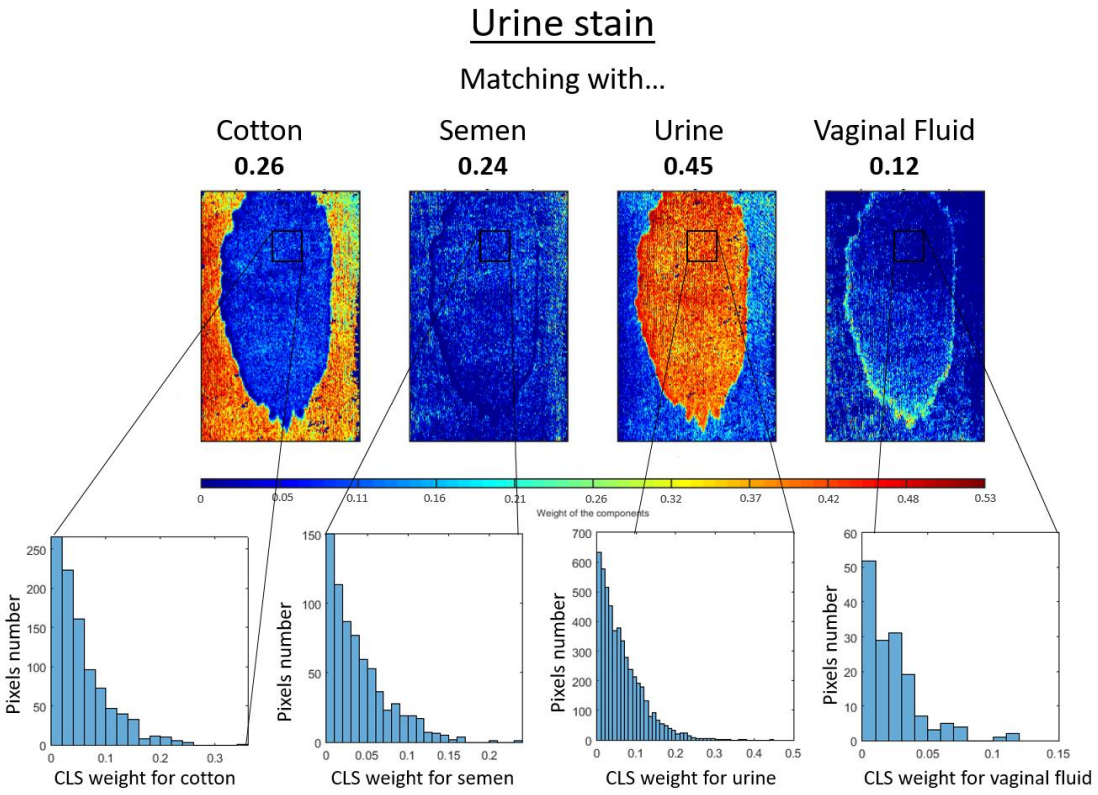

Figure 9.5. CLS classification model applied to a urine stain on cotton fabric. The CLS coloured maps for each class (cotton, semen, urine and vaginal fluid) are displayed. The maximum CLS weight values obtained for each class within the selected stained region is indicated above every colour map. The histogram containing the number of pixels within the selected region and their corresponding CLS weight to each class are provided below every colour map.

With regards to the vaginal fluid stain (Figure 9.6), cotton was classified surrounding the stain, as expected, (and it provided a maximum weight value of 0.34 and 1232 pixels within the selected region) whereas vaginal fluid was classified throughout the stain, with 0.62 of maximum weight and 2923 pixels within the selected region. The matching with semen and urine within the selected region yielded maximum weight values of 0.19 and 0.27, respectively; and 1059 and 1429 pixels, respectively. Although urine was randomly classified along the whole fabric, semen was mostly concentrated in a small well-defined region of the stain, as previously and contrarily occurred with the semen stain in comparison to vaginal fluid. Similar results were obtained for the rest of urine and vaginal fluid stains (see Table 9.2).

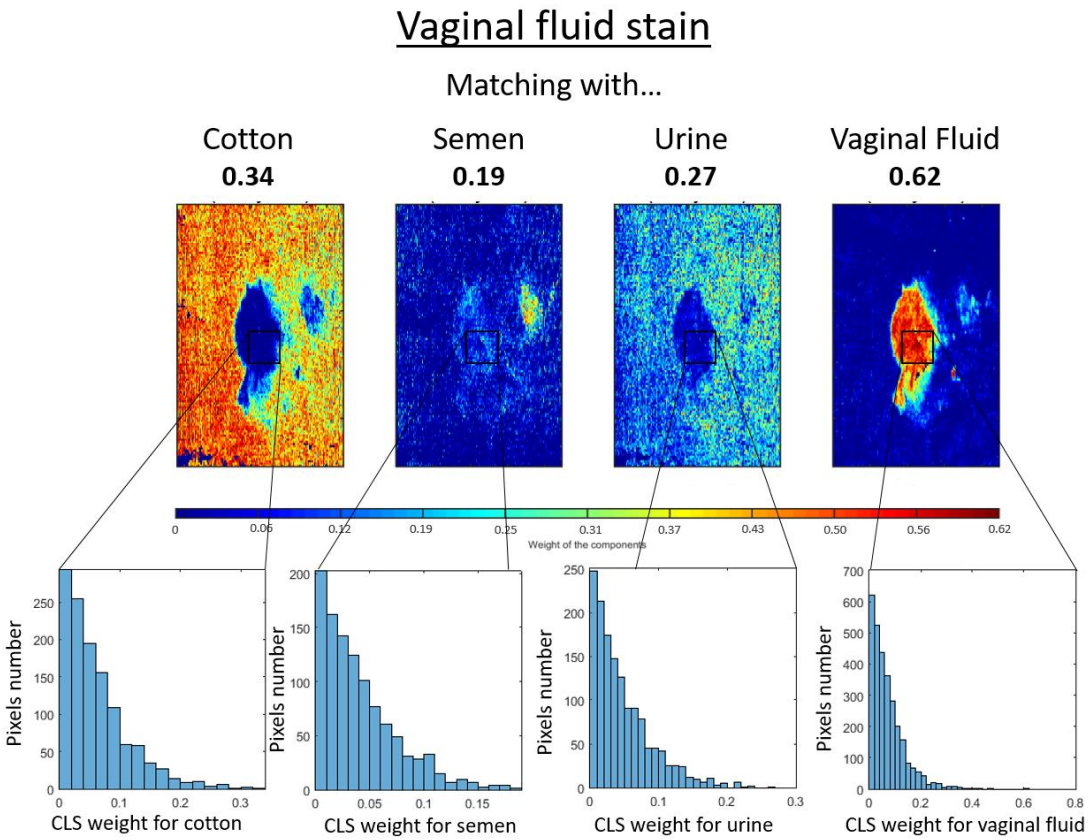

Figure 9.6. CLS classification model applied to a vaginal fluid stain on cotton fabric. The CLS coloured maps for each class (cotton, semen, urine and vaginal fluid) are displayed. The maximum CLS weight values obtained for each class within the selected stained region is indicated above every colour map. The histogram containing the number of pixels within the selected region and their corresponding CLS weight to each class are provided below every colour map.

However, what is the situation when body fluids are mixed? Interestingly, both semen and vaginal fluid were independently identified and located within the semen-vaginal fluid mixture-stain. As expected, the coloured map for cotton was highly-red intense outside the stain and highly-blue inside the alleged stained area, which is due to the presence of the body fluids (Figure 9.7). Within this alleged stained region, both semen and vaginal fluid were identified along clearly defined and independent areas, allowing the visualization of the different distributions of semen and vaginal fluid along the stain. Urine, like cotton, was mostly identified outside the stain; but what is more problematic is the fact that urine was also identified around some semen regions, which is a negative result since urine was not present in this stain. Finally, in order to check the independent distribution of semen and vaginal fluid two regions were selected for comparison purposes: the first region was selected from an area intensely coloured as semen and vaguely coloured as vaginal fluid whereas the second one was selected from an area intensely marked as vaginal fluid. Positively, the maximum weight and number of pixels for semen and vaginal fluid were in accordance with the colour information of the selected region. For instance, within the first region, a maximum weight value of 0.41 and 2639 pixels were obtained for semen, in comparison with the maximum weight value of 0.22 and 707 pixels obtained for vaginal fluid. On the contrary, within the second region, a maximum weight value of 0.36 and 1576 pixels were obtained for semen, in comparison to the overwhelming maximum weight value of 0.69 and 2122 pixels obtained for vaginal fluid. This way, it becomes extremely clear the optimum spot from which collecting the semen remains containing the aggressor's DNA. Even though both regions contained traces of semen, within the second region these traces were hindered by a considerably larger amount of vaginal fluid. Thus, the first region should be chosen for subsequent genetic analysis, *i.e.* this region should be the one that might be selected, cut, separated from the rest of the stain with an excess of vaginal fluid, and subsequently subjected to DNA extraction and typing.

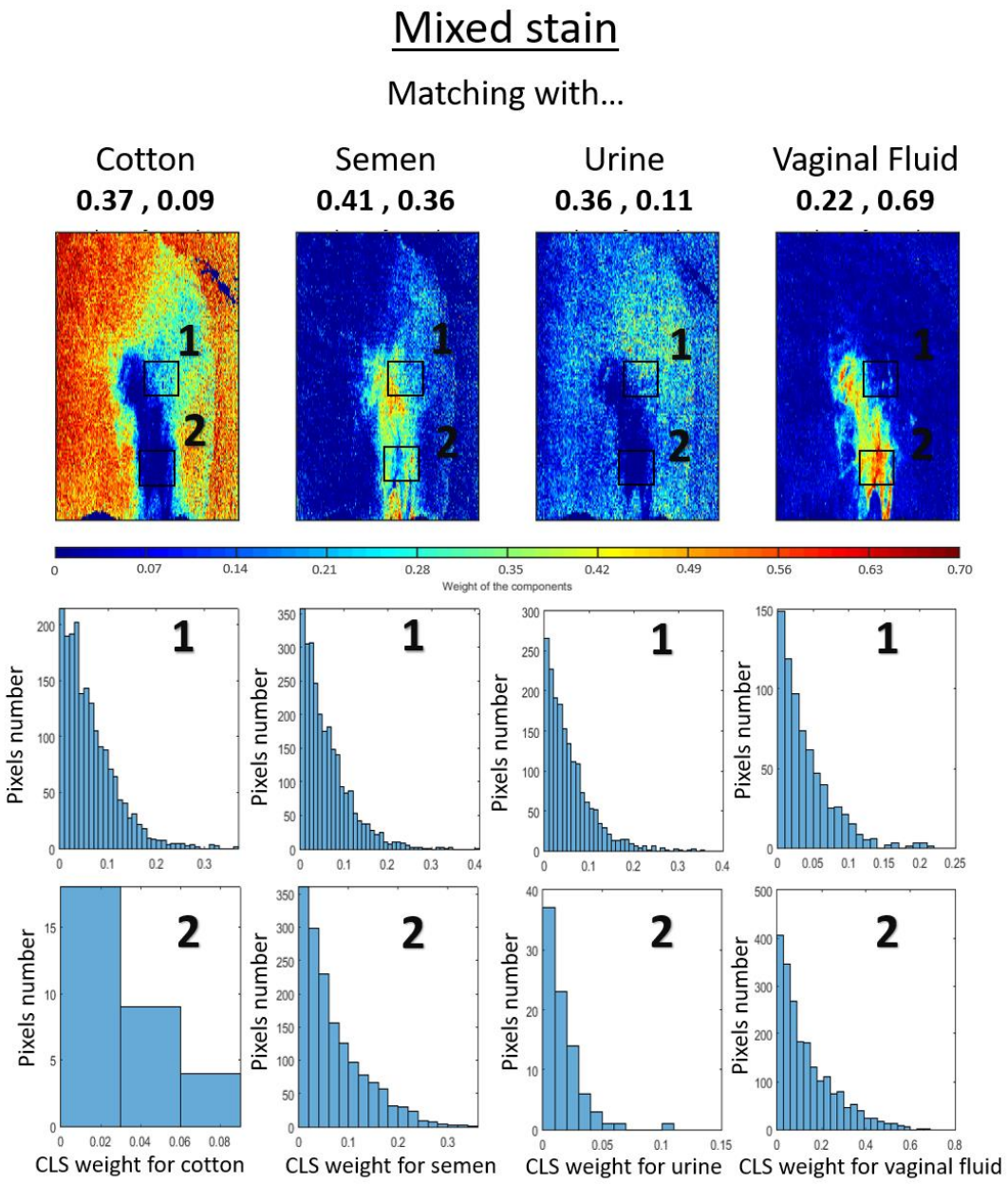

Figure 9.7. CLS classification model applied to a mixture of semen-vaginal fluid on cotton fabric. The CLS coloured maps for each class (cotton, semen, urine and vaginal fluid) are displayed. The maximum CLS weight values obtained for each class within the two selected stained regions are indicated above every colour map, corresponding the first value to region 1 and the second, to region 2. The histograms containing the number of pixels within the selected regions and their corresponding CLS weight to each class are provided below every colour map.

Conclusions

First, this study has demonstrated that invisible stains can be easily visualized under NIR wavelengths, especially when using a chemometric analysis such as PCA that easily discriminates between stain and cotton (background). In fact, UV–Vis light sources are currently being used for detecting invisible stains, thus it is interesting that NIR can also achieve comparable results.

The most significant capability of NIR-HSI in comparison to UV–Vis is its selectivity, which enabled the discrimination of semen from urine and vaginal fluid; a discrimination whose ultimate goal is the confirmatory identification of different body fluids mixed in a unique stain. To this aim, NIR-HSI supported by chemometric classification models such as CLS, has demonstrated to be highly useful to discriminate body fluids even in semen-vaginal fluid mixtures which is challenging for forensic practitioners. Thirty years after the discovery and using of UV light sources to non-selectively detect stains of body fluids, NIR-HSI has appeared as the perfect complementary technique to overcome the crucial aspect of knowing the distribution of the body fluids along the stain. Moreover, this procedure enabled the selective visualization of the individual distribution of each body fluid present on the stain providing useful information to select the optimum region from which recovering the semen traces.

According to the results reported in this work, the identification has not been optimum and thus, this methodology (NIR-HSI-CLS) cannot be considered as a confirmatory technique, but it is proposed as useful complementary technique to visualize a stain after having been confirmed traces of semen in it. Further studies using both more advance chemometric tools and larger NIR spectral libraries need to be accomplished to improve the classification and the identification of body fluids stains in casework.

References

[1] A. Schepers, Trailer CSI The Hague, 2012, from CSI The Hague project (last accessed May 2018). ⟨ https://www.youtube.com/watch?v=um_grUdOx38⟩.

[2] K. Virkler, I.K. Lednev, Analysis of body fluids for forensic purposes: from laboratory testing to non-destructive rapid confirmatory identification at a crime scene, Forensic Sci. Int. 188 (2009) 1-17.

[3] F. Zapata, M.A. Fernández de la Ossa, C. García-Ruiz, Emerging spectrometric techniques for the forensic analysis of body fluids, Trends Anal. Chem. 64 (2015) 53-63.

[4] F. Zapata, I. Gregório, C. García-Ruiz, Body fluids and spectroscopic techniques in forensics: a perfect match?, J. Forensic Med. 1 (2015). DOI:10.4172/jfm.1000101.

[5] G.J. Edelman, E. Gaston, T.G. van Leeuwen, P.J. Cullen, M.C.G. Aalders, Hyperspectral imaging for non-contact analysis of forensic traces, Forensic Sci. Int. 223 (2012) 28-39.

[6] D.G. Nelson, K.A. Santucci, An alternate light source to detect semen, Acad. Emerg. Med. 9 (10) (2002) 1045-1048.

[7] N. Vandenberg, R.A.H. van Oorschot, The use of polilight in the detection of seminal fluid, saliva, and bloodstains and comparison with conventional chemicalbased screening tests, J. Forensic Sci. 51 (2) (2006) 361-370.

[8] A. Fiedler, J. Rehdorf, F. Hilbers, L. Johrdan, C. Stribl, M. Benecke, Detection of semen (human and boar) and saliva on fabrics by a very high powered UV-/VIS Light source, Open Forensic Sci. J. 1 (2008) 12-15.

[9] J. Workman Jr., L. Weyer, Practical Guide and Spectral Atlas for Interpretive Near-Infrared Spectroscopy, Second ed., CRC Press, Taylor & Francis Group, Boca Raton, USA, 2012.

[10] D.A. Burns, E.W. Ciurczak, Handbook of Near Infrared Analysis, Third ed., CRC Press, Taylor & Francis Group, Boca Raton, USA, 2008.

[11] J.M. Amigo, Practical issues of hyperspectral imaging analysis of solid dosage forms, Anal. Bioanal. Chem. 398 (2010) 93-109.

[12] M. Vidal, J.M. Amigo, Pre-processing of hyperspectral images. Essential steps before image analysis, Chemom. Intell. Lab. Syst. 117 (2012) 138-148.

[13] J.M. Amigo, H. Babamoradi, S. Elcoroaristizabal, Hyperspectral image analysis. A tutorial, Anal. Chim. Acta 896 (2015) 34-51.

[14] A.C. Lin, H. Hsieh, L. Tsai, A. Linacre, J.C. Lee, Forensic applications of infrared imaging for the detection and recording of latent evidence, J. Forensic Sci. 52 (2007) 1148-1150.

[15] G.J. Edelman, T.G. van Leeuwen, M.C.G. Aalders, Hyperspectral Imaging of the Crime Scene for Detection and Identification of Blood Stains, Proc. SPIE 8743 (2013), 2013 (87430A/1-87430A/7).

[16] B. Li, P. Beveridge, W.T. O'Hare, M. Islam, The application of visible wavelength reflectance hyperspectral imaging for the detection and identification of blood stains, Sci. Justice 54 (2014) 432-438.

[17] G.J. Edelman, T.G. van Leeuwen, M.C. Aalders, Visualization of latent blood stains using visible reflectance hyperspectral imaging and chemometrics, J. Forensic Sci. 60 (2015) S188-S192.

[18] K. Virkler, I.K. Lednev, Raman spectroscopy offers great potential for the nondestructive confirmatory identification of body fluids, Forensic Sci. Int. 181 (1-3) (2008) e1-e5.

[19] V. Sikirzhytski, K. Virkler, I.K. Lednev, Discriminant analysis of Raman spectra for body fluid identification for forensic purposes, Sensors 10 (4) (2010) 2869-2884.

[20] V. Sikirzhytski, A. Sikirzhytskaya, I.K. Lednev, Multidimensional Raman spectroscopic signatures as a tool for forensic identification of body fluid traces: a review, Appl. Spectrosc. 65 (11) (2011) 1223-1232.

[21] K.M. Elkins, Rapid presumptive “Fingerprinting” of body fluids and materials by ATR FT-IR spectroscopy, J. Forensic Sci. 56 (6) (2011) 1580-1587.

[22] C. Orphanou, The detection and discrimination of human body fluids using ATR FT-IR spectroscopy, Forensic Sci. Int. 252 (2015) e10-e16.

[23] F. Zapata, M.A. Fernández, de la Ossa, C. García-Ruiz, Differentiation of body fluid stains on fabrics using external reflection Fourier Transform Infrared Spectroscopy (FT-IR) and chemometrics, Appl. Spectrosc. 70 (4) (2016) 654-665.

[24] J.M. Amigo, HYPERTools (⟨www.models.life.ku.dk/HYPERTools⟩), Department of Food Science, Faculty of Science, University of Copenhagen, Copenhagen, 2016.

General conclusions

Conclusiones generales

In this Doctoral Thesis, different spectroscopic approaches have been performed to face three currently relevant forensic challenges: the transfer of residues, the identification of explosive residues and the identification of stains of body fluids.

In **Section 1**, new analytical approaches have been developed for the study of different aspects of the transfer of residues, either gunshot residues or explosive residues.

In Chapter 1, it has been possible to correlate the density of GSR with the shooting distance in the range 30-220 cm (for the ammunition, weapon, and conditions used), which comprises the limits between short to long distance. Specifically, it has been demonstrated an exponential decrease of the amount of GSR with the shooting distance, according to the equation $N\ pixels\ with\ GSR = 15016\ e^{-0.04(shooting\ distance)}$.

In Chapter 2, the tendencies displayed by different explosives when being transferred on different surfaces by means of consecutive fingerprints have been determined. Particularly, the finely pulverized explosives (with small particle size) showed an exponential / potential decrease in their transfer on cotton / polycarbonate with the consecutive fingerprints. On the contrary, the oxidizing salts (hygroscopic and with larger particle size) did not show any tendency in their transfer with respect to the ordinal number of the impression. They were transferred to a greater or lesser extent independently of the number of impressions. Likewise, it was found that the variability between people in the transfer was not significant, when following a predefined protocol.

In Chapter 3, the inorganic components of the explosive residues transferred to handprints have been identified and quantified by means of the combined use of Raman spectroscopy and ion chromatography. The limitations of one technique have been profitably compensated with the skills and abilities of the other, and *vice versa*. Specifically, Raman spectroscopy has enabled the identification of the major oxidizing salt (anion + cation), which is only possible when the salt is analysed in solid state. On the contrary, ion chromatography has allowed to quantify the ions in solution, both major and minor ions.

In **Section 2**, significant advances in the characterization and identification of explosives by vibrational spectroscopic techniques have been accomplished.

In Chapter 4, the most relevant key aspects of explosives have been critically revised, including their definition, historical evolution and classification (depending on the velocity of detonation or the application). In the absence of a classification that is useful for the chemical-analytical identification of explosives, this Chapter has proposed a new general classification based on the chemical composition of explosives. The fundament of this new classification lays on the discrimination between individual uni-molecular explosives (organic or inorganic) and oxidizer-fuel explosive mixtures. In addition, Chapter 4 has reviewed and compiled the terrorist attacks committed with explosives in Europe, evidencing a significant increase during the last century. This increase has been partly due to the greater ease to obtain / manufacture a large variety of explosives, most of them discovered during the 19th and 20th centuries.

In Chapter 5, the Raman, IR and NIR spectra of the explosives TNT, RDX, PETN, TATP, HMTD, dynamite, ANFO, ANAl, black powder, chloratite, single, double and triple base smokeless powders, and oxidizing salts of nitrate, chlorate and perchlorate; have been interpreted in terms of the fundamental vibrations, overtones or combination bands that produce them. In addition, the spectra of explosives and oxidizing salts have been verified to be characteristic and selective enough for each explosive, with the exception of some single and double base powders (whose chemical composition was very similar), and some nitrate/perchlorate salts (whose bands, exclusively due to the anion, have not enabled to differentiate the present cation). This Chapter has also constituted a spectral library of explosives with which later comparing the spectra of the post-blast residues collected in Chapter 6.

In Chapter 6, theoretical hypotheses regarding the chemical reactions that occur during the detonation of an explosive have been contrasted with simple empirical observations of real detonations, such as the colour of the smoke. Particularly, it has been verified that not all explosives with negative oxygen balance decompose to carbon particles, which shows that chemical mechanisms of detonation are different between explosives. Interestingly, intact particles of the inorganic components of oxidizing-fuel mixtures have allowed to identify the explosive in the post-blast residues of either pyrotechnic devices or improvised explosive devices by FTIR and Raman spectroscopy. It has been also verified that the identification of residues by means of Raman microscopy strongly depends on the surface on which these have been collected, being the smooth

and homogeneous surfaces (such as glass and wood), those that gave better results. On the other hand, intact particles of uni-molecular organic explosives have not been detected in post-blast residues using spectroscopic techniques, which evidences the greater performance yield in the decomposition of these explosives during detonation compared to oxidizer-fuel mixtures.

In **Section 3**, significant advances in the localization and identification of stains of body fluids by vibrational spectroscopic and imaging techniques have been accomplished.

In Chapter 7, the state of the art on the identification of body fluids by means of spectrometric techniques has been revised. A significant number of studies conclude that spectroscopy in the UV-Vis range is very useful in the presumptive location of stains of body fluids due to the fluorescence they produce. However, this fluorescence is not selective and does not allow confirmatory identification. For this reason, the research that aims to discriminate and unequivocally identify body fluids by selective spectroscopic techniques (mainly IR/Raman) has significantly increased in the last recent years.

In Chapter 8, stains of semen, vaginal fluid and urine on cotton fabrics have been successfully discriminated by FTIR. After establishing the characteristic FTIR spectral signature of each fluid, it has been visually verified that there are perceptible differences among them. However, given the high similarity between the spectra of semen and vaginal fluid (whose bands are due to the peptide bonds of the respective proteins that composed these body fluids), multivariate analysis methods have supported their discrimination (in stains of a single body fluid). However, in mixtures of several body fluids (semen-vaginal fluid) inconclusive results were obtained, since only vaginal fluid was detected.

In Chapter 9, the discrimination of individual stains of semen, vaginal fluid and urine using NIR-HSI has been also demonstrated. Although the NIR spectra of stains of semen/vaginal fluid on cotton are visually indistinguishable, the multivariate analysis of the NIR spectra has allowed to find little but significant differences that allow their identification. In addition, the advantage of NIR-HSI of simultaneously recording the NIR spectra of every pixel in the stain has enabled to discriminate the areas of the stain with a greater proportion of one or another fluid (in mixtures of several body fluids). This allows to select the

zones of the stain where the body fluid of interest is in greater proportion, thus improving the performance and reducing the interferences of other fluids in the extraction and subsequent genetic analysis.

Finally, I want to include in this section my conclusions about the last of the objectives set out in every doctoral Thesis presented by compendium of articles: the publishing of the accomplished research in international journals. After reading and revising hundreds of articles, I have learned that research that is not published in English in an international scientific journal, it simply does not exist. Overcoming the peer review process is a test that requires not only the comprehensive writing and prior critical reading by the authors, but also the correction, improvement and/or discussion of objective critical comments enunciated by unknown reviewers. During my PhD, this formative training has been particularly hard, extensive and multidisciplinary because of the large variety of scientific journals and categories in which I have had the luck to publish my research. In brief, it has been published in the categories of analytical chemistry (*TrAC, Analytical Chemistry, Talanta,* and *Sensors*); spectroscopy (*Spectrochimica Acta A, Applied Spectroscopy, Journal of Raman Spectroscopy,* and *Applied Spectroscopy Reviews*); and forensic sciences (*Forensic Science International, Science and Justice,* and *Journal of Forensic Medicine*). In conclusion, another thing I have also verified during the PhD is that any small scientific advance anyone gets, automatically opens new ideas, new experiments and new horizons to investigate. A Thesis is not the end, but the beginning.

En esta Tesis Doctoral se han investigado distintas aproximaciones espectroscópicas para afrontar tres problemáticas forenses actualmente relevantes: la transferencia de residuos, la identificación de residuos de explosivos y la identificación de manchas de fluidos biológicos.

En la **Sección 1**, se han desarrollado nuevas aproximaciones analíticas para el estudio de distintos aspectos acerca de la transferencia de residuos, bien residuos de disparo o residuos de explosivo.

En el Capítulo 1, se ha podido correlacionar la densidad de GSR con la distancia de disparo en el rango de 30-220 cm (para la munición, arma y condiciones empleadas), abarcando los límites entre corta y larga distancia. Concretamente, se ha comprobado que la cantidad de GSR se reduce exponencialmente con la distancia de disparo de acuerdo con la ecuación $Nº\,pixeles\,con\,GSR = 15016\,e^{-0.04(distancia\,disparo)}$.

En el Capítulo 2, se han determinado, por primera vez, las tendencias que presentan diferentes explosivos al ser transferidos sobre distintas superficies mediante impresiones dactilares consecutivas. Particularmente, los explosivos finamente pulverizados (con pequeño tamaño de partícula) mostraron una tendencia de decrecimiento exponencial/potencial en su transferencia sobre algodón/policarbonato en función de las consecutivas impresiones dactilares. Por el contrario, las sales oxidantes (higroscópicas y con mayor tamaño de partícula) no mostraron ninguna tendencia y se transfirieron en mayor o menor medida con independencia de la impresión realizada. Asimismo, se comprobó que la variabilidad entre personas en la transferencia no era significativa, cuando se sigue un protocolo predefinido.

En el Capítulo 3 se han identificado y cuantificado los componentes inorgánicos de los residuos de explosivo transferidos en las huellas palmares mediante el empleo combinado de la espectroscopía Raman y la cromatografía iónica. Las limitaciones de una técnica han sido provechosamente compensadas con las aptitudes y capacidades de la otra, y viceversa. En concreto, la espectroscopía Raman ha permitido identificar la sal oxidante (anión + catión) mayoritaria, algo que únicamente es posible cuando se analiza la sal en estado sólido. Por el contrario, la cromatografía iónica ha permitido llevar a cabo la cuantificación de los iones en disolución, tanto los mayoritarios como los minoritarios.

En la **Sección 2**, se han realizado significativos avances en el campo de la caracterización e identificación de explosivos mediante técnicas de espectroscopía vibracional.

En el Capítulo 4, se han revisado de forma crítica los aspectos clave más relevantes de los explosivos incluyendo su definición, evolución histórica y clasificación (según la velocidad de detonación o la aplicación). Ante la falta de una clasificación que sea útil en la identificación químico-analítica de los explosivos, en este capítulo se ha propuesto una nueva clasificación general basada en la composición química de los explosivos. Esta nueva clasificación tiene como eje principal la discriminación entre explosivos individuales uni-moleculares (orgánicos o inorgánicos) y mezclas explosivas oxidante-combustible. Asimismo, en el Capítulo 4 se ha revisado y comprobado el incremento que ha habido en el uso ilegal de explosivos en la comisión de atentados terroristas durante el último siglo. Tal incremento ha sido en parte debido a la mayor facilidad de obtener/fabricar una gran variedad de explosivos, la mayoría de ellos descubiertos a lo largo de los siglos XIX y XX.

En el Capítulo 5, se han interpretado pormenorizadamente los espectros Raman, IR y NIR de los explosivos TNT, RDX, PETN, TATP, HMTD, dinamita, ANFO, ANAl, pólvora negra, cloratita, pólvoras de simple, doble y triple base, y sales oxidantes de nitrato, clorato y perclorato; en términos de las vibraciones fundamentales, sobretonos o bandas de combinación que los producen. Se ha comprobado además que los espectros son característicos y selectivos de cada explosivo, a excepción de algunas de las pólvoras de simple y doble base (cuya composición química es muy similar), y de algunas de las sales de nitrato, y de perclorato (cuyas bandas, debidas únicamente a las vibraciones fundamentales del anión, no han permitido diferenciar el catión presente). Este capítulo ha constituido, además, una biblioteca espectral de explosivos con los que poder comparar los espectros de los residuos post-explosión del Capítulo 6.

En el Capítulo 6, se han contrastado, en primer lugar, hipótesis teóricas respecto de las reacciones químicas que ocurren durante la detonación de un explosivo, con observaciones empíricas sencillas de detonaciones reales, tales como el color del humo. En concreto, se ha verificado que no todos los explosivos con balance de oxígeno negativo se descomponen a partículas de carbono, lo que evidencia que los mecanismos químicos de detonación son diferentes entre explosivos. Asimismo, se han identificado, mediante espectroscopía FTIR y

Raman, partículas intactas de los componentes inorgánicos de mezclas oxidante-combustible en residuos post-explosionados de artefactos pirotécnicos y artefactos explosivos improvisados. Se ha comprobado, además, que la identificación de los residuos mediante microscopía Raman depende en gran medida de la superficie sobre la que estos se han recolectado, siendo las superficies lisas y homogéneas las que proporcionaron mejores resultados, (*i.e.* vidrio y madera). Por el contrario, mediante técnicas espectroscópicas no se han detectado partículas de explosivos orgánicos uni-moleculares en restos post-explosionados, lo que evidencia un mayor rendimiento en la descomposición de estos explosivos frente a las mezclas oxidante-combustible.

En la **Sección 3**, se han realizado significativos avances en el campo de la localización e identificación de manchas de fluidos biológicos mediante técnicas de espectroscopía vibracional e imagen.

En el Capítulo 7, se ha profundizado en el conocimiento del estado del arte sobre la identificación de fluidos biológicos mediante técnicas espectrométricas. Una cantidad significativa de estudios concluyen que la espectroscopía UV-Vis, es muy útil en la localización presuntiva de manchas de fluidos biológicos, debido a la fluorescencia que éstas producen. Sin embargo, esta fluorescencia no es selectiva y no permite una identificación confirmatoria. Por ello, se han incrementado enormemente en los últimos años, los estudios que investigan la discriminación e identificación inequívoca de fluidos biológicos mediante técnicas espectroscópicas selectivas (principalmente IR/Raman).

En el Capítulo 8, se han discriminado con éxito manchas de semen, fluido vaginal y orina sobre tejidos de algodón mediante FTIR. Tras establecer la firma espectral FTIR característica de cada fluido, se ha comprobado visualmente que existen diferencias apreciables entre sí. No obstante, dada la elevada similitud entre los espectros de semen y fluido vaginal (cuyas bandas se deben a los enlaces peptídicos de las respectivas proteínas que los componen), los métodos de análisis multivariante empleados han ayudado significativamente en su discriminación (en manchas de un solo fluido). Sin embargo, en mezclas de varios fluidos (semen-fluido vaginal) se obtuvieron resultados no concluyentes, pues únicamente se detectaba el fluido vaginal.

En el Capítulo 9, se ha comprobado que la discriminación de manchas individuales de semen, fluido vaginal y orina, es también posible mediante

imagen NIR-HSI. Aunque se ha comprobado que los espectros NIR de manchas de semen y fluido vaginal sobre algodón son visualmente indistinguibles, el análisis multivariante ha permitido encontrar pequeñas pero significativas diferencias que permiten su identificación. Además, la ventaja de NIR-HSI de registrar simultáneamente los espectros NIR de todos y cada uno de los píxeles de una mancha, ha permitido en aquellas manchas que son una mezcla de varios fluidos, discriminar las zonas de la mancha con mayor proporción de uno u otro fluido. Esto permite seleccionar las zonas de la mancha donde el fluido de interés se encuentra en mayor proporción, mejorando así el rendimiento de la extracción y reduciendo las interferencias de otros fluidos en la posterior secuenciación genética.

Por último, quiero incluir en este apartado mis conclusiones acerca del último de los objetivos planteados en cualquier Tesis doctoral presentada por compendio de artículos: la publicación de la investigación realizada en revistas internacionales. Si algo he aprendido, tras revisar y leer cientos de artículos, es que la investigación que no está publicada en lengua inglesa en una revista científica internacional, sencillamente no existe. Superar la revisión por pares es una prueba que obliga no solo a la escritura y revisión crítica previa por parte de los autores, sino a la corrección, mejora y/o discusión objetiva de comentarios y críticas enunciados por revisores desconocidos. Durante mi doctorado, este aprendizaje formativo ha sido especialmente complicado, extenso y multidisciplinar por la amplia variedad de revistas científicas y categorías en las que he tenido la suerte de publicar mi investigación. En resumen, ésta ha sido publicada en las categorías de química analítica (*TrAC, Analytical Chemistry, Talanta,* y *Sensors*); espectroscopía (*Spectrochimica Acta A, Applied Spectroscopy, Journal of Raman Spectroscopy,* y *Applied Spectroscopy Reviews*); y ciencias forenses (*Forensic Science International, Science and Justice,* y *Journal of Forensic Medicine*). Por último, también he aprendido durante el doctorado que cualquier pequeño avance científico que se consigue, automáticamente abre nuevas ideas, nuevos experimentos y nuevos horizontes en los que investigar. Una Tesis no es el final, sino el principio.

Annexes

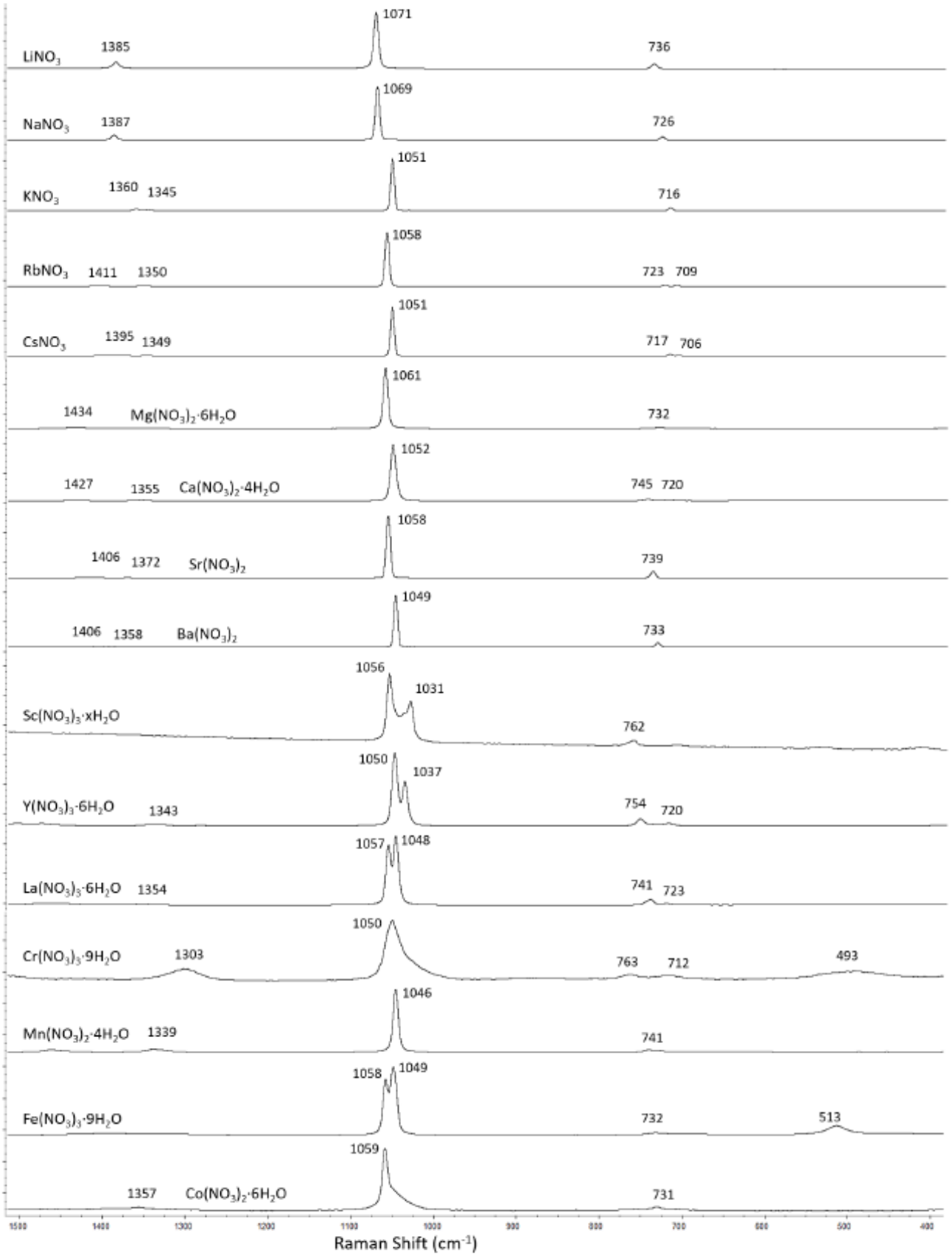
Nitrate salts
LiNO3
1385
1071
736
NaNO3
1387
1069
726
KNO3
1360
1345
1051
716
RbNO3
1411
1350
1058
723
709
CsNO3
1395
1349
1051
717
706
1434
Mg(NO3)2·6H2O
1061
732
1427
1355
Ca(NO3)2·4H2O
1052
745
720
1406
1372
Sr(NO3)2
1058
739
1406
1358
Ba(NO3)2
1049
733
Sc(NO3)3·xH2O
1056
1031
762
Y(NO3)3·6H2O
1343
1050
1037
754
720
La(NO3)3·6H2O
1354
1057
1048
741
723
Cr(NO3)3·9H2O
1303
1050
763
712
493
Mn(NO3)2·4H2O
1339
1046
741
Fe(NO3)3·9H2O
1058
1049
732
513
1357
Co(NO3)2·6H2O
1059
731
1500
1400
1300
1200
1100
1000
900
800
700
600
500
400
Raman Shift (cm-1)

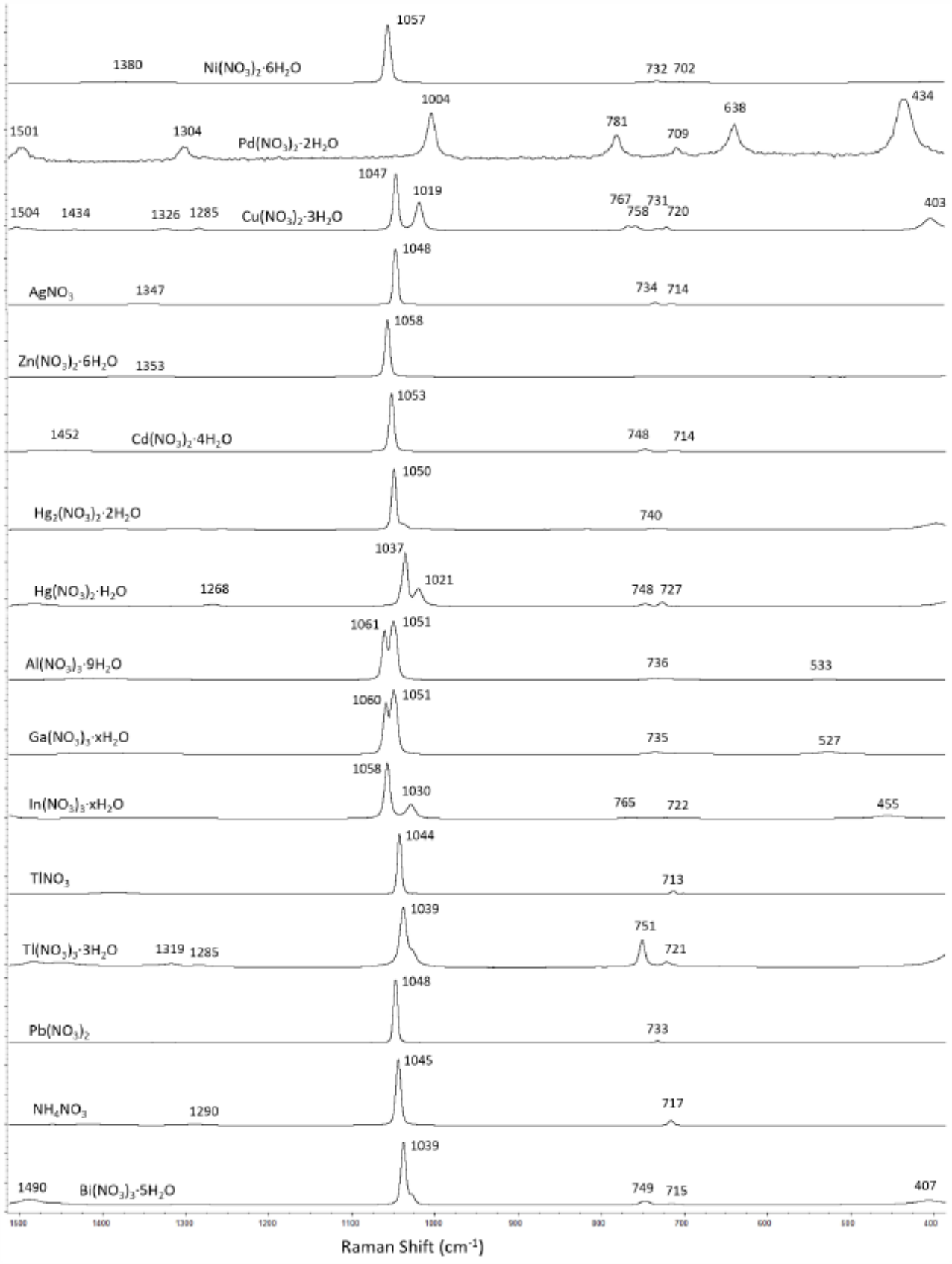
1057
1380
Ni(NO3)2·6H2O
732 702
1004
434
638
781
1501
1304
Pd(NO3)2·2H2O
709
1047
1019
767 731
1504 1434
1326 1285
Cu(NO3)2·3H2O
758 720
403
1048
AgNO3
1347
734 714
1058
Zn(NO3)2·6H2O
1353
1053
1452
Cd(NO3)2·4H2O
748 714
1050
Hg2(NO3)2·2H2O
740
1037
1021
Hg(NO3)2·H2O
1268
748 727
1061
1051
Al(NO3)3·9H2O
736
533
1060
1051
Ga(NO3)3·xH2O
735
527
1058
1030
In(NO3)3·xH2O
765 722
455
1044
TlNO3
713
1039
751
Tl(NO3)3·3H2O
1319 1285
721
1048
Pb(NO3)2
733
1045
NH4NO3
1290
717
1039
1490
Bi(NO3)3·5H2O
749 715
407
1500 1400 1300 1200 1100 1000 900 800 700 600 500 400
Raman Shift (cm-1)

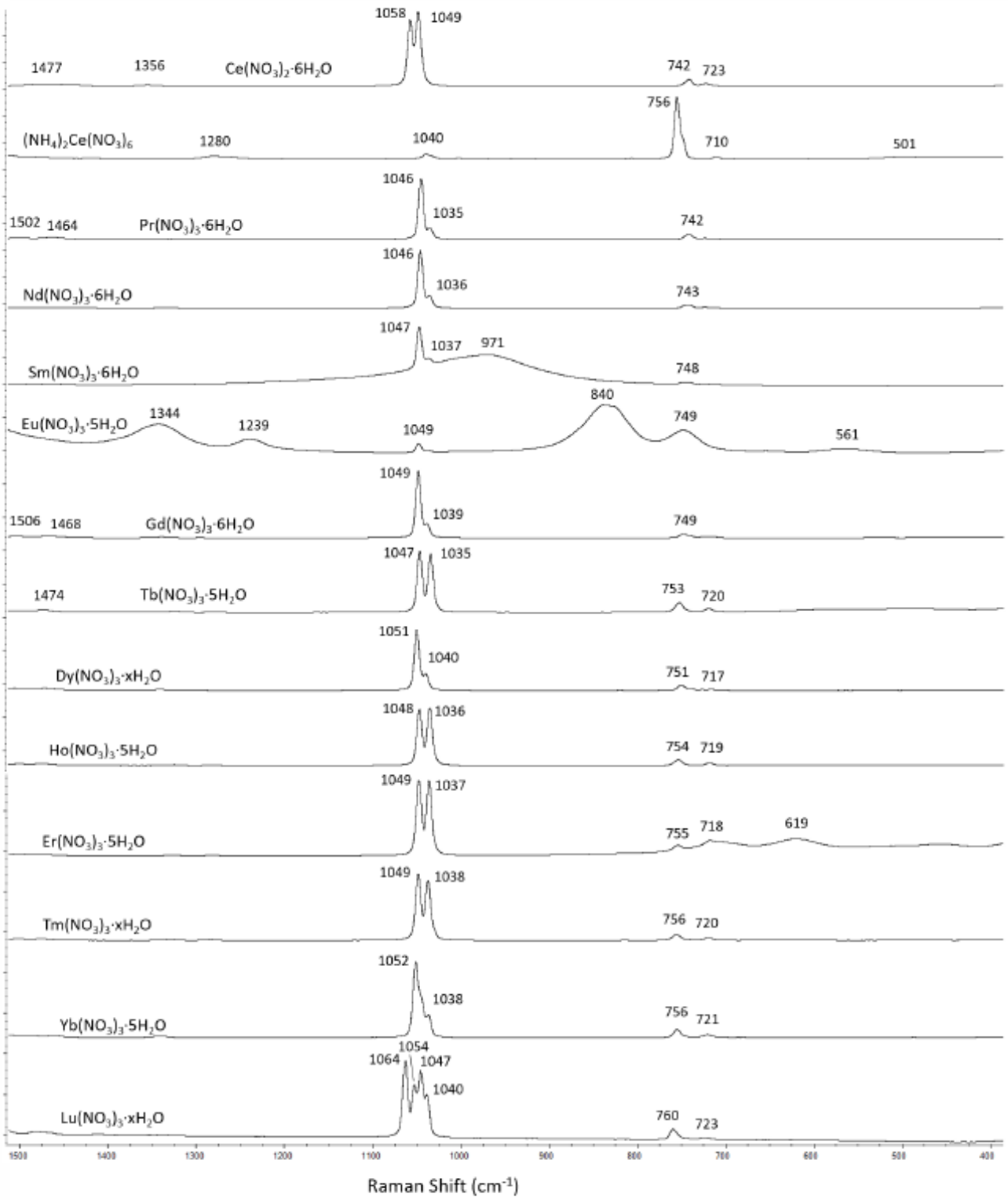
1058
1049
1477
1356
Ce(NO3)2·6H2O
742
723
756
(NH4)2Ce(NO3)6
1280
1040
710
501
1046
1035
1502
1464
Pr(NO3)3·6H2O
742
1046
1036
Nd(NO3)3·6H2O
743
1047
1037
971
Sm(NO3)3·6H2O
748
840
Eu(NO3)3·5H2O
1344
1239
1049
749
561
1049
1039
1506
1468
Gd(NO3)3·6H2O
749
1047
1035
1474
Tb(NO3)3·5H2O
753
720
1051
1040
Dy(NO3)3·xH2O
751
717
1048
1036
Ho(NO3)3·5H2O
754
719
1049
1037
Er(NO3)3·5H2O
755
718
619
1049
1038
Tm(NO3)3·xH2O
756
720
1052
1038
Yb(NO3)3·5H2O
756
721
1054
1064
1047
1040
Lu(NO3)3·xH2O
760
723
1500
1400
1300
1200
1100
1000
900
800
700
600
500
400
Raman Shift (cm-1)

Chlorate salts

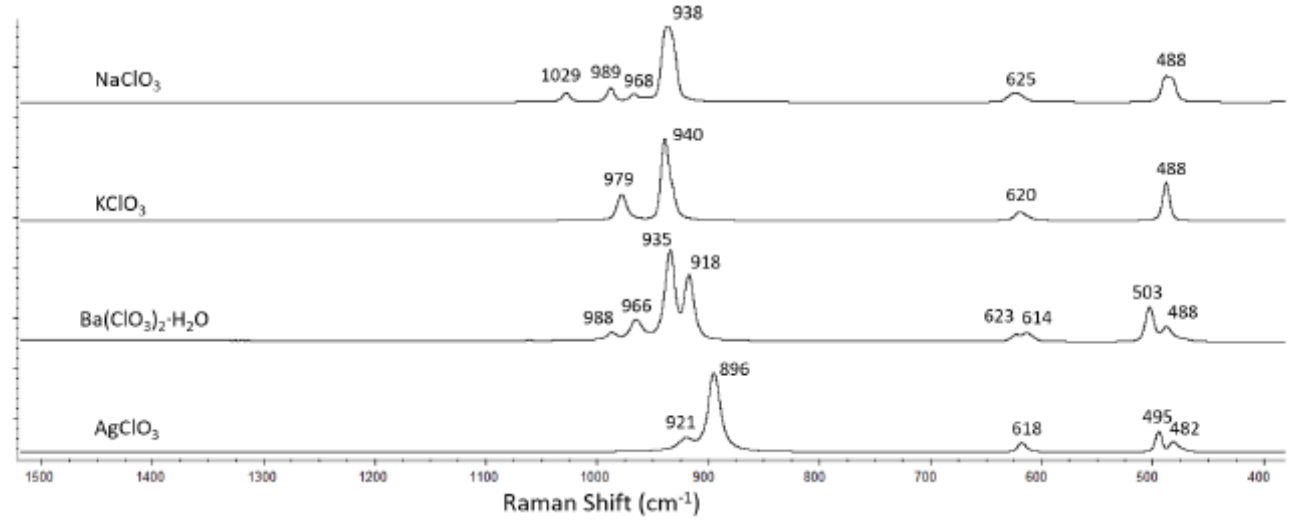

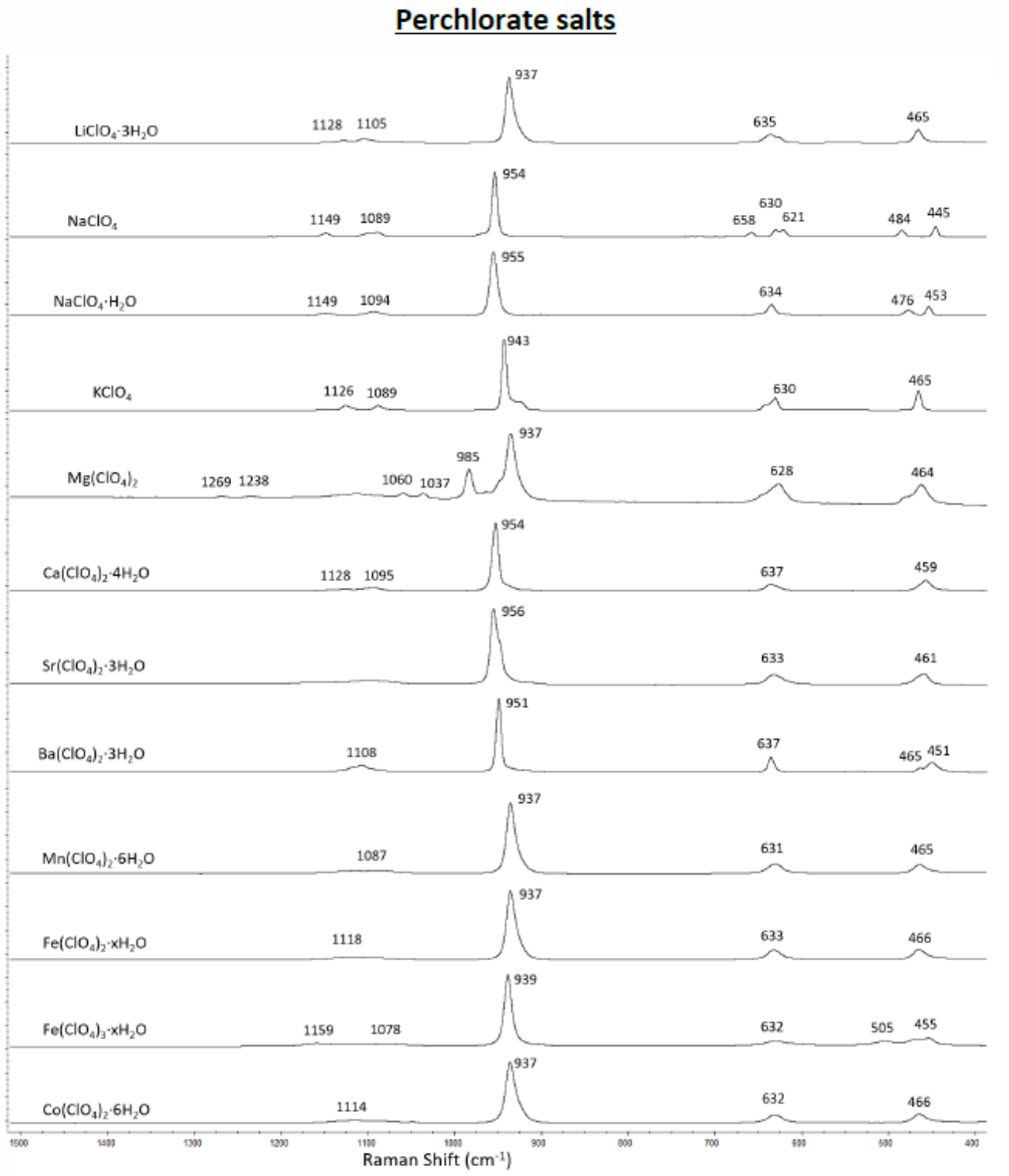
Perchlorate salts
LiClO4·3H2O
937
1128 1105
635
465
NaClO4
954
1149 1089
658 630 621
484 445
NaClO4·H2O
955
1149 1094
634
476 453
KClO4
943
1126 1089
630
465
Mg(ClO4)2
937
985
1269 1238
1060 1037
628
464
Ca(ClO4)2·4H2O
954
1128 1095
637
459
Sr(ClO4)2·3H2O
956
633
461
Ba(ClO4)2·3H2O
951
1108
637
465 451
Mn(ClO4)2·6H2O
937
1087
631
465
Fe(ClO4)2·xH2O
937
1118
633
466
Fe(ClO4)3·xH2O
939
1159 1078
632
505 455
Co(ClO4)2·6H2O
937
1114
632
466
1500 1400 1300 1200 1100 1000 900 800 700 600 500 400
Raman Shift (cm-1)

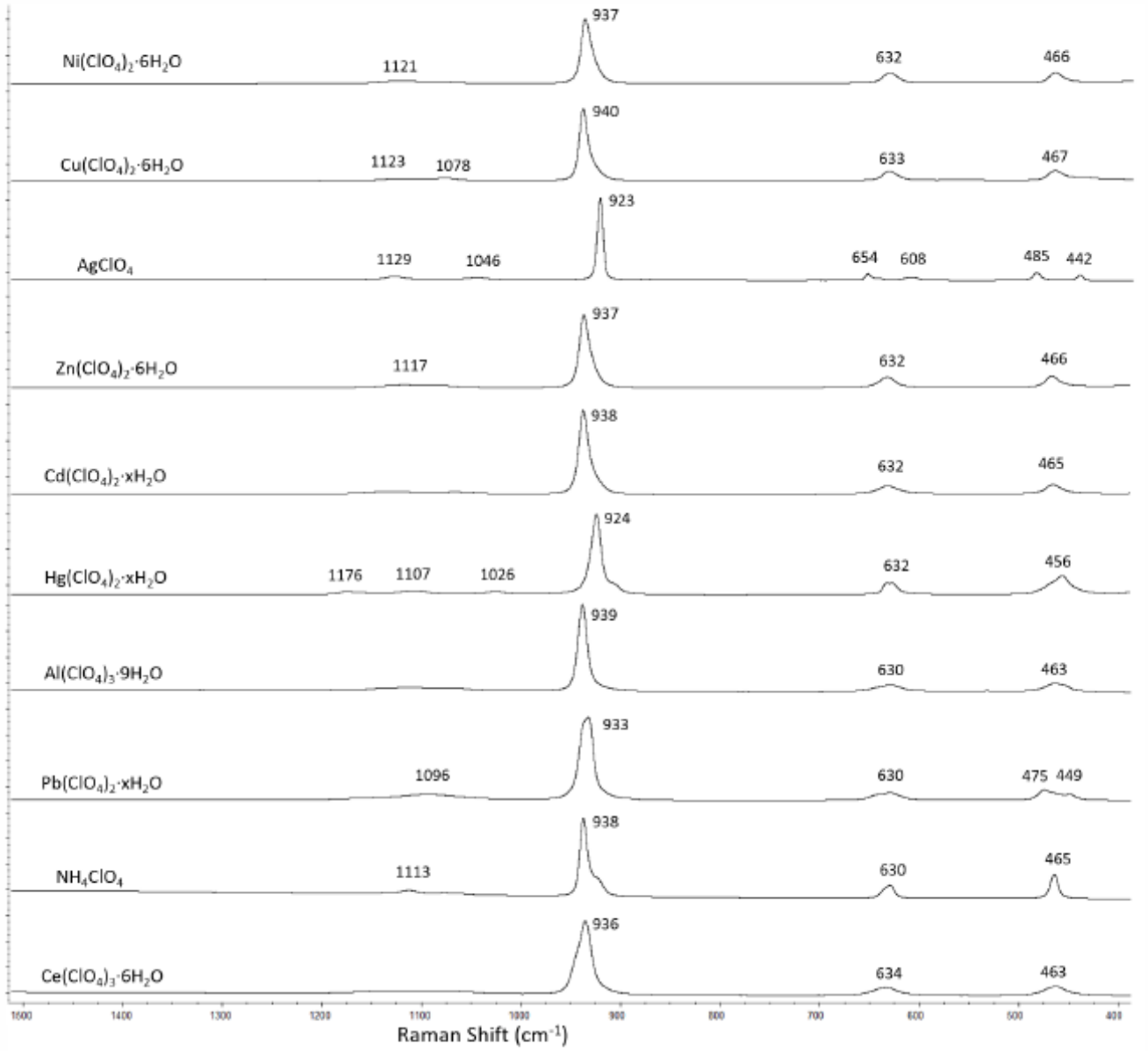
Ni(ClO4)2·6H2O
937
1121
632
466
Cu(ClO4)2·6H2O
940
1123
1078
633
467
AgClO4
923
1129
1046
654
608
485
442
Zn(ClO4)2·6H2O
937
1117
632
466
Cd(ClO4)2·xH2O
938
632
465
Hg(ClO4)2·xH2O
924
1176
1107
1026
632
456
Al(ClO4)3·9H2O
939
630
463
Pb(ClO4)2·xH2O
933
1096
630
475
449
NH4ClO4
938
1113
630
465
Ce(ClO4)3·6H2O
936
634
463
1600
1400
1300
1200
1100
1000
900
800
700
600
500
400
Raman Shift (cm-1)

Nitrate salts

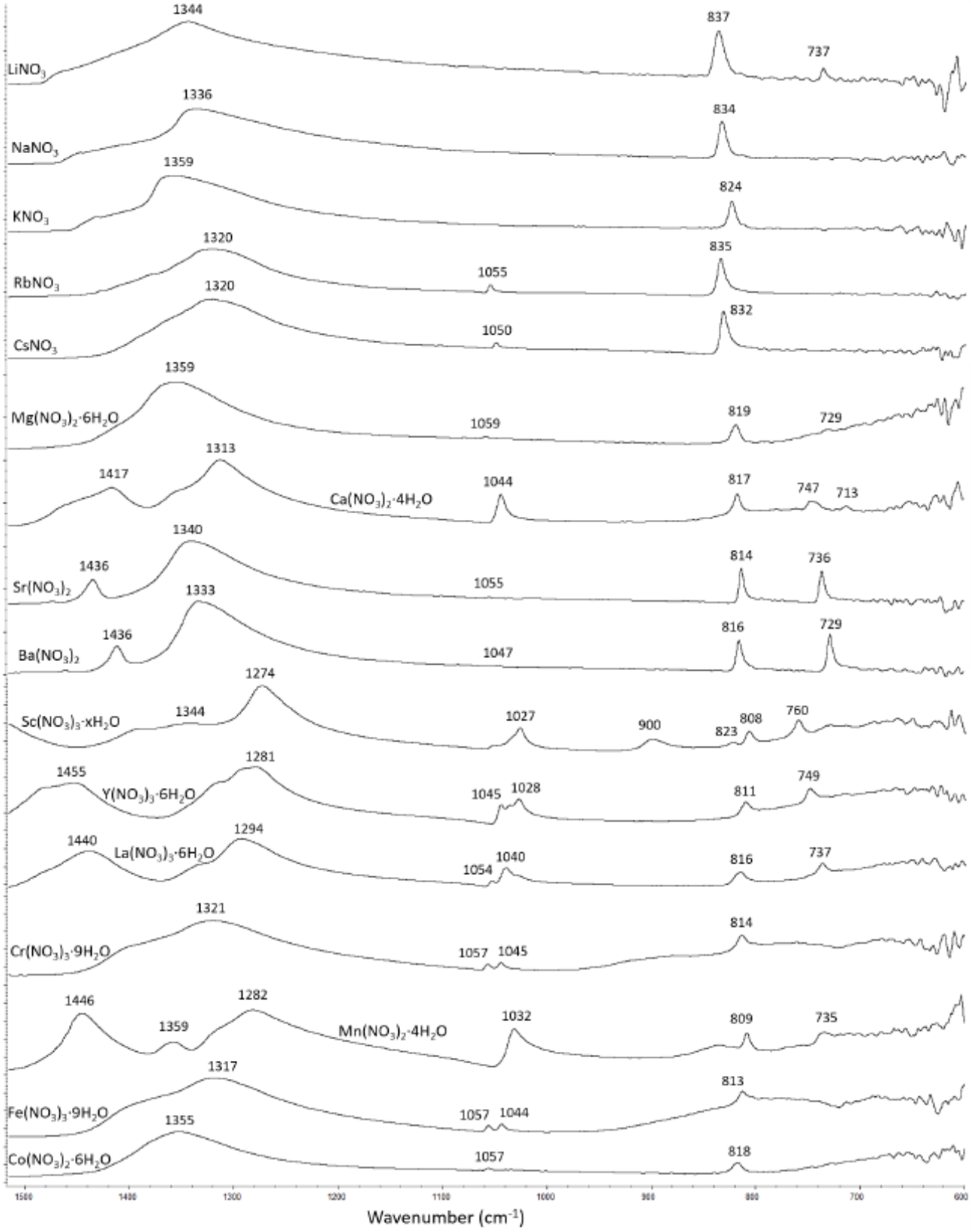

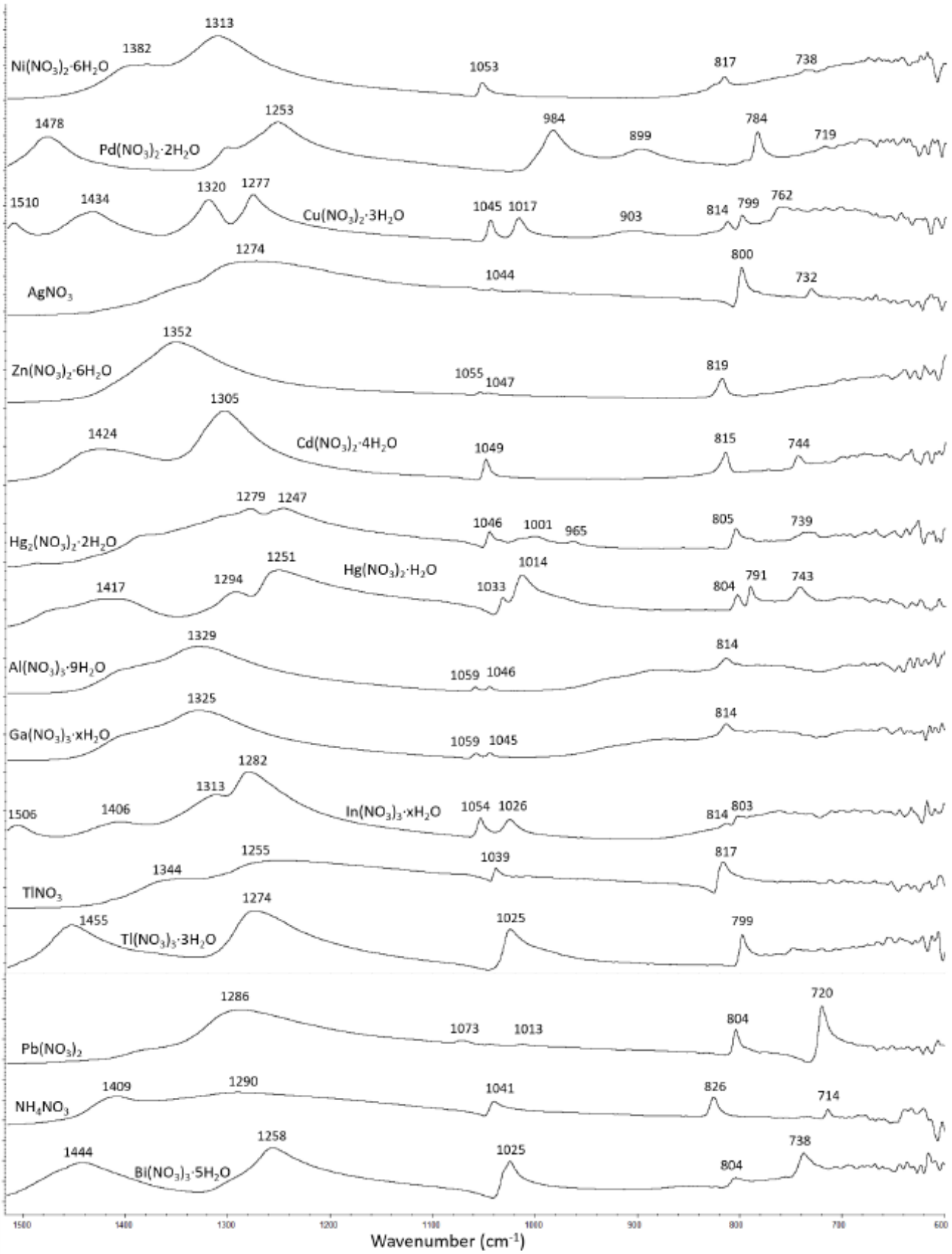
Ni(NO3)2·6H2O
1313
1382
1053
817
738
Pd(NO3)2·2H2O
1478
1253
984
899
784
719
Cu(NO3)2·3H2O
1510
1434
1320
1277
1045
1017
903
814
799
762
AgNO3
1274
1044
800
732
Zn(NO3)2·6H2O
1352
1055
1047
819
Cd(NO3)2·4H2O
1305
1424
1049
815
744
Hg2(NO3)2·2H2O
1279
1247
1046
1001
965
805
739
Hg(NO3)2·H2O
1417
1294
1251
1033
1014
804
791
743
Al(NO3)3·9H2O
1329
1059
1046
814
Ga(NO3)3·xH2O
1325
1059
1045
814
In(NO3)3·xH2O
1506
1406
1313
1282
1054
1026
814
803
TlNO3
1344
1255
1039
817
Tl(NO3)3·3H2O
1455
1274
1025
799
Pb(NO3)2
1286
1073
1013
804
720
NH4NO3
1409
1290
1041
826
714
Bi(NO3)3·5H2O
1444
1258
1025
804
738
1500
1400
1300
1200
1100
1000
900
800
700
600
Wavenumber (cm-1)

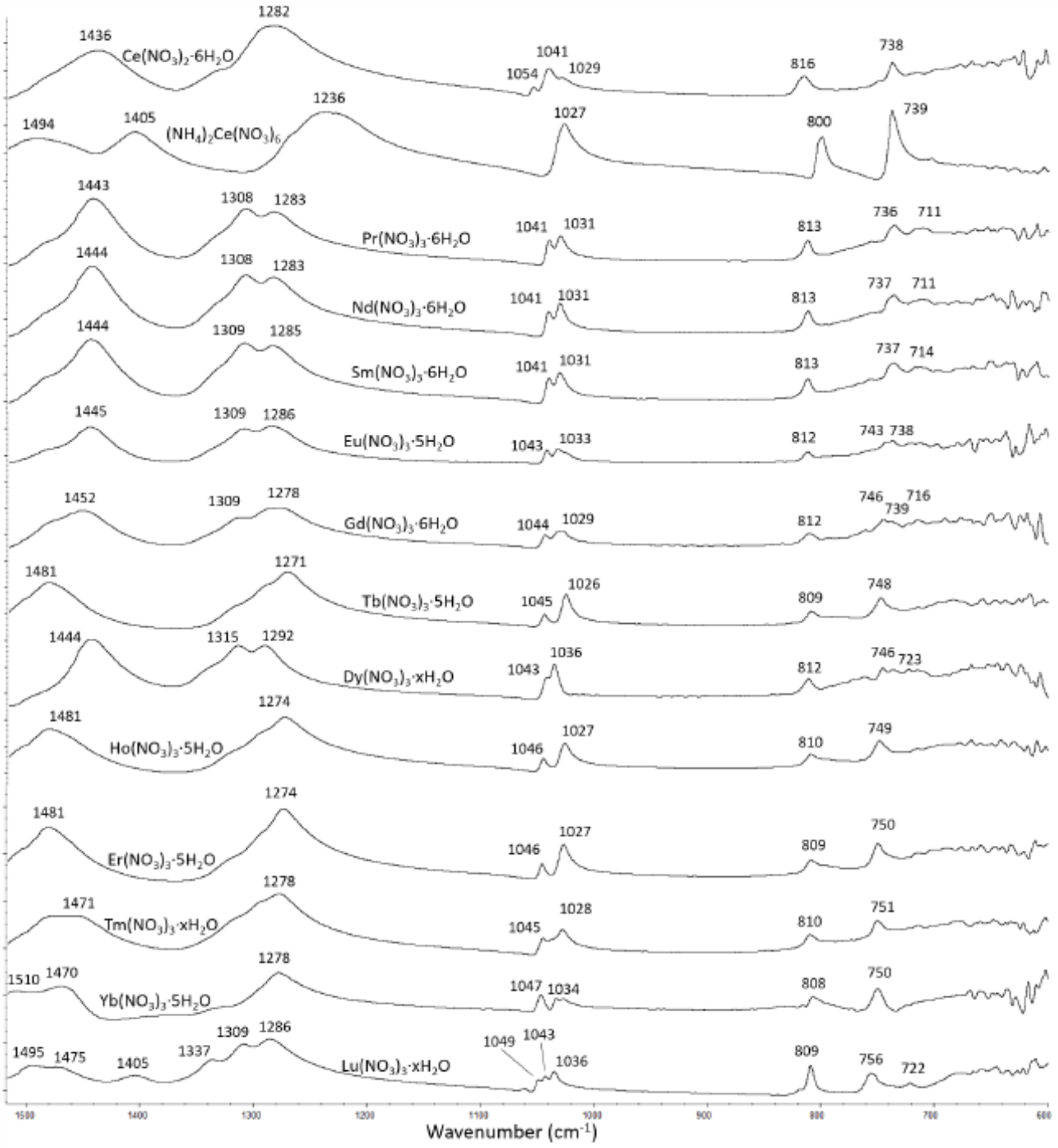
1436
1282
Ce(NO3)2·6H2O
1054
1041
1029
816
738
1494
1405
(NH4)2Ce(NO3)6
1236
1027
800
739
1443
1308
1283
Pr(NO3)3·6H2O
1041
1031
813
736
711
1444
1308
1283
Nd(NO3)3·6H2O
1041
1031
813
737
711
1444
1309
1285
Sm(NO3)3·6H2O
1041
1031
813
737
714
1445
1309
1286
Eu(NO3)3·5H2O
1043
1033
812
743
738
1452
1309
1278
Gd(NO3)3·6H2O
1044
1029
812
746
739
716
1481
1271
Tb(NO3)3·5H2O
1045
1026
809
748
1444
1315
1292
Dy(NO3)3·xH2O
1043
1036
812
746
723
1481
1274
Ho(NO3)3·5H2O
1046
1027
810
749
1481
1274
Er(NO3)3·5H2O
1046
1027
809
750
1471
1278
Tm(NO3)3·xH2O
1045
1028
810
751
1510
1470
1278
Yb(NO3)3·5H2O
1047
1034
808
750
1495
1475
1405
1337
1309
1286
Lu(NO3)3·xH2O
1049
1043
1036
809
756
722
1500
1400
1300
1200
1100
1000
900
800
700
600
Wavenumber (cm-1)

Chlorate salts

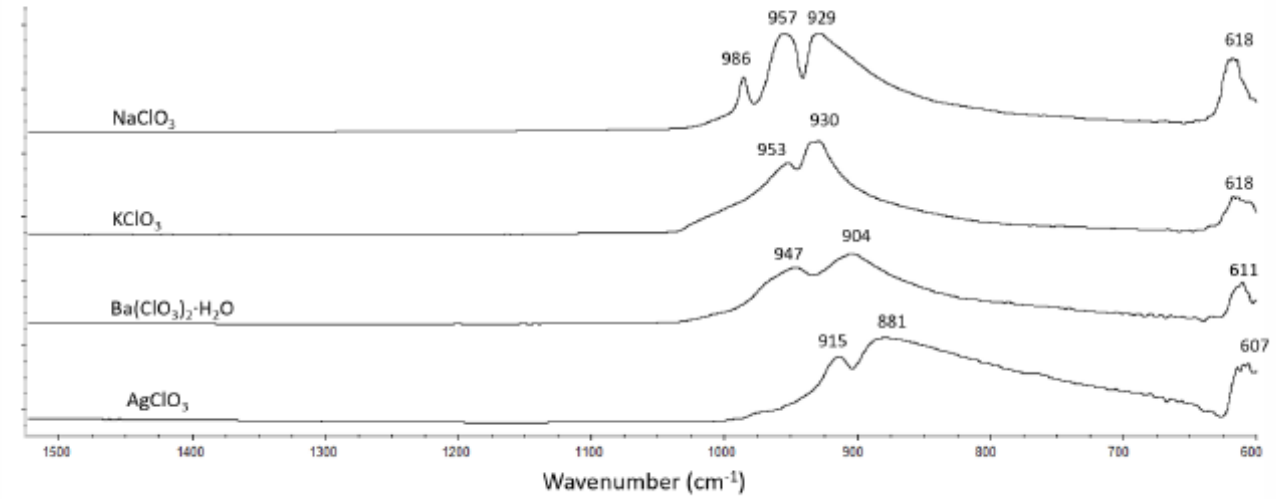

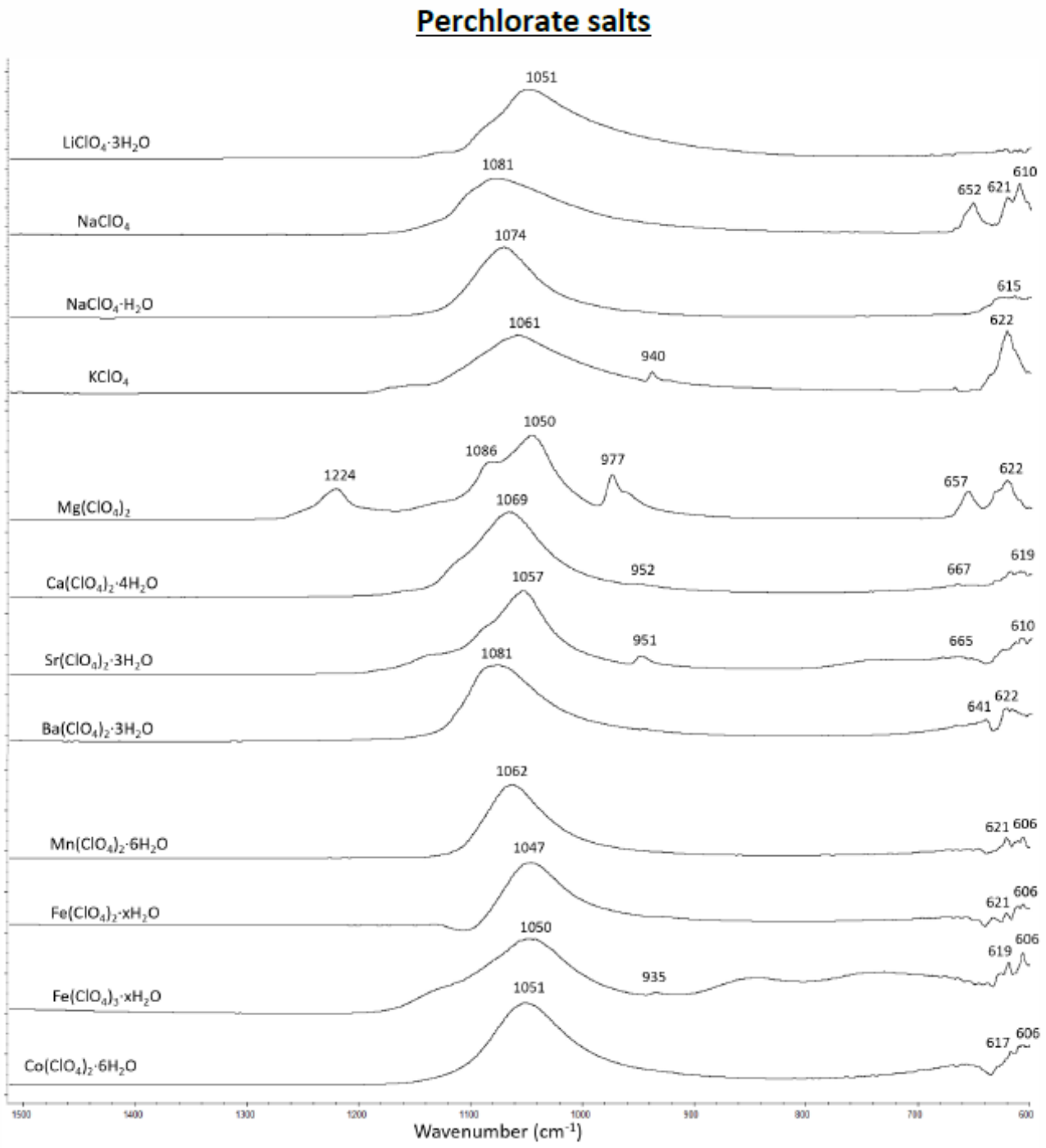
Perchlorate salts
LiClO4·3H2O
1051
NaClO4
1081
652
621
610
NaClO4·H2O
1074
615
KClO4
1061
940
622
Mg(ClO4)2
1224
1086
1050
977
657
622
Ca(ClO4)2·4H2O
1069
952
667
619
Sr(ClO4)2·3H2O
1057
951
665
610
Ba(ClO4)2·3H2O
1081
641
622
Mn(ClO4)2·6H2O
1062
621
606
Fe(ClO4)2·xH2O
1047
621
606
Fe(ClO4)3·xH2O
1050
935
619
606
Co(ClO4)2·6H2O
1051
617
606
1500
1400
1300
1200
1100
1000
900
800
700
600
Wavenumber (cm-1)

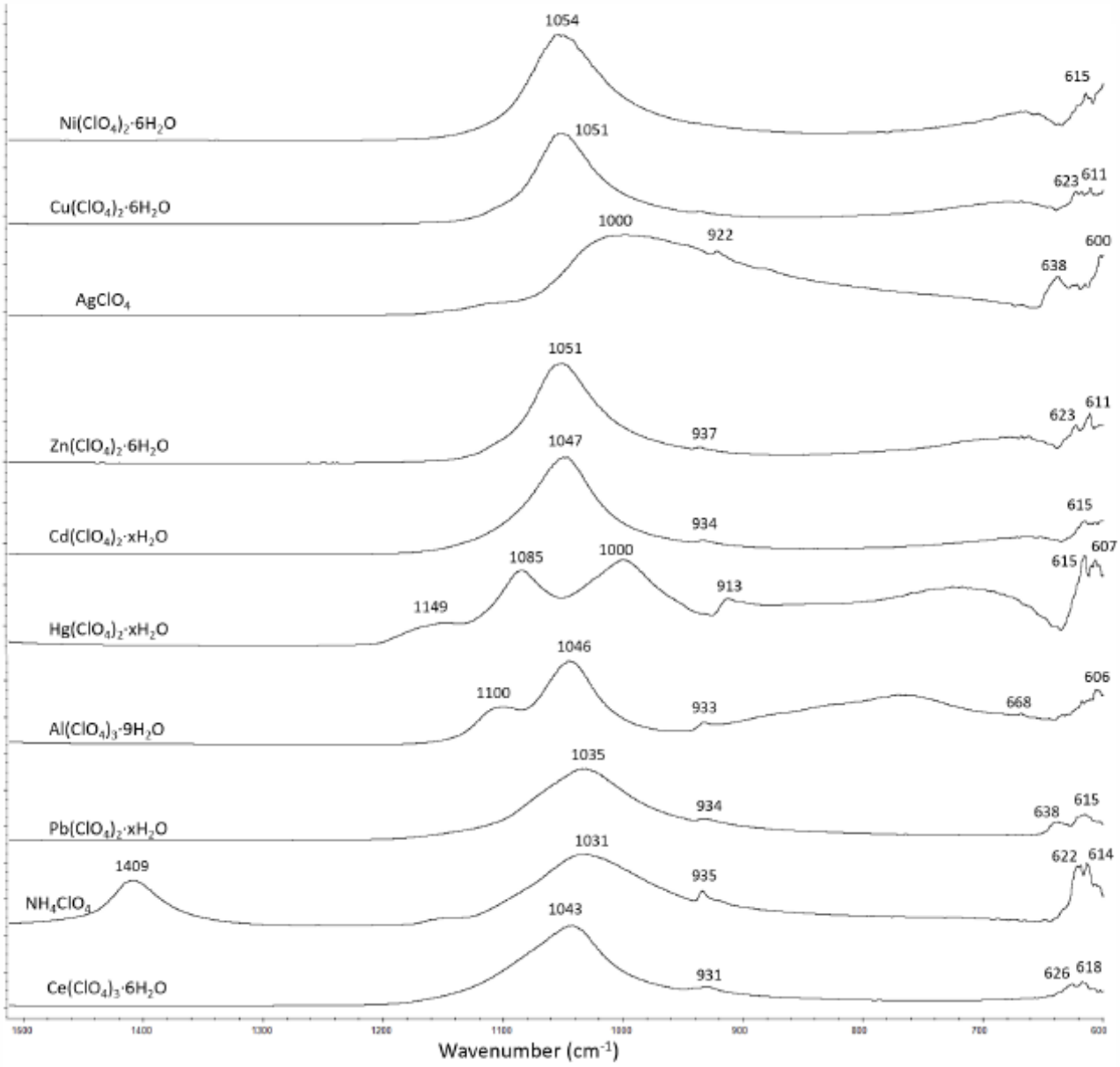
1054
615
Ni(ClO4)2·6H2O
1051
623
611
Cu(ClO4)2·6H2O
1000
922
600
638
AgClO4
1051
623
611
937
Zn(ClO4)2·6H2O
1047
615
934
Cd(ClO4)2·xH2O
1085
1000
615
607
913
1149
Hg(ClO4)2·xH2O
1046
606
1100
933
668
Al(ClO4)3·9H2O
1035
934
638
615
Pb(ClO4)2·xH2O
1031
622
614
1409
935
NH4ClO4
1043
931
626
618
Ce(ClO4)3·6H2O
1500
1400
1300
1200
1100
1000
900
800
700
600
Wavenumber (cm-1)

Annexe 3. IR spectra of stains of body fluids and potential interfering substances (Chapter 8)

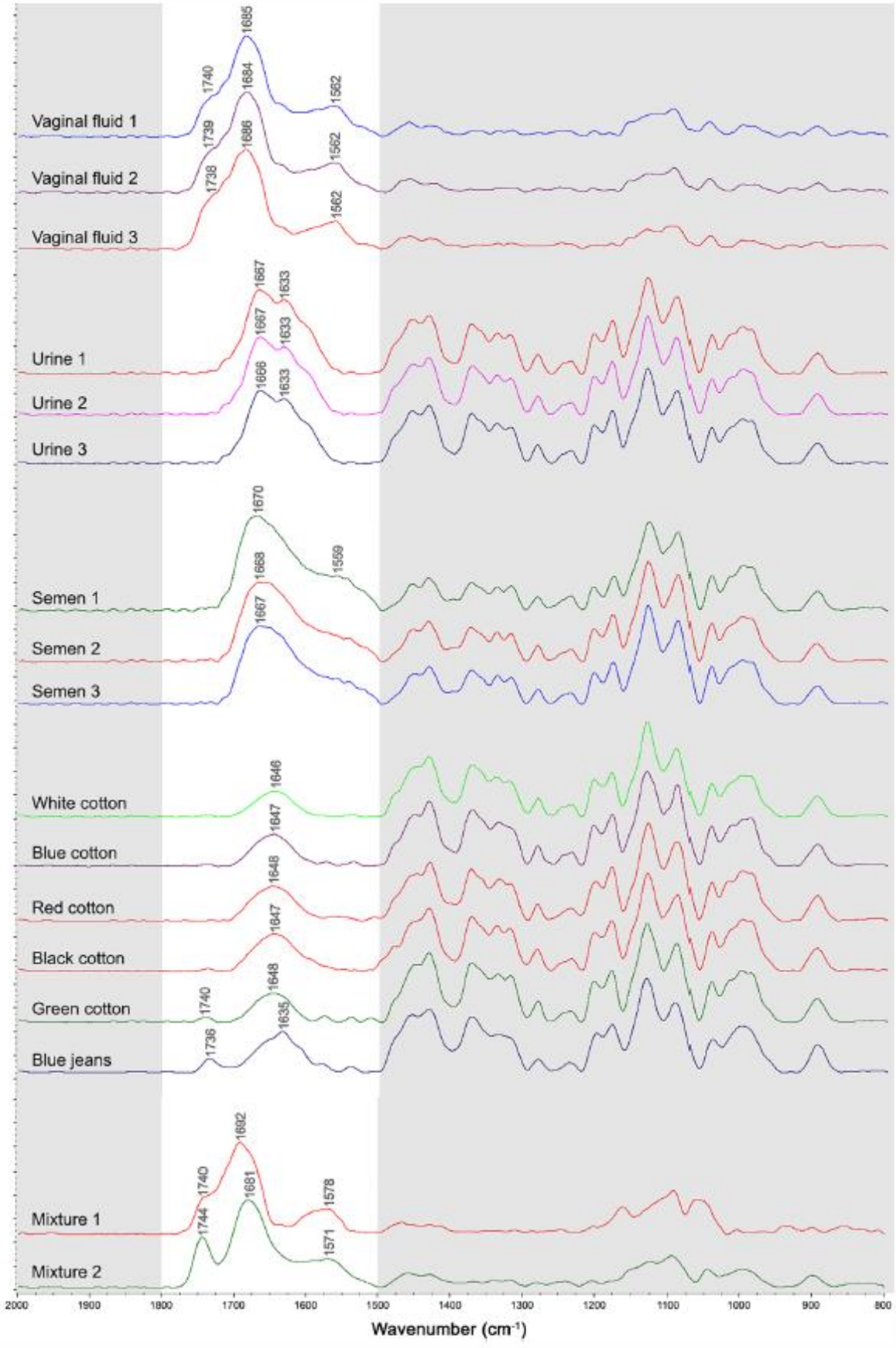

Annexe 3. IR spectra of stains of body fluids and potential interfering substances (Chapter 8)

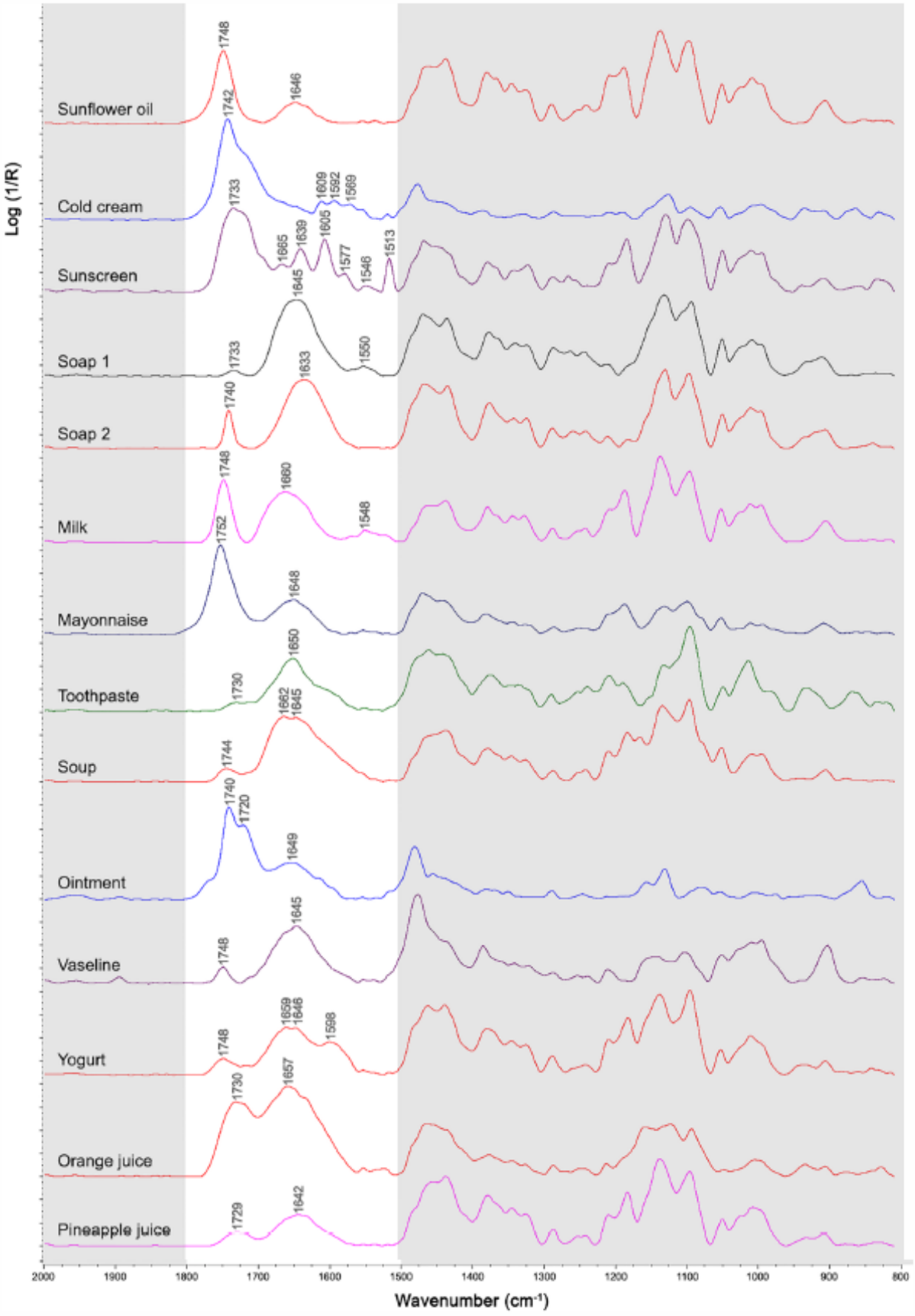

Agradecimientos/Acknowledgements

Aún no he empezado a escribir este apartado y ya se agolpan en mi mente un sinfín de personas, recuerdos e historias que, en mayor o menor medida, han influido en el desarrollo de mi doctorado, tanto a nivel científico/académico como a nivel personal y humano. Si por mi fuera, llenaría decenas de páginas rememorando tales momentos, y agradeciendo a todas y cada una de las personas que conmigo los compartieron, la ayuda que directa o indirectamente me han brindado. A lo largo de estos cuatro años de doctorado, han sido muchas las veces que he dicho agradecido "gracias, *thanks, obrigado, grazie, aitäh, tak* y *mercy*" (creo que no me dejo ninguna :)). Este pequeño diccionario multilingüe muestra a la perfección la ayuda, tanto nacional como internacional, que he recibido de tantas y tantas personas a lo largo de esta etapa de mi vida. Etapa que, con la redacción de esta tesis, toca tristemente a su fin. Y, aunque sea de manera simbólica, poder dedicaros unas líneas en esta tesis mostrando mi agradecimiento es una bonita forma de deciros que un pedacito de ella os corresponde.

El mayor pedacito, sin lugar a dudas, te lo debo a ti, Carmen. Siendo mi directora de tesis, has sido, junto a mí, la persona que más se ha esforzado y más ha trabajado en este proyecto. Te agradezco todo ese esfuerzo y todo ese tiempo que me has dedicado. Pero, sobre todo, quiero agradecerte que hayas sido la directora de tesis que necesitaba. Porque junto con tus directrices, consejos y críticas constructivas, me has dado también la libertad, ya fuera, para aceptarlas, mejorarlas o incluso cuestionarlas; y me has dado la libertad y el apoyo para explorar nuevos horizontes en los que investigar. Y como resultado, algunas veces hemos acertado y otras veces no; lo que ha sido muy positivo porque ha hecho que aprenda doblemente. Desde que me diste clase por primera vez (allá por el año 2009), ya conectamos, y todos estos años no han hecho sino demostrarnos la enriquecedora sinergia y el rápido entendimiento que hay entre nosotros. Tanto es así, que muchas veces nos basta una mirada para entendernos y nos bastan unas pocas palabras para discutir cientos de ideas. Lo que es enormemente práctico. Así pues, aprovechando esa ventaja y puesto que tantos años "soportándonos" dan mucho para agradecer, lo resumiré en pocas palabras diciendo: MUCHÍSIMAS GRACIAS POR TANTO.

En segundo lugar, quiero incluir en mis agradecimientos a todos los miembros de Inquifor. A los primeros… porque fuisteis con los que compartí mis inicios en el grupo. Porque gracias a que Carmen me diera clase en primero de carrera y, como consecuencia, yo empezara a participar en las actividades de divulgación del grupo; he tenido la inmensa suerte de conocer a todos y cada uno de los doctorandos (ahora doctores) que con su dedicación y esfuerzo han enriquecido el grupo a su paso. Porque todos habéis sido, de un modo u otro, ejemplos a seguir y guías valiosas en este difícil camino que supone hacer el doctorado. Aunque ya no estéis en el grupo, para mi sois los pilares fundamentales que lo sustentan… Siempre agradecido le estaré a Mariángeles, una de las personas que más ha contribuido en mi formación como investigador. Gracias por haber sido tú quién supervisó mis inicios y mis primeros años en la investigación, una persona seria, trabajadora y competente. Si hoy estoy terminando esta tesis, sin duda, es gracias a ti, a tu ayuda y a la base que me diste. De verdad, muchísimas gracias... Gracias también a María, por tu ayuda, por tu empatía, por las actividades de divulgación y las investigaciones que hemos compartido. Porque si hoy estoy escribiendo estos agradecimientos, en parte, es por tu culpa, porque la defensa de tu tesis fue la primera que presencié en mi vida y la que terminó de convencerme de la locura de hacer el doctorado… Gracias a Charlie, de quién aprendí que no hay nada imposible (un biólogo al que le asustan los petardos y tras la tesis, el mayor experto en pirotecnia y cócteles molotov del mundo). Gracias por tu amabilidad y por la ayuda mutua en los distintos trabajos, investigaciones y actividades que juntos hemos realizado… Gracias a André, por los años que coincidimos en Alcalá y por hacer mi estancia en Recife tan agradable, fácil y cómoda. *Muito, muito obrigado*… Gracias a Matías, por ser una de las personas con las que más tiempo he compartido el laboratorio, gracias por tu simpatía y tu disposición para ayudarme siempre… Y a Jorge, una de las personas con las que menos tiempo coincidí en el laboratorio, pero con la que compartí mi estreno en las actividades de divulgación del grupo. Muchas gracias a todos.

Igualmente agradecido les estoy a las personas con las que he compartido la mayor parte de mis años de doctorado: A Vale, la persona que, con toda seguridad, mejor comprende las dificultades que entraña la microscopía Raman. Gracias por compartir conmigo, no sólo los momentos divertidos vividos dentro y fuera de la Universidad, sino también esos momentos de frustración "instrumental", llevados con optimismo y buen ánimo. Sé que te debo más de

un baile xD… A Sofía, con quien he compartido un sinfín de aventuras por España, Portugal, Dinamarca y Suecia. Porque hay momentos, buenos y malos, que conectan a las personas y fortalecen la amistad. Podría escribir varias páginas hablando de los buenos momentos que hemos vivido y extrayendo lo positivo de los malos, pero prefiero guardarlos para nosotros. *Mas sim, vou resumir dizendo que um dos maiores presentes que me deu o doutoramento foi ter conhecido uma pessoa tão ótima, excepcional e maravilhosa como tu, e eu estou muito grato por isso…* A Pablo, uno de los mejores compañeros de doctorado que se pueden tener, por aportar la dosis de calma y tranquilidad necesarias para no volverse loco en el estrés que supone hacer una tesis. Porque ya sea para montar en bici, escalar una montaña, atravesar un río a nado o tomar unas tapas y beber unos UBEs, siempre puedo contar contigo. Gracias por ser tan genial y por tener un corazón tan grande… A Fernando, una de las personas de las que más he aprendido, no sin esfuerzo, sobre quimiometría y Matlab. Gracias por tantas investigaciones y resultados que hemos discutido. Porque muchas veces no hemos estado de acuerdo, lo que ha enriquecido nuestras discusiones científicas, nos ha obligado a explicar mejor nuestras posturas y nos ha permitido reenfocar ideas y mejorarlas. Pero sobretodo, gracias por tu optimismo al emprender nuevas investigaciones (por muy locas que éstas sean), y por los momentos de distensión, de bromas y de risas que hemos disfrutado en el laboratorio… A Mercedes, con quien más actividades de divulgación he compartido y que más libros me ha prestado; gracias por, a pesar de tus ocupaciones, buscar siempre un hueco para atenderme cuando he necesitado tu ayuda, por tu apoyo en la docencia de OBL que hemos impartido y por ser un gran ejemplo como docente… A Gemma, por tu buena disposición en las investigaciones, cursos y actividades de divulgación en las que juntos hemos colaborado, por tus comentarios, siempre críticos, para mejorar y re-mejorar cualquier trabajo, y por enseñarme que a pesar del estrés constante en que vivimos, siempre hay tiempo para tomarse un café rápido… A Víctor, nuestro veterinario forense chileno, gracias por tu confianza, tu ayuda desinteresada, tu trabajo y esfuerzo constante por hacer que todo salga adelante, por tu implicación en cualquier actividad de equipo y por ser tan simpático y complaciente. Muchas gracias por todo… Agradezco por último en este apartado a Miguel González y a Gloria Quintanilla por todas las veces que me han ayudado a lo largo de mi doctorado en los distintos temas que hemos colaborado.

Un apartado propio merecen los mejores gestores y técnicos que ha tenido Inquifor, los cuáles han hecho posible que los proyectos, investigaciones, cursos y actividades de divulgación que ha hecho el grupo hayan salido adelante. Un agradecimiento inmenso merece el mejor arquitecto-bombero del mundo. Gracias Ignacio por transformar mis cutres figuras y *graphical abstracts* en figuras magistrales (infinitamente mejor que mi idea original); y por TODA tu ayuda con el trabajo "de campo" de Ramanex que nos ocupó horas y horas de dedicación y esfuerzo, ya fuera transportando ladrillos y neumáticos bajo la lluvia, serrando estacas bajo un sol abrasador o explosionando IEDs con síntomas de congelación. Muchísimas gracias… Gracias también a Laura, con quien he compartido un lugar secreto en la Universidad de Alcalá; exacto, nuestro laboratorio de ciencias, el que ningún repartidor es capaz de encontrar. Gracias Laura por ayudarme y relevarme en un montón de quehaceres, tanto con la supervisión de los espectrofotómetros IR y Raman como con el pedido e inventariado de reactivos… Y a Javier, por tu colaboración y ayuda en la organización de las actividades de divulgación y redacción de proyectos de estos últimos años y por tu constante buen rollo, tanto en las reuniones de grupo como estando cabeza abajo en una montaña rusa. Aprovecho para recordarte que aún me debes un cachopo.

Tampoco puedo olvidarme de los excelentes investigadores y mejores personas que he tenido la suerte de supervisar, dirigir o ayudar en sus respectivos doctorados, trabajos fin de máster o trabajos fin de grado durante estos años. Si de mis profesores aprendí mucho, de vosotros he aprendido mucho más. Ha sido un placer conoceros, supervisar vuestro trabajo y comprobar vuestra brillante evolución como científicos. A Inês, porque nadie mejor que tú podría haber continuado la investigación que empecé sobre *body fluids*. *Porque desde o primeiro dia depositaste em mim, um estudante a começar o doutoramento, a confiança para te guiar na tua investigação, avaliando positivamente os meus comentários e críticas*. Por tu amabilidad, tu buen ánimo, tu interés por aprender y por las cañas que juntos hemos disfrutado. *Muito obrigado*… A Heidi, *the prettiest estonian model scientist, I really enjoyed those months we spent together taking "pictures" every day; our trips and adventures; our research and scientific discussions; our ten thousand days being forever young; our "Tinto de vino" and "Tinto de verano". Thank you for choosing our group to make your stay and demonstrating me that cold pessimist people from the North Pole may be lovely and nice. Aitäh*… A Diogo, *uma das pessoas mais trabalhadoras que*

alguma vez conheci. Porque viniste a Alcalá para trabajar con un "eminente científico" llamado Félix Zapata que resulté ser yo. Solo espero que no te llevaras una gran decepción cuando nos conocimos. Creo que al final hicimos un gran trabajo gracias a tu dedicación, esfuerzo y voluntad de aprender. *Muito obrigado*… A Sergio, el multi-ocupado investigador que amablemente ha contribuido a incrementar también mi multi-ocupación. Gracias por "molestarme" siempre de forma tan educada, tan considerada y avisándome con tanta antelación xD. Pero, gracias sobretodo por esos momentos de terapia motivadora… A Filipe, *um investigador brasileiro brilhante e fluorescente, sempre predisposto a começar novas investigações e a compartilhar bons momentos tanto no laboratório como no trabalho de campo acomphanados por explosivos, bombeiros e aranhas. Muito obrigado*… A Raúl, quien vino de Tarragona a hacer su TFM con nosotros y cuya estancia se pasó realmente rápido. Pero ya dicen, lo bueno, si breve, dos veces bueno. Gracias por tu sentido del humor, tu compañerismo, tu franqueza y tu actitud inteligentemente pragmática y resolutiva… A Irene (mi bióloga favorita), con quien he compartido la frustración e impaciencia ante la falta de resultados que parecen no llegar nunca, y que nos ha obligado a reconsiderar todas las opciones. Muchas gracias por tu capacidad de adaptación a los avatares de la investigación, por tu constancia, tus ganas de aprender, y sobretodo, por tu simpatía, tu naturalidad y tu buen ánimo… A Víctor, quien ha venido desde Perú a trabajar conmigo a Alcalá, no una, sino dos veces. Gracias por tu confianza, tu modestia, tu esfuerzo y tu dedicación minuciosa para hacer cualquier trabajo lo mejor posible… A Marzia, *la mia amica italo-slovena, cosa?* Gracias por esos meses tan divertidos disfrutando de tu compañía, ya fuera degustando una tapa tras otra en los distintos bares de Alcalá (que sé cuánto lo echas de menos), investigando en la Universidad en compañía de nuestra amiga Mª Juana, o riéndonos juntos de tus *figura di merda*. *Grazie grazie mille*… A Vicky, a quien acabo apenas de conocer, pero es como si conociera de toda la vida. Gracias por tu confianza e implicación desde el minuto cero, por esas miradas de "comprensión mutua" en las prácticas de laboratorio, e incluso por esa mezcla de curiosidad, ironía y franqueza infinitas, con la que tanto te "haces querer" xD… A Irene Burgos, y su alter ego (Irene Conflictos), por tu envidiable organización y tu buen ánimo. Nunca olvidaré esas "maravillosas y felices" tardes (tardes que se tornaron noches) que tanto disfrutamos preparando toneladas y toneladas de jabón… A Mireya, ¿cuántos años hace que nos conocemos? Casi la mitad de nuestras vidas metiéndonos el

uno con el otro, siempre con mucho cariño, eso sí. Gracias por tantos momentos divertidos en las clases de inglés, en las clases particulares que algún año te di (no sé si con mucho éxito) o en el laboratorio supervisando tu TFG. Cuán encantadora y pejiguera pudiste llegar a ser :P… A Nacho, por tu gran autonomía e iniciativa en el magnífico TFG que hiciste y tu buena disposición para colaborar en cualquier actividad de grupo… A María Martínez, por elegir Inquifor para hacer tu TFG, teniendo incluso que venir desde Jaén. Gracias por tanto interés y esfuerzo… Y a Paula, la primera estudiante cuyo TFG supervisé y, tal vez por ello, uno de los TFG más queridos para mí. Tuve la suerte de empezar supervisando a una persona inteligente, trabajadora y, en pocas palabras, excelente. Muchas gracias por haber sido tú la primera…

Termino mis agradecimientos al grupo con las personas que por él pasaron y con las que compartí breves pero buenos y divertidos momentos, muy especialmente a Carolina, Joana, Lucía, Héctor, Erika, Karla, Gül Fidan y Kiko; y con las personas que recientemente se han incorporado al grupo, muy especialmente a Jordi y a Germán.

Si esta tesis ha salido adelante ha sido, sin duda, gracias a la colaboración del Servicio de Criminalística de la Guardia Civil, la Comisaría General de Policía Científica y el Instituto Nacional de Toxicología y Ciencias Forenses. Muchas gracias por vuestro apoyo, por compartir vuestra experiencia y por trasladarnos problemáticas forenses reales en las que centrar nuestras investigaciones científicas, siempre con el fin de encontrar soluciones, mejoras y/o métodos complementarios con los que asegurar la correcta detección y análisis del vestigio forense. Sobre todo, gracias a José Luis Ferrando y a todos los compañeros del SEDEX por su inestimable ayuda en todas las investigaciones que implicaron trabajar con explosivos… a los compañeros de balística del CNP y del SECRIM por las investigaciones que implicaron hacer disparos con armas de fuego… y a Pilar Martínez del INTCF, por su apoyo en las investigaciones relativas al análisis de fluidos biológicos. Aprovecho también para agradecer al Instituto Universitario de Investigación en Ciencias Policiales por facilitar dicha comunicación entre los cuerpos policiales y la Universidad y crear ese marco de encuentro tan enriquecedor.

También agradezco el valioso apoyo y ayuda instrumental que he recibido de los técnicos de los distintos espectrómetros que he utilizado: A Sergio, Pedro y Rafa (de Thermo) por el microscopio Raman y el espectrofotómetro FTIR;

especialmente a Sergio, por tantas veces y tantas horas que nos ha visitado y de quien tanto he aprendido sobre Raman… A Carlos Villar (de Bruker) por el espectrofotómetro FTIR portable… y a Jaime de Sousa (de Microbeam) por el espectrómetro Raman portable.

I really want to thank the marvellous people I met during my stay in Copenhagen for their great reception, help and all the fun we had together those months, including Juliana, Carlos, Viola, Neirivaldo, Ecem, Dillen, Luliana, Tina, Rocío y muy especialmente… A José Manuel Amigo, tutor de mi estancia, y de quien más he aprendido sobre análisis de imagen hiperespectral. Gracias por crear hypertools para los que somos principiantes en MatLab y la programación no nos apasiona, y gracias sobre todo por tu buen rollo (tanto en la universidad interpretando algoritmos, como de ocio catando cervezas)… A Davinia, *thank you for your help during my wonderful stay in Ghent…* A Carol, *Oh caralh...! Você já sabe o quão genial você é e o quão grato eu estou de que, durante nossos doutorados, coincidimos em 3 países e 2 continentes compartilhando muitas histórias, risadas, despedidas e reencontros. Muito obrigado…* A Manu, *Allora! You were one of the persons who made my stay in Copenhagen wonderful. Because, even without knowing me, you were so kind to me from the first minute, sharing with me your office, your desktop and your love to CPH. Grazie mille mia carissima amica di Ancona, mi manchi my dear!!…* y a Noe, ¡Dale! Porque vos fuiste la persona que terminó de hacer maravillosa mi estancia en Copenhague. Gracias por las excursiones que hicimos por Dinamarca, por esperarme para comer con el horario español y por enseñarme con tu simple carta de presentación que somos ciudadanos del mundo: "Hola, me llamo Noemí, soy de Paraguay, pero vivo en Barcelona, donde estoy haciendo el doctorado; aunque ahora mismo estoy haciendo una estancia en Copenhague y la próxima semana voy a un congreso a Helsinki", ehhh rebobina…

Eu quero, também, agradecer aos amigos que fiz (ou visitei) durante a minha estância no Brasil. Em primeiro lugar, ao Celio Pasquini *e à* Maria Fernanda Pimentel *por me terem aceite na Universidade Estadual de Campinas (UNICAMP) e na Universidade Federal de Pernambuco, respectivamente. Em segundo lugar, à Cris, porque aqueles dias que estive em Campinas foram ótimos graças a você e por ser a melhor professora de portunhol do mundo. Muito obrigado… E finalmente, para os amigos André, José, Carol e Neirivaldo que vi novamente em*

Recife, e para Marcella, que embora não tendo coincidido em Recife, jamais esqueceremos os dias maravilhosos que passamos em Alcalá. Legau!

Agradezco también, en este apartado de viajes y estancias, a mis amigos de la Universidad de Cádiz, muy especialmente a Marta, por tu amable acogida durante mi visita a Cádiz, por los cursos de verano que hemos compartido y por enseñar a un escéptico en gestores bibliográficos como yo, que Mendeley puede ser el mejor ayudante que se puede tener a la hora de escribir la bibliografía de cualquier trabajo.

Volviendo la vista a Alcalá, quiero incluir en mis agradecimientos a todos mis compañeros de Quimicanal. La verdad es que mi ubicación habitual en el laboratorio de ciencias, mis idas y venidas entre laboratorios, y mis obligaciones diarias como chófer de mediodía, han hecho que nuestros encuentros por los pasillos hayan sido siempre fugaces y ocasionales. No obstante, me quedo con nuestras fantásticas cenas de Navidad, con nuestras barbacoas universitarias, con esos días de celebración siempre que alguien defendía una tesis y con esa esperanza ciega de hacernos millonarios cada 22 de Diciembre. Muchas gracias por todos esos buenos momentos. No citaré los nombres de todos los Quimicanalíticos para no extenderme indefinidamente, salvo el de una persona con la que compartí más de una desventura. Gracias Romy por visitarme en Copenhague (me alegro de que todo se quedara en un susto…), y porque siempre podremos sentirnos orgullosos de lograr lo imposible: encontrar una pizzería en Malmö que aún estuviera abierta a las 18:00 de la tarde un sábado.

Hago extensivo mi agradecimiento a los profesores del Departamento de Química Analítica, muy especialmente a Alberto Escarpa, coordinador del Doctorado y Director del Departamento; y a las profesoras Mª Paz, Nines y Mª Sol con quienes he compartido varias horas de prácticas en el laboratorio y de las que, día tras día, sigo aprendiendo para ser un buen profesor. Gracias Mª Paz, además, por ser mi tutora durante el doctorado; y gracias Nines, por contar conmigo cada año en la actividad del nitrógeno líquido de química en acción con la que siempre triunfamos. Agradezco también en este apartado a Ana, Vanesa y María José, las técnico de laboratorio de química analítica, química inorgánica y química física, que en más de una ocasión me han brindado su ayuda.

A mis compañeros del máster, por vuestra cercanía y vuestra humildad sin importar el número de estrellas que llevéis en el uniforme. Gracias sobre todo a

Emilio, el mejor delegado que una clase puede tener… a Carmen, ¡qué suerte tuve de coincidir con otra química en el máster y que resultara ser una persona tan maravillosa como eres! Gracias por todos los buenos momentos que hemos disfrutado… y a Bernardo, el incansable abogado siempre ocupado, pero que aun así saca tiempo para invitarme a una cerveza cada vez que nos vemos. Lo que daría por que el tiempo me cundiera la mitad que a ti. Gracias por todo.

A mi gran amigo Alberto, con quién he compartido la ESO, Bachillerato y Universidad; un gran ejemplo de voluntad, dedicación y esfuerzo.

A mis amigos del grado en química con los que pasé tantas horas aprendiendo esta ciencia, compartiendo no solo un sinfín de asignaturas y prácticas de laboratorio, sino también noches de ocio y diversión. Las cuales, aunque con menor frecuencia, han continuado durante estos años de doctorado. Muchas gracias a todos, especialmente a Nerea, María, Sergio y Erika. A todos os digo: Siempre quedará la "química" entre nosotros. E igualmente partícipes de este agradecimiento os podéis sentir todos los "no químicos" del grupo. Gracias sobre todo a Marta, con quien siempre compartiré mi pasión por los patines y el hielo.

Por último y más importante, agradezco a mi familia el amor y apoyo incondicional que siempre me han dado. Ellos son el pilar fundamental que me sustenta. A mis padres. Se dice que somos un 50% genética y un 50% ambiente (influyendo en nosotros desde la infancia), lo que quiere decir que prácticamente todo (bueno y malo) os lo debo a vosotros. Y ciertamente puedo decir que me siento muy afortunado y agradecido porque lo mucho bueno ha superado con creces lo poco malo. Cómplices necesarias de ese buenísimo ambiente son mis dos hermanas, quienes lo son todo para mí. Ellas lo saben perfectamente, pero aun así dirán que pocas veces se lo digo… y puede que tengan razón. No soy de los que pregonan sus sentimientos a los cuatro vientos, y mi familia lo sabe; de la misma forma que sabe, sin necesidad de palabras, que un amor incondicional es inefable, servicial y constante… A mis abuelos, muy especialmente a los que ya no están aquí, los mejores ejemplos de superación que pude conocer y a quienes pude disfrutar por tantos años… A mi tía Loli, por tantas geniales visitas, excursiones y viajes… A mis primos y tíos navarros, claros sinónimos de divertidas e inolvidables vacaciones. ¡Aúpa ahí!… Y sobre todo, a mi tía Rosa, quien mejor puede comprender lo que supone terminar una tesis…

Universidad de Alcalá

Facultad de Ciencias
Departamento de Química Analítica, Química Física e Ingeniería Química
Área de Química Analítica